ANL/FE-80-10

ANL/FE-80-10

SULFUR CONTROL IN FLUIDIZED-BED COMBUSTORS: METHODOLOGY FOR PREDICTING THE PERFORMANCE OF LIMESTONE AND DOLOMITE SORBENTS

by

Darrell C. Fee, Kevin M. Myles, W. Ira Wilson,
Liang-Shih Fan, Gregory W. Smith, Samuel H. Wong,
John A. Shearer, John F. Lenc, and Irving Johnson

RETURN TO REFERENCE FILE
TECHNICAL PUBLICATIONS
DEPARTMENT

FOSSIL ENERGY PROGRAM

ARGONNE NATIONAL LABORATORY, ARGONNE, ILLINOIS

Prepared for the U. S. DEPARTMENT OF ENERGY
under Contract W-31-109-Eng-38

DISCLAIMER

This report was prepared as an account of work sponsored by an agency of the United States Government. Neither the United States Government nor any agency thereof, nor any of their employees, makes any warranty, express or implied, or assumes any legal liability or responsibility for the accuracy, completeness, or usefulness of any information, apparatus, product, or process disclosed, or represents that its use would not infringe privately owned rights. Reference herein to any specific commercial product, process, or service by trade name, trademark, manufacturer, or otherwise, does not necessarily constitute or imply its endorsement, recommendation, or favoring by the United States Government or any agency thereof. The views and opinions of authors expressed herein do not necessarily state or reflect those of the United States Government or any agency thereof.

Printed in the United States of America
Available from
National Technical Information Service
U. S. Department of Commerce
5285 Port Royal Road
Springfield, VA 22161

NTIS price codes
Printed copy: A20
Microfiche copy: A01

Distribution Category:
Coal Conversion and Utilization—
Direct Combustion of Coal
(UC-90e)

ANL/FE-80-10

ARGONNE NATIONAL LABORATORY
9700 South Cass Avenue
Argonne, Illinois 60439

SULFUR CONTROL IN FLUIDIZED-BED COMBUSTORS: METHODOLOGY FOR PREDICTING THE PERFORMANCE OF LIMESTONE AND DOLOMITE SORBENTS

by

Darrell C. Fee, Kevin M. Myles, W. Ira Wilson,
Liang-Shih Fan,* Gregory W. Smith, Samuel H. Wong,
John A. Shearer, John F. Lenc, and Irving Johnson

Chemical Technology Division

September 1982

This report supersedes ANL/CEN/FE-80-10

*Consultant, The Ohio State University, Columbus

TABLE OF CONTENTS

		Page
ABSTRACT		1
1.0	SUMMARY	2
	1.1 How to Use this Book	5
	1.2 Comparisons with Plant Operation Data	7
2.0	SUMMARY OF SORBENT SELECTION	14
	2.1 Limestone Formation and General Properties	15
	2.2 Sorbents Included in this Book	18
	2.3 Sorbent Ranking	27
3.0	SUMMARY OF STANDARD TESTS	64
	3.1 Thermogravimetric Analyzer Test	65
	3.2 Attrition	70
	3.3 Petrographic Analysis	74
	3.4 Porosity, Pore Size Distribution, Surface Area, Density	76
	3.5 Decrepitation Test	80
4.0	SUMMARY OF TEST RESULTS	81
	4.1 Analysis of TGA Test Data	82
	4.2 Analysis of Attrition Data	97
5.0	LIMESTONE SUMMARY	110
	5.1 Standard Sorbent Data Format	111
	5.2 Test Data on Limestones	113
6.0	DOLOMITE SUMMARY	273
	6.1 Standard Sorbent Data Format	274
	6.2 Test Data on Dolomites	276
7.0	SUMMARY OF PREDICTION MODELS	360
	7.1 In-Bed Sulfation	361
	How to Determine γ and $(1 - \beta)$	367
	7.2 Freeboard and In-Bed Sulfation	378
	7.3 In-Bed Sulfation: Multiple Particle Sizes	390
	7.4 Limitations of Thermogravimetric Analyzer Data	400
	7.5 Attrition	412
	7.6 Elutriation	425
	7.7 Elutriation Coupled with Attrition	435
8.0	FBC PLANT DATA	443

(see Addendum, ANL/FE-80-10, "Compilation of Sorbent Performance Data from Atmospheric Fluidized-Bed Combustor," 1982)

ABSTRACT

The ANL methodology significantly simplifies predictions of sulfur capture in fluidized-bed coal combustors. This section summarizes how to use the methodology to make predictions. The details of the method development and supporting data are given in the later sections. In addition, comparisons between predicted sorbent performance and actual FBC plant data are shown to support the methodology. The method adequately describes the experimental results and thus can be used with some confidence to compare sorbent performance, provided, of course, that the limitations of the methodology are recognized.

1.0 SUMMARY

The ANL methodology significantly simplifies predictions of sulfur capture in fluidized-bed coal combustors. Fluidized-bed combustion of coal is one of the more promising new technologies for steam and power generation. In this process, coal is burned in a fluidized-bed composed mainly of calcined limestone sorbent. The calcium oxide reacts chemically to capture the sulfur dioxide formed during combustion and to maintain the stack gas sulfur emissions at acceptable levels. The spent sulfur sorbent, containing calcium sulfate, is a dry solid that can be disposed of with coal ash or potentially used as a commercially attractive material. Other major advantages of fluidized-bed combustion are the reduction in nitrogen oxide emissions because of the relatively low combustion temperatures, the capability of burning wide varieties of fuel, the high carbon combustion efficiencies, and the high heat-transfer coefficients. The ANL effort clearly enhances the commercialization of fluidized-bed coal combustion by providing a simple, yet reliable, user-oriented methodology that allows performance of a sorbent to be simply predicted.

Standardized laboratory tests rapidly define the three essential sorbent parameters utilized by the ANL methodology. These low cost tests form the basis for predicting sorbent performance. The standard tests and the subsequent method of data analysis are described in detail in the handbook (ANL/FE-80-10, "Sulfur Control in Fluidized-Bed Combustors: Methodology for Predicting the Performance of Limestone and Dolomite Sorbents," 1982, supersedes ANL/CEN/FE-80-10, "Sulfur Control in Fluidized-Bed Combustors: Sorbent Utilization Prediction Methodology," 1980). The principal test measures the reactivity and capacity of the sorbent with sulfur dioxide using a laboratory thermogravimetric analyzer. A second test measures the durability of the sorbent particle under the mixing and grinding action of a fluidized bed. The reactivity, capacity, and durability are the three essential sorbent parameters defined by standardized laboratory tests.

Sorbents clearly exhibit a wide range of behavior. The standard tests show several orders of magnitude variation in sorbent durability and in sorbent reactivity and capacity for sulfur dioxide. Sorbent specific data must be used to predict the sulfur capture performance in a particular fluidized-bed combustor and at particular operating conditions. Testing of sorbents is a cost-effective means of ensuring optimal sorbent performance. Severe negative economic impacts usually arise from less than optimal performance. The wide range of sorbent behavior must be taken into account in successfully designing and operating a fluidized-bed coal combustor.

The simple ANL methodology adequately predicts combustor sulfur capture performance. The ANL methodology is sufficiently accurate to identify the best sorbent among several. Further, the economics of various alternative scenarios of combustor operation can be evaluated in terms of limestone utilization, quarrying/transportation costs, and waste management. The ANL methodology is part of a limestone evaluation and advisory service which is available to assist with the decisions concerning sorbent selection for the optimization of existing plants and for the optimization of the site of future facilities. Using the ANL methodology, predictions have been made for sorbent performance in large scale fluidized-bed combustors. The correlation

between these predictions and previously reported observed sorbent performance is better than previous models. Thus, some confidence has been established that this simple, easy to use methodology is adequate for evaluating sorbent performance.

Darrell C. Fee, Coordinator
Kevin M. Myles
W. Ira Wilson
Liang-Shih Fan*
Gregory W. Smith
Samuel H. Wong
John A. Shearer
John F. Lenc
Irving Johnson

Chemical Technology Division
Argonne National Laboratory
September 1982

*Consultant, The Ohio State University, Columbus, OH

CONTRIBUTORS AND ACKNOWLEDGMENTS

In addition to the authors listed in the Summary, the following individuals have made significant contributions to the preparation of this handbook.

Roy A. Benson

Paul T. Champagne (1)

Scott L. MacKenzie (2)

Daniel C. Brennan (3)

(1) Student Aide, University of Illinois, Urbana, IL

(2) Undergraduate Research Participant, Wheaton College, Wheaton, IL

(3) Student Aide, Cornell College, Mount Vernon, IA

The authors wish to express their appreciation to Michael Petrick, Director, Fossil Energy Program; Albert A. Jonke, Associate Director for Coal Combustion and Conversion, Chemical Technology Division; and Leslie Burris, Director, Chemical Technology Division, of the Argonne National Laboratory for their encouragement and support.

The authors are grateful for the cooperation they have received from all the various industrial and governmental organizations that have participated in this effort. Special recognition is extended to the U.S. Department of Energy Morgantown Energy Technology Center and the U.S. Environmental Protection Agency without whose patient sponsorship this project would not have been undertaken.

1.1 HOW TO USE THIS BOOK

Predictions of sorbent performances in atmospheric fluidized-bed combustors (AFBC) are made with the ANL methodology using the following equation:

$$Ca/S = \frac{1}{\frac{D}{R} - \frac{U\gamma}{H\,b\,(1 - R)(1 - \beta)}}$$

where Ca/S is the molar ratio of calcium in the sorbent feed to sulfur in the coal feed to the bed.

H = combustion bed height (meters or feet).

U = fluidizing gas velocity (meters/second or feet/second; depending on units of bed height).

R = fraction of sulfur retained in the bed (i.e., 0.85 for 85% retention).

$1-\beta$ = fractional volume of the bed occupied by sorbent (i.e., excluding the bed volume occupied by gas bubbles, heat exchange tubes, and inert particles such as ash and rocks). For a fluidizing gas velocity of 2 to 2.5 meter/second and an average bed particle diameter of 1000 to 1200 μm, $(1 - \beta)$ is approximately 0.25. Formulas for calculating $(1 - \beta)$ for specific fluidized-bed operating conditions are given in Section 7.1 of this handbook.

D = maximum sorbent fractional utilization parameter, as determined from thermogravimetric analysis.

b = sorbent sulfur capture rate parameter (sec^{-1}) as determined from thermogravimetric analysis. The D and b values, unique to each sorbent, are tabulated in Section 4.1 for selected sorbents.

γ = a scaling parameter to account for bubbles in the bed, specifically to account for the possible difference in sulfur dioxide concentrations between the bubbles and the remainder of the bed (emulsion phase). For a fluidizing gas velocity of 2 to 2.5 meter/sec and an average bed particle diameter of 1000 to 1200 μm, γ is approximately 0.25 to 0.30 (i.e., TWO PHASE is the descriptor given to bubbles and emulsion). Formulas for calculating γ for specific operating conditions are given in Section 7.1 of this book. In this case, γ is 1.0 (i.e., ONE PHASE is the descriptor given to bubbles and emulsion).

To use this methodology:

1. Determine the sorbent parameters D and b. These parameters are tabulated in Section 4.1 for selected sorbents.

2. Determine the fluidized bed parameters γ and $(1 - \beta)$. These may be calculated for the particular operating conditions of interest with the formulas in Section 7.1. For a quick prediction with a combustor having a fluidizing gas velocity of 2 to 2.5 meter/sec and an average particle size of 1000 to 1200 μm, use $(1 - \beta) = 0.25$ and $\gamma = 0.25$.

3. Select the desired fractional sulfur retention R. For the New Source Performance Standards of 90% removal of the sulfur in the coal feed, R = 0.90.

4. Calculate the predicted Ca/S ratio for the bed height, H, and fluidizing gas velocity, U of the AFBC.

As an example, for D = 0.21, b = 430, $\gamma = 0.25$ and $(1 - \beta) = 0.25$, H = 1.2 m, U = 2.0 m/s, and R = 0.85, the required Ca/S is predicted to be 4.3.

The amount of sorbent that is required for a given amount of coal of known sulfur content can be calculated with the following equation:

$$\text{Weight sorbent} = (\text{weight coal})\left(\frac{Ca}{S}\right)\left(\frac{\text{wt \% sulfur in coal}}{\text{wt \% } CaCO_3 \text{ in sorbent}}\right)\left(\frac{100}{32}\right).$$

Thus, 0.25 ton of sorbent would be required for each ton of 3.2 wt % sulfur coal, if the concentration of $CaCO_3$ in the sorbent is 100 wt % and the predicted Ca/S ratio is 2.5.

1.2 COMPARISONS WITH PLANT OPERATING DATA

Confidence in the predictive capability of any model can be established only through a comparison between the model predictions and actual experience. To provide the basis for comparison in this handbook, an extensive review of the literature on sorbent performance in atmospheric fluidized-bed combustors has been undertaken; a compilation of the data is provided in (ANL/FE-10; "Sulfur Control in Fluidized-Bed Combustors: Methodology for Predicting the Performance of Limestone and Dolomite Sorbents," Addendum, Compilation of Sorbent Performance Data from Atmospheric Fluidized-Bed Combustors, supersedes ANL/CEN/FE-80-10, "Sulfur Control in Fluidized-Bed Combustors: Sorbent Utilization Prediction Methodology," 1980), FBC PLANT DATA. Selected combustor performance data has been extracted from the data base and compared with predicted sorbent performance data. The comparisons are made for larger scale combustors, although several smaller-scale combustors are included in the literature review, to avoid the problems associated with channeling and slugging found in smaller combustors. The comparisons are made as a plot of sulfur retention versus calcium to sulfur molar ratio in the feed.

For each combustor and sorbent selected, the combustor data and the model predictions are shown for the same set of operating conditions, listed at the bottom of the figure. The conditions listed represent the midpoint of narrow ranges of the actual operating conditions; for example, a temperature of 850°C represents a range of 840 to 860°C, approximately. The model predictions for the ANL methodology are shown in Figs. 1.2.1, 1.2.2, and 1.2.3.

In general, the ANL model under-predicts the sulfur retention for a given Ca/S ratio in the feed. Several possible explanations are as follows: (1) Freeboard sulfation - The model deals solely with sulfur capture within the fluidized-bed. However, sulfur capture above the bed, in the freeboard region, has been reported to be as high as 25% of the total [Babcock and Wilcox L/R:79: 4775:03(1979)]; (2) Compositional and reactivity differences in sorbent and coal, and (3) Inadequate Standard TGA Test - The model predictions are based on thermogravimetric analyzer (TGA) data. However, even though great care is taken in an attempt to make the conditions identical in terms of temperature, CO_2, SO_2, and N_2 pressure, etc., the calcination/sulfation conditions are apparently different in the TGA and in the fluidized-bed combustors. Quite wide differences in reactivity of a given commercial limestone have been noticed in this laboratory arising from compositional variability in some cases and, in others, arising from no obvious differences in physical character. A detailed discussion of limitations and qualifications of the TGA technique can be found in Section 7.4.

Part of the difference between TGA and FBC appears in the utilization of the calcium in the sorbent in that the maximum calcium utilization achieved in the combustor is much higher than in the TGA test. For example, sorbent 9202, Lowellville limestone, achieves a maximum utilization of only 31% of the calcium in the TGA test while utilizations of 35% were reported in the Babcock and Wilcox (B&W) 6'x6' combustor at steady-state conditions [Babcock and Wilcox LR:79:4775:01(1979)]. A difference in the maximum utilization of this magnitude would increase the predicted retention at a Ca/S feed ratio of 3.0 of S to 8% of the sulfur fed to the bed in Fig. 1.2.2 and yield retentions that fall closer within the scatter of the B&W FBC data. Another part of the difference results from attrition. The abrasive action of particle-particle contact in a fluidized-bed tends to remove the outer calcium sulfate layer on the sorbent particle and

the sorbent particle and expose the unreacted core of calcium oxide to SO_2. The attrition process thus rejuvenates the reactive surface area of the sorbent to increase the overall sulfur dioxide adsorption capacity. A similar mechanism does not exist in the standard TGA test where the sorbent particles are not in motion (see Section 4, STANDARD TESTS).

In summary, predictions of sorbent performance in AFBCs based on TGA data are subject to several limitations.

First, it has been observed, by several Laboratories, that the TGA test consistency under estimates the performance of sorbents as compared to that found in an AFBC. We believe that the alkali metal content in the coal enlarges the pore structure of the sorbents in a manner similar to that of salt enhancement additives (see ANL/CEN/FE-80-19). To date, we have not been able to satisfactorily redefine the standardized TGA test to quantitatively factor in the alkali content of the coal under consideration. Of course, the TGA test does remain an excellent method of comparing the relative performance of sorbents or materials.

Second, limestone is highly variable. The chemical composition and sulfation behavior of limestone varies significantly from strata to strata within a given limestone bed. Attempting to characterize many tons of limestone through a few TGA tests on 0.5 gm samples is clearly subject to great potential error. Finally, care must be taken when using TGA data for predictions because, in most cases, large increases in Ca/S molar ratio yield only small increases in sulfur retention, especially above 80 to 90% retention. Small changes in operating condition may shift this flat portion of the (retention versus Ca/S) curve, upward or down slightly. When the whole curve is analyzed, the change in operating conditions had little effect. However, if only the Ca/S ratio for 85% sulfur retention is reported, a large change in Ca/S ratio may be indicated due solely to the flatness of the curve. Recognition must be given this potentially misleading feature when analyzing the data.

The predicted elutriation rate of the smaller and lighter sorbent particles from the bed is also an important consideration. The calculations show that sorbent particles less than 150 μm in diameter are generally not retained in the bed. These finely sized particles are from three sources: (1) fine particles in the raw sorbent feed stock; (2) fine particles produced by calcination induced breakup as the sorbent enters the bed; and (3) fine particles produced by the abrasive action of particle-particle contact within the fluidized-bed. The first contribution is determined from sieve analysis of the sorbent feed; the latter two contributions are determined from the results of a standard laboratory attrition test (see Section 4, STANDARD TESTS). The three contributions are calculated and summed by the procedure described in Section 7, PREDICTION MODELS.

There are only a few cases where there is sufficient data in the literature to allow any comparison to be made between the predicted and the observed elutriation. Unfortunately, some of the cases do not represent steady-state elutriation conditions since the model indicates that steady state is reached

only after about 100 to 200 hours of FBC operation if the bed is fed sorbent 1/4- to 3/8-inch or larger in diameter top size. Several obvious cases of nonsteady state conditions were uncovered where between 4 to 5 wt % of the sorbent particles in the bed were found to be larger than the original sorbent feed for the particular test reported. In the final analyses, only the data reported on one sorbent and one combustor, B&W 6'x6' and 9202 - Lowellville, proved satisfactory. For this case the ANL model predicts a calcium elutriation rate that is 50% of the observed rate.

Although a single sorbent and a single combustor are obviously an insufficient basis for judging the ANL model, several reasons have been proposed for the underprediction. These are: (1) Transport Attrition - Fine particles produced during the transport of the sorbent into the bed are not taken into account. Heretofore, the size distribution of sorbent in the feed bunker prior to transport is used which probably results in the feed rate of fine particles to the bed being underestimated. (2) Calcination - Differences in calcination conditions, such as the rate of heating, between the Standard Attrition Test and the fluidized bed combustor, may significantly affect the extent of sorbent breakup on calcination and lead to an underprediction of this source of fine particles.

The ANL methodology in this handbook is adequate for ranking the suitability of limestones and dolomites as sorbents in fluidized-bed combustors. The model is accurate as any model in existence and yet is easier to use. Further, the ANL model shows explicitly the sorbent and FBC parameters which affect sorbent performance. This is advantageous in rapidly screening and selecting candidate sorbents. The standard tests utilized by the models are undergoing refinement to improve the accuracy of the predictions.

References for Section 1.2

Babcock and Wilcox LR:70:4775:03 Fluidized-Bed Combustor Facility and Commercial Utility AFBC Design Assessment, Babcock and Wilcox Annual Report 1978 (1979).

Babcock and Wilcox LR:79:4775:01 Fluidized-Bed Combustor Development Facility and Commercial Utility AFBC Design Assessment, Babcock and Wilcox Quarterly Report, January thru March, 1979 (1979).

Figure 1.2.1

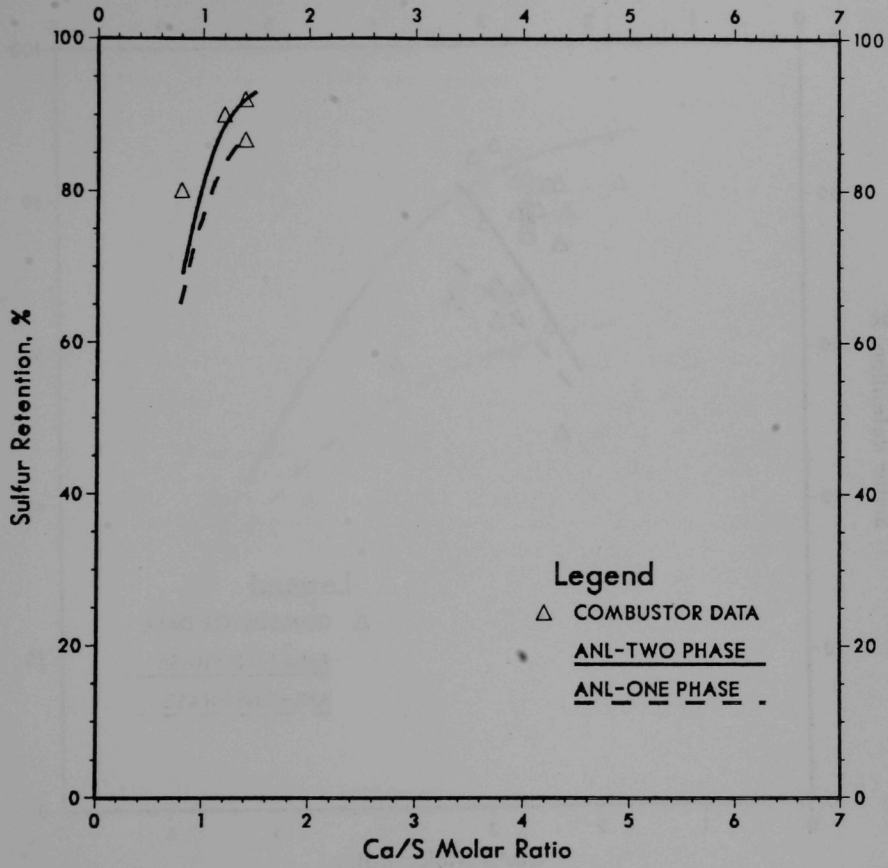

Fluidized Bed Operating Conditions

Temperature = 850. C = 1562. F

Pressure = 101. kPa = 1.0 atm

Fluidizing Velocity = 1.12 m/sec = 3.67 ft/sec

Bed Height = 0.91 Meters = 2.98 ft

Coal Feed Rate = 19.8 kg/hr = 43.6 lb/hr

Sulfur Content in Coal = 4.50 wt%

Bed Area = 0.21 sq. meter = 2.2 sq. ft.

Sorbent Particle Dia. = 1100. micron = 0.0433 inch

Figure 1.2.2

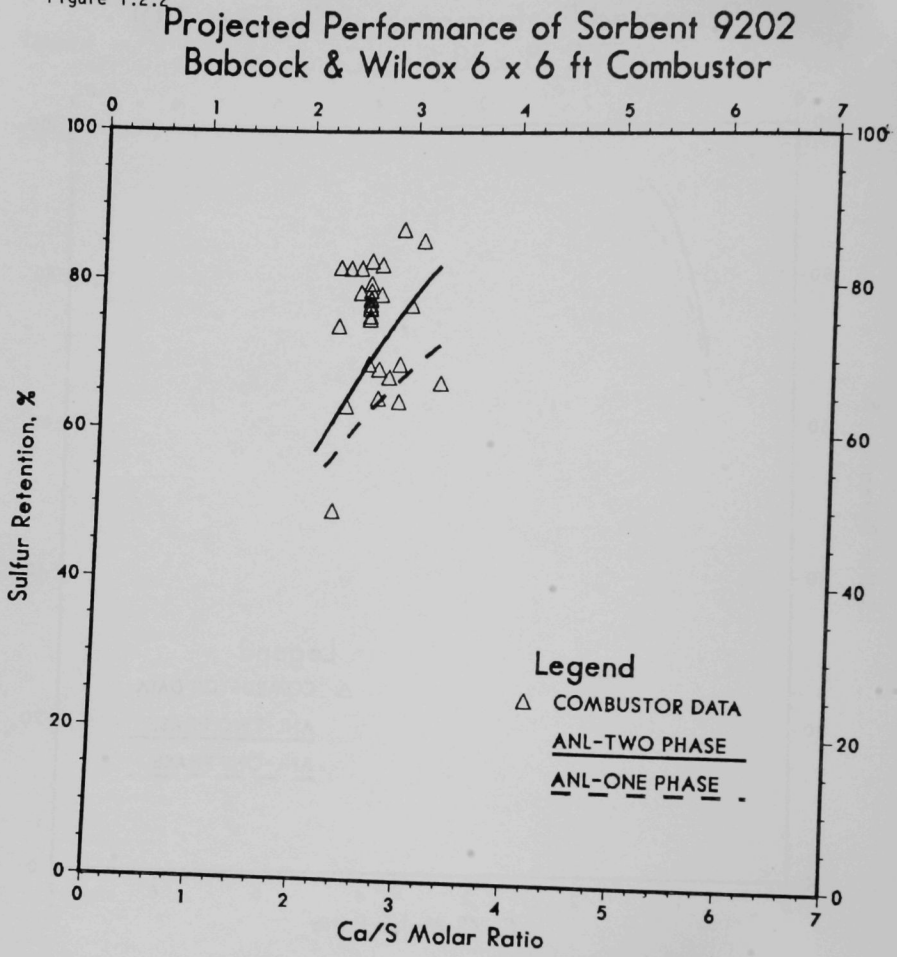

Fluidized Bed Operating Conditions

Temperature = 850. C = 1562. F

Pressure = 101. kPa = 1.0 atm

Fluidizing Velocity = 2.44 m/sec = 8.00 ft/sec

Bed Height = 1.20 Meters = 3.93 ft

Coal Feed Rate = 900.0 kg/hr = 1982.4 lb/hr

Sulfur Content in Coal = 3.60 wt%

Bed Area = 3.34 sq. meter = 36.0 sq. ft.

Sorbent Particle Dia. = 1050. micron = 0.0413 inch

Figure 1.2.3

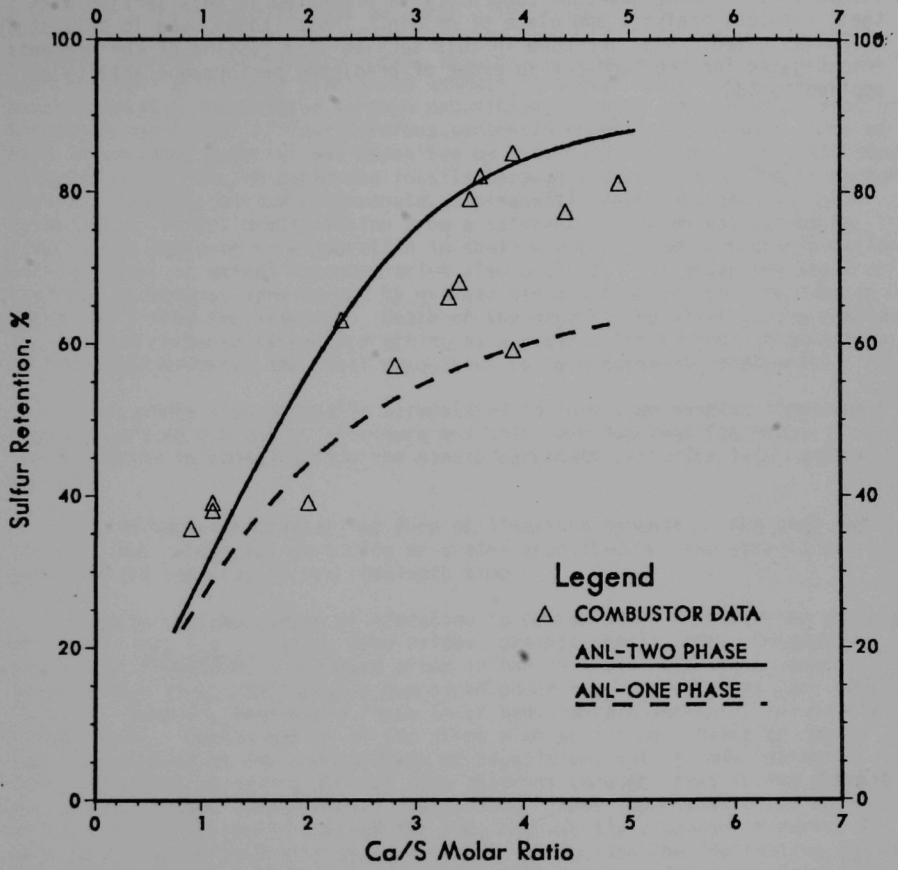

Fluidized Bed Operating Conditions

Temperature = 850. C = 1562. F

Pressure = 101. kPa = 1.0 atm

Fluidizing Velocity = 2.54 m/sec = 8.33 ft/sec

Bed Height = 0.42 Meters = 1.38 ft

Coal Feed Rate = 221.0 kg/hr = 486.9 lb/hr

Sulfur Content in Coal = 3.00 wt%

Bed Area = 0.98 sq. meter = 10.5 sq. ft.

Sorbent Particle Dia. = 880. micron = 0.0346 inch

2.0 SUMMARY OF SORBENT SELECTION

This section gives a general background on limestone and dolomite properties and deposit locations in the United States. A listing of sorbents assembled at Argonne National Laboratory is presented in this section with their chemical analysis and place of origin. Those stones used in this study are highlighted. Also included in this section is a listing of the sorbents investigated for the handbook in order of predicted performance ability as applied to FBC.

2.1 LIMESTONE FORMATION AND GENERAL PROPERTIES

The composition and properties of limestones vary greatly from quarry to quarry and to a lesser extent vary within a particular quarry. The variation reflects the nonuniform processes which resulted in limestone formation. This nonuniformity must be taken into account when predicting the performance of a sorbent in a fluidized-bed combustor. Limestone, one of the most abundant sedimentary rocks, is usually of organic origin. Shells and skeletons of diverse plants and animals in oceans and fresh bodies of water gradually accumulated through deposition, forming layered beds, some of massive proportions, of fossiliferous sediments known as limestone. Some of this accumulated material was deposited by chemical reactions, i.e., the slow dissolution of calcium carbonate fossils through the solvent action of carbon dioxide, forming calcium bicarbonate, subsequently reprecipitated as solid carbonates. Direct precipitation from a saturated solution was caused by temperature increase or evaporation in shallow water. Indirect precipitation through plant or animal intermediaries also occured. The organisms shell or skeletal structures were formed by gradual assimilation of the carbonate as bicarbonate from the seawater. Death of the organism resulted in the remaining calcium carbonate structure acting as a nucleus for further accumulation of carbonate material and final deposition to form carbonate sediments.

Coral reefs also gradually accumulated to form some massive limestone deposits around the world. Pressure and heat have supplemented chemical precipitation in consolidating the minute carbonate particles into compact masses.

The texture and crystalline form of limestone depends on the size and shape of the calcareous particles or grains deposited and the effects of pressure and temperature over geologic time.

Usually the deposition of limestone is contaminated with varying amounts of impurities, i.e., silica, iron oxides, organic debris, etc. Generally, the purest formations occur more often in the thickest beds up to several hundred feet thick continuously deposited under stable conditions over eons of time. However, frequently these thick beds contain strata of relatively impure stone. Contamination of the stone with soil clays, salts or sands usually occurred at the commencement of deposition, but in some instances impurities such as silica alumina were absorbed through pores in the deposit and cracks between strata during deposition. These impurities occur both vertically and laterally through the bed, but usually a change in purity is much more gradual laterally than vertically reflecting the fluctuating levels of the shallow sea environment associated with the deposition of limestones.

The limestone sediment may remain soft and porus, like chalks or marls, or it may be metamorphosized through high temperature and pressure and fused into a highly crystalline form, such as marble. All intermediate forms are also possible.

The other common constituent of limestone, magnesium carbonate, is formed in a related manner to calcium carbonate deposition but it is also theorized that much of it was formed by chemical displacement of calcium with magnesium salts in seawater. Dolomitic stones having mixtures of calcium and magnesium carbonates are formed in this way. Iron may also be introduced as an impurity by chemical displacement of the calcium, making iron carbonates. Iron oxide may also be distributed heterogeneously from minerals such as pyrite, limonite, magnetite and hematite. Phosphorous and sulfur usually occur but generally in small amounts. Remaining impurities could be considered as trace elements in relatively pure stone matrices. One exception would be higher content of the soluble alkali salts present in clay or shale seams of the more impure stones. These salts are usually carbonates and chlorides of sodium and potassium.

Some organic matter may also be present in limestone associated with deposition as intergranules of material or the residue of marine organisms not fully oxidized or decomposed.

The predominate chemical property of calcium limestone and dolomitic limestone is that they can be thermally decomposed to form the oxides of calcium and magnesium which are both chemically very reactive as are their hydroxides. Some of the variability in reactivity associated with the oxides is due in part to the physical properties, i.e., porosity and purity, of the original limestone and dolomite, and on a great number of other variables including elemental composition, type and distribution of impurity species, and the technique of producing the oxide, i.e., temperature, pressure, atmospheric, etc. As in any other natural system quantitative relationships between chemical composition and reactivity are not straight-forward due to the many other associated variables.

References for Section 2.1

R. S. Boynton, Ed., Chemistry and Technology of Lime and Limestone, 2nd Ed., John Wiley and Sons, Inc., New York, pp. 5-34 (1980).

D. Graf and J. Lamer, "Properties of Ca and Mg Carbonates and Their Bearing on Some Uses of Carbonate Rocks," Econ. Geol. 50, 639-713 (1955).

R. Mayer and R. Stowe, Physical Characterizations of Limestone and Lime, Azbe Award No. 4A, National Limestone Association (1964).

2.2 SORBENTS INCLUDED IN THIS BOOK

Over the past decade, a collection of limestone and dolomite rock samples have been assembled at this laboratory in connection with research work on fluidized-bed coal combustion and the sulfur dioxide absorption capabilities of calcium-containing sorbents. Table 2.1.1 is a listing of the samples with their chemical compositions and their source names and location. The ANL number designation indexes the samples by their nominal calcium carbonate composition (indicated by the first two digits). The variability in sorbent composition is discussed in the next section "Limestone Formation and General Properties." The last two digits indicate the chronological order in which the samples were received at the laboratory.

Figure 2.2.1 is a plot of the quarry locations for all the samples listed in Table 2.2.1 showing their geographical distribution across the continental United States. The eastern half of the nation is more heavily represented, in part determined by the source location of sorbents commonly used in the fluidized-bed combustion research field. The distribution of major U.S. power plants also influenced the eastern bias as indicated in Fig. 2.2.2. Major deposits of limestones and dolomites are also located east of the Mississippi River (Figs. 2.2.3 and 2.2.4). The distribution of major coal deposits is also included here in Fig. 2.2.5 as a general guide. Power plants are by choice located at sites convenient to coal deposits, although locations are generally determined by the power needs of a locality and questions of siting. Limestone and dolomite deposits are associated with coal deposits in many cases, and virtually every state in the Union has some carbonate deposits that can be mined. The present collection of sorbent materials at Argonne National Laboratory covers most of the major deposits of limestone and dolomite in the eastern United States along with the stones from other localities and of unusual composition.

From this collection a representative group of stones was selected for detailed study on the basis of a broad range of chemical composition, geographical location and common usage in the field of fluidized-bed combustion. The stones selected for inclusion in this handbook are marked with an asterisk in Table 2.2.1. The data obtained are presented in Section 5, LIMESTONES, and Section 6, DOLOMITES, of this report.

Table 2.2.1. Composition and Location of Sorbents

Stone ANL-	Chemical Compositions, wt %							Source	Common Name and/or Reference Number
	$CaCO_3$	$MgCO_3$	SiO_2	Fe_2O_3	Al_2O_3	Na_2O	K_2O		
4601*	46.0	42.0	-	-	-	-	-	Dolio and Metz LTD, Chicago, IL	
4801*	48.7	40.2	7.00	0.66	1.81	0.09	0.38	Midwest Aggregates Corp., Fort Wayne, IN	
4901	49.9	43.0	1.69	1.69	0.93	0.05	0.12	Monroe, WI	
4902	49.7	43.8	5.71	0.43	0.87	0.03	0.30	Vulcan Materials Corp., McCook, IL	
4903	49.2	44.6	8.77	0.52	0.90	0.05	0.50	Black Creek Limestone Co., Black Creek, IL	
5001*	50.4	43.0	3.52	0.37	0.98	0.34	0.10	Harris Limestone Co., Piedmont, MO	
5101*	51.8	43.3	3.61	0.41	1.46	0.07	0.22	E. E. Duff & Sons, Huntsville, OH	Tymochtee
5102	51.2	43.4	1.20	0.62	0.43	0.05	0.19	Porter Limestone Co., Rockton, IL	
5201	52.2	43.0	1.22	0.26	0.68	0.07	0.13	Midwest Aggregates Corp., Fort Wayne, IN	
5202	52.7	42.0	1.60	0.34	0.87	0.11	0.15	Midwest Aggregates Corp., Fort Wayne, IN	
5203	52.6	36.4	8.77	0.58	1.13	0.04	0.18	Bullitt County Stone Co., Shephardville, KY	
5204	52.9	45.8	0.54	0.25	0.04	0.04	0.01	James River Limestone Co., Buchanan, VA	
5205	52.1	41.0	3.79	0.07	0.16	0.04	0.01	Mayville White Lime Works, Mayville, WI	
5206	52.7	42.2	1.14	0.13	0.25	0.05	0.02	Mayville White Lime Works, Mayville, WI	
5207	52.3	37.5	3.64	2.35	1.00	0.09	0.16	Quapaw Co., Drumright, OK	
5301*	53.4	45.4	0.69	0.07	0.08	0.05	0.03	Chas. Pfizer Co., Gibsonburg, OH	1337
5302	53.9	44.9	1.35	0.16	0.43	0.03	0.07	Vulcan Materials Co., Helena, AL	
5303	53.7	42.8	2.94	0.30	0.31	0.40	0.10	May Stone and Sands, Fort Wayne, IN	
5304	53.6	3.71	36.12	3.33	0.73	0.16	0.41	Vulcan Materials Co., Medley, FL	
5401	54.5	42.9	1.04	0.07	0.34	0.04	0.10	Delta Mining Co., Mill Creek, OK	
5403	54.0	44.1	0.62	0.08	0.17	0.03	0.07	U.S. Steel Corp., Chicago, IL	
5501*	55.6	43.3	2.97	0.23	0.18	0.03	0.03	Lime Products Corp., Union, ME	
5601*	56.8	45.6	0.18	0.09	0.01	0.02	0.01	Kaiser Refractories, Salinas, CA	Dolowhite
5602	56.6	43.8	1.05	0.33	0.18	0.03	0.09	G&WH Corson, Inc., Plymouth Meeting PA	
5603	56.3	41.7	1.08	0.46	0.60	0.20	0.22	York Stone Co., York, PA	
5901*	59.1	35.7	3.48	0.68	0.34	0.27	0.53	Road Materials Co., Cumberland City, TN	
6001	60.0	27.7	6.29	5.30	3.06	0.24	0.43	Raid Quarries (Medusa Aggregates) Burlington, IA	
6101*	61.2	28.7	3.15	5.56	0.51	0.13	0.18	Jeffery Limestone Co., Parma, MI	1351
6301	63.2	32.6	2.54	0.39	0.28	0.04	0.05	Meshberger Stone Inc., Columbus, IN	
6401*	64.2	29.5	5.10	0.33	0.69	0.15	0.31	G&WH Corson, Inc., Plymouth Meeting, PA	
6501	65.9	31.5	2.08	0.38	0.28	0.04	0.05	Meshberger Stone, Inc., Columbus, IN	

*Denotes sorbents included in this handbook.

(contd)

Table 2.2.1. (contd)

Stone ANL-	Chemical Compositions, wt %							Source	Common Name and/or Reference Number
	$CaCO_3$	$MgCO_3$	SiO_2	Fe_2O_3	Al_2O_3	Na_2O	K_2O		
6701*	67.3	31.5	1.25	0.37	0.22	0.04	0.15	Osmundson Bros., Adams, MN	
6702	67.5	0.9	30.22	0.08	0.18	0.08	0.13	Vulcan Materials Co., Knoxville, TN	
7301*	73.1	12.5	12.94	1.14	0.67	0.65	0.32	Denny & Simpson, Harrisburg, IL	
7302	73.7	9.6	13.4	1.36	2.32	0.89	0.49	Hopkinsville Aggregate Co., Berry, TN	
7401	74.7	10.2	11.2	1.07	1.82	0.19	0.36	Fort Calhoun Limestone Co., Fort Calhoun, NE	
7402*	74.4	18.2	5.64	0.87	0.57	0.41	0.23	Williams Quarries, Harrisburgh, IL	
7901*	79.8	3.2	15.8	0.98	0.36	0.94	0.17	Kentucky Stone Co., Canton, KY	
8001*	80.4	3.5	10.32	1.24	3.18	0.23	0.72	Greer Limestone Co., Morgantown, WV	Greer
8002	80.8	4.0	11.07	1.82	1.79	0.70	0.52	Rigsby & Barnard, Cave in Rock, IL	
8101*	81.6	11.6	1.86	0.86	0.19	0.10	0.07	Monmouth Stone Co., Monmouth, IL	1360
8201*	82.5	7.8	8.06	0.91	1.53	0.48	0.32	Three Rivers, Smithland, KY	
8301	83.9	13.4	1.24	0.14	0.42	0.02	0.02	Vulcan Materials Co., Calera, AL	
8401	84.8	5.8	8.36	0.60	0.40	0.54	0.20	Kentucky Stone Co., Canton, KY	
8501	85.3	5.6	6.98	0.83	0.48	0.36	0.14	Columbia Quarry Co., Cypress, IL	
8601	86.9	4.6	5.15	0.88	0.98	0.35	0.16	Mid-South Co., Carthage, TN	
8701*	87.0	1.2	7.10	3.40	2.00	<0.13	0.19	Pope, Evans, and Robbins, Inc., Alexandria, VA	Chaney
8702	87.6	5.7	5.66	0.65	0.83	0.32	0.23	Wilson County Rock Products, Lebanon, TN	
8703	87.9	1.7	8.53	1.00	0.20	0.45	0.09	Reed Crushed Stone Co., Gilbertsville, IL	
8801	88.9	5.8	4.19	0.58	0.76	0.07	0.20	Fredonia Valley Blue Ledge, Fredonia, KY	
8802	88.9	5.4	3.26	0.68	0.62	0.21	0.22	Wilson County Rock Products, Lebanon, TN	
8901*	98.8	2.5	4.0	0.66	1.04	0.10	0.19	Hooper Brothers Quarry, Weeping Water, NE	1343
8902	89.6	3.0	5.06	0.37	0.79	0.03	0.29	Vulcan Materials Co., Holladay, TN	
8903	89.3	1.2	5.50	0.98	0.83	0.12	0.22	Curl Bend Bethany Falls, Bethany, MD	
9101	91.0	2.5	5.01	0.77	0.94	0.11	0.19	Kentucky Stone Co., Princeton, KY	
9102	91.5	2.9	4.01	0.58	0.23	0.23	0.10	Reed Crushed Stone Co., Gilbertsville, IL	
9201*	92.6	5.3	1.26	0.20	0.42	0.10	0.02	Georgia Marble Co., Tate, GA	1336
9202*	93.2	1.6	1.84	7.18	1.12	0.03	0.18	Carbon Limestone Co., Lowellville, OH	Lowellville
9203	92.1	3.9	3.12	0.60	0.47	0.28	0.17	Hopkinsville Aggregate Co., Berry TN	
9301	93.0	2.9	2.94	0.59	0.30	0.22	0.11	Rigsby & Barnard, Hole in Rock, IL	
9401	94.1	1.0	3.18	0.35	0.51	0.05	0.10	Pete Lien & Sons, Rapid Cit, SD	

*Denotes sorbent included in this handbook.

(contd)

Table 2.2.1. (contd)

Stone ANL-	Chemical Compositions, wt %							Source	Common Name and/or Reference Number
	$CaCO_3$	$MgCO_3$	SiO_2	Fe_2O_3	Al_2O_3	Na_2O	K_2O		
9402*	94.7	0.9	0.63	0.14	0.23	0.02	0.02	Lime Products Corp., Union, ME	
9403	94.1	2.3	2.31	0.55	0.21	0.14	0.09	Denny & Simpson, Harrisburg, IL	
9501*	95.3	1.3	0.77	0.09	0.25	0.03	0.06	Grove Lime Co., Stephens City, VA	
9502	95.6	3.4	0.42	0.05	0.11	0.02	0.04	American Aggregates, Indianapolis, IN	
9503	95.5	0.8	0.15	0.05	0.13	0.02	<0.01	Southern Materials, Ocala, FL	
9504	95.8	0.6	2.71	0.30	0.36	0.05	0.13	Rose Equipment, Inc., Weeping Water, NE	
9505	95.1	3.5	0.70	0.90	0.29	0.04	0.03	Midwest Minerals, Pittsburgh, KS	
9506	95.6	2.7	1.24	0.45	0.21	0.04	0.08	Fredonia Valley Quarries (Upper) Fredonia, KY	
9601*	96.0	3.6	0.20	0.17	<0.01	0.05	0.01	Columbia Quarry Co., Valmeyer, IL	2203
9602	96.2	0.4	0.19	0.12	0.21	0.03	0.01	Delta Mining Corp., Mill Creek, OK	
9603	96.4	1.6	0.70	0.10	0.30	0.05	0.11	G&WH Corson, Inc., Plymouth Meeting, PA	
9701*	97.8	0.6	0.20	0.10	1.80	0.25	0.47	Greer Limestone Co., Morgantown, WV	Germany Valley
9702	97.5	0.7	0.21	0.05	0.05	0.01	0.01	Hemphill Bros., Seattle, WA	
9703	97.6	0.6	1.08	0.19	0.50	0.03	0.17	Austin White Lime Co., McNeil, TX	
9704	97.8	0.3	0.15	0.30	0.05	0.04	0.02	Midwest Limestone Co., Gilmore City, IA	
9705	97.3	0.5	0.20	0.17	0.35	0.05	0.01	Western Materials Co., Orleans, IN	
9706	97.3	1.0	0.23	0.23	0.08	0.03	0.01	U.S. Steel Corp., Chicago, IL	
9707	97.1	2.0	1.14	0.41	0.13	0.06	0.08	Fredonia Valley (Lower White) Fredonia, KY	
9708	97.3	1.80	-	0.15	0.10	-	-	Columbia Quarry Co., Columbia, IL	
9709	97.8	1.47	0.60	0.05	0.08	-	-	Calcium Carbonate Co., Quincy, IL	
9801*	98.3	0.6	0.20	0.15	0.16	0.04	0.20	Iowa Limestone Co., Alden, IA	
9802	98.2	0.5	0.29	0.18	0.10	0.04	0.01	Chem. Lime Inc., Clifton, TX	
9803	98.0	1.3	1.47	0.07	0.14	0.02	0.02	Rigsby & Barnard Quarry, Cave in Rock, IL	
9804	98.3	0.50	0.30	0.03	0.02	-	-	Calcium Carbonate Co., Quincy, IL	
9806	98.1	1.16	0.06	0.01	0.02	-	-	(Aragonite) General Electric Co., Schenectedy, NY	
9901	99.1	0.60	0.17	0.05	0.06	<0.01	<0.01	Western Materials Co., Orleans, IN	
9902	99.1	0.4	0.13	0.05	0.04	0.04	0.01	Southern materials, Ocala, FL	
9903*	99.8	0.5	0.24	0.02	0.16	0.20	0.01	Calcium Carbonate Co., Fort Dodge, IA	
1000	100.0	0.0	0.00	0.00	0.00	0.00	0.00	Mexico (Ward's Scientific Equip Co.)	

*Denotes sorbents included in this handbook.

(contd)

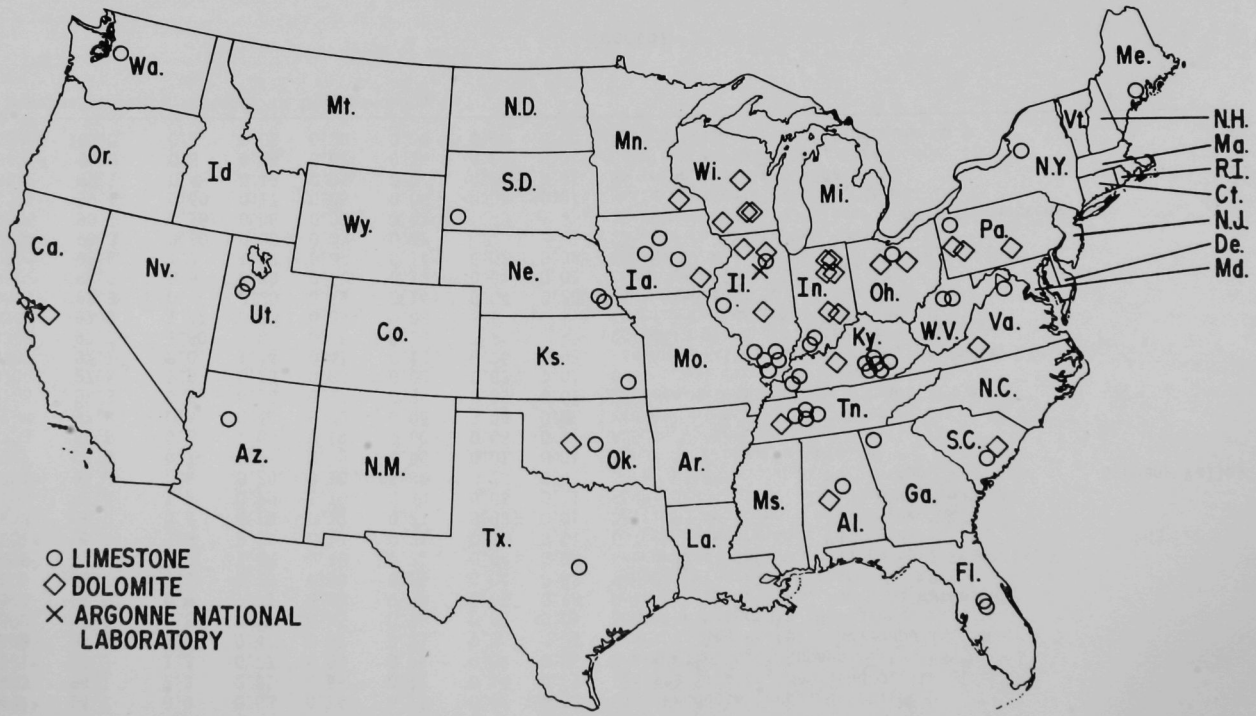

Fig. 2.2.1. DISTRIBUTION OF LIMESTONE AND DOLOMITE SAMPLES PRESENTLY AT ARGONNE NATIONAL LABORATORY CHEMICAL ENGINEERING DIVISION

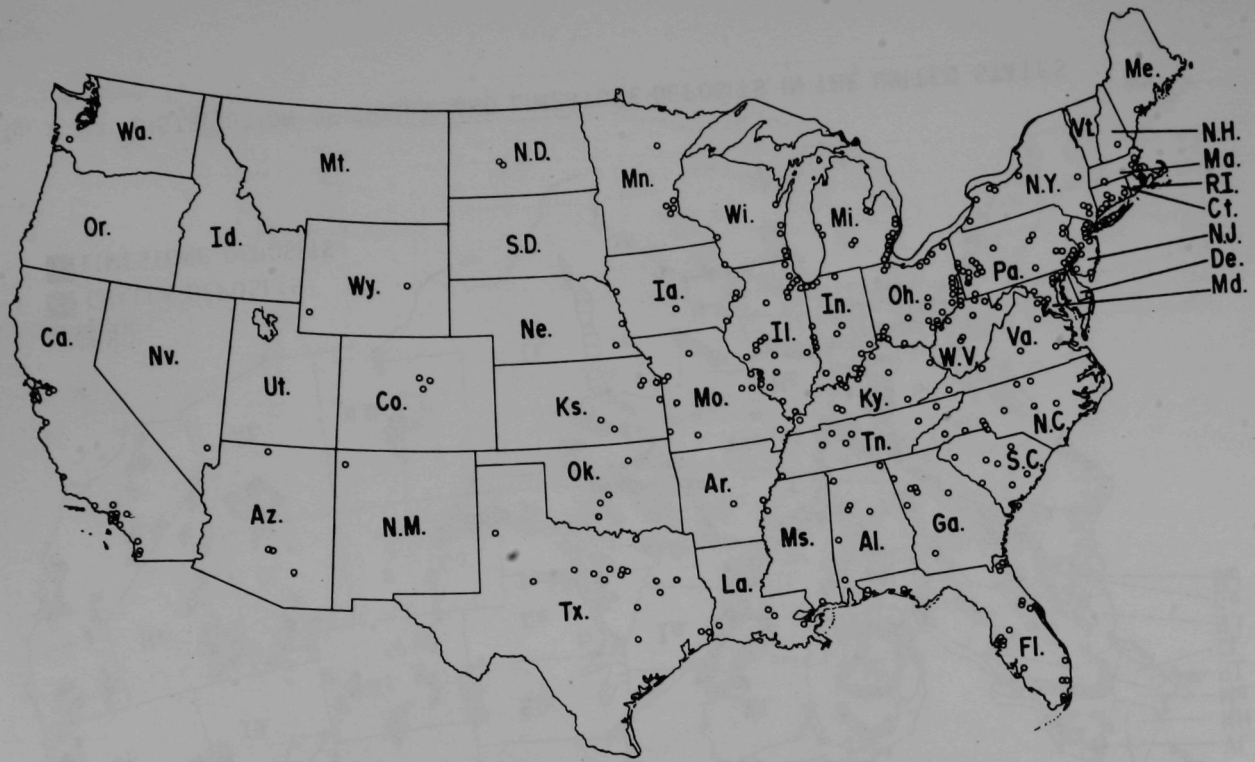

Fig. 2.2.2. MAJOR THERMAL POWER PLANTS IN THE UNITED STATES DESIGNED TO BURN COAL AND/OR OIL

Fig. 2.2.3. DISTRIBUTION OF CHAULK AND LIMESTONE DEPOSITS IN THE UNITED STATES

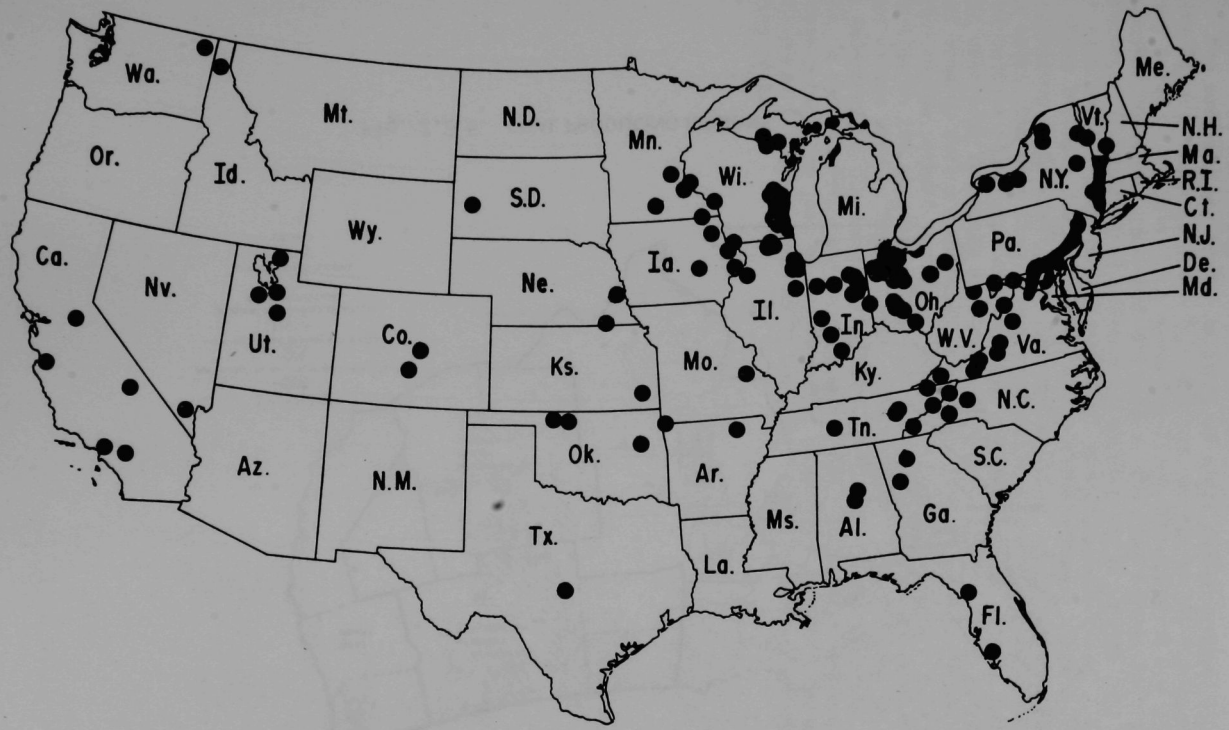

Fig. 2.2.4. LOCATION OF HIGH-GRADE DOLOMITE QUARRIES IN THE UNITED STATES

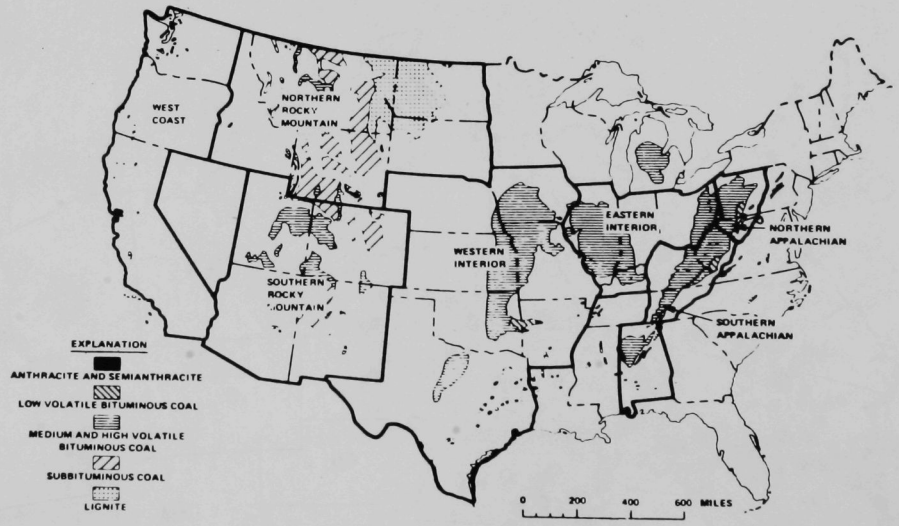

Fig. 2.2.5. **COAL PRODUCING REGIONS**

2.3 SORBENT RANKING

The sorbents are ranked in terms of their sulfur capture capability using the ANL model (Section 7.1) and the results of the standard tests (Sections 5 and 6). Table 2.3.1 gives the fixed dimensions of the fluidized-bed combustor and other data that are used as the common basis for ranking the sorbents. The ranking is achieved by showing the projected feed requirements for each sorbent under the standard FBC operating conditions. The ranking is shown in Table 2.3.2 and the figures which follow. Table 2.3.2 allows comparisons to be easily made between sorbents. Also shown in Table 2.3.2 is the calculated attrition loss of sorbent from the bed at 85% sulfur retention (the calcium elutriated expressed as a percent of the calcium fed to the bed). This attrition loss data includes only the elutriated fines arising from sorbent breakup during shock calcination and from particle-particle contact. Any fines in the sorbent feedstack (12% in the example, Table 2.3.1) would be in addition to the attrition loss data in Table 2.3.2. The calculated attrition loss values were as high as 76% (sorbent 5001). However, the ANL model appears to underpredict the amount of sorbent being eluted. As a result, for sorbent 5001, a sorbent feed rate greater than that required for sulfur capture is probably required just to maintain the bed height. This factor must also be considered for other sorbents which show a high fraction of the sorbent feed being eluted.

Table 2.3.1. Nominal Values Employed for Ranking the Sorbents

Temperature = 850°C = 1562 °F

Pressure = 101 kPa = 1.0 atm

Fluidizing Gas Velocity = 2.00 m/sec = 6.56 ft/sec

Bed Height = 1.20 Meters = 3.93 ft

Coal Feed Rate = 897.6 kg/hr = 1977.0 lb/hr

Sulfur Content of Coal = 2.58 wt%

Bed Area = 3.34 sq meter = 36.0 sq ft

Sorbent Particle Dia.= 1000. μm = 0.0394 inch

Volume fraction voidage in emulsion phase:	E	= 0.45 estimated
Volume fraction inerts in bed:	F_I	= 0.05 estimated
Volume fraction heat exchange tubes in bed:	F_H	= 0.04 estimated
Gas density:	ρ_g	= 0.33 kg/m^3
Acceleration of gravity:	g	= 9.80 m/sec^2
Gas viscosity:	μ	= 4.5 x 10^{-5} kg/m -sec (450 micropoise)
Bed diameter:	D_R	= 1.82 meter (6 ft)
Number of orifice openings in distributor plate	N_D	= 3580
Freeboard height	7.9 m	(26 ft)

Sorbent feed size distribution:	0 to 150 μm	12 wt %
	150 to 930 μm	38 wt %
	930 to 1720 μm	38 wt %
	1720 to 2500 μm	12 wt %

Table 2.3.2. Predicted Ca/S Ratio and Calcium Elutriation for Selected Sorbents[a]

Sorbent	Ca/S Molar Ratio (85% Retention) ANL-Two Phase	Attrition Loss, Calcium Elutriated Expressed as Percent Calcium Fed[b]
9903	4.6	3
9806	1.5	c
9804	3.6	3
9801	3.5	16
9709	3.1	23
9708	3.9	28
9705	3.3	5
9701	16.8	1
9601	4.6	21
9504	2.7	2
9501	7.3	1
9402	8.0	7
9202	4.5	1
9201	7.1	c
9101	5.9	0
8901	3.6	4
8701	3.6	b
8201	4.3	3
8101	2.2	43
8001	5.4	2
7901	3.5	4
7402	4.8	5
7301	3.9	1
6701	2.0	2
6401	5.4	1
6101	1.5	6
5901	2.4	5
5601	14.8	6
5501	6.4	7
5301	1.8	12
5101	1.1	1
5001	1.6	76
4801	1.0	c
4601	1.3	17

[a]Reference combustor related parameters are given in Table 2.3.1. Predictions are made using the ANL model (Section 7.1). All sorbents are predicted to achieve a retention greater than 96% when an unlimited sorbent feed rate is employed.

[b]Excluding the fines in the sorbent feed which would be elutriated immediately. The attrition loss data includes only the fines arising from sorbent breakup during shock calcination and from particle-particle contact.

[c]Data not available.

Predicted Performance of Sorbent 9903

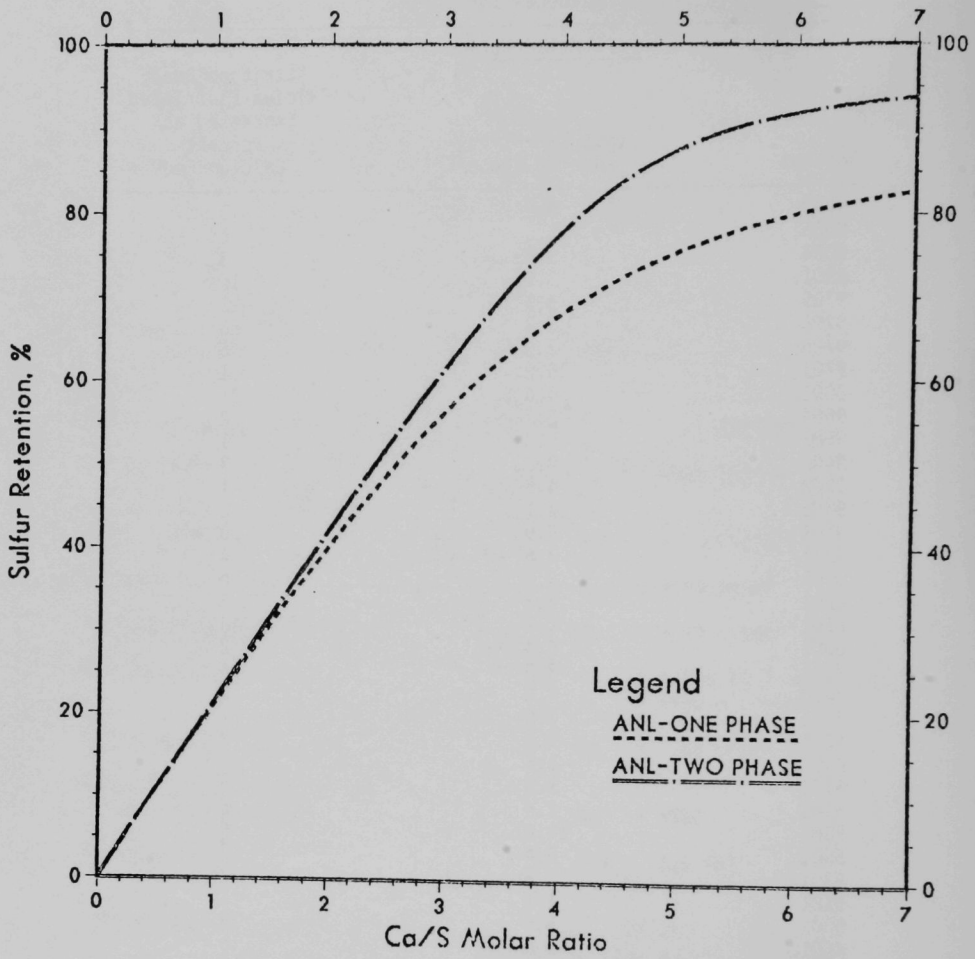

Fluidized Bed Operating Conditions

Temperature = 850. C = 1562. F

Pressure = 101. kPa = 1.0 atm

Fluidizing Velocity = 2.00 m/sec = 6.56 ft/sec

Bed Height = 1.20 Meters = 3.93 ft

Coal Feed Rate = 897.6 kg/hr = 1977.0 lb/hr

Sulfur Content in Coal = 2.58 wt%

Bed Area = 3.34 sq. meter = 36.0 sq. ft.

Sorbent Particle Dia. = 1000. micron = 0.0394 inch

Predicted Performance of Sorbent 9806

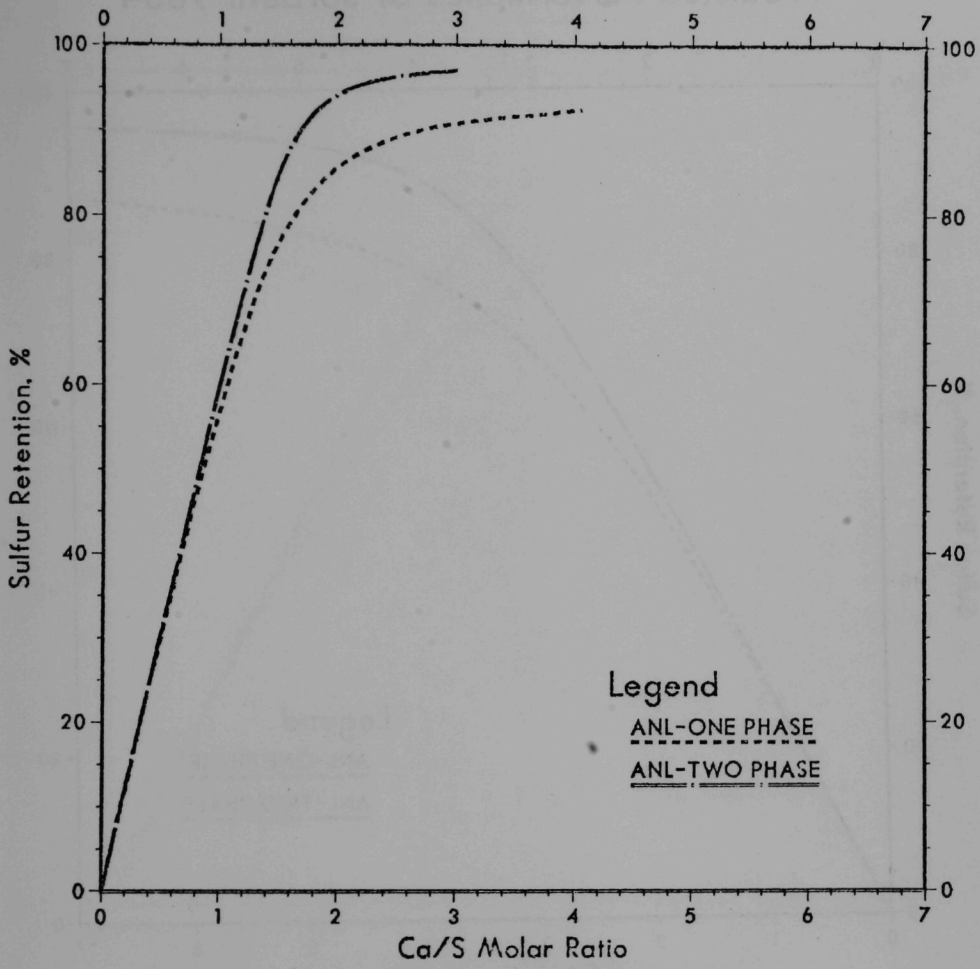

Fluidized Bed Operating Conditions

Temperature = 850. C = 1562. F

Pressure = 101. kPa = 1.0 atm

Fluidizing Velocity = 2.00 m/sec = 6.56 ft/sec

Bed Height = 1.20 Meters = 3.93 ft

Coal Feed Rate = 897.6 kg/hr = 1977.0 lb/hr

Sulfur Content in Coal = 2.58 wt%

Bed Area = 3.34 sq. meter = 36.0 sq. ft.

Sorbent Particle Dia. = 1000. micron = 0.0394 inch

Predicted Performance of Sorbent 9804

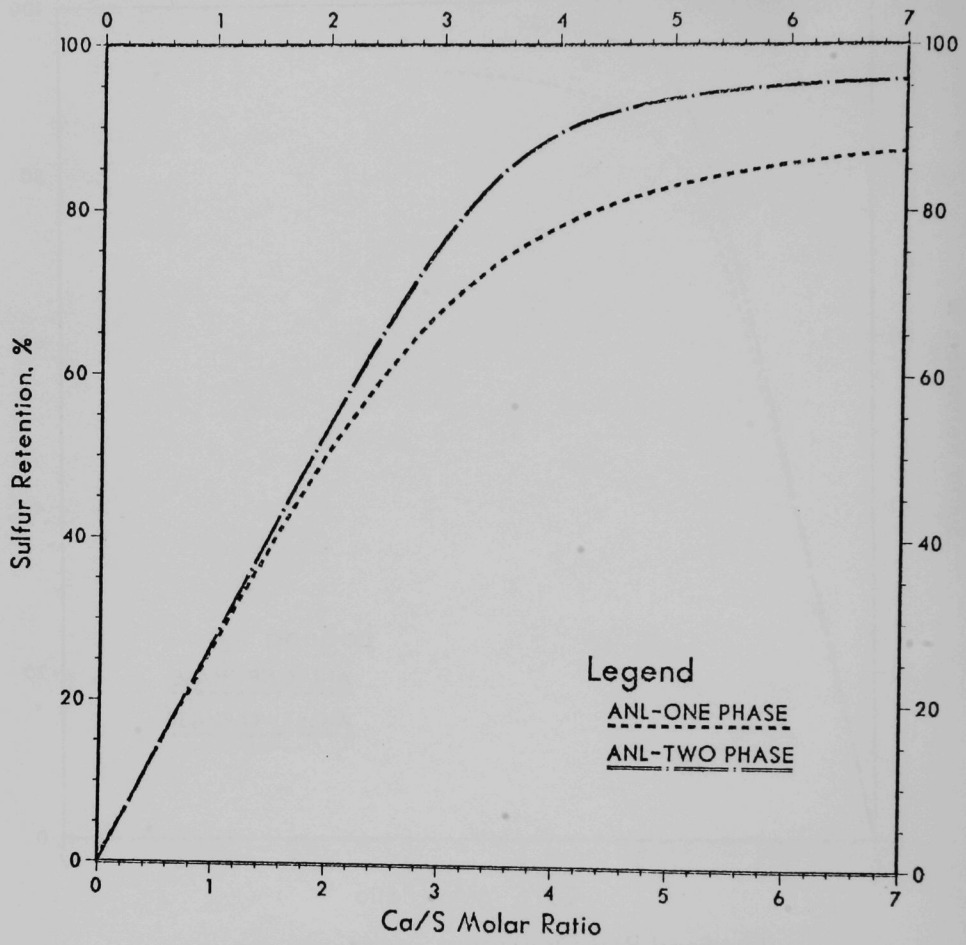

Fluidized Bed Operating Conditions

Temperature = 850. C = 1562. F

Pressure = 101. kPa = 1.0 atm

Fluidizing Velocity = 2.00 m/sec = 6.56 ft/sec

Bed Height = 1.20 Meters = 3.93 ft

Coal Feed Rate = 897.6 kg/hr = 1977.0 lb/hr

Sulfur Content in Coal = 2.58 wt%

Bed Area = 3.34 sq. meter = 36.0 sq. ft.

Sorbent Particle Dia. = 1000. micron = 0.0394 inch

Predicted Performance of Sorbent 9801

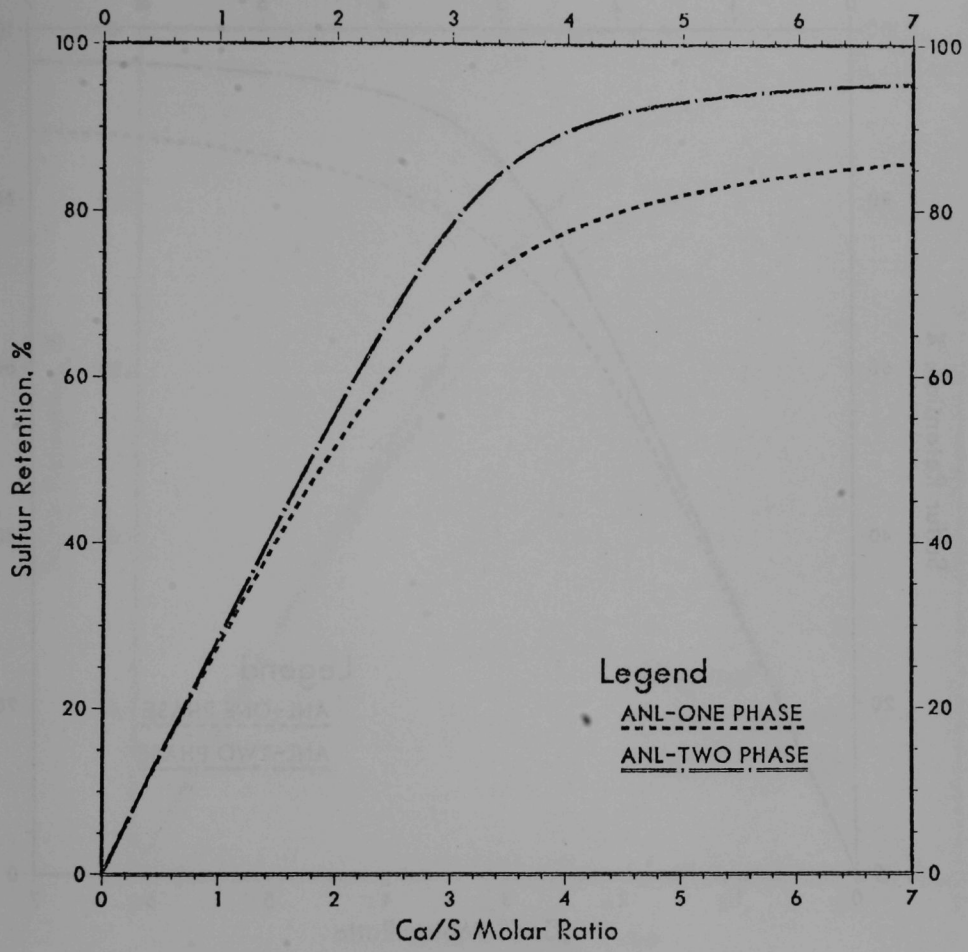

Fluidized Bed Operating Conditions

Temperature = 850. C = 1562. F

Pressure = 101. kPa = 1.0 atm

Fluidizing Velocity = 2.00 m/sec = 6.56 ft/sec

Bed Height = 1.20 Meters = 3.93 ft

Coal Feed Rate = 897.6 kg/hr = 1977.0 lb/hr

Sulfur Content in Coal = 2.58 wt%

Bed Area = 3.34 sq. meter = 36.0 sq. ft.

Sorbent Particle Dia. = 1000. micron = 0.0394 inch

Predicted Performance of Sorbent 9709

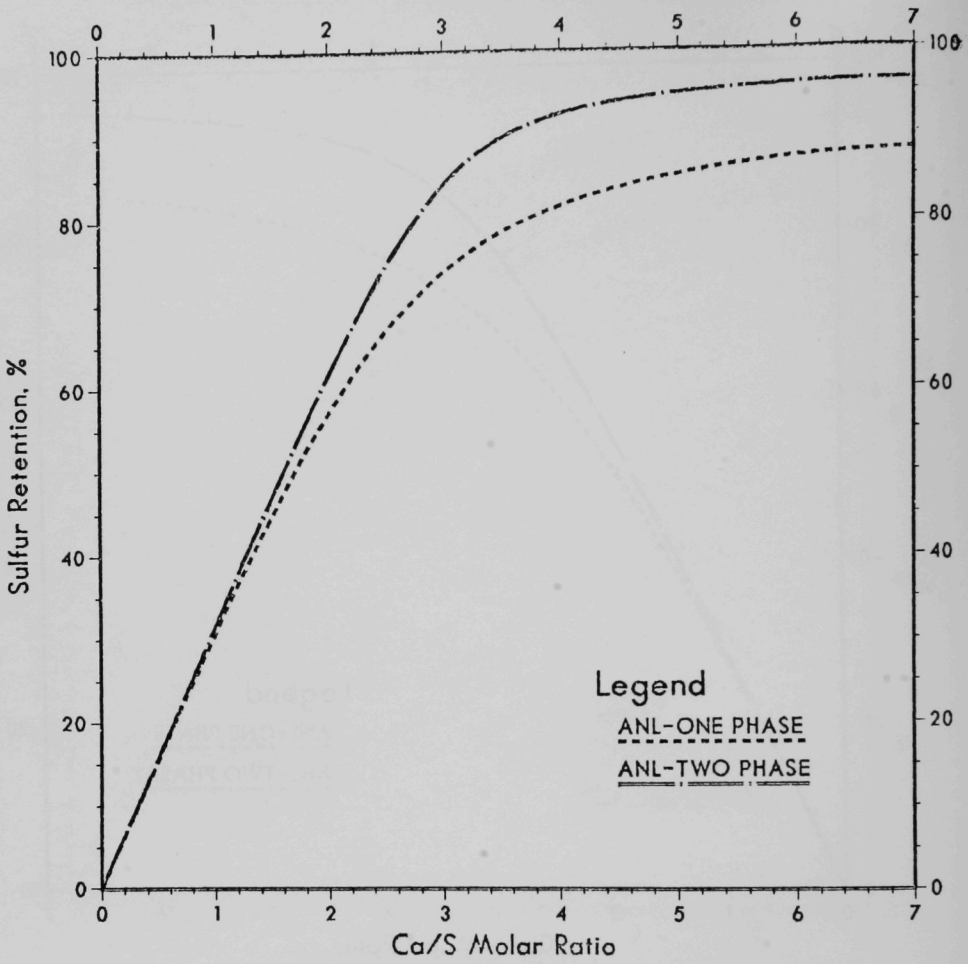

Fluidized Bed Operating Conditions

Temperature = 850. C = 1562. F

Pressure = 101. kPa = 1.0 atm

Fluidizing Velocity = 2.00 m/sec = 6.56 ft/sec

Bed Height = 1.20 Meters = 3.93 ft

Coal Feed Rate = 897.6 kg/hr = 1977.0 lb/hr

Sulfur Content in Coal = 2.58 wt%

Bed Area = 3.34 sq. meter = 36.0 sq. ft.

Sorbent Particle Dia. = 1000. micron = 0.0394 inch

Predicted Performance of Sorbent 9708

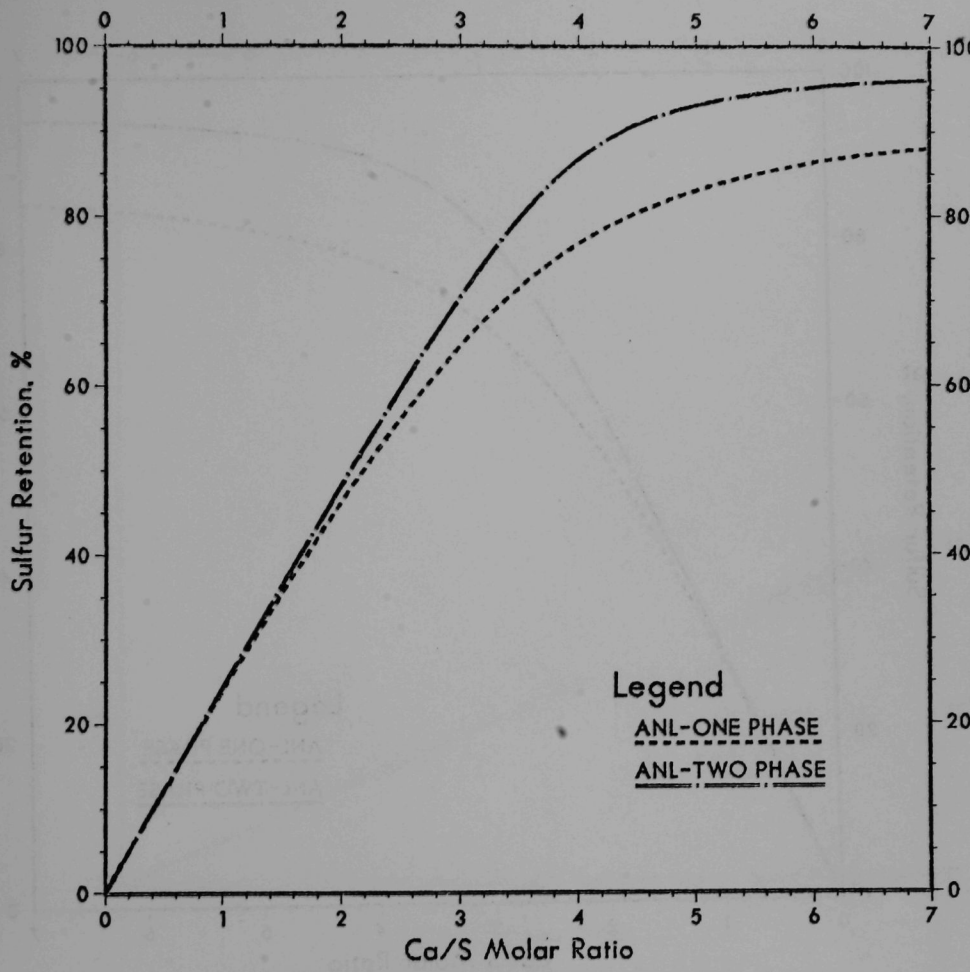

Fluidized Bed Operating Conditions

Temperature = 850. C = 1562. F

Pressure = 101. kPa = 1.0 atm

Fluidizing Velocity = 2.00 m/sec = 6.56 ft/sec

Bed Height = 1.20 Meters = 3.93 ft

Coal Feed Rate = 897.6 kg/hr = 1977.0 lb/hr

Sulfur Content in Coal = 2.58 wt%

Bed Area = 3.34 sq. meter = 36.0 sq. ft.

Sorbent Particle Dia. = 1000. micron = 0.0394 inch

Predicted Performance of Sorbent 9705

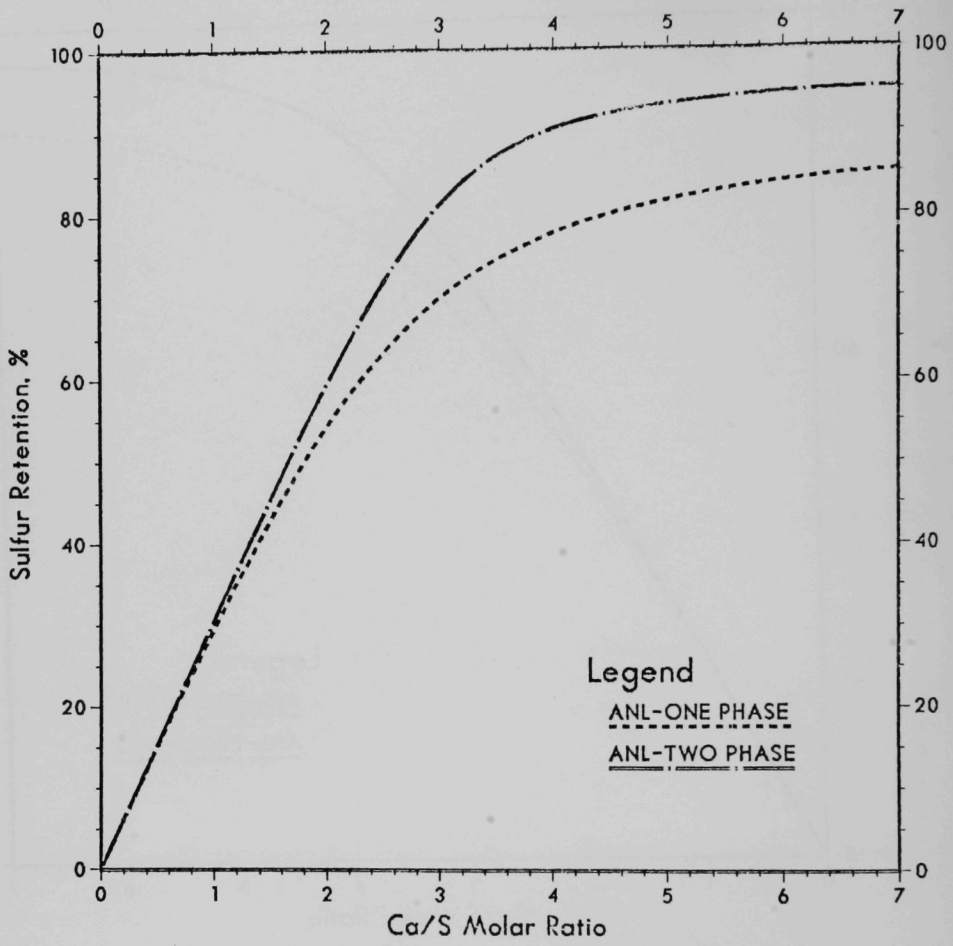

Fluidized Bed Operating Conditions

Temperature = 850. C = 1562. F

Pressure = 101. kPa = 1.0 atm

Fluidizing Velocity = 2.00 m/sec = 6.56 ft/sec

Bed Height = 1.20 Meters = 3.93 ft

Coal Feed Rate = 897.6 kg/hr = 1977.0 lb/hr

Sulfur Content in Coal = 2.58 wt%

Bed Area = 3.34 sq. meter = 36.0 sq. ft.

Sorbent Particle Dia. = 1000. micron = 0.0394 inch

Predicted Performance of Sorbent 9701

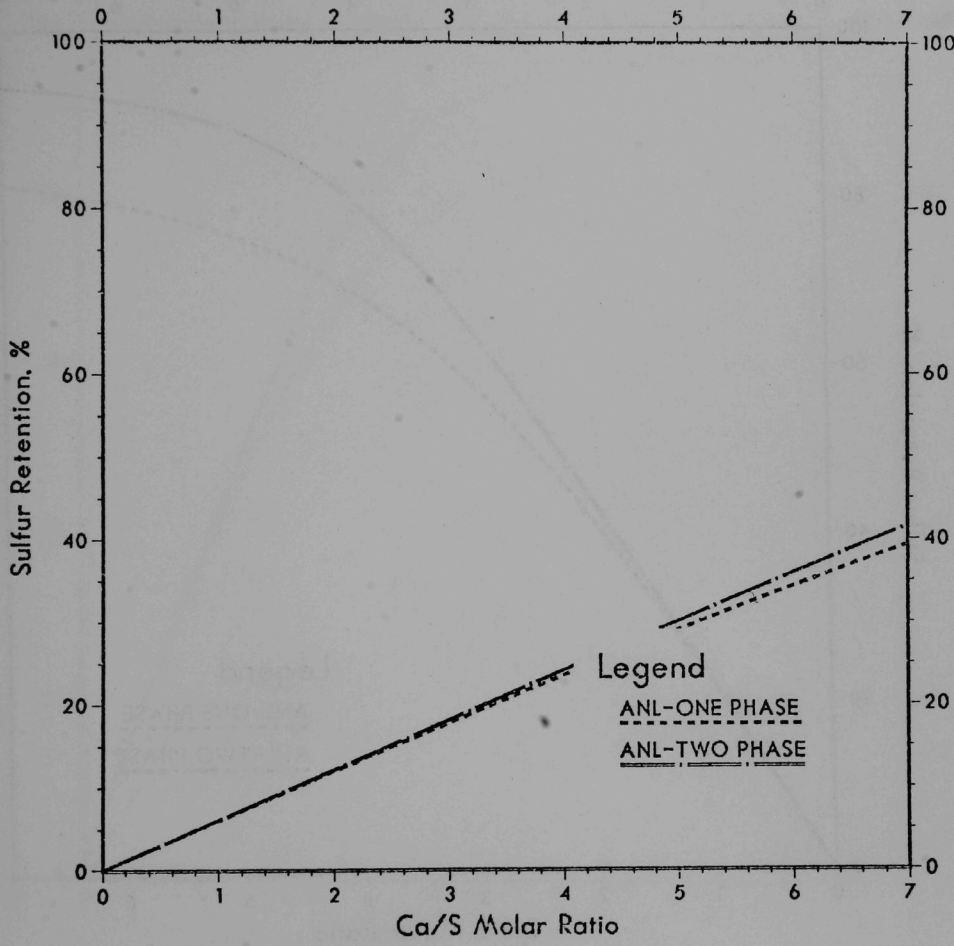

Fluidized Bed Operating Conditions

Temperature = 850. C = 1562. F

Pressure = 101. kPa = 1.0 atm

Fluidizing Velocity = 2.00 m/sec = 6.56 ft/sec

Bed Height = 1.20 Meters = 3.93 ft

Coal Feed Rate = 897.6 kg/hr = 1977.0 lb/hr

Sulfur Content in Coal = 2.58 wt%

Bed Area = 3.34 sq. meter = 36.0 sq. ft.

Sorbent Particle Dia. = 1000. micron = 0.0394 inch

Predicted Performance of Sorbent 9601

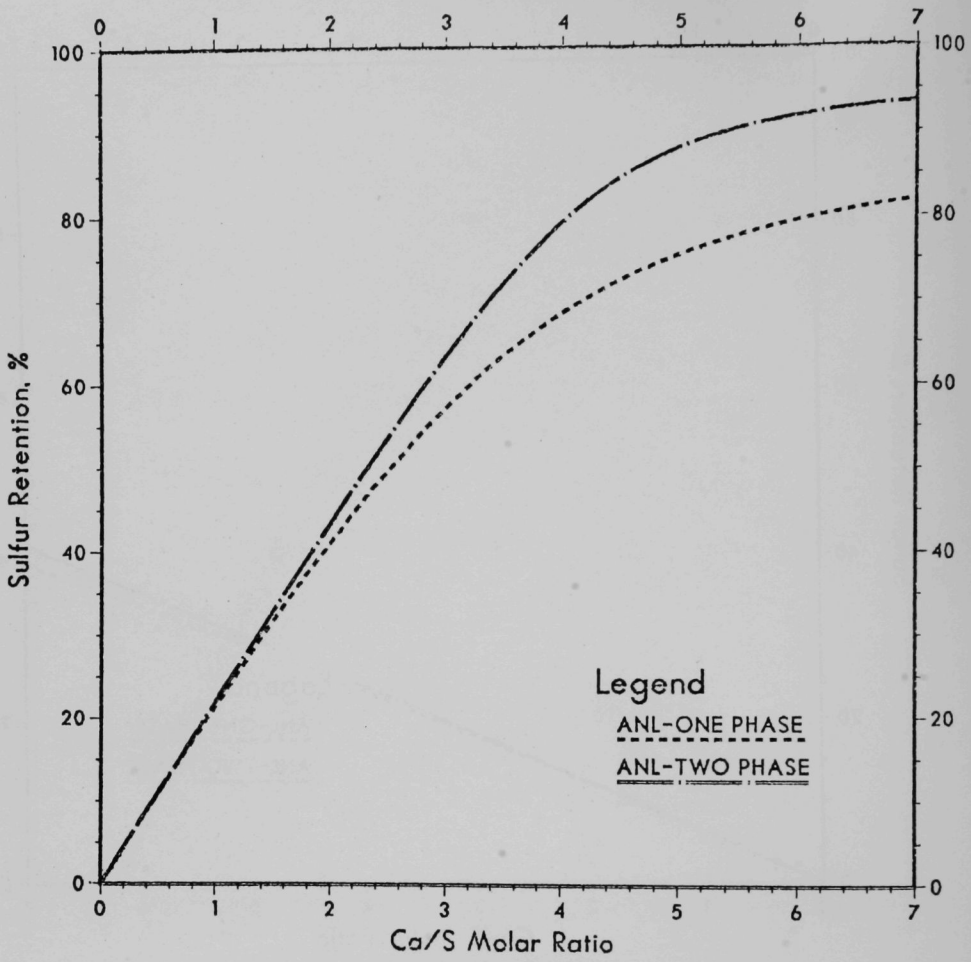

Fluidized Bed Operating Conditions

Temperature = 850. C = 1562. F

Pressure = 101. kPa = 1.0 atm

Fluidizing Velocity = 2.00 m/sec = 6.56 ft/sec

Bed Height = 1.20 Meters = 3.93 ft

Coal Feed Rate = 897.6 kg/hr = 1977.0 lb/hr

Sulfur Content in Coal = 2.58 wt%

Bed Area = 3.34 sq. meter = 36.0 sq. ft.

Sorbent Particle Dia. = 1000. micron = 0.0394 inch

Predicted Performance of Sorbent 9504

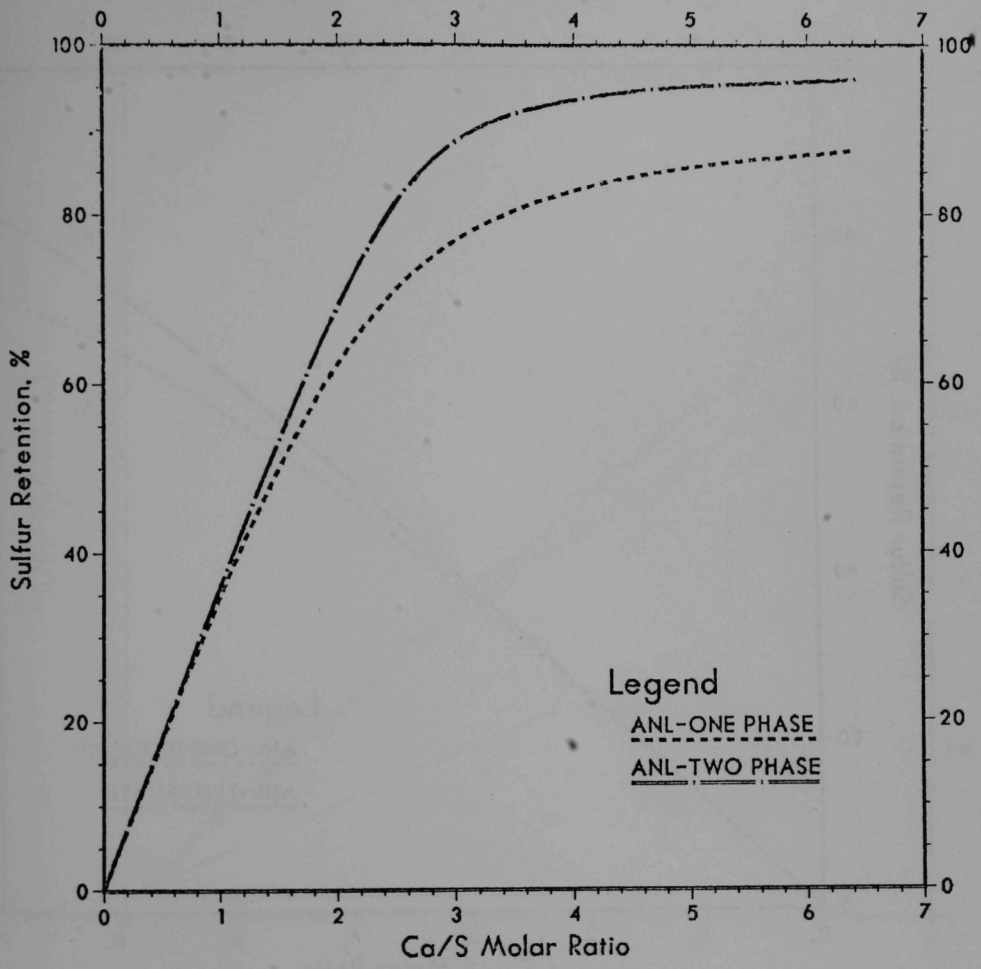

Fluidized Bed Operating Conditions

Temperature = 850. C = 1562. F

Pressure = 101. kPa = 1.0 atm

Fluidizing Velocity = 2.00 m/sec = 6.56 ft/sec

Bed Height = 1.20 Meters = 3.93 ft

Coal Feed Rate = 897.6 kg/hr = 1977.0 lb/hr

Sulfur Content in Coal = 2.58 wt%

Bed Area = 3.34 sq. meter = 36.0 sq. ft.

Sorbent Particle Dia. = 1000. micron = 0.0394 inch

Predicted Performance of Sorbent 9501

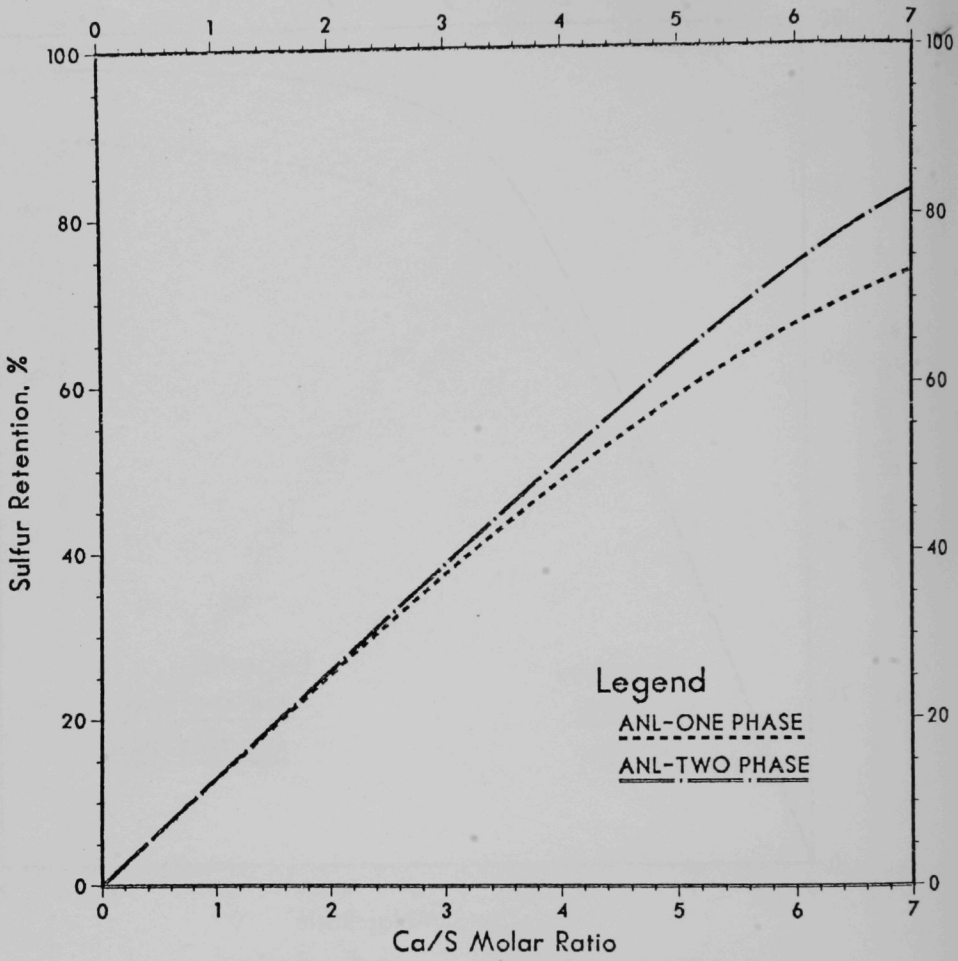

Fluidized Bed Operating Conditions

Temperature = 850. C = 1562. F

Pressure = 101. kPa = 1.0 atm

Fluidizing Velocity = 2.00 m/sec = 6.56 ft/sec

Bed Height = 1.20 Meters = 3.93 ft

Coal Feed Rate = 897.6 kg/hr = 1977.0 lb/hr

Sulfur Content in Coal = 2.58 wt%

Bed Area = 3.34 sq. meter = 36.0 sq. ft.

Sorbent Particle Dia. = 1000. micron = 0.0394 inch

Predicted Performance of Sorbent 9402

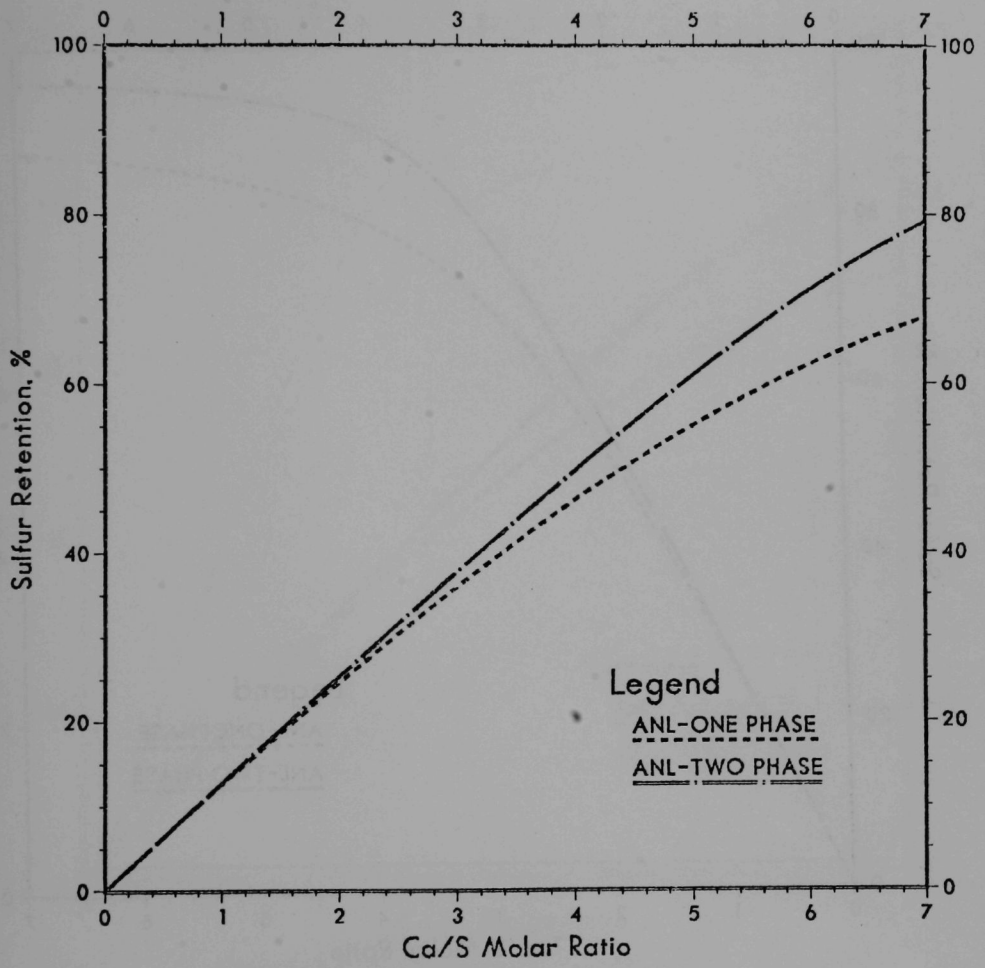

Fluidized Bed Operating Conditions

Temperature = 850. C = 1562. F

Pressure = 101. kPa = 1.0 atm

Fluidizing Velocity = 2.00 m/sec = 6.56 ft/sec

Bed Height = 1.20 Meters = 3.93 ft

Coal Feed Rate = 897.6 kg/hr = 1977.0 lb/hr

Sulfur Content in Coal = 2.58 wt%

Bed Area = 3.34 sq. meter = 36.0 sq. ft.

Sorbent Particle Dia. = 1000. micron = 0.0394 inch

Predicted Performance of Sorbent 9202

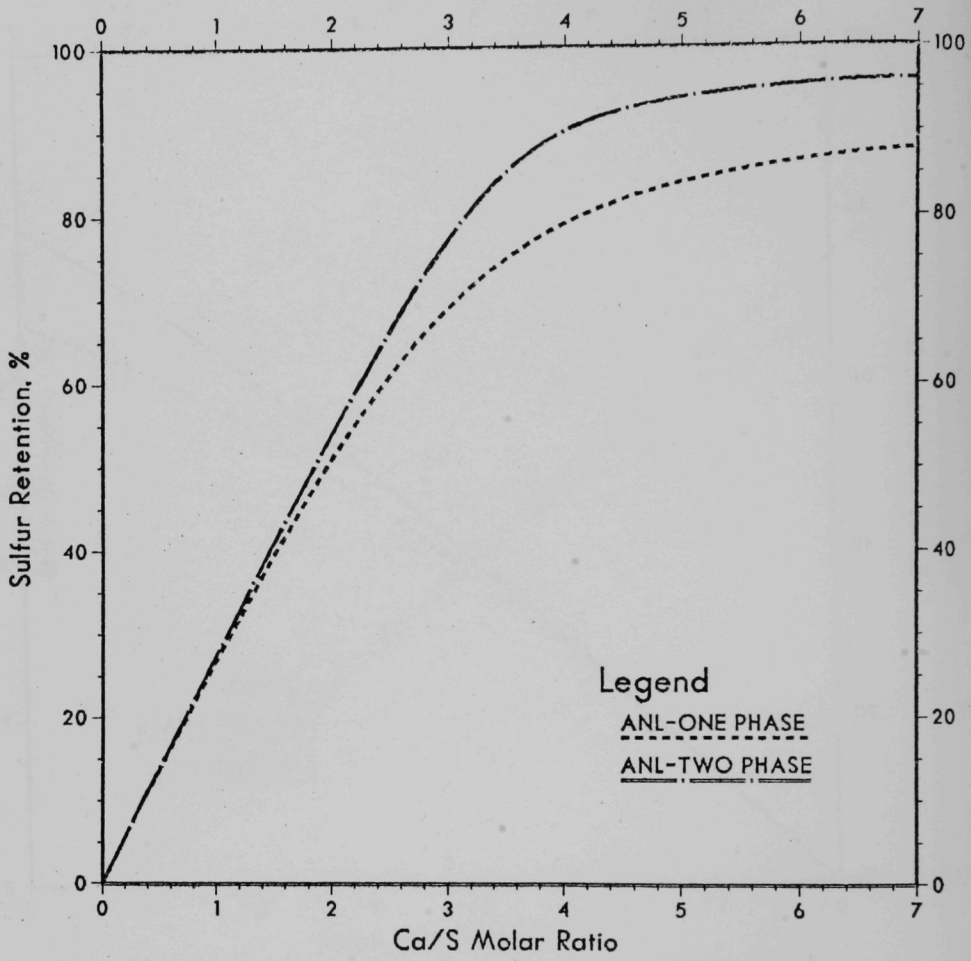

Fluidized Bed Operating Conditions

Temperature = 850. C = 1562. F

Pressure = 101. kPa = 1.0 atm

Fluidizing Velocity = 2.00 m/sec = 6.56 ft/sec

Bed Height = 1.20 Meters = 3.93 ft

Coal Feed Rate = 897.6 kg/hr = 1977.0 lb/hr

Sulfur Content in Coal = 2.58 wt%

Bed Area = 3.34 sq. meter = 36.0 sq. ft.

Sorbent Particle Dia. = 1000. micron = 0.0394 inch

Predicted Performance of Sorbent 9201

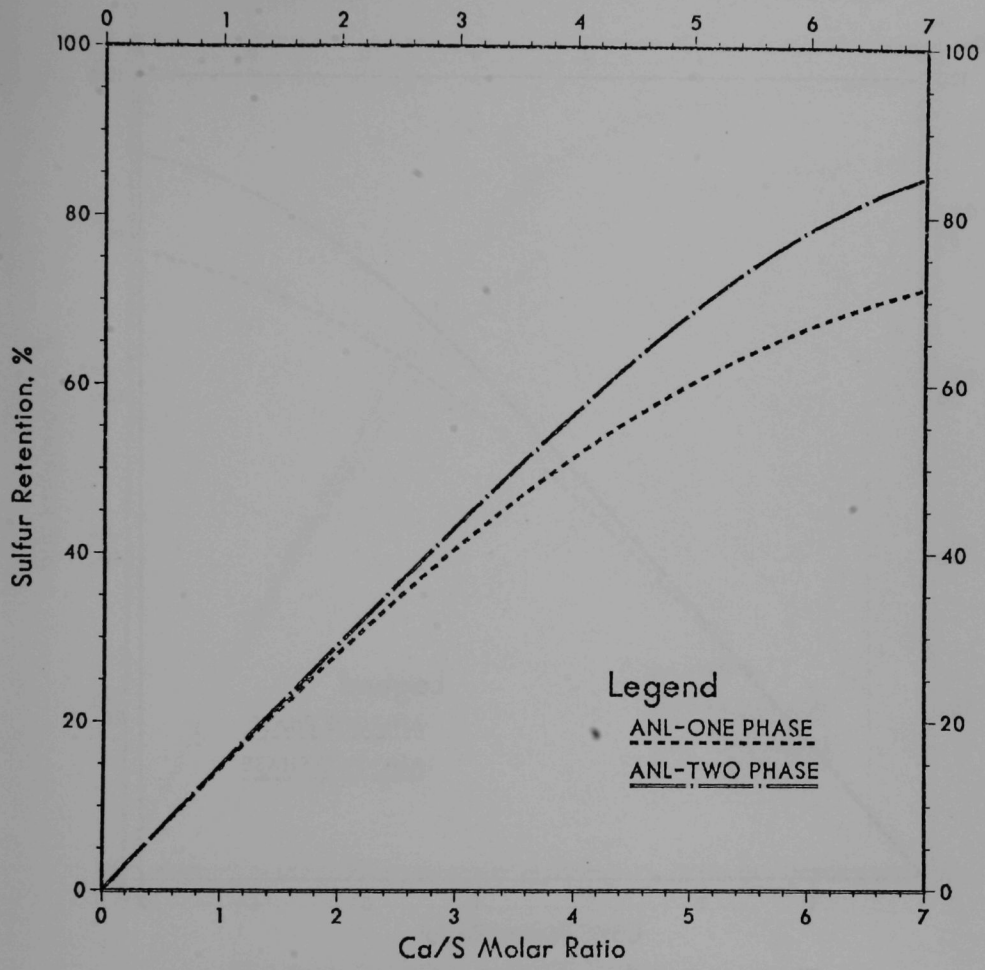

Fluidized Bed Operating Conditions

Temperature = 850. C = 1562. F

Pressure = 101. kPa = 1.0 atm

Fluidizing Velocity = 2.00 m/sec = 6.56 ft/sec

Bed Height = 1.20 Meters = 3.93 ft

Coal Feed Rate = 897.6 kg/hr = 1977.0 lb/hr

Sulfur Content in Coal = 2.58 wt%

Bed Area = 3.34 sq. meter = 36.0 sq. ft.

Sorbent Particle Dia. = 1000. micron = 0.0394 inch

Predicted Performance of Sorbent 9101

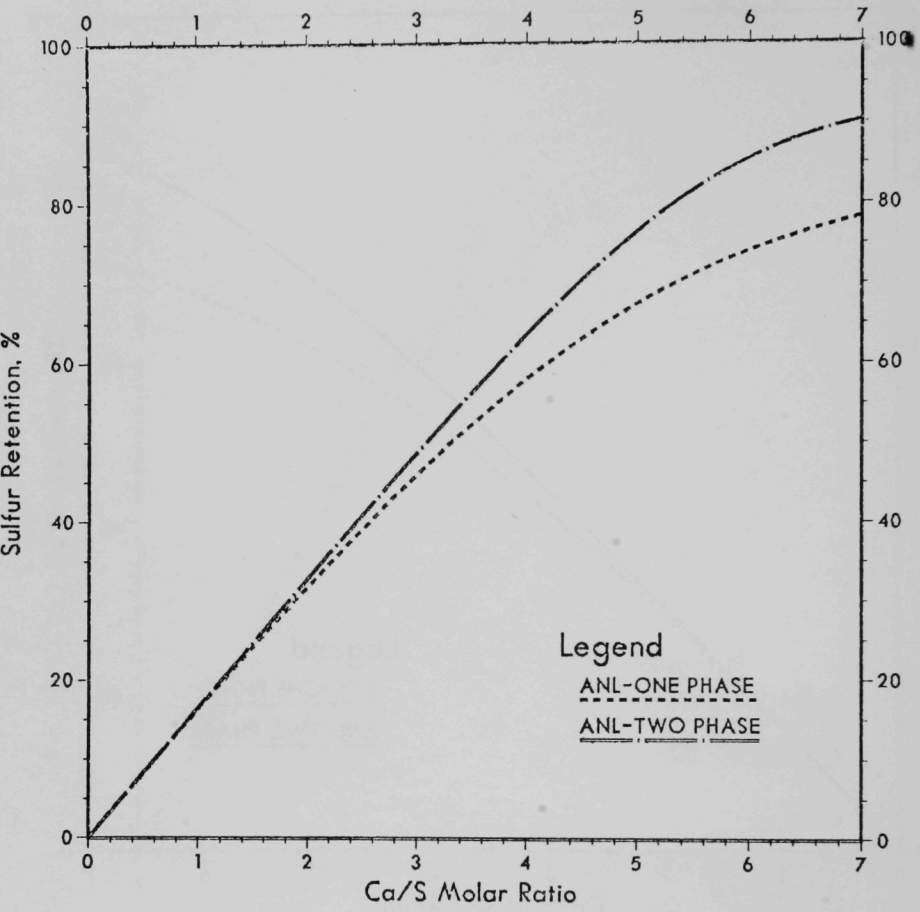

Fluidized Bed Operating Conditions

Temperature = 850. C = 1562. F

Pressure = 101. kPa = 1.0 atm

Fluidizing Velocity = 2.00 m/sec = 6.56 ft/sec

Bed Height = 1.20 Meters = 3.93 ft

Coal Feed Rate = 897.6 kg/hr = 1977.0 lb/hr

Sulfur Content in Coal = 2.58 wt%

Bed Area = 3.34 sq. meter = 36.0 sq. ft.

Sorbent Particle Dia. = 1000. micron = 0.0394 inch

Predicted Performance of Sorbent 8901

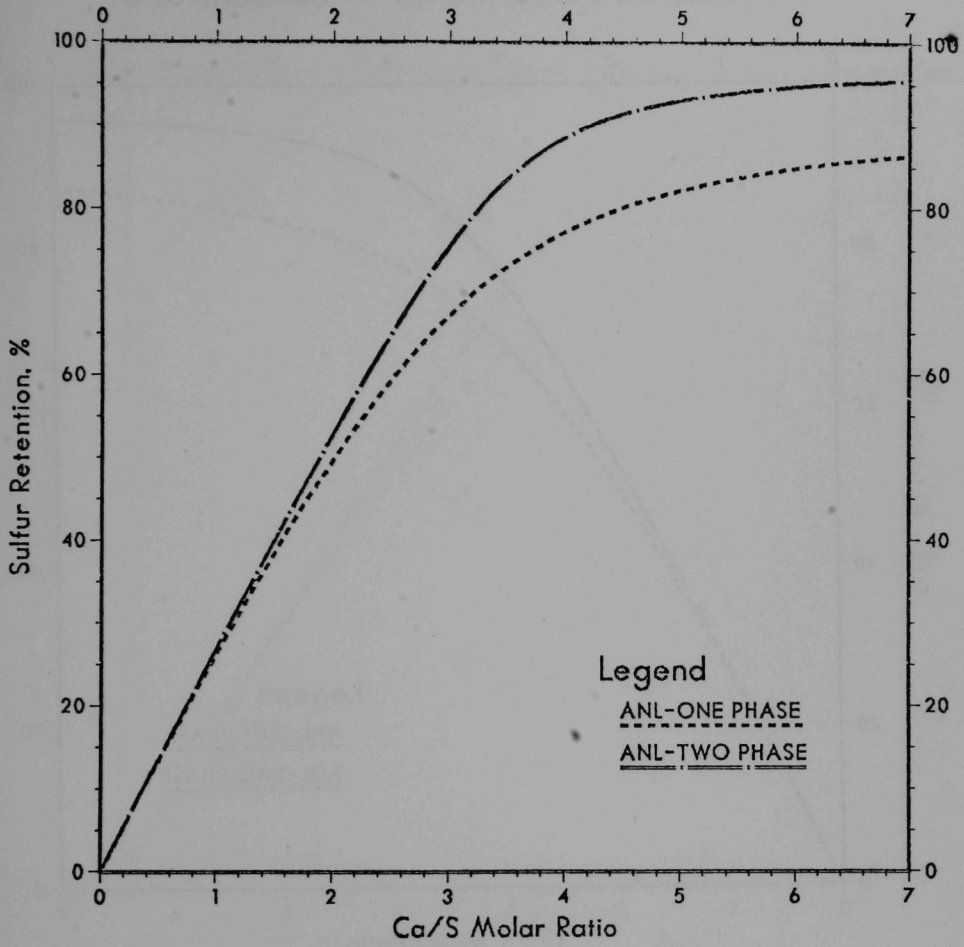

Fluidized Bed Operating Conditions

Temperature = 850. C = 1562. F

Pressure = 101. kPa = 1.0 atm

Fluidizing Velocity = 2.00 m/sec = 6.56 ft/sec

Bed Height = 1.20 Meters = 3.93 ft

Coal Feed Rate = 897.6 kg/hr = 1977.0 lb/hr

Sulfur Content in Coal = 2.58 wt%

Bed Area = 3.34 sq. meter = 36.0 sq. ft.

Sorbent Particle Dia. = 1000. micron = 0.0394 inch

Predicted Performance of Sorbent 8701

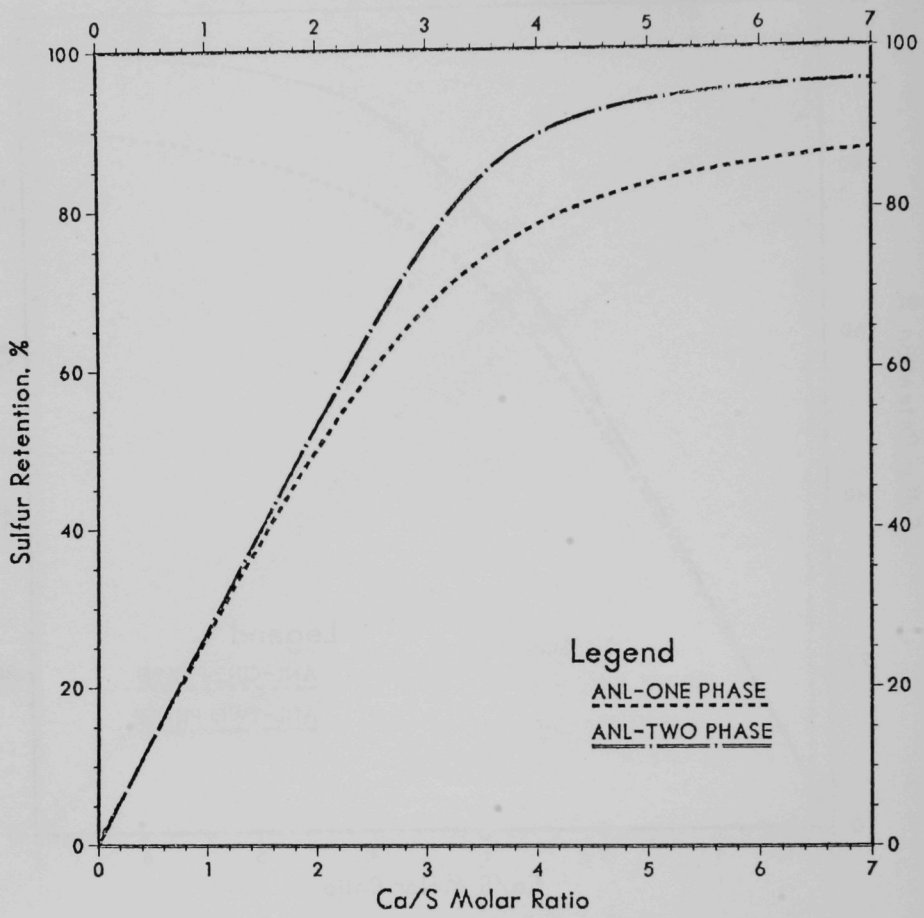

Fluidized Bed Operating Conditions

Temperature = 850. C = 1562. F

Pressure = 101. kPa = 1.0 atm

Fluidizing Velocity = 2.00 m/sec = 6.56 ft/sec

Bed Height = 1.20 Meters = 3.93 ft

Coal Feed Rate = 897.6 kg/hr = 1977.0 lb/hr

Sulfur Content in Coal = 2.58 wt%

Bed Area = 3.34 sq. meter = 36.0 sq. ft.

Sorbent Particle Dia. = 1000. micron = 0.0394 inch

Predicted Performance of Sorbent 8201

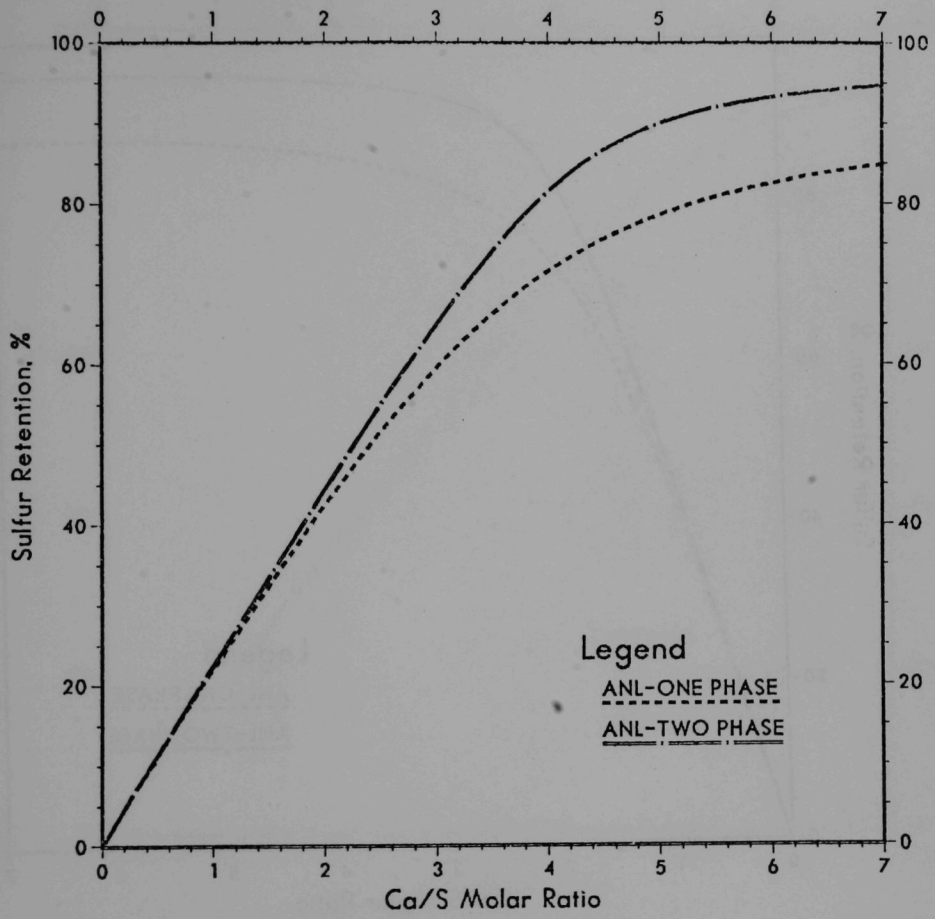

Fluidized Bed Operating Conditions

Temperature = 850. C = 1562. F

Pressure = 101. kPa = 1.0 atm

Fluidizing Velocity = 2.00 m/sec = 6.56 ft/sec

Bed Height = 1.20 Meters = 3.93 ft

Coal Feed Rate = 897.6 kg/hr = 1977.0 lb/hr

Sulfur Content in Coal = 2.58 wt%

Bed Area = 3.34 sq. meter = 36.0 sq. ft.

Sorbent Particle Dia. = 1000. micron = 0.0394 inch

Predicted Performance of Sorbent 8101

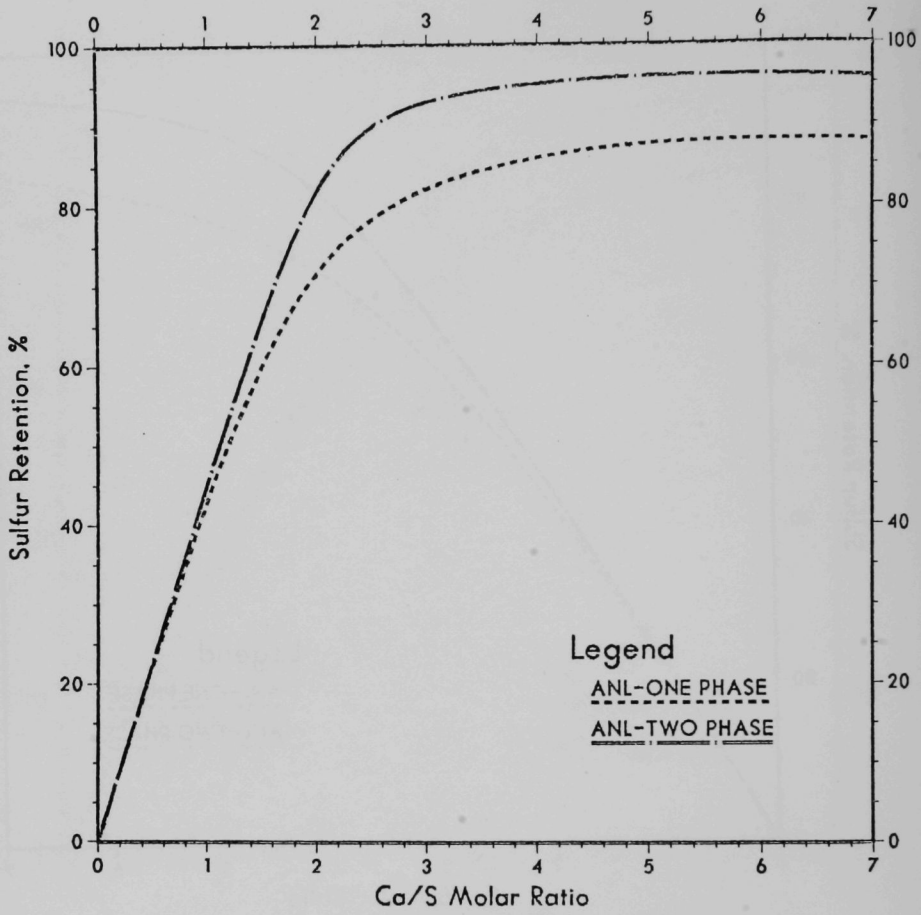

Fluidized Bed Operating Conditions

Temperature = 850. C = 1562. F

Pressure = 101. kPa = 1.0 atm

Fluidizing Velocity = 2.00 m/sec = 6.56 ft/sec

Bed Height = 1.20 Meters = 3.93 ft

Coal Feed Rate = 897.6 kg/hr = 1977.0 lb/hr

Sulfur Content in Coal = 2.58 wt%

Bed Area = 3.34 sq. meter = 36.0 sq. ft.

Sorbent Particle Dia. = 1000. micron = 0.0394 inch

Predicted Performance of Sorbent 8001

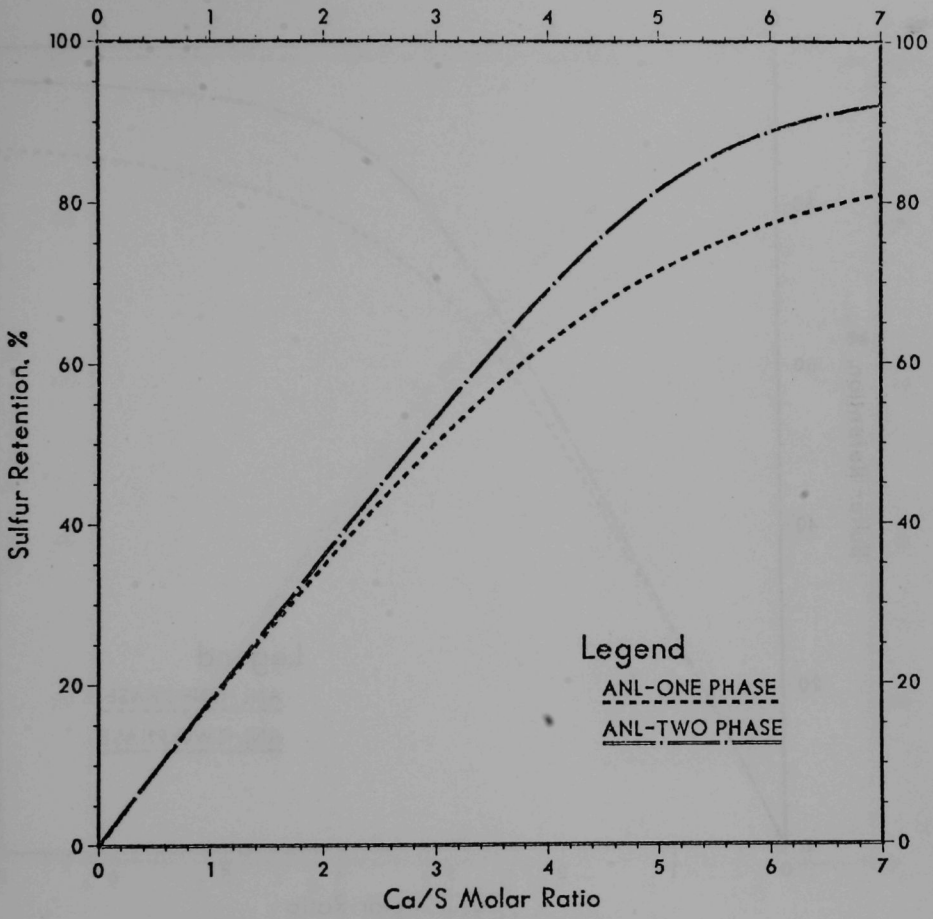

Fluidized Bed Operating Conditions

Temperature = 850. C = 1562. F

Pressure = 101. kPa = 1.0 atm

Fluidizing Velocity = 2.00 m/sec = 6.56 ft/sec

Bed Height = 1.20 Meters = 3.93 ft

Coal Feed Rate = 897.6 kg/hr = 1977.0 lb/hr

Sulfur Content in Coal = 2.58 wt%

Bed Area = 3.34 sq. meter = 36.0 sq. ft.

Sorbent Particle Dia. = 1000. micron = 0.0394 inch

Predicted Performance of Sorbent 7901

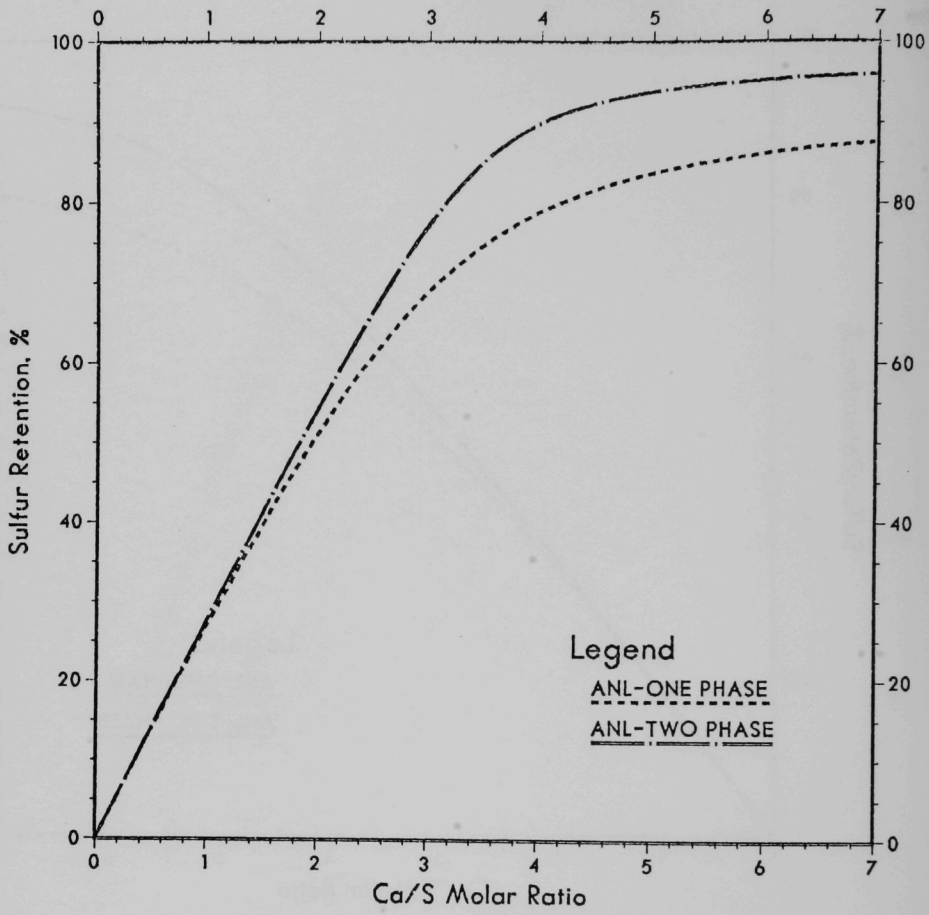

Fluidized Bed Operating Conditions

Temperature = 850. C = 1562. F

Pressure = 101. kPa = 1.0 atm

Fluidizing Velocity = 2.00 m/sec = 6.56 ft/sec

Bed Height = 1.20 Meters = 3.93 ft

Coal Feed Rate = 897.6 kg/hr = 1977.0 lb/hr

Sulfur Content in Coal = 2.58 wt%

Bed Area = 3.34 sq. meter = 36.0 sq. ft.

Sorbent Particle Dia. = 1000. micron = 0.0394 inch

Predicted Performance of Sorbent 7402

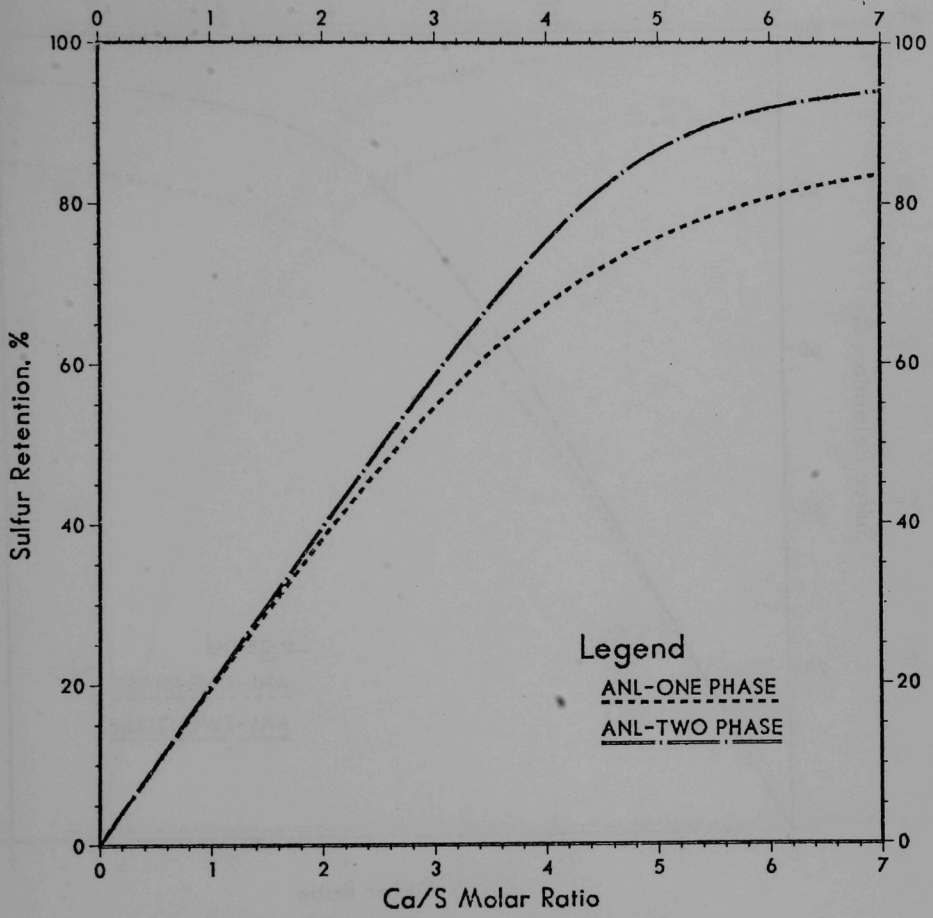

Fluidized Bed Operating Conditions

Temperature = 850. C = 1562. F

Pressure = 101. kPa = 1.0 atm

Fluidizing Velocity = 2.00 m/sec = 6.56 ft/sec

Bed Height = 1.20 Meters = 3.93 ft

Coal Feed Rate = 897.6 kg/hr = 1977.0 lb/hr

Sulfur Content in Coal = 2.58 wt%

Bed Area = 3.34 sq. meter = 36.0 sq. ft.

Sorbent Particle Dia. = 1000. micron = 0.0394 inch

Predicted Performance of Sorbent 7301

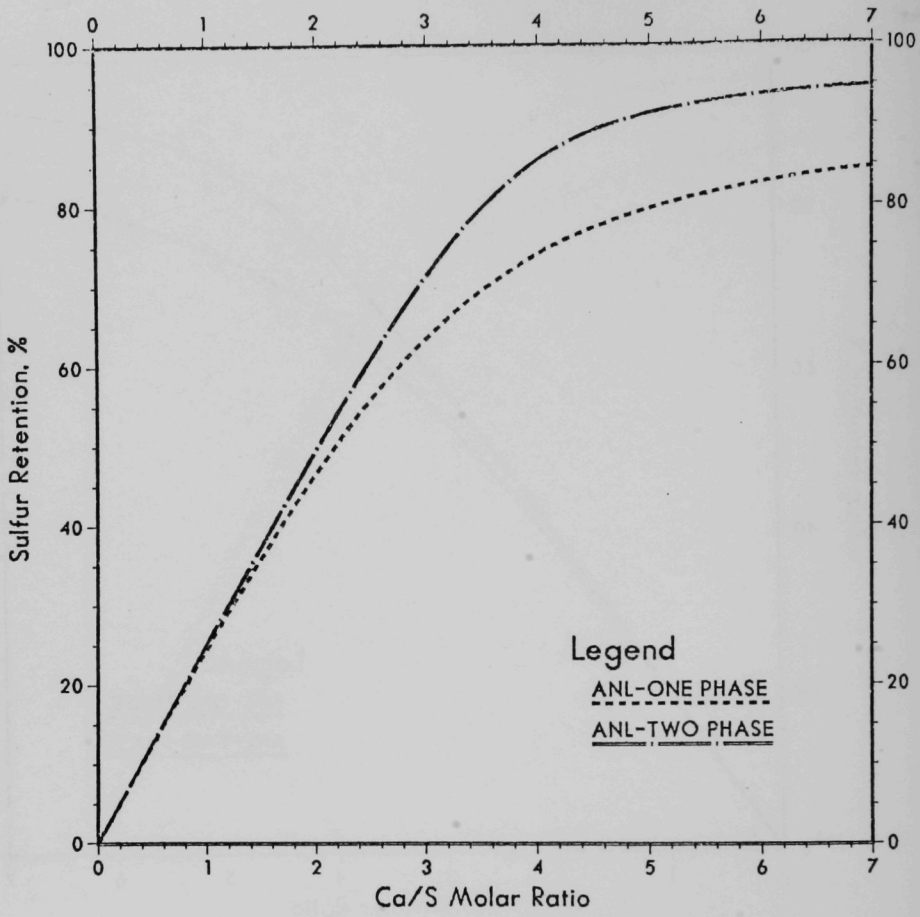

Fluidized Bed Operating Conditions

Temperature = 850. C = 1562. F

Pressure = 101. kPa = 1.0 atm

Fluidizing Velocity = 2.00 m/sec = 6.56 ft/sec

Bed Height = 1.20 Meters = 3.93 ft

Coal Feed Rate = 897.6 kg/hr = 1977.0 lb/hr

Sulfur Content in Coal = 2.58 wt%

Bed Area = 3.34 sq. meter = 36.0 sq. ft.

Sorbent Particle Dia. = 1000. micron = 0.0394 inch

Predicted Performance of Sorbent 6701

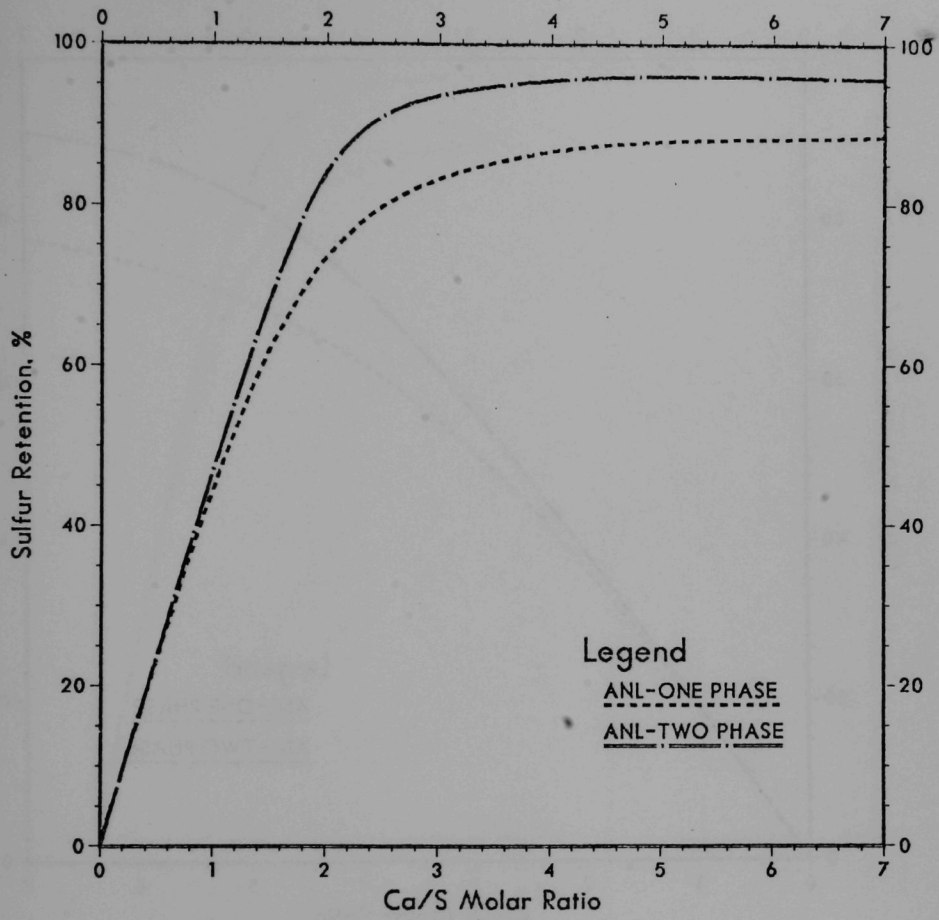

Fluidized Bed Operating Conditions

Temperature = 850. C = 1562. F

Pressure = 101. kPa = 1.0 atm

Fluidizing Velocity = 2.00 m/sec = 6.56 ft/sec

Bed Height = 1.20 Meters = 3.93 ft

Coal Feed Rate = 897.6 kg/hr = 1977.0 lb/hr

Sulfur Content in Coal = 2.58 wt%

Bed Area = 3.34 sq. meter = 36.0 sq. ft.

Sorbent Particle Dia. = 1000. micron = 0.0394 inch

Predicted Performance of Sorbent 6401

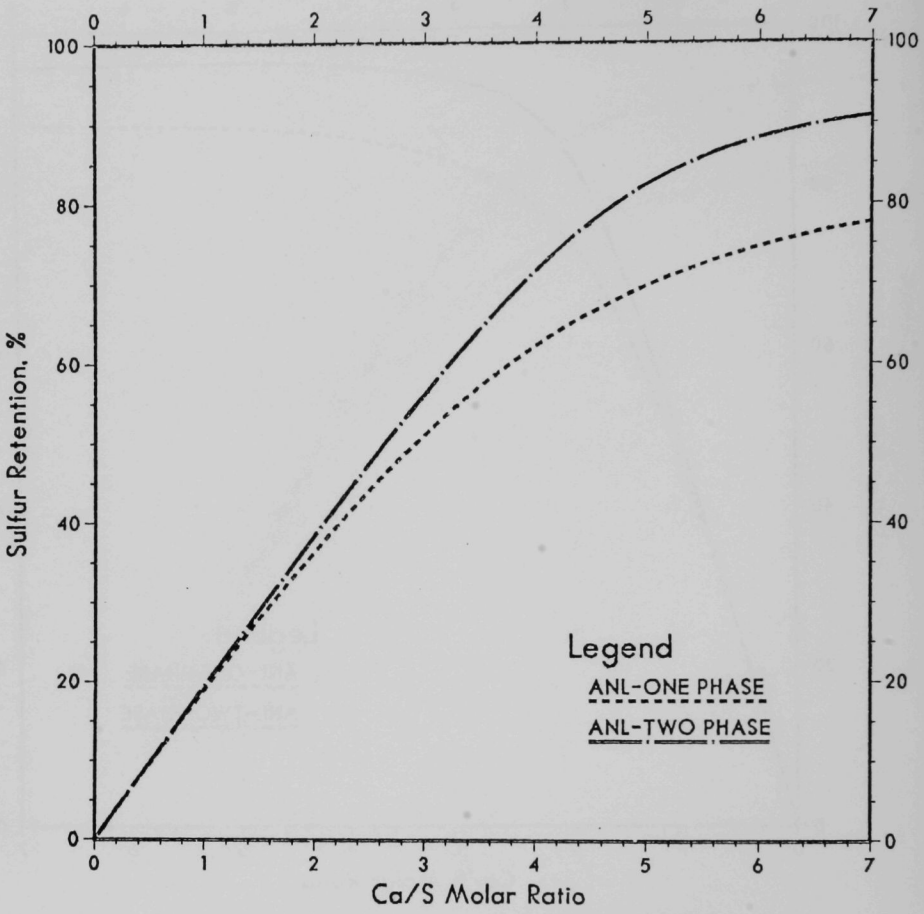

Fluidized Bed Operating Conditions

Temperature = 850. C = 1562. F

Pressure = 101. kPa = 1.0 atm

Fluidizing Velocity = 2.00 m/sec = 6.56 ft/sec

Bed Height = 1.20 Meters = 3.93 ft

Coal Feed Rate = 897.6 kg/hr = 1977.0 lb/hr

Sulfur Content in Coal = 2.58 wt%

Bed Area = 3.34 sq. meter = 36.0 sq. ft.

Sorbent Particle Dia. = 1000. micron = 0.0394 inch

Predicted Performance of Sorbent 6101

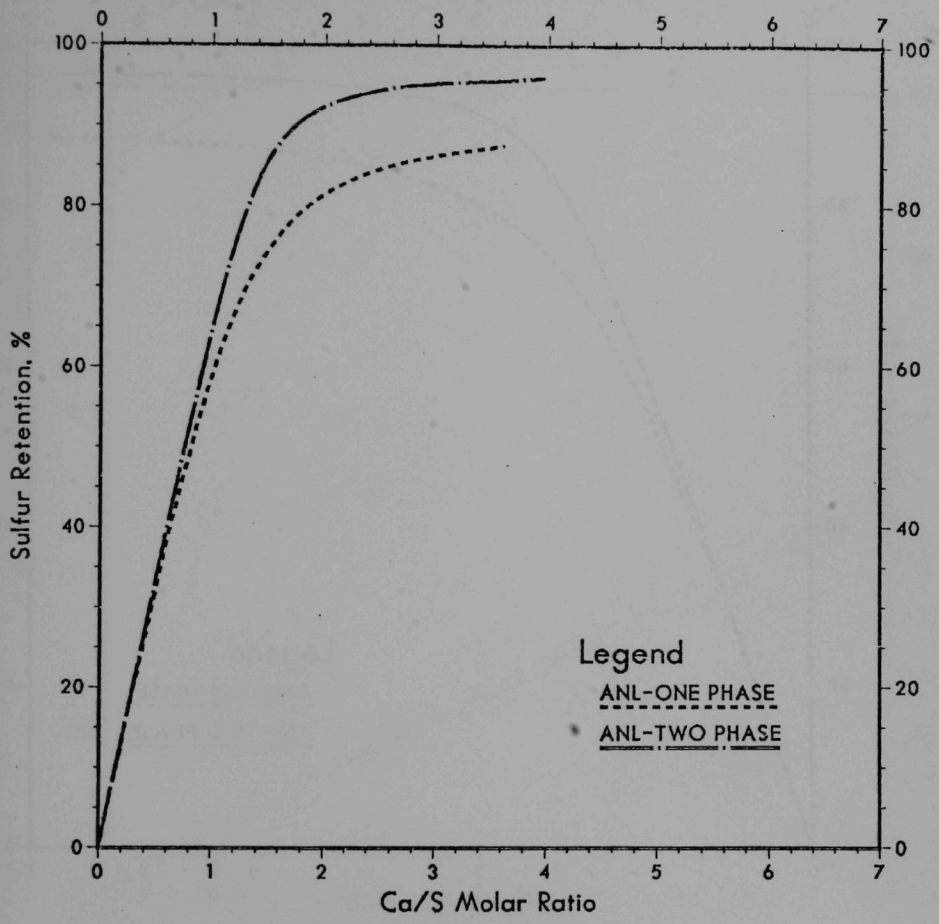

Fluidized Bed Operating Conditions

Temperature = 850. C = 1562. F

Pressure = 101. kPa = 1.0 atm

Fluidizing Velocity = 2.00 m/sec = 6.56 ft/sec

Bed Height = 1.20 Meters = 3.93 ft

Coal Feed Rate = 897.6 kg/hr = 1977.0 lb/hr

Sulfur Content in Coal = 2.58 wt%

Bed Area = 3.34 sq. meter = 36.0 sq. ft.

Sorbent Particle Dia. = 1000. micron = 0.0394 inch

Predicted Performance of Sorbent 5901

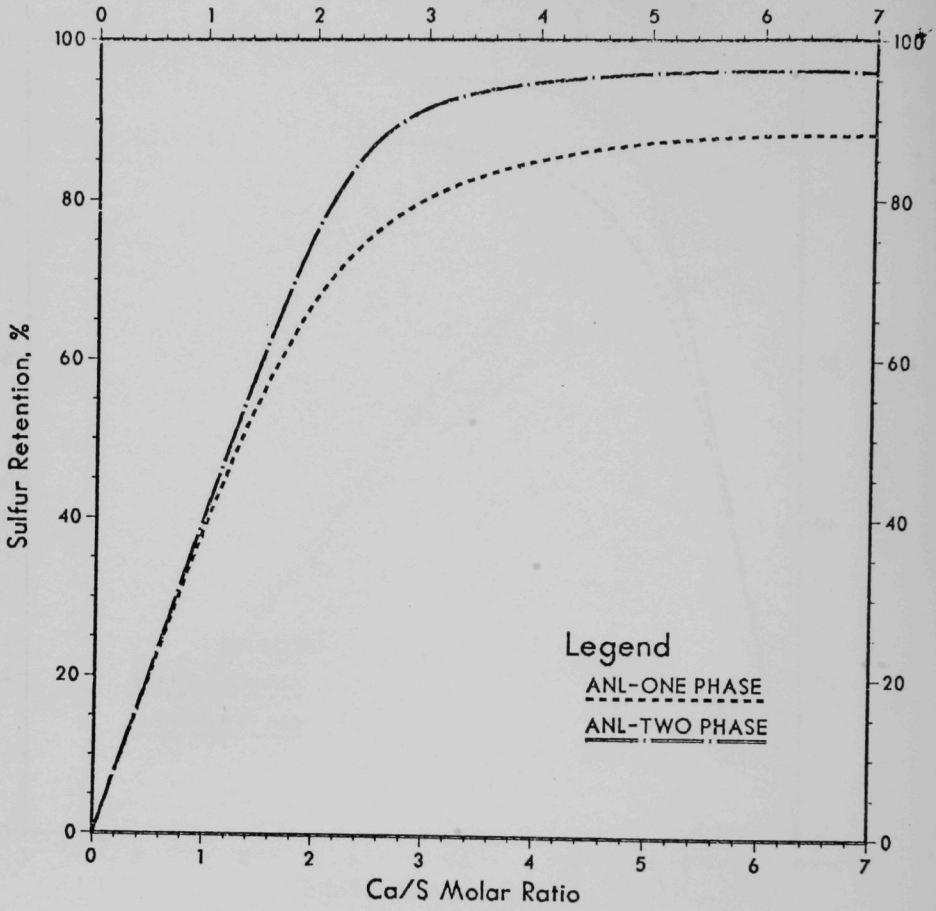

Fluidized Bed Operating Conditions

Temperature = 850. C = 1562. F

Pressure = 101. kPa = 1.0 atm

Fluidizing Velocity = 2.00 m/sec = 6.56 ft/sec

Bed Height = 1.20 Meters = 3.93 ft

Coal Feed Rate = 897.6 kg/hr = 1977.0 lb/hr

Sulfur Content in Coal = 2.58 wt%

Bed Area = 3.34 sq. meter = 36.0 sq. ft.

Sorbent Particle Dia. = 1000. micron = 0.0394 inch

Predicted Performance of Sorbent 5601

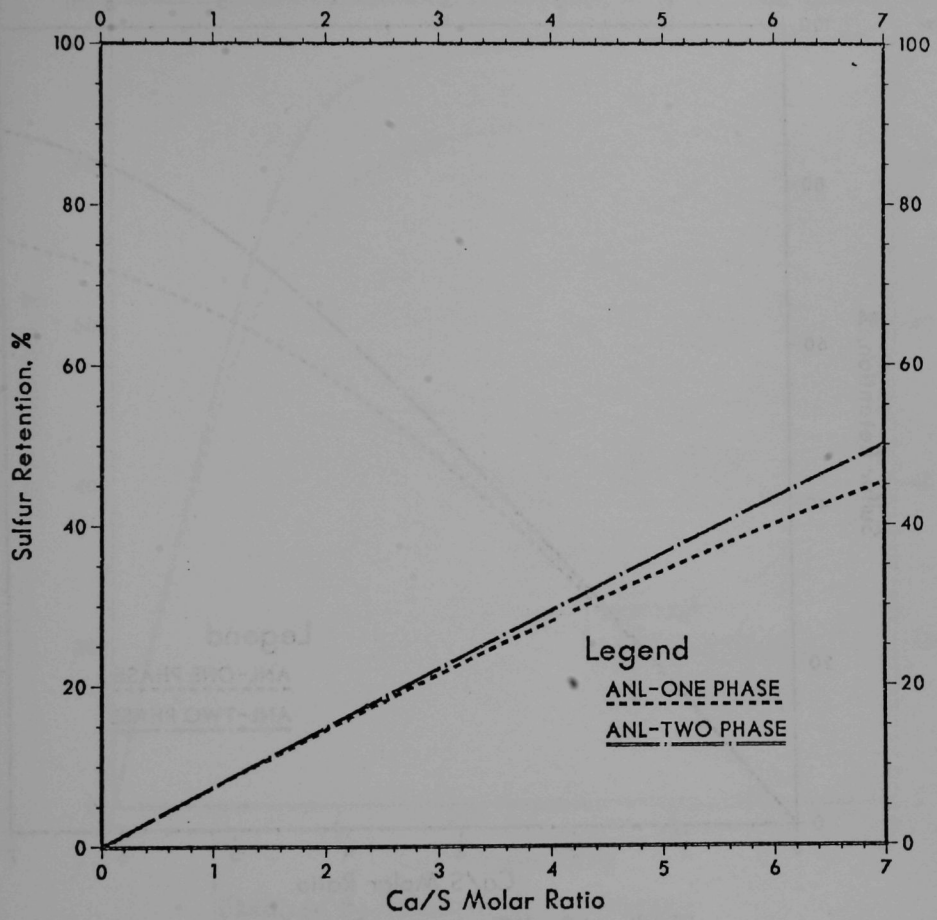

Fluidized Bed Operating Conditions

Temperature = 850. C = 1562. F

Pressure = 101. kPa = 1.0 atm

Fluidizing Velocity = 2.00 m/sec = 6.56 ft/sec

Bed Height = 1.20 Meters = 3.93 ft

Coal Feed Rate = 897.6 kg/hr = 1977.0 lb/hr

Sulfur Content in Coal = 2.58 wt%

Bed Area = 3.34 sq. meter = 36.0 sq. ft.

Sorbent Particle Dia. = 1000. micron = 0.0394 inch

Predicted Performance of Sorbent 5501

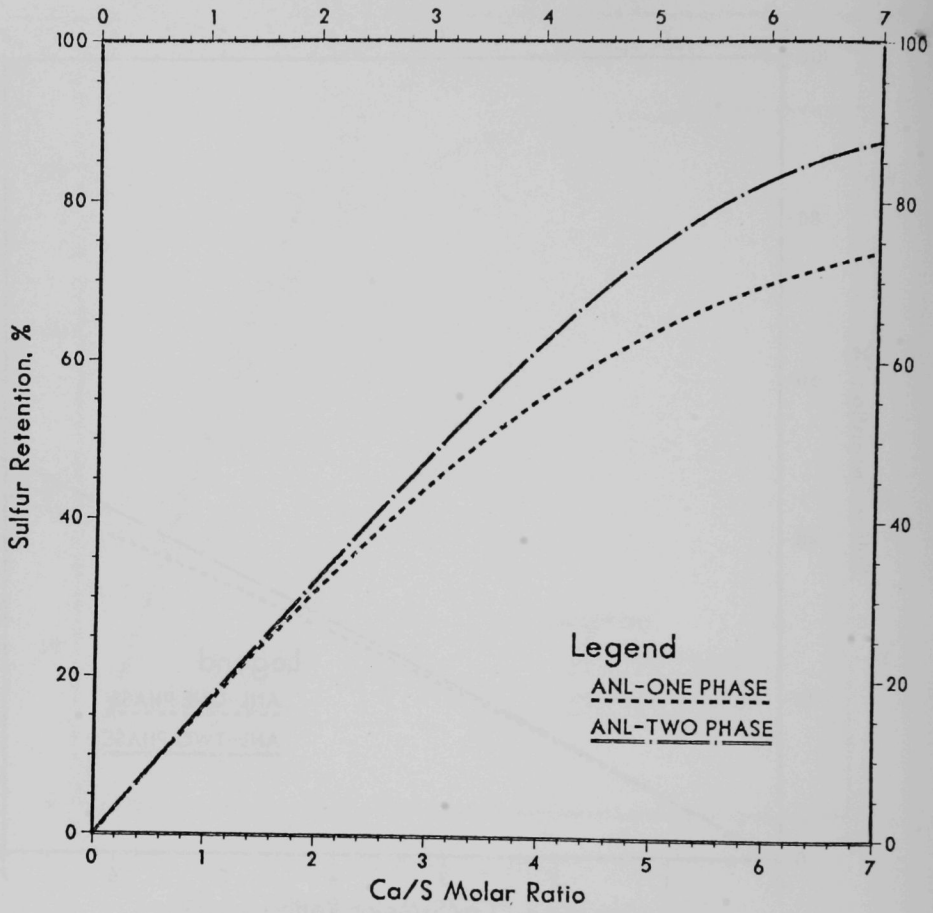

Fluidized Bed Operating Conditions

Temperature = 850. C = 1562. F

Pressure = 101. kPa = 1.0 atm

Fluidizing Velocity = 2.00 m/sec = 6.56 ft/sec

Bed Height = 1.20 Meters = 3.93 ft

Coal Feed Rate = 897.6 kg/hr = 1977.0 lb/hr

Sulfur Content in Coal = 2.58 wt%

Bed Area = 3.34 sq. meter = 36.0 sq. ft.

Sorbent Particle Dia. = 1000. micron = 0.0394 inch

Predicted Performance of Sorbent 5301

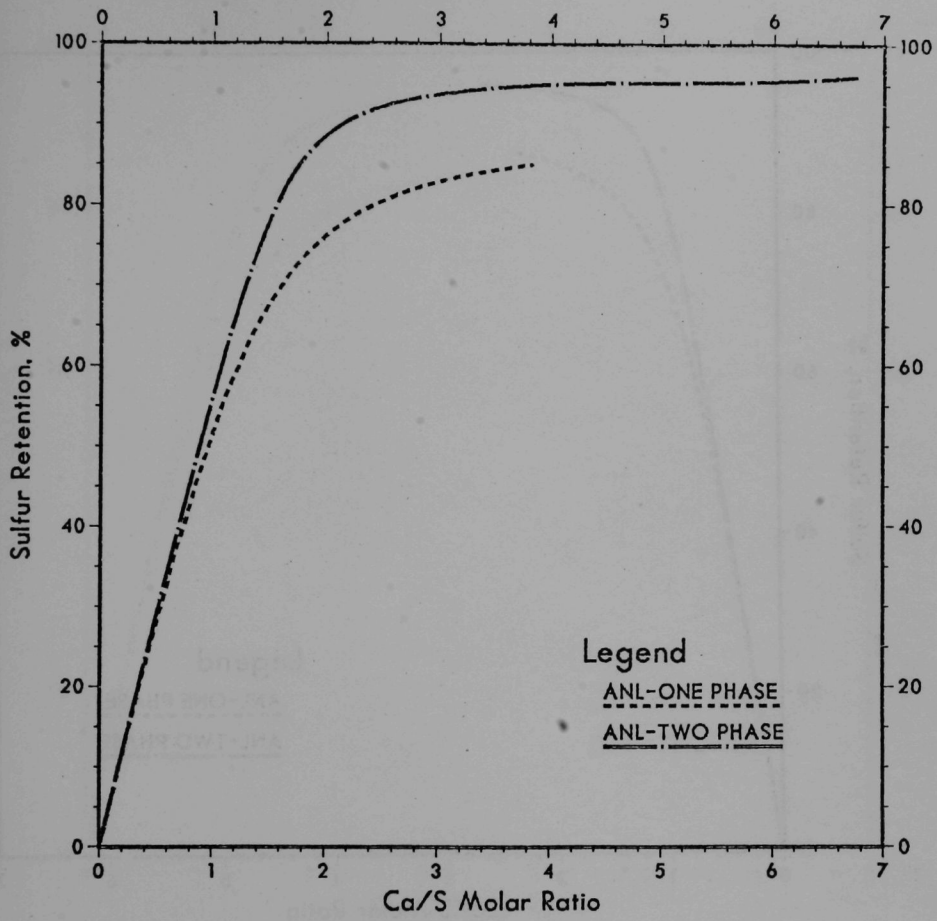

Fluidized Bed Operating Conditions

Temperature = 850. C = 1562. F

Pressure = 101. kPa = 1.0 atm

Fluidizing Velocity = 2.00 m/sec = 6.56 ft/sec

Bed Height = 1.20 Meters = 3.93 ft

Coal Feed Rate = 897.6 kg/hr = 1977.0 lb/hr

Sulfur Content in Coal = 2.58 wt%

Bed Area = 3.34 sq. meter = 36.0 sq. ft.

Sorbent Particle Dia. = 1000. micron = 0.0394 inch

Predicted Performance of Sorbent 5101

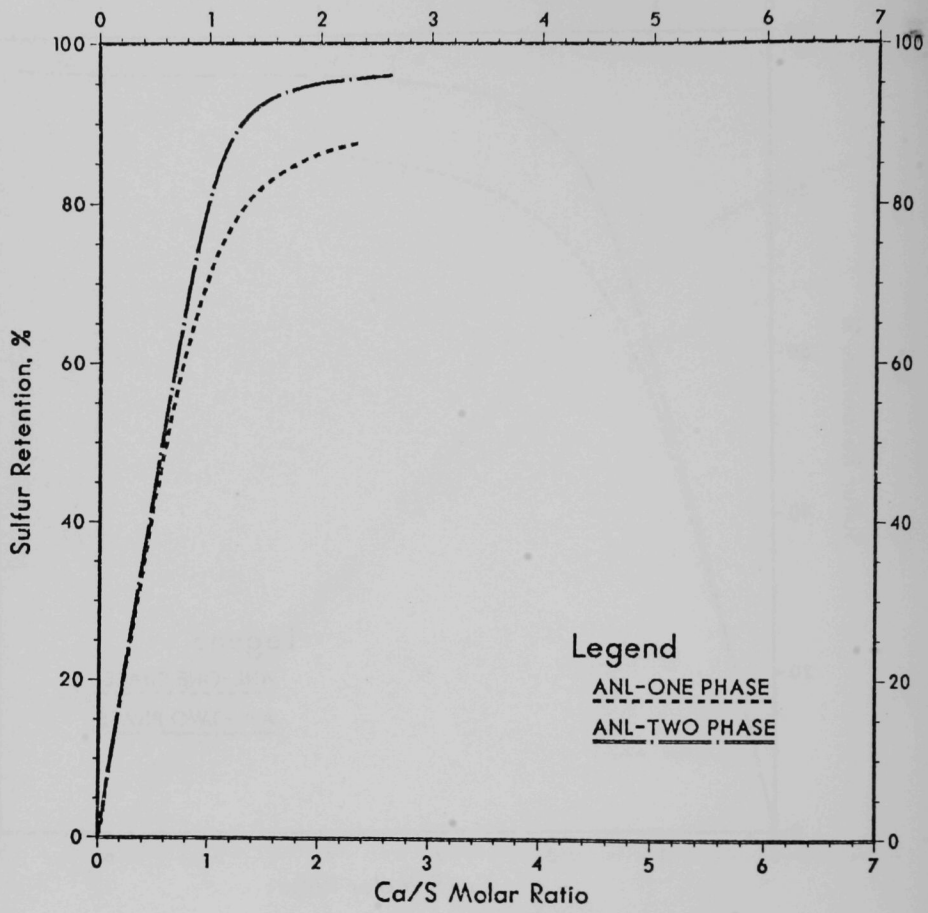

Fluidized Bed Operating Conditions

Temperature = 850. C = 1562. F

Pressure = 101. kPa = 1.0 atm

Fluidizing Velocity = 2.00 m/sec = 6.56 ft/sec

Bed Height = 1.20 Meters = 3.93 ft

Coal Feed Rate = 897.6 kg/hr = 1977.0 lb/hr

Sulfur Content in Coal = 2.58 wt%

Bed Area = 3.34 sq. meter = 36.0 sq. ft.

Sorbent Particle Dia. = 1000. micron = 0.0394 inch

Predicted Performance of Sorbent 5001

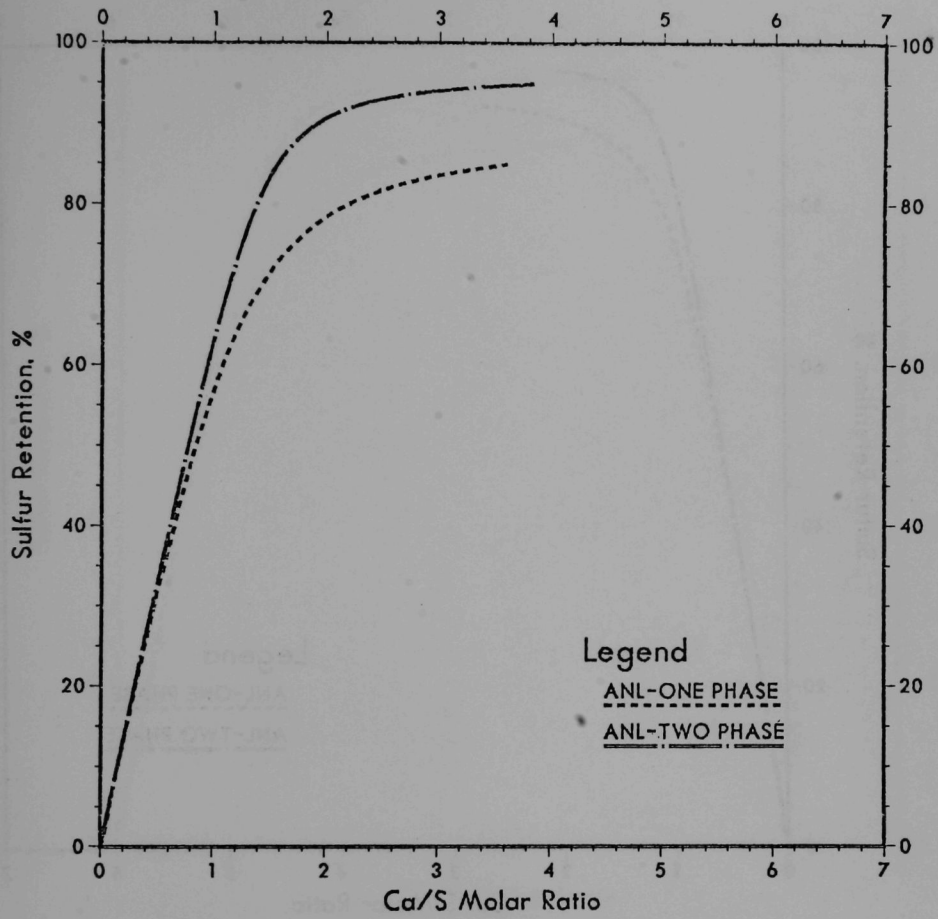

Fluidized Bed Operating Conditions

Temperature = 850. C = 1562. F

Pressure = 101. kPa = 1.0 atm

Fluidizing Velocity = 2.00 m/sec = 6.56 ft/sec

Bed Height = 1.20 Meters = 3.93 ft

Coal Feed Rate = 897.6 kg/hr = 1977.0 lb/hr

Sulfur Content in Coal = 2.58 wt%

Bed Area = 3.34 sq. meter = 36.0 sq. ft.

Sorbent Particle Dia. = 1000. micron = 0.0394 inch

Predicted Performance of Sorbent 4801

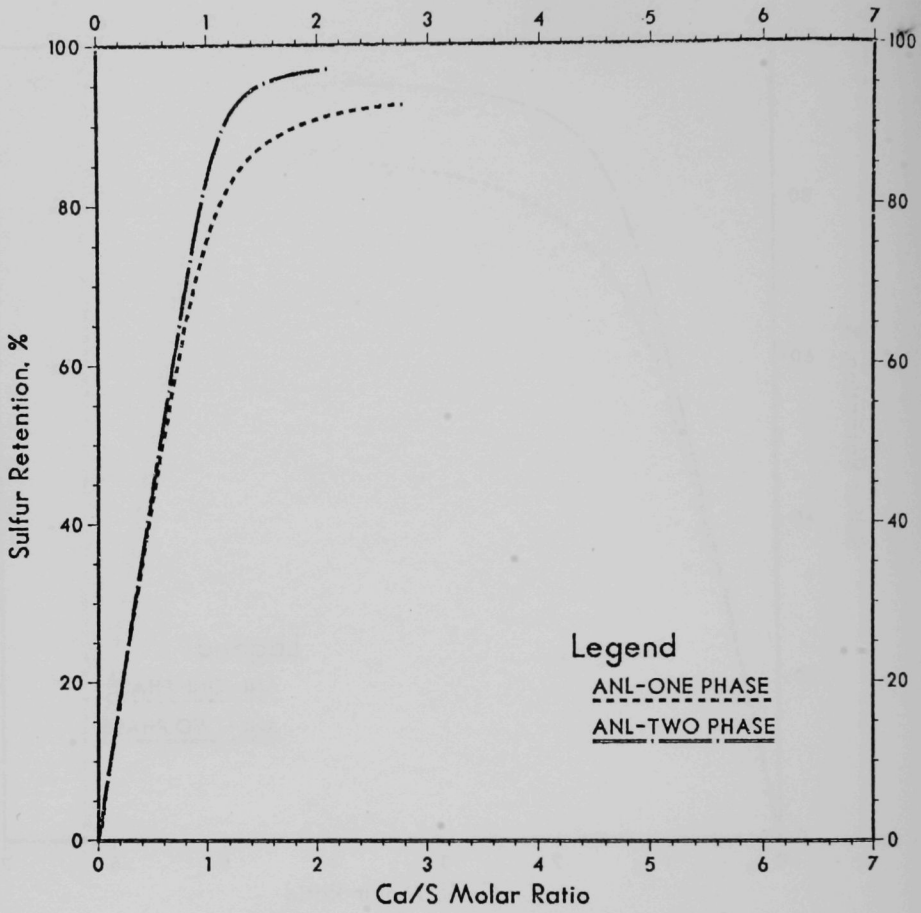

Fluidized Bed Operating Conditions

Temperature = 850. C = 1562. F

Pressure = 101. kPa = 1.0 atm

Fluidizing Velocity = 2.00 m/sec = 6.56 ft/sec

Bed Height = 1.20 Meters = 3.93 ft

Coal Feed Rate = 897.6 kg/hr = 1977.0 lb/hr

Sulfur Content in Coal = 2.58 wt%

Bed Area = 3.34 sq. meter = 36.0 sq. ft.

Sorbent Particle Dia. = 1000. micron = 0.0394 inch

Predicted Performance of Sorbent 4601

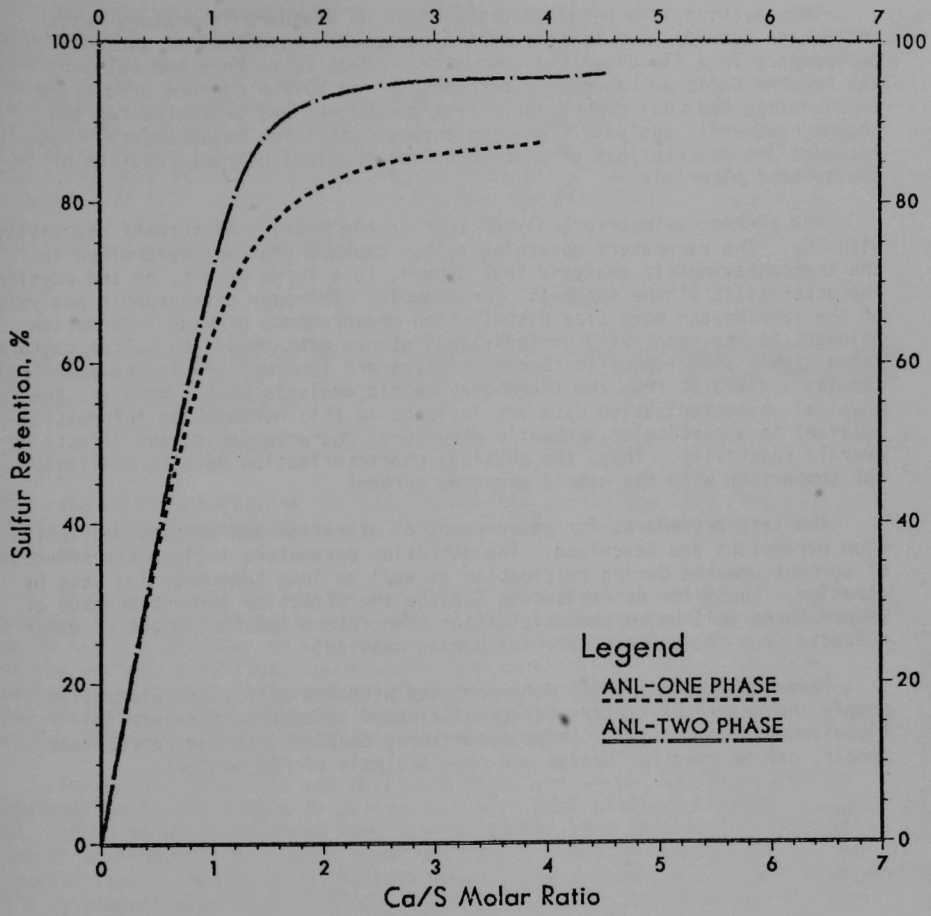

Fluidized Bed Operating Conditions

Temperature = 850. C = 1562. F

Pressure = 101. kPa = 1.0 atm

Fluidizing Velocity = 2.00 m/sec = 6.56 ft/sec

Bed Height = 1.20 Meters = 3.93 ft

Coal Feed Rate = 897.6 kg/hr = 1977.0 lb/hr

Sulfur Content in Coal = 2.58 wt%

Bed Area = 3.34 sq. meter = 36.0 sq. ft.

Sorbent Particle Dia. = 1000. micron = 0.0394 inch

3.0 SUMMARY OF STANDARD TESTS

This section is a detailed description of standard laboratory tests which have been devised to measure the parameters essential to sorbent performance in a fluidized-bed combustor. These tests form the basis of the Argonne National Laboratory methodology for sulfur capture prediction in fluidized-bed coal combustion. Test procedures are presented for the thermogravimetric analysis (TGA) and sorbent attrition measurements. Also included are descriptions of procedures for physical characterization of the sorbent materials.

The thermogravimetric analyzer test is the measure of sorbent reactivity with SO_2. The parameters governing sulfur capture that are determined in the thermogravimetric analysis test depend, to a large extent, on the physical characteristics of the sorbent. For example: Thorough petrographic analysis of the samples and pore size distribution measurements provide information relevant to the reactivity of individual stones with regard to sulfur capture. These highly stone-specific characteristics are incorporated in the numerical results arrived at from the thermogravimetric analysis test. However, the physical characterization data are included in this handbook as information relevant to a particular sorbent's structural characteristics and effects on overall reactivity. Thus, the physical characterization data is available for comparison with the user's proposed sorbent.

The test procedures for measurement of attrition and sorbent decrepitation parameters are described. The attretion parameters include the effects of sorbent breakup during calcination as well as long term material loss by abrasion. Those for decrepitation include the effect of sorbent breakup at temperatures well below the calcination temperature and the amount of water released from the sorbent material during heating.

Thermogravimetric (TGA) data combined with the attrition information supply the needed parameters for prediction of sorbent performance in fluidized-bed combustion. These parameters, coupled with the appropriate models, can be used for design and cost analysis of FBC systems.

3.1 THERMOGRAVIMETRIC ANALYZER TEST

The intrinsic reactivity of a sorbent with sulfur dioxide is a primary consideration in sorbent selection since feed rates will be lower for sorbents with greater reactivity and capacity for sulfur dioxide. This has a favorable impact on the overall economics of the fluidized bed combustion process. The laboratory test selected to compare the relative reactivities and capacities of sorbents for sulfur dioxide utilizes a thermogravimetric analyzer (TGA). The standardized laboratory test procedure for the apparatus has two steps: The first step is calcining the sorbent; the second step is reaction of this calcine with SO_2. Calcination involves heating the sorbent, which in an atmospheric FBC is accompanied by evolution of CO_2 from the $CaCO_3$ in the sorbent, according to the reaction

$$CaCO_3(c) \rightarrow CaO(c) + CO_2(g) \qquad 1$$

A decrease in molar volume of the solid occurs during calcination, giving rise to significant porosity of the calcined material. This porous calcine is then reacted with SO_2 according to Eq. 2

$$CaO(c) + SO_2(g) + 1/2\ O_2(g) \rightarrow CaSO_4(c) \qquad 2$$

The rate of this sulfation reaction is monitored with the TGA. The rate of sulfation depends strongly on the degree to which the sorbent has already been sulfated.

In general, not all of the CaO in the sorbent reacts with SO_2 (i.e., sorbent utilization is less than 100%). This occurs because the product, which has a high molar volume, blocks the gas diffusional paths along pores in the sorbent particles, causing reaction to virtually cease. Maximum sorbent utilization is a capacity factor which is also determined with the TGA apparatus. Thus, both the reactivity and the capacity of a sorbent for sulfur dioxide are determined in a single experiment.

For both calcination and sulfation reactions in the thermogravimetric analyzer test, the sample is placed in a wire mesh platinum basket (0.5-cm ID, 1.8-cm height) suspended in a quartz reactor tube (2.5-cm ID) from one arm of an Ainsworth Model RVA recording microbalance as in Fig. 3.1.1. The reactor tube is heated by a platinum-wound furnace which is controlled within 5°C at temperatures up to 1200°C. Two Pt, Pt-10% Rh thermocouples are used for temperature monitoring and control. The gas mixture passes upward through the heated reaction tube and reacts with the samples, then exits through a condenser and a series of scrubbers. A nitrogen purge gas stream that flows countercurrently through the microbalance bell jar keeps it free of corrosive reactant gases.

The gas mixtures are prepared by blending streams of the individual gaseous constituents. Water, when a part of the mixture, is added to the blend of the other gases by passage through a humidifier upstream from the point of introduction of SO_2. The gas lines leading from the humidifier

are heated to prevent condensation of the water and to minimize corrosion. Mass spectrometric analyses of samples of the feed gas mixtures are made to verify their composition; the measured values of the SO_2 and O_2 concentrations are within 5% of the values computed from the flow rates. (The H_2 and CO lines shown in Fig. 3.1.1 are not used in the calcination or sulfation experiments.)

In the calcination step, a sample of each stone is initially screened to -18 +20 mesh (1000-841 μm) particle size. This particle size represents an average particle size of material used in a fluidized-bed combustor (i.e., -14 +30 mesh). A sample of each stone (300-400 mg) is calcined at 850°C in 20% CO_2-N_2. After calcination is completed, the sample is exposed to a gaseous mixture consisting of 0.3% SO_2 - 5% O_2 - 20% CO_2 in N_2 at 850°C. These standardized conditions, summarized in Table 3.1.1, are representative of conditions encountered in a fluidized bed coal combustor.

The TGA unit continuously records the weight change of the sample during its reaction with a gas mixture. Typical data are shown in the Test Results section. At the completion of a TGA run, chemical analyses of the sample are performed to help determine and quantify chemical changes which have occurred. The precision of the TGA measurements is approximately 2 mg or approximately 5% of the total weight change. This precision is typical of sulfation data in the literature [Borgwardt (1970), Borgwardt and Harvey (1972) Yang et al. (1979), and James and Hughes (1976)].

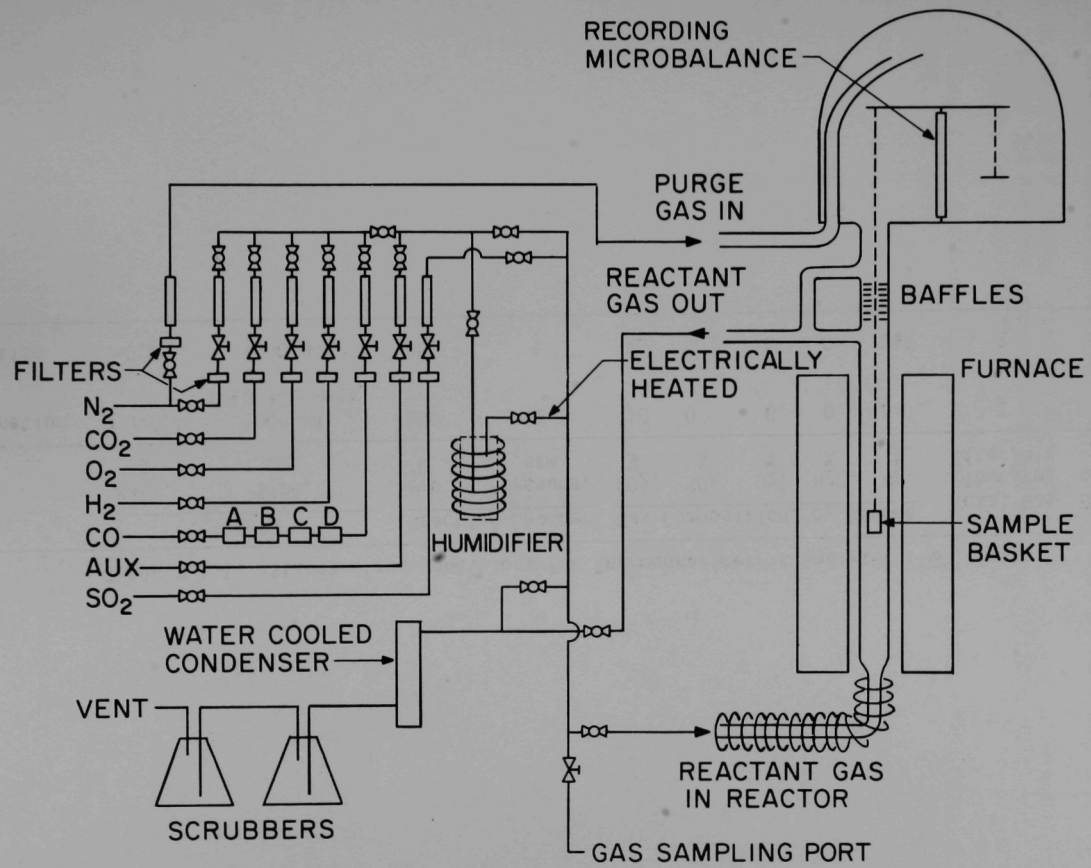

Fig. 3.1.1. TGA Apparatus

Table 3.1.1. Standardized Conditions for Thermogravimetric Analyzer (TGA) Tests

Step	Sample		Reaction Chamber		Gas Composition, by Volume					Total Gas Flowrate, liter/min	Duration of Expt., h
	Mass, g	Size, μm	Temp., °C	Pressure, atm	CO_2, %	SO_2, %	O_2, %	H_2O, %	N_2, %		
Calcination	0.3-0.4	1000-841 (-18 +20 mesh)	850	1	20	0	0	0	bal.	1	0.3
Sulfation	~0.2	1000-841	850	1	20	0.3	5	0	bal.	2	≥5

References for Section 3.1

R. H. Borgwardt, Environ. Sci. Tech. 4, 59 (1970).

R. H. Borgwardt and R. D. Harvey, Environ. Sci. Tech. 6, 350 (1972).

N. J. James and R. Hughes, 2nd Int. Conference on The Control of Gaseous Sulfur and Nitrogen Compound Emissions (Vol. 1), Salford, United Kingdom, April 6-8 (1976).

R. T. Yang, P. T. Cunningham, W. I. Wilson and S. A. Johnson, Adv. Chem. 139, 149 (1975).

3.2 ATTRITION

The attrition resistance of a sorbent is an important consideration in sorbent selection. Sorbent utilization decreases when fine sorbent particles are entrained in the gas stream and carried away from the fluidized bed. Such elutriation of fine particles greatly reduces the average residence time of sorbent in the bed and thus reduces the effectiveness of the sorbent in the bed. Fine particles are generated in the bed by the attrition of large sorbent particles [Merrick and Highly (1974), Austin et al. (1976), Wei et al. (1977), Fan and Srivastava (1980), Wells et al. (1980)]. Attrition encompasses the abrasive action of particle-particle and particle-wall contact in the bed, as well as sorbent fracture arising from thermal shock and decrepitation during calcination. The attrition behavior is also dependent on the sulfation of the sorbent. The calcium sulfate product layer which forms on the outer surface of the sorbent particle (and penetrates into the particle to some extent) gives the sulfated particle an attrition behavior different from that of the unsulfated calcine.

The laboratory test device used to measure the attrition characteristics of a sorbent is a small fluidized bed. The experimental apparatus is schematically depicted in Fig. 3.2.1. The column has a 1.2-m (49-in) height that is composed of two sections. The bottom section is 45-7 cm (18 in.) high and has an I.D. of 5.08 cm (2 in.). The top section is 76.2 cm (30 in.) high and has an I.D. of 7.62 cm (3 in.). The top portion of the bed is a disengagement section that functions to decrease the velocity of the fluidizing gas, minimizing particle entrainment. At the bottom of the bed, there is a porous metal plate that functions as a gas distributor. A pressure regulator (not shown) controls the fluidizing gas flow. The experimental system also consists of a rotameter that monitors the SO_2, allowing its concentration in the fluidizing gas to be calculated; an external electric furnace for heating the bed; and a preheater for preheating the fluidizing gas. Cyclones are located downstream from the bed to collect the overhead material.

The procedure is as follows: Carefully sized sorbent material (see Table 3.2.1) is weighed and placed in the test apparatus after the test device has been heated to the desired temperature. Next, the fluidizing gas is passed through the bed for the duration of the test. At the end of the test, the material remaining in the bed is sieved and the mass of each sieve fraction is determined. Similarly, the particle sizes and mass fractions of the overhead material collected hourly in the cyclone system are determined. Representative samples are analyzed to determine the chemical composition of bed and overhead materials. Typical data and subsequent analysis are shown in Section 4, Test Results. Attrition data for each sorbent are included in Sections 5 and 6, LIMESTONES and DOLOMITES, respectively, of this book.

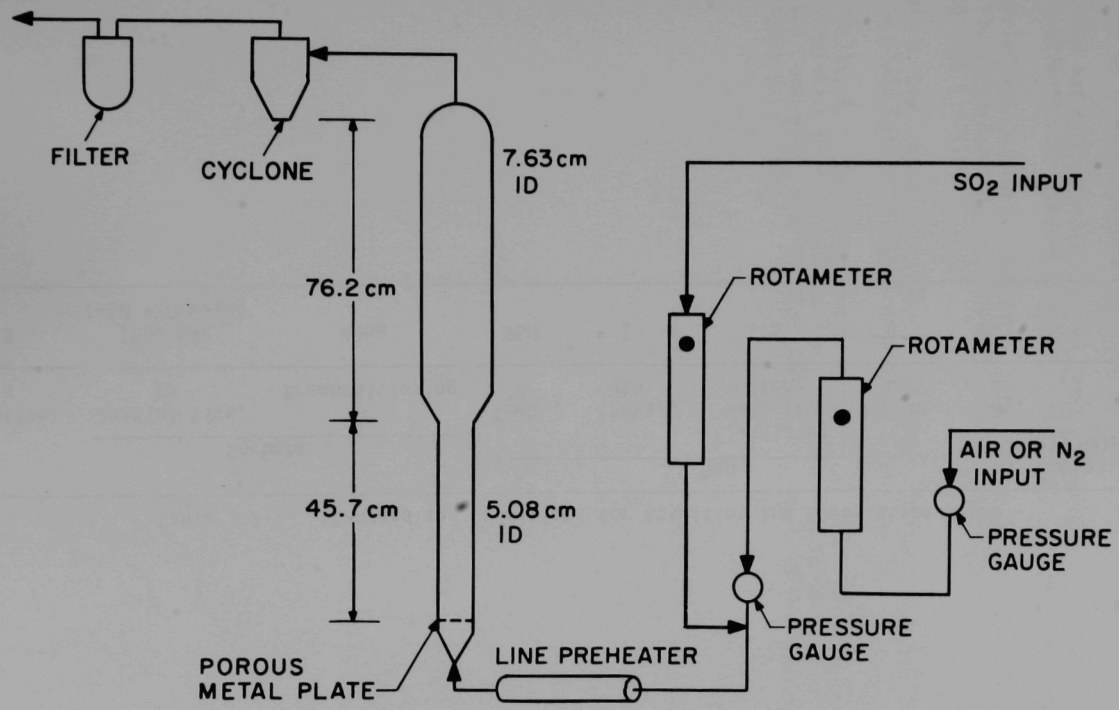

Fig. 3.2.1. Attrition Test Apparatus

Table 3.2.1. Standardized Conditions for Attrition and Elutriation Tests

Duration, h	Sorbent		Bed				Gas Composition, by Volume		
	Initial Size, μm	Preconditioning	Temp., °C	Press., atm	Fluidizing Velocity m/sec	Height, cm	SO_2, %	O_2, %	N_2, %
8	1000-841 (-18 +20 mesh)	none	850	1	1.5	6	0.3	5	6.1

References for Section 3.2

L. Austin, K. Shoji, V. Bhatia, V. Jindal, and K. Savage, "Some Results on the Description of Size Reduction as a Rate Process in Various Mills," I & EC Process Des. Dev. 15, 187 (1976).

L. S. Fan and R. C. Serivastava, "A Stochastic Model for Particle Disintegration I. Grinding Mechanism," Chem. Eng. Sci. 36, 1091-1096 (1981).

D. Merrick and J. Highly, "Particle Reduction and Elutriation in a Fluidized-Bed Process," AIChE Symposium Series No. 137, Vol. 70, p .366 (1974).

J. Wei, W. Lee, and R. F. Krambeck, "Catalyst Attrition and Deactivation in Fluid Catalytic Cracking System," Chem. Eng. Sci. 32, 1211 (1977).

J. R. Wells, R. P. Krishnan, and C. E. Ball, "A Mathematical Model for Simulation of AFBC Systems," 6th International Conference on Fluidized-Bed Combustion, CONF-8000428 (1980), p. 773, Atlanta, Georgia, April 9-11, 1980.

3.3 PETROGRAPHIC ANALYSIS

The size of the grains in a sorbent particle has a significant effect on the overall sulfur-capture ability of that sorbent. Complete utilization of the sorbent is accomplished only when each sorbent grain is completely reacted. Because the main resistance to reaction is from the product layer formed on each grain, grain size is important. Larger grains may support thicker product layers and result in less overall reactivity.

The grain size of the sorbent is determined by petrographic analysis of the raw stone and is assumed to be left as a remnant structure after calcination of the material. Petrographic analysis is performed as follows [Harvey et al. (1968, 1973)]. An -18 +30 mesh size fraction is prepared for examination by vacuum impregnation with epoxy resin in a standard metallography mount. After polishing, the samples are examined in reflected polarized light. The predominant particle size of the grains present is determined by inspection. The grains are assigned to one of three size categories: (1) fine--5 to 60 μm diameter, (2) medium--60 to 250 μm diameter, and (3) coarse--larger than 250 μm diameter. In addition, textural features of the surface are noted.

Petrographic descriptions of sorbents are included in Sections 5 and 6, LIMESTONES and DOLOMITES, of this book.

References for Section 3.3

Richard D. Harvey, "Mineralogy and Petrography of Carbonate Rocks Related to Control of Sulfur Dioxide in Flue Gases," Illinois State Geological Survey (March, 1968).

Richard D. Harvey, Robert R. Frost, and Josephus Thomas, Jr., "Petrographic Characteristics and Physical Properties of Marls, Chalks, Shells, and their Calcines Related to Desulfurization of Flue Gases," Final Report to U.S. Environment Protection Agency (Sept. 1973).

3.4 POROSITY, PORE SIZE DISTRIBUTION, SURFACE AREA, DENSITY

One of the more important considerations affecting the reactivity of calcium-containing sorbents in fluidized-bed combustion is the porosity of the material before and after calcination. It has been shown by many investigators [Borgwardt (1970), Borgwardt and Harvey (1972), Shearer et al. (1978)] that the pore size distribution of a limestone or dolomite greatly affects its ability to absorb SO_2 in a combustor. Pores larger than 0.03 μm have been found to be more important because these pores are not rapidly plugged by the high-molar-volume product. Therefore, measurement of the pore size distribution and total porosity of candidate sorbents would be worthwhile for comparing potential sorbent reactivities.

An American Instrument Company mercury porosimeter has been used to make the standardized measurement of pore size distribution. The 30,000-psi porosimeter uses the mercury intrusion technique to measure the pore volume distribution as a function of pore diameter in solids and powders. This technique involves forcing mercury under increasing pressure into successively smaller pores of a sample. The sizes of the filled pores are obtained from the measured pressures since for each given pressure, all pores equal to or larger than a corresponding minimum diameter will be filled. The volume of these filled pores is obtained directly from the measured volume of mercury intrusion. Mercury porosimeter data can also be used to calculate sorbent density and surface area.

For surface area determination, the mercury porosimetry technique is preferred to gas adsorption techniques. The latter techniques include the surface area due to extremely small pores as well as large pores. Although this area may be substantial, it does not contribute greatly to sulfur capture because the small pores are rapidly plugged by the high-molar-volume product. Thus, the mercury porosimetry technique gives a more realistic assessment of the surface area available for sulfur capture.

The conditions for calcination prior to mercury porosimetry are given in Table 3.4.1. The standardized laboratory method for determining porosity, pore size distribution, surface area, and density is as follows: Sorbent samples are ground to -18 +20 mesh size and are measured on the porosimeter either as raw material or after calcination in a simulated flue gas with no SO_2 present. The gas for calcination contains 5% O_2, 20% CO_2, and the balance N_2. Samples are calcined at 850°C for 60 min. These conditions are summarized in Table 3.4.1. Following calcination, the sample is quickly introduced into the porosimeter to avoid pickup of water or CO_2 by the lime. Data is directly recorded as a plot of cumulative pore volume versus pore diameter. A pore size distribution graph for each sorbent is included in Sections 5 and 6, LIMESTONES and DOLOMITES, respectively, of this book.

Table 3.4.1. Standardized Conditions for Calcination Prior to Mercury Porosimetry

Step	Sample		Reaction Chamber		Gas Composition, by Volume					Total Gas Flowrate, liter/min	Duration of Expt., h
	Mass, g	Size, µm	Temp., °C	Pressure, atm	CO_2, %	SO_2, %	O_2, %	N_2, %	H_2O, %		
Calcination	0.5	1000-841 (-18 +20 mesh)	850	1	20	0	5	0	bal.	1	1.0

Total Porosity. The total porosity is read directly from the graph of data as the total cumulative volume.

Surface Area. Surface area may be calculated from the data, using a pore model of a right circular frustrum whose area is given by

$$S_{ij} = \sum \pi (r_i + r_j) \sqrt{h^2 + (r_i - r_j)^2} \qquad 1$$

and whose volume by

$$V = \sum \frac{\pi h}{3} (r_i^2 + r_i r_j + r^2) \qquad 2$$

where h is the length of the pore, and r_i and r_j are the radii of the two circular ends of the pore. In terms of the actual volume and pressure measurements, the surface area of the calcined material is given by

$$S = \sum \pi (r_i + r_j) \sqrt{\left[\frac{3(V_j - V_i)}{\pi (r_i^2 + r_i r_j + r_j^2)}\right]^2 + (r_i - r_j)^2} \qquad 3$$

where $(V_j - V_i)$ is the incremental volume measurement as recorded on the porosimeter, $r_i = \frac{0.0087}{P_i}$, P_i is the measured pressure corresponding to V_i, and $j = i + 1$.

Pore Size Distribution. The pore size distribution is shown directly by the graph of the data. Further, from the calculated surface area and the measured volume, an average pore diameter can be calculated as a single numerical designation of the pore size distribution for a given sample.

Density. The density of the material is also calculated from the mercury volume displacement measurements on the mercury porosimeter, combined with weights of sample, mercury, and container. Standard pycnometer formulas are utilized.

References for Section 3.4

R. H. Borgwardt, Environ. Sci. Tech. 4, 59 (1970).

R. H. Boregwardt and R. D. Harvey, Environ. Sci. Tech. 6, 350 (1972).

J. A. Shearer, I. Johnson, and C. B. Turner, ANL/CEN/FE-78-8 (1978).

3.5 DECREPITATION TEST

The attrition of a sorbent due to thermal stress is a physical property that must be assessed before a sorbent can be used in the fluidized-bed combustor (FBC). Fine particles capable of escaping from the FBC are produced, in part, by the build up of internal pressure due to water vapor expansion as a result of an increase in termperature. As a sorbent breaks down into finer particles upon heating (decrepitates), the finer particles are carried out of the combustor by the fluidizing air. This ultimately leads to an increase in the limestone feed rate which in turn increases operational and maintenance costs. The ideal sorbent should show minimal thermal decrepitation in order to alleviate these problems.

The laboratory test procedures to measure the decrepitation characteristics of a sorbent and the total amount of water released from the sorbent material during heating are as follows:

Decrepitation Test - A sample of each sorbent of about 20 g of -18 +20 mesh (-1000 +841 μm) limestone is placed in a combustion boat (38.1 mm x 50.8 mm) and covered with a 30-mesh platinum wire gauge. This apparatus is placed in a furnace at room temperature with a 20% CO_2 balance N_2 gas mixture flowing through the furnace. The furnace temperature is then raised slowly to 850°C at intervals of 200, 300, 400, 600, 750 and 850°C. After the furnace has reached each interval, the temperature is maintained for about 30 minutes. The sorbent material is then removed, sieved in three sieve sizes, -18 +20 (1000 -841 μm), -20 +30 (841-595 μm), and less than 30 mesh (595 μm), and returned to the furnace. The percentage decrepitation of sorbent material is calculated from the quantity of fines produced at each temperature interval.

Water Analysis Test - A thermogravimetric analyzer (TGA) was used to determine the total amount of water released from the sorbent materials. Measurements were made using samples of particles in the size range -18 +20 mesh (-1000 +841 μm diameter). A sample of each sorbent was placed in the reactor tube of the TGA at room temperature. A 20% CO_2, balance N_2 gas mixture was passed through the reactor tube during the duration of the experimental test. The reactor tube temperature was then raised slowly to 850°C using a platinum wound furnace. The weight loss (the removal of water from the sample and the evolution of CO_2 as a result of calcination) was determined by continuous measurement of the sample weight using a recording balance. At the conclusion of the experimental test, the sample was removed, weighed and the total amount of water released from the sorbent sample was determined as follows. From the known calcium carbonate and magnesium carbonate content of each stone and the weight change, the quantity of CO_2 driven off during calcination (i.e., stone in which $CaCO_3$ and $MgCO_3$ has been converted to CaO and MgO) is calculated. The difference between the calculated weight loss and the observed weight loss is taken as the total amount of water released from the sorbent sample.

4.0 SUMMARY OF TEST RESULTS

Proper analysis of thermogravimetric analyzer (TGA) and attrition test data significantly enhances the utility of laboratory tests in the prediction of fluidized-bed combustor performance. The analysis of the TGA and attrition test data is detailed in this section. The test results are summarized to show wide ranges of behavior of the sorbents with regard to their sulfation and attrition behavior. The effects of such variables as particle size and SO_2 partial pressure on sulfation are also presented.

4.1 ANALYSIS OF TGA DATA

The reactivity of a sorbent to sulfur dioxide as a function of time is monitored with a thermogravimetric analyzer. The TGA sample gains weight during the experiment due to the pickup of SO_2 to form $CaSO_4$. The observed weight gains are converted, using the sample weight and chemical composition, into the fractions of the total original calcium that reacted to yield calcium utilizations (sulfations). The calcium utilization data, $\alpha(t)$, are least squares curve fitted by the following empirical equation:

$$\alpha(t) = a - ae^{-kt^n} = a(1 - e^{-kt^n}) \qquad 1$$

where t is time and a, k, and n are fitting constants. The constant a equals the maximum utilization a sorbent can achieve in infinite time under the standard test conditions. A typical plot is shown in Fig. 4.1.1; the two solid curves show the same utilizations over durations of 100 and 300 minutes. The appropriatiness of the use of Eq. 1 to represent the utilization is clearly indicated by the smoothness of the fit of the experimental values in Fig. 1 especially over the sensitive early periods of the test. The rate of calcium utilization is obtained by differentiating Eq. 1:

$$\frac{d\alpha(t)}{dt} = nake^{-kt^n} t^{n-1} = nk[a - \alpha(t)]t^{n-1} \qquad 2$$

If n is equal one, the rate of calcium utilization decreases linearly as the extent of calcium utilization, $\alpha(t)$, increases; for values of n less than one, the rate will also decrease as the calcium utilization increases, but not linearly. For sorbents recently studied, the average value of n was 0.75 with a range from 0.6 to 1.1. The dashed curve in Fig. 4.1.1 represents the utilization reaction rate (percent utilization/minute) as a function of the extent of calcium utilization (percent) as defined by Eq. 1.

It is highly desirable to define the constants a, k, and n in terms of the experimental conditions associated with the standard TGA test that strongly affect the calcium utilization and, therefore, the rate of utilization. Two such conditions are the sulfur dioxide concentration and the sorbent particle size. Over the range of sulfur dioxide concentrations of interest, the sulfur capture reaction, is first order in SO_2. This conclusion was reached after observing, for two different sorbents, the linear relationship between the sulfation reaction rate (% utilization/ minute) and the sulfur dioxide concentration in the TGA gas stream (ppm), as illustrated in Figs. 4.1.2 and 4.1.3. For a given sorbent, the reaction was measured for each SO_2 pressure at the same fractional utilization of sorbent. This fractional utilization was chosen to give a reaction rate which falls within the range of reactivity required for effective sulfur capture in a fluidized-bed combustor. The first order dependence is constant with previously published results [Borgwardt (1970), Borgwardt and Harvey (1972), Yang et al. (1979), and James and Hughes (1976)].

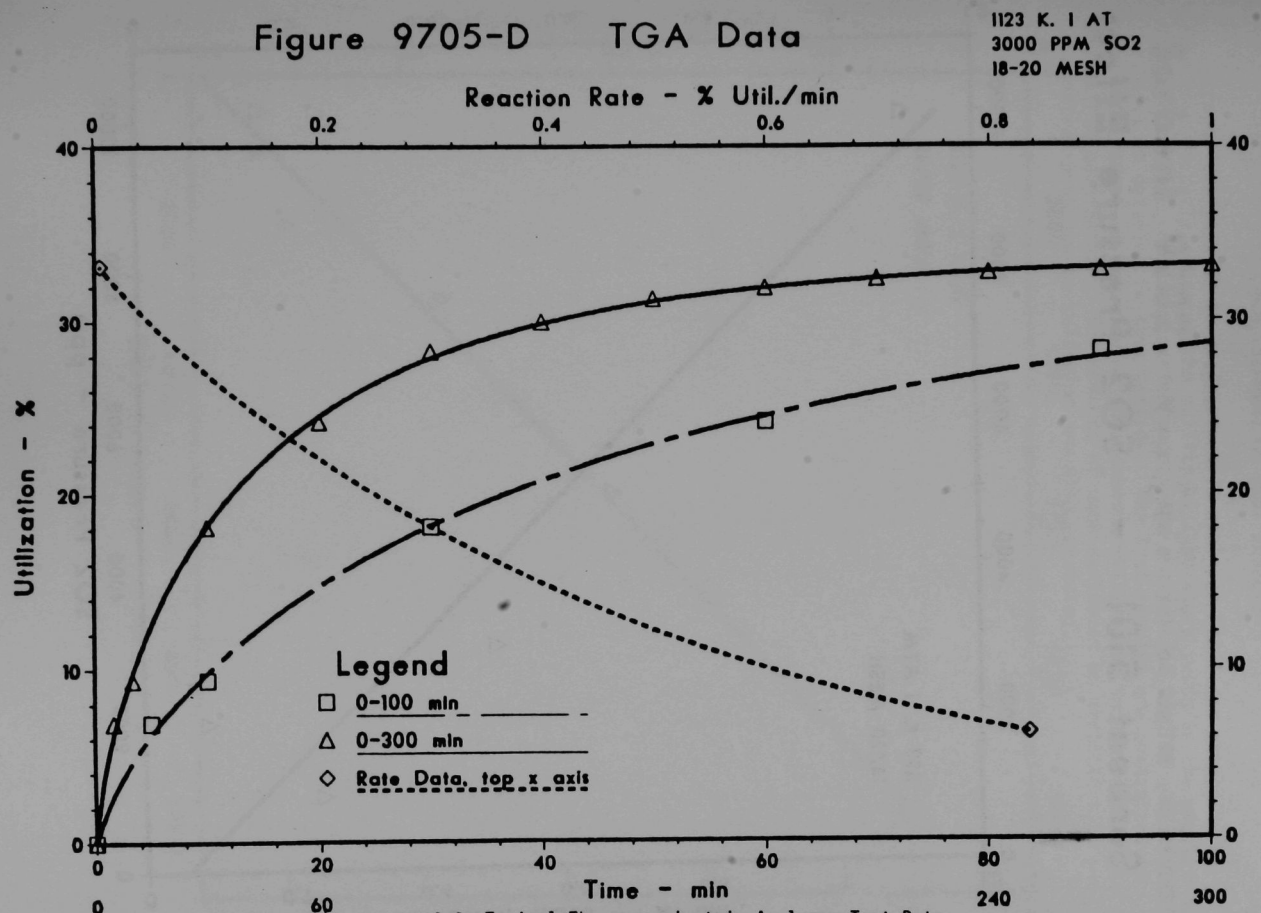

Fig. 4.1.1 Typical Thermogravimetric Analyzer Test Data

Fig. 4.1.2

Sorbent 5101 - SO2 Pressure Effect

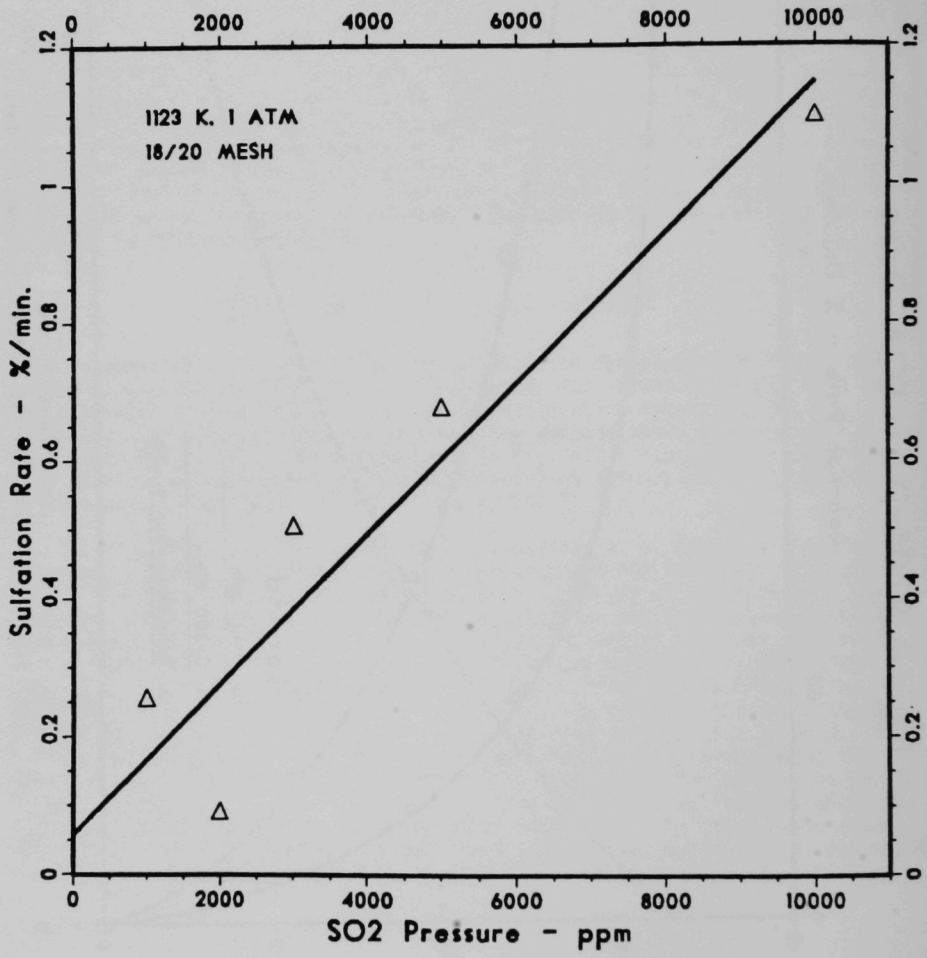

Fig. 4.1.3

Sorbent 9202 - SO2 Pressure Effect

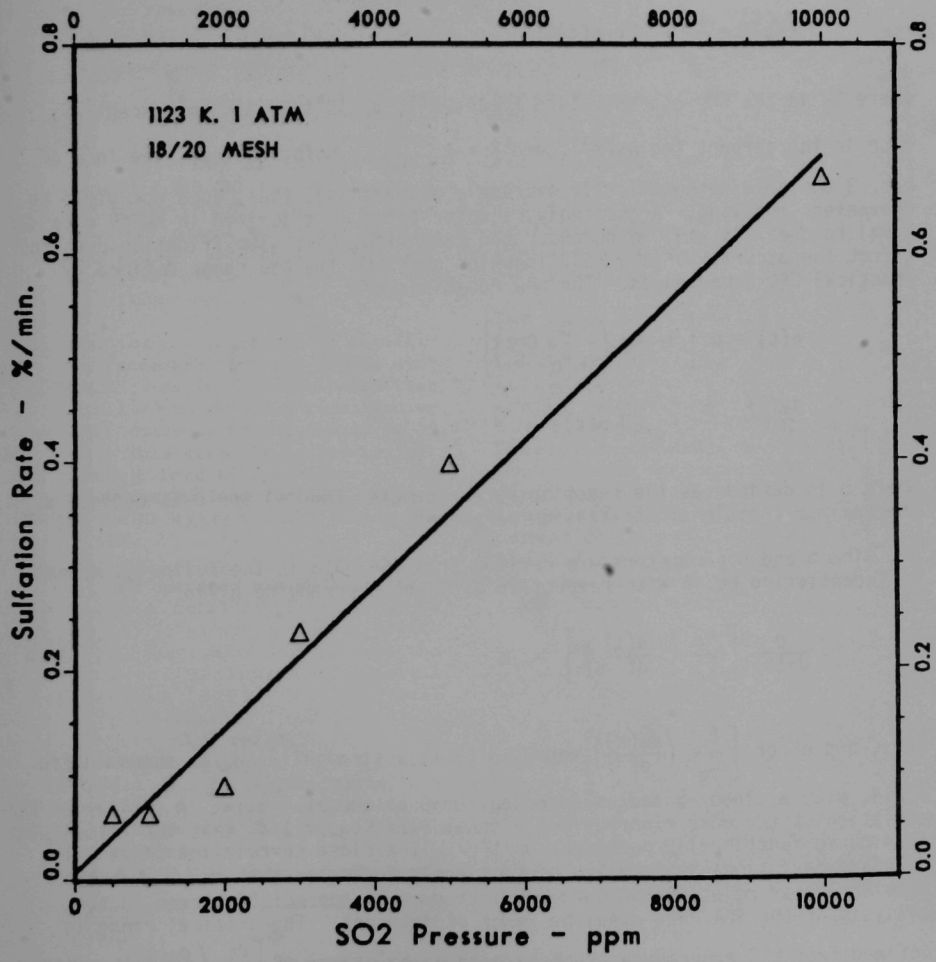

Reformulations of Eqs. 1 and 2 that reflect the first order sulfur dioxide concentration dependence are, respectively, as follows:

$$\alpha(t) = a \left[1-\exp\left(- \frac{K}{\rho_c} C_g t^n \right) \right] \qquad 3$$

and

$$\frac{d\alpha(t)}{dt} = \frac{K}{\rho_c} C_g \, [a-\alpha(t)] t^{n-1} \qquad 4$$

where C_g is the SO_2 concentration (moles/m^3), ρ_c is the calcium concentration in the sorbent (moles/m^3), and $K = k \frac{\rho_c}{C_g}$. Unfortunately, the form of Eqs. 3 and 4 is mathematically extremely awkward and, thus, does not yield to convenient modeling. Accordingly, simpler forms were derived in which n is set equal to one. As will be demonstrated forthwith, this simplification does not affect the accuracy of the relationships over the limited range defined by practical FBC experiences. The new equations are:

$$\alpha(t) = D \left[1-\exp\left(- \frac{b}{\rho_c} C_g t \right) \right] \qquad 5$$

$$\frac{d\alpha(t)}{dt} = \frac{b}{p_c} C_g \, [D-\alpha(t)] \qquad 6$$

where b is defined as the reaction rate parameter (sec^{-1}) and D is defined as the maximum fractional utilization parameter.

The b and D parameters are derived from TGA data in the following manner. Differentiating Eq. 6 with respect to $\alpha(t)$ and rearranging gives

$$\frac{d}{d\alpha(t)} \left[\frac{\rho_c}{C_g} \left(\frac{d\alpha(t)}{dt} \right) \right] = -b \qquad 7$$

Thus, a plot of $\left[\frac{\rho_c}{C_g} \left(\frac{d\alpha(t)}{dt} \right) \right]$ versus $\alpha(t)$ is a straight line, as shown in Fig. 4.2.4, with a slope -b and on intercept of D on the $\alpha(t)$ axis. A similar differentiation of the more rigorous Eq. 4 shows (see Fig. 4.1.4) that the actual plot is a curve functionally dependent on t^{n-1}. The close correlation (± 3% = 1 standard deviation) between two plots clearly indicates that the use of the simpler linear relationship does not introduce an appreciable error to the analysis of the TGA data over the range of interest. The critical range is defined from FBC experience as corresponding to values of $\left[\frac{\rho_c}{C_g} \left(\frac{d\alpha(t)}{dt} \right) \right]$ ranging from approximately 10 to 50 sec^{-1}.

Fig. 4.1.4

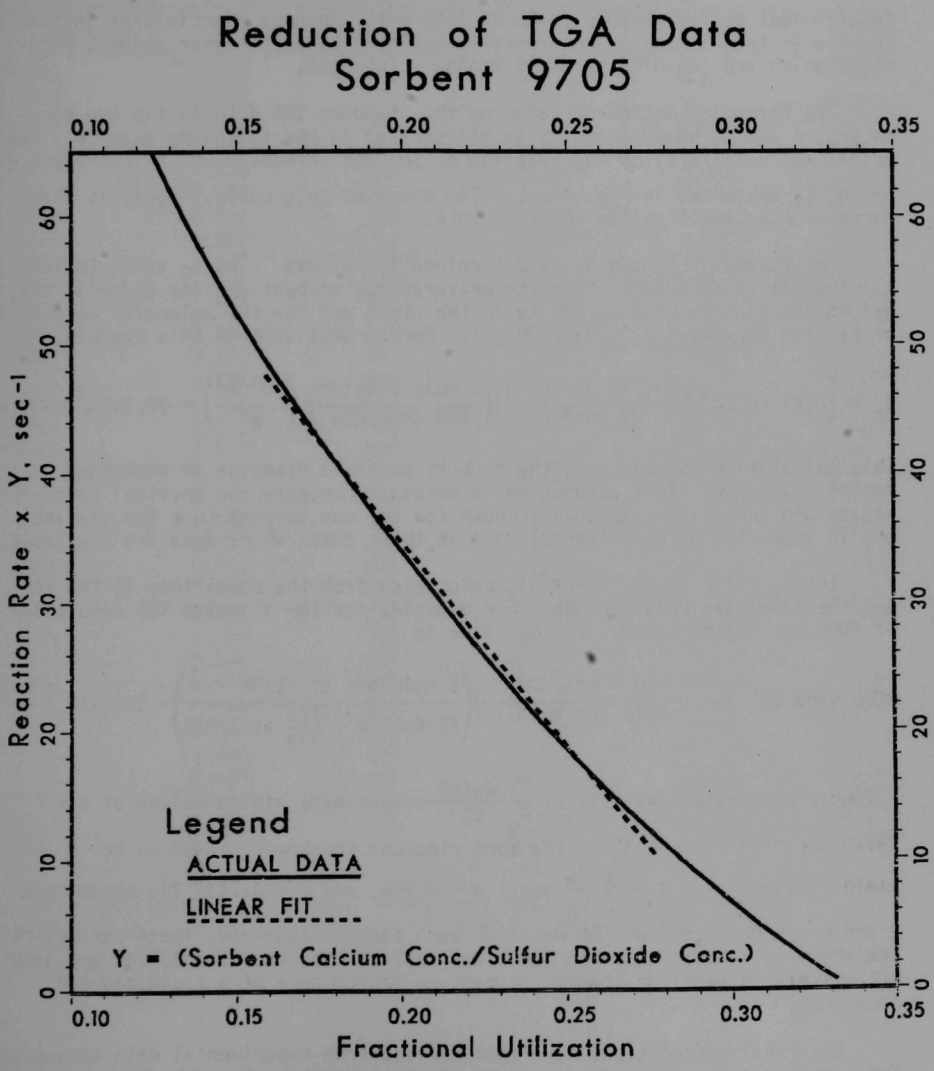
Reduction of TGA Data
Sorbent 9705
0.10
0.15
0.20
0.25
0.30
0.35
Reaction Rate x Y, sec-1
0
10
20
30
40
50
60
Legend
ACTUAL DATA
LINEAR FIT
Y = (Sorbent Calcium Conc./Sulfur Dioxide Conc.)
Fractional Utilization

With a ratio of bed height (H, m) to fluidizing velocity (u, m/sec) ranging from 0.3 to 1.25 in the AFBC, this sorbent reactivity range will result in achieving the mandatory new source performance standards of 90% sulfur capture. Lower sorbent reactivity $\left[\frac{\rho_c}{C_g}\left(\frac{d\alpha(t)}{dt}\right)\right]$ values than 10 sec^{-1} result in insuf-insufficient sulfur capture to be of interest. Sorbent reactivities in the bed higher than 50 sec^{-1} are generally achieved by only higher sorbent feed rates which are too high to be of economic interest.

The foregoing method of reducing the standard TGA data to the two parameters, D and b, based on Eq. 5 is illustrated in the following example. The actual TGA data, $\alpha(t)$ on the reaction of SO_2 and Sorbent 9705 (as represented by Eq. 1) are shown in Fig. 4.1.1. The slope of this curve, $\frac{d\alpha(t)}{dt}$, is also shown in Fig. 4.1.1 as the reaction rate.

The values of ρ_c and C_g is determined as follows. The ρ_c value (moles calcium/m^3) is calculated from the measured raw sorbent density (g/cm^3), the weight fraction calcium carbonate in the stone and the the molecular weights of calcium (40 gm) and $CaCO_3$ (100 gm). For Sorbent 9705 in this example,

$$\rho_c = \left[2.29\ (g/cm^3)\right]\left(\frac{0.973\ gm\ CaCO_3}{gm\ sorbent}\right)\left(\frac{1\ mole\ calcium}{100\ gm\ CaCO_3}\right)\left(\frac{10^6 cm^3}{m^3}\right) = 22.3x10^3\ mole/m^3$$

This calculation assumes that the sorbent particle diameter is unchanged during calcining. This assumption is necessary because the chemical composition and density are generally known for the raw sorbent (not the calcine) and is supported by experimental data in those cases where data are available.

The C_g value (moles SO_2/m^3 is calculated from the conditions in the TGA and the ideal gas relationship. For example, for the standard TGA conditions of 3000 ppm SO_2 by volume, the C_g value is

$$3000\ vppm\ SO^2 = \left(\frac{3000x10^{-6}\ mole\ SO_2}{1\ mole\ gas\ total}\right)\left(\frac{1\ mole\ gas\ at\ 1123K}{22.4x10^3 m^3\ \frac{1123}{273}\ at\ 1123K}\right) = 3.25x10^{-2}\ \frac{moles\ SO_2}{m^3}$$

A linear regression analysis of $\frac{\rho_c}{C_g}\frac{d\alpha(t)}{dt}$ versus $\alpha(t)$ yields values of b = 267.9 sec^{-1} and D = 0.309. The more rigorous treatment, based on Eq. 3 yields value of K = 0.0621 $\frac{\rho_c}{C_g}$ sec^{-1} a = 0.336, and n = 0.74. The parameters D and b are derived from TGA data for each sorbent examined. These parameters are shown in Tables 4.1.1 and 4.1.2 and in Test Results, item 8, and are used extensively in modeling the sulfur capture performance of a fluidized-bed combustor.

Empirical correlations have been derived from experimental data to express the particle size dependence in terms of the parameters D and b. The correlation of the particle size effect on parameter b is shown in Eq. 8 and Figs. 4.1.5 and 4.1.6. The correlation of the particle size effect on the parameter D is shown in Eq. 9 and Figs. 4.1.7 and 4.1.8.

Table 4.1.1 Summary of TGA Data

1123K, 1 Atm, 3000 ppm SO_2, 18/20 Mesh

Sorbent	D	b	A	k	n
9903	0.214	431	0.238	0.0858	0.713
9806	0.614	277	0.603	0.040	0.844
9804	0.272	401	0.287	0.066	0.786
9801	0.288	320	0.307	0.0588	0.777
9709	0.318	338	0.325	0.0888	0.6392
9708	0.245	542	0.250	0.170	0.542
9705	0.309	268	0.336	0.0621	0.744
9701	0.0607	1266	0.0874	0.207	0.520
9601	0.222	377	0.247	0.0702	0.744
9504	0.366	266	0.382	0.0484	0.818
9501	0.130	945	0.158	0.274	0.495
9402	0.128	594	0.164	0.108	0.637
9202	0.277	415	0.289	0.066	0.808
9201	0.148	484	0.183	0.0709	0.723
9101	0.166	583	0.192	0.145	0.632
8901	0.271	379	0.267	0.0225	1.085
8701	0.272	405	0.274	0.0426	0.967
8201	0.226	466	0.258	0.143	0.614
8101	0.461	213	0.506	0.0652	0.704
8001	0.182	560	0.193	0.0900	0.808
7901	0.278	399	0.290	0.0772	0.803
7402	0.201	548	0.199	0.0495	1.036
7301	0.254	357	0.286	0.108	0.672
6701	0.481	212	0.501	0.0479	0.829
6401	0.196	356	0.262	0.0853	0.646
6101	0.684	137	0.689	0.0205	0.967
5901	0.411	246	0.459	0.116	0.639
5601	0.0745	747	0.149	0.091	0.594
5501	0.164	421	0.209	0.100	0.676
5301	0.586	135	0.630	0.0355	0.825
5101	0.899	115	0.950	0.0422	0.782
5001	0.669	113	0.807	0.0504	0.668
4801	0.904	186	0.894	0.0152	1.130
4601	0.767	110	0.838	0.0557	0.665

$\alpha(t)$ = utilization = $A(1 - \exp(-kt^n))$ over entire reactivity range.
$\alpha(t) = D\,(1 - \exp(-bt))$ over the reactivity range of interest to fluidized-bed combustion.

Table 4.1.2 Summary of TGA Data at 1123K, 1 Atm

Sorbent	Mesh	SO_2, ppm	D	b	A	k	n
9701	50/70	3,000	0.358	426	0.369	0.0798	0.7741
	140/170	3,000	0.555	176	0.595	0.0346	0.770
9202	14/16	3,000	0.172	671	0.198	0.179	0.590
	10/16	3,000	0.135	675	0.195	0.179	0.467
	6/8	3,000	0.110	817	0.231	0.165	0.359
	50/70	3,000	0.344	308	0.456	0.155	0.456
	140/170	3,000	0.374	291	0.470	0.144	0.488
	<10 micron	3,000	0.922	150	0.970	0.052	0.704
8001	50/70	3,000	0.571	258	0.578	0.0286	0.951
	140/170	3,000	0.700	192	0.715	0.0332	0.858
7301	12/14	3,000	0.180	403	0.226	0.092	0.663
	50/70	3,000	0.508	169	0.581	0.0678	0.508
	140/170	3,000	0.642	122	0.642	0.0392	0.730
6401	12/14	3,000	0.090	732	0.152	0.1185	0.583
	50/70	3,000	0.391	165	0.744	0.0510	0.535
	140/170	3,000	0.721	113	0.721	0.0418	0.684
5301	50/70	3,000	0.668	116	0.819	0.0573	0.646
	140/170	3,000	0.740	114	0.740	0.0574	0.625
5101	50/70	3,000	0.944	135	0.966	0.0357	0.862
	140/170	3,000	0.989	117	0.995	0.0194	0.965
	18/20	10,000	0.835	99	0.980	0.128	0.645
	18/20	5,000	0.892	96	0.940	0.0409	0.843
	18/20	2,000	0.648	95	0.868	0.0296	0.667
	18/20	1,000	0.861	197	0.857	0.0070	1.049
	18/20	500	0.723	101	1.015	0.0054	0.791

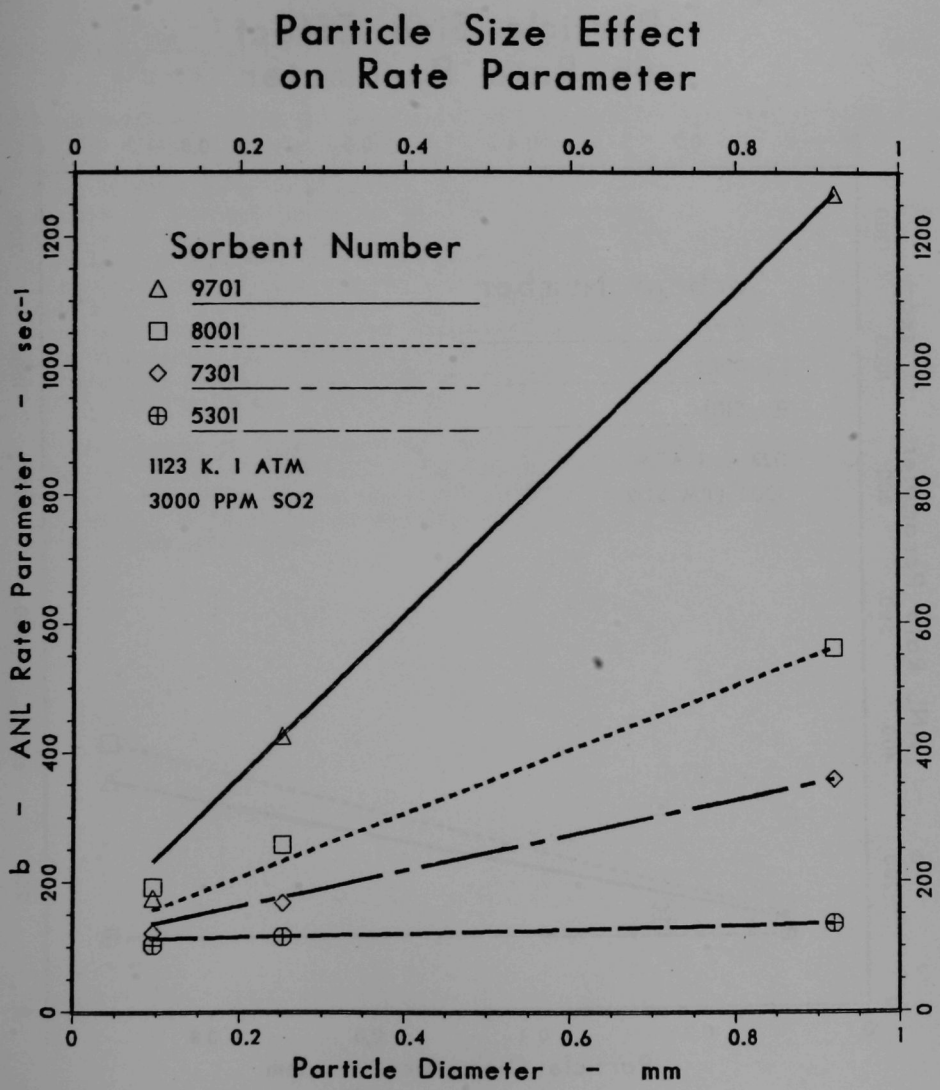
Particle Size Effect
on Rate Parameter
Sorbent Number
9701
8001
7301
5301
1123 K. 1 ATM
3000 PPM SO2
b - ANL Rate Parameter - sec-1
Particle Diameter - mm
0
0.2
0.4
0.6
0.8
1
200
400
600
800
1000
1200

Fig. 4.1.5

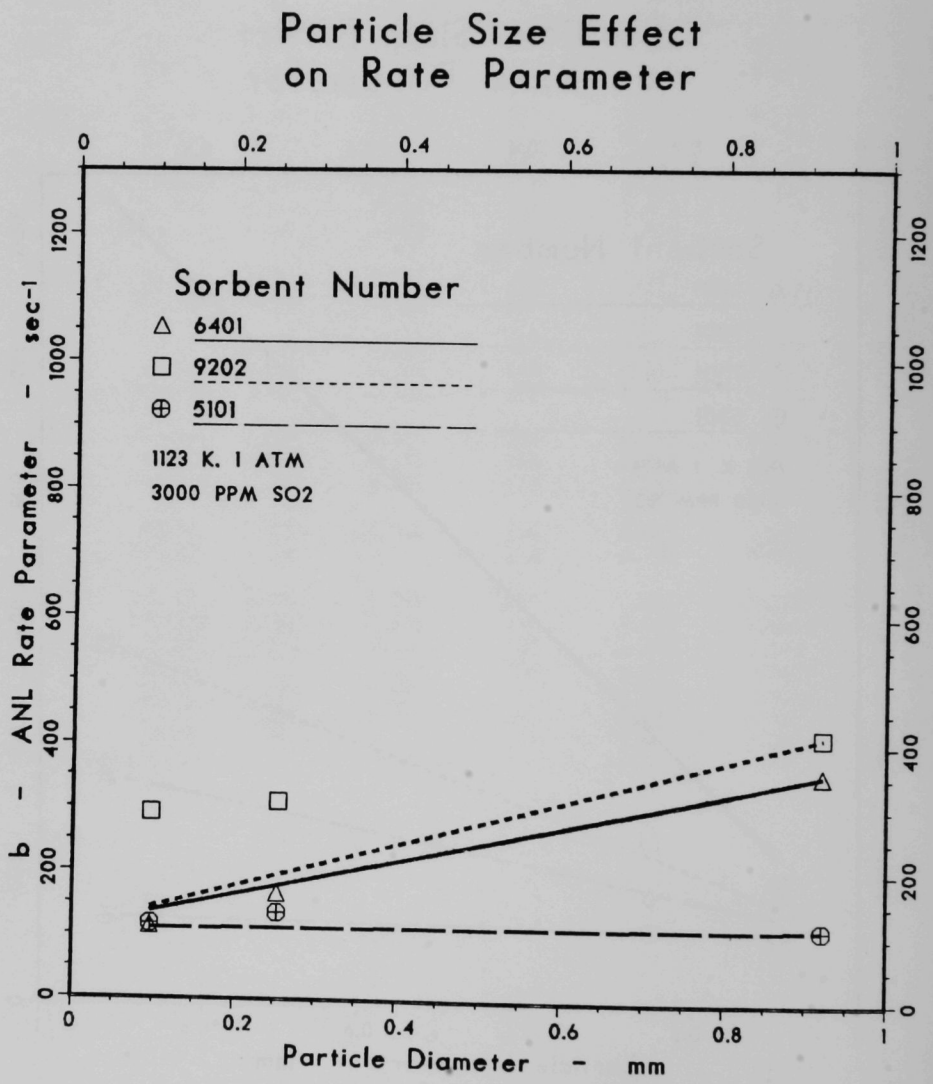
Particle Size Effect
on Rate Parameter
Sorbent Number
6401
9202
5101
1123 K. 1 ATM
3000 PPM SO2
b - ANL Rate Parameter - sec-1
Particle Diameter - mm
0
0.2
0.4
0.6
0.8
1
200
400
600
800
1000
1200

Fig. 4.1.6

$$b = \left[\frac{b_{std} - 110}{d_{p,std}}\right] d_p + 110 \qquad 8$$

$$D = \left[\frac{D_{std} - 1}{d_{p,std}^{1/3}}\right] (d_p)^{1/3} + 1 \qquad 9$$

The correlations allows the results for the standard TGA test that utilizes a particle diameter, $d_{p,std}$, of 920 μm on the average and the corresponding D and b values, D_{std} and b_{std} respectively, to be used to predict d and b values at other particle diameters, d_p. Thus, the maximum utilization of the particle, D, increases while the reaction rate parameter, b, generally decreases slightly as the particle size decreases. However, since the change in D with particle size dominates in the rate expression, Eq. 6, the rate of sulfation increases as the particle size decreases. Smaller sorbent particles react more rapidly and to a greater extent, i.e., achieve higher calcium utilizations than larger particles. The trends of increasing maximum sulfation parameter and decreasing reaction rate parameter with decreasing particle size are consistent with previous results in the literature [Borgwardt (1970), Borgwardt and Harvey (1972), Hartman (1976), O'Neill et al. (1979)].

Data exists at larger particle sizes (>920 μm diameter) for only a few stones as listed in Table 4.1.2. The numbers indicate that for very large particles the effect on rate and sulfation parameters begins to level off, such that maximum sulfation values do not go to zero as indicated by the small particle size correlation.

Particle Size Effect on Maximum Sulfation

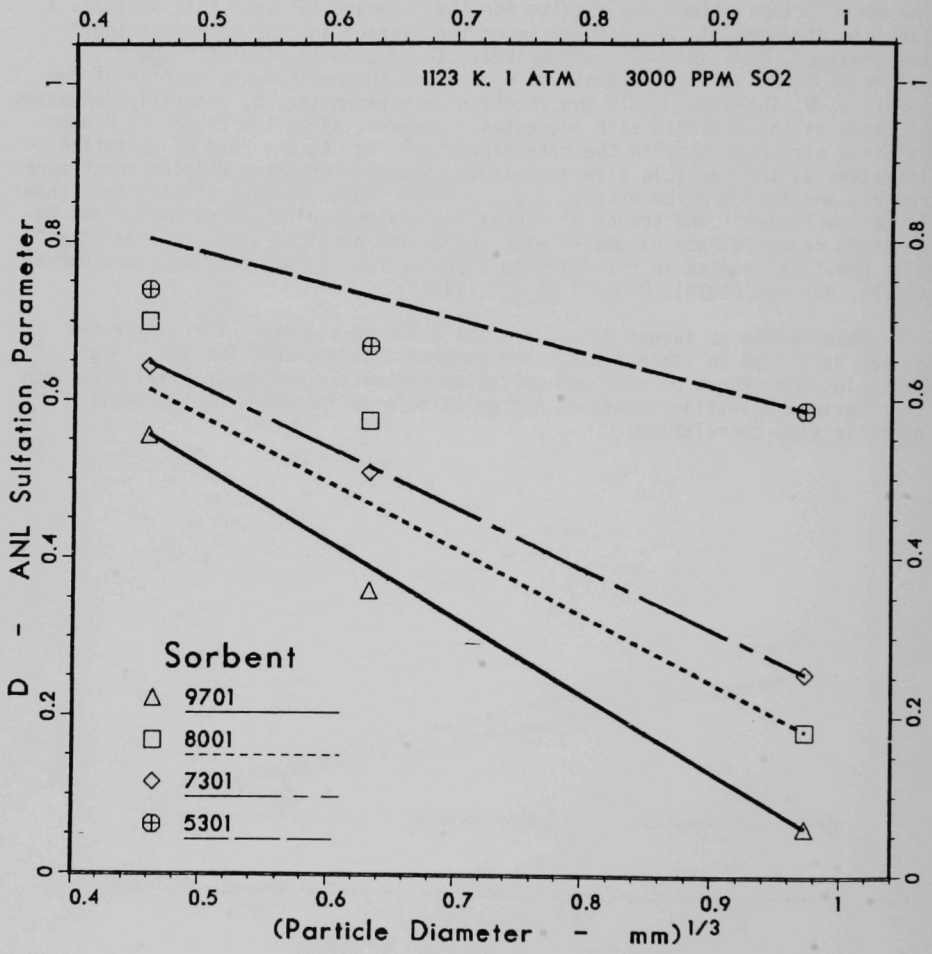

4.1.7

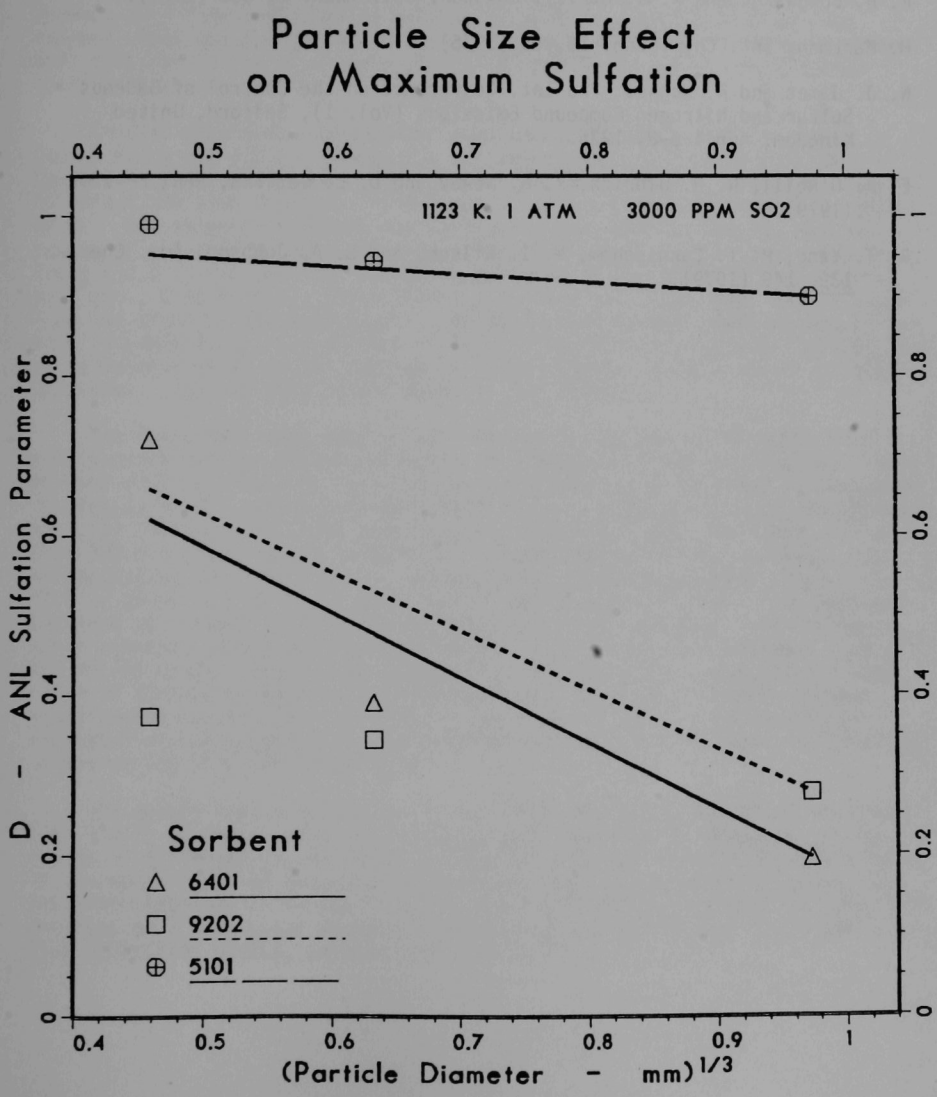
Particle Size Effect
on Maximum Sulfation
1123 K. 1 ATM 3000 PPM SO2
D - ANL Sulfation Parameter
(Particle Diameter - mm)^1/3
Sorbent
6401
9202
5101
0.4
0.5
0.6
0.7
0.8
0.9
1
0
0.2
0.4
0.6
0.8
1

Fig. 4.1.8

References for Section 4.1

R. H. Borgwardt, Environ. Sci. Tech. 4, 59 (1970).

R. H. Borgwardt and R. D. Harvey, Environ. Sci. Tech. 6, 350 (1972).

M. Hartman, Int. Chem. Eng. 16, 86 (1976).

N. J. James and R. Hughes, 2nd Int. Conference on the Control of Gaseous Sulfur and Nitrogen Compound Emissions (Vol. 1), Salford, United Kingdom, April 6-8, 1976.

E. P. O'Neill, N. H. Ulerich, R. A. Newby and D. L. Keairns, EPRI FP-1307 (1979).

R. T. Yang, P. T. Cunningham, W. I. Wilson, and S. A. Johnson, Adv. Chem. 139, 149 (1979).

4.2 ANALYSIS OF ATTRITION DATA

In fluidized-bed combustion, the fine particles may come directly from the feed or be generated in the bed by attrition [Wilson, et al. (1981)]. Attrition in a fluidized bed occurs by abrasion of the coarse particles to produce very fine particles as well as by sorbent fracture arising from thermal shock and decrepitation during calcination. Both of these phenomena were measured in the laboratory attrition test described in the STANDARD TESTS section.

Typical data from the standard laboratory attrition test are shown in Tables 4.2.1 and 4.2.2. These data are the measured weight of material in the initial bed, final bed, and overhead (cyclone catch) at different time intervals and size fraction. The chemical analysis of the material is also given. One chemical analysis was routinely performed on a representative sample of all the overhead material. So the chemical composition given in Table 4.2.1 is the same for the overhead material collected in the interval 0 to 5 min., 5 to 10 min., 10 to 15 min., 30 min. to 1 hour, etc. (times given from the start of the experiment). Using the weight and chemical composition data in Table 4.2.1, the percent of the calcium that was carried overhead can be calculated based on the calcium initially loaded into the attrition test apparatus. Typical results are shown in Fig. 4.2.1.

The fractional mass loss of the calcium in the bed in the early part of the standard test is due to breakup of the sorbent during calcination. (This breakup results primarily from sorbent decrepitation on heating, as discussed separately at the end of this section.) This calcination loss is determined by: (1) fitting a straight line to the experimental data for times greater than 100 min (times where abrasion is the dominant attrition process), (2) extrapolating the linear fit to the beginning of the experiment (time = 0). This is shown in Fig. 4.2.1 where 18% of the initial calcium in the bed goes overhead as a result of breakup due to calcination. Similar data for the other sorbents tested are shown in Table 4.2.3. The fractional mass loss of the stones tested ranged from 0.0092 to 0.62 (0.9 to 62%) indicating a wide range of sorbent breakup during calcination. The breakup affects sorbent requirements because this fraction of the sorbent fed to a fluidized-bed combustor may be immediately entrained and carried from the bed, limiting the amount of SO_2 that can be captured.

The weight loss from the bed in the flat portion of the attrition curve, Fig. 4.2.1, is due to abrasion. The abrasion behavior is dependent on the degree of sulfation of the sorbent. The calcium sulfate product, which forms in the outer layer of the sorbent particle, gives the sulfated particle an attrition behavior different from that of the unreacted calcine. The attrition constant of a particular sorbent is determined using the attrition model (see PREDICTION MODELS, Section 7 of this book).

Table 4.2.1 Typical Attrition Data (Standard Eight-Hour Test)

	Grams Total	wt%	
		Ca	S
Initial Bed	160.733	38.60	0.0
Final Bed[a]	88.009	58.0	7.10
Total Overhead[a]	24.684	47.2	1.98
Overhead, 5 min	9.158	47.2	1.98
10 min	7.226	47.2	1.98
15 min	2.217	47.2	1.98
30 min	3.163	47.2	1.98
1 h	1.014	47.2	1.98
1.5 h	0.302	47.2	1.98
2 h	0.652	47.2	1.98
4 h	0.503	47.2	1.98
6 h	0.251	47.2	1.98
8 h	0.198	47.2	1.98

[a]Includes weight loss due to calcination and weight gain due to sulfation.

Table 4.2.2. Typical Attrition Data Weights of Size Fractions

Weight in Grams, Particle Diameter in μm

Sample	-1000 +840	-841 +707	-707 +595	-595 +420	-420 +297	-297 +250
Overhead, first 30 min	0.000	0.0034	0.0046	0.0043	0.0516	0.1717
Overhead, remaining 7.5 h	0.0009	0.0005	0.0013	0.0038	0.182	0.512
Final Bed, post test	50.56	11.55	6.38	7.26	7.11	2.42

Sample	-250 +210	-210 +74	-74 +63	-63 +53	-53 +44	-44 +37	-37 +0
Overhead, first 30 min	1.016	12.75.	0.048	0.564	1.377	0.516	1.504
Overhead, remaining 7.5 h	1.414	2.31	0.017	0.097	0.169	0.102	0.232
Final Bed, post test	1.97	0.529	0.0036	0.0133	0.0124	0.0031	0.0091

Table 4.2.3. Summary of Attrition Data

1123K, 1 Atm, Initially 10/20 Mesh, 3000 ppm SO_2

Sorbent	Attrition Constant, λ_4 Sec^{-1}	Bed Loss Due to Calcination Breakup, %
9903	1.4×10^{-7}	2.1
9806	-	-
9804	1.7×10^{-7}	1.7
9801	3.7×10^{-7}	13.0
9709	2.4×10^{-7}	22.8
9708	1.1×10^{-7}	20.7
9705	2.1×10^{-7}	2.5
9701	8.8×10^{-7}	0.6
9601	1.9×10^{-7}	18.0
9504	1.3×10^{-7}	0.5
9501	6.7×10^{-8}	0.5
9402	4.7×10^{-7}	5.5
9202	9.2×10^{-8}	0.2
9201	-	-
9101	2.9×10^{-8}	1.0
8901	1.9×10^{-7}	2.5
8701	-	-
8201	2.3×10^{-7}	1.0
8101	2.8×10^{-7}	44.4
8001	1.9×10^{-7}	0.8
7901	2.4×10^{-7}	2.2
7402	2.6×10^{-7}	3.9
7301	7.8×10^{-8}	0.6
6701	8.1×10^{-8}	0.6
6401	6.8×10^{-8}	0.3
6101	2.8×10^{-8}	1.1
5901	4.0×10^{-7}	0.6
5601	4.8×10^{-7}	5.9
5501	9.0×10^{-7}	3.9
5301	2.5×10^{-7}	10.0
5101	3.8×10^{-9}	0.7
5001	1.5×10^{-6}	61.6
4801	-	-
4601	1.6×10^{-7}	16.0

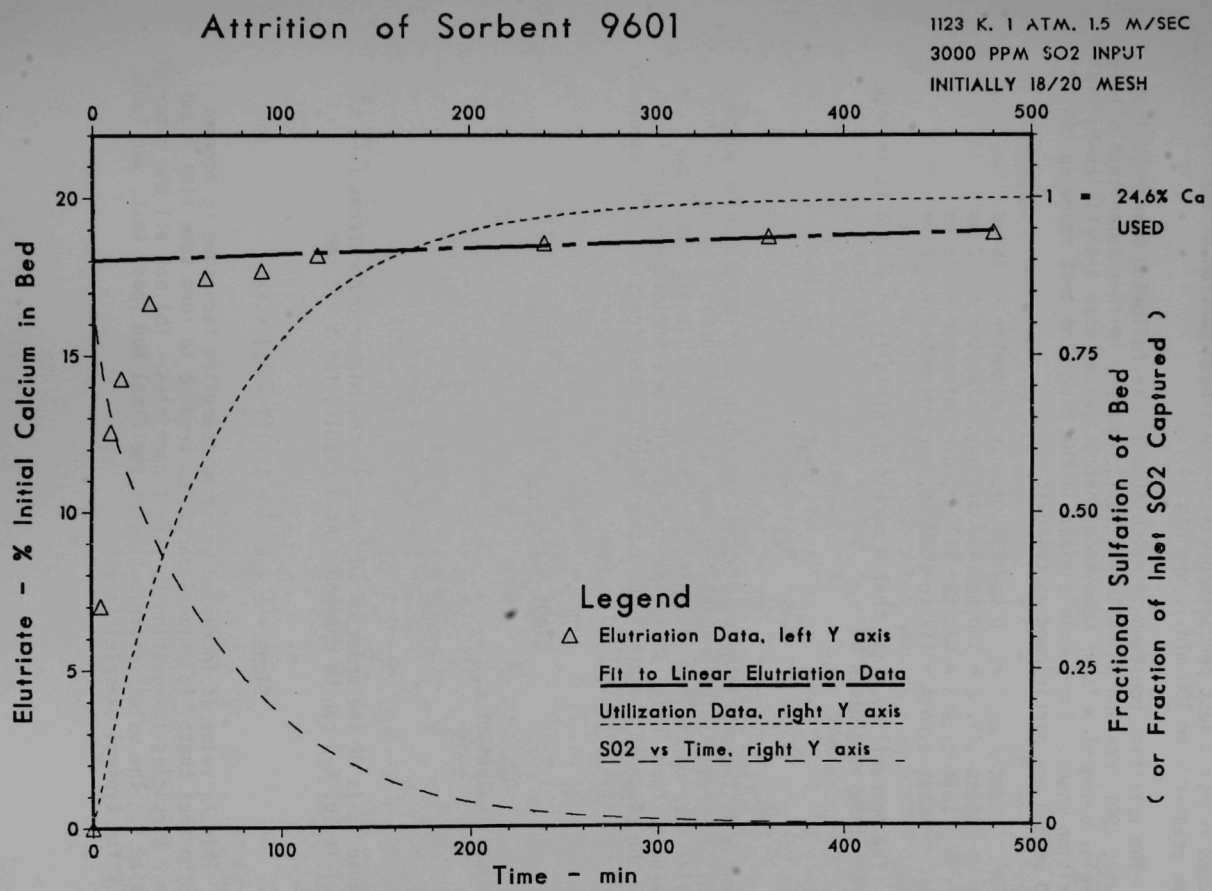

Fig. 4.2.1 Typical Attrition Data

The attrition rate constant was determined after the material loss from the bed had reached a steady state, i.e., the rate constant was calculated when the bed fraction lost per second was in the linear portion of the curve (i.e., times greater than 100 min.), see Fig. 4.2.1.

The attrition constant is calculated in the following manner [Wilson et al., 1981, Fan and Srivastava (1981)]. First, it is assumed that all the material being elutriated come from what is called size 4 particles in the attrition model. The particle sizes in the attrition test range up to 1000 μm and are partitioned as follows:

test size 1 = 0 to 150 μm, ave. diameter = 75 μm
test size 2 = 150 to 433 μm, ave. diameter = 292 μm
test size 3 = 433 to 717 μm, ave. diameter = 575 μm
test size 4 = 717 to 1000 μm, ave. diameter = 858 μm

The probability, P_{44}, that a particle initially in size 4 is in size 4 after time t is given by

$$P_{44} = e^{-\lambda_4 t} \qquad 1$$

where λ_4 is the characteristic attrition constant of a particular sorbent. Thus, $(1 - P_{44})$ is the probability that a size 4 particle breaks up into smaller size particles. Assuming for the moment that all size 4 particles breakup to form (only) size 1 particles which are immediately elutriated, then the slope of the attrition curve (Slope = bed fraction elutriated/sec) is $(1 - P_{44})$. Thus

$$\text{Slope} = 1 - P_{44} = 1 - e^{-\lambda_4 t} \qquad 2$$

For small values of x,

$$e^{-x} = 1 - x + \frac{x^2}{2} - \frac{x^3}{6} \qquad 3$$

Because λ_4 is of the order of 10^{-6} sec^{-1}, the higher order terms (x^2, x^3, etc.) in Eq. A-3 can be dropped. As a result, for t = 1 sec

$$\text{Slope} = 1 - e^{-\lambda_4} = 1 - (1 - \lambda_4) = \lambda_4 \qquad 4$$

This λ_4 value is increased using an iterative technique to account for the fact that: (a) size 4 particles breakup to form some size 3 and size 2 particles in addition to size 1 particles. (b) not all the material is size 4. The weight distribution of the final bed (post test, see Table 4.2.2 for typical example) is used.

The attrition constant of the stones tested ranged from 1.5×10^{-6} to 3.3×10^{-8} sec $^{-1}$ as shown in Table 4.2.3. So a wide range of behavior was also observed in the linear portion of the attrition test curve where abrasion predominates.

The calculated SO_2 concentration in the bed during the flat portion of the attrition curve was generally close to the inlet value of 3000 ppm. This is shown in Fig. 4.2.1 where the fraction of inlet SO_2 captured (right Y axis) is 0.1 or less for the flat portion of the curve.

The sorbent was generally sulfated at or near its maximum value during the flat portion of the curve. Fig. 4.3.1 shows a typical example of the calculated average calcium utilization in the sorbent bed versus time (right Y axis). The calculation was made using thermogravimetric analyzer (TGA) data. After 100 minutes, the average sulfation of the bed was greater than 80% of the maximum sulfation observed for sorbent 9601 during the TGA test.

The experimental maximum bed sulfation value from the attrition tests was only 75-85% of that determined from the TGA. The calcination conditions in the attrition test may be different from those employed in the TGA test. Any difference would produce a different pore structure in the calcined sorbent, and consequently, different capacity for SO_2 (i.e., a different maximum sulfation value). The small differences between the observed and calculated average sulfation values for the bed material at the end of the test do not affect the interpretation of the data. The attrition constant in each case was determined for partially sulfated material.

Sieve analyses were performed on all bed and overhead material to determine particle size reduction and distribution as a result of attrition. The mass fraction of bed material at the end of the test which retained its initial particle size ranged between 0.577 and 0.989 for the sorbents tested. Wet chemical analyses were performed on the final bed and overhead material to ascertain the mass fraction of calcium in the attrited sorbent at the end of each test. The results of the analysis were used to determine a complete mass balance of calcium in each test. The mass of calcium in the final material, bed and overhead, were combined and compared to the mass of calcium in the initial material. The mass of calcium in the final material, bed and overhead, of all stones tested was 94 ± 10 (one standard deviation) percent of the initial material.

Decrepitation. One of the major criteria by which natural sorbents are selected for use in a fluidized-bed combustor (FBC), is resistance to decrepitation. Decrepitation (Internal Attrition) may arise due to two effects, internal gas evolution and thermal shock. The two effects, both due to a sudden rise in temperature, occur when uncalcined sorbent is initially introduced into a combustor. One is evolution of gases (such as steam) from within the particles. If those gases have no easy way to escape through the pores, they will generate forces which may weaken the internal structure of the particles. Temperatures where decrepitation occurs for some sorbents have been found to be well below the calcination temperature. Laboratory tests to measure the decrepitation of sorbent materials and the total amount of water released from the sorbent during heating are described in STANDARD TESTS, Section.3.

Typical data from the standard laboratory decrepitation test are shown in Table 4.2.4. These data are the measured weight fraction of material at different temperature intervals for three size fractions, -1000 +841μm, -841 +595 μm, and -595 +0 μm. Using the weight fraction data in Table 4.2.4, the percent of fine produced as a result of decrepitation less than 595 μm can be plotted as a function of temperature. Typical results are shown in Fig. 4.2.2.

It is observed that the decrepitation process begins arount 600K and continues into the calcination temperatures near 1000K.

Data from the standard water determination test are shown in Table 4.2.5. These data are the measured weight loss as a result of water being released from the sorbent and the weight loss due to calcination (evolution of CO_2 from the dissociation of $CaCO_3$ and $MgCO_3$ to CaO and MgO) as a function of temperature. The numerical value obtained by getting the difference between the calculated weight loss and the observed weight loss is taken as the total amount of water released from the sorbent. Using the data in Table 4.2.5, the percent of water loss from the sorbent can be calculated based on the weight of the sorbent initially used in the experimental test. Typical results are shown in Fig. 4.2.4.

The decrepitation of sorbent materials may be due to the presence of water within the stone, and the releasing of the water during heating. The water may be chemically bonded as water of hydration or adsorbed water in isolated pockets of porosity. Release of this water by thermal decomposition of the hydrate or thermal desorption creates internal pressure which enhances the breakup of the sorbent particle. Experimental test methods were devised and performed to verify that water was indeed released from the sorbents during heating.

The sorbent material was placed in a quartz reaction tube that was inserted into a platinum-wound furnace. The temperature of the furnace was then raised slowly from room temperature to 600°C. A cold trap, cooled by a dry ice/methanol mixture, collected the water vapors released from the heated sorbent. The water that was released from the sorbent material was collected at temperature intervals of 373, 473, 573, 673, and 873K. The results showed that the largest

Table 4.2.4. Typical Decrepitation Data -8101

Temp. °C	Weight Percent of Size Fractions, Particle Diameter in µm -1000 +841	-841 +595	-595 +0
200	99.60	0.32	0.09
300	96.68	1.86	1.46
400	64.13	5.67	30.20
600	57.58	5.30	37.13
750	52.57	6.11	41.32
850	49.15	8.61	42.25

Table 4.2.5. Water Determination Data -8101

Initially 18/20 mesh
Initial Weight of Sorbent - 69.6 mg
Theoretical Weight Loss Due to Calcination 29.2 mg
Observed Weight Loss - 34.1 mg

Temp. °C	Observed Weight Loss, (mg)	Percent Weight Loss
20	0	0
30	0	0
70	0	0
110	0.2	0.29
200	0.7	1.01
250	1.1	1.58
295	1.7	2.44
340	1.9	2.73
395	5.3	7.61
440	6.0	8.62
480	6.0	8.62
525	6.1	8.76
570	6.2	8.91
610	6.3	9.05
655	12.3	17.67
730	17.8	17.25
850	34.1	48.99

Figure 8101-F Decrepitation Data

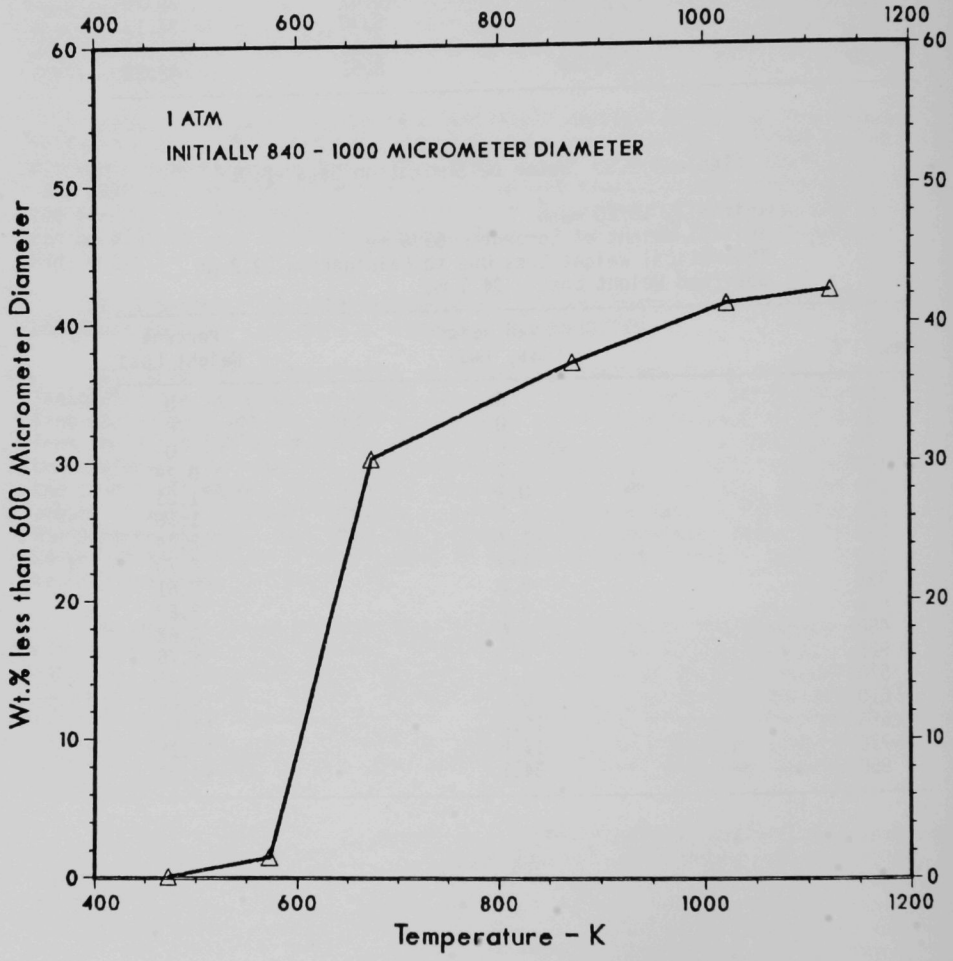

Fig. 4.2.2

quantity of water released from the sorbent materials occurred between the 373 to 673 K temperature range. The results of the experimental investigation clearly demonstrates that water was released from sorbents during heating. Therefore, the fractional mass loss, as illustrated in Fig. 4.2.3 in the early part of the test, is due to the evolution of water during heating-up of the sorbent material.

Figure 8101-G Water Loss Data

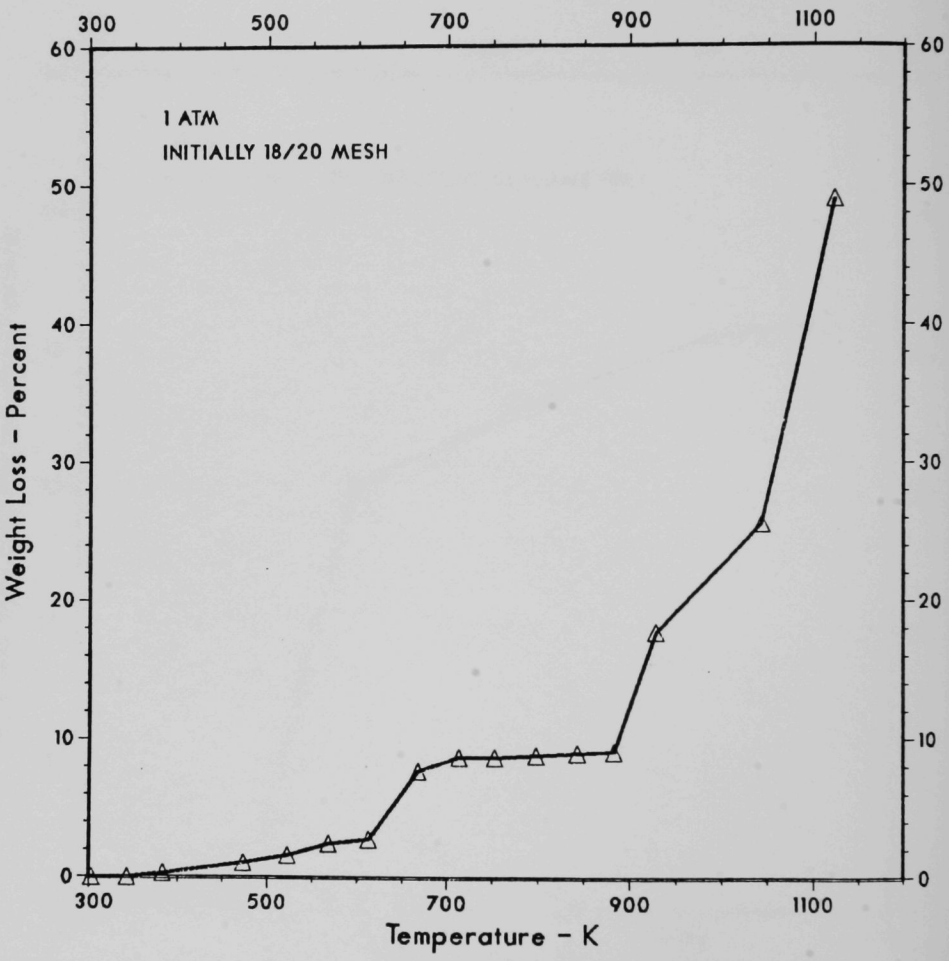

Fig. 4.2.3

References for Section 4.2

L. S. Fan and R. C. Srivastava, Chemical Engineering Science 36, 1091 (1981).

W. I. Wilson, D. C. Fee, and K. M. Myles, Proc. Int. Powder and Bulk Solids Handling and Processing Conference, Rosemont, IL, May 12-14, 1981, Cahners Exposition Group, (1981), p. 127.

5.0 LIMESTONE SUMMARY

This section gives the standard format used for reporting the data collected on each limestone sorbent using the standard tests. Also included in this section is a description of each item of the standard tests.

5.1 STANDARD SORBENT DATA FORMAT

A standard format has been devised for reporting the data collected on each sorbent using the standard tests. This format, and a description of each item are as follows:

1.	Name, ANL Number, Source,	- The commonly used name of the sorbent is given. Often this is the name of the quarry or otherwise reflects on the source of the sorbent. The first two digits of the ANL number signify the nominal amount of calcium carbonate (wt %) in the sorbent.
2.	Chemical Composition	- The nominal chemical composition of the sorbent is given. This is an average composition. Variations of composition within the particular limestone formation or particular quarry certainly exist and must be taken into account when using this handbook.
3.	Density	- The density of the raw and calcined sorbent are given.
4.	Petrographic Description	- Photomicrographs are given of both the raw (Fig. A) and the calcined sorbent (Fig. B). The sorbent microstructure is described and the average grain size is given.
5.	Pore Size Distribution	- The pore size distribution of the calcined material is given as a plot of cumulative pore volume versus pore diameter (Fig. C).
6.	Surface Area	- The surface area is given both for the raw and the calcined sorbent.
7.	Total Porosity	- The total pore volume is given for both the raw and calcined sorbent.
8.	Thermogravimetric Analysis	- The TGA data is plotted as calcium utilization versus time (Fig. D). The parameters D and b, described in the section "Analysis of TGA Data", are given.

9. Attrition

- The data from the standard laboratory attrition test and the interpretation are as previously discussed in the "Analysis of Attrition Data" section. The cumulative fraction of the initial bed which goes overhead during the test is shown in Fig. E. The intercept on this figure is taken as the "bed loss due to calcination breakup (%)." The slope of linear fit in Fig. E is taken as the "bed mass lost per minute in the linear portion (%/min)." The "Attrition constant, $\lambda_4(sec^{-1})$," is derived from this portion of the curve using the attrition model.

10. Other Data

- a. Decrepitation data is plotted as the percent of fines particles produced less than 595 μm diameter as a function of temperature. The measured weight loss as a result of water being released from the sorbent and the weight loss due to calcination is also described in the section "Analysis of Decrepitation Data."

- b. Additional TGA data, if any, is presented here. This data is for sorbent particle size and sulfur dioxide concentrations other than the standard 1000-840 μm and 3000 ppm, respectively.

5.2 TEST DATA ON LIMESTONES

1. NAME: ANL-9903

   SOURCE: Calcium Carbonate Co., Fort Dodge, IA

2. CHEMICAL COMPOSITION, wt %

$CaCO_3$	$MgCO_3$	SiO_2	Fe_2O_3	Al_2O_3	Na_2O	K_2O
99.8	0.53	0.24	0.02	0.16	0.20	0.01

3. DENSITY: RAW SORBENT 2.588 g/cm^3 161.6 lb/ft^3

   CALCINED 1.479 g/cm^3 92.33 lb/ft^3

4. PETROGRAPHIC DESCRIPTION: AVERAGE GRAIN SIZE 250 μm, SEE FIG. 9903 A & B

   Coarse-grained; loosely packed inequigranular particles.

5. PORE SIZE DISTRIBUTION: SEE FIG. 9903-C

   AVERAGE PORE DIAMETER - RAW SORBENT 0.471 μm

   CALCINED 0.091 μm

6. SURFACE AREA: RAW SORBENT 0.205 m^2/g 1 x 10^3 ft^2/lb

   CALCINED 19.01 m^2/g 9.28 x 10^4 ft^2/lb

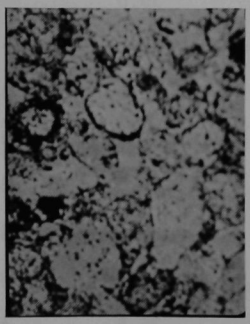

Fig. 9903A
Raw Limestone
50X

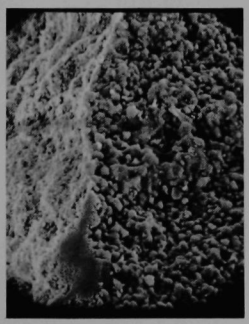

Fig. 9903B
Calcined Limestone 1 h 850°C
1100X

7. TOTAL POROSITY: RAW SORBENT 0.029 cm^3/g 4.6×10^{-4} ft^3/lb

CALCINED 0.445 cm^3/g 7.13×10^{-3} ft^3/lb

8. THERMOGRAVIMETRIC ANALYSIS: SEE FIG. 9903-D

(1123 K, 1 atm, 3000 ppm SO_2, -18 +20 mesh)

FRACTIONAL UTILIZATION = $\alpha(t, min) = 0.238 [1 - exp (-0.0858 t^{0.713})]$

ANL PARAMETERS: D = 0.214 b = 431.4

9. ATTRITION: SEE FIG. 9903-E

Bed loss due to calcination breakup (%) = 2.1

Bed mass lost in linear portion (%/min.) = 6.1×10^{-4}

Attrition constant, λ_4 (sec^{-1}) = 1.4×10^{-7}

ATTRITION DATA

	Grams Total	wt %	
		Ca	S
Initial Bed	160.405	39.9	0.00
Final Bed	109.850	57.1	5.77
Total Overhead	4.327	35.6	4.79
Overhead, 5 min	1.841	35.6	4.79
10 min	0.823	35.6	4.79
15 min	0.613	35.6	4.79
30 min	0.221	35.6	4.79
1 h	0.269	35.6	4.79
1.5 h	0.082	35.6	4.79
2 h	0.091	35.6	4.79
4 h	0.140	35.6	4.79
6 h	0.170	35.6	4.79
8 h	0.078	35.6	4.79

Attrition Data, continued for Sorbent 9903

Weight in Grams, Particle Diameter, μm

Sample	-1000 +840	-841 +707	-707 +595	-595 +420	-420 +297	-297 +250
Overhead, first 30 min	0.000	0.000	0.000	0.055	0.132	0.237
Overhead, remaining 7.5 h	0.000	0.000	0.000	0.014	0.078	0.099
Final Bed, post test	93.123	10.231	2.904	1.349	1.224	0.340

Sample	-250 +210	-210 +74	-74 +63	-63 +53	-53 +44	-44 +37	-37 +0
Overhead, first 30 min	0.380	1.952	0.072	0.103	0.152	0.093	0.039
Overhead, remaining 7.5 h	0.116	0.465	0.025	0.046	0.042	0.042	0.009
Final Bed, post test	0.214	0.591	0.016	0.031	0.029	0.025	0.006

Figure 9903-C
Pore Size Distribution

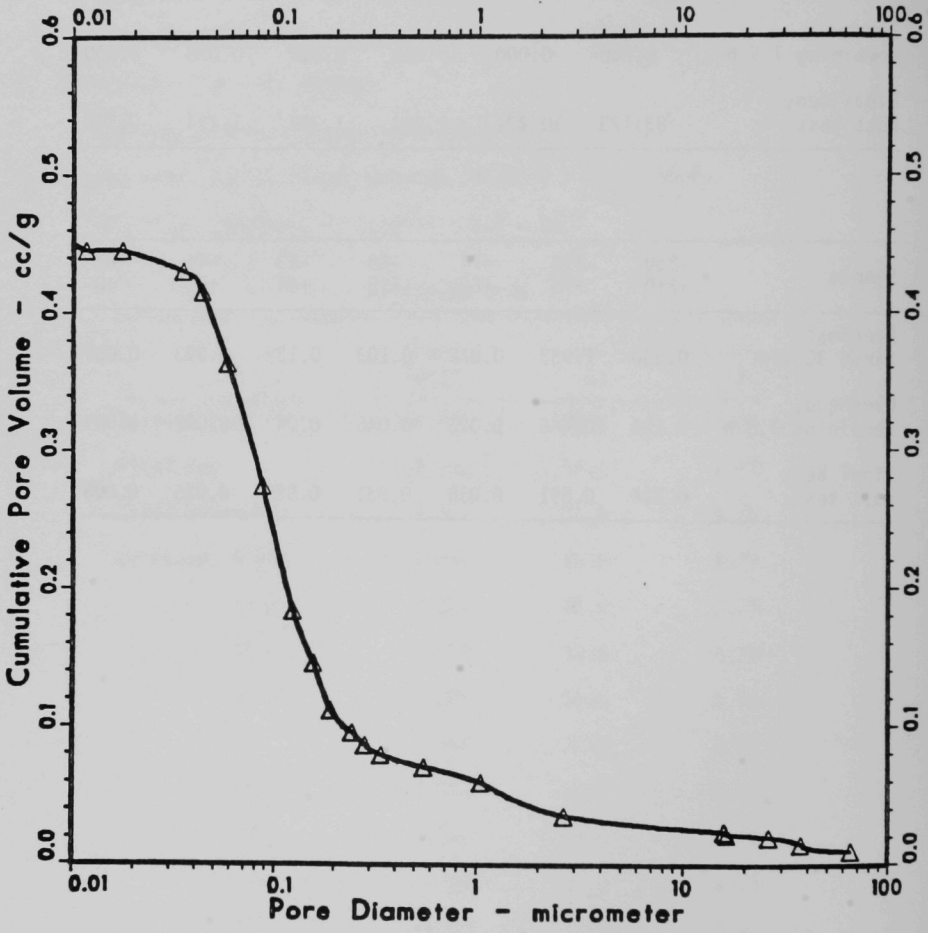

Figure 9903-D TGA Data

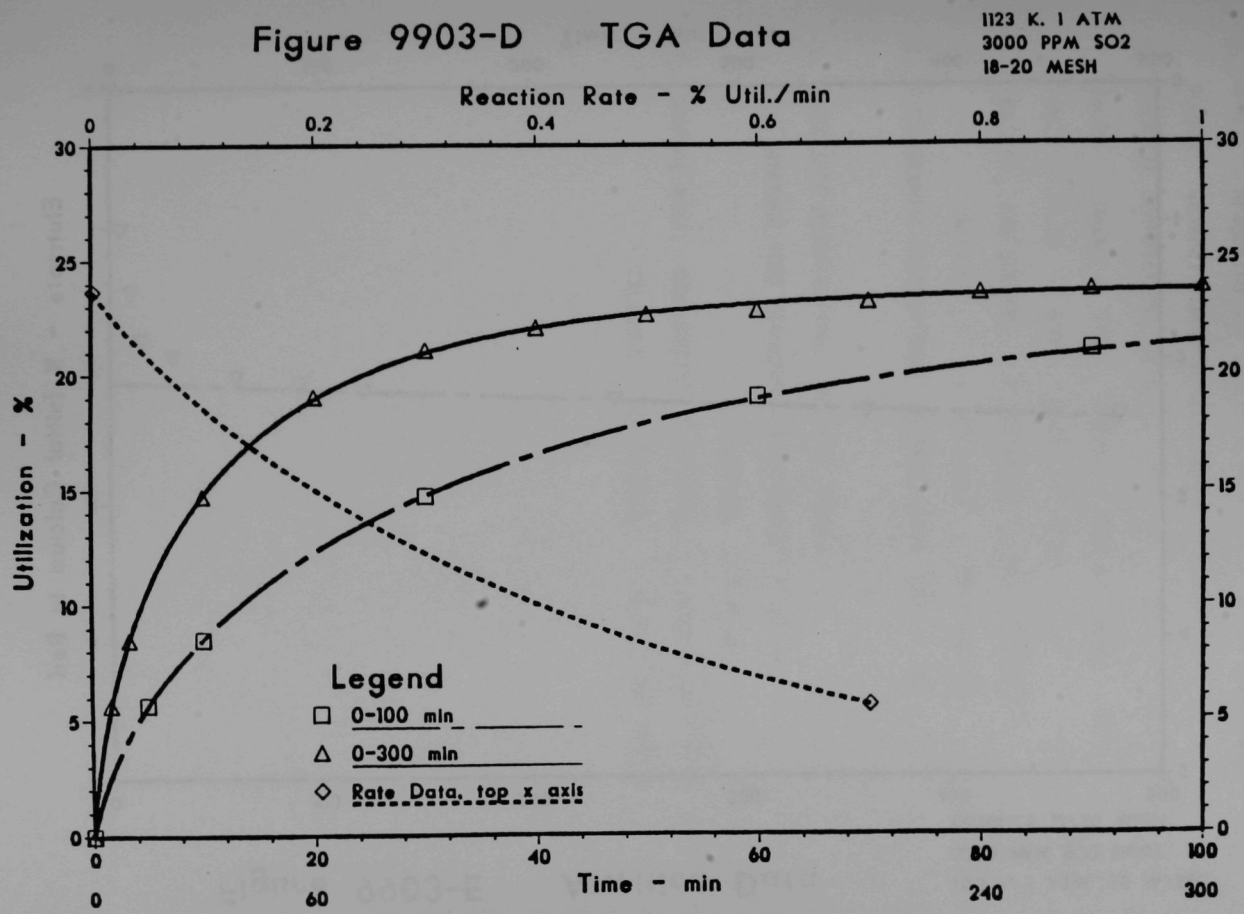

Figure 9903-E Attrition Data

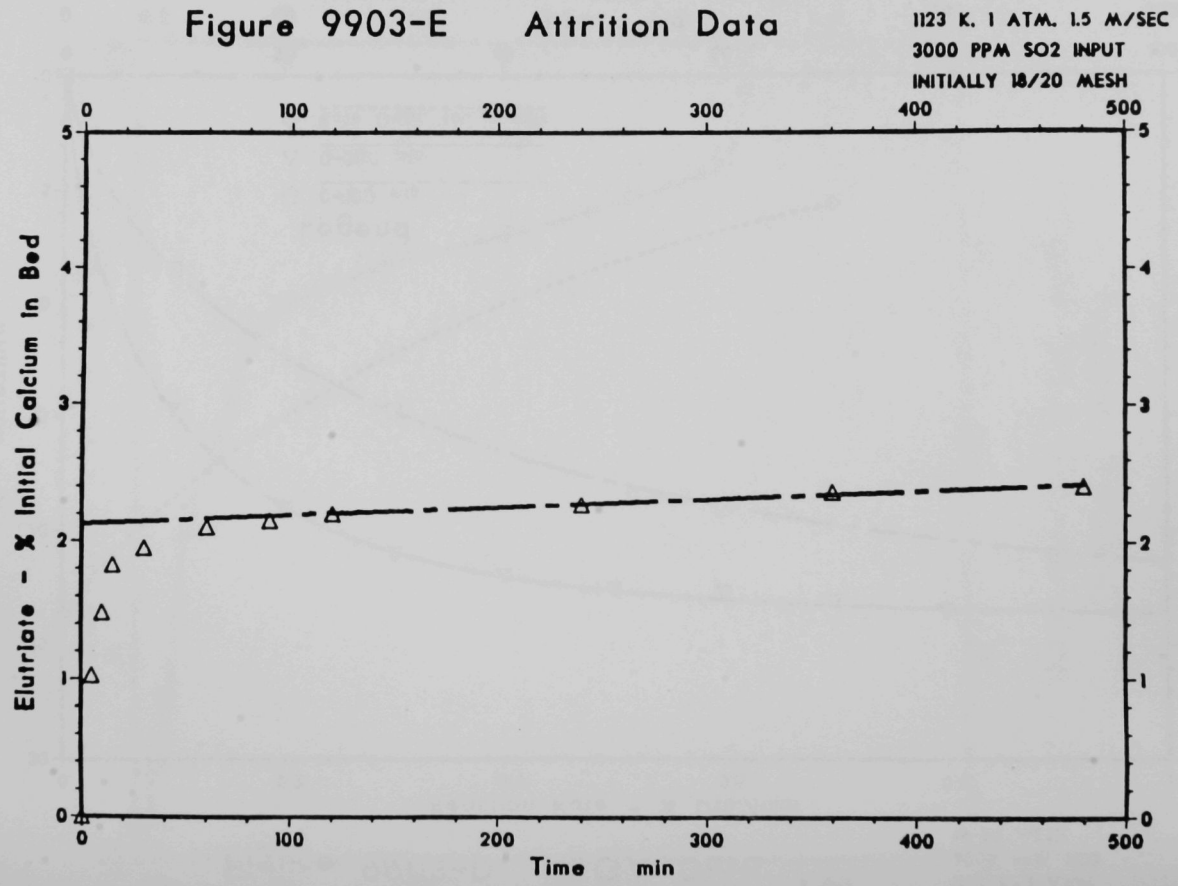

1. NAME: Aragonite ANL-9806

   SOURCE: General Electric Co., Schenectedy, NY

2. CHEMICAL COMPOSITION, wt %

$CaCO_3$	$MgCO_3$	SiO_2	Fe_2O_3	Al_2O_3	Na_2O	K_2O
98.1	1.16	0.06	0.01	0.02	--	--

3. DENSITY: RAW SORBENT 2.343 g/cm^3 146.2 lb/ft^3

   CALCINED 1.385 g/cm^3 86.5 lb/ft^3

4. PETROGRAPHIC DESCRIPTION: AVERAGE GRAIN SIZE -- μm,

5. PORE SIZE DISTRIBUTION: SEE FIG. 9806-C

   AVERAGE PORE DIAMETER - RAW SORBENT 0.56 μm

   CALCINED 2.5 μm

6. SURFACE AREA: RAW SORBENT 0.39 m^2/g 2.65 x 10^3 ft^2/lb

   CALCINED 13.55 m^2/g 6.65 x 10^4 ft^2/lb

7. TOTAL POROSITY: RAW SORBENT 0.040 cm^3/g 6.4×10^{-4} ft^3/lb

CALCINED 0.245 cm^3/g 3.9×10^{-3} ft^3/lb

8. THERMOGRAVIMETRIC ANALYSIS: SEE FIG. 9806-D

(1123 K, 1 atm, 3000 ppm SO_2, -18 +20 mesh)

FRACTIONAL UTILIZATION = $\alpha(t, \text{min}) = 0.603\ [1 - \exp(-0.0401\ t^{0.844})]$

ANL PARAMETERS: D = 0.614 b = 277

9. ATTRITION: SEE FIG. --

Bed loss due to calcination breakup (%) = --

Bed mass lost in linear portion (%/min.) = --

Attrition constant, λ_4 (sec^{-1}) = --

ATTRITION DATA

	Grams Total	wt % Ca	wt % S
Initial Bed			
Final Bed			
Total Overhead			
Overhead, 5 min			
10 min			
15 min			
30 min			
1 h			
1.5 h			
2 h			
4 h			
6 h			
8 h			

Figure 9806-C
Pore Size Distribution

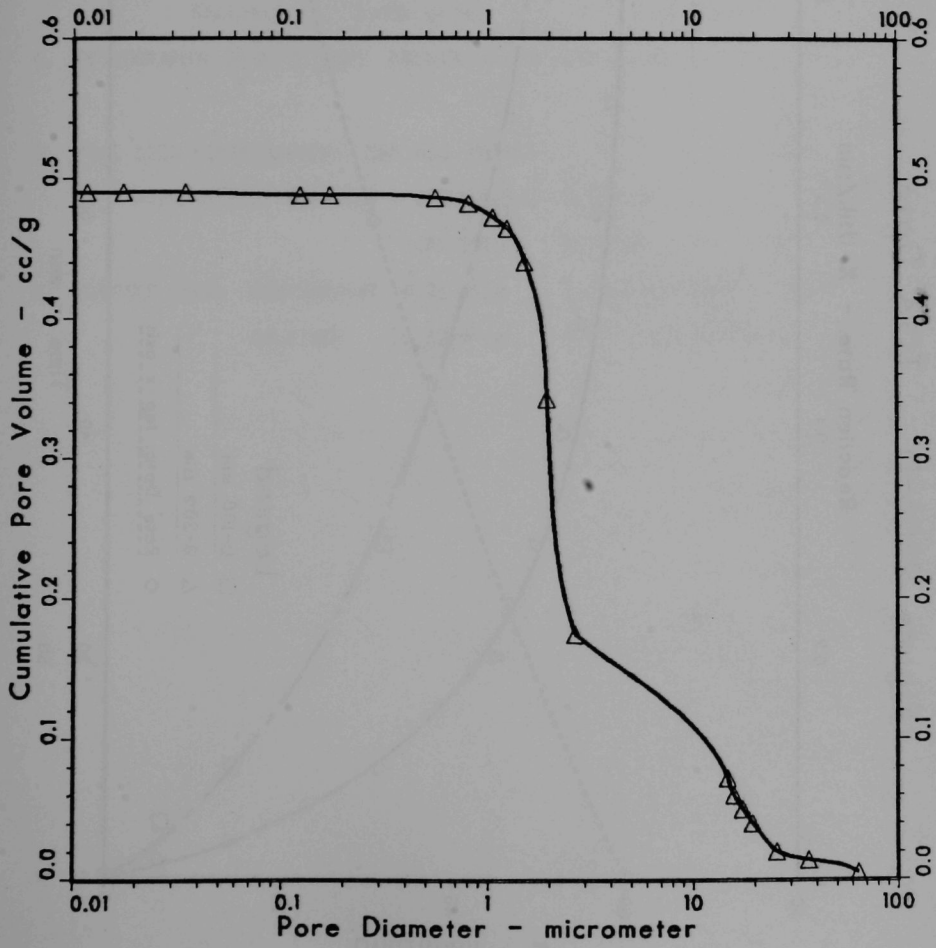

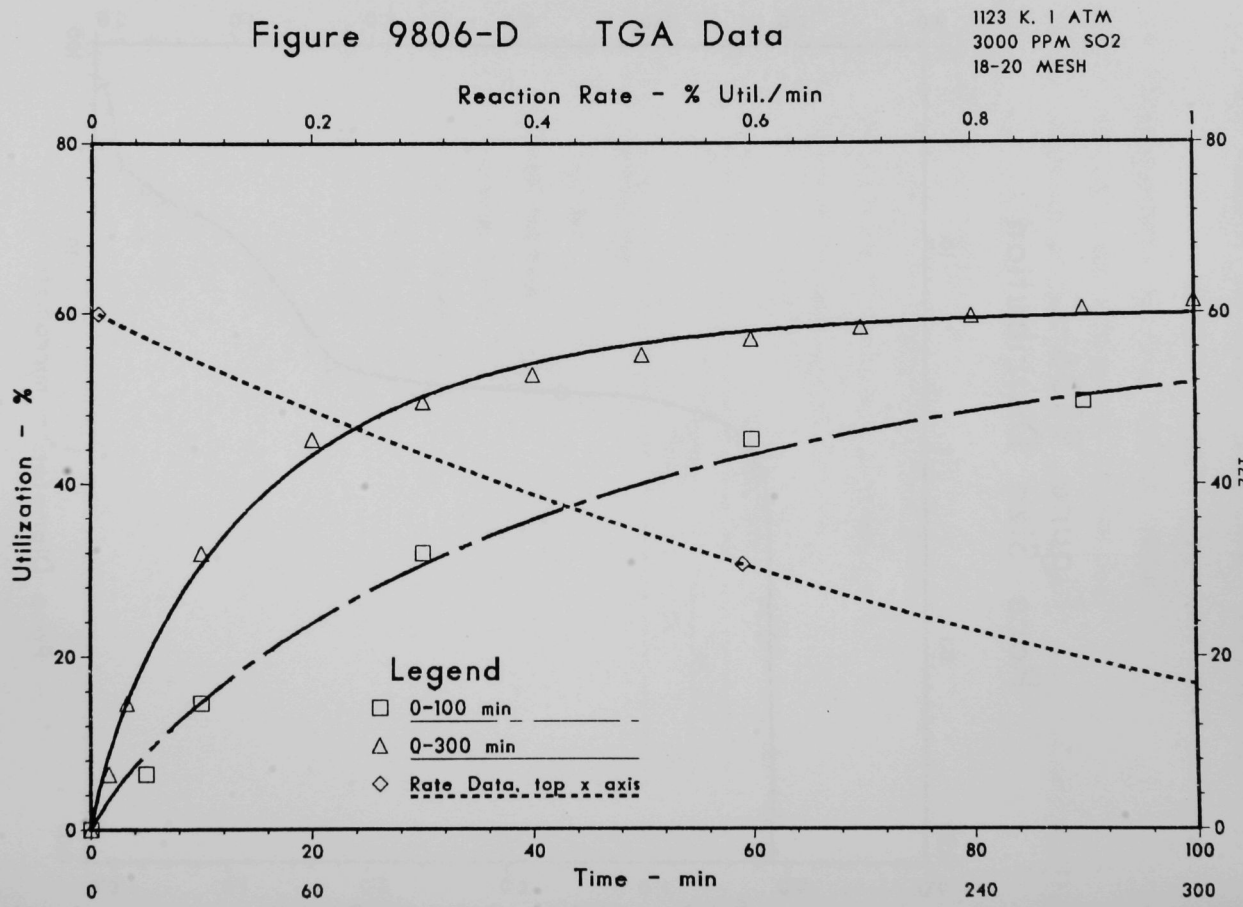
Figure 9806-D TGA Data
1123 K. 1 ATM
3000 PPM SO2
18-20 MESH
Reaction Rate - % Util./min
0
0.2
0.4
0.6
0.8
1
Utilization - %
80
60
40
20
0
Time - min
0
20
40
60
80
100
0
60
240
300
Legend
0-100 min
0-300 min
Rate Data, top x axis

1. NAME: ANL-9804

   SOURCE: Calcium Carbonate Co., Quincy, IL

2. CHEMICAL COMPOSITION, wt %

$CaCO_3$	$MgCO_3$	SiO_2	Fe_2O_3	Al_2O_3	Na_2O	K_2O
98.3	0.5	0.30	0.03	0.02	--	--

3. DENSITY: RAW SORBENT 2.573 g/cm^3 160.6 lb/ft^3

   CALCINED 1.451 g/cm^3 90.6 lb/ft^3

4. PETROGRAPHIC DESCRIPTION: AVERAGE GRAIN SIZE -- μm, --

5. PORE SIZE DISTRIBUTION: SEE FIG. 9804-C

   AVERAGE PORE DIAMETER - RAW SORBENT 0.453 μm

   CALCINED 0.10 μm

6. SURFACE AREA: RAW SORBENT 0.25 m^2/g 1.18 x 10^3 ft^2/lb

   CALCINED 12.13 m^2/g 5.95 x 10^4 ft^2/lb

7. TOTAL POROSITY: RAW SORBENT 0.034 cm^3/g 5.4×10^{-4} ft^3/lb

CALCINED 0.195 cm^3/g 3.13×10^{-3} ft^3/lb

8. THERMOGRAVIMETRIC ANALYSIS: SEE FIG. 9804-D

(1123 K, 1 atm, 3000 ppm SO_2, -18 +20 mesh)

FRACTIONAL UTILIZATION = $\alpha(t, min) = 0.287 [1 - exp (-0.0644 t^{0.786})]$

ANL PARAMETERS: D = 0.273 b = 401

9. ATTRITION: SEE FIG. 9804-E

Bed loss due to calcination breakup (%) = 1.7

Bed mass lost in linear portion (%/min.) = 8.5×10^{-4}

Attrition constant, λ_4 (sec^{-1}) = 1.7×10^{-7}

ATTRITION DATA

	Grams Total	wt %	
		Ca	S
Initial Bed	159.999	39.32	0.00
Final Bed	124.816	48.1	11.2
Total Overhead	2.705	49.3	4.23
Overhead, 5 min	0.890	49.3	4.23
10 min	0.476	49.3	4.23
15 min	0.367	49.3	4.23
30 min	0.278	49.3	4.23
1 h	0.167	49.3	4.23
1.5 h	0.082	49.3	4.23
2 h	0.061	49.3	4.23
4 h	0.116	49.3	4.23
6 h	0.188	49.3	4.23
8 h	0.079	49.3	4.23

Attrition Data, continued for Sorbent 9804

Weight in Grams, Particle Diameter, μm

Sample	-1000 +840	-841 +707	-707 +595	-595 +420	-420 +297	-297 +250
Overhead, first 30 min	0.00	0.00	0.00	0.0010	0.0058	0.0059
Overhead, remaining 7.5 h	0.00	0.00	0.00	0.00	0.00	0.044
Final Bed, post test	112.315	6.034	2.701	0.261	1.413	0.523

Sample	-250 +210	-210 +74	-74 +63	-63 +53	-53 +44	-44 +37	-37 +0
Overhead, first 30 min	0.117	1.047	0.118	0.166	0.118	0.057	0.076
Overhead, remaining 7.5 h	0.120	0.562	0.116	0.137	0.041	0.028	0.047
Final Bed, post test	0.718	1.141	0.010	0.026	0.020	0.009	0.005

Figure 9804-C
Pore Size Distribution

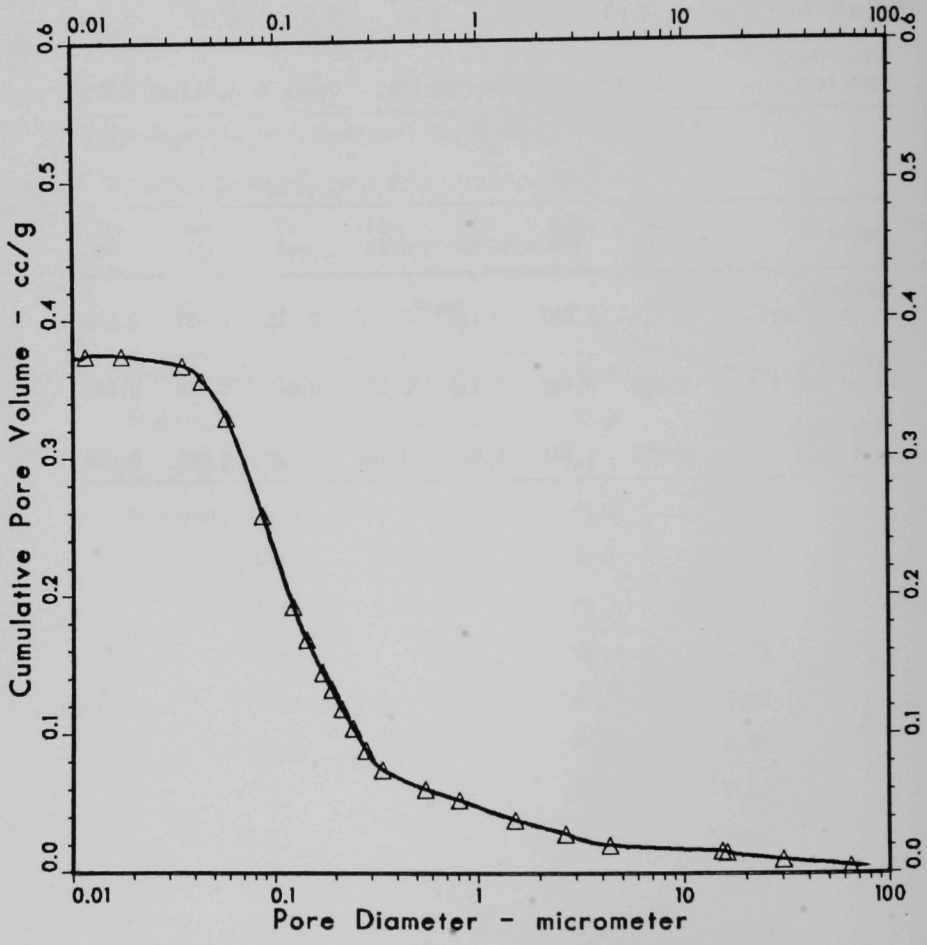

Figure 9804-D TGA Data

1123 K. 1 ATM
3000 PPM SO2
18-20 MESH

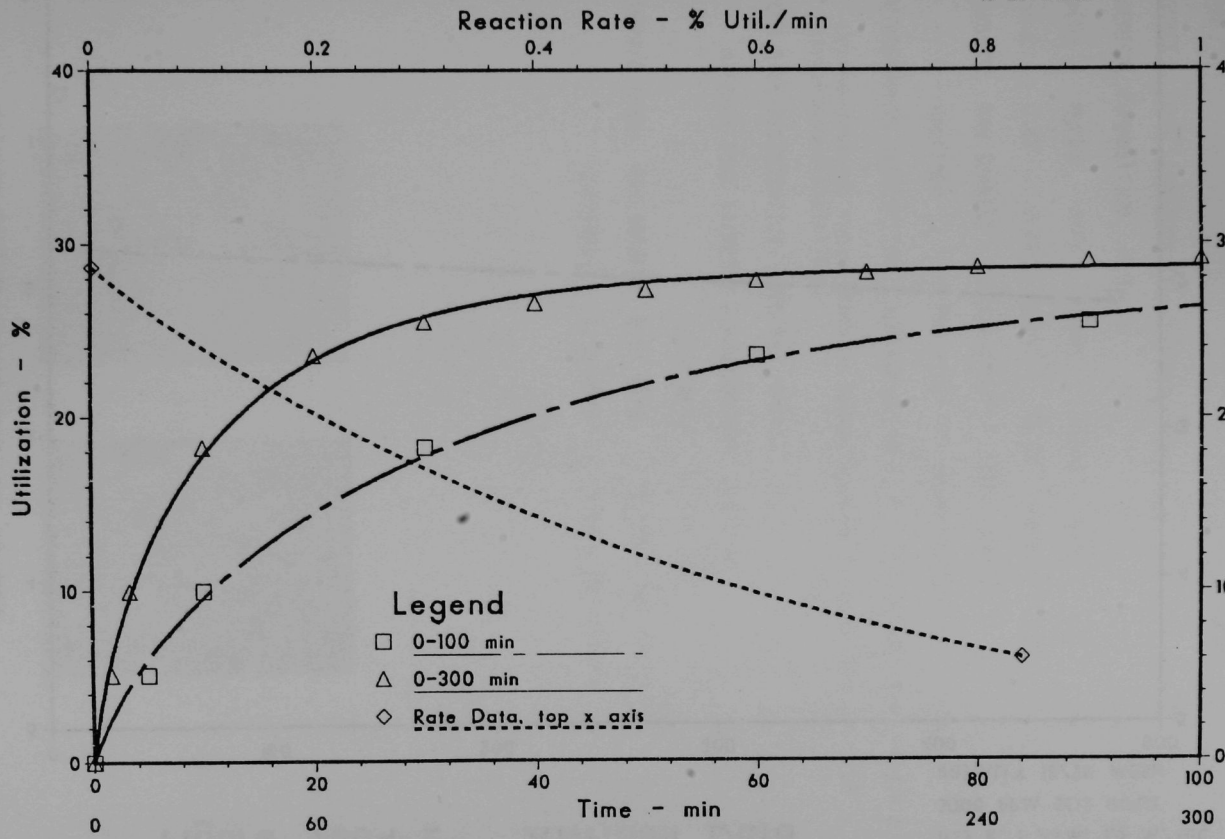

Figure 9804-E Attrition Data

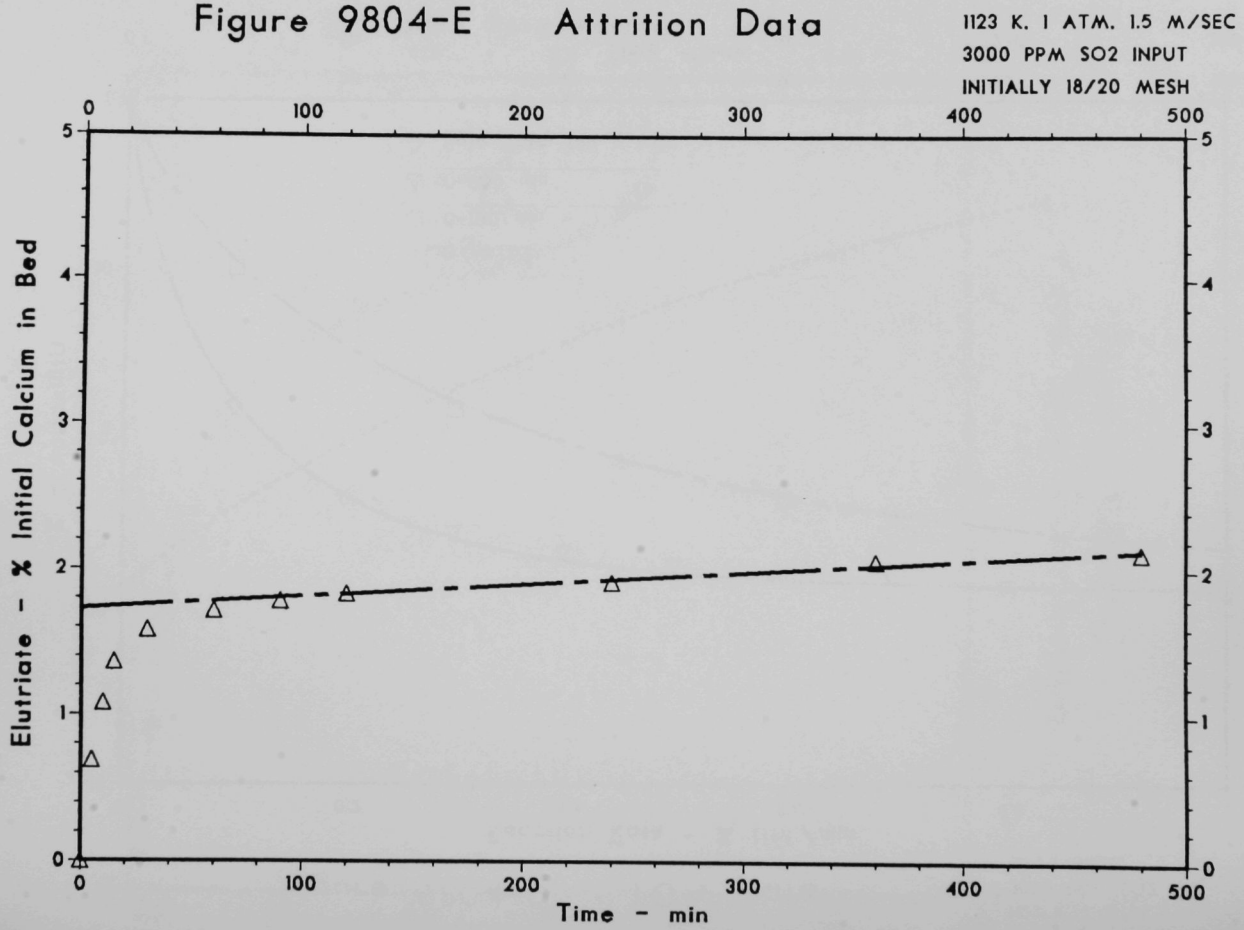

1. NAME: ANL-9801

   SOURCE: Iowa Limestone Co., Alden, IA

2. CHEMICAL COMPOSITION, wt %

$CaCO_3$	$MgCO_3$	SiO_2	Fe_2O_3	Al_2O_3	Na_2O	K_2O
98.2	0.47	0.29	0.18	0.10	0.04	0.01

3. DENSITY: RAW SORBENT 2.539 g/cm^3 158.5 lb/ft^3

   CALCINED 1.456 g/cm^3 90.90 lb/ft^3

4. PETROGRAPHIC DESCRIPTION: AVERAGE GRAIN SIZE > 250 μm, SEE FIG. 9801 A & B

   Coarse-grained; inequigranular stone; appears to have some veins of carbonaceous stylolites.

5. PORE SIZE DISTRIBUTION: SEE FIG. 9801-C

   AVERAGE PORE DIAMETER - RAW SORBENT 0.531 μm

   CALCINED 0.146 μm

6. SURFACE AREA: RAW SORBENT 0.24 m^2/g 1.170 x 10^3 ft^2/lb

   CALCINED 11.35 m^2/g 5.54 x 10^4 ft^2/lb

Fig. 9801A
Raw Limestone
50X

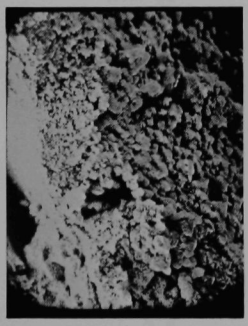

Fig. 9801B
Calcined Limestone 1 h 850°C
1100X

7. TOTAL POROSITY: RAW SORBENT 0.0330 cm^3/g 5.29×10^{-4} ft^3/lb

CALCINED 0.430 cm^3/g 6.89×10^{-3} ft^3/lb

8. THERMOGRAVIMETRIC ANALYSIS: SEE FIG. 9801-D

(1123 K, 1 atm, 3000 ppm SO_2, -18 +20 mesh)

FRACTIONAL UTILIZATION = $\alpha(t, min) = 0.307 [1 - exp (-0.0588 t^{0.777})]$

ANL PARAMETERS: D = 0.288 b = 320.5

9. ATTRITION: SEE FIG. 9801-E

Bed loss due to calcination breakup (%) = 13.0

Bed mass lost in linear portion (%/min.) = 1.46×10^{-3}

Attrition constant, λ_4 (sec^{-1}) = 3.74×10^{-7}

ATTRITION DATA

	Grams Total	wt % Ca	wt % S
Initial Bed	160.065	39.28	0.00
Final Bed	109.476	47.2	5.13
Total Overhead	19.343	44.6	5.13
Overhead, 5 min	12.278	44.6	5.13
10 min	3.716	44.6	5.13
15 min	1.530	44.6	5.13
30 min	0.534	44.6	5.13
1 h	0.289	44.6	5.13
1.5 h	0.123	44.6	5.13
2 h	0.123	44.6	5.13
4 h	0.311	44.6	5.13
6 h	0.219	44.6	5.13
8 h	0.221	44.6	5.13

Attrition Data, continued for Sorbent 9801

Weight in Grams, Particle Diameter, μm

Sample	-1000 +840	-841 +707	-707 +595	-595 +420	-420 +297	-297 +250
Overhead, first 30 min	0.000	0.000	0.000	0.000	0.364	0.551
Overhead, remaining 7.5 h	0.000	0.000	0.000	0.007	0.101	0.238
Final Bed, post test	87.406	6.269	3.365	4.335	4.955	1.533

Sample	-250 +210	-210 +74	-74 +63	-63 +53	-53 +44	-44 +37	-37 +0
Overhead, first 30 min	2.338	12.341	0.126	0.150	0.804	0.354	0.637
Overhead, remaining 7.5 h	0.326	0.744	0.015	0.026	0.023	0.004	0.000
Final Bed, post test	0.941	0.591	0.014	0.028	0.024	0.012	0.000

10. OTHER DATA

See Figs. 9801-F and 9801-G for decrepitation data.

Figure 9801-C
Pore Size Distribution

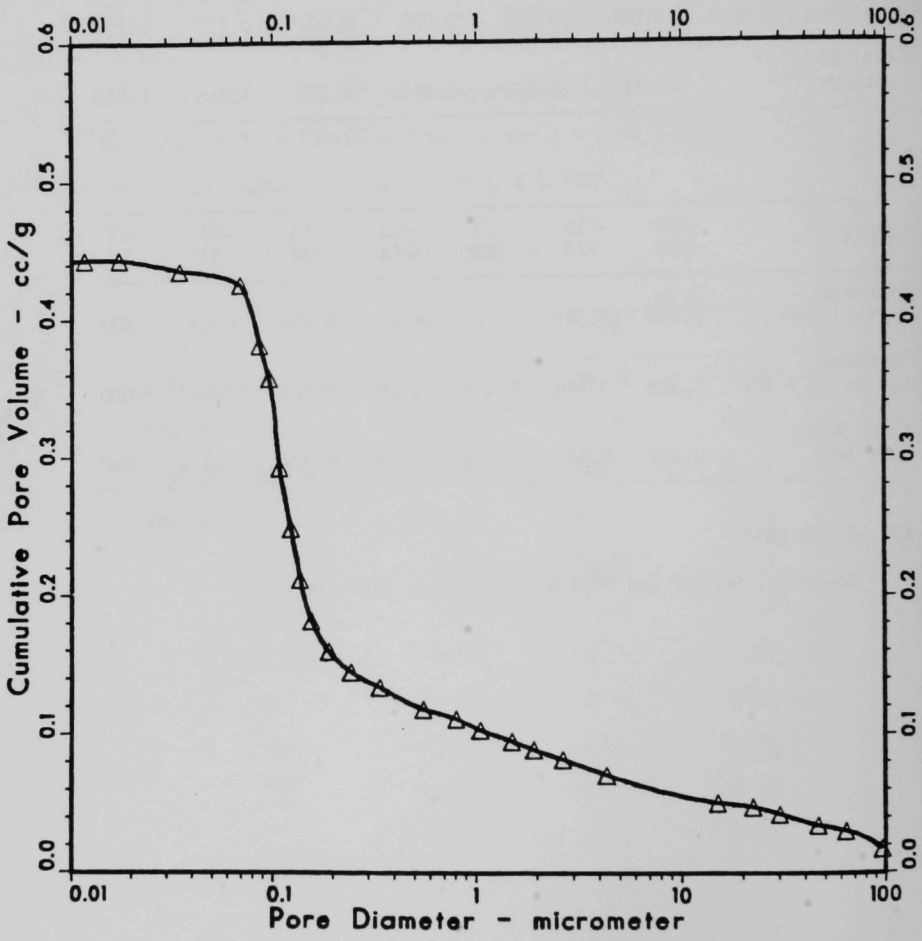

Figure 9801-D TGA Data

1123 K. 1 ATM
3000 PPM SO2
18-20 MESH

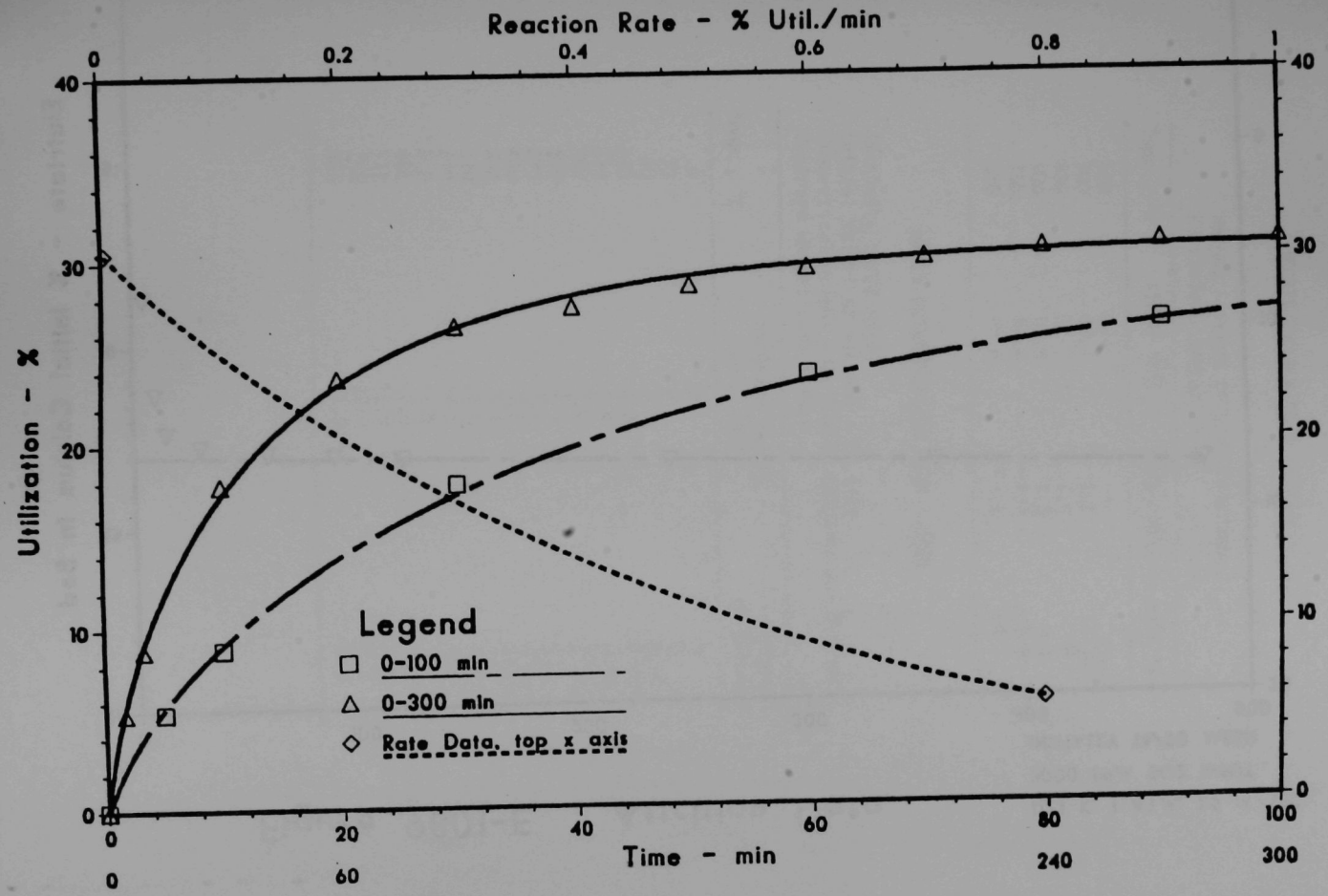

Figure 9801-E Attrition Data

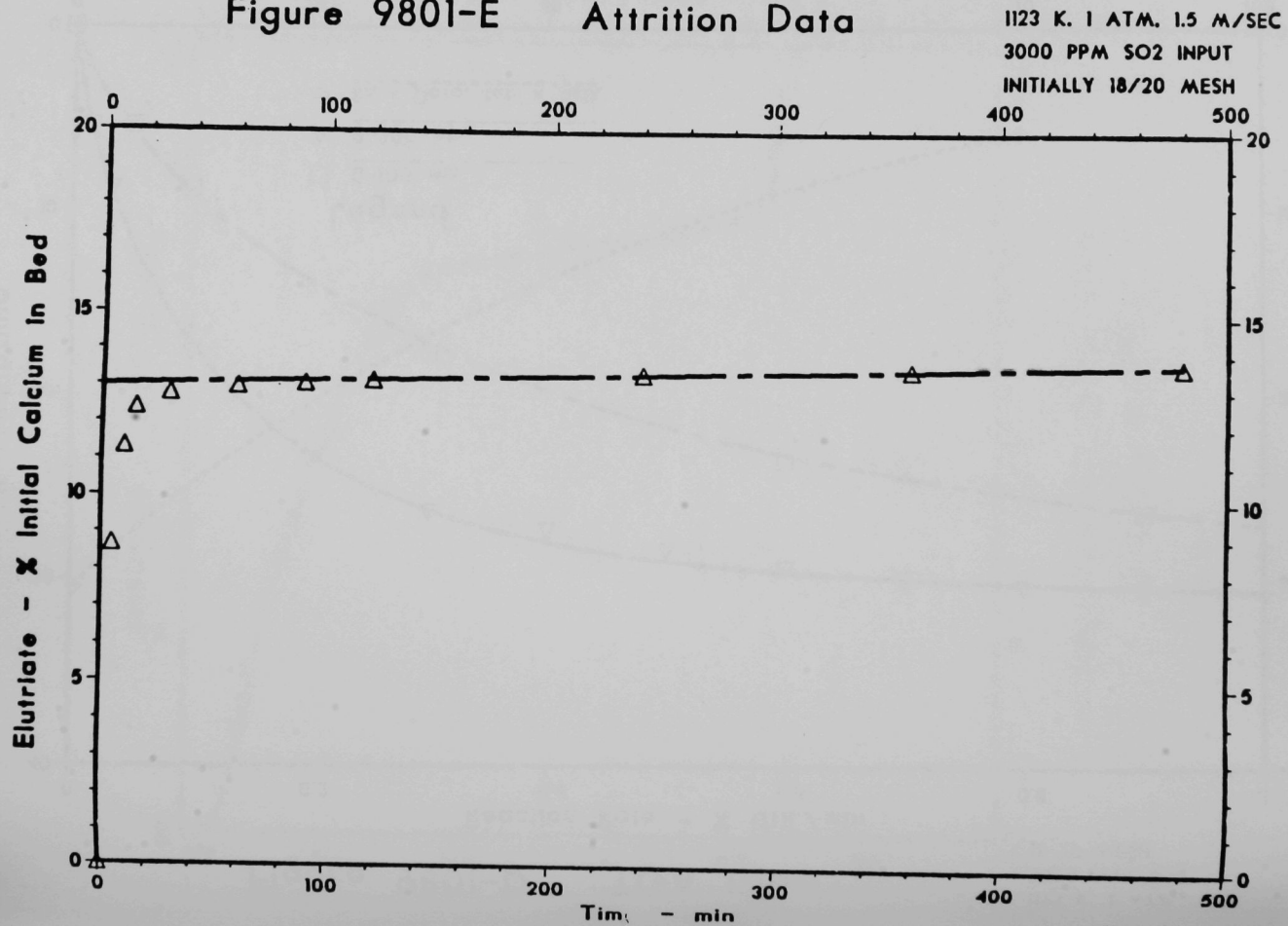

DECREPITATION DATA - 9801

Temp., °C	Weight Percent of Size Fractions, Particle Diameter in µm -1000 +841	-841 +595	-595 +0
200	--	--	--
300	98.7	1.2	0.10
400	87.7	4.5	7.8
600	87.0	4.6	8.4
750	86.4	4.7	9.0
850	85.4	4.8	10.1

WATER DETERMINATION DATA - 9801

Initially 18/20 mesh
Initial Weight of Sorbent - 89.4 mg
Theoretical Weight Loss Due to Calcination 38.9 mg
Observed Weight Loss - 41.0

Temp., °C	Observed Weight Loss, (mg)	Percent Weight Loss
0	0	0
30	0	0
80	0.1	0.11
130	0.2	0.22
230	0.4	0.45
280	1.0	1.1
330	1.3	1.5
390	2.1	2.3
440	3.0	3.4
480	3.4	3.8
520	3.8	4.3
570	4.2	4.7
610	5.0	5.6
660	6.5	7.3
710	11.3	12.6
790	37.7	42.2
850	41.0	45.9

Figure 9801-F Decrepitation Data

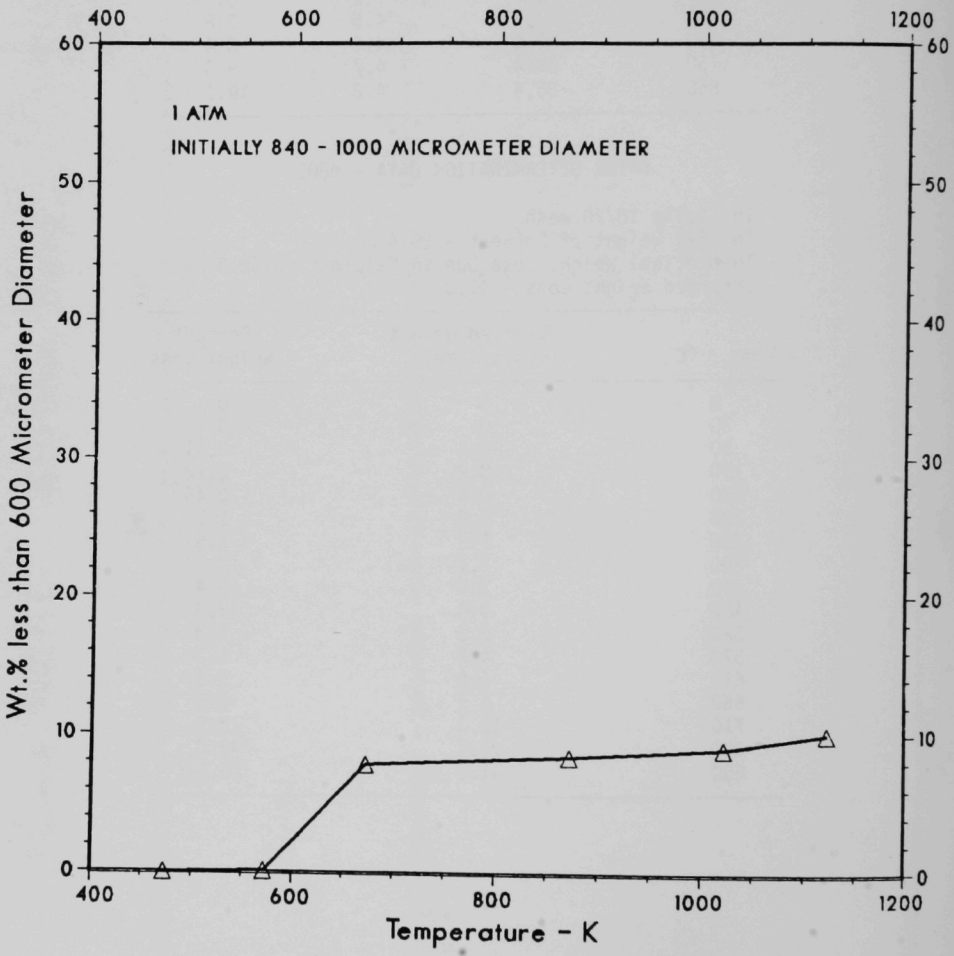

Figure 9801-G Water Loss Data

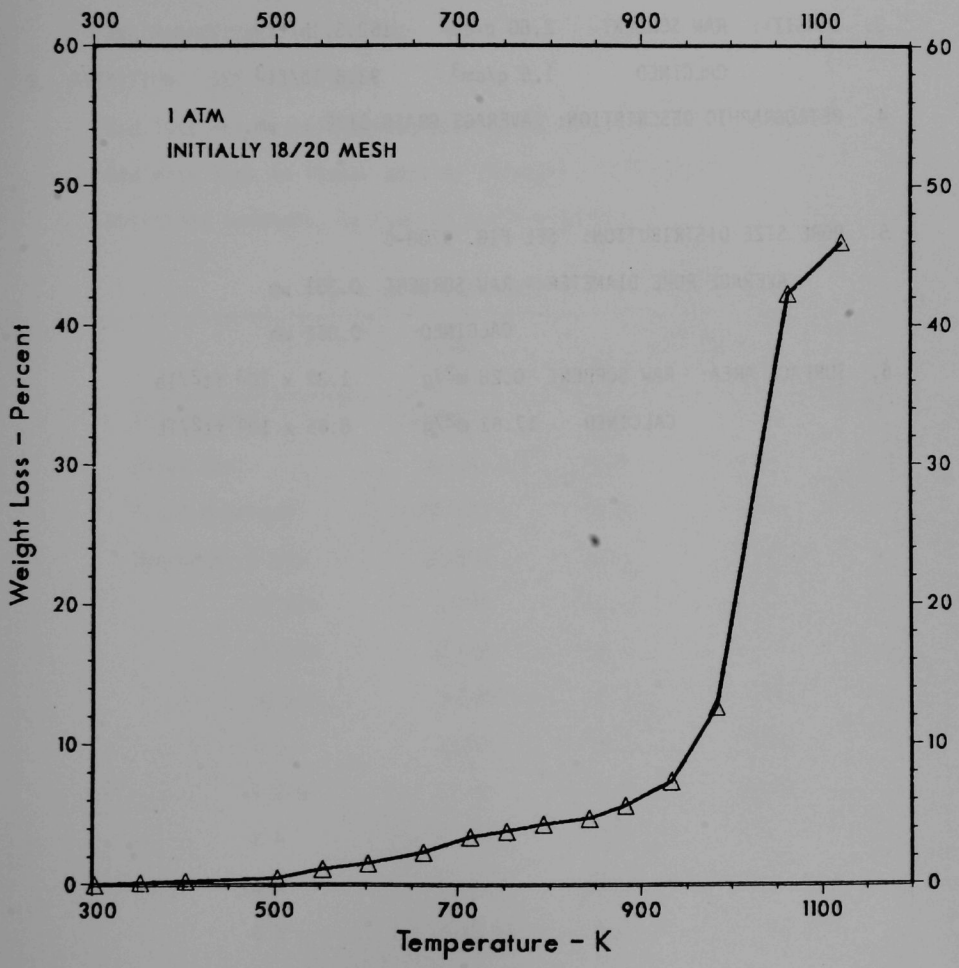

1. NAME: ANL-9708

   SOURCE: Columbia Quarry Co., Columbia, IL

2. CHEMICAL COMPOSITION, wt %

$CaCO_3$	$MgCO_3$	SiO_2	Fe_2O_3	Al_2O_3	Na_2O	K_2O
97.3	1.80	--	0.15	0.10	--	--

3. DENSITY: RAW SORBENT 2.60 g/cm^3 162.3 lb/ft^3

   CALCINED 1.5 g/cm^3 93.6 lb/ft^3

4. PETROGRAPHIC DESCRIPTION: AVERAGE GRAIN SIZE -- μm, --

5. PORE SIZE DISTRIBUTION: SEE FIG. 9708-C

   AVERAGE PORE DIAMETER - RAW SORBENT 0.331 μm

   CALCINED 0.052 μm

6. SURFACE AREA: RAW SORBENT 0.28 m^2/g 1.32 x 10^3 ft^2/lb

   CALCINED 17.62 m^2/g 8.65 x 10^4 ft^2/lb

7. TOTAL POROSITY: RAW SORBENT 0.027 cm^3/g 4.3×10^{-4} ft^3/lb

CALCINED 0.198 cm^3/g 3.2×10^{-3} ft^3/lb

8. THERMOGRAVIMETRIC ANALYSIS: SEE FIG. 9708-D

(1123 K, 1 atm, 3000 ppm SO_2, -18 +20 mesh)

FRACTIONAL UTILIZATION = $\alpha(t, min) = 0.250 [1 - exp (-0.170 t^{0.542})]$

ANL PARAMETERS: D = 0.245 b = 542

9. ATTRITION: SEE FIG. 9708-E

Bed loss due to calcination breakup (%) = 20.78

Bed mass lost in linear portion (%/min.) = 3.7×10^{-3}

Attrition constant, λ_4 (sec^{-1}) = 1.1×10^{-6}

ATTRITION DATA

	Grams Total	wt % Ca	wt % S
Initial Bed	160.003	38.92	0.00
Final Bed	93.371	51.5	8.86
Total Overhead	27.075	42.7	1.26
Overhead, 5 min	12.388	42.7	1.26
10 min	3.440	42.7	1.26
15 min	2.104	42.7	1.26
30 min	5.174	42.7	1.26
1 h	1.663	42.7	1.26
1.5 h	0.443	42.7	1.26
2 h	0.049	42.7	1.26
4 h	0.610	42.7	1.26
6 h	0.442	42.7	1.26
8 h	0.353	42.7	1.26

Attrition Data, continued for Sorbent 9708

Weight in Grams, Particle Diameter, μm

Sample	-1000 +840	-841 +707	-707 +595	-595 +420	-420 +297	-297 +250
Overhead, first 30 min	0.00	0.007	0.007	0.008	0.013	0.029
Overhead, remaining 7.5 h	0.00	0.00	0.008	0.010	0.044	0.198
Final Bed, post test	43.226	13.885	8.157	9.892	9.128	3.852

Sample	-250 +210	-210 +74	-74 +63	-63 +53	-53 +44	-44 +37	-37 +0
Overhead, first 30 min	0.160	14.140	0.151	0.331	0.987	0.803	1.358
Overhead, remaining 7.5 h	1.173	6.809	0.029	0.134	0.219	0.143	0.304
Final Bed, post test	3.312	1.771	0.006	0.048	0.045	0.044	0.001

Figure 9708-C
Pore Size Distribution

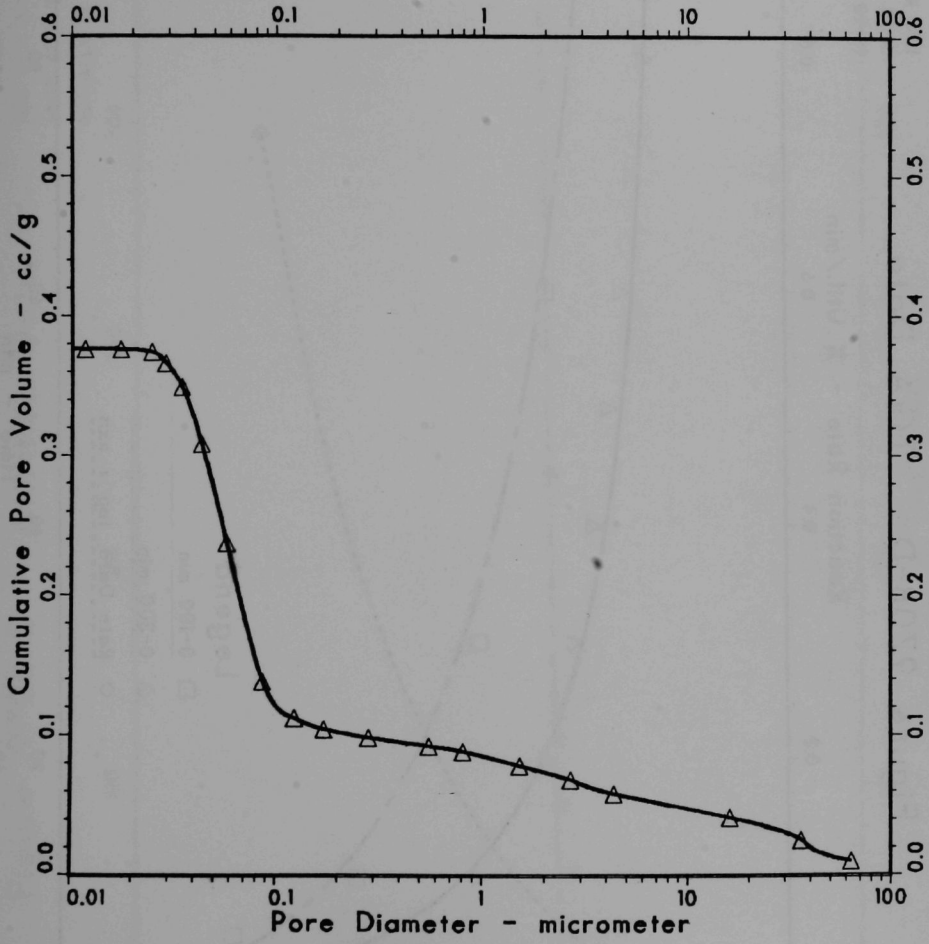

Figure 9708-D TGA Data

1123 K. 1 ATM
3000 PPM SO2
18-20 MESH

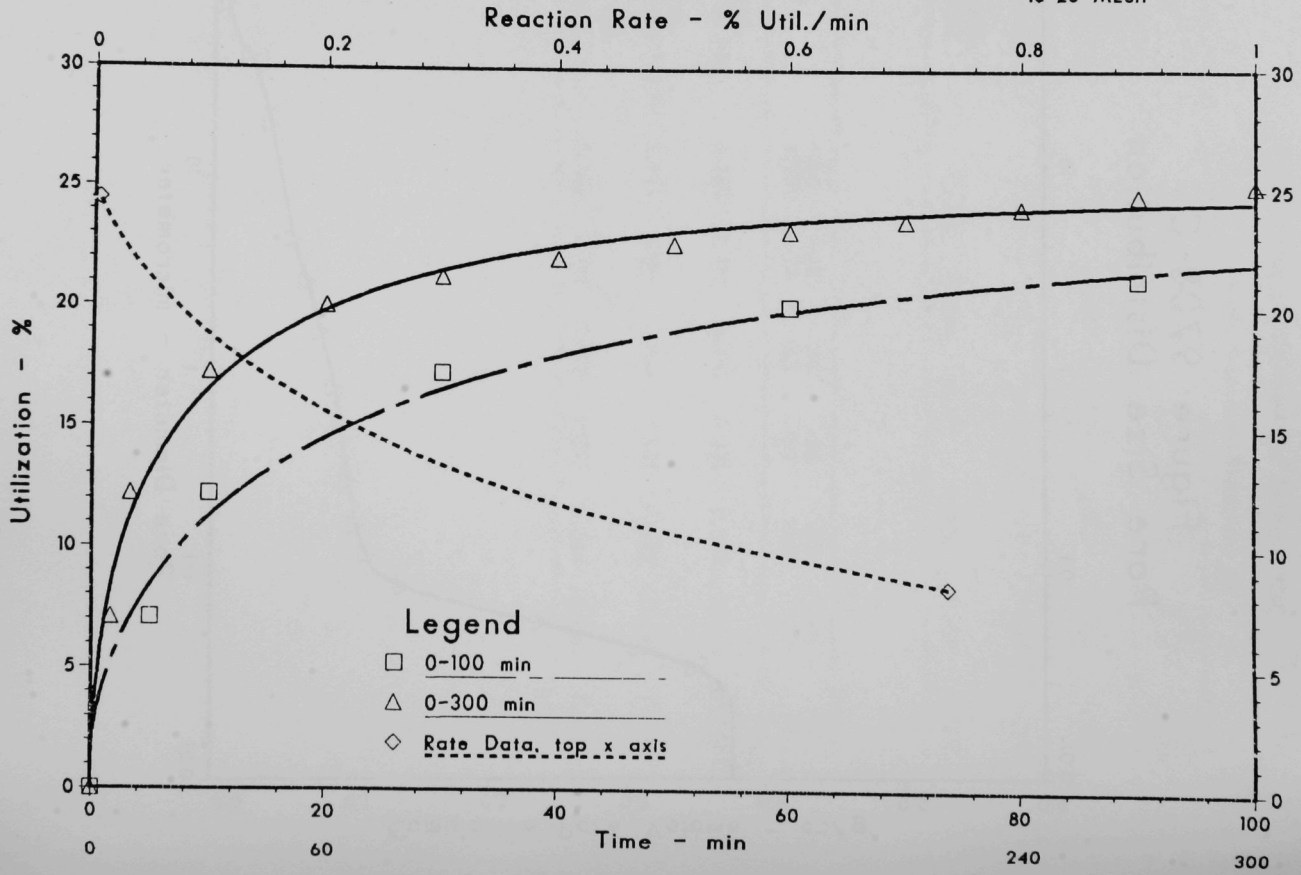

Figure 9708-E Attrition Data

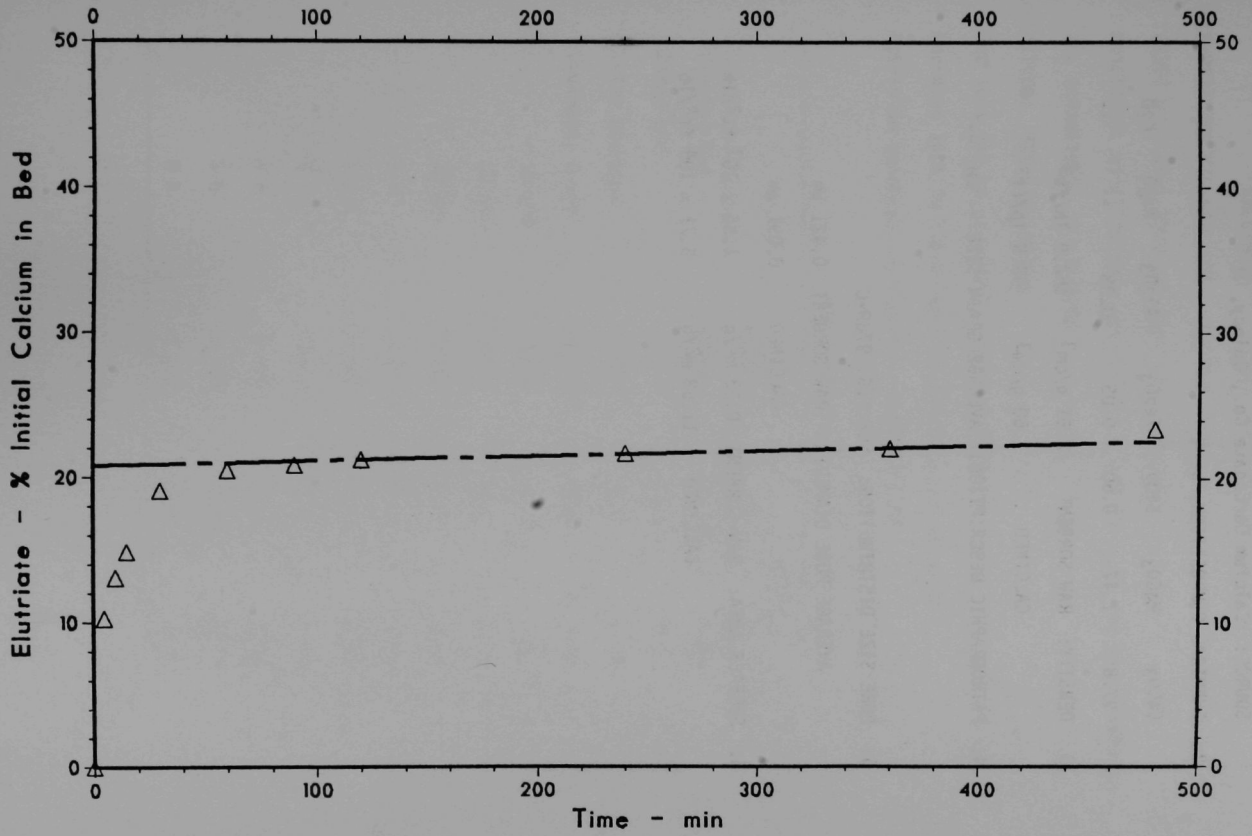

1. NAME: ANL-9709

   SOURCE: Calcium Carbonate Co., Quincy, IL

2. CHEMICAL COMPOSITION, wt %

$CaCO_3$	$MgCO_3$	SiO_2	Fe_2O_3	Al_2O_3	Na_2O	K_2O
97.8	1.47	0.60	0.05	0.08	--	--

3. DENSITY: RAW SORBENT 2.61 g/cm^3 162.9 lb/ft^3

   CALCINED 1.60 g/cm^3 99.9 lb/ft^3

4. PETROGRAPHIC DESCRIPTION: AVERAGE GRAIN SIZE -- μm, --

5. PORE SIZE DISTRIBUTION: SEE FIG. 9709-C

   AVERAGE PORE DIAMETER - RAW SORBENT 0.421 μm

   CALCINED 0.091 μm

6. SURFACE AREA: RAW SORBENT 0.33 m^2/g 1.56 x 10^3 ft^2/lb

   CALCINED 11.63 m^2/g 5.71 x 10^4 ft^2/lb

7. TOTAL POROSITY: RAW SORBENT 0.032 cm^3/g 5.1×10^{-4} ft^3/lb

CALCINED 0.320 cm^3/g 5.1×10^{-3} ft^3/lb

8. THERMOGRAVIMETRIC ANALYSIS: SEE FIG. 9709-D

(1123 K, 1 atm, 3000 ppm SO_2, -18 +20 mesh)

FRACTIONAL UTILIZATION = $\alpha(t, \text{min}) = 0.325\ [1 - \exp(-0.089\ t^{0.639})]$

ANL PARAMETERS: D = 0.3180 b = 338

9. ATTRITION: SEE FIG. 9709-E

Bed loss due to calcination breakup (%) = 22.8

Bed mass lost in linear portion (%/min.) = 1.03×10^{-3}

Attrition constant, λ_4 (sec^{-1}) = 2.429×10^{-7}

ATTRITION DATA

	Grams Total	wt % Ca	wt % S
Initial Bed	163.455	39.12	0.00
Final Bed	98.374	49.8	10.1
Total Overhead	36.107	41.3	1.13
Overhead, 5 min	24.704	41.3	1.13
10 min	5.146	41.3	1.13
15 min	2.279	41.3	1.13
30 min	2.526	41.3	1.13
1 h	0.574	41.3	1.13
1.5 h	0.180	41.3	1.13
2 h	0.123	41.3	1.13
4 h	0.248	41.3	1.13
6 h	0.186	41.3	1.13
8 h	0.140	41.3	1.13

Attrition Data, continued for Sorbent 9709

Weight in Grams, Particle Diameter, μm

Sample	-1000 +840	-841 +707	-707 +595	-595 +420	-420 +297	-297 +250
Overhead, first 30 min	0.006	0.006	0.006	0.007	0.035	0.295
Overhead, remaining 7.5 h	0.000	0.000	0.002	0.010	0.042	0.176
Final Bed, post test	70.199	11.471	4.186	4.178	4.240	1.468

Sample	-250 +210	-210 +74	-74 +63	-63 +53	-53 +44	-44 +37	-37 +0
Overhead, first 30 min	0.649	25.964	0.278	0.352	1.446	1.175	2.030
Overhead, remaining 7.5 h	0.856	2.300	0.019	0.170	0.108	0.084	0.089
Final Bed, post test	1.623	0.931	0.011	0.021	0.025	0.015	0.007

Figure 9709-C
Pore Size Distribution

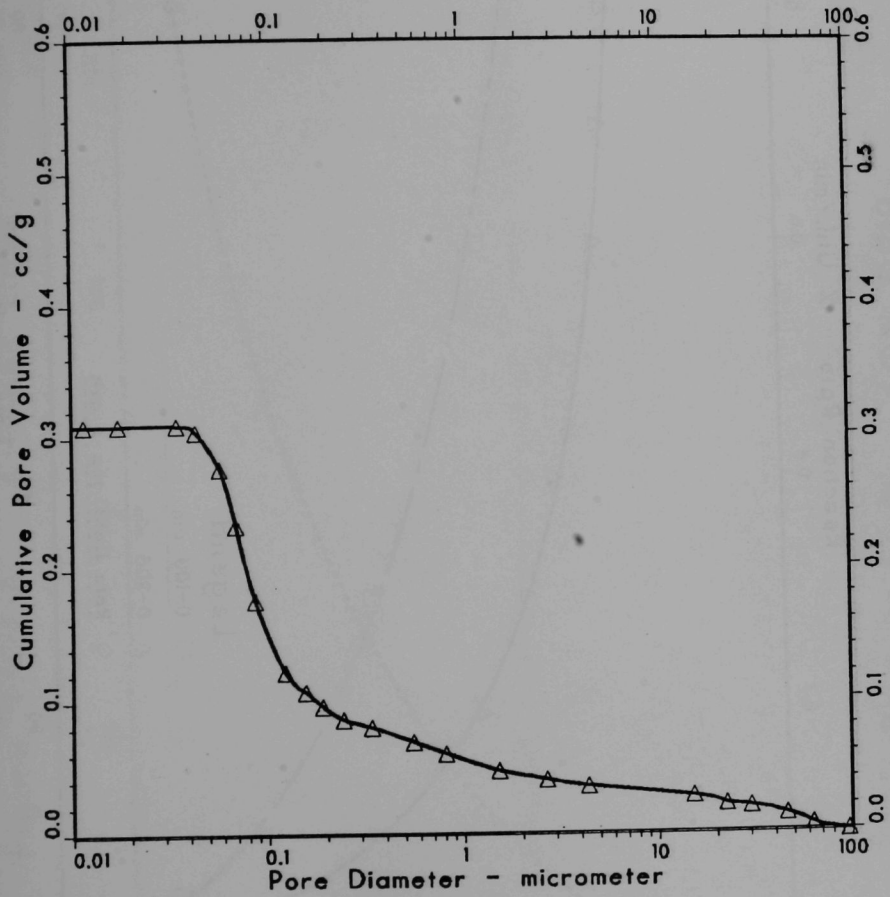

Figure 9709-D TGA Data

1123 K. 1 ATM
3000 PPM SO2
18-20 MESH

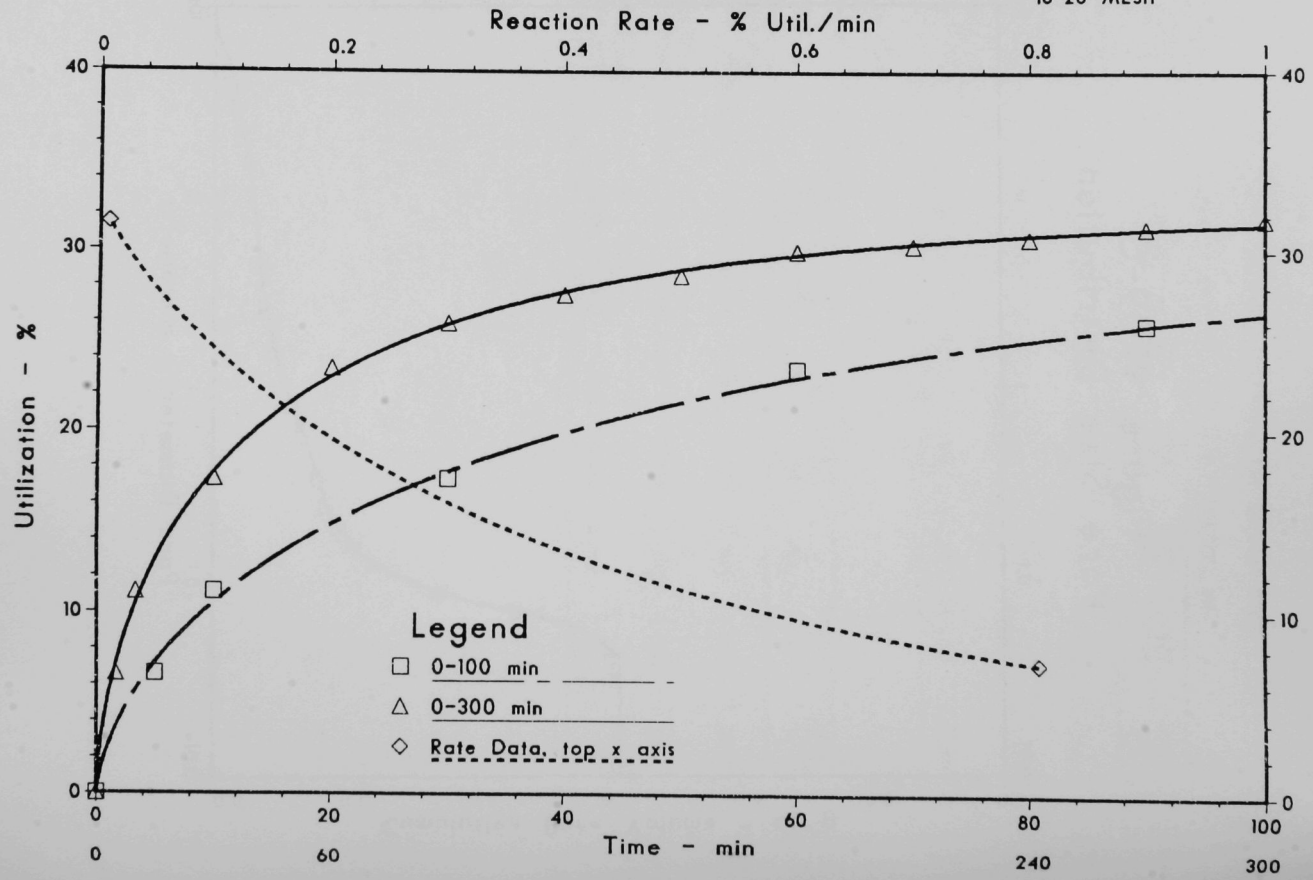

Figure 9709-E Attrition Data

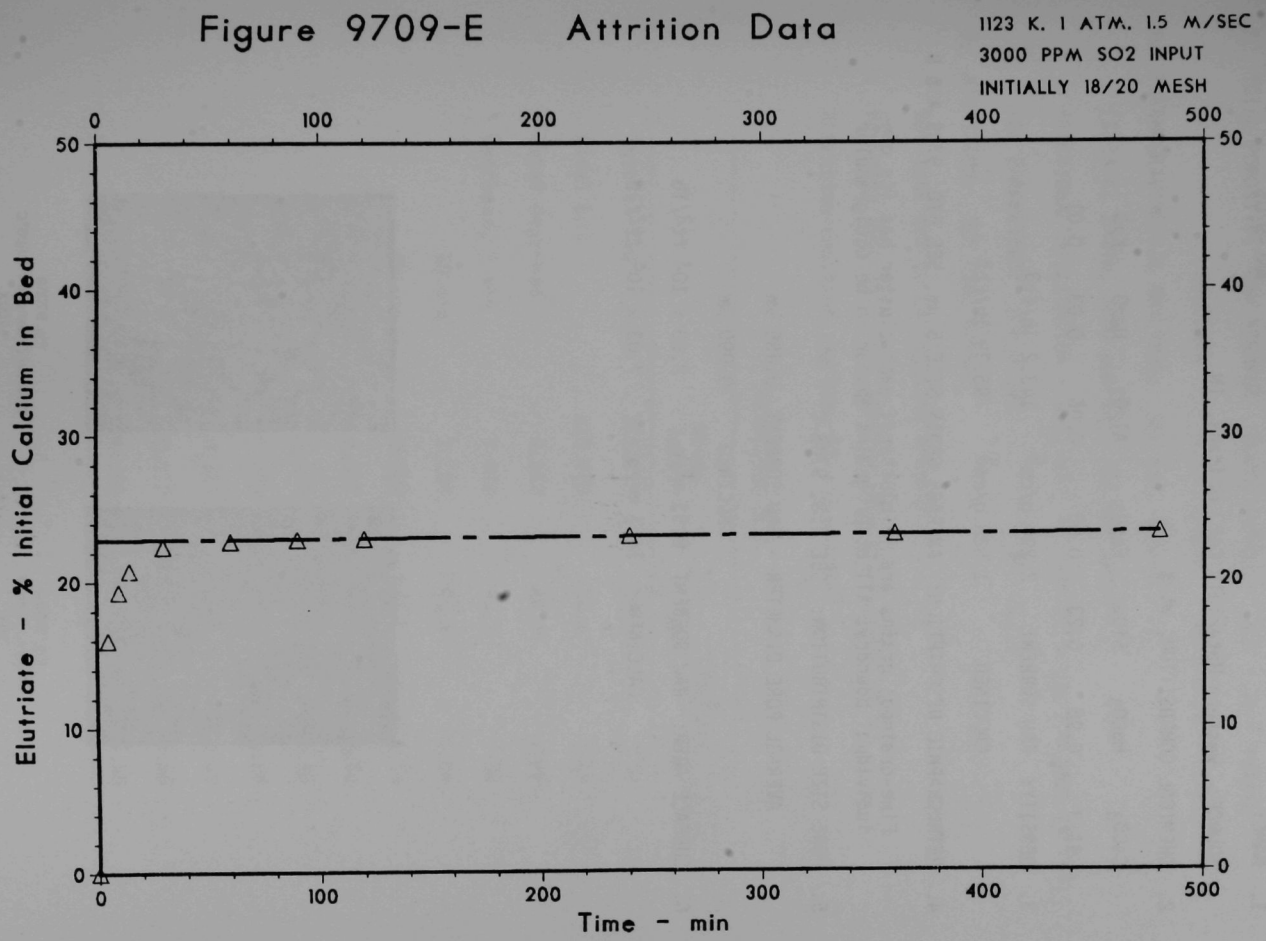

1. NAME: ANL-9705

SOURCE: Western Materials Co., Orleans, IN

2. CHEMICAL COMPOSITION, wt %

$CaCO_3$	$MgCO_3$	SiO_2	Fe_2O_3	Al_2O_3	Na_2O	K_2O
97.3	0.98	0.23	0.08	0.06	0.03	0.01

3. DENSITY: RAW SORBENT 2.294 g/cm^3 143.2 lb/ft^3

CALCINED 1.528 g/cm^3 95.39 lb/ft^3

4. PETROGRAPHIC DESCRIPTION: AVERAGE GRAIN SIZE 5 μm, SEE FIG. 9705 A & B

Fine-grained; grains are in clusters; each cluster has its own individual boundry; all other grains appear to be equigranular

5. PORE SIZE DISTRIBUTION: SEE FIG. 9705-C

AVERAGE PORE DIAMETER - RAW SORBENT 0.406 μm

CALCINED 0.090 μm

6. SURFACE AREA: RAW SORBENT 0.53 m^2/g 2.60 x 10^3 ft^2/lb

CALCINED 14.4 m^2/g 7.03 x 10^4 ft^2/lb

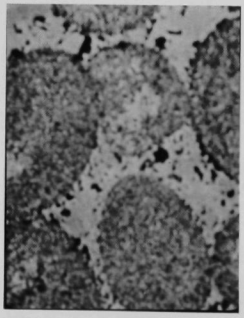

Fig. 9705A
Raw Limestone
50X

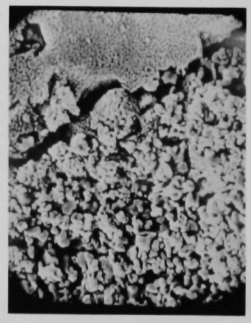

Fig. 9705B
Calcined Limestone 1 h 850°C
1100X

7. TOTAL POROSITY: RAW SORBENT 0.059 cm^3/g 9.4×10^{-4} ft^3/lb

CALCINED 0.330 cm^3/g 5.29×10^{-3} ft^3/lb

8. THERMOGRAVIMETRIC ANALYSIS: SEE FIG. 9705-D

(1123 K, 1 atm, 3000 ppm SO_2, -18 +20 mesh)

FRACTIONAL UTILIZATION = $\alpha(t, min) = 0.336 [1 - exp (-0.0621 t^{0.744})]$

ANL PARAMETERS: D = 0.309 b = 267.9

9. ATTRITION: SEE FIG. 9705-E

Bed loss due to calcination breakup (%) = 2.5

Bed mass lost in linear portion (%/min.) = 8.7×10^{-4}

Attrition constant, λ_4 (sec^{-1}) = 2.1×10^{-7}

ATTRITION DATA

	Grams Total	wt % Ca	wt % S
Initial Bed	161.051	38.92	0.00
Final Bed	118.485	51.2	9.19
Total Overhead	4.522	40.4	5.56
Overhead, 5 min	1.510	40.4	5.56
10 min	1.100	40.4	5.56
30 min	0.502	40.4	5.56
1 h	0.328	40.4	5.56
1.5 h	0.109	40.4	5.56
2 h	0.093	40.4	5.56
4 h	0.161	40.4	5.56
6 h	0.172	40.4	5.56
8 h	0.161	40.4	5.56

Attrition Data, continued for Sorbent 9705

Weight in Grams, Particle Diameter, μm

Sample	-1000 +840	-841 +707	-707 +595	-595 +420	-420 +297	-297 +250
Overhead, first 30 min	0.000	0.000	0.000	0.040	0.704	0.191
Overhead, remaining 7.5 h	0.000	0.000	0.000	0.005	0.148	0.161
Final Bed, post test	105.327	5.289	1.786	2.343	2.491	0.442

Sample	-250 +210	-210 +74	-74 +63	-63 +53	-53 +44	-44 +37	-37 +0
Overhead, first 30 min	0.355	1.699	0.047	0.104	0.156	0.178	0.142
Overhead, remaining 7.5 h	0.146	0.611	0.019	0.036	0.055	0.038	0.026
Final Bed, post test	0.237	0.586	0.011	0.022	0.019	0.008	0.000

Figure 9705-C
Pore Size Distribution

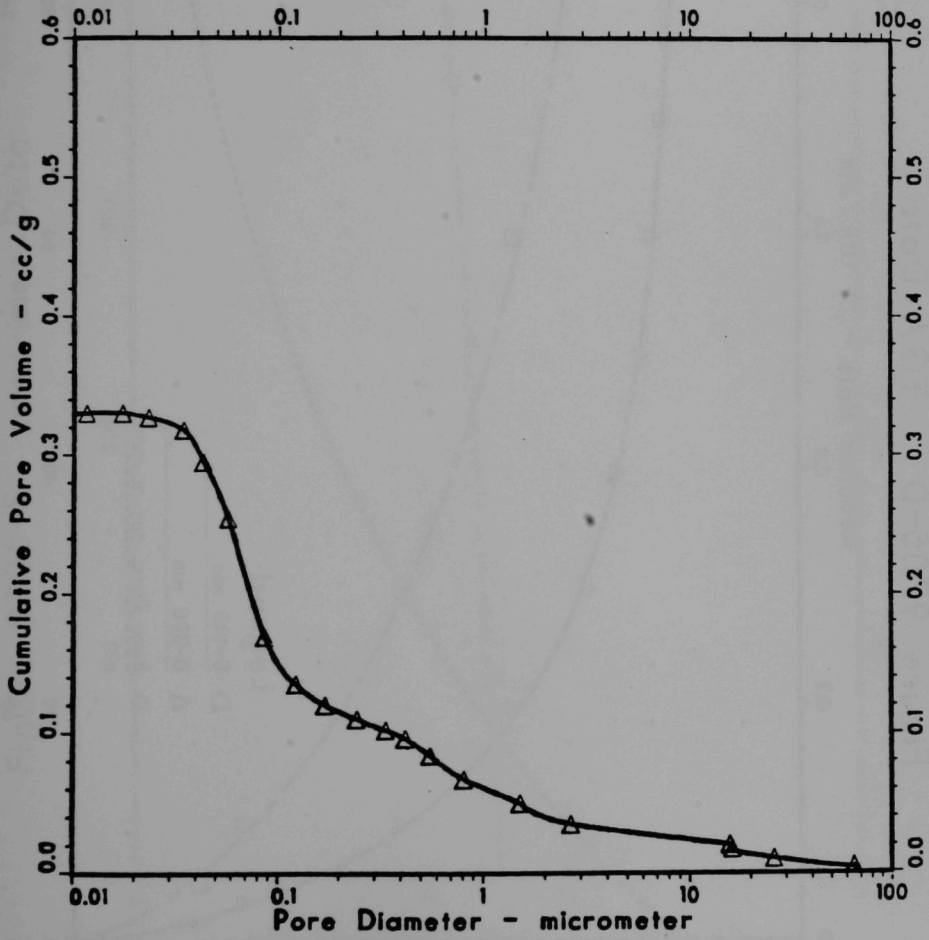

Figure 9705-D TGA Data

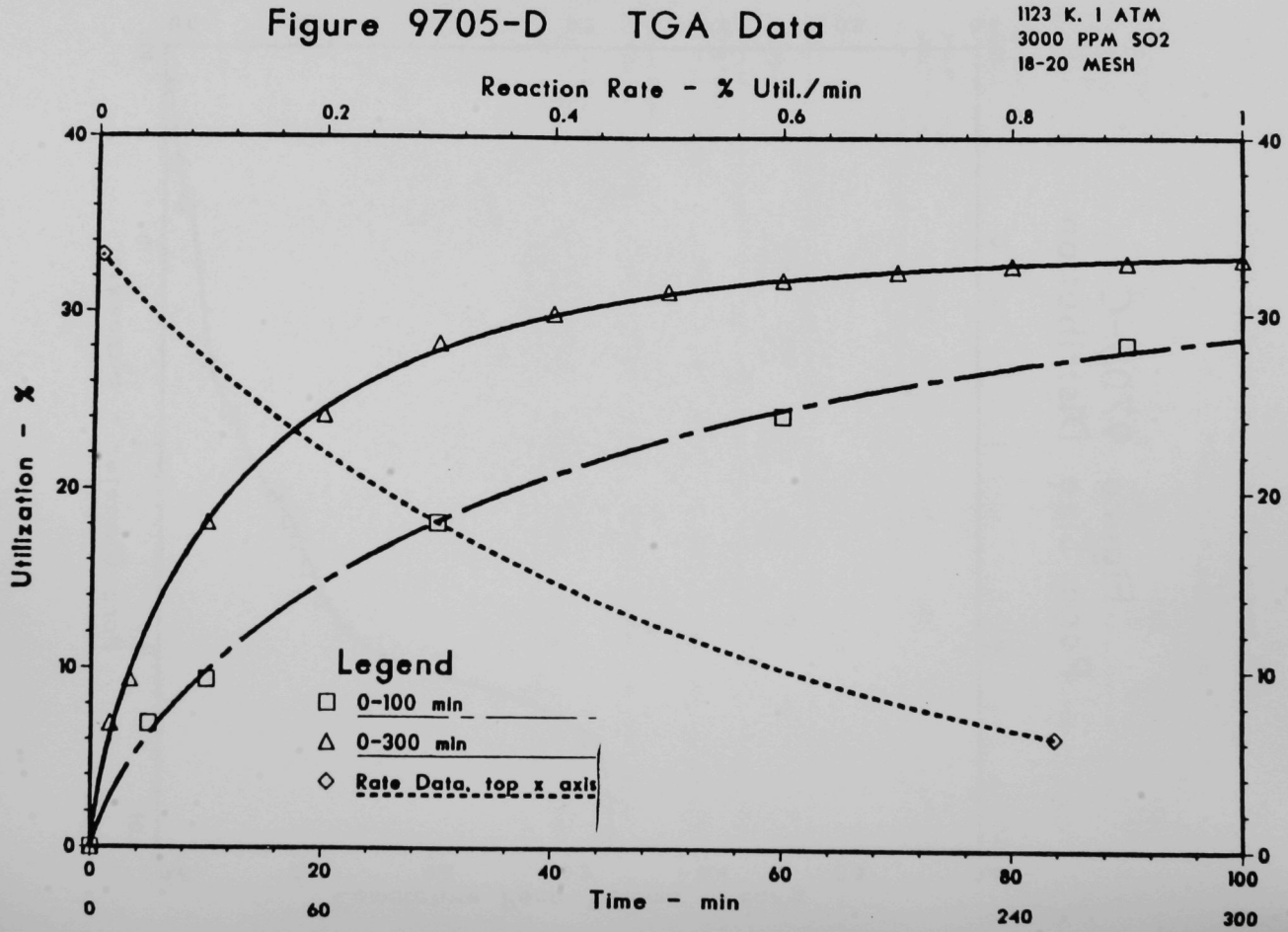

Figure 9705-E Attrition Data

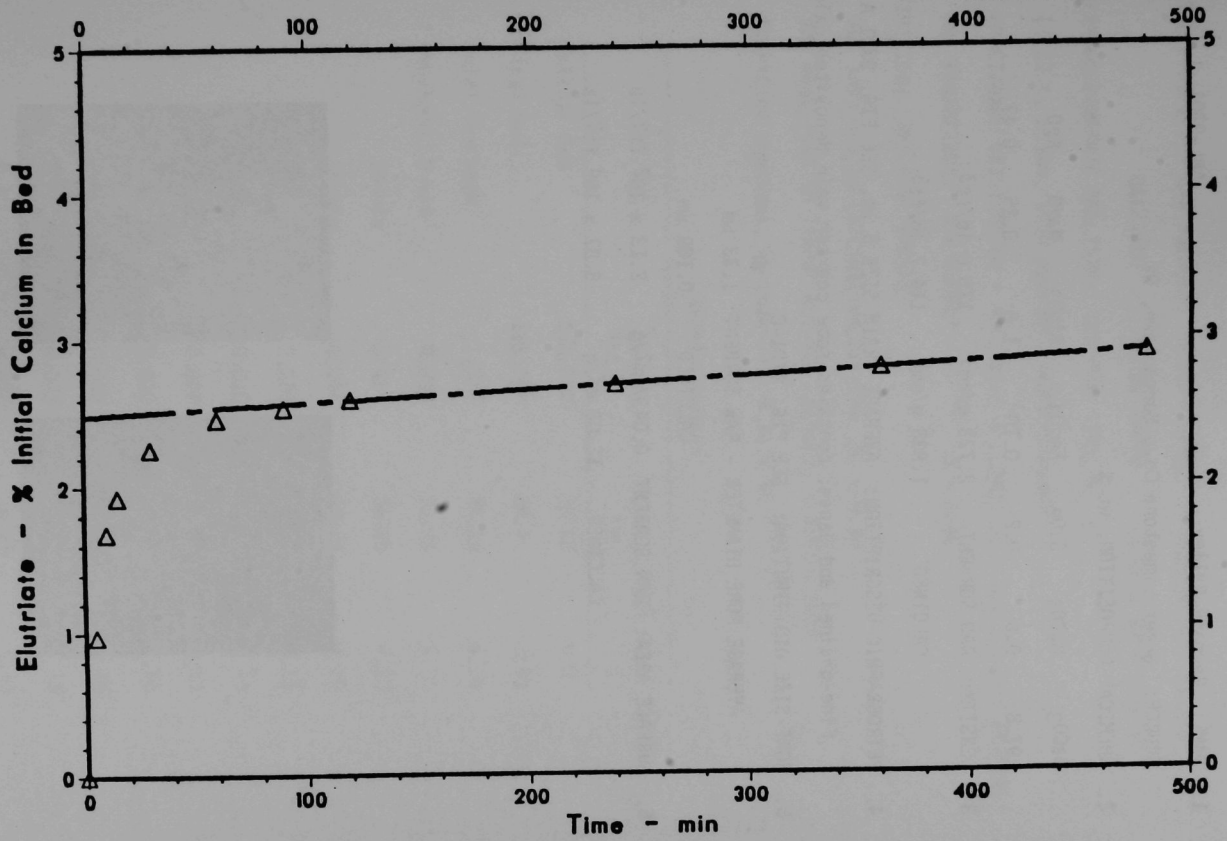

1. NAME: Germany Valley ANL-9701

   SOURCE: Greer Limestone Co., Morgantown, WV

2. CHEMICAL COMPOSITION, wt %

$CaCO_3$	$MgCO_3$	SiO_2	Fe_2O_3	Al_2O_3	Na_2O	K_2O
97.8	0.6	0.2	0.10	1.8	0.25	0.47

3. DENSITY: RAW SORBENT 2.723 g/cm^3 170.0 lb/ft^3

   CALCINED 1.838 g/cm^3 114.7 lb/ft^3

4. PETROGRAPHIC DESCRIPTION: AVERAGE GRAIN SIZE 5 μm, SEE FIG. 9701 A & B

   Fine-grained and dense; contains some coarser vein deposited calcite.

5. PORE SIZE DISTRIBUTION: SEE FIG. 9701-C

   AVERAGE PORE DIAMETER - RAW SORBENT 1.33 μm

   CALCINED 0.109 μm

6. SURFACE AREA: RAW SORBENT 0.0437 m^2/g 2.13 x 10^2 ft^2/lb

   CALCINED 12.02 m^2/g 5.87 x 10^4 ft^2/lb

Fig. 9701A
Raw Limestone
50X

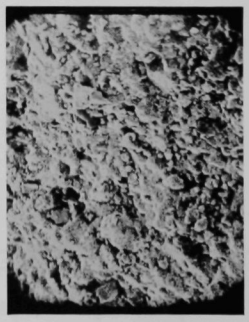

Fig. 9701B
Calcined Limestone 1 h 850°C
1100X

7. TOTAL POROSITY: RAW SORBENT 0.0194 cm^3/g 3.11×10^{-4} ft^3/lb

CALCINED 0.351 cm^3/g 5.62×10^{-3} ft^3/lb

8. THERMOGRAVIMETRIC ANALYSIS: SEE FIG. 9701-D

(1123 K, 1 atm, 3000 ppm SO_2, -18 +20 mesh)

FRACTIONAL UTILIZATION = $\alpha(t, \text{min}) = 0.0874\ [1 - \exp(-0.207\ t^{0.520})]$

ANL PARAMETERS: D = 0.0607 b = 1266

9. ATTRITION: SEE FIG. 9701-E

Bed loss due to calcination breakup (%) = 0.60

Bed mass lost in linear portion (%/min.) = 3.83×10^{-4}

Attrition constant, λ_4 (sec^{-1}) = 8.81×10^{-8}

ATTRITION DATA

	Grams Total	wt % Ca	wt % S
Initial Bed	160.000	39.12	0.0
Final Bed	106.765	58.2	3.93
Total Overhead	1.355	36.25	4.15
Overhead, 5 min	0.395	36.25	4.15
10 min	0.415	36.25	4.15
15 min	0.094	36.25	4.15
30 min	0.083	36.25	4.15
1 h	0.052	36.25	4.15
1.5 h	0.027	36.25	4.15
2 h	0.030	36.25	4.15
4 h	0.089	36.25	4.15
6 h	0.072	36.25	4.15
8 h	0.098	36.25	4.15

Attrition Data, continued for Sorbent 9701

Weight in Grams, Particle Diameter, μm

Sample	-1000 +840	-841 +707	-707 +595	-595 +420	-420 +297	-297 +250
Overhead, first 30 min	0.001	0.001	0.001	0.001	0.002	0.004
Overhead, remaining 7.5 h	0.001	0.001	0.000	0.002	0.005	0.005
Final Bed, post test	96.695	2.399	0.332	0.269	0.286	0.066

Sample	-250 +210	-210 +74	-74 +63	-63 +53	-53 +44	-44 +37	-37 +0
Overhead, first 30 min	0.020	0.292	0.006	0.032	0.043	0.039	0.029
Overhead, remaining 7.5 h	0.002	0.135	0.004	0.008	0.004	0.004	0.000
Final Bed, post test	0.076	0.320	0.027	0.002	0.014	0.000	0.000

10. OTHER DATA: TGA data: 1123 K, 1 atm, 3000 ppm SO_2

See Fig. 9701-F $\alpha(t, \text{min}) = 0.3695\,[1 - \exp(-0.0798\, t^{0.7741})]$

-50 +70 mesh $D = 0.3577$ $b = 426$

See Fig. 9701-G $\alpha(t, \text{min}) = 0.595\,[1 - \exp(-0.0346\, t^{0.770})]$

-140 +170 mesh $D = 0.555$ $b = 176$

Figure 9701-C
Pore Size Distribution

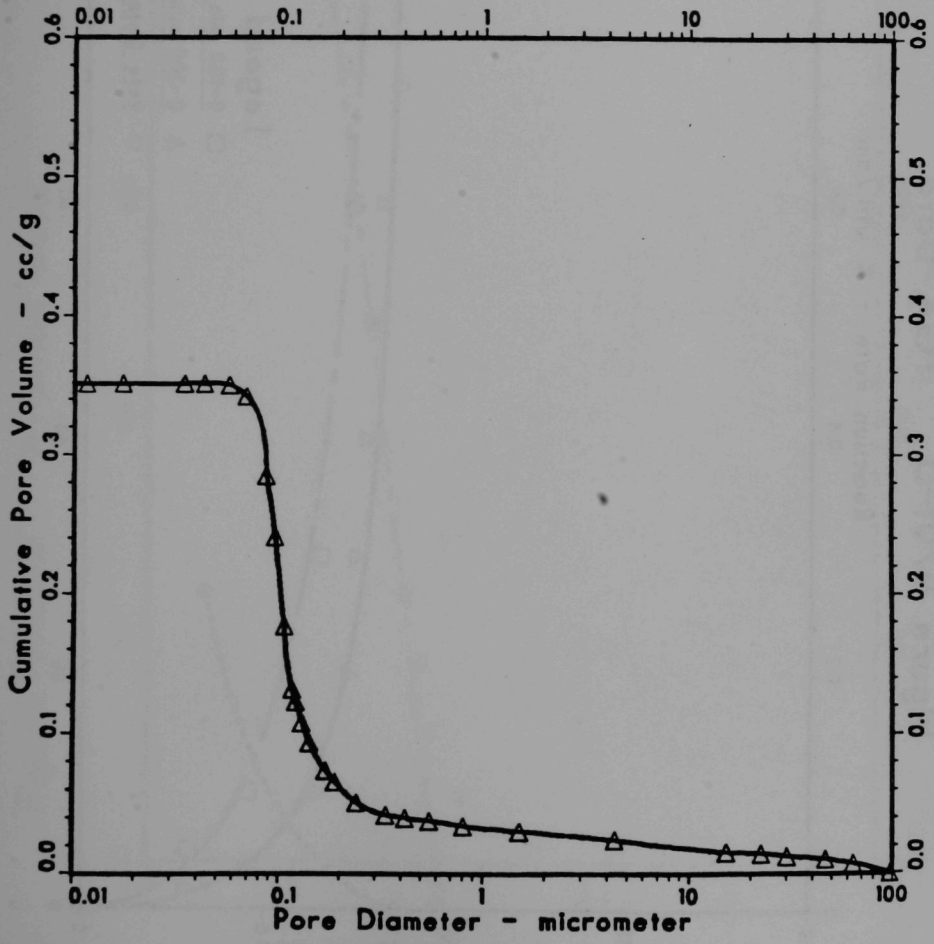

Figure 9701-D TGA Data

1123 K. 1 ATM
3000 PPM SO2
18-20 MESH

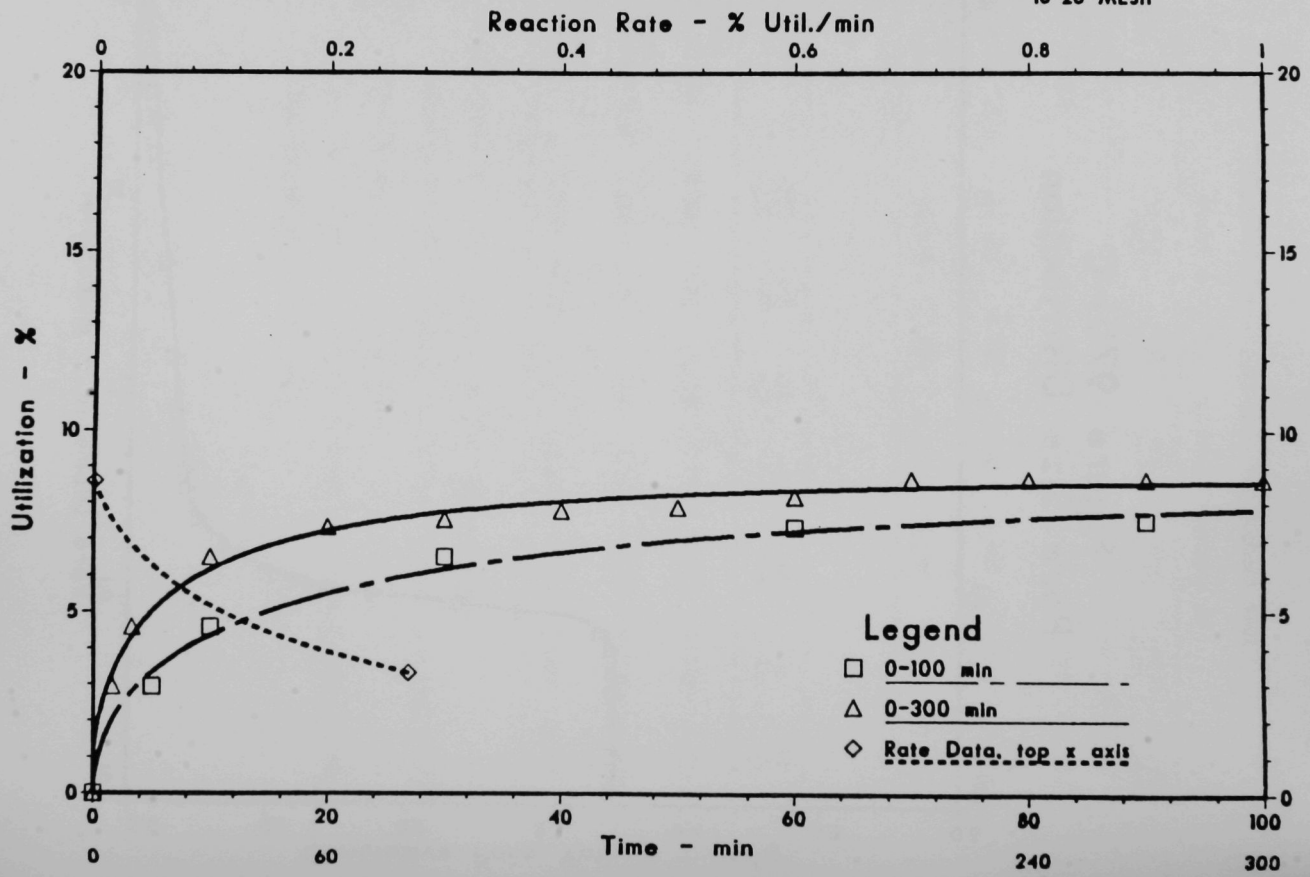

Figure 9701-E Attrition Data

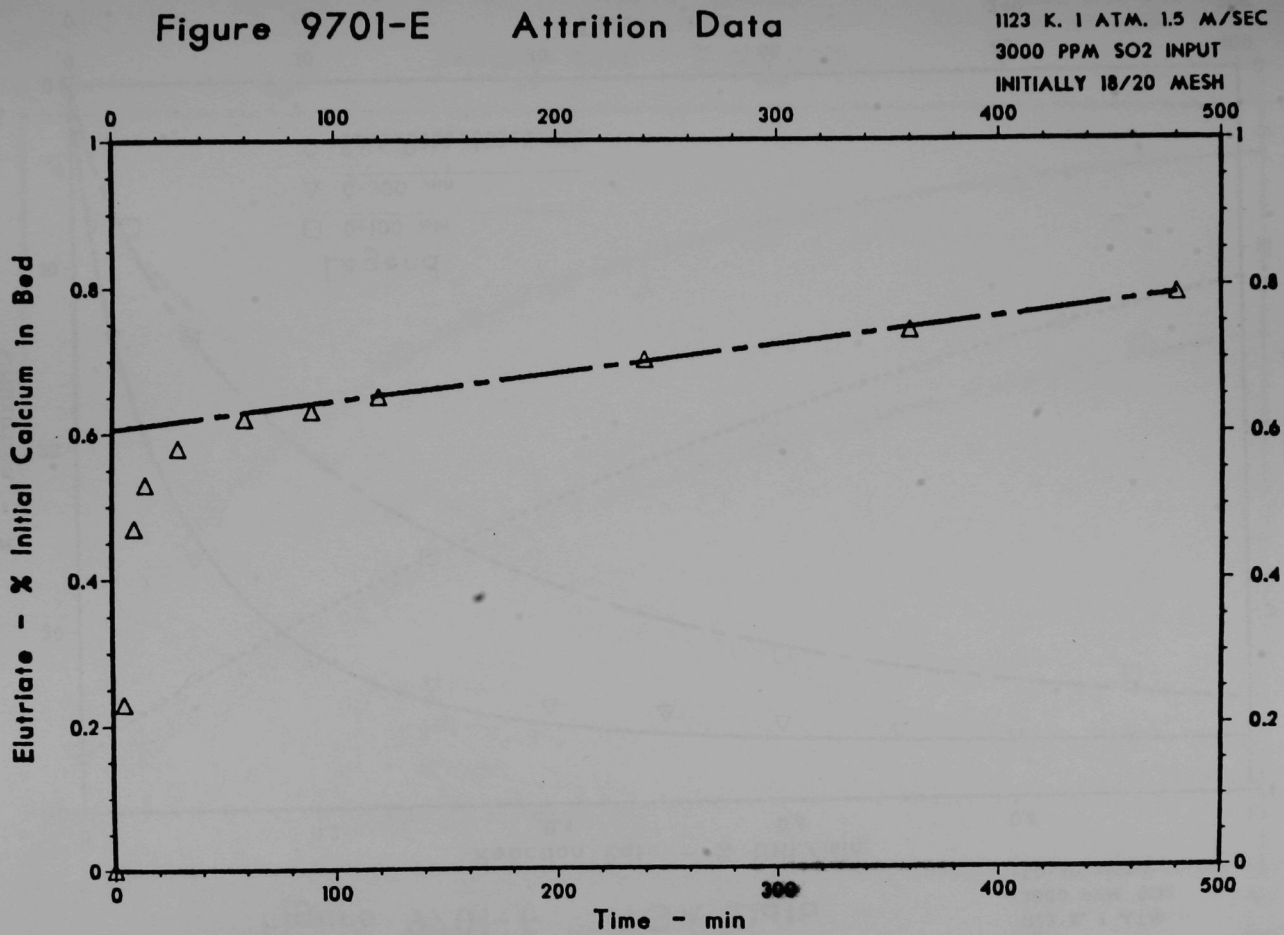

Figure 9701-F TGA Data

1123 K. 1 ATM
3000 PPM SO2
50-70 MESH

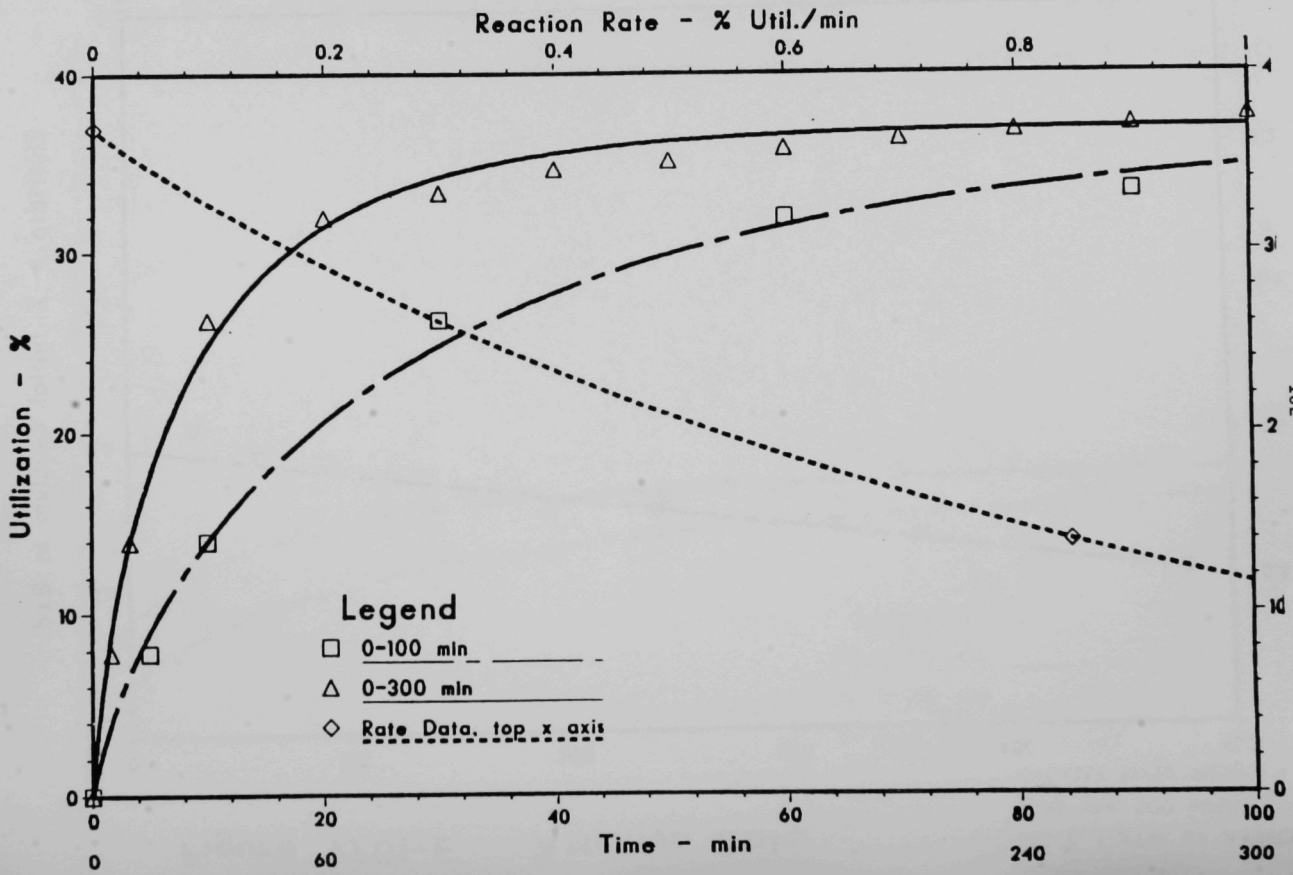

Figure 9701-G TGA Data

1123 K. 1 ATM
3000 PPM SO2
140-170 MESH

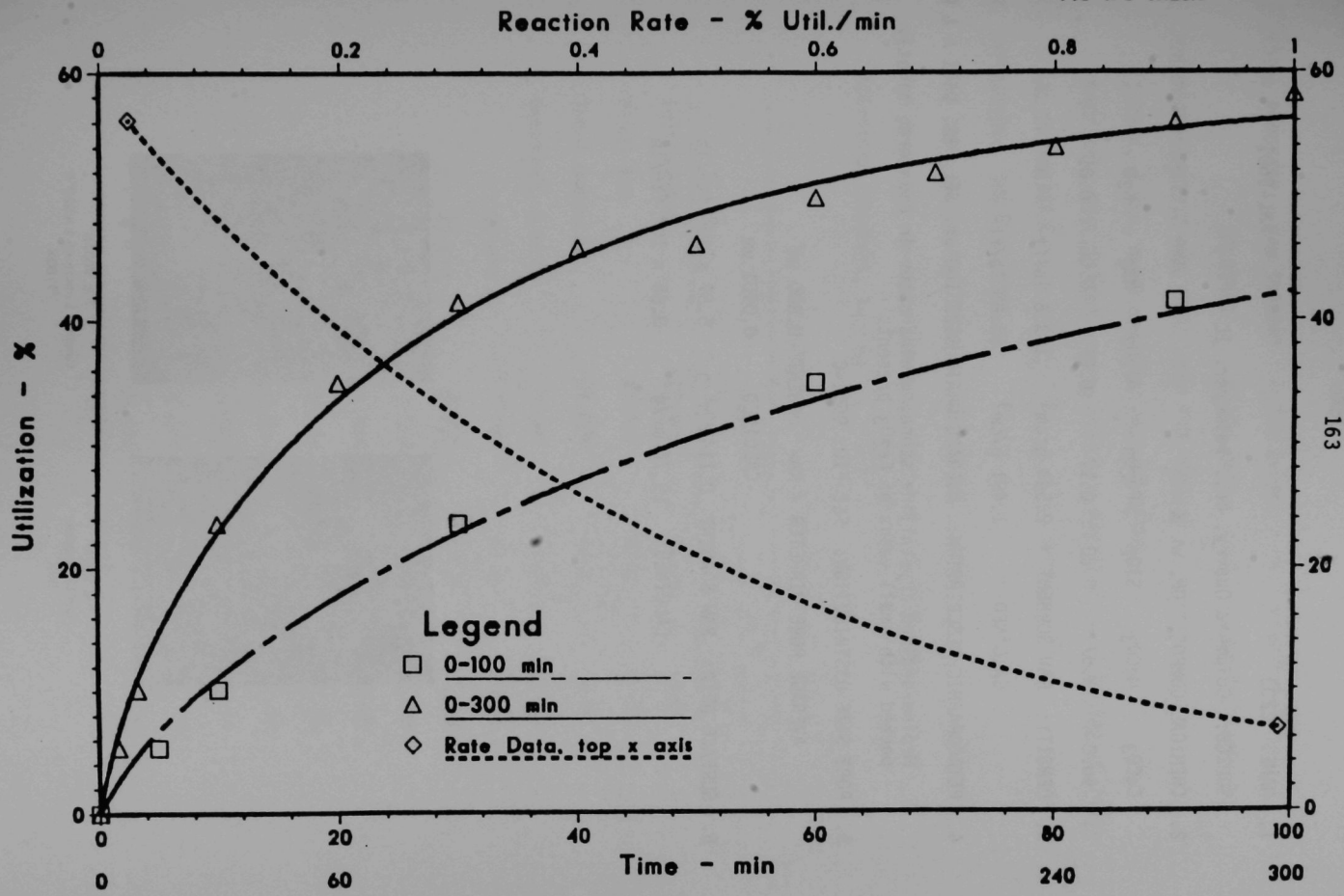

1. NAME: 2203 ANL-9601

SOURCE: Columbia Quarry, Co., Valmeyer, IL

2. CHEMICAL COMPOSITION, wt %

$CaCO_3$	$MgCO_3$	SiO_2	Fe_2O_3	Al_2O_3	Na_2O	K_2O
96.0	3.57	0.20	0.17	<0.01	0.05	0.01

3. DENSITY: RAW SORBENT 2.544 g/cm^3 158.8 lb/ft^3

CALCINED 1.491 g/cm^3 93.08 lb/ft^3

4. PETROGRAPHIC DESCRIPTION: AVERAGE GRAIN SIZE 100 μm, SEE FIG. 9601 A & B

Medium-grained crystalline stone; grains occur in clusters; tightly packed with small veins of Fe_2O_3 present.

5. PORE SIZE DISTRIBUTION: SEE FIG. 9601-C

AVERAGE PORE DIAMETER - RAW SORBENT 0.800 μm

CALCINED 0.0901 μm

6. SURFACE AREA: RAW SORBENT 0.1141 m^2/g 5.57 x 10^2 ft^2/lb

CALCINED 19.76 m^2/g 9.65 x 10^4 ft^2/lb

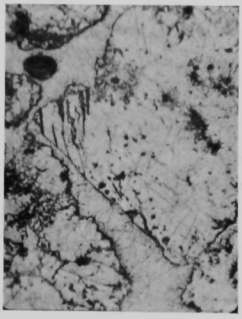

Fig. 9601A
Raw Limestone
50X

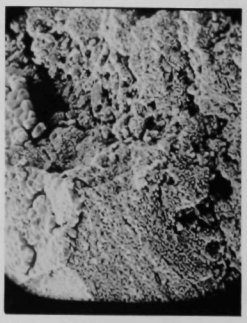

Fig. 9601B
Calcined Limestone 1 h 850°C
1100X

7. TOTAL POROSITY: RAW SORBENT 0.023 cm^3/g 3.7×10^{-4} ft^3/lb

CALCINED 0.454 cm^3/g 7.27×10^{-3} ft^3/lb

8. THERMOGRAVIMETRIC ANALYSIS: SEE FIG. 9601-D

(1123 K, 1 atm, 3000 ppm SO_2, -18 +20 mesh)

FRACTIONAL UTILIZATION = $\alpha(t, \text{min}) = 0.247\ [1 - \exp(-0.0702\ t^{0.744})]$

ANL PARAMETERS: D = 0.222 b = 377.2

9. ATTRITION: SEE FIG. 9601-E

Bed loss due to calcination breakup (%) = 18.0

Bed mass lost in linear portion (%/min.) = 1.95×10^{-3}

Attrition constant, λ_4 (sec^{-1}) = 5.74×10^{-7}

ATTRITION DATA

	Grams Total	wt % Ca	wt % S
Initial Bed	160.733	38.60	0.0
Final Bed	88.009	58.0	7.10
Total Overhead	24.684	47.2	1.98
Overhead, 5 min	9.158	47.2	1.98
10 min	7.226	47.2	1.98
15 min	2.217	47.2	1.98
30 min	3.163	47.2	1.98
1 h	1.014	47.2	1.98
1.5 h	0.302	47.2	1.98
2 h	0.652	47.2	1.98
4 h	0.503	47.2	1.98
6 h	0.251	47.2	1.98
8 h	0.198	47.2	1.98

Attrition Data, continued for Sorbent 9601

Weight in Grams, Particle Diameter, μm

Sample	-1000 +840	-841 +707	-707 +595	-595 +420	-420 +297	-297 +250
Overhead, first 30 min	0.000	0.003	0.005	0.004	0.052	0.172
Overhead, remaining 7.5 h	0.001	0.000	0.001	0.004	0.182	0.512
Final Bed, post test	50.647	11.550	6.385	7.260	7.106	2.415

Sample	-250 +210	-210 +74	-74 +63	-63 +53	-53 +44	-44 +37	-37 +0
Overhead, first 30 min	1.016	12.751	0.048	0.564	1.377	0.516	1.504
Overhead, remaining 7.5 h	1.414	2.313	0.017	0.097	0.169	0.102	0.232
Final Bed, post test	1.973	0.529	0.004	0.013	0.012	0.003	0.009

10. OTHER DATA

See Figs. 9601-F and 9601-G for decrepitation data.

Figure 9601-C
Pore Size Distribution

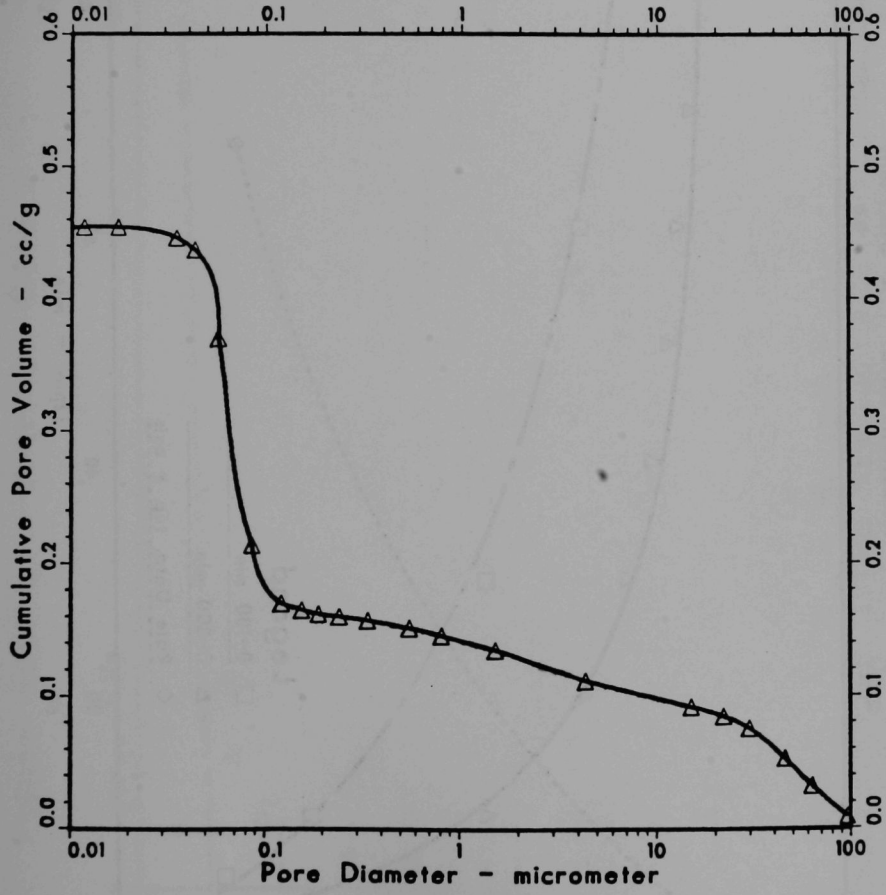

Figure 9601-D TGA Data

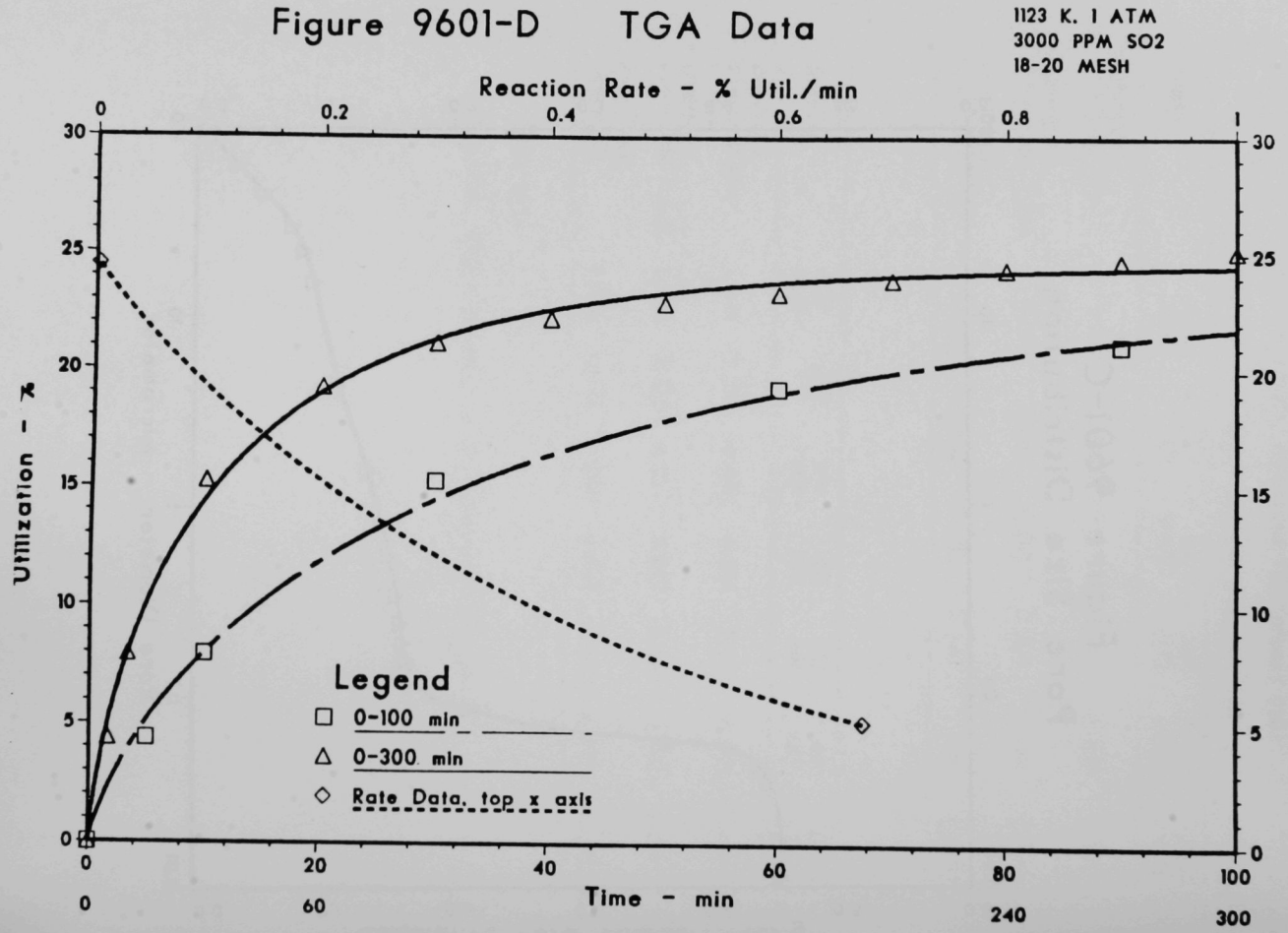

Figure 9601-E Attrition Data

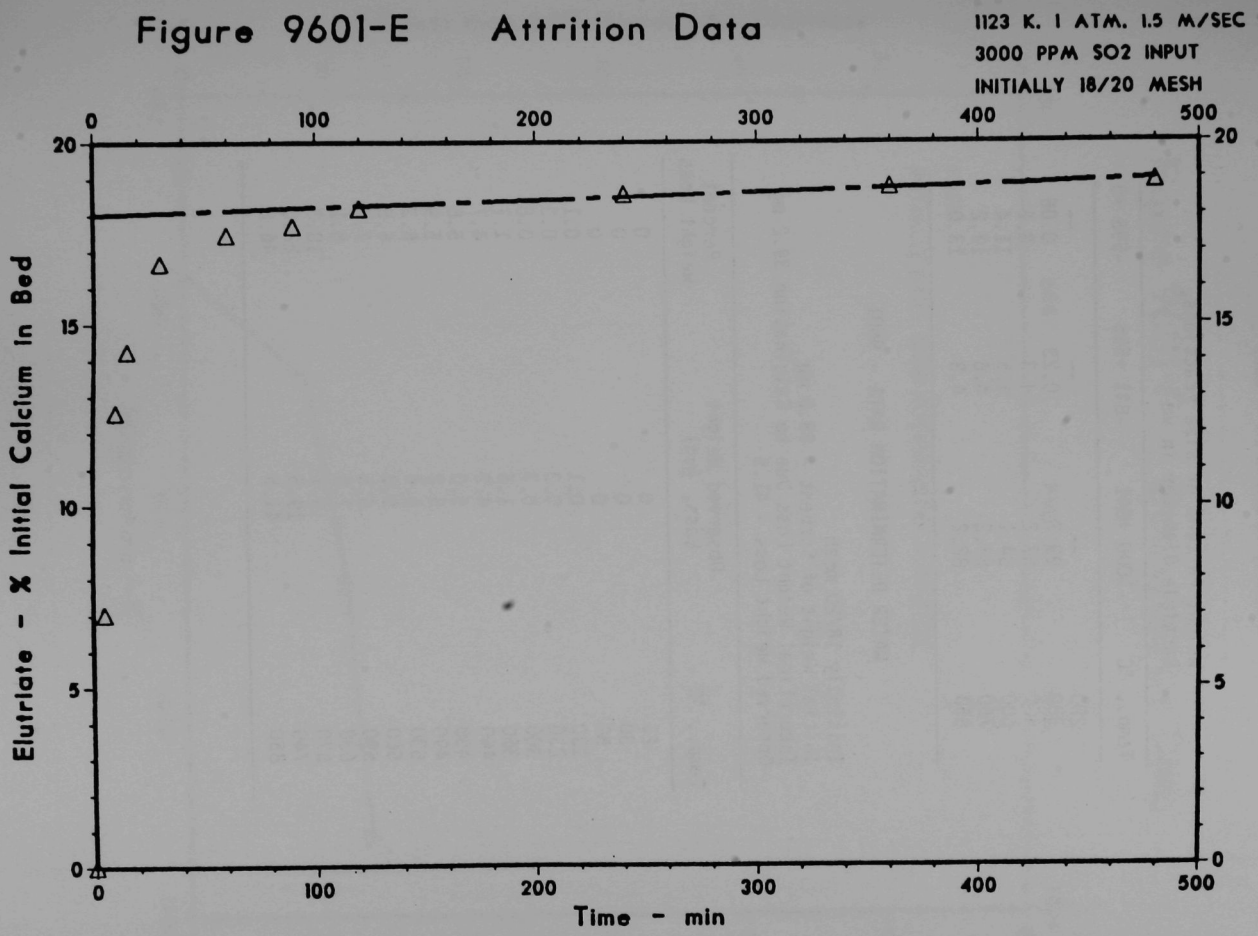

DECREPITATION DATA - 9601

Temp., °C	Weight Percent of Size Fractions, Particle Diameter in μm -1000 +841	-841 +595	-595 +0
200	--	--	--
300	99.7	0.23	0.06
400	87.2	4.3	8.5
600	84.1	4.5	11.4
750	83.2	4.6	12.2
850	82.2	4.8	13.0

WATER DETERMINATION DATA - 9601

Initially 18/20 mesh
Initial Weight of Sorbent - 88.6 mg
Theoretical Weight Loss Due to Calcination 39.2 mg
Observed Weight Loss - 41.5

Temp., °C	Observed Weight Loss, (mg)	Percent Weight Loss
25	0	0
30	0	0
80	0	0
130	0.1	0.1
230	0.3	0.3
300	0.7	0.8
350	1.5	1.7
400	4.2	4.7
450	5.0	5.6
490	5.2	5.9
530	5.6	6.3
560	5.8	6.5
590	6.5	7.3
630	7.2	8.1
670	9.1	10.3
740	19.5	22.0
850	41.5	46.8

Figure 9601-F Decrepitation Data

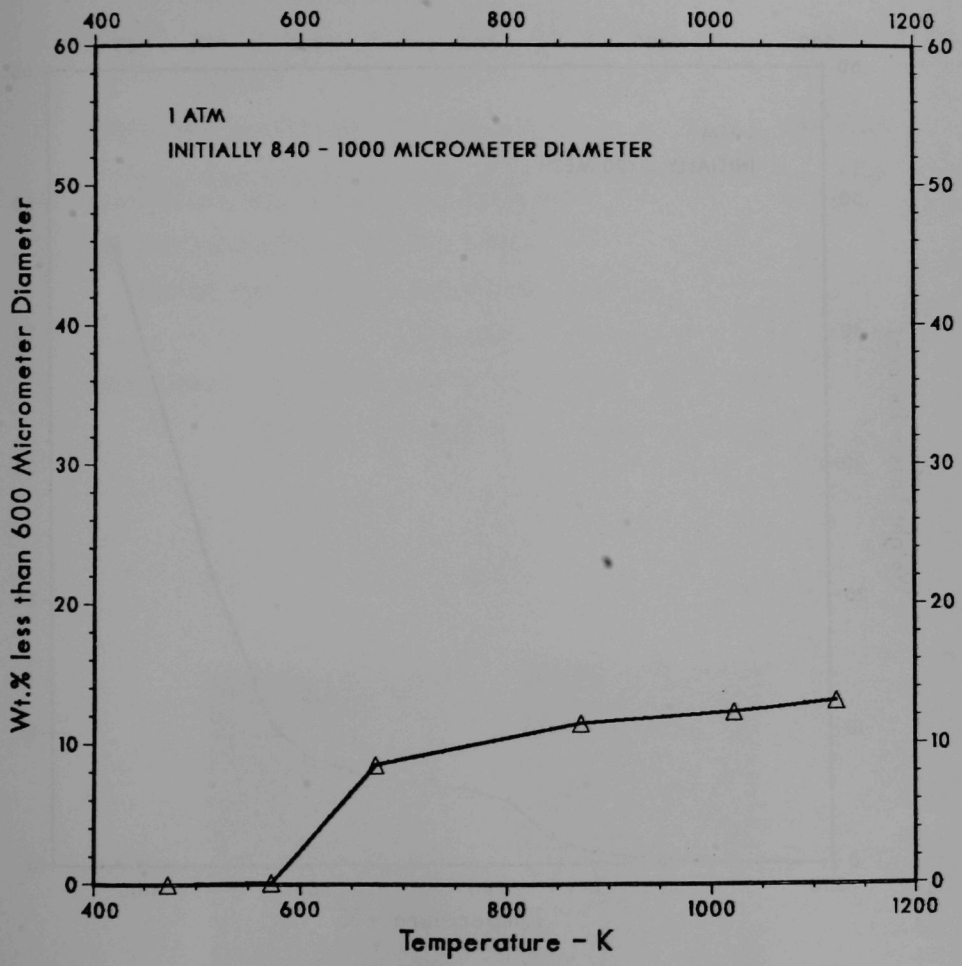

Figure 9601-G Water Loss Data

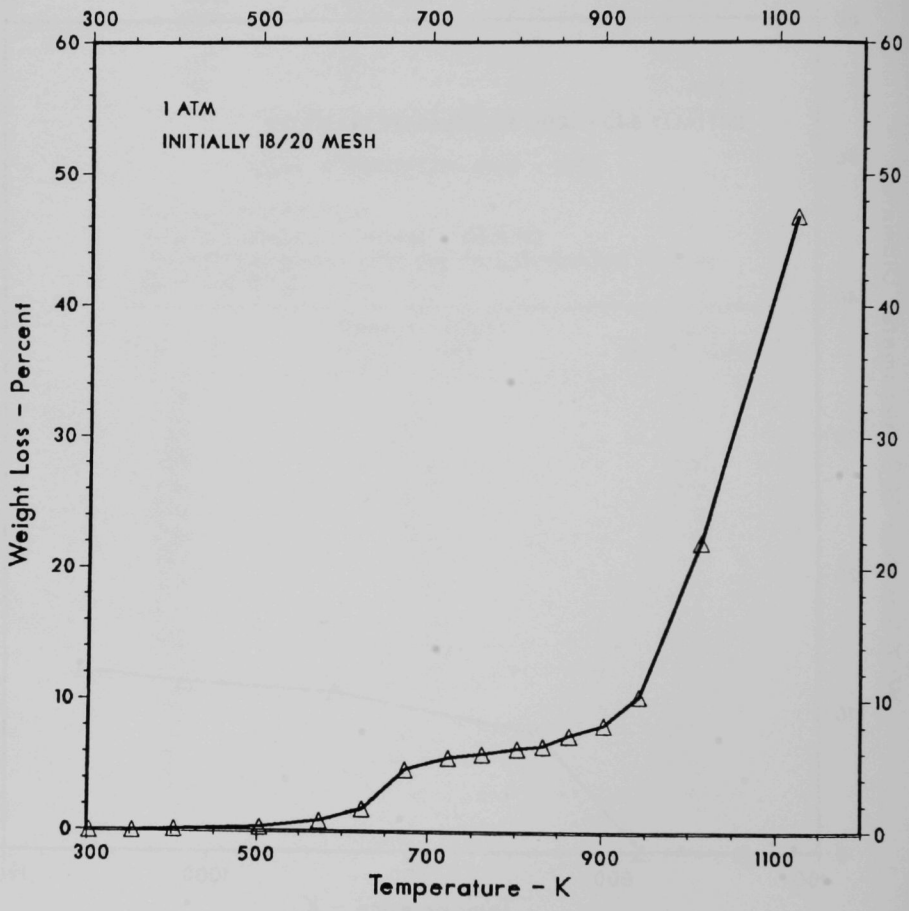

1. NAME: ANL-9504

   SOURCE: Rose Equipment, Inc., Weeping Water, NE

2. CHEMICAL COMPOSITION, wt %

$CaCO_3$	$MgCO_3$	SiO_2	Fe_2O_3	Al_2O_3	Na_2O	K_2O
95.8	0.58	2.71	0.30	0.36	0.05	0.13

3. DENSITY: RAW SORBENT 2.367 g/cm^3 147.8 lb/ft^3

   CALCINED 1.679 g/cm^3 104.8 lb/ft^3

4. PETROGRAPHIC DESCRIPTION: AVERAGE GRAIN SIZE 8 μm, SEE FIG. 9504 A & B

   Fine grained with veins of coarse-grains throughout the stone; fine grains are loosely packed and equigranular.

5. PORE SIZE DISTRIBUTION: SEE FIG. 9504-C

   AVERAGE PORE DIAMETER - RAW SORBENT 0.532 μm

   CALCINED 0.124 μm

6. SURFACE AREA: RAW SORBENT 0.47 m^2/g 2.31 x 10^3 ft^2/lb

   CALCINED 11.26 m^2/g 5.50 x 10^4 ft^2/lb

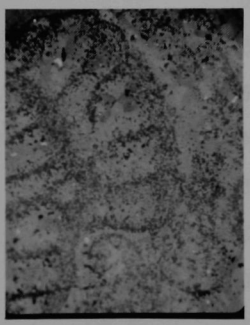

Fig. 9504A
Raw Limestone
50X

Fig. 9504B
Calcined Limestone 1 h 850°C
1100X

7. TOTAL POROSITY: RAW SORBENT 0.068 cm^3/g 1.1×10^{-3} ft^3/lb

CALCINED 0.351 cm^3/g 5.627×10^{-3} ft^3/lb

8. THERMOGRAVIMETRIC ANALYSIS: SEE FIG. 9504-D

(1123 K, 1 atm, 3000 ppm SO_2, -18 +20 mesh)

FRACTIONAL UTILIZATION = $\alpha(t, min) = 0.382 [1 - exp (-0.0484 t^{0.818})]$

ANL PARAMETERS: D = 0.366 b = 265.6

9. ATTRITION: SEE FIG. 9504-E

Bed loss due to calcination breakup (%) = 0.52

Bed mass lost in linear portion (%/min.) = 5.5×10^{-3}

Attrition constant, λ_4 (sec^{-1}) = 1.3×10^{-7}

ATTRITION DATA

	Grams Total	wt %	
		Ca	S
Initial Bed	160.951	38.32	0.00
Final Bed	111.367	53.1	7.24
Total Overhead	0.932	51.5	1.92
Overhead, 5 min	0.360	51.5	1.92
10 min	0.083	51.5	1.92
15 min	0.060	51.5	1.92
30 min	0.065	51.5	1.92
1 h	0.046	51.5	1.92
1.5 h	0.034	51.5	1.92
2 h	0.055	51.5	1.92
4 h	0.073	51.5	1.92
6 h	0.090	51.5	1.92
8 h	0.067	51.5	1.92

Attrition Data, continued for Sorbent 9504

Weight in Grams, Particle Diameter, μm

Sample	-1000 +840	-841 +707	-707 +595	-595 +420	-420 +297	-297 +250
Overhead, first 30 min	0.000	0.000	0.000	0.009	0.014	0.017
Overhead, remaining 7.5 h	0.000	0.000	0.000	0.000	0.013	0.015
Final Bed, post test	104.088	5.480	0.403	0.280	0.248	0.082

Sample	-250 +210	-210 +74	-74 +63	-63 +53	-53 +44	-44 +37	-37 +0
Overhead, first 30 min	0.023	0.192	0.046	0.028	0.038	0.026	0.013
Overhead, remaining 7.5 h	0.020	0.104	0.013	0.008	0.010	0.012	0.004
Final Bed, post test	0.106	0.400	0.013	0.051	0.076	0.058	0.034

Figure 9504-C
Pore Size Distribution

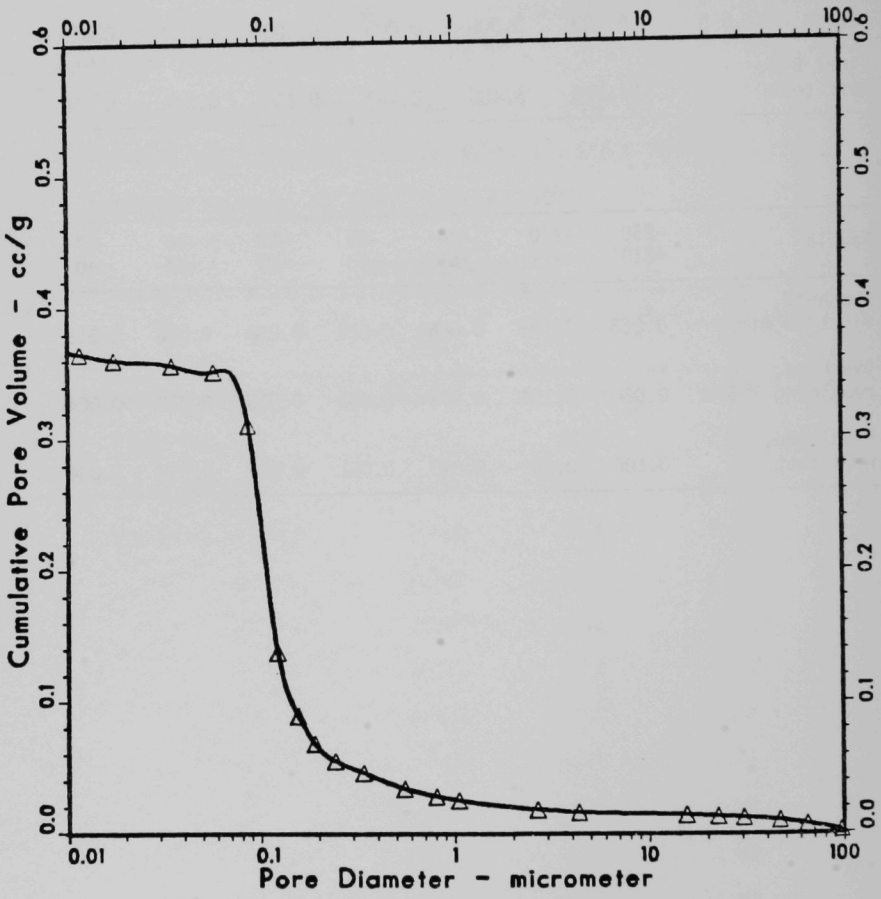

Figure 9504-D TGA Data

1123 K. 1 ATM
3000 PPM SO2
18-20 MESH

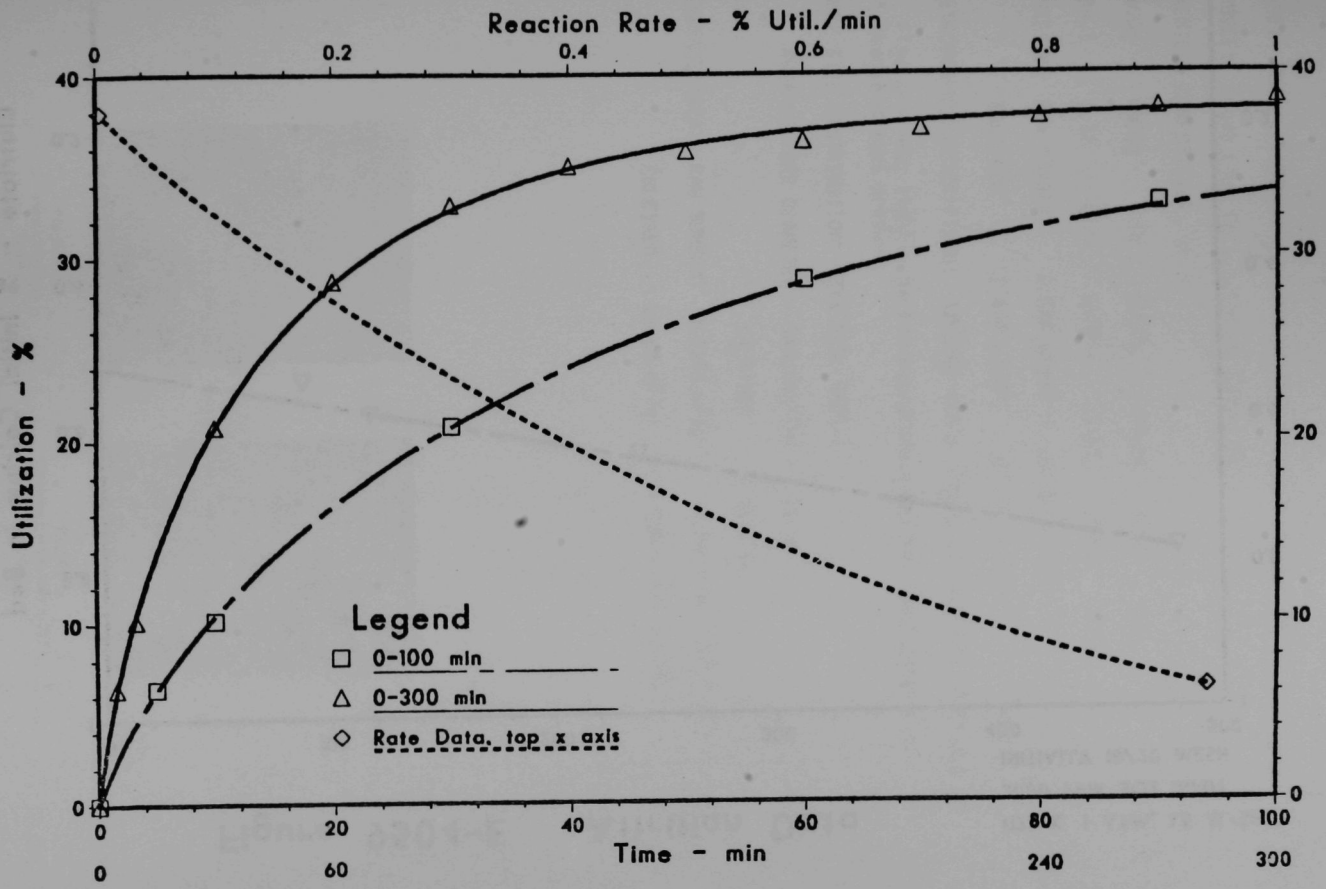

Figure 9504-E Attrition Data

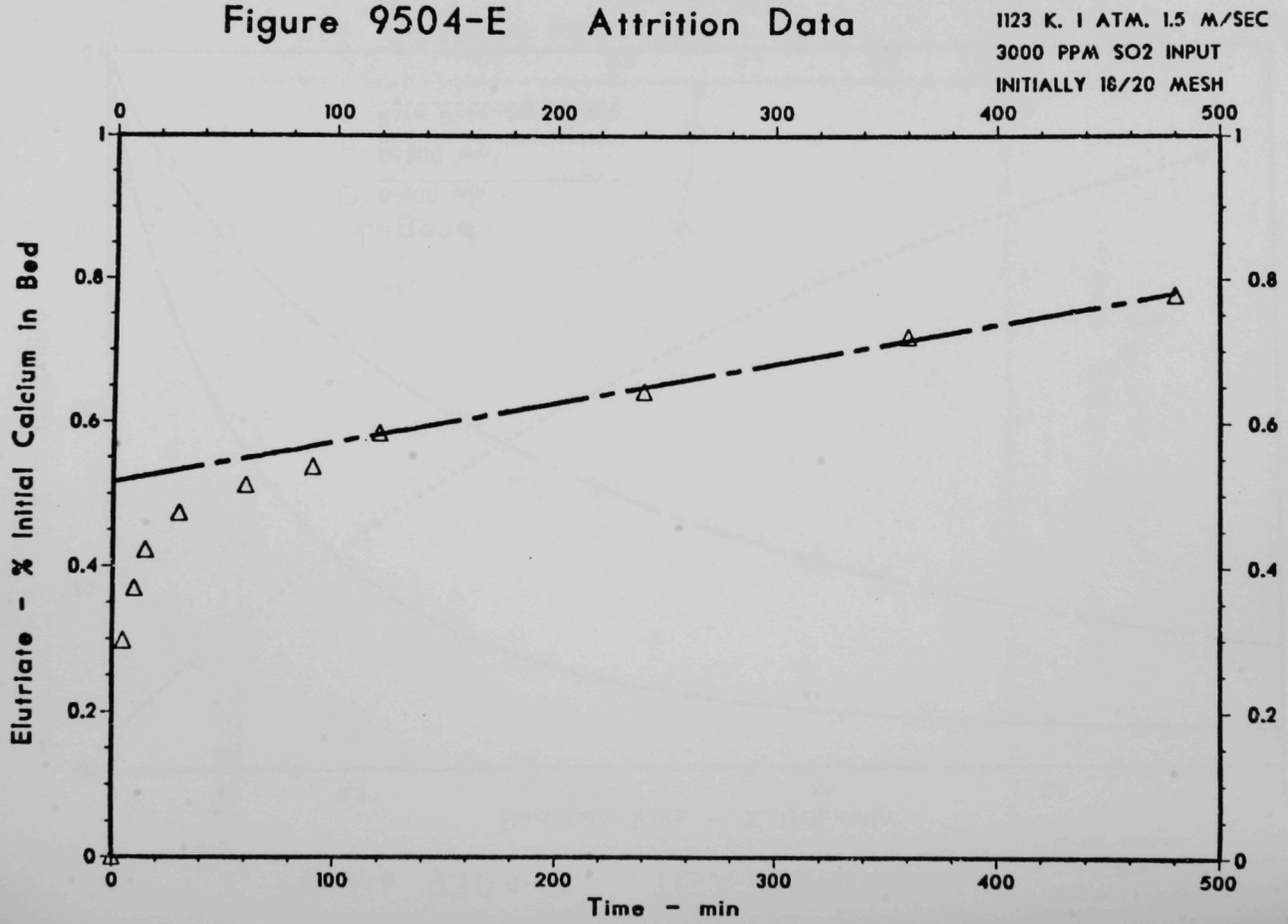

1. NAME: Grove, 1359 ANL-9501

   SOURCE: Grove Lime Co., Stephens City, VA

2. CHEMICAL COMPOSITION, wt %

$CaCO_3$	$MgCO_3$	SiO_2	Fe_2O_3	Al_2O_3	Na_2O	K_2O
95.3	1.32	0.77	0.09	0.25	0.03	0.06

3. DENSITY: RAW SORBENT 2.624 g/cm^3 163.8 lb/ft^3

   CALCINED 1.499 g/cm^3 93.58 lb/ft^3

4. PETROGRAPHIC DESCRIPTION: AVERAGE GRAIN SIZE 5 μm, SEE FIG. 9501 A & B

   Fine grained; tightly packed equigranular stone; some patches of coarse-grains present.

5. PORE SIZE DISTRIBUTION: SEE FIG. 9501-C

   AVERAGE PORE DIAMETER - RAW SORBENT 1.15 μm

   CALCINED 0.0964 μm

6. SURFACE AREA: RAW SORBENT 0.0868 m^2/g 4.24 x 10^2 ft^2/lb

   CALCINED 18.84 m^2/g 9.204 x 10^2 ft^2/lb

Fig. 9501A
Raw Limestone
50X

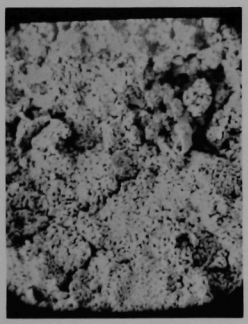

Fig. 9501B
Calcined Limestone 1 h 850°C
1100X

7. TOTAL POROSITY: RAW SORBENT 0.035 cm^3/g 5.6×10^{-3} ft^3/lb

CALCINED 0.375 cm^3/g 6.01×10^{-3} ft^3/lb

8. THERMOGRAVIMETRIC ANALYSIS: SEE FIG. 9501-D

(1123 K, 1 atm, 3000 ppm SO_2, -18 +20 mesh)

FRACTIONAL UTILIZATION = $\alpha(t, min) = 0.130 [1 - exp (-0.274 t^{0.495})]$

ANL PARAMETERS: D = 0.130 b = 945

9. ATTRITION: SEE FIG. 9501-E

Bed loss due to calcination breakup (%) = 0.48

Bed mass lost in linear portion (%/min.) = 2.90×10^{-4}

Attrition constant, λ_4 (sec^{-1}) = 6.66×10^{-8}

ATTRITION DATA

	Grams Total	wt % Ca	wt % S
Initial Bed	160.001	38.12	0.00
Final Bed	109.235	52.4	7.47
Total Overhead	1.086	34.93	3.22
Overhead, 5 min	0.220	34.93	3.22
10 min	0.270	34.93	3.22
15 min	0.151	34.93	3.22
30 min	0.145	34.93	3.22
1 h	0.055	34.93	3.22
1.5 h	0.028	34.93	3.22
2 h	0.036	34.93	3.22
4 h	0.046	34.93	3.22
6 h	0.057	34.93	3.22
8 h	0.078	34.93	3.22

Attrition Data, continued for Sorbent 9501

Weight in Grams, Particle Diameter, μm

Sample	-1000 +840	-841 +707	-707 +595	-595 +420	-420 +297	-297 +250
Overhead, first 30 min	0.001	0.000	0.000	0.001	0.004	0.007
Overhead, remaining 7.5 h	0.000	0.000	0.001	0.003	0.003	0.006
Final Bed, post test	105.746	1.193	1.165	0.995	0.089	0.007

Sample	-250 +210	-210 +74	-74 +63	-63 +53	-53 +44	-44 +37	-37 +0
Overhead, first 30 min	0.022	0.202	0.004	0.020	0.031	0.040	0.001
Overhead, remaining 7.5 h	0.020	0.154	0.002	0.016	0.020	0.017	0.006
Final Bed, post test	0.007	0.027	0.002	0.003	0.002	0.002	0.000

Figure 9501-C
Pore Size Distribution

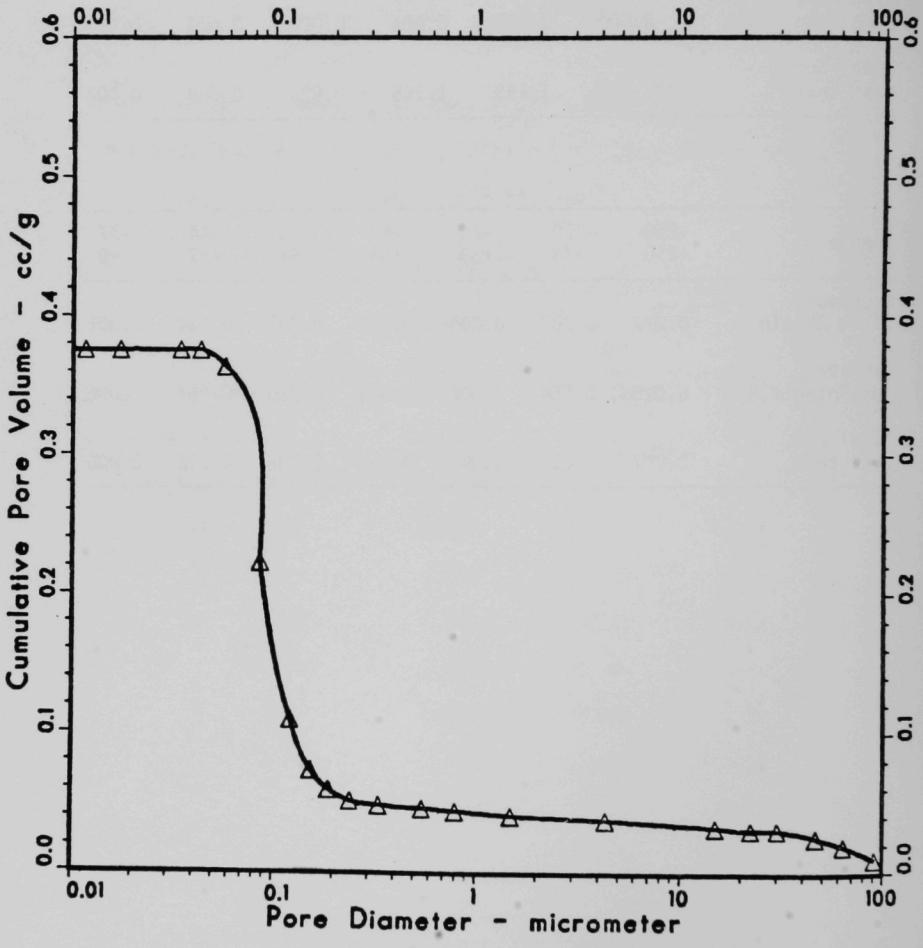

Figure 9501-D TGA Data

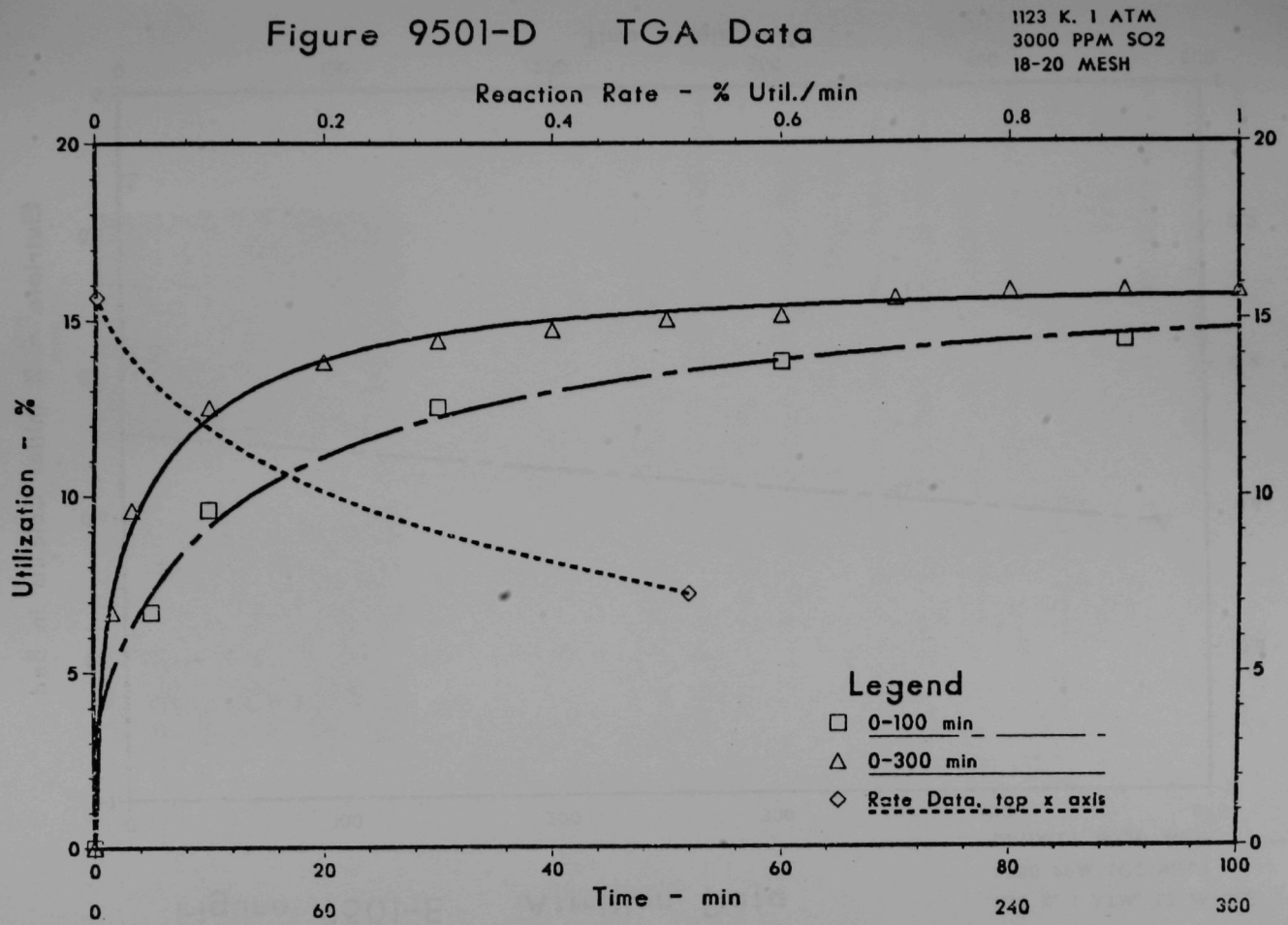

Figure 9501-E Attrition Data

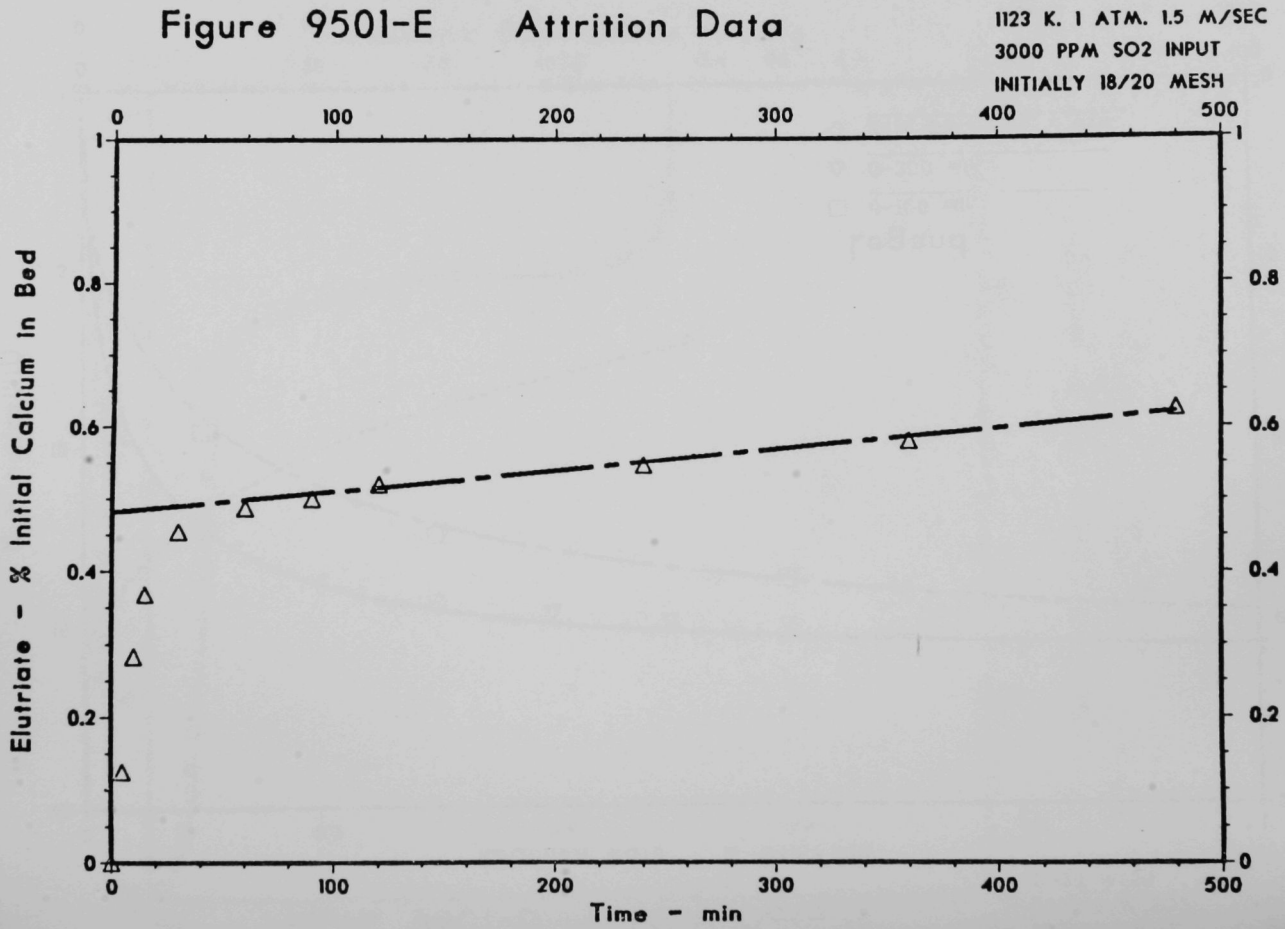

1. NAME: ANL-9402

   SOURCE: Limestone Products Corp., Union, ME

2. CHEMICAL COMPOSITION, wt %

$CaCO_3$	$MgCO_3$	SiO_2	Fe_2O_3	Al_2O_3	Na_2O	K_2O
94.7	0.87	0.63	0.14	0.23	0.02	0.02

3. DENSITY: RAW SORBENT 2.698 g/cm^3 168.4 lb/ft^3

   CALCINED 1.620 g/cm^3 101.1 lb/ft^3

4. PETROGRAPHIC DESCRIPTION: AVERAGE GRAIN SIZE >250 μm, SEE FIG. 9402 A & B

   Very coarse grained; shows a twinning lamellae characteristic.

5. PORE SIZE DISTRIBUTION: SEE FIG. 9402-C

   AVERAGE PORE DIAMETER - RAW SORBENT 1.930 μm

   CALCINED 0.089 μm

6. SURFACE AREA: RAW SORBENT 0.039 m^2/g 1.89 x 10^2 ft^2/lb

   CALCINED 12.48 m^2/g 6.09 x 10^4 ft^2/lb

Fig. 9402A
Raw Limestone
50X

Fig. 9402B
Calcined Limestone 1 h 850°C
1100X

7. TOTAL POROSITY: RAW SORBENT 0.024 cm^3/g 3.80×10^{-4} ft^3/lb

CALCINED 0.277 cm^3/g 4.44×10^{-3} ft^3/lb

8. THERMOGRAVIMETRIC ANALYSIS: SEE FIG. 9402-D

(1123 K, 1 atm, 3000 ppm SO_2, -18 +20 mesh)

FRACTIONAL UTILIZATION = $\alpha(t, \text{min}) = 0.164\ [1 - \exp(-0.108\ t^{0.637})]$

ANL PARAMETERS: D = 0.128 b = 594.2

9. ATTRITION: SEE FIG. 9402-E

Bed loss due to calcination breakup (%) = 5.5

Bed mass lost in linear portion (%/min.) = 1.8×10^{-3}

Attrition constant, λ_4 (sec^{-1}) = 4.7×10^{-7}

ATTRITION DATA

	Grams Total	wt % Ca	wt % S
Initial Bed	160.463	37.92	0.00
Final Bed	95.319	44.0	4.18
Total Overhead	10.639	36.03	5.05
Overhead, 5 min	5.813	36.03	5.05
10 min	1.240	36.03	5.05
15 min	0.504	36.03	5.05
30 min	0.927	36.03	5.05
1 h	0.440	36.03	5.05
1.5 h	0.305	36.03	5.05
2 h	0.275	36.03	5.05
4 h	0.543	36.03	5.05
6 h	0.279	36.03	5.05
8 h	0.313	36.03	5.05

Attrition Data, continued for Sorbent 9402

Weight in Grams, Particle Diameter, μm

Sample	-1000 +840	-841 +707	-707 +595	-595 +420	-420 +297	-297 +250
Overhead, first 30 min	0.000	0.000	0.000	0.080	0.162	0.387
Overhead, remaining 7.5 h	0.000	0.000	0.000	0.059	0.691	0.462
Final Bed, post test	60.489	18.309	6.879	5.505	3.460	0.576

Sample	-250 +210	-210 +74	-74 +63	-63 +53	-53 +44	-44 +37	-37 +0
Overhead, first 30 min	0.875	4.260	0.099	0.254	0.360	0.265	0.594
Overhead, remaining 7.5 h	0.292	1.021	0.048	0.072	0.121	0.113	0.058
Final Bed, post test	0.254	0.489	0.010	0.024	0.023	0.013	0.008

Figure 9402-C
Pore Size Distribution

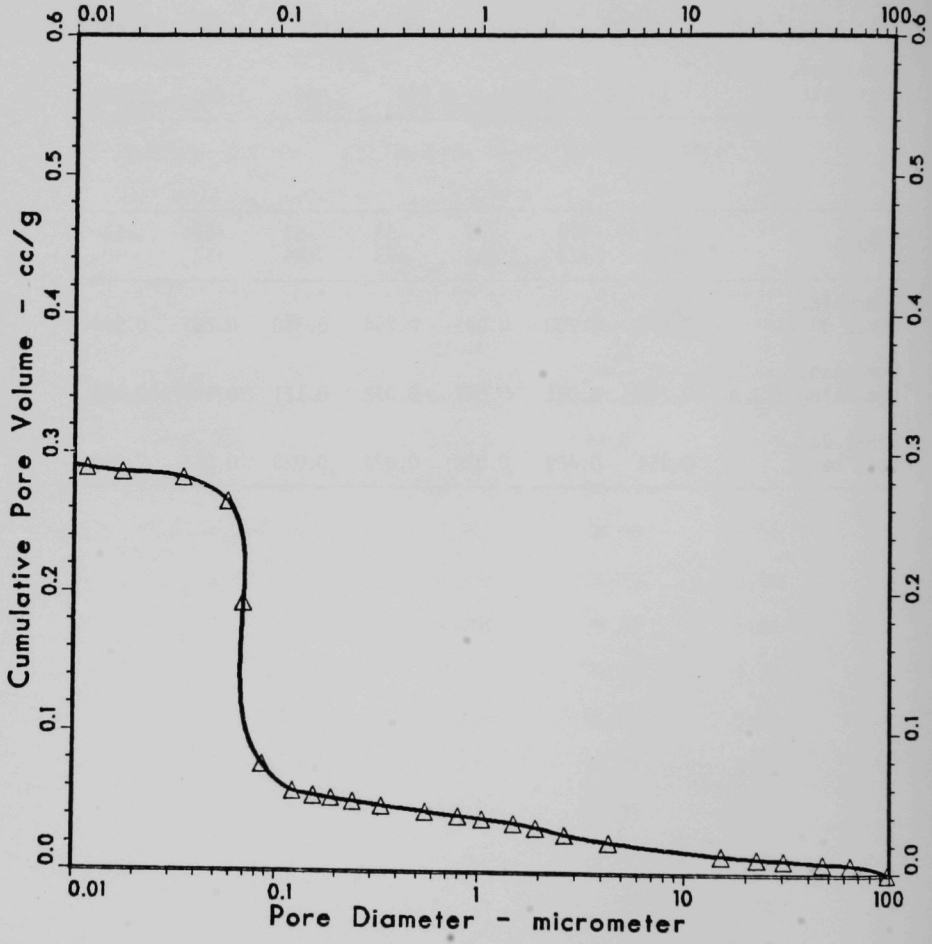

Figure 9402-D TGA Data

1123 K. 1 ATM
3000 PPM SO2
18-20 MESH

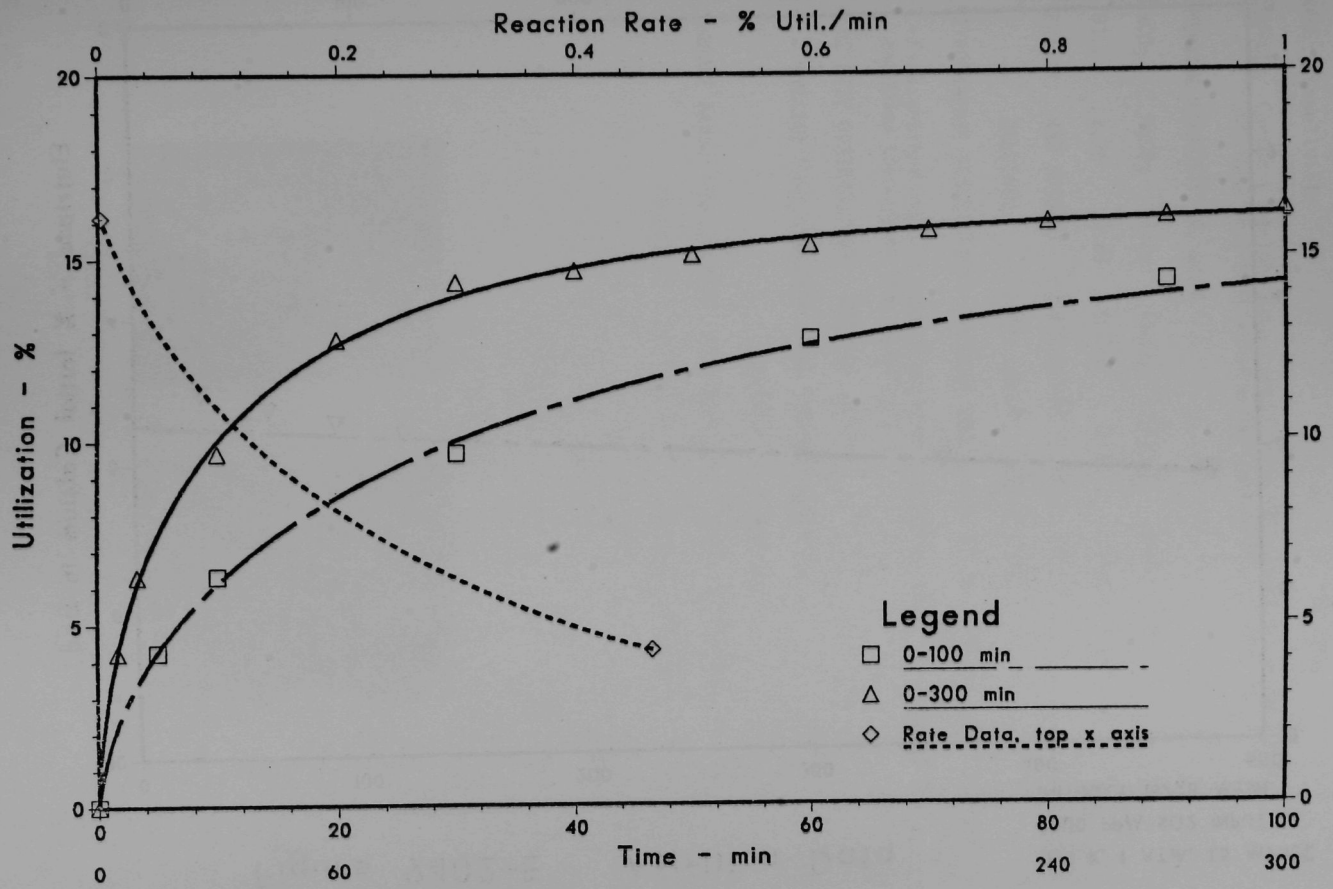

Figure 9402-E Attrition Data

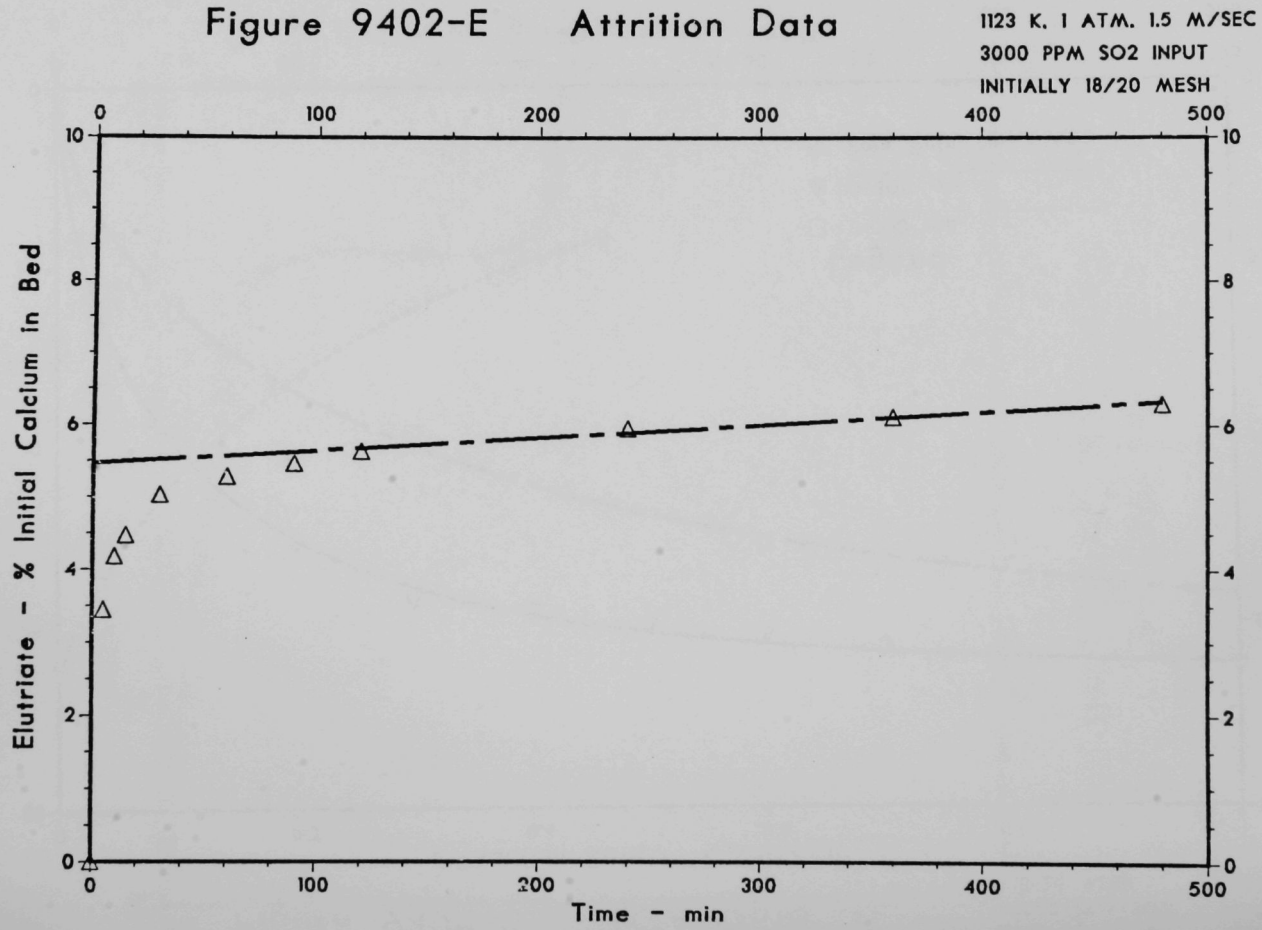

1. NAME: Lowellville ANL-9202

SOURCE: Carton Limestone Co., Lowellville, OH, representative sample obtained from Westinghouse R&D Center Pittsburgh, PA

2. CHEMICAL COMPOSITION, wt %

$CaCO_3$	$MgCO_3$	SiO_2	Fe_2O_3	Al_2O_3	Na_2O	K_2O
93.2	1.58	1.84	0.718	1.12	0.032	0.18

3. DENSITY: RAW SORBENT 2.633 g/cm^3 164.4 lb/ft^3

CALCINED 1.676 g/cm^3 121.5 lb/ft^3

4. PETROGRAPHIC DESCRIPTION: AVERAGE GRAIN SIZE 10 μm, SEE FIG. 9202 A & B

Fine grained loosely packed equigranular stone with coarse grains embedded throughout the particles.

5. PORE SIZE DISTRIBUTION: SEE FIG. 9202-C

AVERAGE PORE DIAMETER - RAW SORBENT 0.243 μm

CALCINED 0.106 μm

6. SURFACE AREA: RAW SORBENT 0.21 m^2/g 1.04 x 10^3 ft^2/lb

CALCINED 17.7 m^2/g 8.64 x 10^4 ft^2/lb

Fig. 9202A
Raw Limestone
50X

Fig. 9202B (Lowellville)
Calcined Limestone 1 h 850°C
1000X

7. TOTAL POROSITY: RAW SORBENT 0.018 cm^3/g 2.9×10^{-4} ft^3/lb

CALCINED 0.331 cm^3/g 7.74×10^{-3} ft^3/lb

8. THERMOGRAVIMETRIC ANALYSIS: SEE FIG. 9202-D

(1123 K, 1 atm, 3000 ppm SO_2, -18 +20 mesh)

FRACTIONAL UTILIZATION = $\alpha(t, min) = 0.223 [1 - exp (-0.0452 t^{0.928})]$

ANL PARAMETERS: D = 0.218 b = 436.8

9. ATTRITION: SEE FIG. 9202-E

Bed loss due to calcination breakup (%) = 0.22

Bed mass lost in linear portion (%/min.) = 4.00×10^{-4}

Attrition constant, λ_4 (sec^{-1}) = 9.20×10^{-8}

ATTRITION DATA

	Grams Total	wt % Ca	wt % S
Initial Bed	160.000	37.06	0.0
Final Bed	112.788	50.4	7.29
Total Overhead	0.730	34.75	3.59
Overhead, 5 min	0.162	34.75	3.59
10 min	0.080	34.75	3.59
15 min	0.052	34.75	3.59
30 min	0.039	34.75	3.59
1 h	0.038	34.75	3.59
1.5 h	0.048	34.75	3.59
2 h	0.070	34.75	3.59
4 h	0.058	34.75	3.59
6 h	0.087	34.75	3.59
8 h	0.096	34.75	3.59

Attrition Data, continued for Sorbent 9202

Weight in Grams, Particle Diameter, μm

Sample	-1000 +840	-841 +707	-707 +595	-595 +420	-420 +297	-297 +250
Overhead, first 30 min	0.000	0.000	0.000	0.000	0.001	0.001
Overhead, remaining 7.5 h	0.014	0.001	0.006	0.007	0.007	0.004
Final Bed, post test	107.858	3.066	0.493	0.390	0.240	0.052

Sample	-250 +210	-210 +74	-74 +63	-63 +53	-53 +44	-44 +37	-37 +0
Overhead, first 30 min	0.005	0.118	0.003	0.010	0.015	0.006	0.004
Overhead, remaining 7.5 h	0.024	0.204	0.008	0.007	0.010	0.002	0.001
Final Bed, post test	0.080	0.052	0.005	0.030	0.016	0.007	0.012

10. OTHER DATA: TGA Data: 1123 K, 1 atm, $\alpha(t,min) = C_1[1 - \exp(-C_2 t^{C_3})]$

Fig.	ppm SO_2	Mesh	C_1	C_2	C_3	D	b
9202-F	3,000	50/70	0.456	0.155	0.456	0.344	308
9202-G	3,000	140/170	0.470	0.144	0.819	0.374	291
9202-H	3,000	14/16	0.198	0.179	0.590	0.172	671
9202-I	3,000	10/16	0.195	0.179	0.467	0.135	675
9202-J	3,000	6/8	0.231	0.165	0.359	0.110	817
9202-K	3,000	<10 microns	0.970	0.052	0.704	0.922	150

See Figs. 9202-L and 9202-M for decrepitation data.

Figure 9202-C
Pore Size Distribution

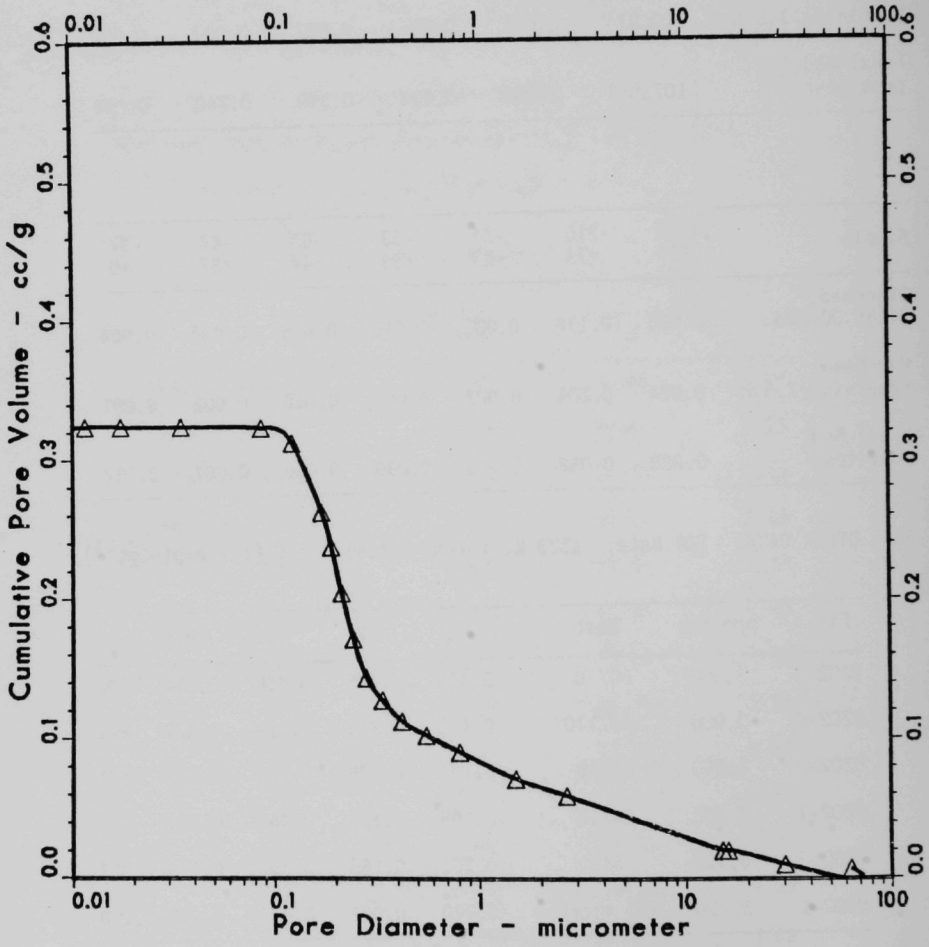

Figure 9202-D TGA Data

1123 K. 1 ATM
3000 PPM SO2
18-20 MESH

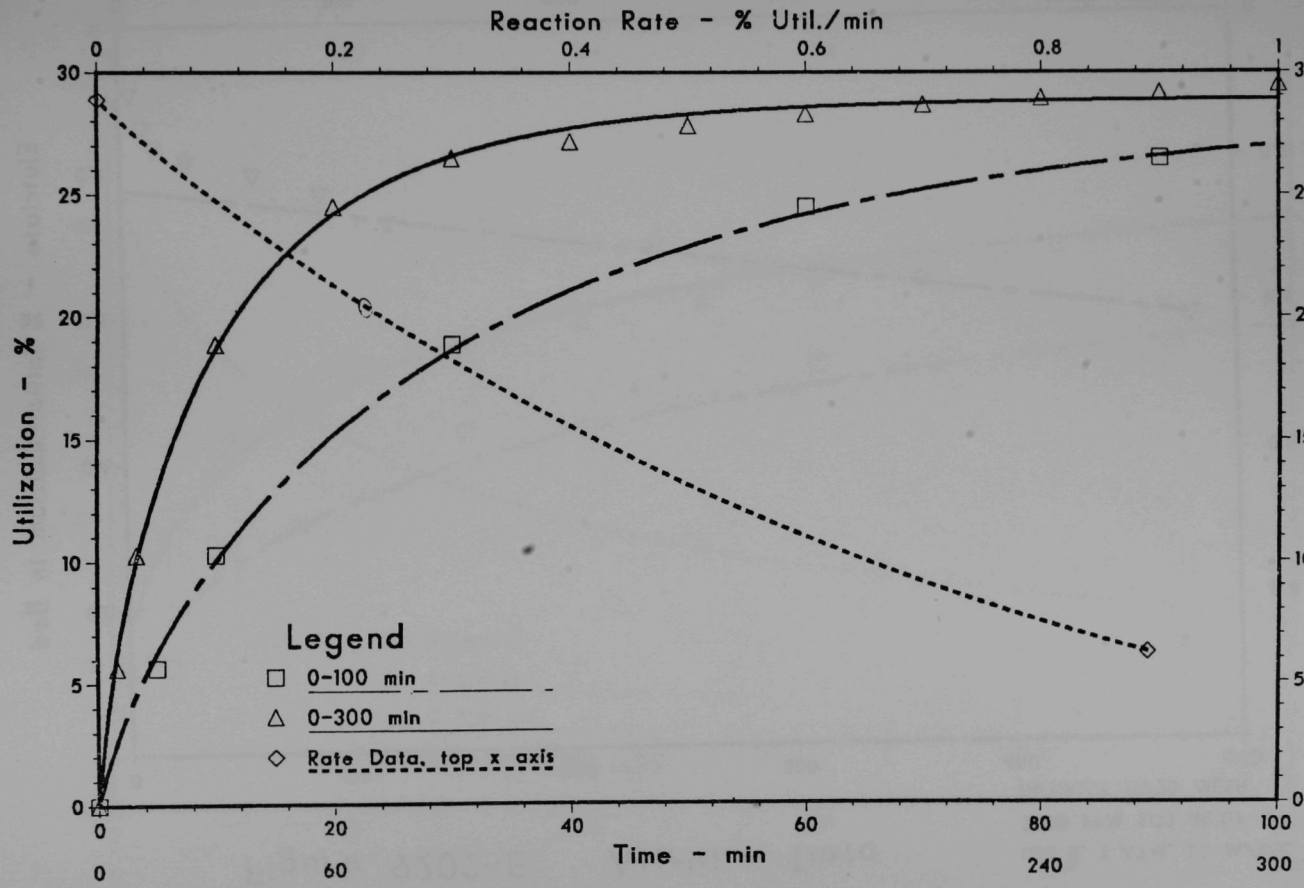

Figure 9202-E Attrition Data

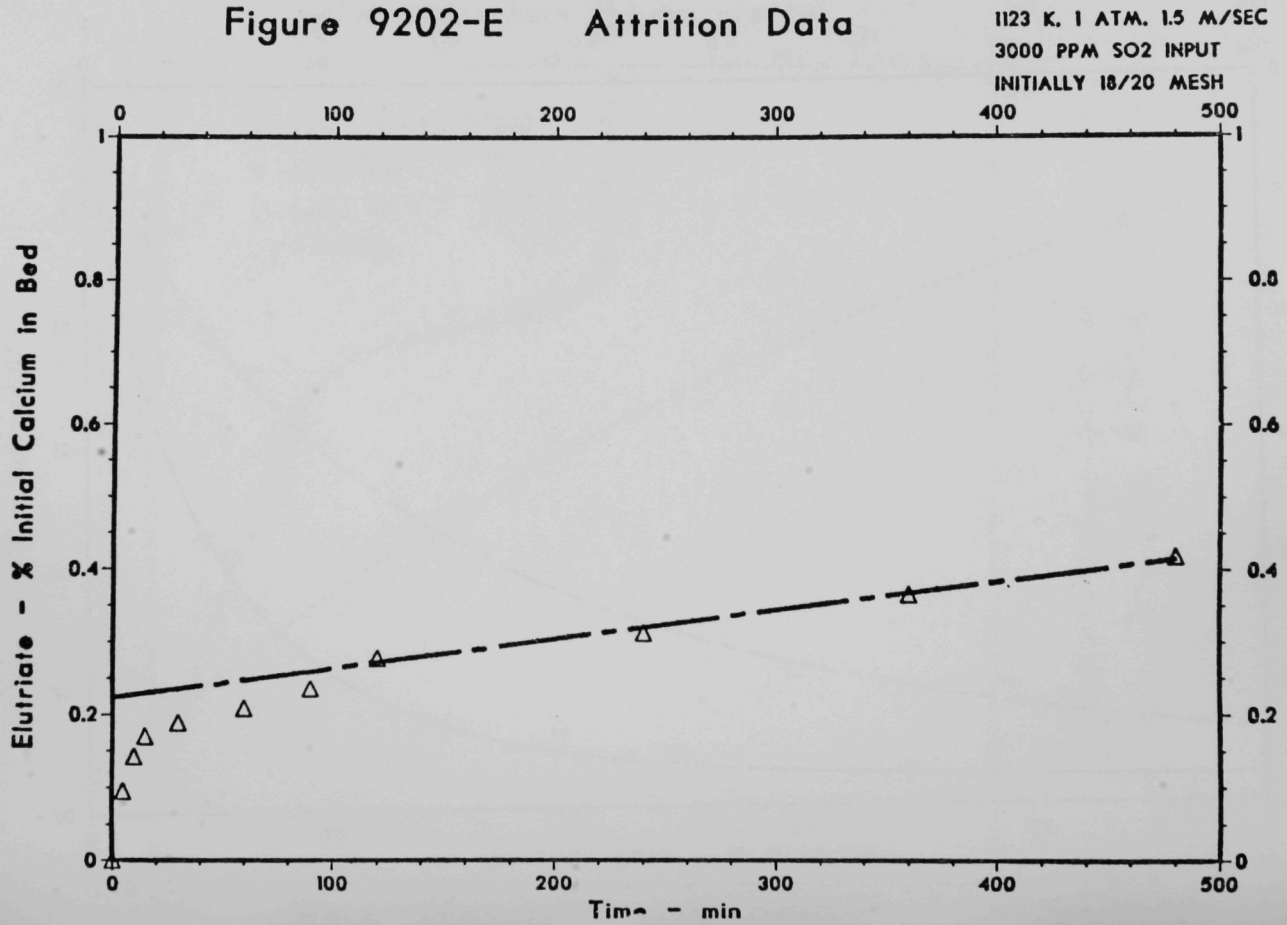

Figure 9202-F TGA Data

1123 K. 1 ATM
3000 PPM SO2
50-70 MESH

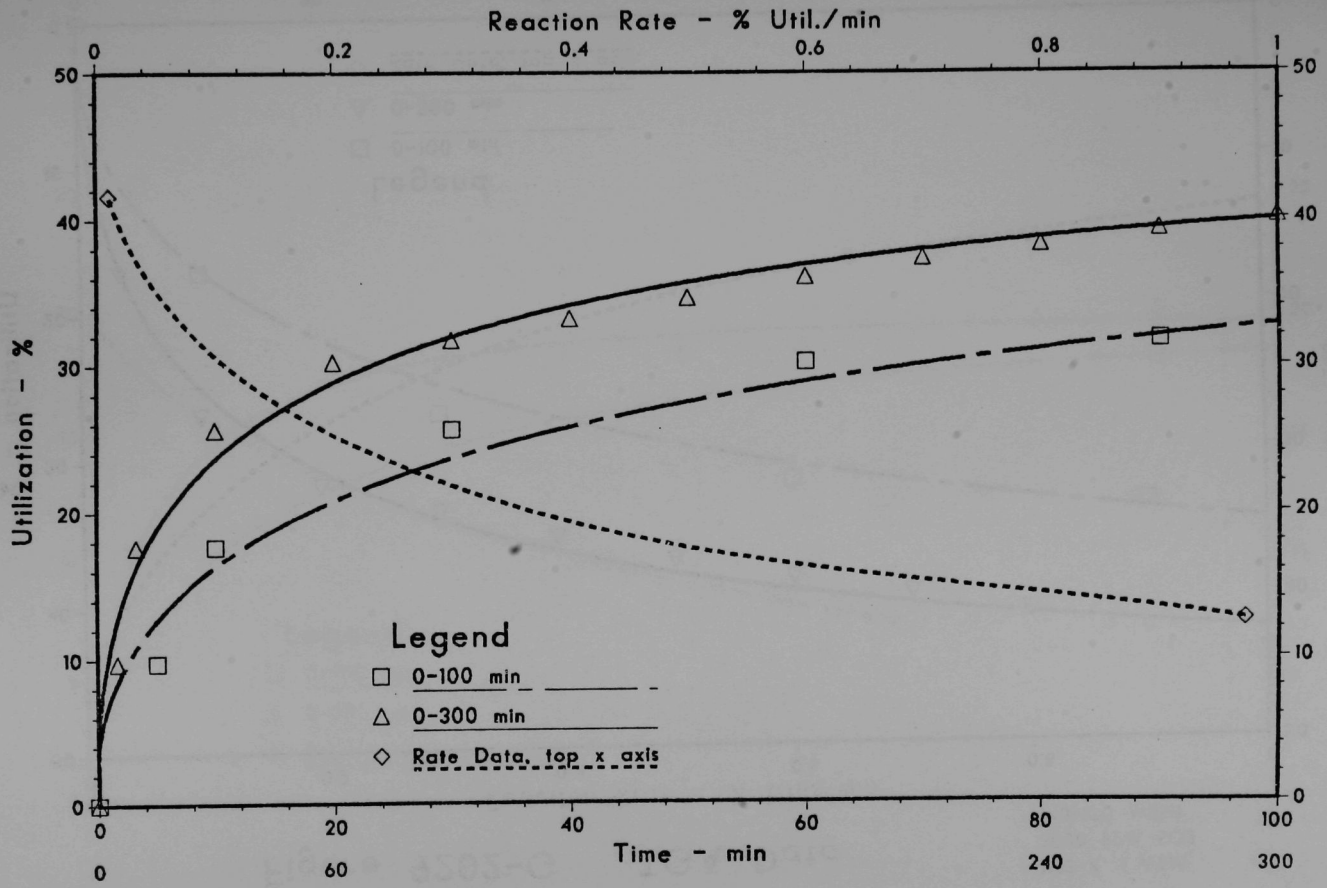

Figure 9202-G TGA Data

1123 K. 1 ATM
3000 PPM SO2
140-170 MESH

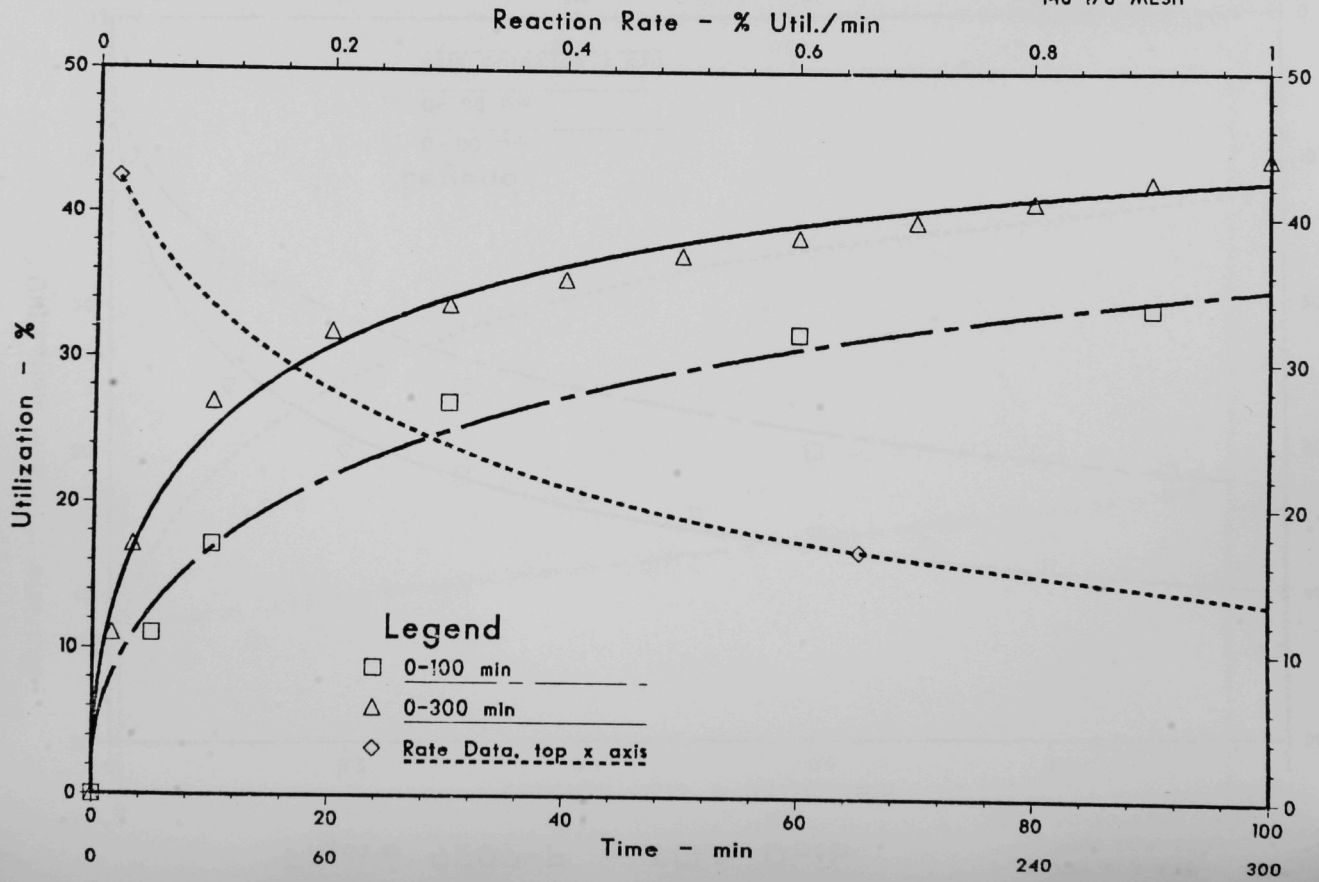

Figure 9202-H TGA Data

1123 K. 1 ATM
3000 PPM SO2
14-16 MESH

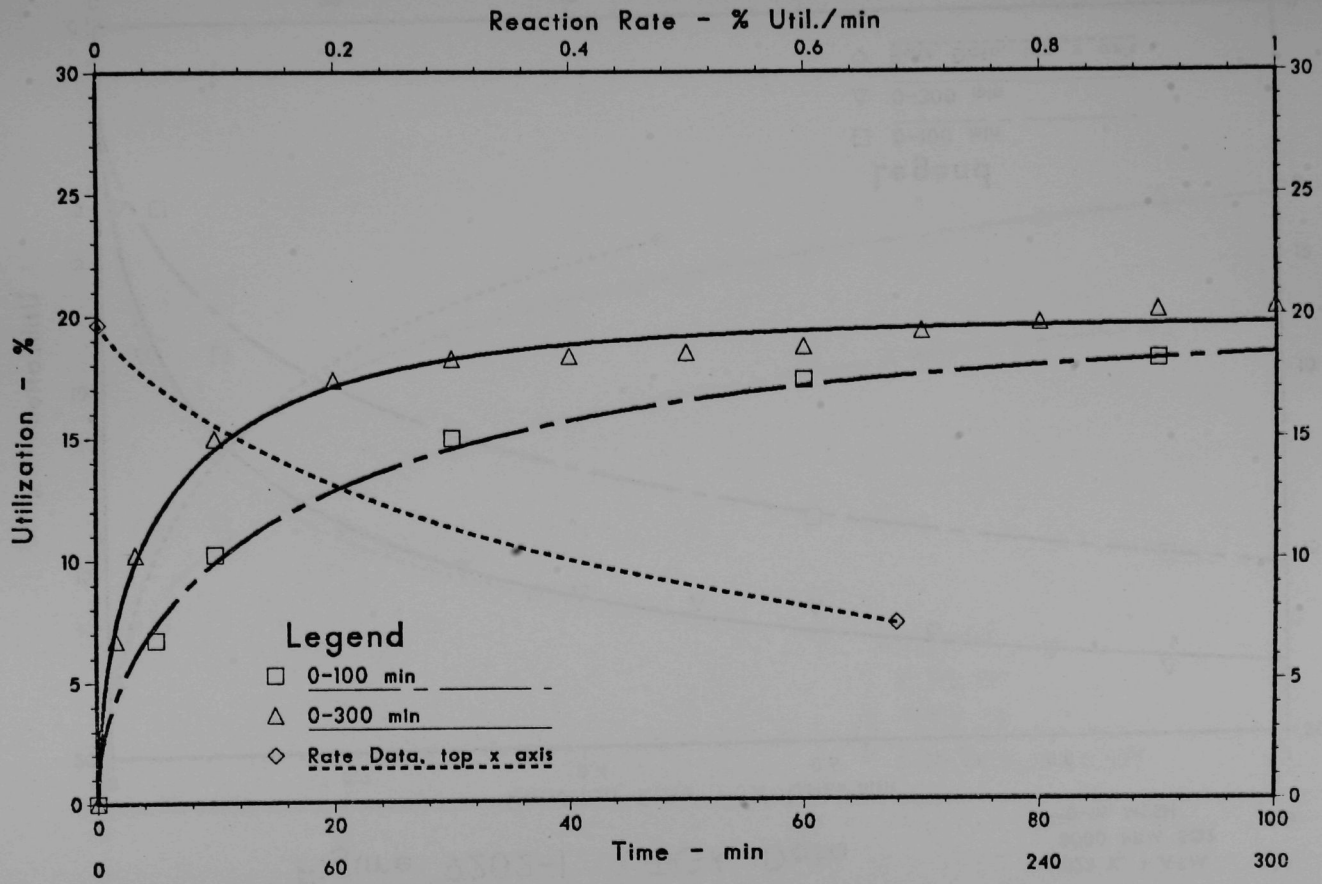

Figure 9202-1 TGA Data

1123 K. 1 ATM
3000 PPM SO2
10-16 MESH

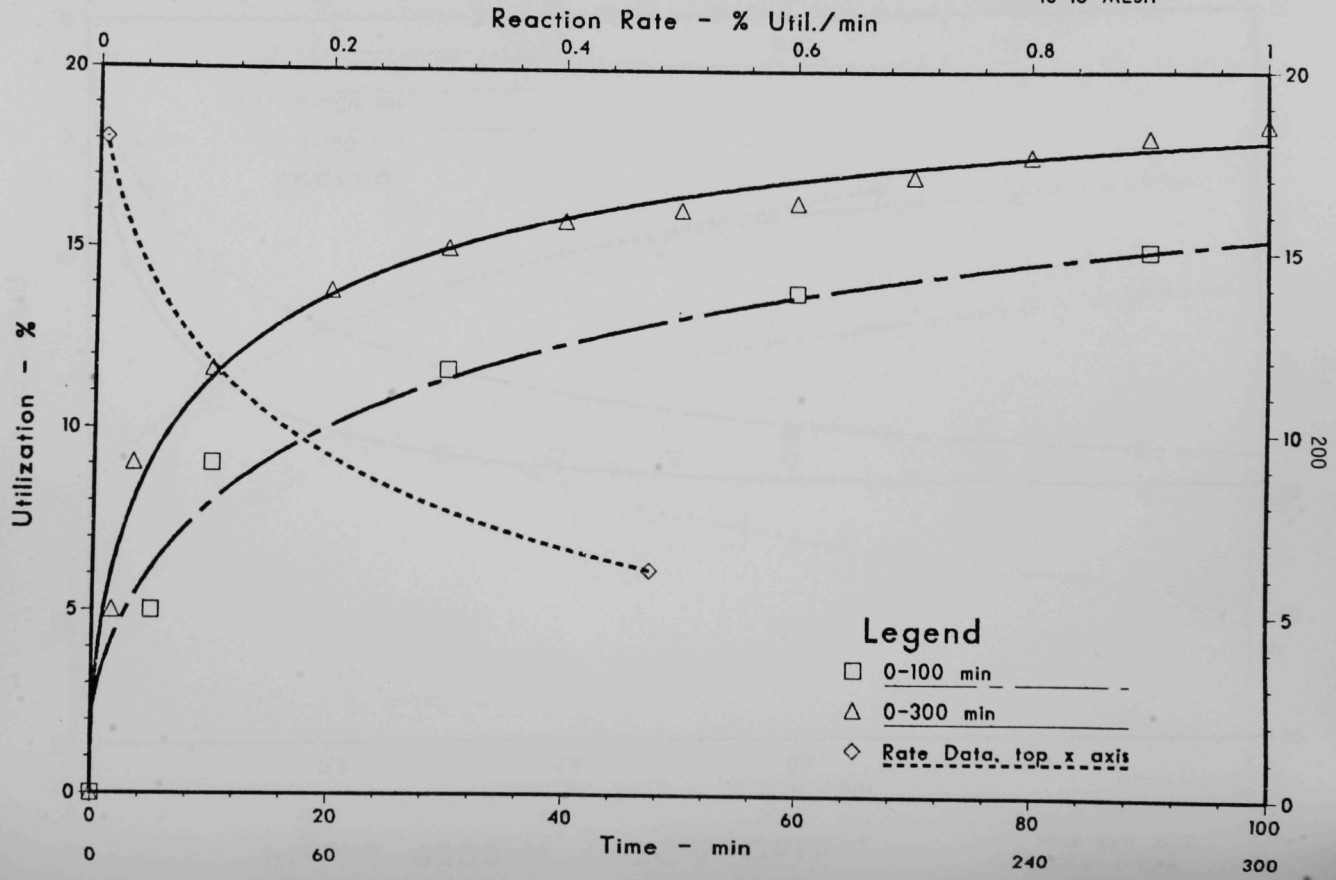

Figure 9202-J TGA Data

1123 K. 1 ATM
3000 PPM SO2
6-8 MESH

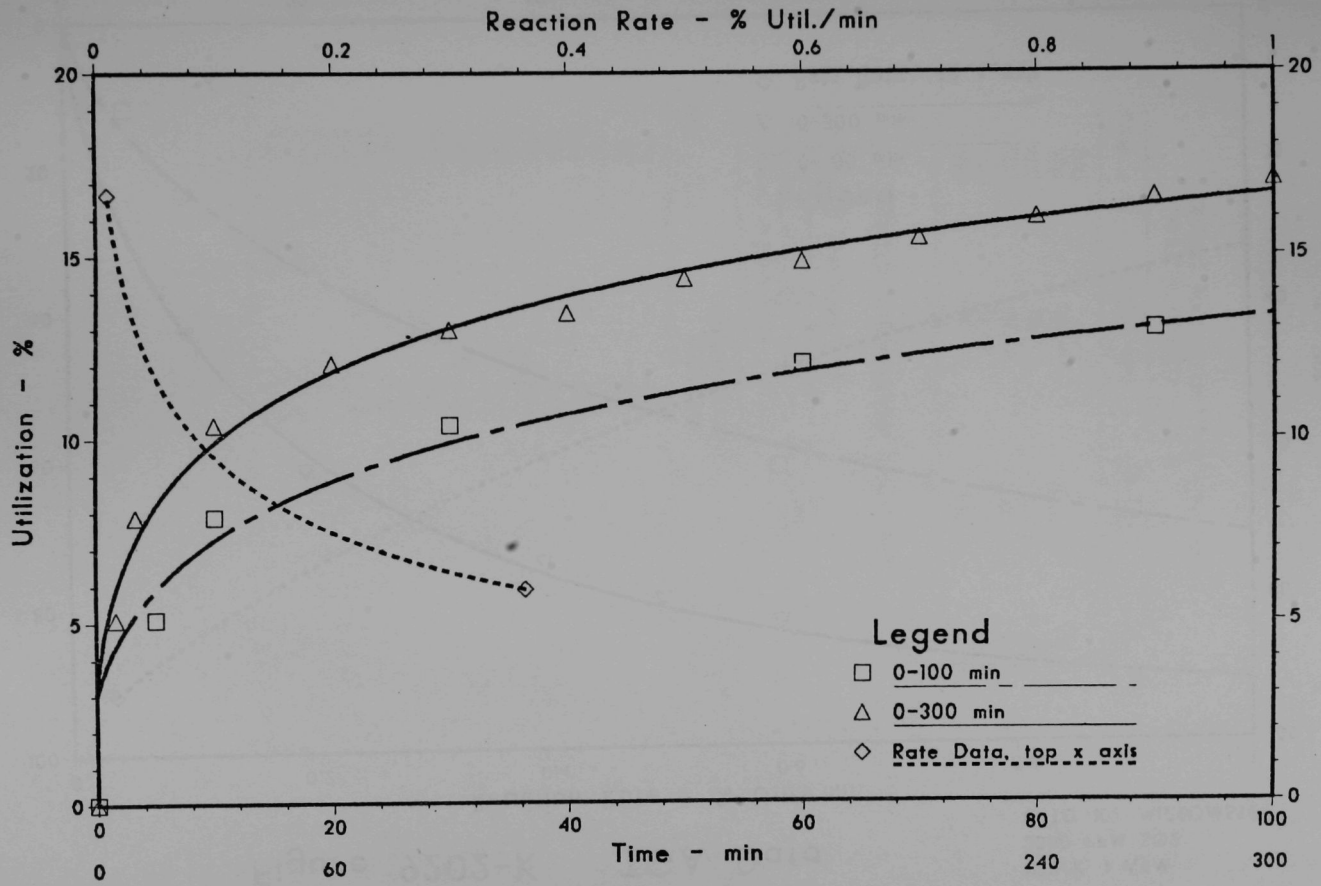

Figure 9202-K TGA Data

1123 K. 1 ATM
3000 PPM SO2
0 TO 10 MICROMETER

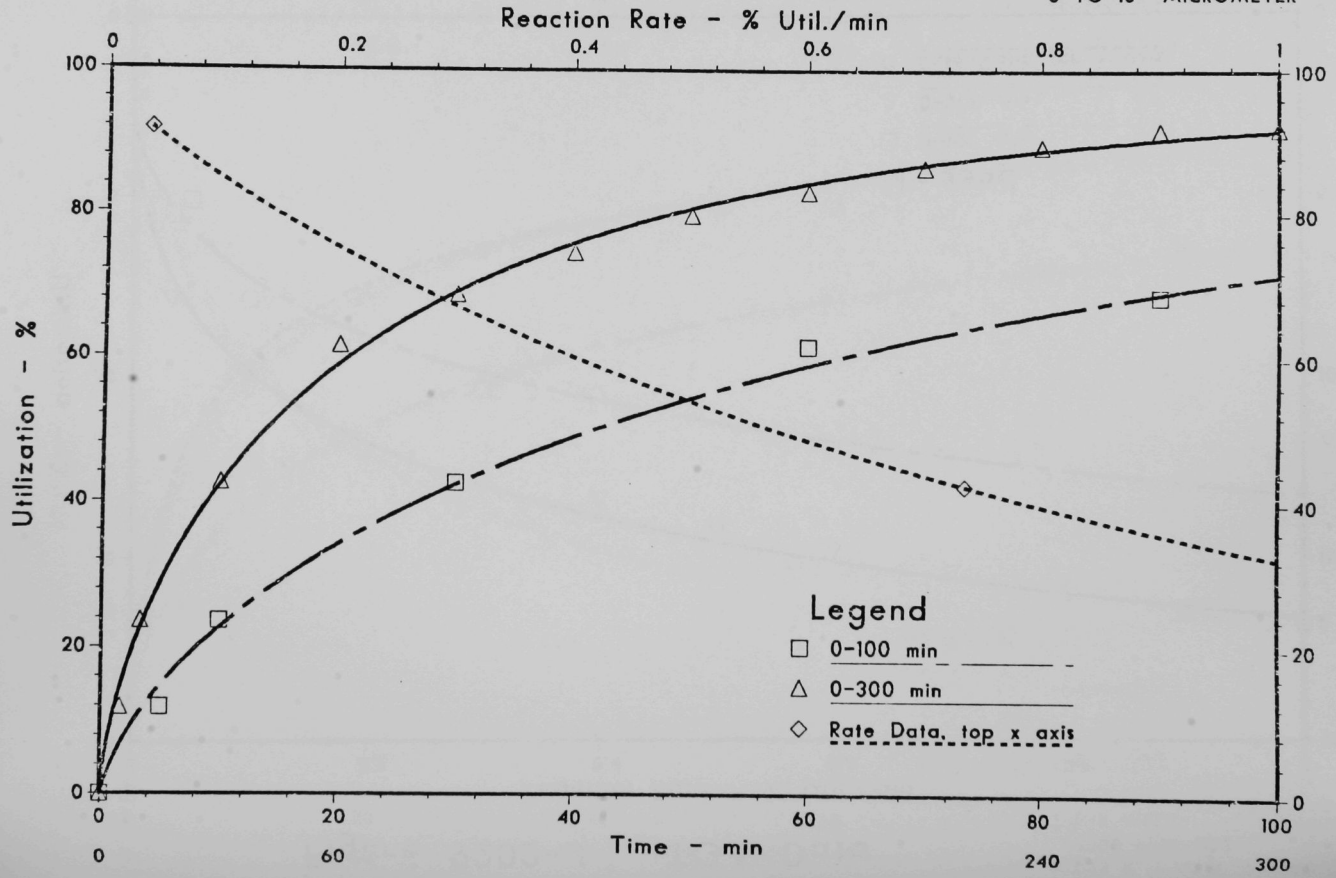

DECREPITATION DATA - 9202

Temp., °C	Weight Percent of Size Fractions, Particle Diameter in µm -1000 +841	-841 +595	-595 +0
200	--	--	--
300	98.7	1.2	0.07
400	98.1	1.7	0.22
600	97.8	1.8	0.42
750	97.2	2.0	0.80
850	96.9	2.1	1.00

WATER DETERMINATION DATA - 9202

Initially 18/20 mesh
Initial Weight of Sorbent - 94.7 mg
Theoretical Weight Loss Due to Calcination 39.6 mg
Observed Weight Loss - 41.0

Temp., °C	Observed Weight Loss, (mg)	Percent Weight Loss
25	0	0
40	0	0
80	0.1	0.11
130	0.4	0.42
230	0.6	0.63
290	0.9	0.95
340	1.3	1.4
390	1.7	1.8
440	2.0	2.1
490	2.5	2.6
540	2.8	3.0
580	3.5	3.7
620	4.6	4.9
650	6.9	7.3
690	15.0	15.8
730	32.3	34.1
850	41.0	43.3

Figure 9202-L Decrepitation Data

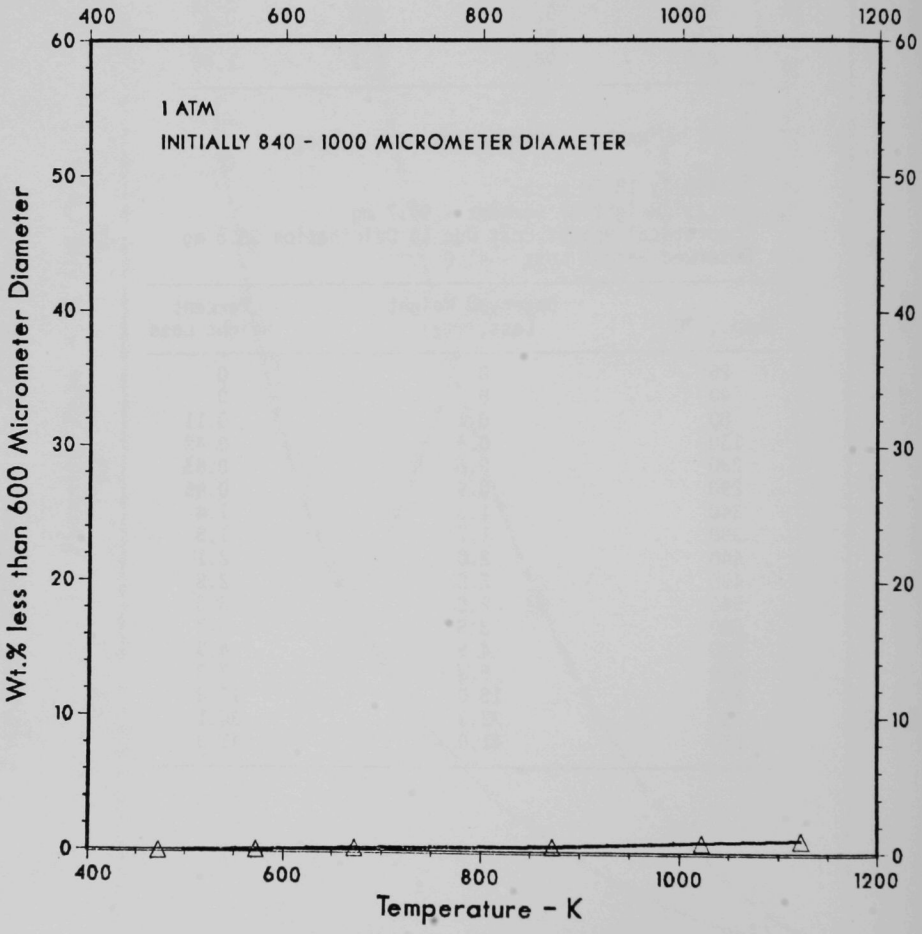

Figure 9202-M Water Loss Data

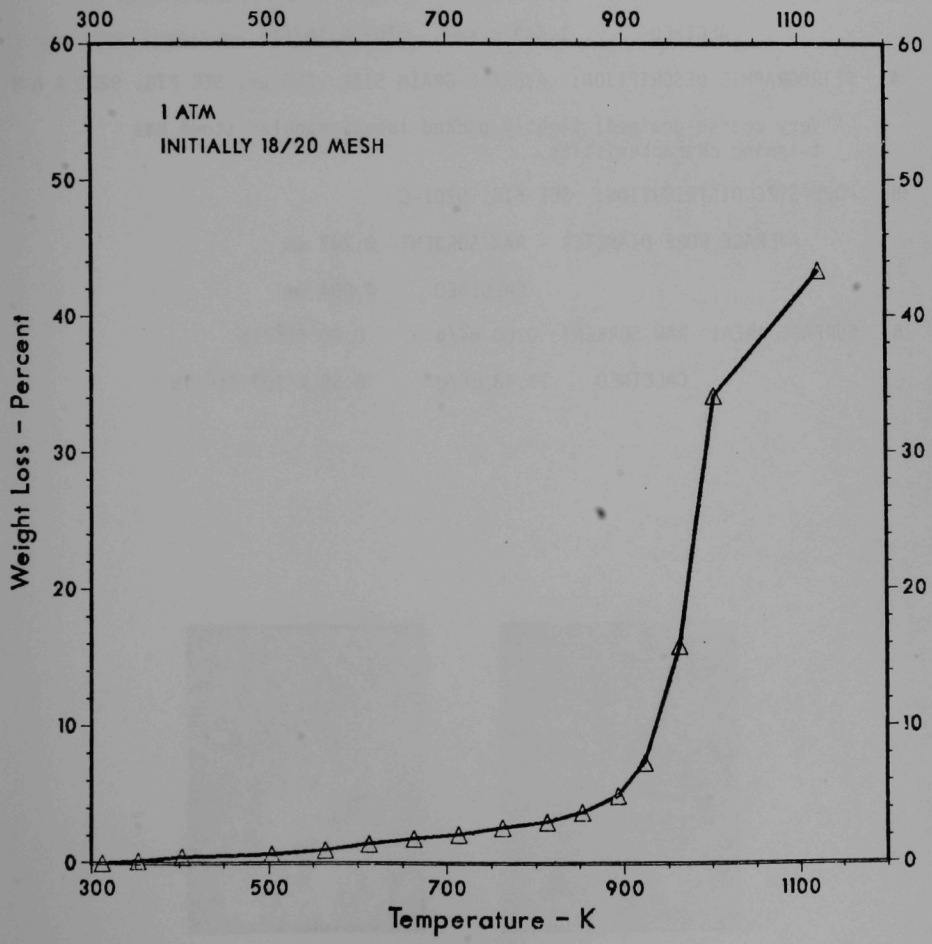

1. NAME: 1336 ANL-9201

   SOURCE: Georgia Marble Co., Tate, GA

2. CHEMICAL COMPOSITION, wt %

$CaCO_3$	$MgCO_3$	SiO_2	Fe_2O_3	Al_2O_3	Na_2O	K_2O
92.6	5.33	1.26	0.2	0.42	0.10	0.02

3. DENSITY: RAW SORBENT 2.788 g/cm^3 174.0 lb/ft^3

   CALCINED 1.649 g/cm^3 102.9 lb/ft^3

4. PETROGRAPHIC DESCRIPTION: AVERAGE GRAIN SIZE >250 μm, SEE FIG. 9201 A & B

   Very coarse-grained; tightly packed inequigranular stone has twinning characteristics.

5. PORE SIZE DISTRIBUTION: SEE FIG. 9201-C

   AVERAGE PORE DIAMETER - RAW SORBENT 0.747 μm

   CALCINED 0.094 μm

6. SURFACE AREA: RAW SORBENT 0.00 m^2/g 0.00 ft^2/lb

   CALCINED 13.48 m^2/g 6.58 x 10^4 ft^2/lb

Fig. 9201A
Raw Limestone
50X

Fig. 9201B
Calcined Limestone 1 h 850°C
1100X

7. TOTAL POROSITY: RAW SORBENT 0.006 cm^3/g 9.9×10^{-5} ft^3/lb

CALCINED 0.325 cm^3/g 5.21×10^{-3} ft^3/lb

8. THERMOGRAVIMETRIC ANALYSIS: SEE FIG. 9201-D

(1123 K, 1 atm, 3000 ppm SO_2, -18 +20 mesh)

FRACTIONAL UTILIZATION = $\alpha(t, \text{min}) = 0.183\ [1 - \exp(-0.0709\ t^{0.723})]$

ANL PARAMETERS: D = 0.148 b = 483.8

9. ATTRITION: No data available

Figure 9201-C
Pore Size Distribution

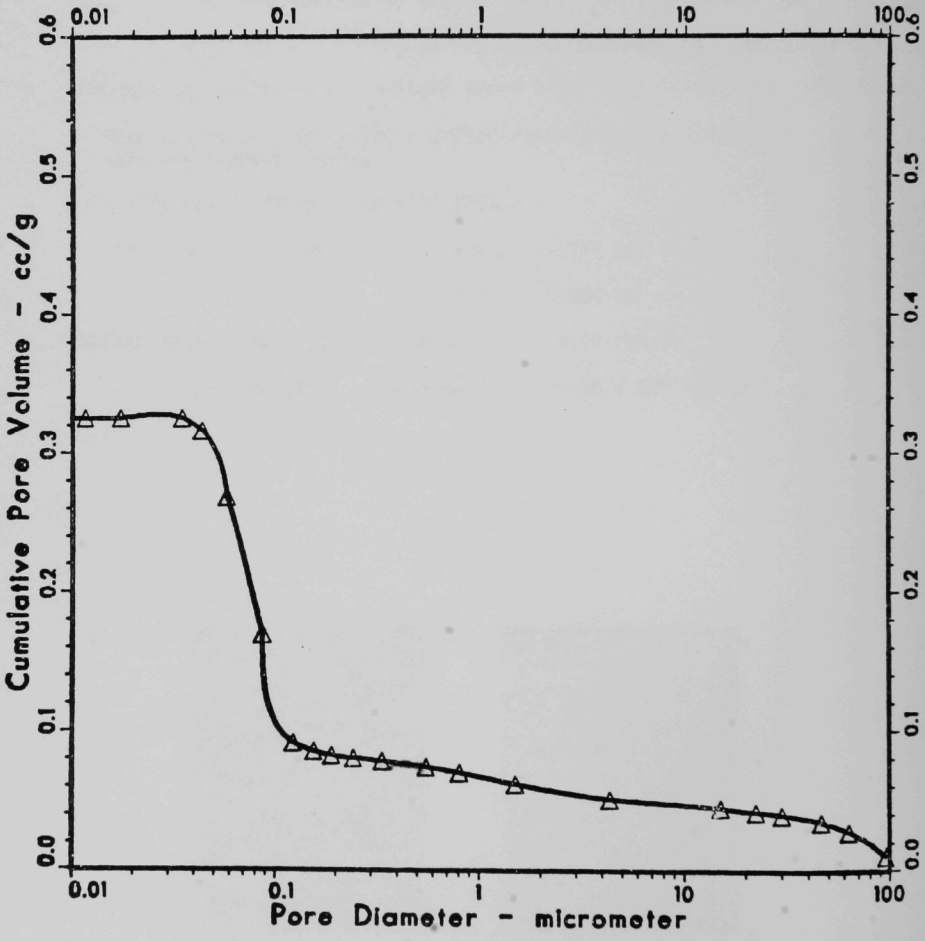

Figure 9201-D TGA Data

1123 K. 1 ATM
3000 PPM SO2
18-20 MESH

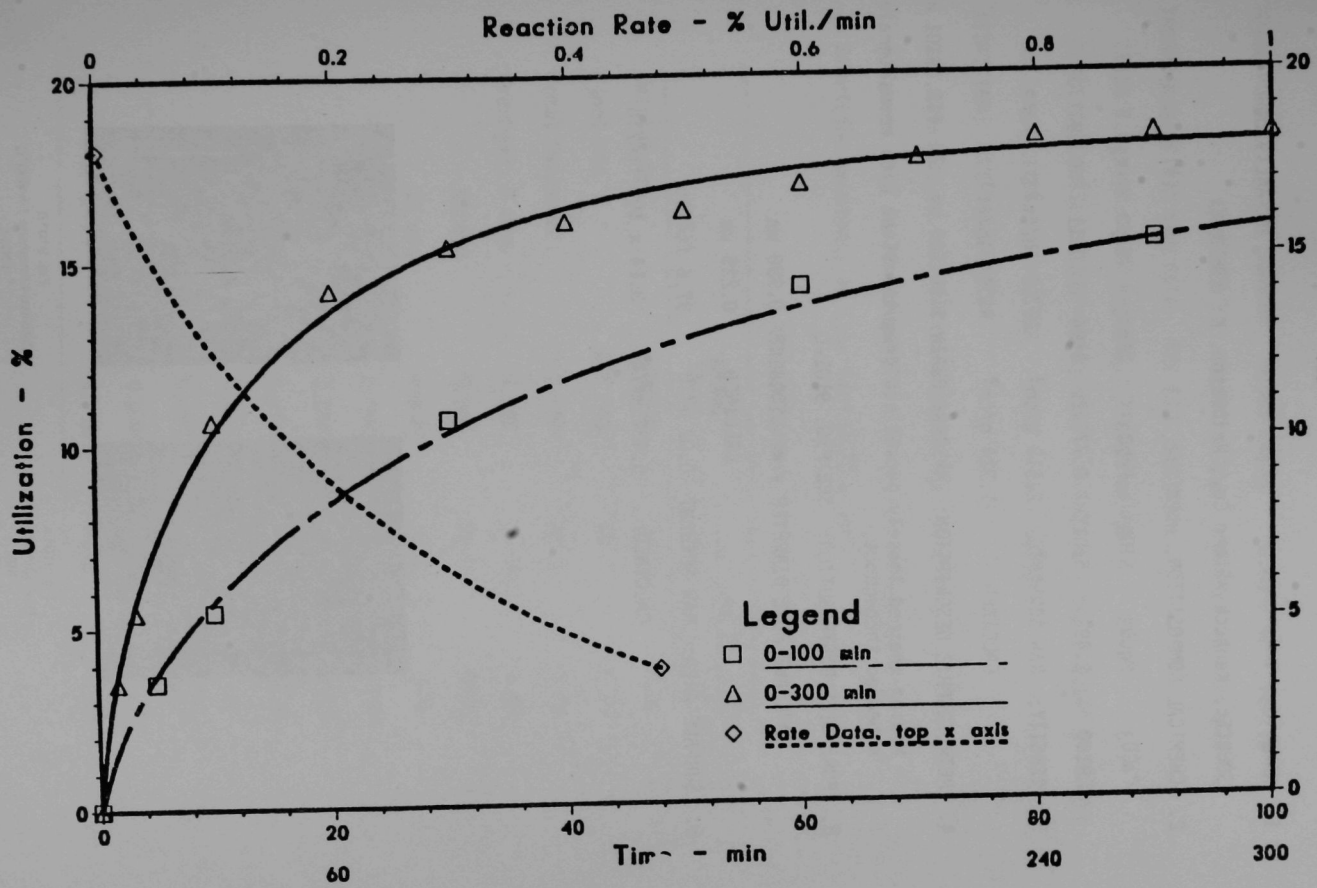

1. NAME: ANL-9101

SOURCE: Kentucky Stone Co., Princeton, KY

2. CHEMICAL COMPOSITION, wt %

$CaCO_3$	$MgCO_3$	SiO_2	Fe_2O_3	Al_2O_3	Na_2O	K_2O
91.0	2.49	5.01	0.77	0.94	0.11	0.19

3. DENSITY: RAW SORBENT 2.518 g/cm^3 157.2 lb/ft^3

CALCINED 1.524 g/cm^3 95.14 lb/ft^3

4. PETROGRAPHIC DESCRIPTION: AVERAGE GRAIN SIZE 120 μm, SEE FIG. 9101 A & B

Medium-grained loosely packed equigranular stone with coarse grains embedded throughout.

5. PORE SIZE DISTRIBUTION: SEE FIG. 9101-C

AVERAGE PORE DIAMETER - RAW SORBENT 0.990 μm

CALCINED 0.225 μm

6. SURFACE AREA: RAW SORBENT 0.02 m^2/g 97.6 ft^2/lb

CALCINED 6.437 m^2/g 3.14 x 10^4 ft^2/lb

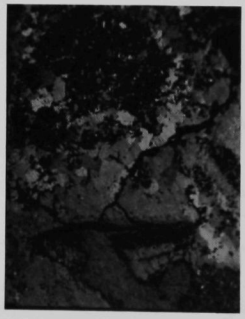

Fig. 9101A
Raw Limestone
50X

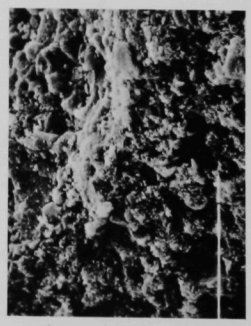

Fig. 9101B
Calcined Limestone 1 h 850°C
1000X

7. TOTAL POROSITY: RAW SORBENT 0.015 cm^3/g 2.40×10^{-4} ft^3/lb

CALCINED 0.367 cm^3/g 5.88×10^{-3} ft^3/lb

8. THERMOGRAVIMETRIC ANALYSIS: SEE FIG. 9101-D

(1123 K, 1 atm, 3000 ppm SO_2, -18 +20 mesh)

FRACTIONAL UTILIZATION = $\alpha(t, min) = 0.192 [1 - exp (-0.145 t^{0.632})]$

ANL PARAMETERS: D = 0.166 b = 582.8

9. ATTRITION: SEE FIG. 9101-E

Bed loss due to calcination breakup (%) = 0.092

Bed mass lost in linear portion (%/min.) = 1.26×10^{-4}

Attrition constant, λ_4 (sec^{-1}) = 2.87×10^{-8}

ATTRITION DATA

	Grams Total	wt % Ca	wt % S
Initial Bed	160.002	36.40	0.00
Final Bed	112.243	49.7	5.76
Total Overhead	0.252	36.0	3.66
Overhead, 5 min	0.066	36.0	3.66
10 min	0.080	36.0	3.66
15 min	0.009	36.0	3.66
30 min	0.000	36.0	3.66
1 h	0.008	36.0	3.66
1.5 h	0.015	36.0	3.66
2 h	0.001	36.0	3.66
4 h	0.009	36.0	3.66
6 h	0.006	36.0	3.66
8 h	0.056	36.0	3.66

Attrition Data, continued for Sorbent 9101

Weight in Grams, Particle Diameter, μm

Sample	-1000 +840	-841 +707	-707 +595	-595 +420	-420 +297	-297 +250
Overhead, first 30 min	0.001	0.000	0.001	0.000	0.002	0.004
Overhead, remaining 7.5 h	0.000	0.000	0.000	0.000	0.000	0.000
Final Bed, post test	110.364	1.341	0.088	0.118	0.058	0.028

Sample	-250 +210	-210 +74	-74 +63	-63 +53	-53 +44	-44 +37	-37 +0
Overhead, first 30 min	0.008	0.109	0.004	0.010	0.022	0.008	0.000
Overhead, remaining 7.5 h	0.000	0.000	0.000	0.000	0.000	0.000	0.000
Final Bed, post test	0.037	0.183	0.005	0.015	0.021	0.008	0.001

Figure 9101-C
Pore Size Distribution

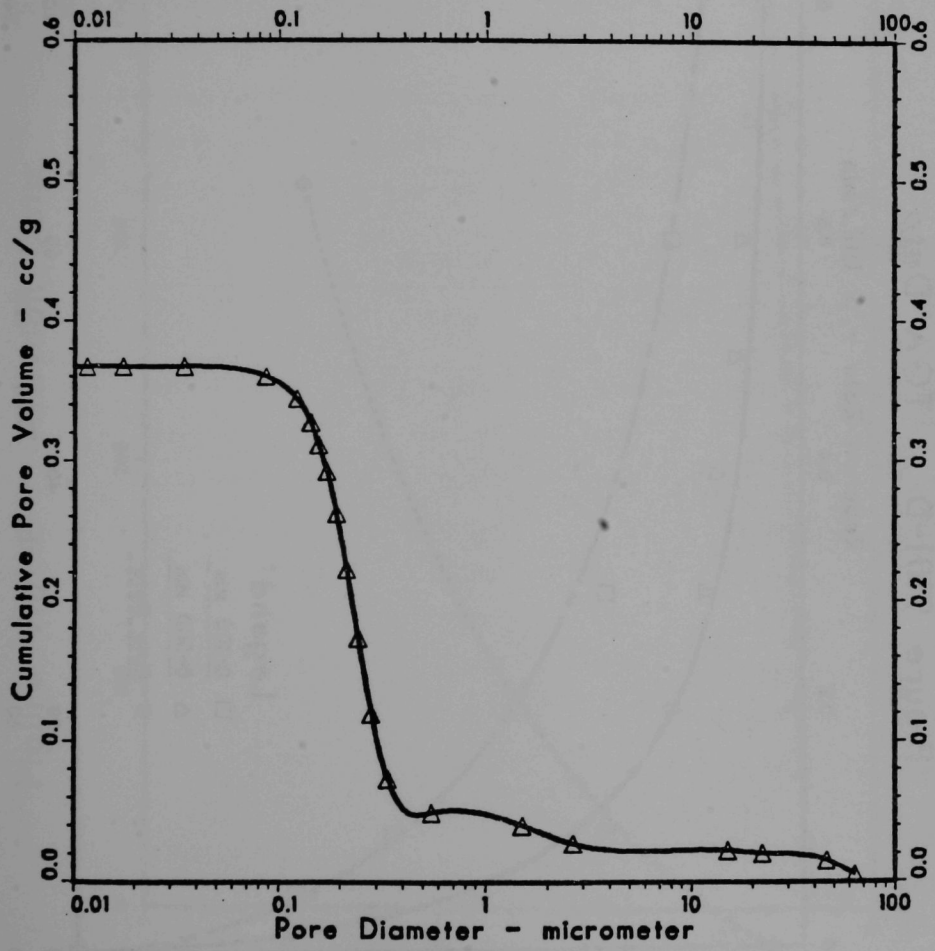

Figure 9101-D TGA Data

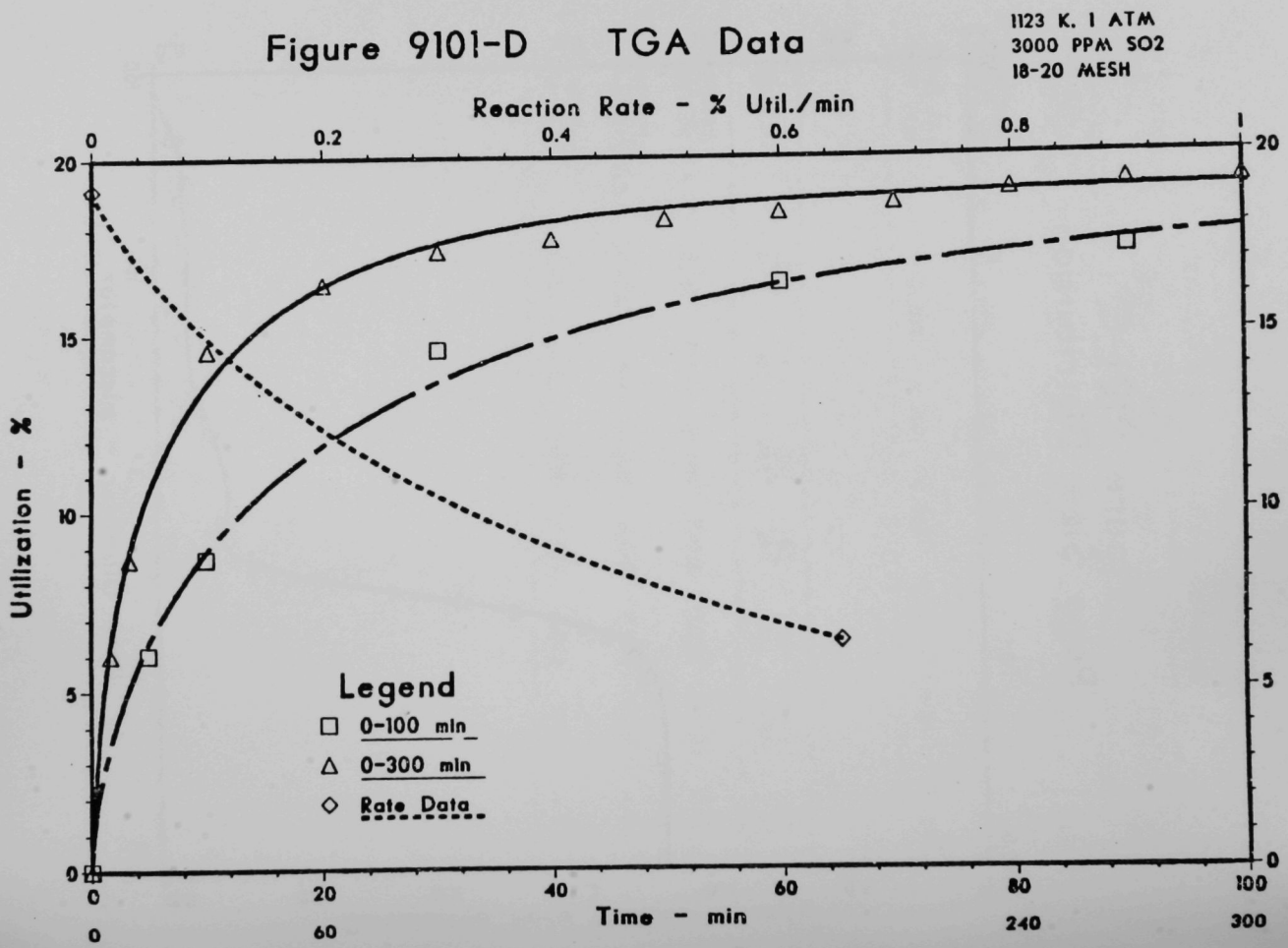

Figure 9101-E Attrition Data

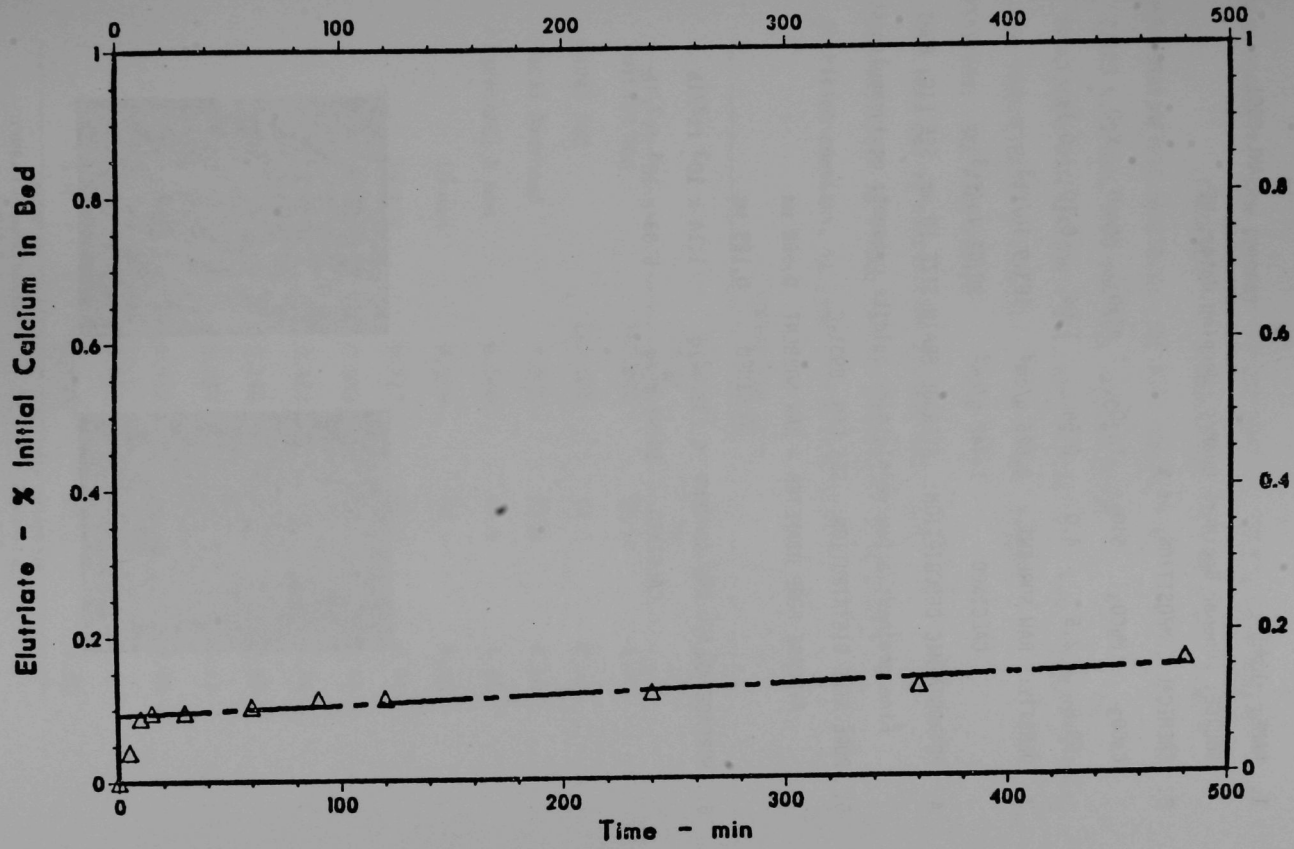

1. NAME: 1343 ANL-8901

SOURCE: Hooper Brothers Quarry, Weeping Water, NE

2. CHEMICAL COMPOSITION, wt %

$CaCO_3$	$MgCO_3$	SiO_2	Fe_2O_3	Al_2O_3	Na_2O	K_2O
89.8	2.5	4.0	0.66	1.04	0.10	0.19

3. DENSITY: RAW SORBENT 2.625 g/cm^3 163.9 lb/ft^3

CALCINED 1.442 g/cm^3 90.02 lb/ft^3

4. PETROGRAPHIC DESCRIPTION: AVERAGE GRAIN SIZE 10 μm, SEE FIG. 8901 A & B

Fine grained; a few veinlets of calcite present; equigranular stone.

5. PORE SIZE DISTRIBUTION: SEE FIG. 8901-C

AVERAGE PORE DIAMETER - RAW SORBENT 0.568 μm

CALCINED 0.129 μm

6. SURFACE AREA: RAW SORBENT 0.232 m^2/g 1.14 x 10^3 ft^2/lb

CALCINED 10.92 m^2/g 5.33 x 10^4 ft^2/lb

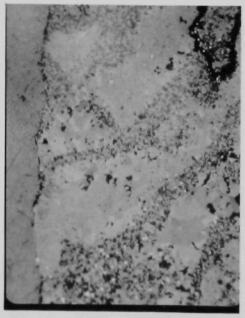

Fig. 8901A
Raw Limestone
50X

Fig. 8901B
Calcined Limestone 1 h 850°C
1100X

7. TOTAL POROSITY: RAW SORBENT 0.038 cm^3/g 6.1×10^{-4} ft^3/lb

CALCINED 0.353 cm^3/g 5.65×10^{-3} ft^3/lb

8. THERMOGRAVIMETRIC ANALYSIS: SEE FIG. 8901-D

(1123 K, 1 atm, 3000 ppm SO_2, -18 +20 mesh)

FRACTIONAL UTILIZATION = $\alpha(t, min) = 0.267 [1 - exp (-0.0225 t^{1.085})]$

ANL PARAMETERS: D = 0.271 b = 379.3

9. ATTRITION: SEE FIG. 8901-E

Bed loss due to calcination breakup (%) = 2.5

Bed mass lost in linear portion (%/min.) = 8.42×10^{-4}

Attrition constant, λ_4 (sec^{-1}) = 1.95×10^{-7}

ATTRITION DATA

	Grams Total	wt % Ca	wt % S
Initial Bed	160.001	35.92	0.00
Final Bed	126.501	43.3	8.51
Total Overhead	4.072	40.9	4.46
Overhead, 5 min	0.540	40.9	4.46
10 min	0.816	40.9	4.46
15 min	0.773	40.9	4.46
30 min	0.880	40.9	4.46
1 h	0.423	40.9	4.46
1.5 h	0.146	40.9	4.46
2 h	0.057	40.9	4.46
4 h	0.182	40.9	4.46
6 h	0.121	40.9	4.46
8 h	0.134	40.9	4.46

Attrition Data, continued for Sorbent 8901

Weight in Grams, Particle Diameter, μm

Sample	-1000 +840	-841 +707	-707 +595	-595 +420	-420 +297	-297 +250
Overhead, first 30 min	0.003	0.002	0.001	0.001	0.004	0.008
Overhead, remaining 7.5 h	0.002	0.001	0.001	0.004	0.030	0.064
Final Bed, post test	119.816	3.636	0.869	0.738	0.759	0.110

Sample	-250 +210	-210 +74	-74 +63	-63 +53	-53 +44	-44 +37	-37 +0
Overhead, first 30 min	0.042	0.937	0.029	0.087	0.210	0.137	0.422
Overhead, remaining 7.5 h	0.137	0.757	0.019	0.099	0.187	0.090	0.206
Final Bed, post test	0.194	0.328	0.008	0.015	0.017	0.004	0.004

Figure 8901-C
Pore Size Distribution

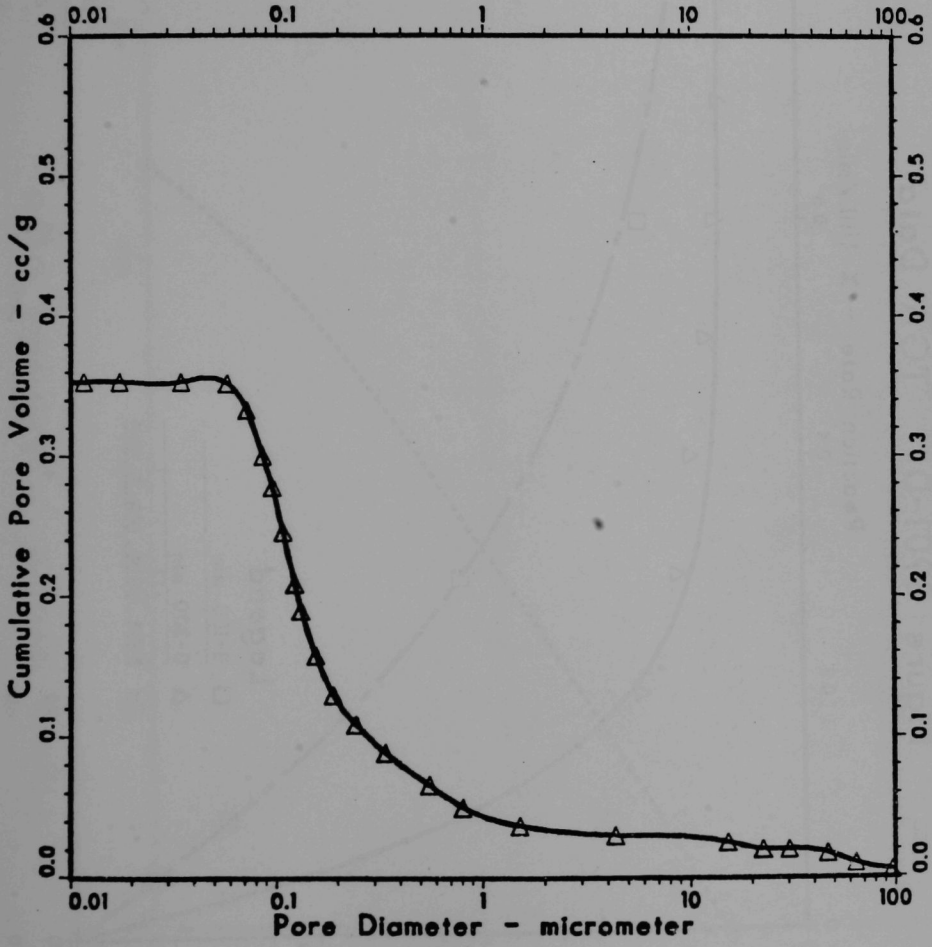

Figure 8901-D TGA Data

1123 K. 1 ATM
3000 PPM SO2
18-20 MESH

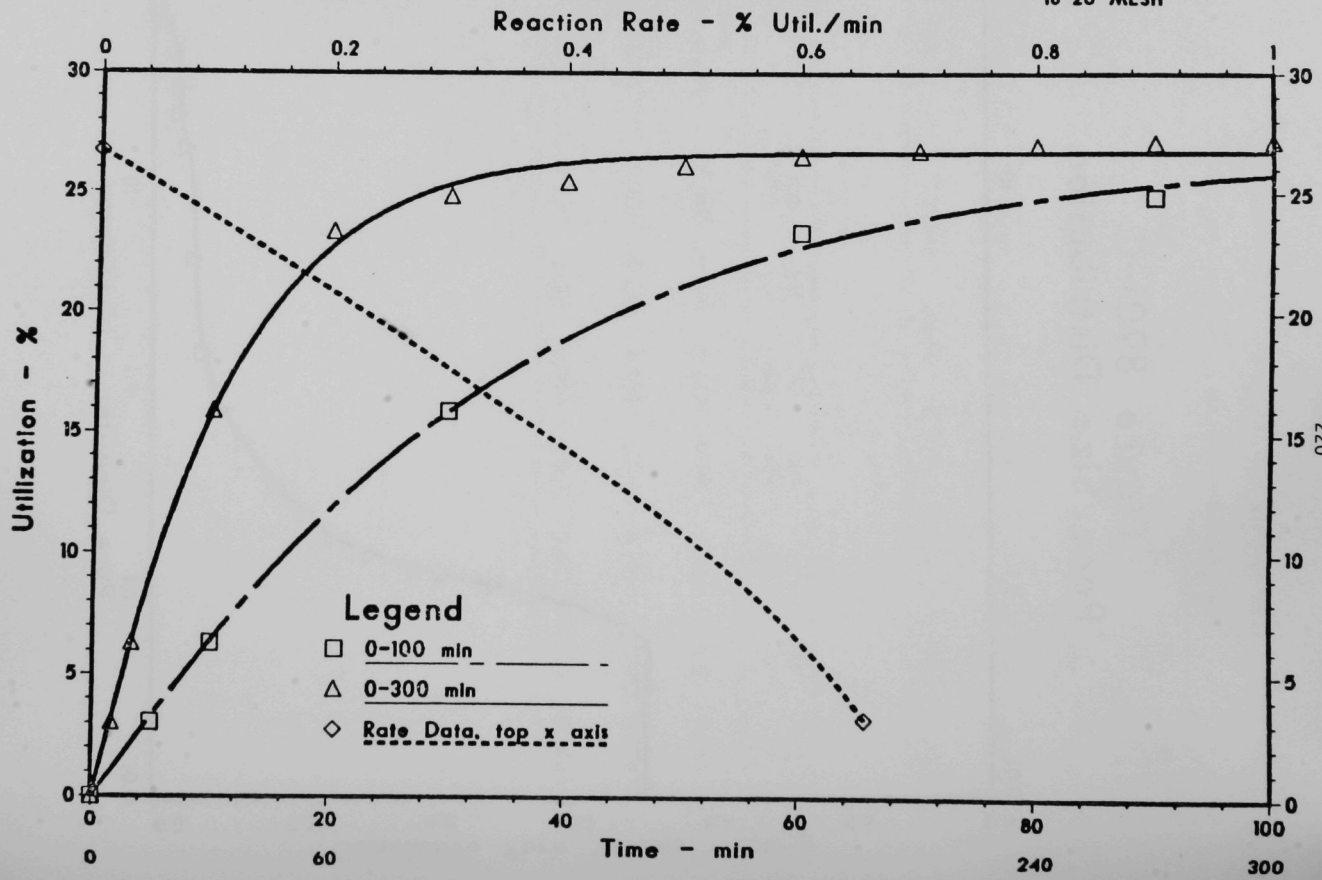

Figure 8901-E Attrition Data

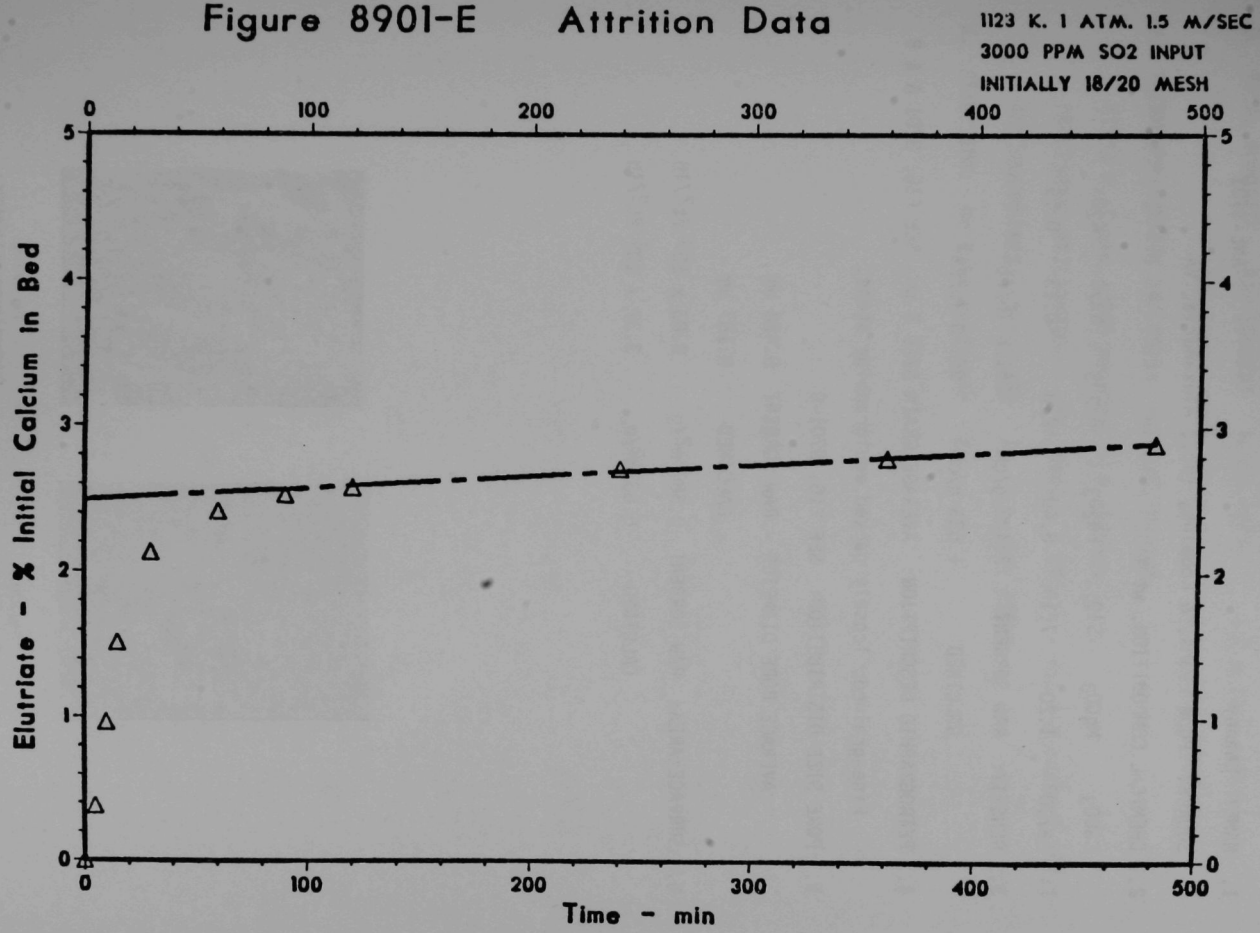

1. NAME: Chaney ANL-8701

SOURCE: Pope Evans, & Robbins, Inc., Alexandria, VA

2. CHEMICAL COMPOSITION, wt %

$CaCO_3$	$MgCO_3$	SiO_2	Fe_2O_3	Al_2O_3	Na_2O	K_2O
87.0	1.20	7.10	3.40	2.0	<0.13	0.19

3. DENSITY: RAW SORBENT 2.428 g/cm^3 151.6 lb/ft^3

CALCINED 1.533 g/cm^3 95.70 lb/ft^3

4. PETROGRAPHIC DESCRIPTION: AVERAGE GRAIN SIZE 5 μm, SEE FIG. 8701 A & B

Fine-grained; loosely packed equigranular stone.

5. PORE SIZE DISTRIBUTION: SEE FIG. 8701-C

AVERAGE PORE DIAMETER - RAW SORBENT 0.428 μm

CALCINED 0.187 μm

6. SURFACE AREA: RAW SORBENT 0.580 m^2/g 2.83 x 10^3 ft^2/lb

CALCINED 6.83 m^2/g 3.37 x 10^4 ft^2/lb

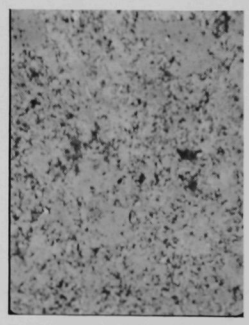

Fig. 8701A
Raw Limestone
50X

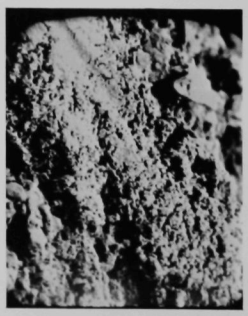

Fig. 8701B
Calcined Limestone 1 h 850°C
1100X

7. TOTAL POROSITY: RAW SORBENT 0.072 cm^3/g 1.2×10^{-5} ft^3/lb

CALCINED 0.396 cm^3/g 6.34×10^{-3} ft^3/lb

8. THERMOGRAVIMETRIC ANALYSIS: SEE FIG. 8701-D

(1123 K, 1 atm, 3000 ppm SO_2, -18 +20 mesh)

FRACTIONAL UTILIZATION = $\alpha(t, \text{min}) = 0.274\ [1 - \exp(-0.0426\ t^{0.967})]$

ANL PARAMETERS: D = 0.272 b = 405.3

9. ATTRITION: No data available

Figure 8701-C
Pore Size Distribution

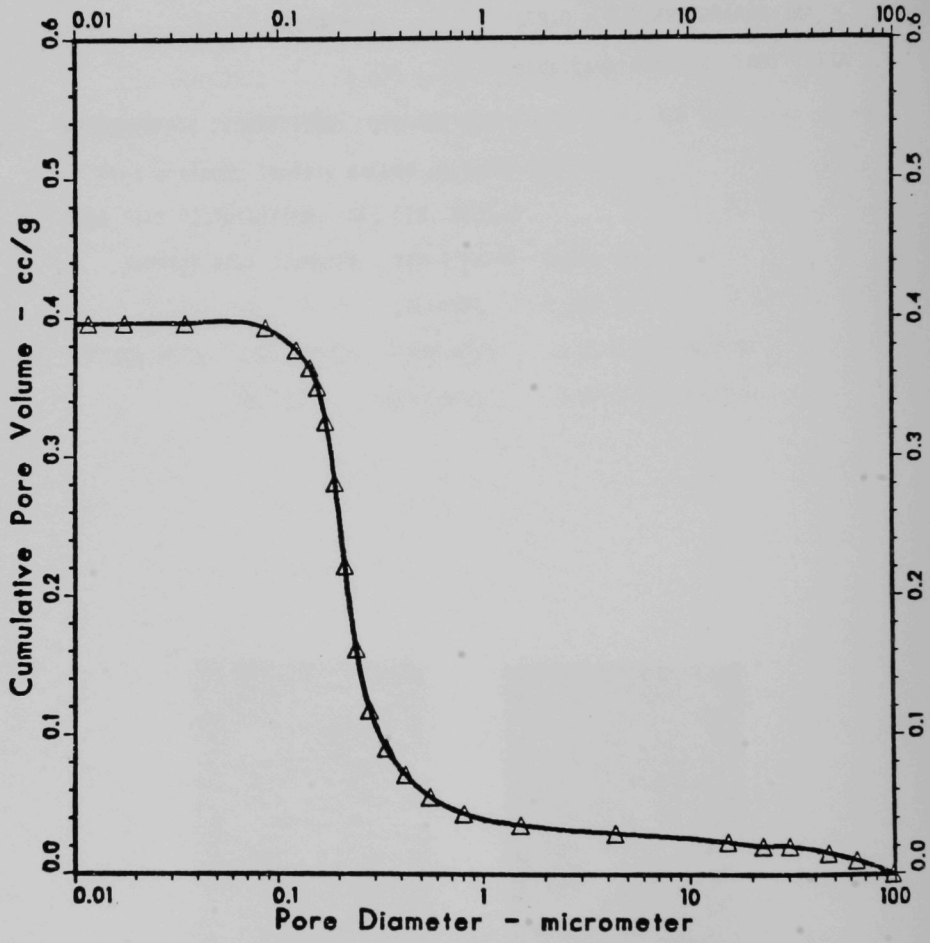

Figure 8701-D TGA Data

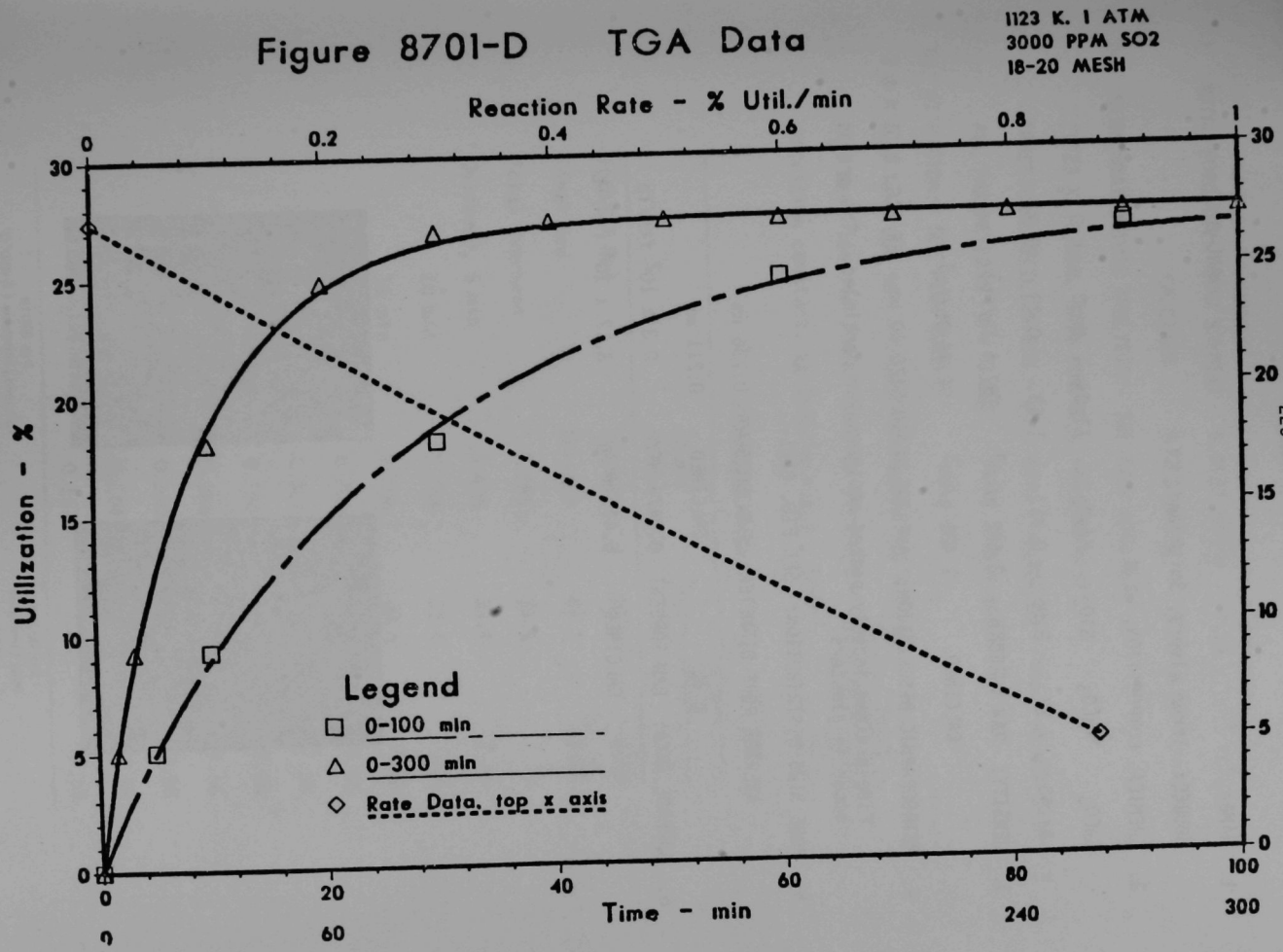

1. NAME: ANL-8201

   SOURCE: Three Rivers, Smithland, KY

2. CHEMICAL COMPOSITION, wt %

$CaCO_3$	$MgCO_3$	SiO_2	Fe_2O_3	Al_2O_3	Na_2O	K_2O
82.50	7.27	8.06	0.91	1.53	0.48	0.32

3. DENSITY: RAW SORBENT 2.682 g/cm^3 167.4 lb/ft^3

   CALCINED 1.481 g/cm^3 92.46 lb/ft^3

4. PETROGRAPHIC DESCRIPTION: AVERAGE GRAIN SIZE 40 μm, SEE FIG. 8201 A & B

   Fine-grained loosely packed equigranular particles. The grains occur in clusters.

5. PORE SIZE DISTRIBUTION: SEE FIG. 8201-C

   AVERAGE PORE DIAMETER - RAW SORBENT 0.736 μm

   CALCINED 0.211 μm

6. SURFACE AREA: RAW SORBENT 0.0473 m^2/g 2.3 x 10^2 ft^2/lb

   CALCINED 6.495 m^2/g 3.17 x 10^4 ft^2/lb

Fig. 8201A
Raw Limestone
50X

Fig. 8201B
Calcined Limestone 1 h 850°C
1000X

7. TOTAL POROSITY: RAW SORBENT 0.0137 cm^3/g 2.19×10^{-4} ft^3/lb

CALCINED 0.353 cm^3/g 5.65×10^{-3} ft^3/lb

8. THERMOGRAVIMETRIC ANALYSIS: SEE FIG. 8202-D

(1123 K, 1 atm, 3000 ppm SO_2, -18 +20 mesh)

FRACTIONAL UTILIZATION = $\alpha(t, \text{min}) = 0.258\ [1 - \exp(-0.143\ t^{0.614})]$

ANL PARAMETERS: D = 0.226 b = 465.9

9. ATTRITION: SEE FIG. 8202-E

Bed loss due to calcination breakup (%) = 0.96

Bed mass lost in linear portion (%/min.) = 1.0×10^{-3}

Attrition constant, λ_4 (sec^{-1}) = 2.3×10^{-7}

ATTRITION DATA

	Grams Total	wt % Ca	wt % S
Initial Bed	160.449	33.06	0.00
Final Bed	117.293	41.2	6.61
Total Overhead	2.295	33.5	7.58
Overhead, 5 min	0.406	33.5	7.58
10 min	0.264	33.5	7.58
15 min	0.196	33.5	7.58
30 min	0.200	33.5	7.58
1 h	0.306	33.5	7.58
1.5 h	0.158	33.5	7.58
2 h	0.188	33.5	7.58
4 h	0.260	33.5	7.58
6 h	0.166	33.5	7.58
8 h	0.151	33.5	7.58

Attrition Data, continued for Sorbent 8201

Weight in Grams, Particle Diameter, μm

Sample	-1000 +840	-841 +707	-707 +595	-595 +420	-420 +297	-297 +250
Overhead, first 30 min	0.000	0.000	0.000	0.004	0.021	0.038
Overhead, remaining 7.5 h	0.000	0.000	0.000	0.013	0.060	0.070
Final Bed, post test	110.663	4.025	0.653	0.493	0.433	0.204

Sample	-250 +210	-210 +74	-74 +63	-63 +53	-53 +44	-44 +37	-37 +0
Overhead, first 30 min	0.061	0.502	0.021	0.042	0.051	0.027	0.010
Overhead, remaining 7.5 h	0.090	0.682	0.019	0.042	0.062	0.041	0.049
Final Bed, post test	0.189	0.413	0.027	0.019	0.027	0.013	0.000

Figure 8201-C
Pore Size Distribution

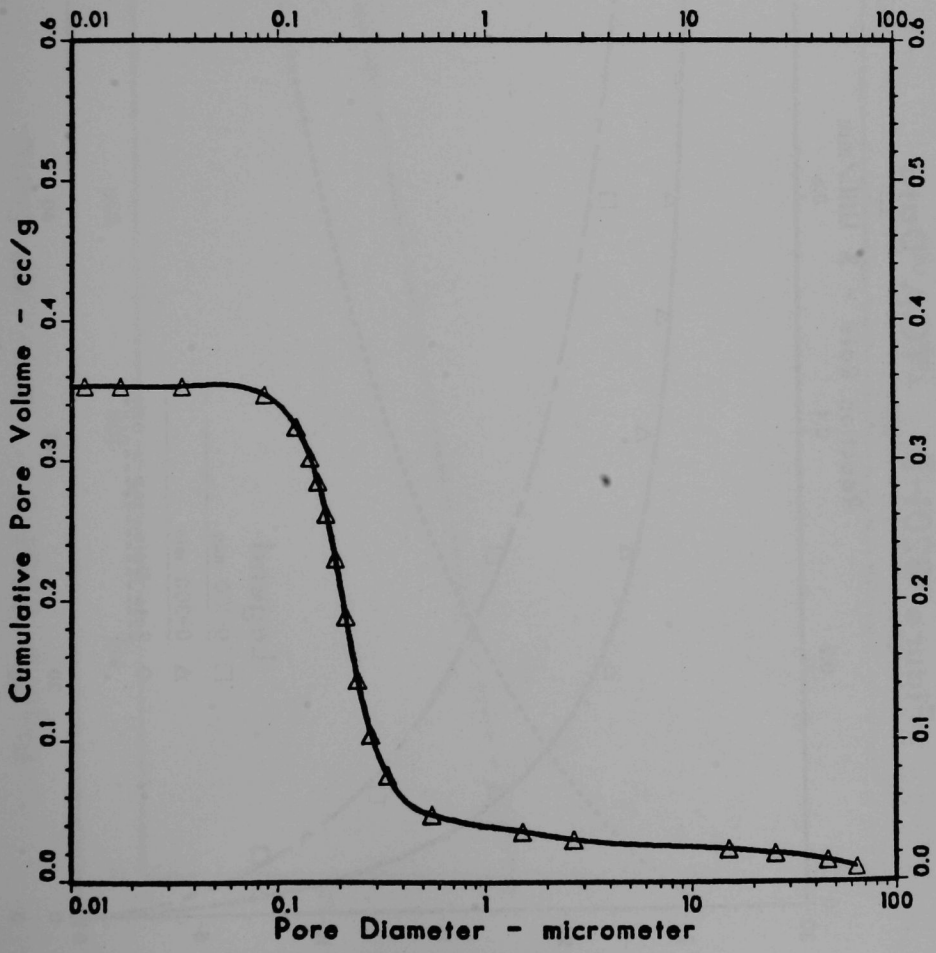

Figure 8201-D TGA Data

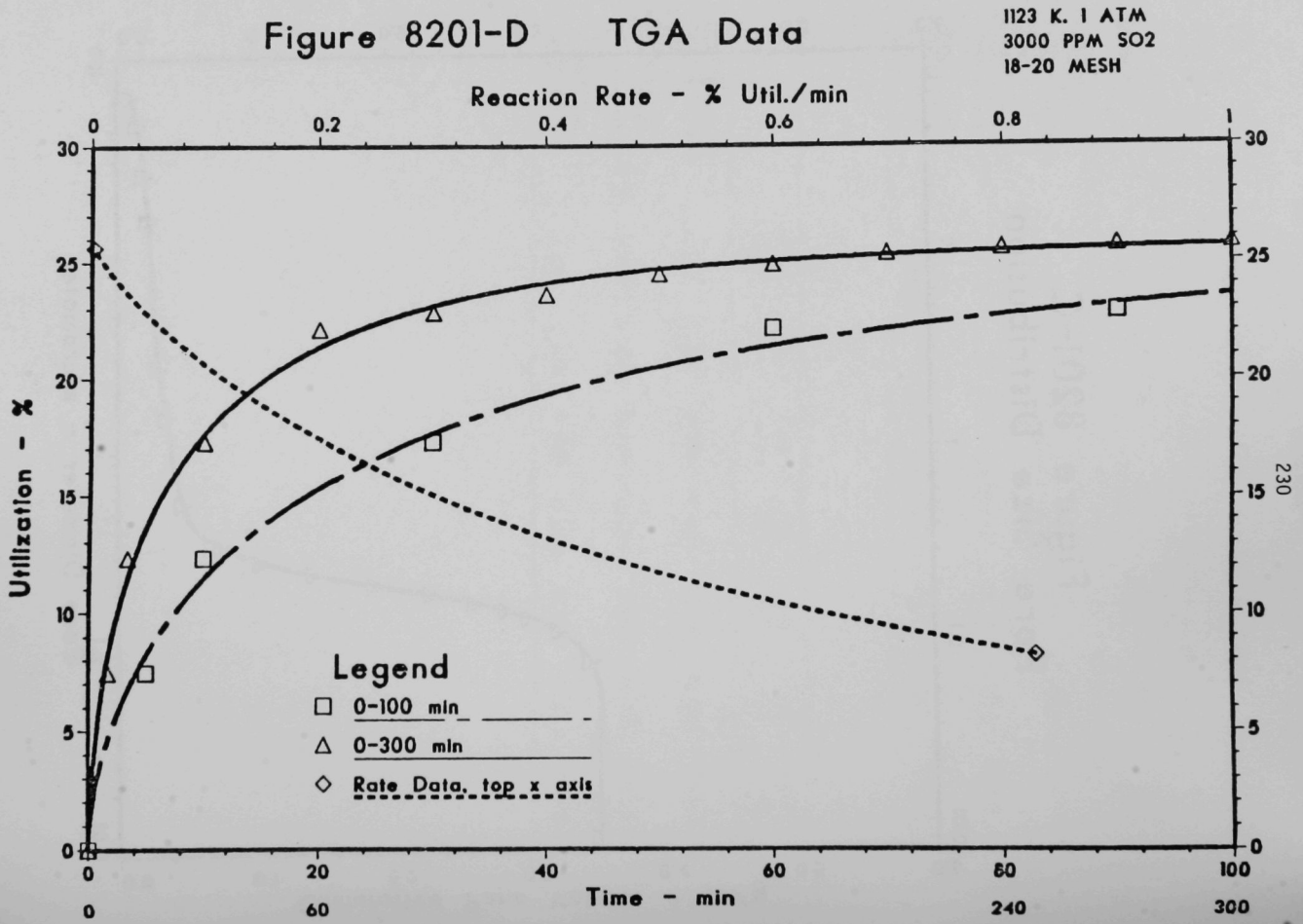

Figure 8201-E Attrition Data

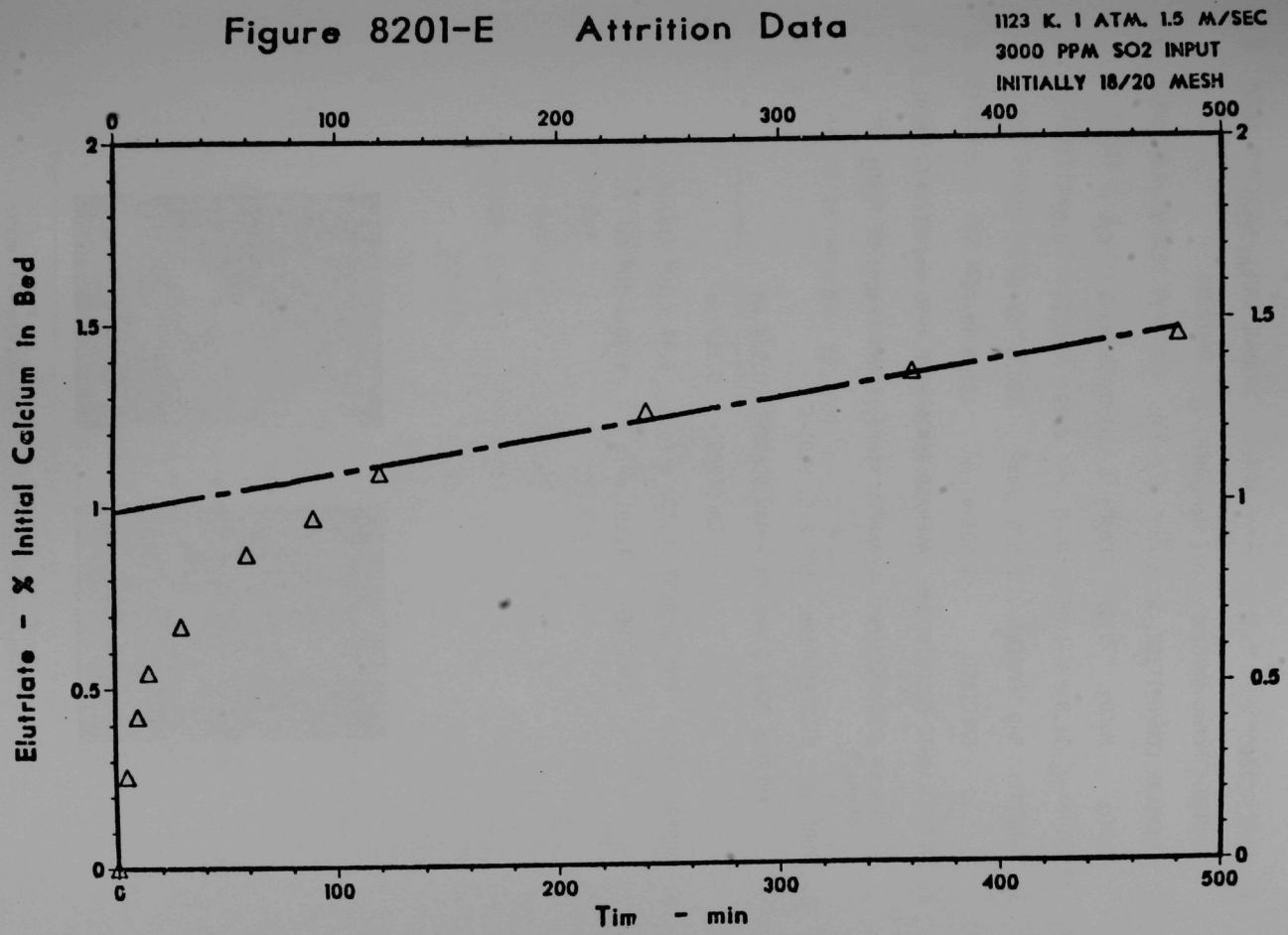

1. NAME: 1360 ANL-8101

SOURCE: Monmouth Stone Co., Monmouth, IL

2. CHEMICAL COMPOSITION, wt %

$CaCO_3$	$MgCO_3$	SiO_2	Fe_2O_3	Al_2O_3	Na_2O	K_2O
81.6	11.6	1.86	0.86	0.19	0.10	0.07

3. DENSITY: RAW SORBENT 2.576 g/cm^3 160.8 lb/ft^3

CALCINED 1.631 g/cm^3 101.8 lb/ft^3

4. PETROGRAPHIC DESCRIPTION: AVERAGE GRAIN SIZE >250 μm, SEE FIG. 8101 A & B

Coarse-grained; inequigranular stone; small traces of Fe_2O_3 present.

5. PORE SIZE DISTRIBUTION: SEE FIG. 8101-C

AVERAGE PORE DIAMETER - RAW SORBENT 0.954 μm

CALCINED 0.117 μm

6. SURFACE AREA: RAW SORBENT 0.132 m^2/g 6.47 x 10^2 ft^2/lb

CALCINED 12.91 m^2/g 6.30 x 10^4 ft^2/lb

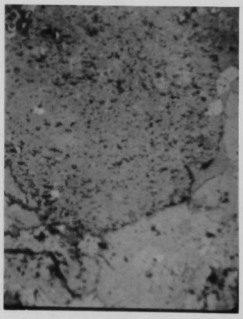

Fig. 8101A
Raw Limestone
50X

Fig. 8101B
Calcined Limestone 1 h 850°C
1100X

7. TOTAL POROSITY: RAW SORBENT 0.039 cm^3/g 6.2×10^{-4} ft^3/lb

CALCINED 0.453 cm^3/g 7.26×10^{-3} ft^3/lb

8. THERMOGRAVIMETRIC ANALYSIS: SEE FIG. 8101-D

(1123 K, 1 atm, 3000 ppm SO_2, -18 +20 mesh)

FRACTIONAL UTILIZATION = $\alpha(t, \text{min}) = 0.506\ [1 - \exp(-0.0652\ t^{0.704})]$

ANL PARAMETERS: D = 0.461 b = 213.3

9. ATTRITION: SEE FIG. 8101-E

Bed loss due to calcination breakup (%) = 44.4

Bed mass lost in linear portion (%/min.) = 9.83×10^{-4}

Attrition constant, λ_4 (sec^{-1}) = 2.76×10^{-7}

ATTRITION DATA

	Grams Total	wt %	
		Ca	S
Initial Bed	160.001	32.64	0.00
Final Bed	67.940	35.3	8.83
Total Overhead	56.561	41.6	2.35
Overhead, 5 min	39.768	41.6	2.35
10 min	5.425	41.6	2.35
15 min	3.968	41.6	2.35
30 min	5.633	41.6	2.35
1 h	0.837	41.6	2.35
1.5 h	0.389	41.6	2.35
2 h	0.086	41.6	2.35
4 h	0.200	41.6	2.35
6 h	0.126	41.6	2.35
8 h	0.130	41.6	2.35

Attrition Data, continued for Sorbent 8101

Weight in Grams, Particle Diameter, μm

Sample	-1000 +840	-841 +707	-707 +595	-595 +420	-420 +297	-297 +250
Overhead, first 30 min	0.002	0.001	0.002	0.007	0.155	0.491
Overhead, remaining 7.5 h	0.003	0.001	0.001	0.011	1.271	1.681
Final Bed, post test	45.939	5.670	2.621	4.538	6.400	1.795

Sample	-250 +210	-210 +74	-74 +63	-63 +53	-53 +44	-44 +37	-37 +0
Overhead, first 30 min	3.288	39.391	0.075	0.587	1.799	1.194	1.901
Overhead, remaining 7.5 h	1.747	1.911	0.050	0.113	0.199	0.093	0.162
Final Bed, post test	0.821	0.185	0.006	0.020	0.040	0.010	0.011

10. OTHER DATA

See Figs. 8101-F and 8101-G for decrepitation data.

Figure 8101-C
Pore Size Distribution

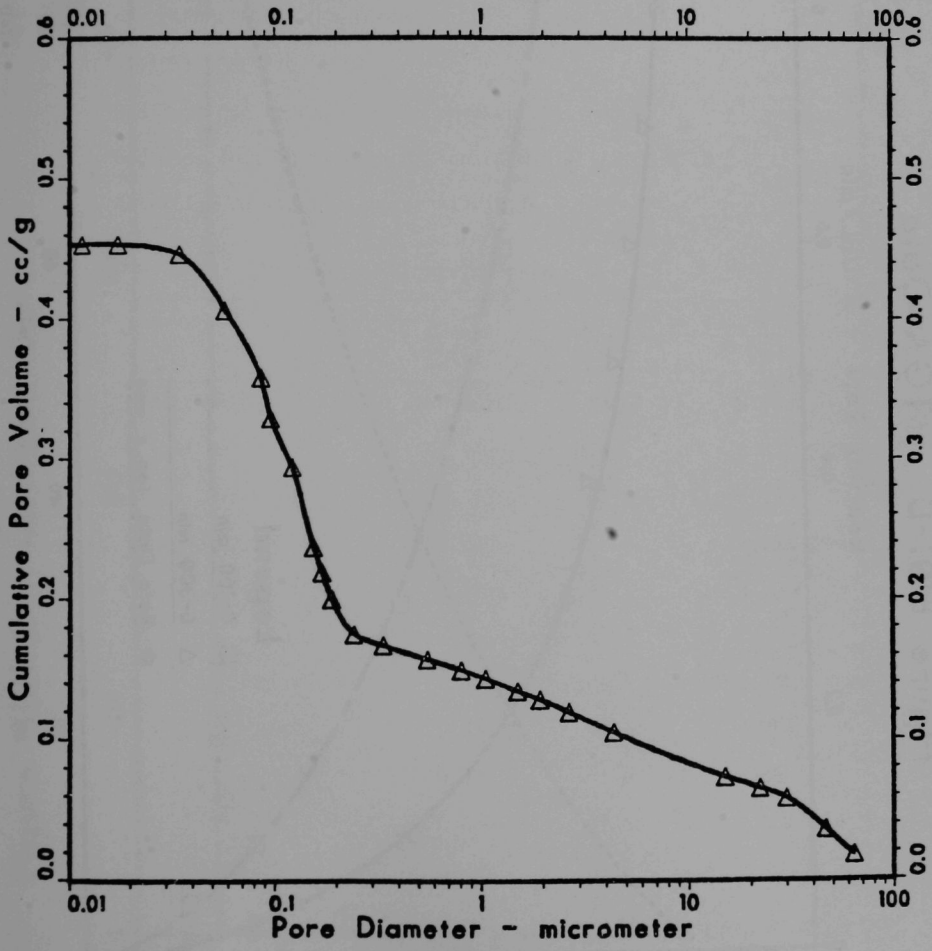

Figure 8101-D TGA Data

1123 K. 1 ATM
3000 PPM SO2
18-20 MESH

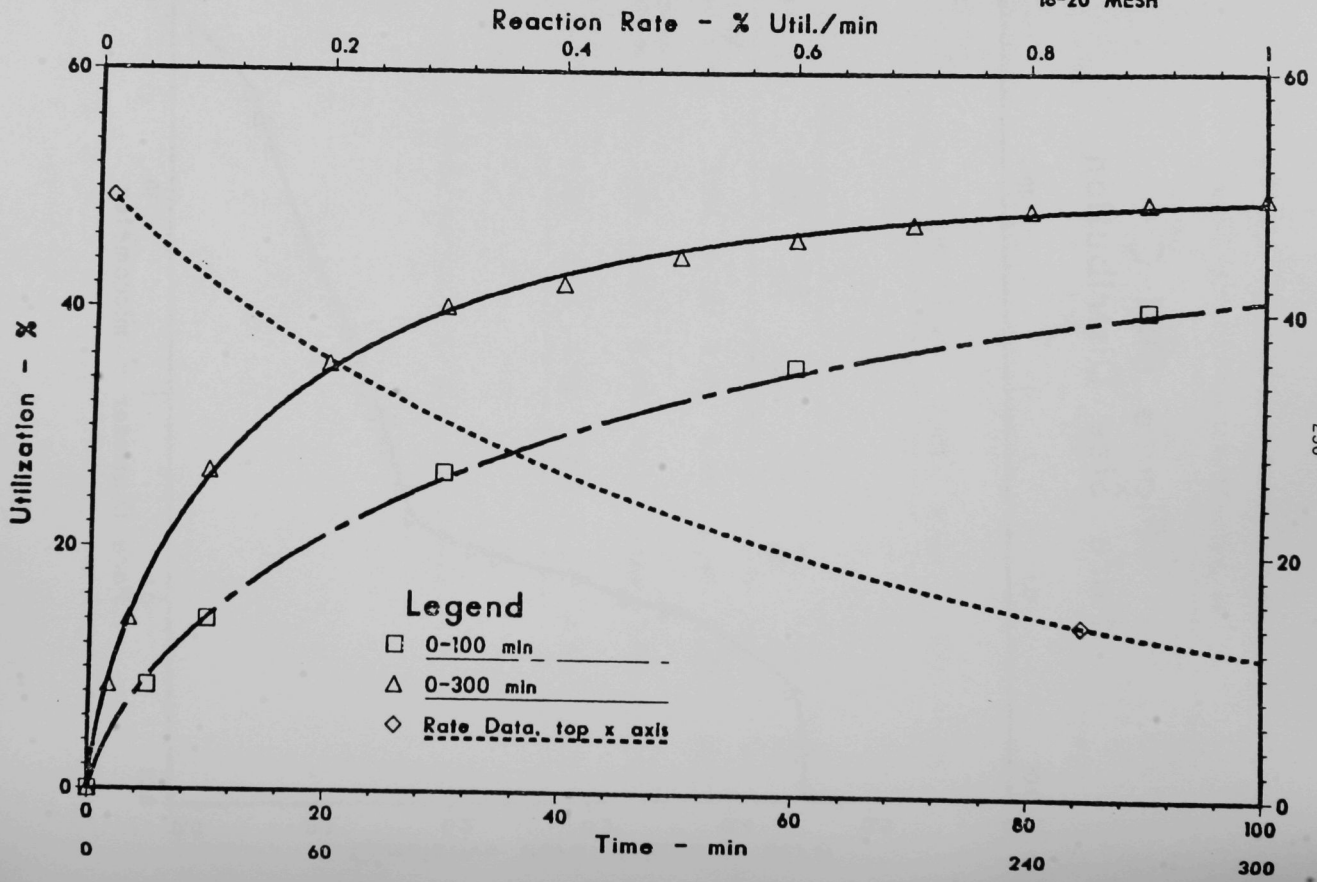

Figure 8101-E Attrition Data

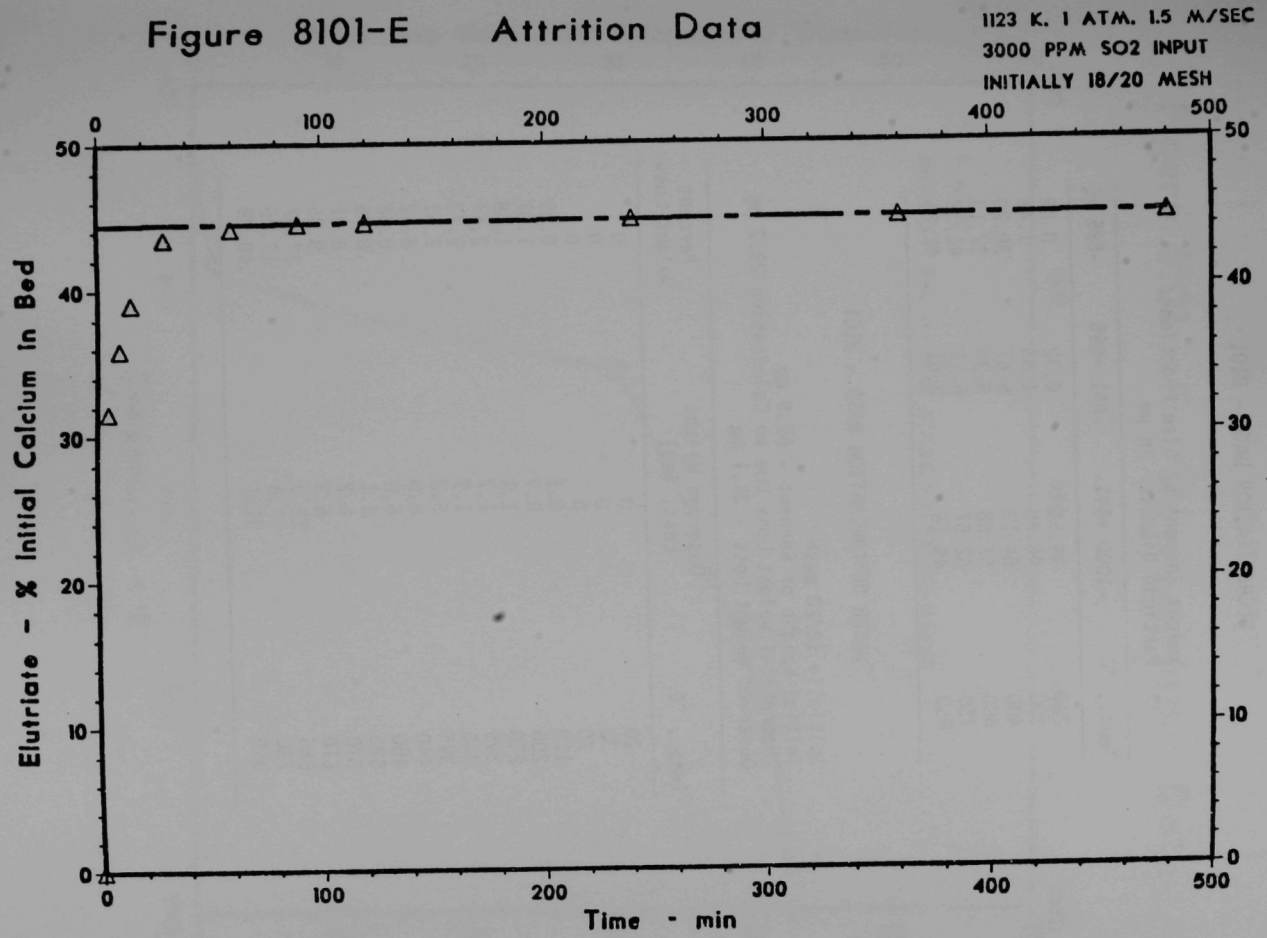

DECREPITATION DATA - 8101

Temp., °C	Weight Percent of Size Fractions, Particle Diameter in µm -1000 +841	-841 +595	-595 +0
200	99.60	0.32	0.09
300	96.68	1.86	1.46
400	64.13	5.67	30.20
600	57.58	5.30	37.13
750	52.57	6.11	41.32
850	49.15	8.61	42.25

WATER DETERMINATION DATA - 8101

Initially 18/20 mesh
Initial Weight of Sorbent - 69.6 mg
Theoretical Weight Loss Due to Calcination 29.2 mg
Observed Weight Loss - 34.1 mg

Temp., °C	Observed Weight Loss, (mg)	Percent Weight Loss
20	0	0
30	0	0
70	0	0
110	0.2	0.29
200	0.7	1.01
250	1.1	1.58
295	1.7	2.44
340	1.9	2.73
395	5.3	7.61
440	6.0	8.62
480	6.0	8.62
525	6.1	8.76
570	6.2	8.91
610	6.3	9.05
655	12.3	17.67
730	17.8	17.25
850	34.1	48.99

Figure 8101 -F Decrepitation Data

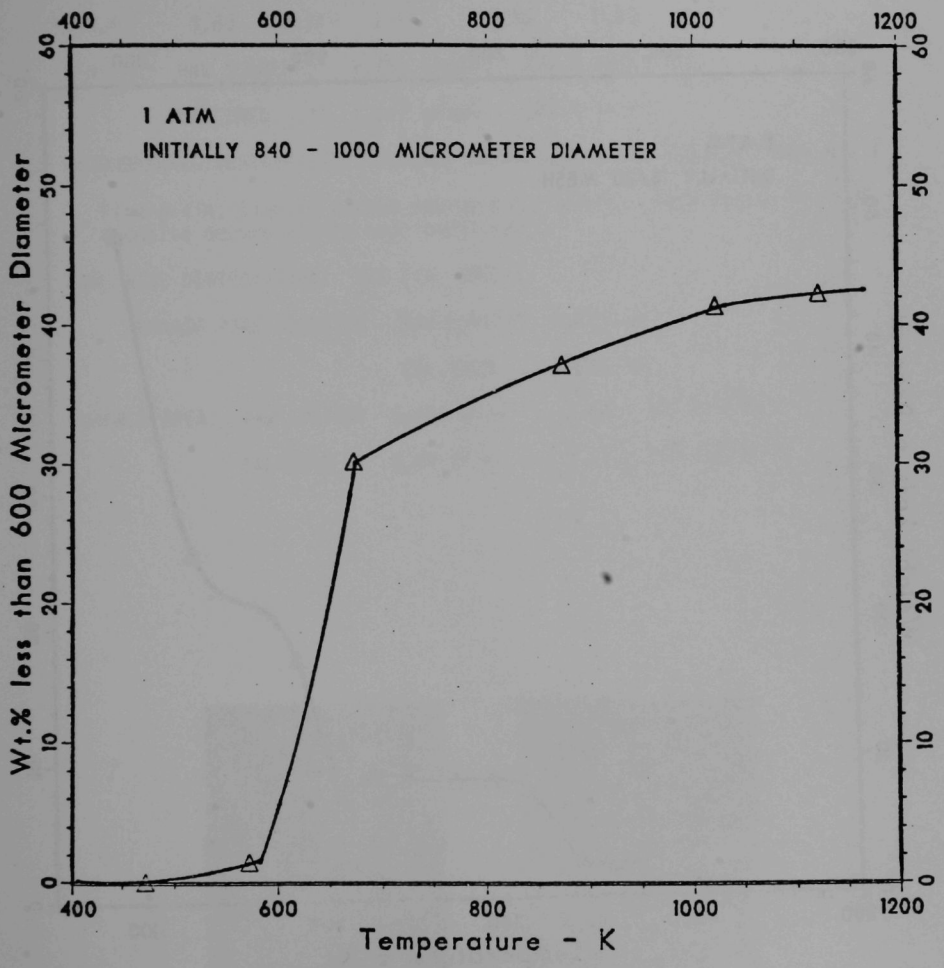

Figure 8101 -G Water Loss Data

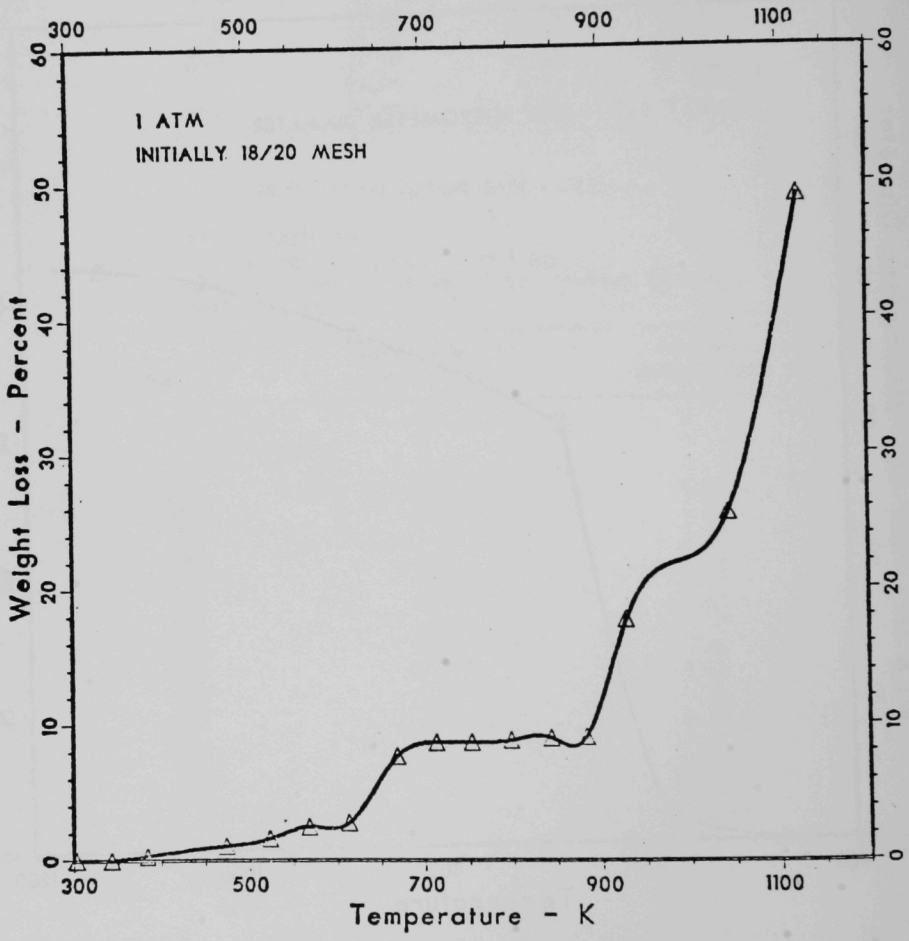

1. NAME: Greer ANL-8001

   SOURCE: Greer Limestone Co., Morgantown, WV

2. CHEMICAL COMPOSITION, wt %

$CaCO_3$	$MgCO_3$	SiO_2	Fe_2O_3	Al_2O_3	Na_2O	K_2O
80.4	3.50	10.34	1.24	3.18	0.23	0.72

3. DENSITY: RAW SORBENT 2.752 g/cm^3 171.8 lb/ft^3

   CALCINED 1.637 g/cm^3 102.2 lb/ft^3

4. PETROGRAPHIC DESCRIPTION: AVERAGE GRAIN SIZE 5 μm, SEE FIG. 8001 A & B

   Fine-grain; tightly packed equigranular stone. Some coarse grained deposite occurs within some particles.

5. PORE SIZE DISTRIBUTION: SEE FIG. 8001-C

   AVERAGE PORE DIAMETER - RAW SORBENT 0.223 μm

   CALCINED 0.211 μm

6. SURFACE AREA: RAW SORBENT 0.054 m^2/g 2.63 x 10^2 ft^2/lb

   CALCINED 6.64 m^2/g 3.24 x 10^4 ft^2/lb

Fig. 8001A
Raw Limestone
50X

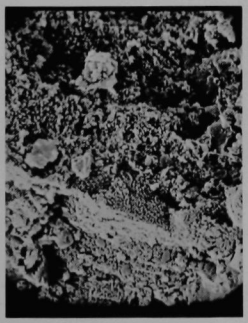

Fig. 8001B
Calcined Limestone 1 h 850°C
1100X

7. TOTAL POROSITY: RAW SORBENT 0.003 cm^3/g 4.8×10^{-5} ft^3/lb

CALCINED 0.325 cm^3/g 5.21×10^{-3} ft^3/lb

8. THERMOGRAVIMETRIC ANALYSIS: SEE FIG. 8001-D

(1123 K, 1 atm, 3000 ppm SO_2, -18 +20 mesh)

FRACTIONAL UTILIZATION = $\alpha(t, min) = 0.193 [1 - exp (-0.090 t^{0.808})]$

ANL PARAMETERS: D = 0.182 b = 560.2

9. ATTRITION: SEE FIG. 8001-E

Bed loss due to calcination breakup (%) = 0.82

Bed mass lost in linear portion (%/min.) = 8.42×10^{-4}

Attrition constant, λ_4 (sec^{-1}) = 1.92×10^{-7}

ATTRITION DATA

	Grams Total	wt % Ca	wt % S
Initial Bed	160.001	32.16	0.00
Final Bed	124.410	41.9	6.57
Total Overhead	1.824	34.5	3.14
Overhead, 5 min	0.460	34.5	3.14
10 min	0.126	34.5	3.14
15 min	0.150	34.5	3.14
30 min	0.142	34.5	3.14
1 h	0.127	34.5	3.14
1.5 h	0.218	34.5	3.14
2 h	0.152	34.5	3.14
4 h	0.157	34.5	3.14
6 h	0.161	34.5	3.14
8 h	0.131	34.5	3.14

Attrition Data, continued for Sorbent 8001

Weight in Grams, Particle Diameter, μm

Sample	-1000 +840	-841 +707	-707 +595	-595 +420	-420 +297	-297 +250
Overhead, first 30 min	0.006	0.006	0.005	0.004	0.003	0.003
Overhead, remaining 7.5 h	0.011	0.009	0.006	0.011	0.007	0.022
Final Bed, post test	122.950	0.814	0.105	0.068	0.034	0.018

Sample	-250 +210	-210 +74	-74 +63	-63 +53	-53 +44	-44 +37	-37 +0
Overhead, first 30 min	0.002	0.203	0.024	0.002	0.010	0.005	0.000
Overhead, remaining 7.5 h	0.201	0.004	0.012	0.007	0.007	0.000	0.000
Final Bed, post test	0.034	0.310	0.008	0.035	0.028	0.016	0.010

10. OTHER DATA: TGA Data: 1123 K, 1 atm, 3000 ppm SO_2

See Fig. 8001-F $\alpha(t,min) = 0.578\ [1 - \exp(-0.0286\ t^{0.951})]$

-50 +70 mesh $D = 0.571$ $b = 258$

See Fig. 8001-G $\alpha(t,min) = 0.7155\ [1 - \exp(-0.03318\ t^{0.8575})]$

-140 +170 mesh $D = 0.700$ $b = 192$

See Figs. 8001-H and 8001-I for decrepitation data.

Figure 8001-C
Pore Size Distribution

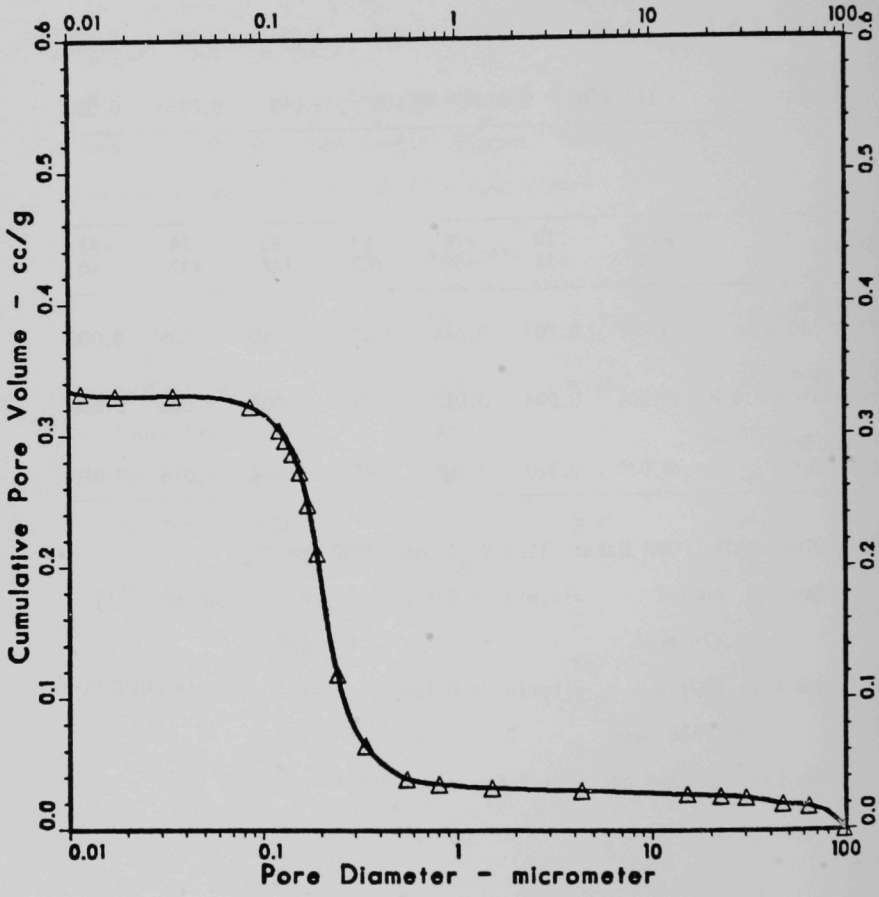

Figure 8001-D TGA Data

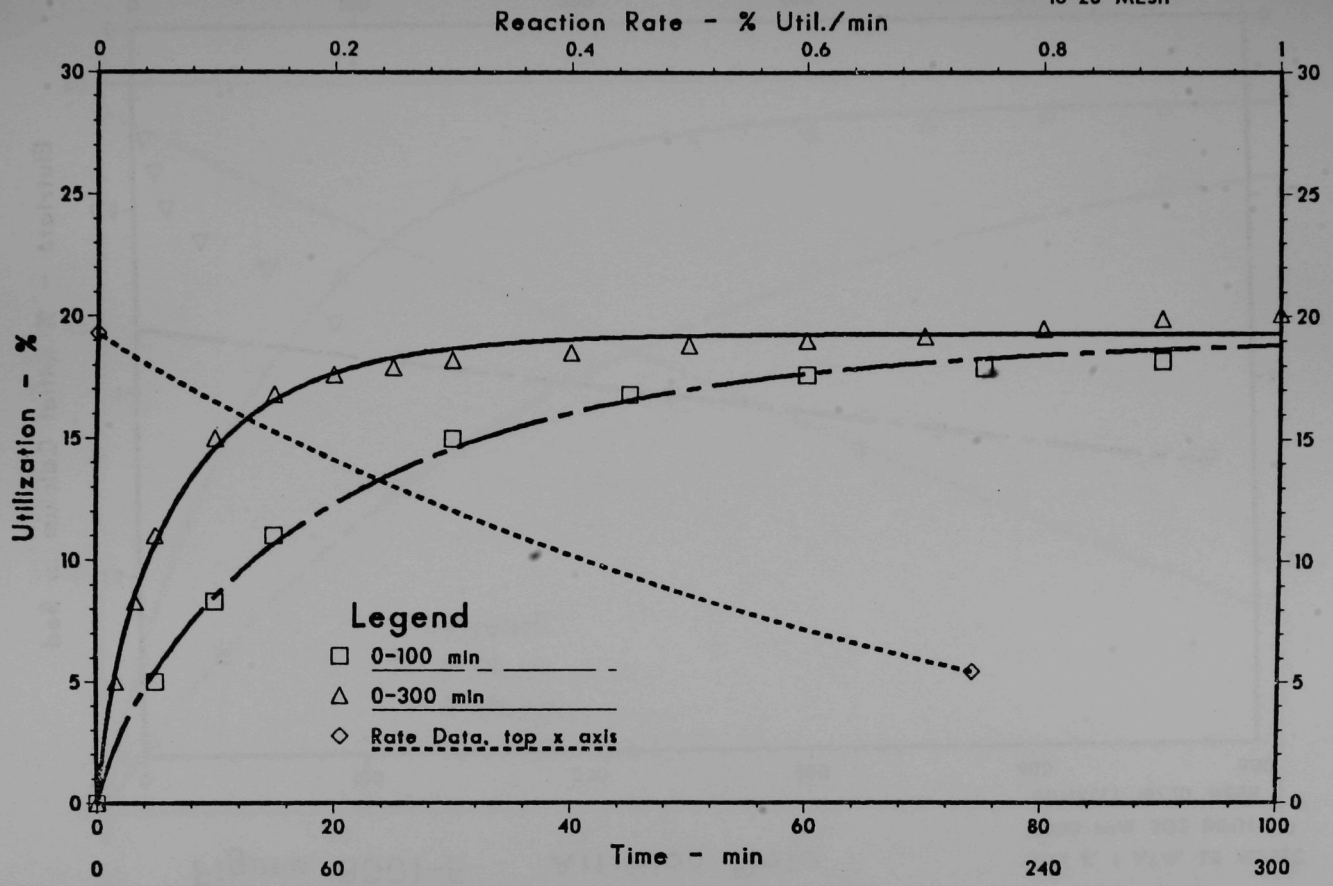

Figure 8001-E Attrition Data

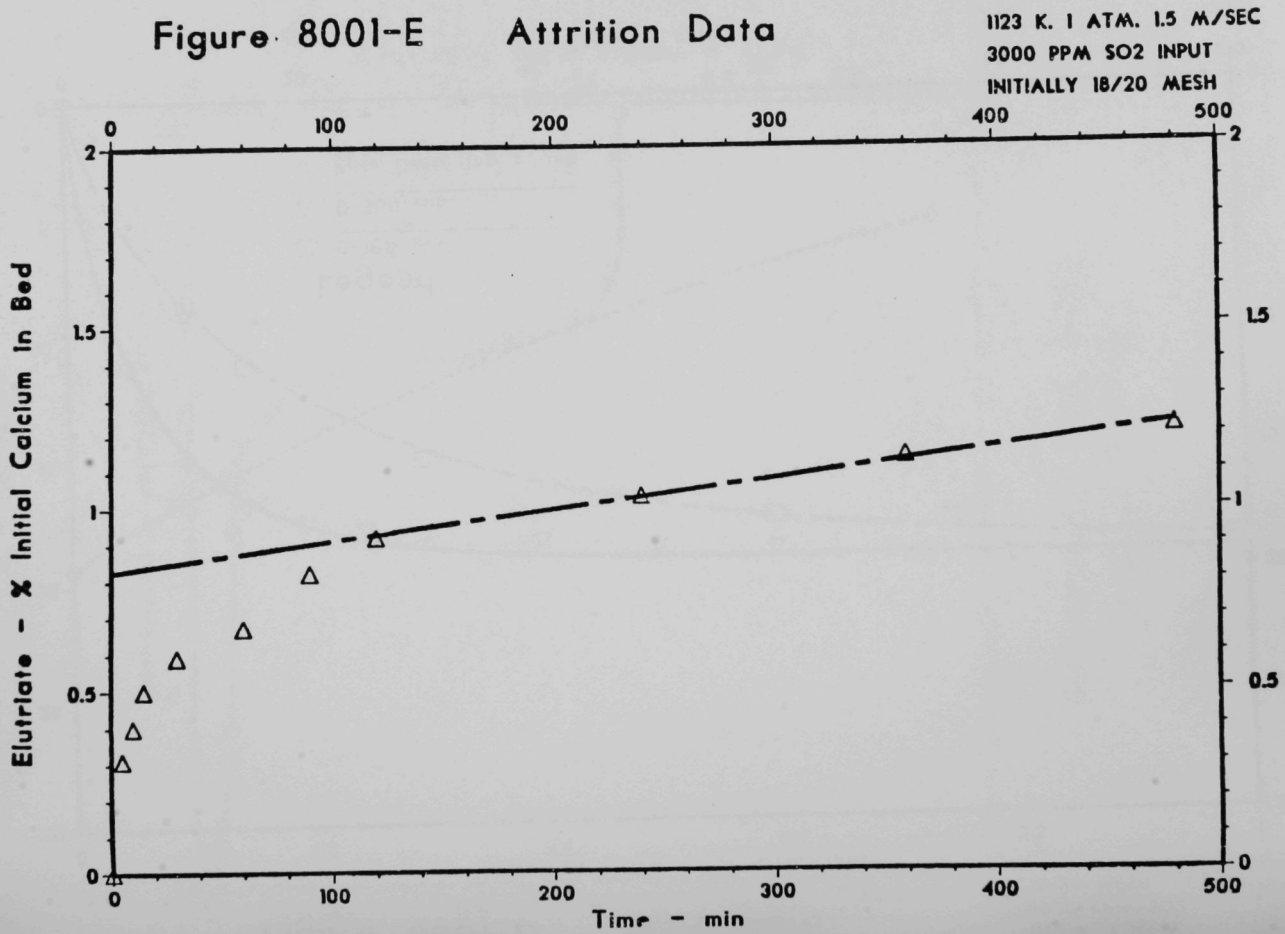

Figure 8001-F TGA Data

1123 K. 1 ATM
3000 PPM SO2
50-70 MESH

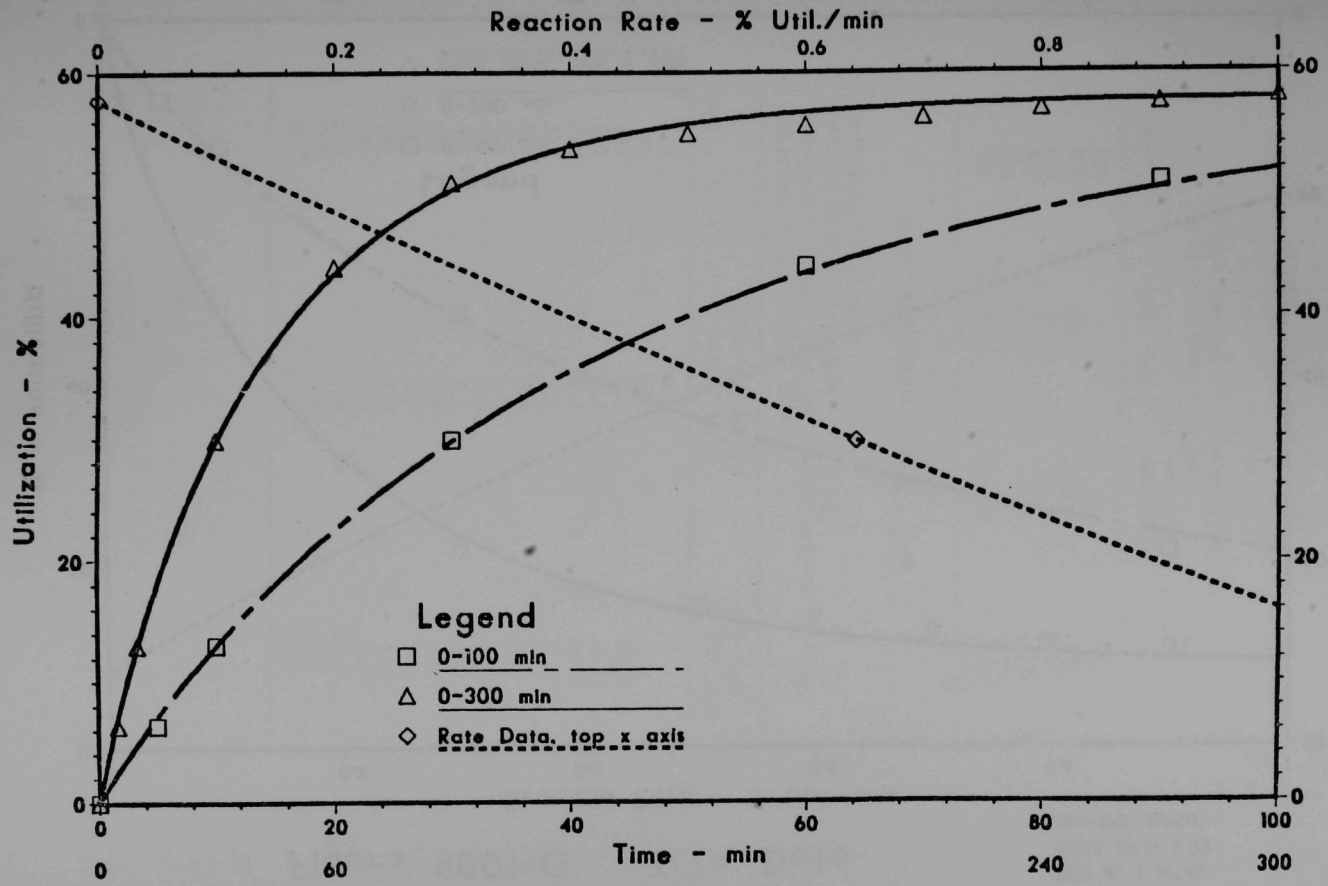

Figure 8001-G TGA Data

1123 K. 1 ATM
3000 PPM SO2
140-170 MESH

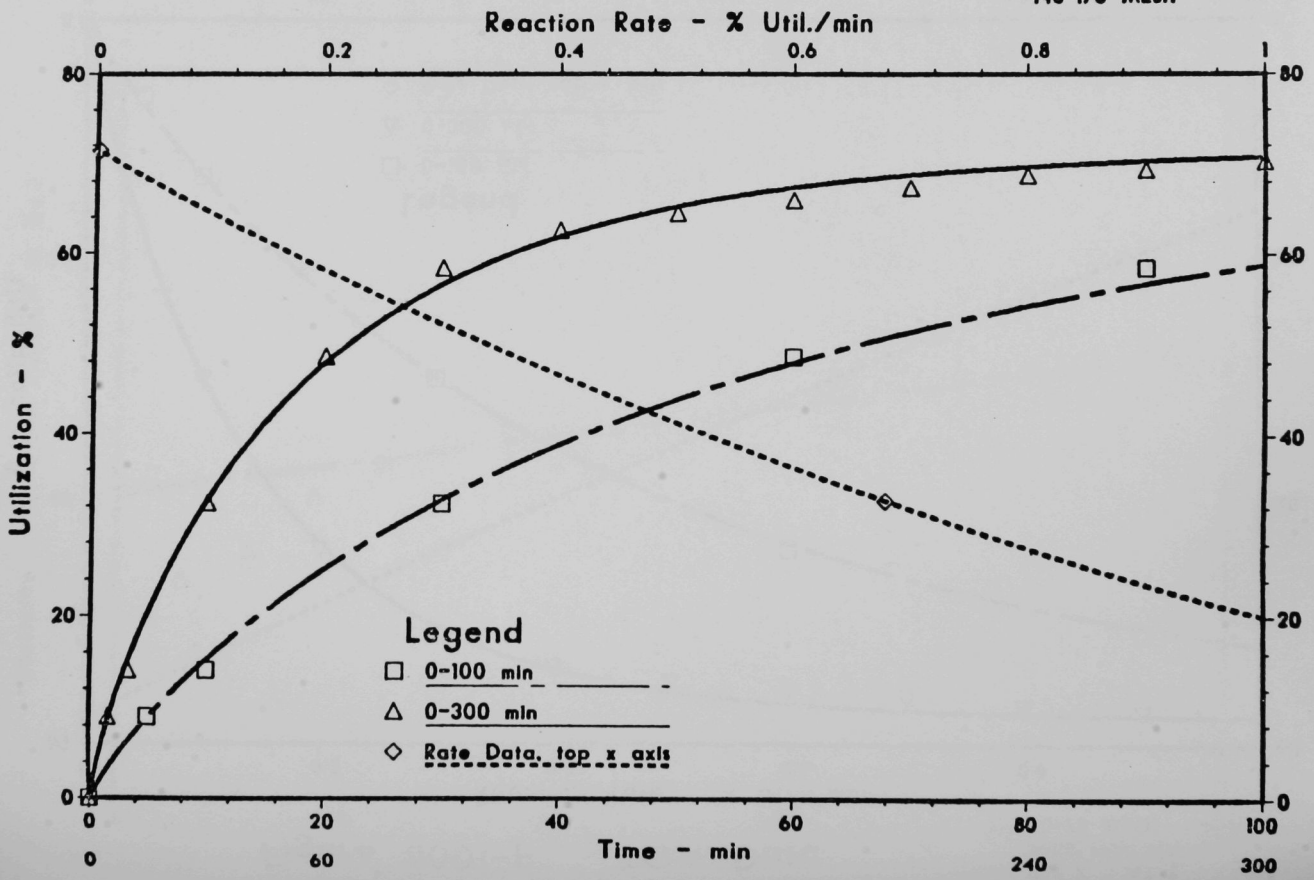

DECREPITATION DATA - 8001

Weight Percent of Size Fractions,
Particle Diameter in μm

Temp., °C	-1000 +841	-841 +595	-595 +0
200	--	--	--
300	99.2	0.74	0.02
400	98.7	1.3	0.07
600	98.4	1.4	0.24
750	98.2	1.4	0.30
850	98.1	1.5	0.42

WATER DETERMINATION DATA - 8001

Initially 18/20 mesh
Initial Weight of Sorbent - 97.9 mg
Theoretical Weight Loss Due to Calcination 36.4 mg
Observed Weight Loss - 37.9 mg

Temp., °C	Observed Weight Loss, (mg)	Percent Weight Loss
0	0	0
30	0	0
90	0.2	0.20
140	0.3	0.30
230	0.7	0.70
310	1.2	1.2
360	1.5	1.5
410	1.8	1.8
460	2.2	2.2
490	2.8	2.9
520	3.2	3.3
550	3.8	3.9
580	4.9	5.0
630	8.5	8.75
670	14.5	14.8
740	33.5	34.2
850	37.9	38.7

Figure 8001-H Decrepitation Data

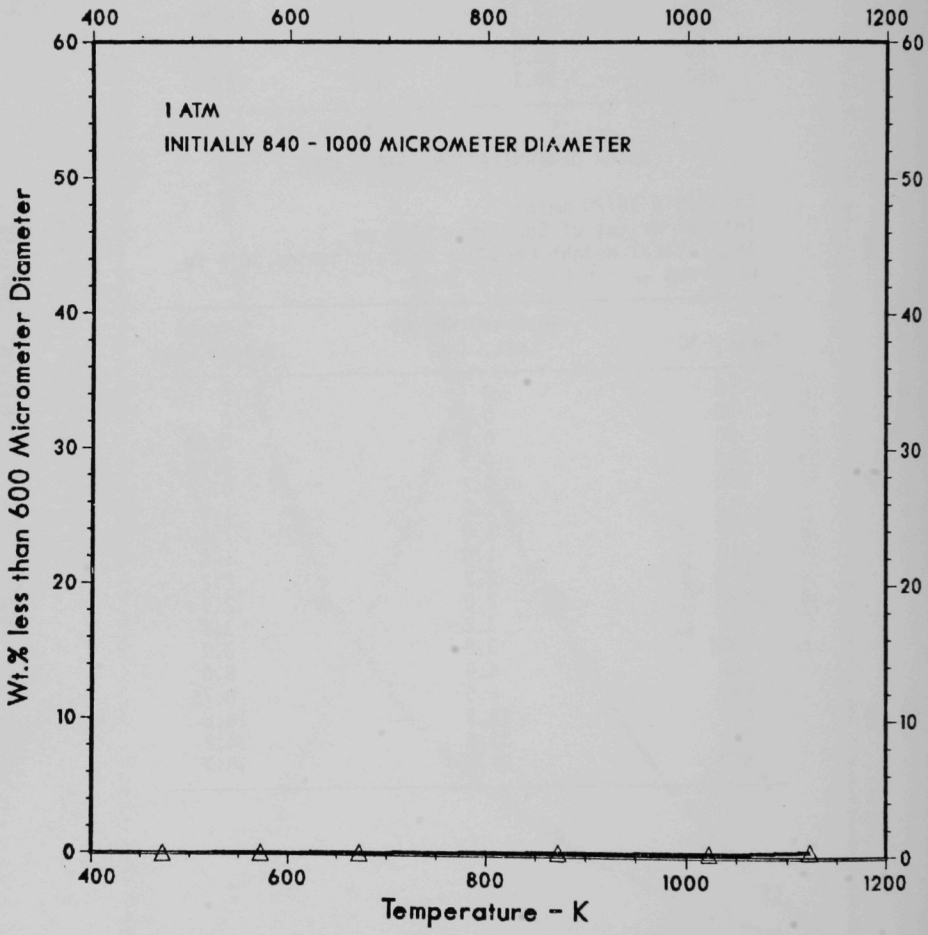

Figure 8001-1 Water Loss Data

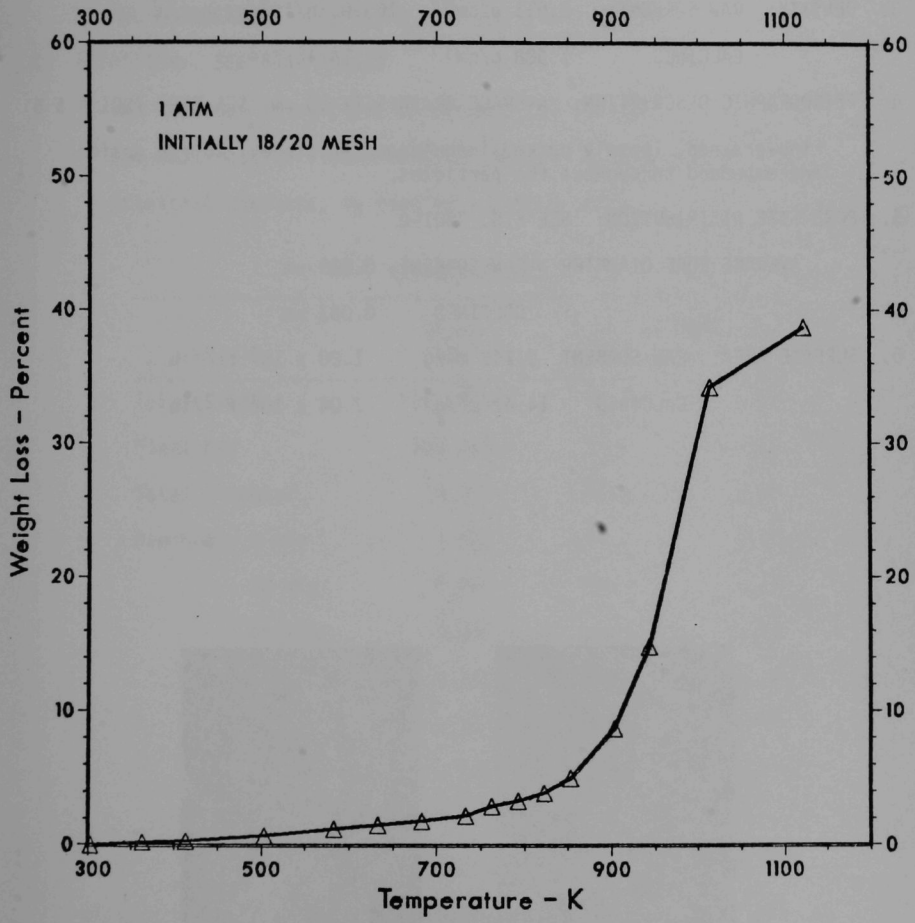

1. NAME: ANL-7901

SOURCE: Kentucky Stone Co., Canton, KY

2. CHEMICAL COMPOSITION, wt %

$CaCO_3$	$MgCO_3$	SiO_2	Fe_2O_3	Al_2O_3	Na_2O	K_2O
79.8	3.18	15.8	0.98	0.36	0.94	0.17

3. DENSITY: RAW SORBENT 2.611 g/cm^3 163.0 lb/ft^3

CALCINED 1.588 g/cm^3 99.14 lb/ft^3

4. PETROGRAPHIC DESCRIPTION: AVERAGE GRAIN SIZE 30 μm, SEE FIG. 7901 A & B

Fine-grained, loosely packed inequigranular stone. Coarse grains are embedded throughout the particles.

5. PORE SIZE DISTRIBUTION: SEE FIG. 7901-C

AVERAGE PORE DIAMETER - RAW SORBENT 0.209 μm

CALCINED 0.083 μm

6. SURFACE AREA: RAW SORBENT 0.245 m^2/g 1.20 x 10^3 ft^2/lb

CALCINED 14.42 m^2/g 7.04 x 10^4 ft^2/lb

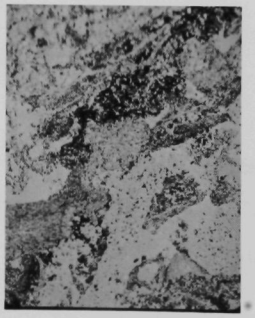

Fig. 7901A
Raw Limestone
50X

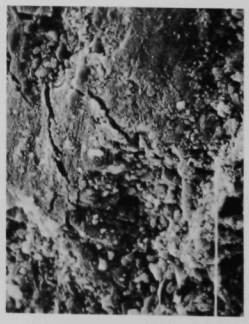

Fig. 7901B
Calcined Limestone 1 h 850°C
1000X

7. TOTAL POROSITY: RAW SORBENT 0.013 cm^3/g 2.1×10^{-4} ft^3/lb

CALCINED 0.309 cm^3/g 4.95×10^{-3} ft^3/lb

8. THERMOGRAVIMETRIC ANALYSIS: SEE FIG. 7901-D

(1123 K, 1 atm, 3000 ppm SO_2, -18 +20 mesh)

FRACTIONAL UTILIZATION = $\alpha(t, min) = 0.290 [1 - exp (-0.0772 t^{0.803})]$

ANL PARAMETERS: D = 0.278 b = 398.9

9. ATTRITION: SEE FIG. 7901-E

Bed loss due to calcination breakup (%) = 2.25

Bed mass lost in linear portion (%/min.) = 1.05×10^{-3}

Attrition constant, λ_4 (sec^{-1}) = 2.40×10^{-7}

ATTRITION DATA

	Grams Total	wt % Ca	wt % S
Initial Bed	161.276	31.92	0.00
Final Bed	123.966	43.4	8.45
Total Overhead	3.527	40.3	6.42
Overhead, 5 min	1.520	40.3	6.42
10 min	0.700	40.3	6.42
15 min	0.200	40.3	6.42
30 min	0.266	40.3	6.42
1 h	0.187	40.3	6.42
1.5 h	0.104	40.3	6.42
2 h	0.073	40.3	6.42
4 h	0.126	40.3	6.42
6 h	0.182	40.3	6.42
8 h	0.168	40.3	6.42

Attrition Data, continued for Sorbent 7901

Weight in Grams, Particle Diameter, μm

Sample	-1000 +840	-841 +707	-707 +595	-595 +420	-420 +297	-297 +250
Overhead, first 30 min	0.000	0.000	0.000	0.000	0.027	0.068
Overhead, remaining 7.5 h	0.000	0.000	0.000	0.014	0.047	0.058
Final Bed, post test	121.435	1.040	0.176	0.232	0.380	0.189

Sample	-250 +210	-210 +74	-74 +63	-63 +53	-53 +44	-44 +37	-37 +0
Overhead, first 30 min	0.182	1.533	0.071	0.115	0.140	0.072	0.056
Overhead, remaining 7.5 h	0.082	0.344	0.015	0.023	0.022	0.005	0.000
Final Bed, post test	0.158	0.370	0.007	0.016	0.017	0.004	0.000

Figure 7901-C
Pore Size Distribution

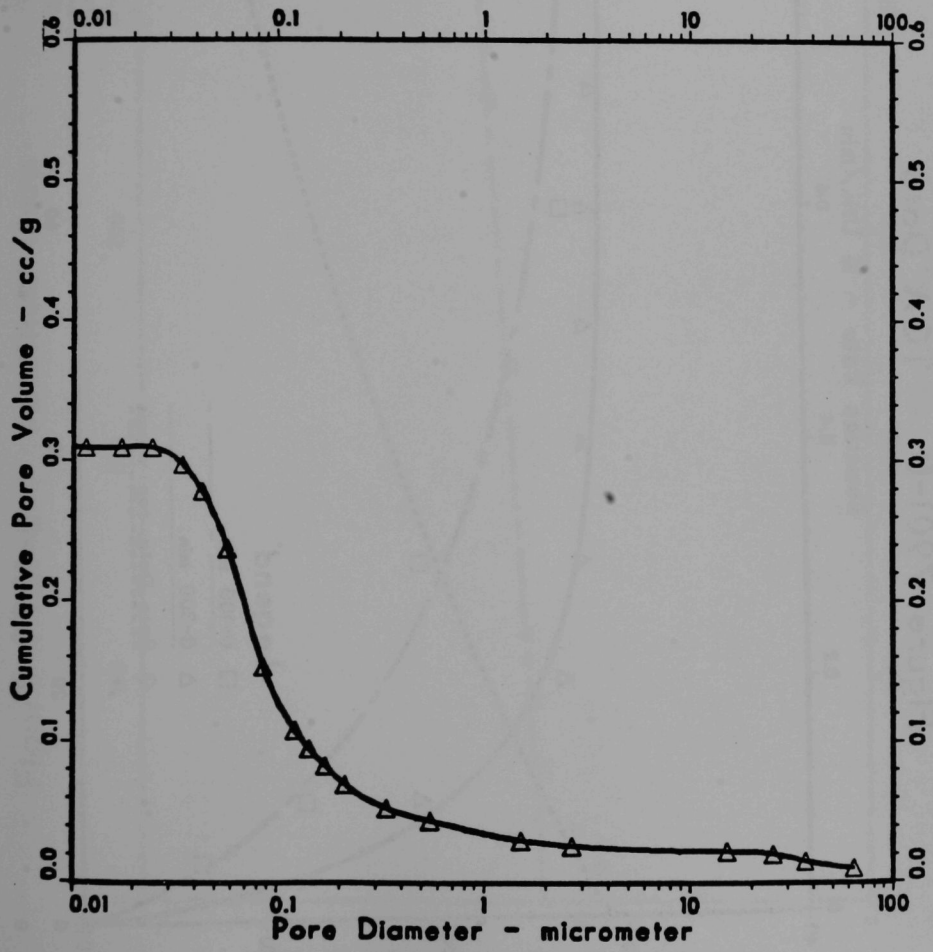

Figure 7901-D TGA Data

1123 K. 1 ATM
3000 PPM SO2
18-20 MESH

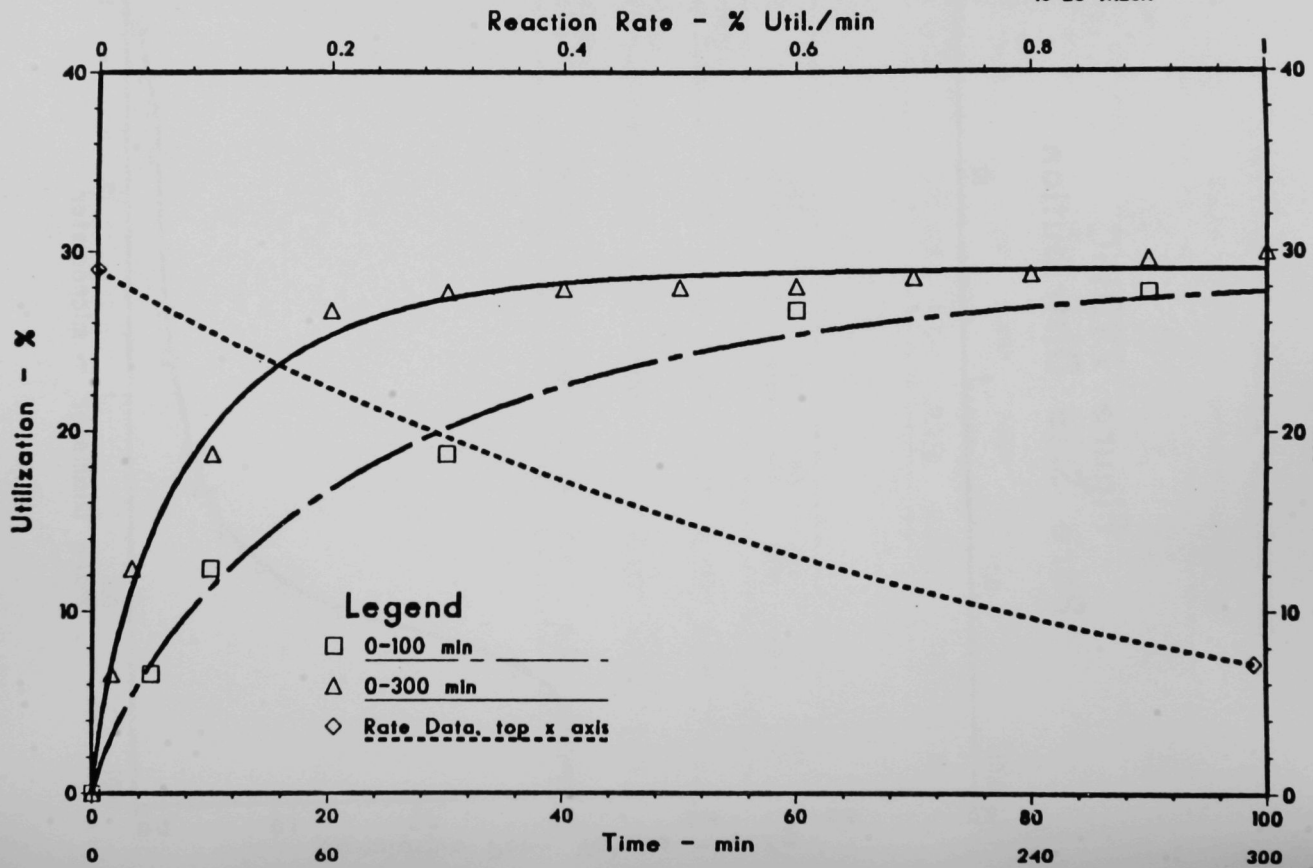

Figure 7901-E Attrition Data

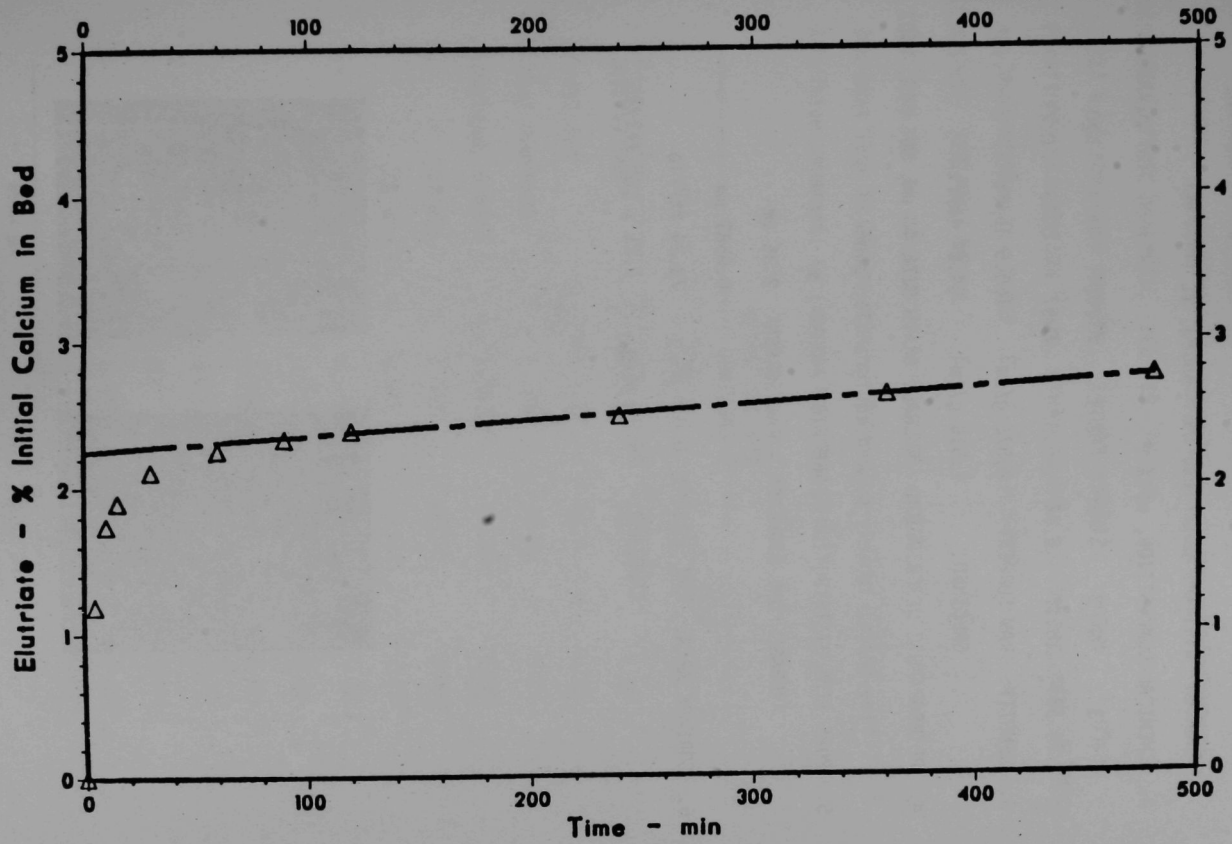

1. NAME: ANL-7402

   SOURCE: Williams Quarries, Harrisburg, IL

2. CHEMICAL COMPOSITION, wt %

$CaCO_3$	$MgCO_3$	SiO_2	Fe_2O_3	Al_2O_3	Na_2O	K_2O
74.38	18.17	5.64	0.87	0.57	0.43	0.23

3. DENSITY: RAW SORBENT 2.571 g/cm^3 160.5 lb/ft^3

   CALCINED 1.516 g/cm^3 94.64 lb/ft^3

4. PETROGRAPHIC DESCRIPTION: AVERAGE GRAIN SIZE 40 μm, SEE FIG. 7402 A & B

   Fine-grain, loosely packed equigranular stone.

5. PORE SIZE DISTRIBUTION: SEE FIG. 7402-C

   AVERAGE PORE DIAMETER - RAW SORBENT 2.35 μm

   CALCINED 0.0581 μm

6. SURFACE AREA: RAW SORBENT 0.015 m^2/g 73.24 ft^2/lb

   CALCINED 24.95 m^2/g 1.21 x 10^5 ft^2/lb

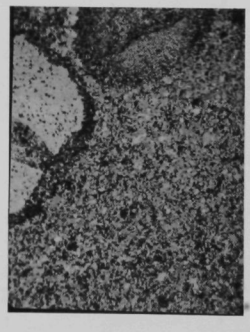

Fig. 7402A
Raw Limestone
50X

Fig. 7402B
Calcined Limestone 1 h 850°C
1000X

7. TOTAL POROSITY: RAW SORBENT 0.014 cm^3/g 2.24×10^{-4} ft^3/lb

CALCINED 0.365 cm^3/g 5.85×10^{-3} ft^3/lb

8. THERMOGRAVIMETRIC ANALYSIS: SEE FIG. 7402-D

(1123 K, 1 atm, 3000 ppm SO_2, -18 +20 mesh)

FRACTIONAL UTILIZATION = $\alpha(t, \text{min}) = 0.199\ [1 - \exp(-0.0495\ t^{1.036})]$

ANL PARAMETERS: D = 0.201 b = 547.6

9. ATTRITION: SEE FIG. 7402-E

Bed loss due to calcination breakup (%) = 3.9

Bed mass lost in linear portion (%/min.) = 1.12×10^{-3}

Attrition constant, λ_4 (sec^{-1}) = 2.59×10^{-7}

ATTRITION DATA

	Grams Total	wt % Ca	wt % S
Initial Bed	160.001	29.75	0.00
Final Bed	107.701	44.8	6.06
Total Overhead	4.794	43.55	4.86
Overhead, 5 min	1.267	43.55	4.86
10 min	1.459	43.55	4.86
15 min	0.725	43.55	4.86
30 min	0.346	43.55	4.86
1 h	0.286	43.55	4.86
1.5 h	0.150	43.55	4.86
2 h	0.116	43.55	4.86
4 h	0.178	43.55	4.86
6 h	0.145	43.55	4.86
8 h	0.122	43.55	4.86

Attrition Data, continued for Sorbent 7402

Weight in Grams, Particle Diameter, μm

Sample	-1000 +840	-841 +707	-707 +595	-595 +420	-420 +297	-297 +250
Overhead, first 30 min	0.003	0.001	0.000	0.002	0.023	0.079
Overhead, remaining 7.5 h	0.000	0.000	0.001	0.003	0.058	0.085
Final Bed, post test	102.389	2.693	0.620	0.565	0.640	0.224

Sample	-250 +210	-210 +74	-74 +63	-63 +53	-53 +44	-44 +37	-37 +0
Overhead, first 30 min	0.250	1.654	0.032	0.126	0.272	0.167	0.730
Overhead, remaining 7.5 h	0.122	0.605	0.013	0.041	0.070	0.052	0.073
Final Bed, post test	0.144	0.455	0.004	0.021	0.025	0.019	0.004

Figure 7402-C
Pore Size Distribution

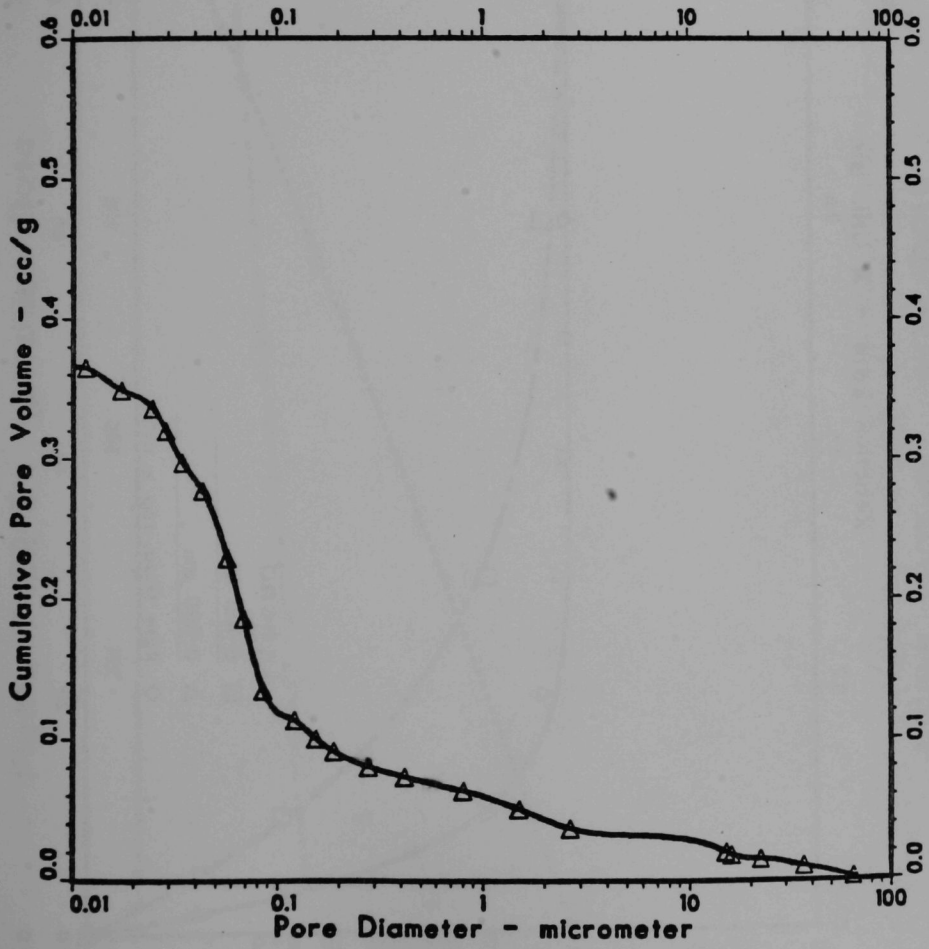

Figure 7402-D TGA Data

1123 K. 1 ATM
3000 PPM SO2
18-20 MESH

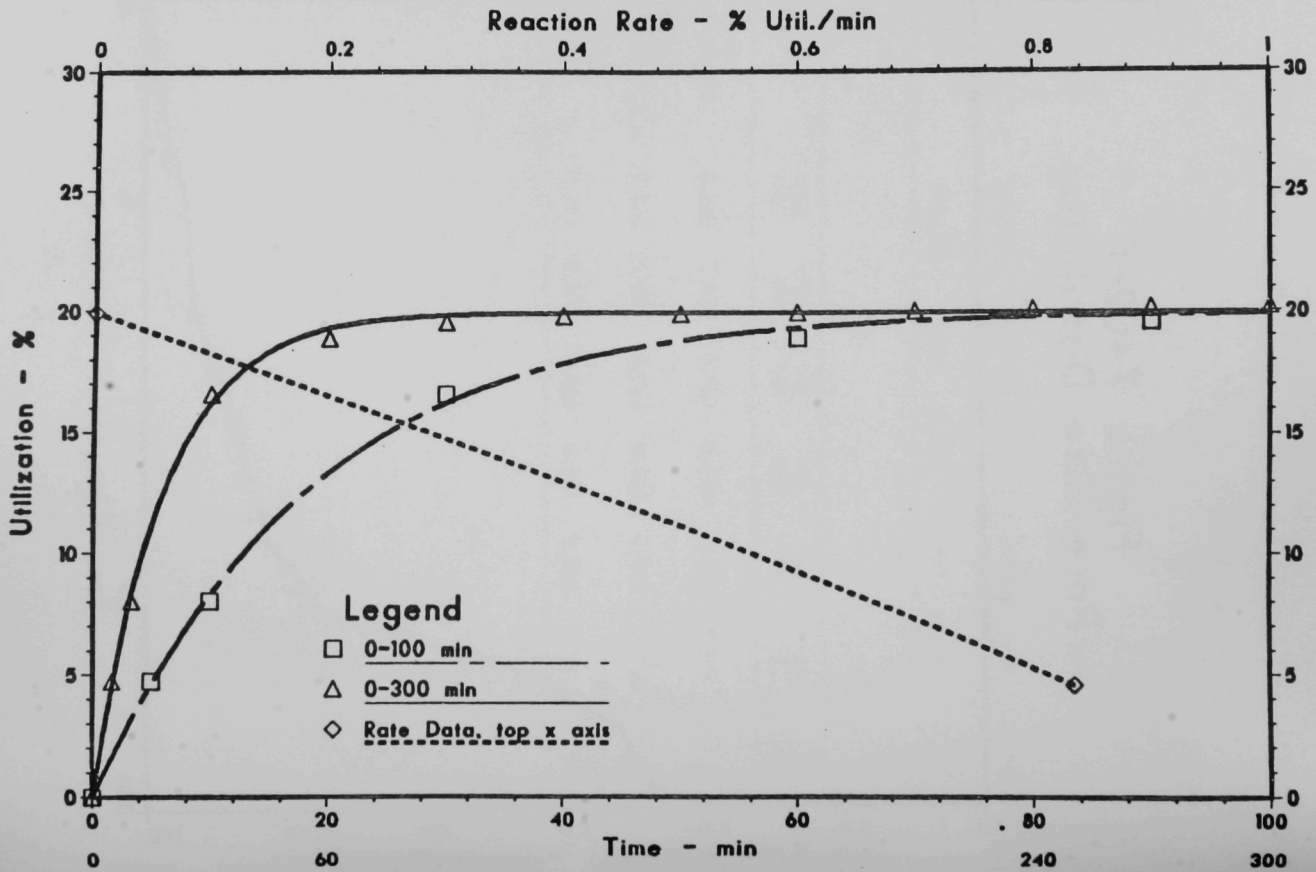

Figure 7402-E Attrition Data

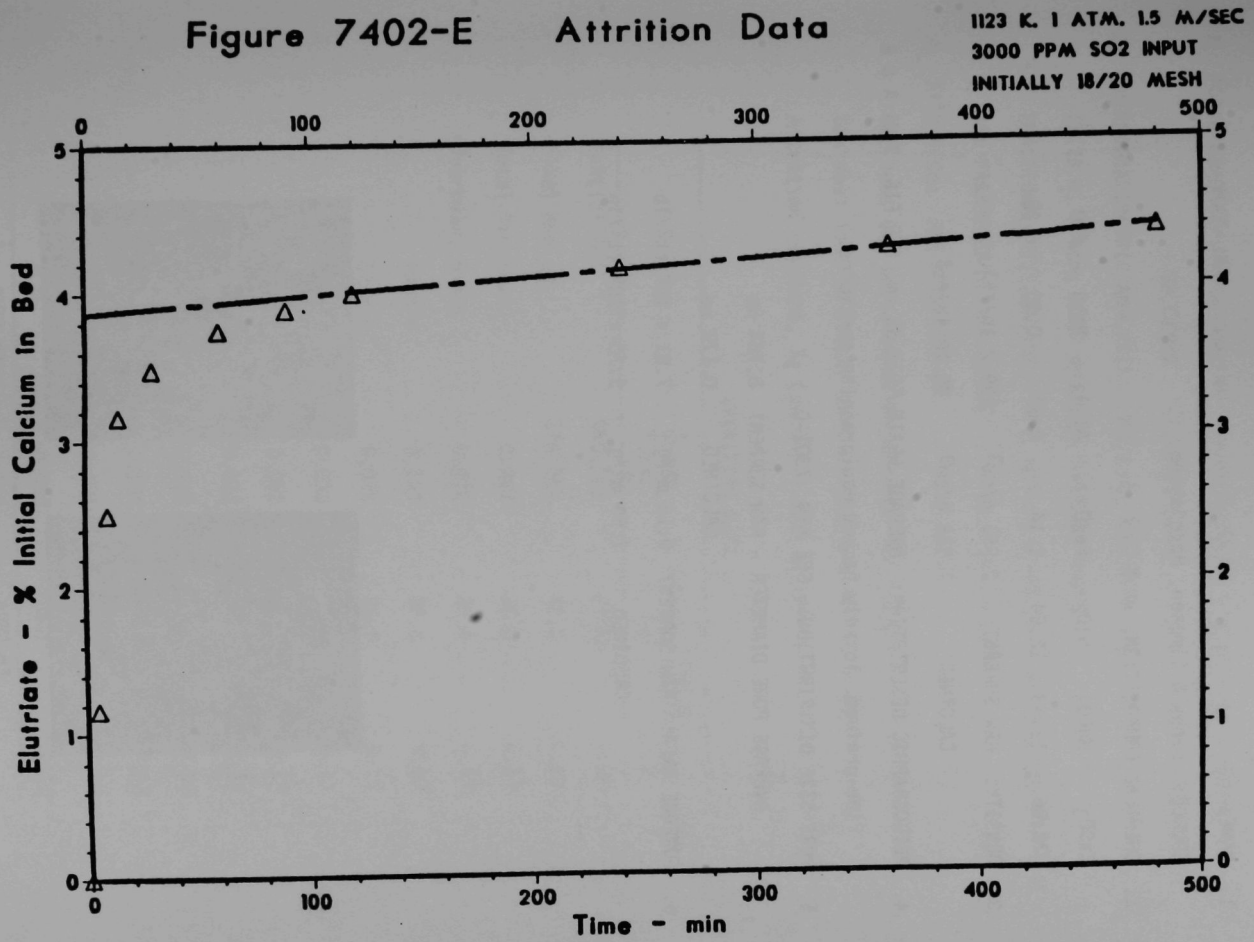

1. NAME: ANL-7301

SOURCE: Denny & Simpson, Harrisburg, IL

2. CHEMICAL COMPOSITION, wt %

$CaCO_3$	$MgCO_3$	SiO_2	Fe_2O_3	Al_2O_3	Na_2O	K_2O
73.06	12.53	12.94	1.14	0.67	0.65	0.32

3. DENSITY: RAW SORBENT 2.551 g/cm^3 159.2 lb/ft^3

CALCINED 1.525 g/cm^3 95.18 lb/ft^3

4. PETROGRAPHIC DESCRIPTION: AVERAGE GRAIN SIZE 35 μm, SEE FIG. 7301 A & B

Fine-grained, loosely packed equigranular particles.

5. PORE SIZE DISTRIBUTION: SEE FIG. 7301-C

AVERAGE PORE DIAMETER - RAW SORBENT 0.764 μm

CALCINED 0.172 μm

6. SURFACE AREA: RAW SORBENT 0.16 m^2/g 7.81 x 10^2 ft^2/lb

CALCINED 7.59 m^2/g 3.70 x 10^4 ft^2/lb

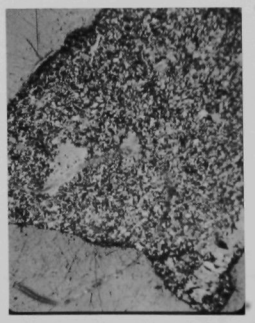

Fig. 7301A
Raw Limestone
50X

Fig. 7301B
Calcined Limestone 1 h 850°C
1000X

7. TOTAL POROSITY: RAW SORBENT 0.035 cm^3/g 5.60×10^{-4} ft^3/lb

CALCINED 0.331 cm^3/g 5.30×10^{-3} ft^3/lb

8. THERMOGRAVIMETRIC ANALYSIS: SEE FIG. 7301-D

(1123 K, 1 atm, 3000 ppm SO_2, -18 +20 mesh)

FRACTIONAL UTILIZATION = $\alpha(t, min) = 0.286 [1 - exp (-0.108 t^{0.672})]$

ANL PARAMETERS: D = 0.254 b = 357.0

9. ATTRITION: SEE FIG. 7301-E

Bed loss due to calcination breakup (%) = 0.65

Bed mass lost in linear portion (%/min.) = 3.41×10^{-4}

Attrition constant, λ_4 (sec^{-1}) = 7.82×10^{-8}

ATTRITION DATA

	Grams Total	wt % Ca	wt % S
Initial Bed	160.168	29.22	0.00
Final Bed	114.749	43.0	6.53
Total Overhead	0.982	38.0	4.13
Overhead, 5 min	0.412	38.0	4.13
10 min	0.185	38.0	4.13
15 min	0.021	38.0	4.13
30 min	0.030	38.0	4.13
1 h	0.052	38.0	4.13
1.5 h	0.017	38.0	4.13
2 h	0.109	38.0	4.13
4 h	0.105	38.0	4.13
6 h	0.031	38.0	4.13
8 h	0.019	38.0	4.13

Attrition Data, continued for Sorbent 7301

Weight in Grams, Particle Diameter, μm

Sample	-1000 +840	-841 +707	-707 +595	-595 +420	-420 +297	-297 +250
Overhead, first 30 min	0.009	0.008	0.007	0.005	0.005	0.008
Overhead, remaining 7.5 h	0.001	0.004	0.003	0.003	0.002	0.006
Final Bed, post test	112.291	0.899	0.163	0.170	0.231	0.094

Sample	-250 +210	-210 +74	-74 +63	-63 +53	-53 +44	-44 +37	-37 +0
Overhead, first 30 min	0.023	0.097	0.099	0.047	0.081	0.001	0.000
Overhead, remaining 7.5 h	0.011	0.018	0.017	0.017	0.018	0.006	0.000
Final Bed, post test	0.120	0.467	0.008	0.027	0.038	0.009	0.012

10. OTHER DATA: TGA Data: 1123 K, 1 atm, 3000 ppm SO_2

See Fig. 7301-F $\alpha(t,min) = 0.581\ [1 - \exp(-0.0678\ t^{0.508})]$

-50 +70 mesh $D = 0.508$ $b = 169$

See Fig. 7301-G $\alpha(t,min) = 0.720\ [1 - \exp(-0.0392\ t^{0.730})]$

-140 +170 mesh $D = 0.642$ $b = 122$

See Fig. 7301-H $\alpha(t,min) = 0.226\ [1 - \exp(-0.092\ t^{0.663})]$

-12 +14 mesh $D = 0.180$ $b = 402$

Figure 7301-C
Pore Size Distribution

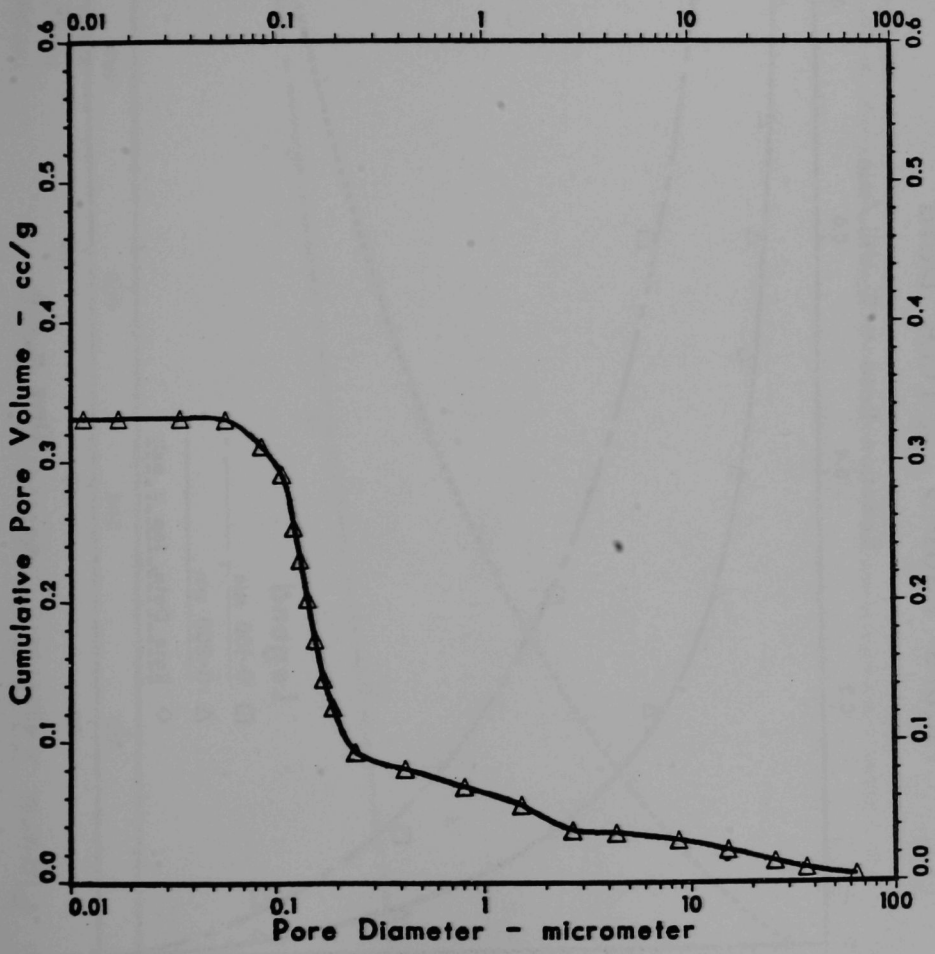

Figure 7301-D TGA Data

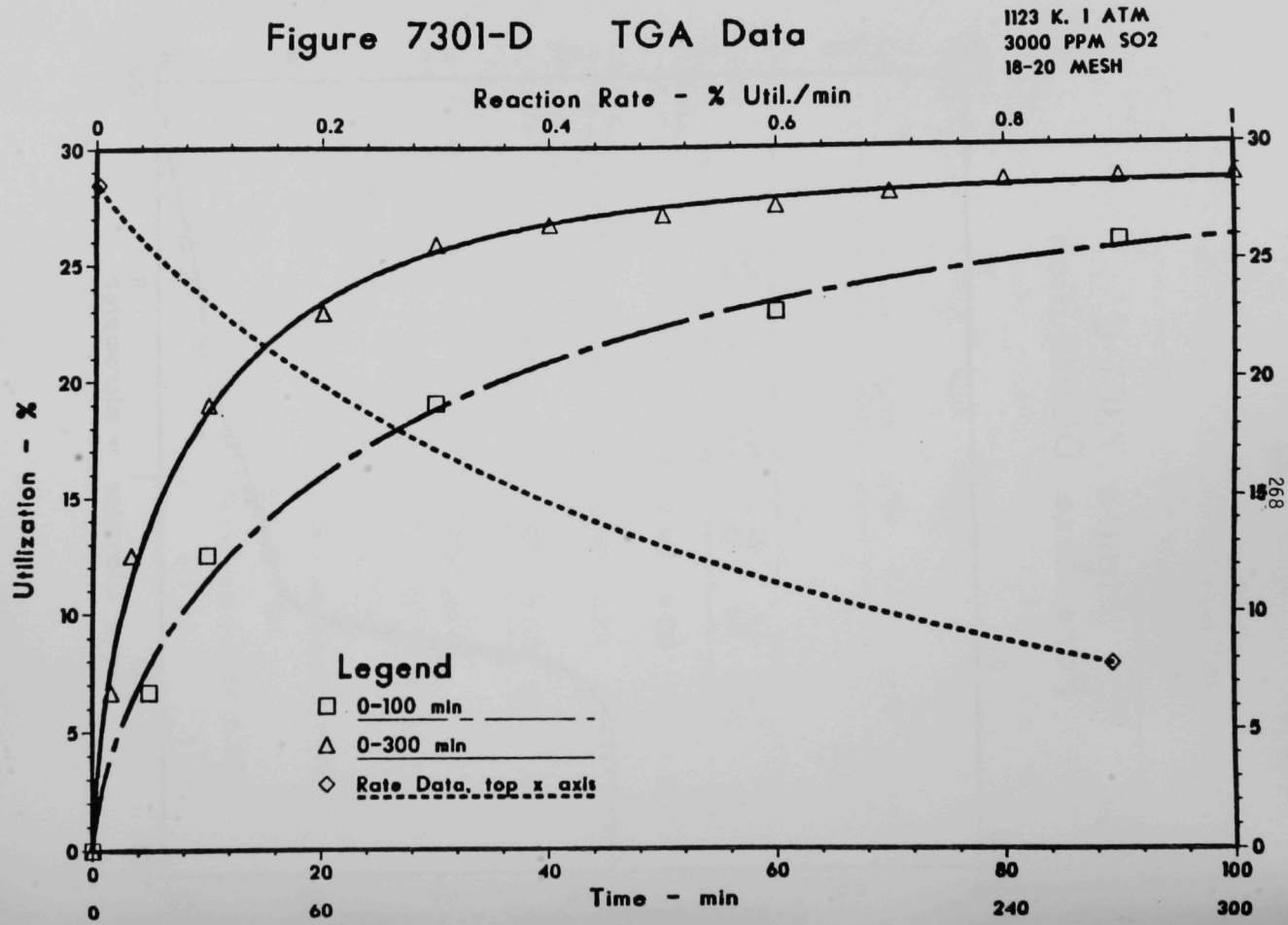

Figure 7301-E Attrition Data

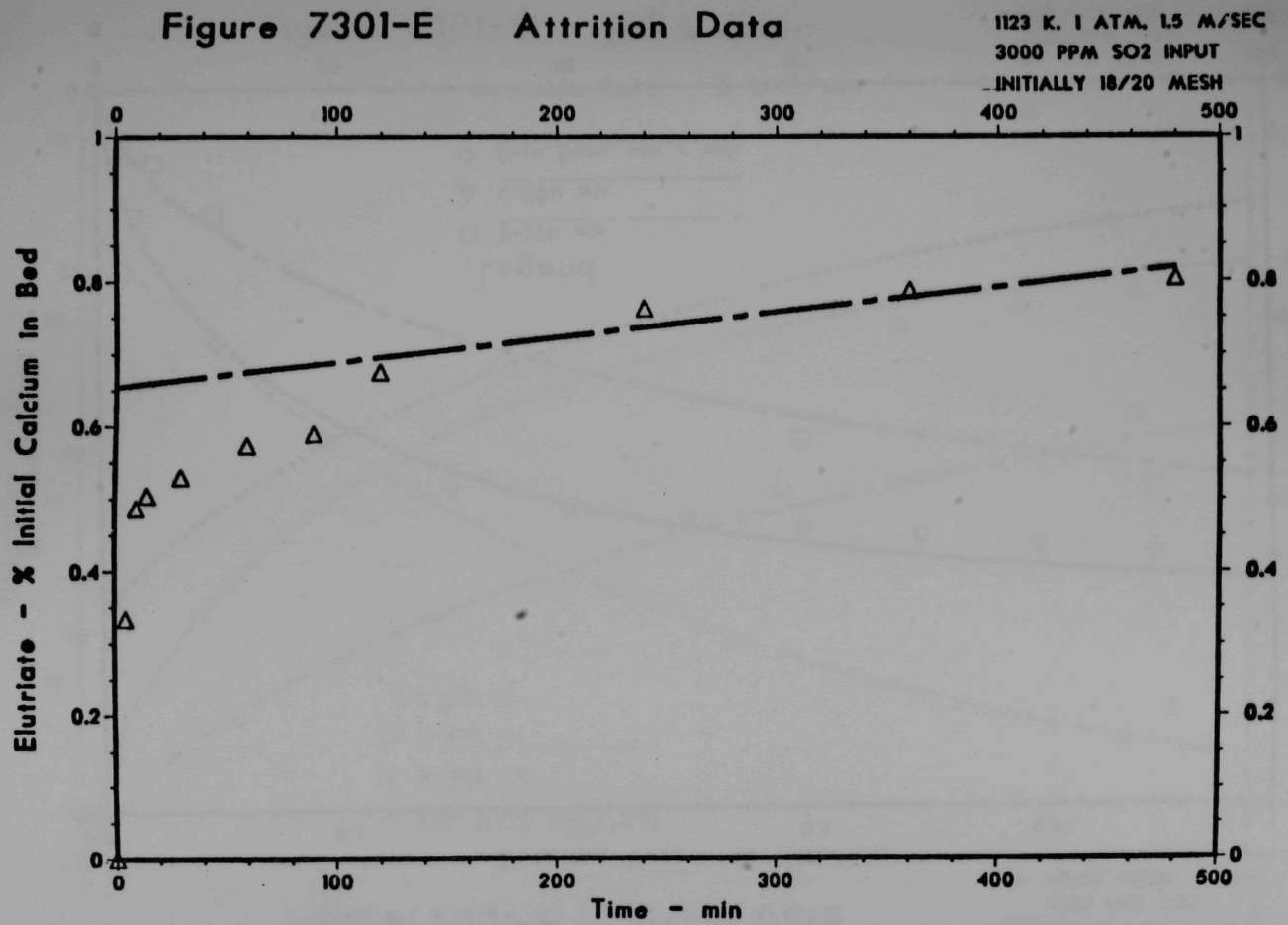

Figure 7301-F TGA Data

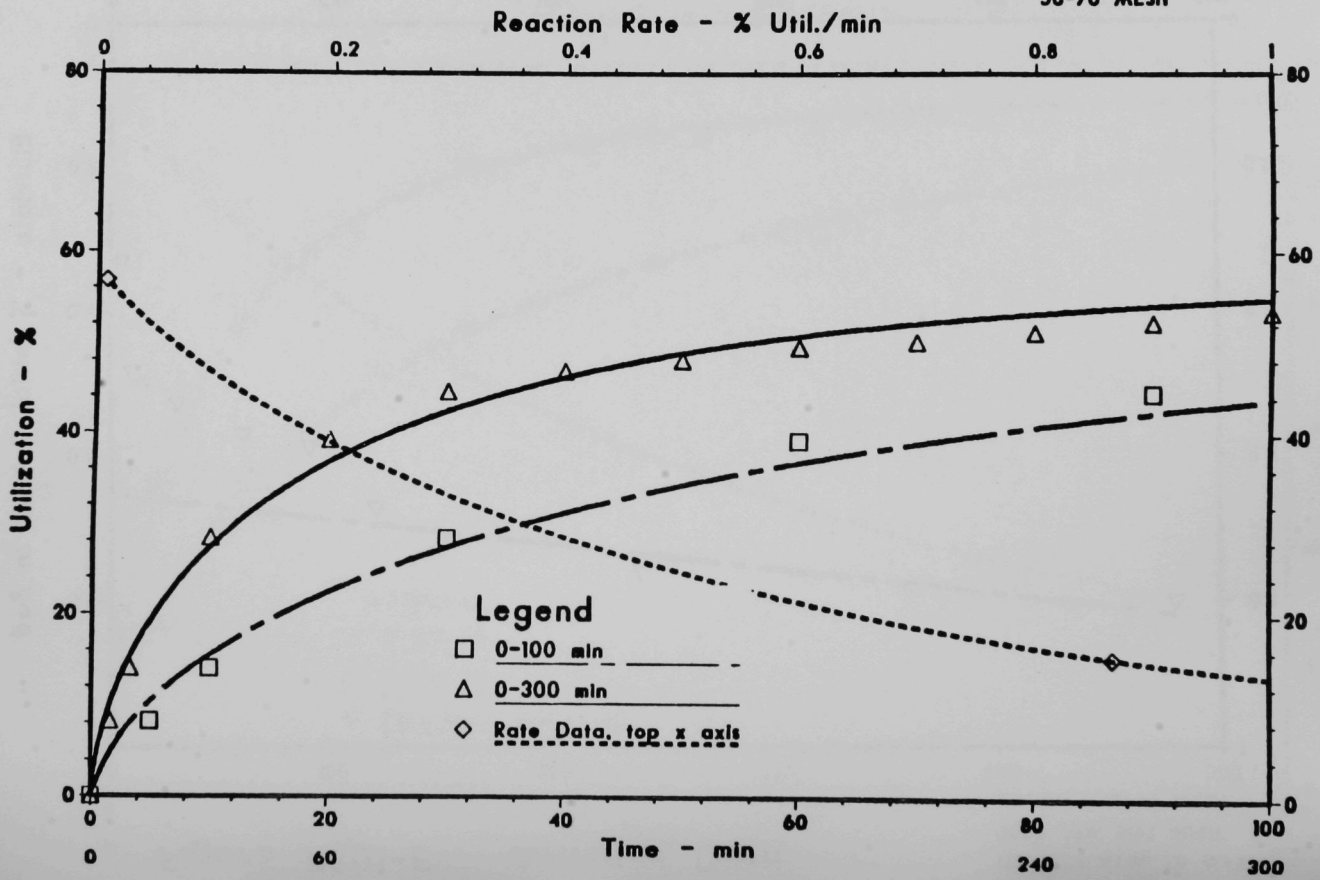

Figure 7301-G TGA Data

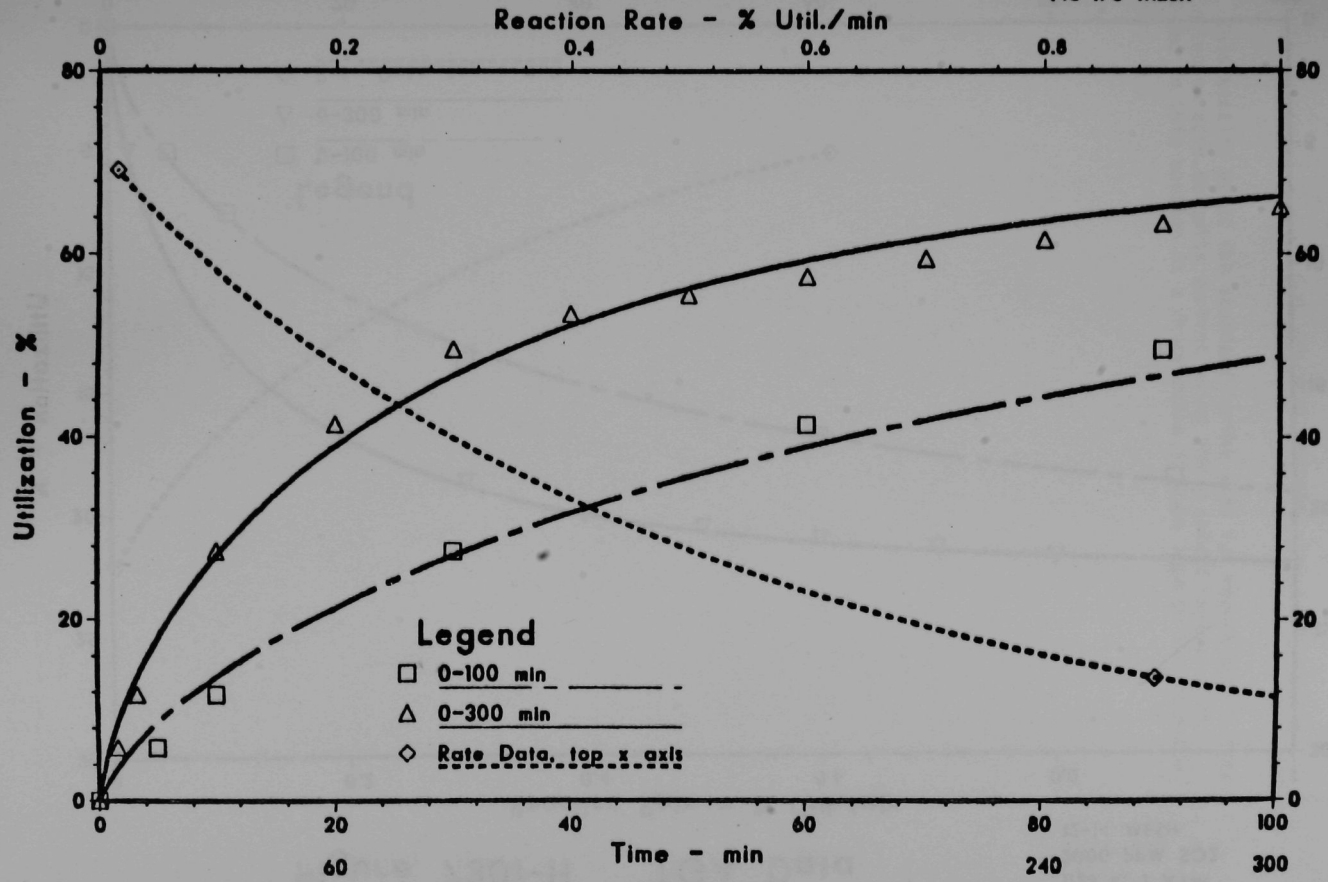

Figure 7301-H TGA Data

1123 K. 1 ATM
3000 PPM SO2
12-14 MESH

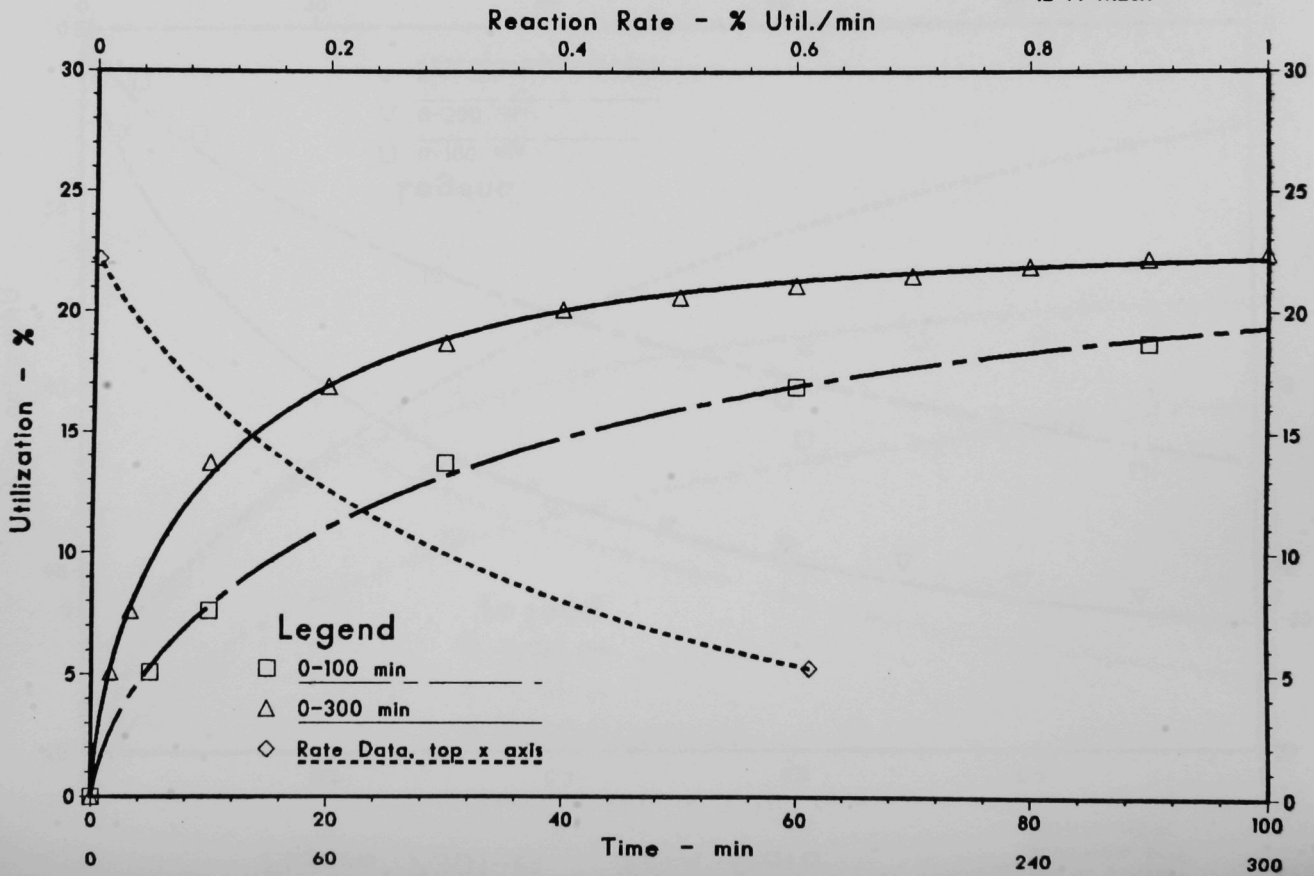

6.0 DOLOMITE SUMMARY

This section gives the standard format used for reporting the data collected on each dolomite sorbent using the standard tests. Also included in this section is a description of each item of the standard tests.

6.1 STANDARD SORBENT DATA FORMAT

A standard format has been devised for reporting the data collected on each sorbent using the standard tests. This format, and a description of each item are as follows:

1.	Name, ANL Number, Source,	- The commonly used name of the sorbent is given. Often this is the name of the quarry or otherwise reflects on the source of the sorbent. The first two digits of the ANL number signify the nominal amount of calcium carbonate (wt %) in the sorbent.
2.	Chemical Composition	- The nominal chemical composition of the sorbent is given. This is an average composition. Variations of composition within the particular limestone formation or particular quarry certainly exist and must be taken into account when using this handbook.
3.	Density	- The density of the raw and calcined sorbent are given.
4.	Petrographic Description	- Photomicrographs are given of both the raw (Fig. A) and the calcined sorbent (Fig. B). The sorbent microstructure is described and the average grain size is given.
5.	Pore Size Distribution	- The pore size distribution of the calcined material is given as a plot of cumulative pore volume versus pore diameter (Fig. C).
6.	Surface Area	- The surface area is given both for the raw and the calcined sorbent.
7.	Total Porosity	- The total pore volume is given for both the raw and calcined sorbent.
8.	Thermogravimetric Analysis	- The TGA data is plotted as calcium utilization versus time (Fig. D). The parameters D and b, described in the section "Analysis of TGA Data," are given.

9. Attrition

- The data from the standard laboratory attrition test and the interpretation are as previously discussed in the "Analysis of Attrition Data" section. The cumulative fraction of the initial bed which goes overhead during the test is shown in Fig. E. The intercept on this figure is taken as the "bed loss due to calcination breakup (%)." The slope of linear fit in Fig. E is taken as the "bed mass lost per minute in the linear portion (%/min)." The "Attrition constant, $\lambda_4(sec^{-1})$, is derived from this portion of the curve using the attrition model.

10. Other Data

- a. Decrepitation data is plotted as the percent of fines particles produced less than 595 μm diameter as a function of temperature. The measured weight loss as a result of water being released from the sorbent and the weight loss due to calcination is also described in the section "Analysis of Decrepitation Data."

- b. Additional TGA data, if any, is presented here. This data is for sorbent particle size and sulfur dioxide concentrations other than the standard 1000-840 μm and 3000 ppm, respectively.

6.2 TEST DATA ON DOLOMITES

1. NAME: ANL-6701

   SOURCE: Osmundson, Bros., Adams, MN

2. CHEMICAL COMPOSITION, wt %

$CaCO_3$	$MgCO_3$	SiO_2	Fe_2O_3	Al_2O_3	Na_2O	K_2O
67.3	31.5	1.25	0.37	0.22	0.04	0.15

3. DENSITY: RAW SORBENT 2.570 g/cm^3 160.42 lb/ft^3

   CALCINED 1.477 g/cm^3 92.21 lb/ft^3

4. PETROGRAPHIC DESCRIPTION: AVERAGE GRAIN SIZE 100 μm, SEE FIG. 6701 A & B

   Medium-grained; loosely packed inequigranular stone; contain small traces of Fe_2O_3.

5. PORE SIZE DISTRIBUTION: SEE FIG. 6701-C

   AVERAGE PORE DIAMETER - RAW SORBENT 0.717 μm

   CALCINED 0.090 μm

6. SURFACE AREA: RAW SORBENT 0.181 m^2/g 8.85 x 10^2 ft^2/lb

   CALCINED 19.90 m^2/g 9.72 x 10^4 ft^2/lb

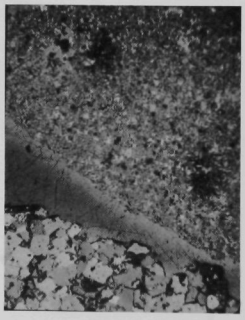

Fig. 6701A
Raw Dolomite
50X

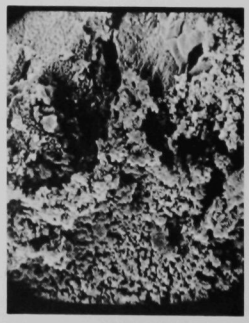

Fig. 6701B
Calcined Dolomite 1 h 850°C
1100X

7. TOTAL POROSITY: RAW SORBENT 0.035 cm^3/g 5.6×10^{-4} ft^3/lb

CALCINED 0.457 cm^3/g 7.32×10^{-3} ft^3/lb

8. THERMOGRAVIMETRIC ANALYSIS: SEE FIG. 6701-D

(1123 K, 1 atm, 3000 ppm SO_2, -18 +20 mesh)

FRACTIONAL UTILIZATION = $\alpha(t, \text{min}) = 0.501\ [1 - \exp(-0.0479\ t^{0.829})]$

ANL PARAMETERS: D = 0.481 b = 211.6

9. ATTRITION: SEE FIG. 6701-E

Bed loss due to calcination breakup (%) = 0.65

Bed mass lost in linear portion (%/min.) = 3.5×10^{-4}

Attrition constant, λ_4 (sec^{-1}) = 8.1×10^{-8}

ATTRITION DATA

	Grams Total	wt % Ca	wt % S
Initial Bed	160.789	26.9	0.00
Final Bed	129.278	32.4	11.50
Total Overhead	0.910	31.1	3.95
Overhead, 5 min	0.435	31.1	3.95
10 min	0.143	31.1	3.95
15 min	0.077	31.1	3.95
30 min	0.006	31.1	3.95
1 h	0.038	31.1	3.95
1.5 h	0.018	31.1	3.95
2 h	0.013	31.1	3.95
4 h	0.051	31.1	3.95
6 h	0.059	31.1	3.95
8 h	0.070	31.1	3.95

Attrition Data, continued for Sorbent 6701

Weight in Grams, Particle Diameter, μm

Sample	-1000 +840	-841 +707	-707 +595	-595 +420	-420 +297	-297 +250
Overhead, first 30 min	0.000	0.000	0.000	0.000	0.010	0.018
Overhead, remaining 7.5 h	0.000	0.000	0.000	0.000	0.012	0.008
Final Bed, post test	119.442	8.313	0.379	0.250	0.248	0.075

Sample	-250 +210	-210 +74	-74 +63	-63 +53	-53 +44	-44 +37	-37 +0
Overhead, first 30 min	0.014	0.171	0.036	0.067	0.074	0.062	0.014
Overhead, remaining 7.5 h	0.007	0.027	0.003	0.005	0.004	0.002	0.004
Final Bed, post test	0.097	0.417	0.021	0.059	0.087	0.068	0.017

Figure 6701-C
Pore Size Distribution

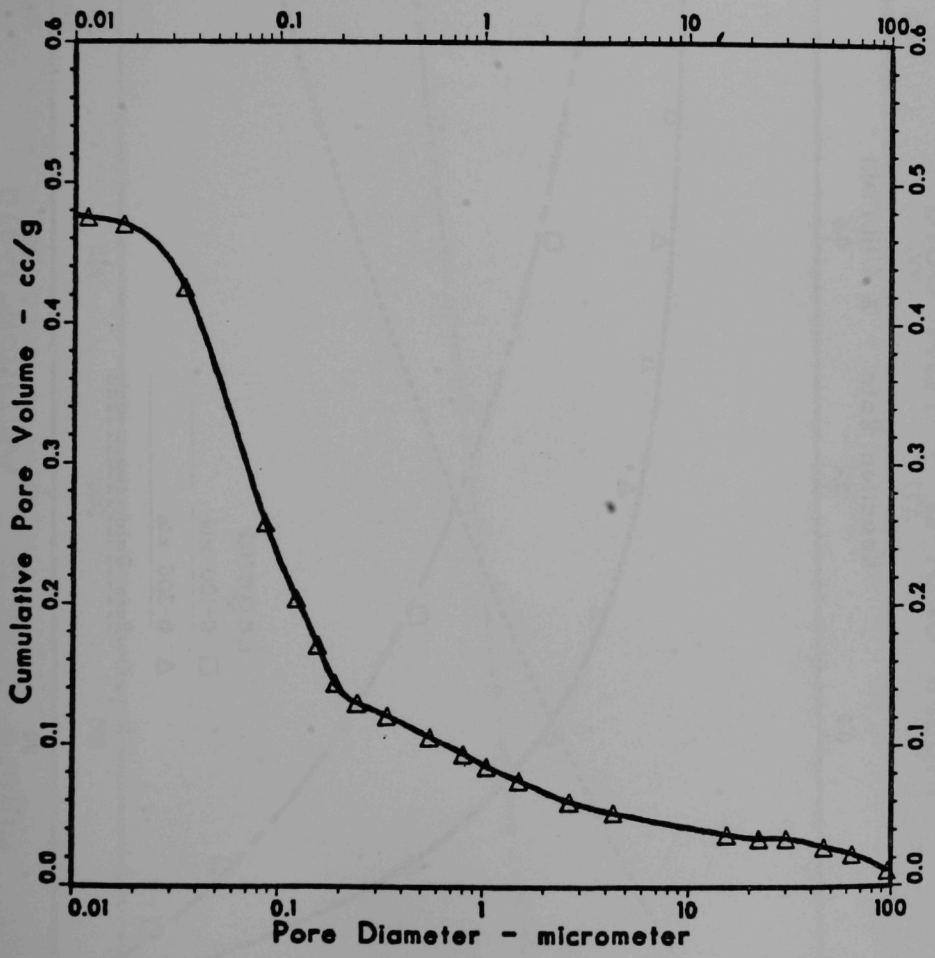

Figure 6701-D TGA Data

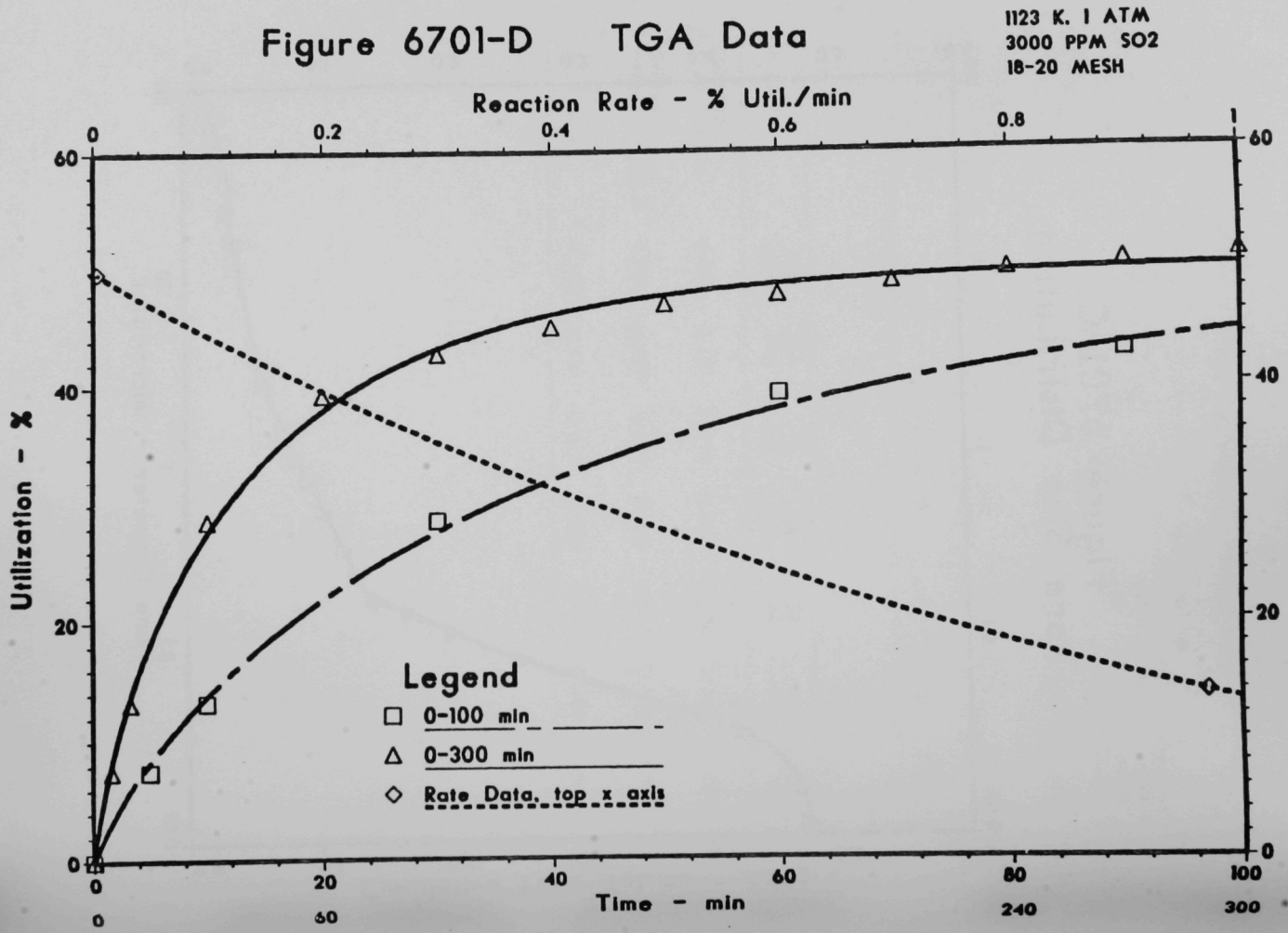

Figure 6701-E Attrition Data

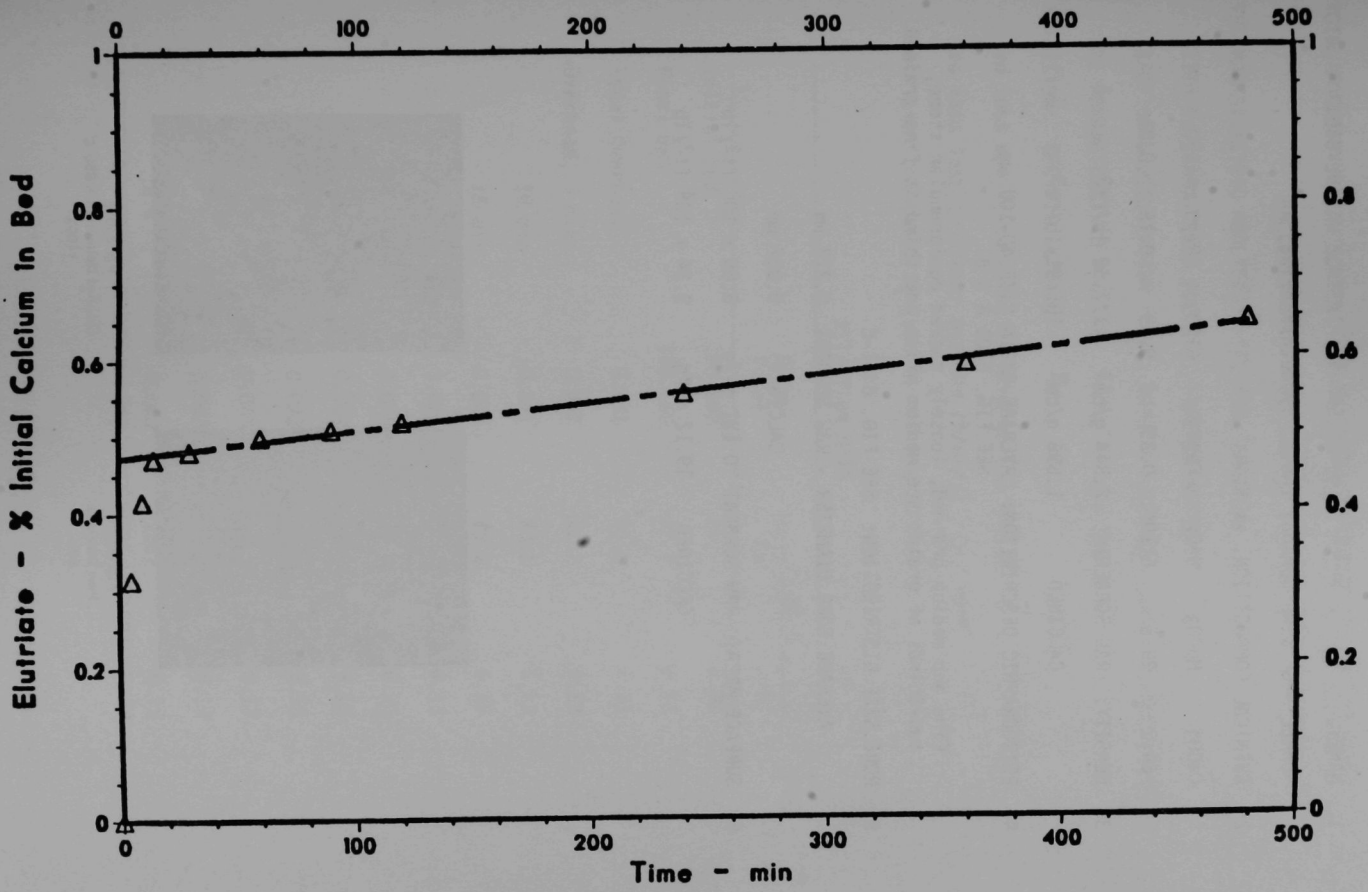

1. NAME: ANL-6401

   SOURCE: G. & WH Corson, Inc., Plymouth/Meeting, PA

2. CHEMICAL COMPOSITION, wt %

$CaCO_3$	$MgCO_3$	SiO_2	Fe_2O_3	Al_2O_3	Na_2O	K_2O
64.2	29.5	5.10	0.33	0.69	0.15	0.31

3. DENSITY: RAW SORBENT 2.844 g/cm^3 177.52 lb/ft^3

   CALCINED 1.696 g/cm^3 105.91 lb/ft^3

4. PETROGRAPHIC DESCRIPTION: AVERAGE GRAIN SIZE 40-100 μm, SEE FIG. 6701 A & B

   Fine and medium grained, loosely packed equigranular stone; two-thirds of grains are medium while one third is fine-grained.

5. PORE SIZE DISTRIBUTION: SEE FIG. 6401-C

   AVERAGE PORE DIAMETER - RAW SORBENT 0.277 μm

   CALCINED 0.067 μm

6. SURFACE AREA: RAW SORBENT 0.137 m^2/g 6.69 x 10^2 ft^2/lb

   CALCINED 19.12 m^2/g 9.34 x 10^4 ft^2/lb

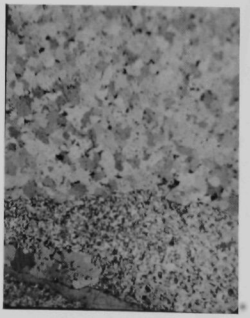

Fig. 6401A
Raw Dolomite
50X

Fig. 6401B
Calcined Dolomite 1 h 850°C
1100X

7. TOTAL POROSITY: RAW SORBENT 0.012 cm^3/g 1.91×10^{-4} ft^3/lb

CALCINED 0.328 cm^3/g 5.25×10^{-3} ft^3/lb

8. THERMOGRAVIMETRIC ANALYSIS: SEE FIG. 6401-D

(1123 K, 1 atm, 3000 ppm SO_2, -18 +20 mesh)

FRACTIONAL UTILIZATION = $\alpha(t, \text{min}) = 0.262\ [1 - \exp(-0.0853\ t^{0.646})]$

ANL PARAMETERS: D = 0.196 b = 356.2

9. ATTRITION: SEE FIG. 6401-E

Bed loss due to calcination breakup (%) = 0.27

Bed mass lost in linear portion (%/min.) = 3×10^{-4}

Attrition constant, λ_4 (sec^{-1}) = 6.8×10^{-8}

ATTRITION DATA

	Grams Total	wt % Ca	wt % S
Initial Bed	160.692	25.7	0.00
Final Bed	108.160	37.7	5.92
Total Overhead	0.731	23.2	6.13
Overhead, 5 min	0.257	23.2	6.13
10 min	0.061	23.2	6.13
15 min	0.025	23.2	6.13
30 min	0.062	23.2	6.13
1 h	0.075	23.2	6.13
1.5 h	0.054	23.2	6.13
2 h	0.022	23.2	6.13
4 h	0.043	23.2	6.13
6 h	0.063	23.2	6.13
8 h	0.069	23.2	6.13

Attrition Data, continued for Sorbent 8001

Weight in Grams, Particle Diameter, μm

Sample	-1000 +840	-841 +707	-707 +595	-595 +420	-420 +297	-297 +250
Overhead, first 30 min	0.000	0.000	0.000	0.000	0.009	0.012
Overhead, remaining 7.5 h	0.000	0.000	0.000	0.000	0.014	0.015
Final Bed, post test	103.247	4.091	0.360	0.102	0.091	0.039

Sample	-250 +210	-210 +74	-74 +63	-63 +53	-53 +44	-44 +37	-37 +0
Overhead, first 30 min	0.010	0.104	0.021	0.042	0.048	0.023	0.004
Overhead, remaining 7.5 h	0.018	0.074	0.012	0.007	0.009	0.009	0.007
Final Bed, post test	0.060	0.151	0.010	0.029	0.046	0.030	0.013

10. OTHER DATA: TGA Data: 1123 K, 1 atm, 3000 ppm SO_2

See Fig. 6401-F $\alpha(t,min) = 0.744\ [1 - \exp(-0.0510\ t^{0.535})]$

-50 +70 mesh $D = 0.391$ $b = 165$

See Fig. 6401-G $\alpha(t,min) = 0.858\ [1 - \exp(-0.0418\ t^{0.684})]$

-140 +170 mesh $D = 0.721$ $b = 113$

See Fig. 6401-H $\alpha(t,min) = 0.152\ [1 - \exp(-0.1185\ t^{0.583})]$

-12 +14 mesh $D = 0.090$ $b = 732$

Figure 6401-C
Pore Size Distribution

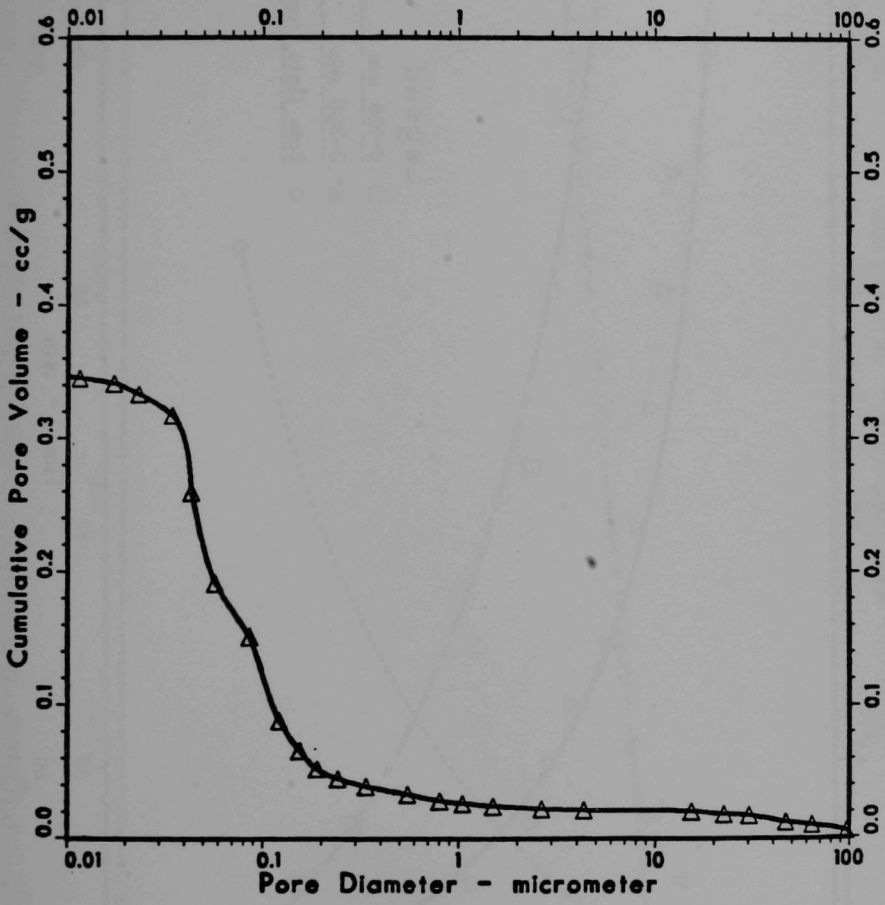

Figure 6401-D TGA Data

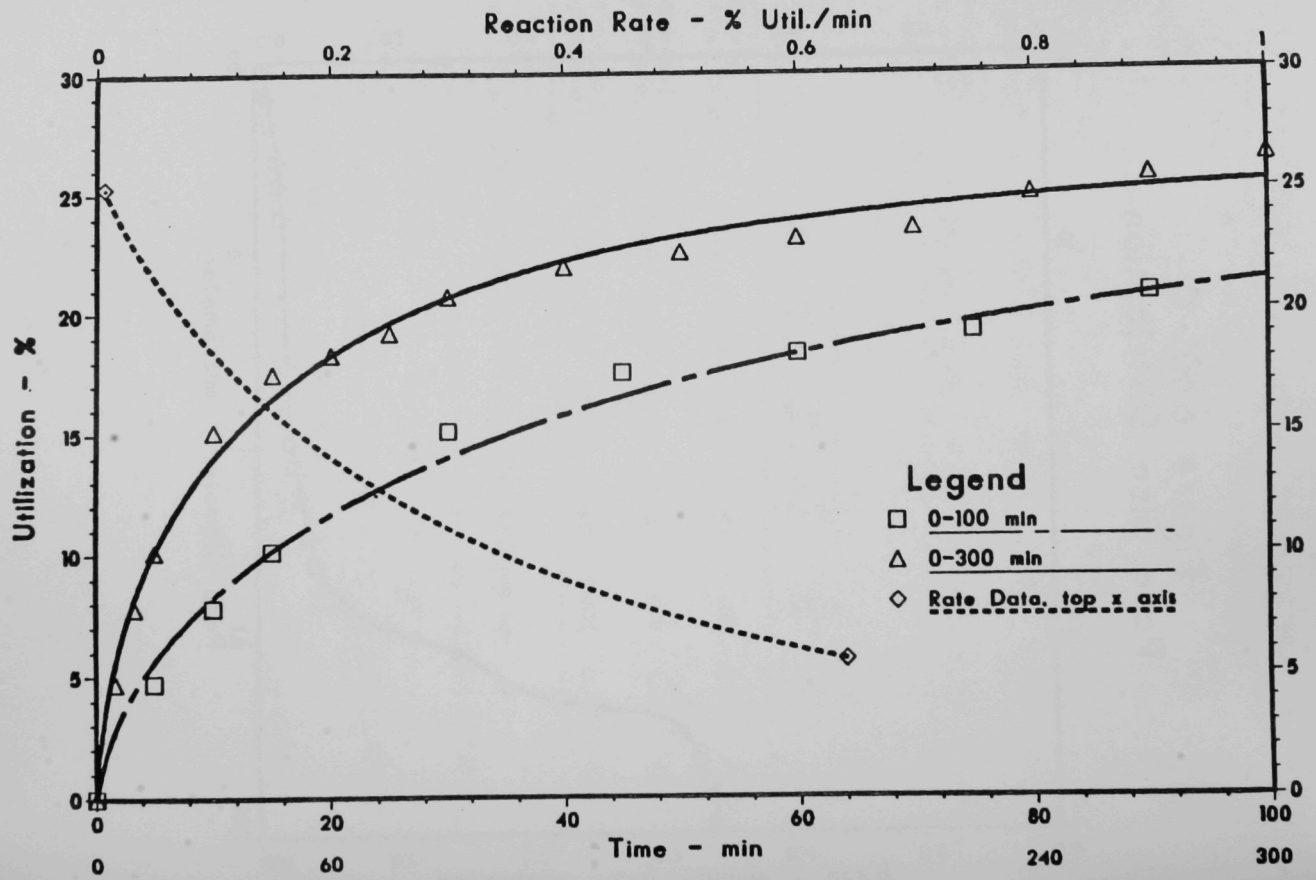

Figure 6401-E Attrition Data

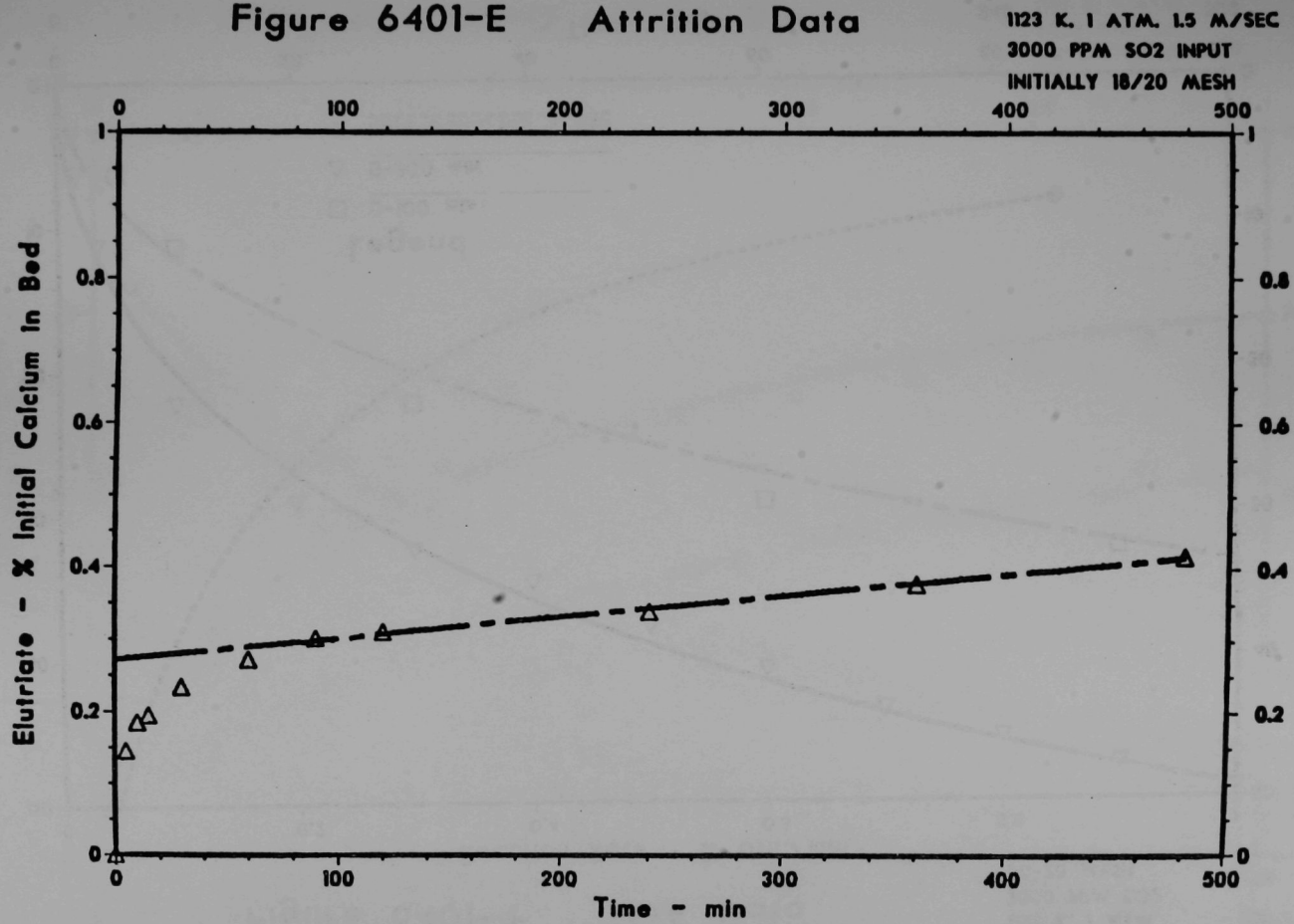

Figure 6401-F TGA Data

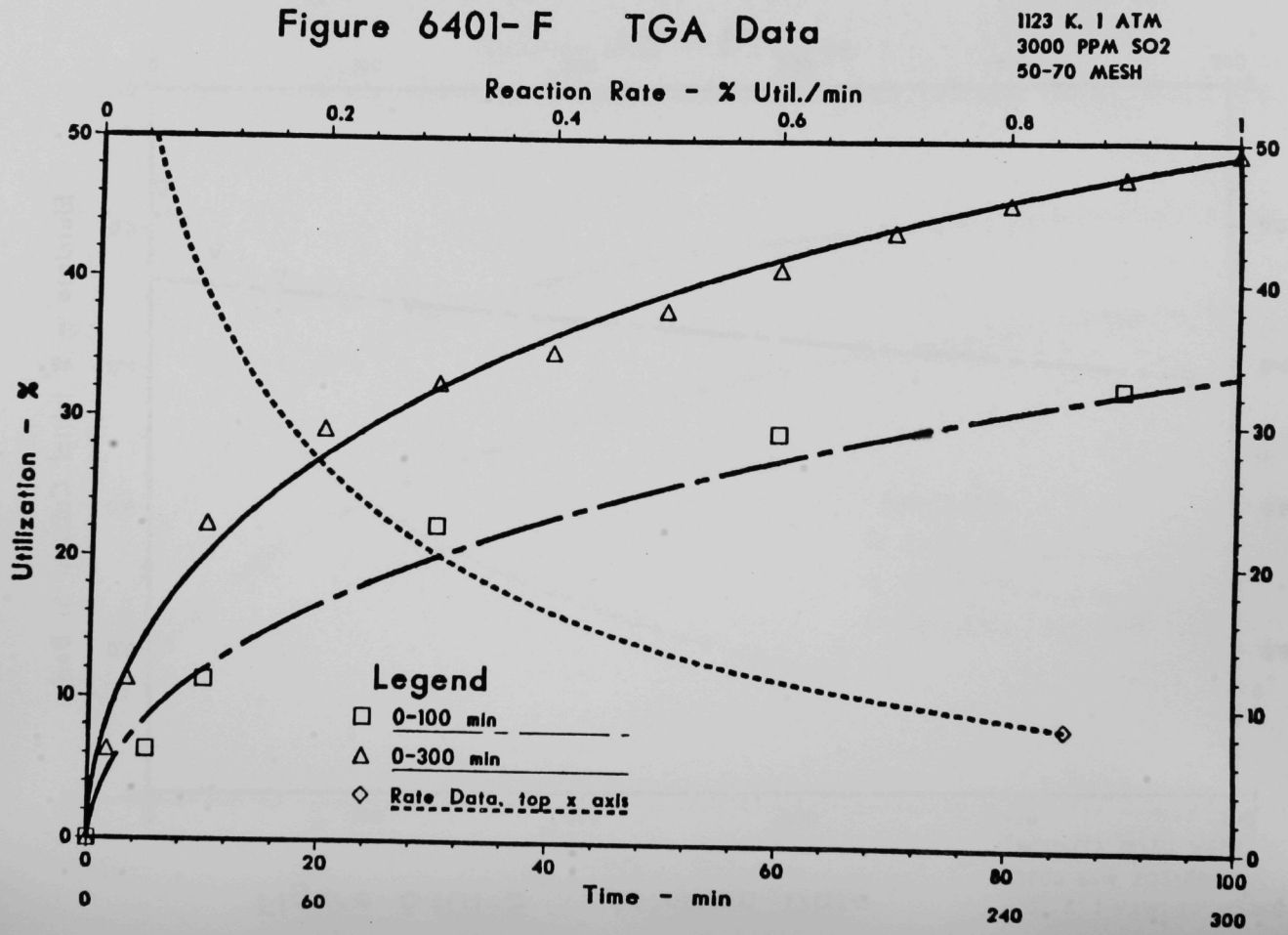

Figure 6401-G TGA Data

1123 K. 1 ATM
3000 PPM SO2
140-170 MESH

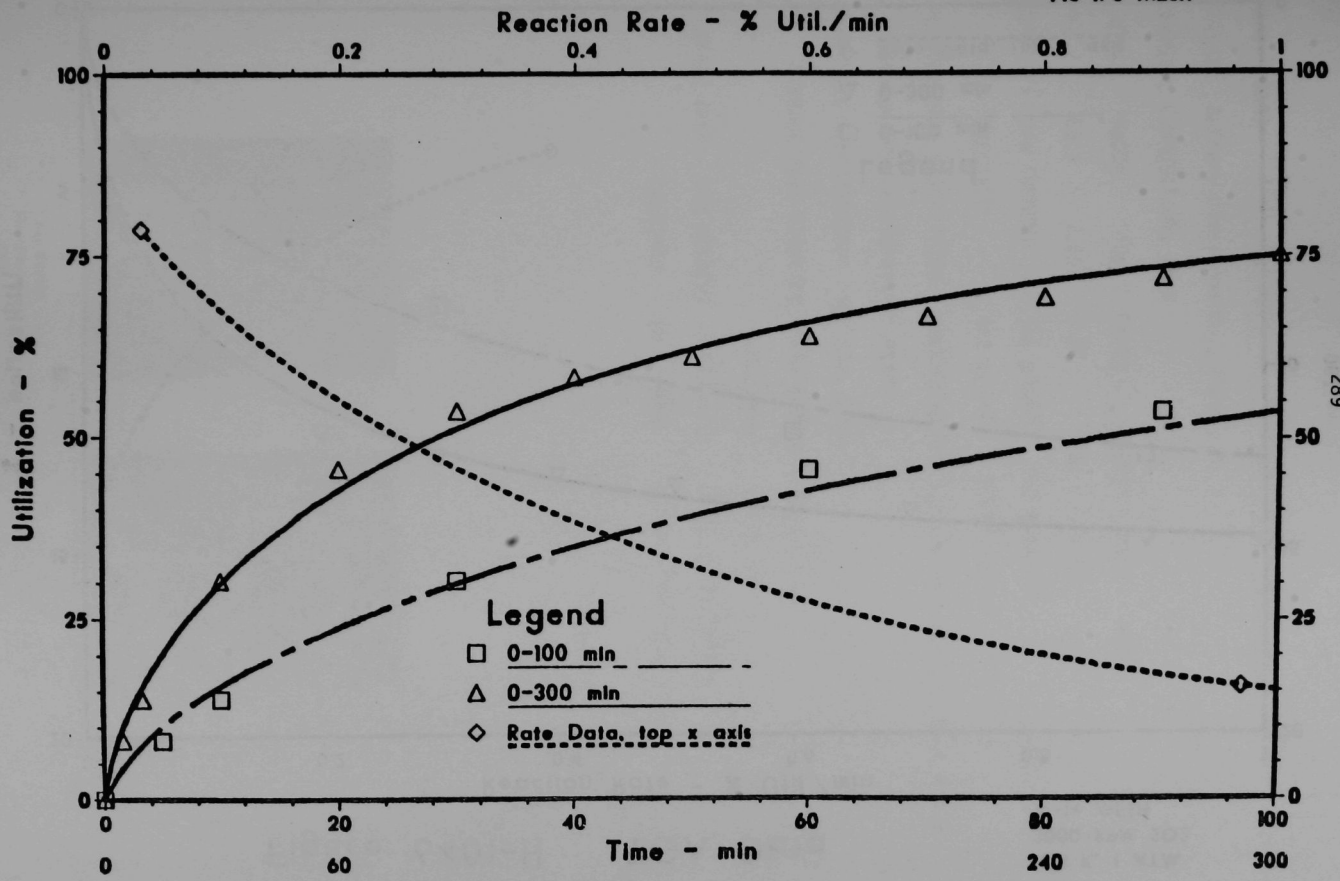

Figure 6401-H TGA Data

1123 K. 1 ATM
3000 PPM SO2
12-14 MESH

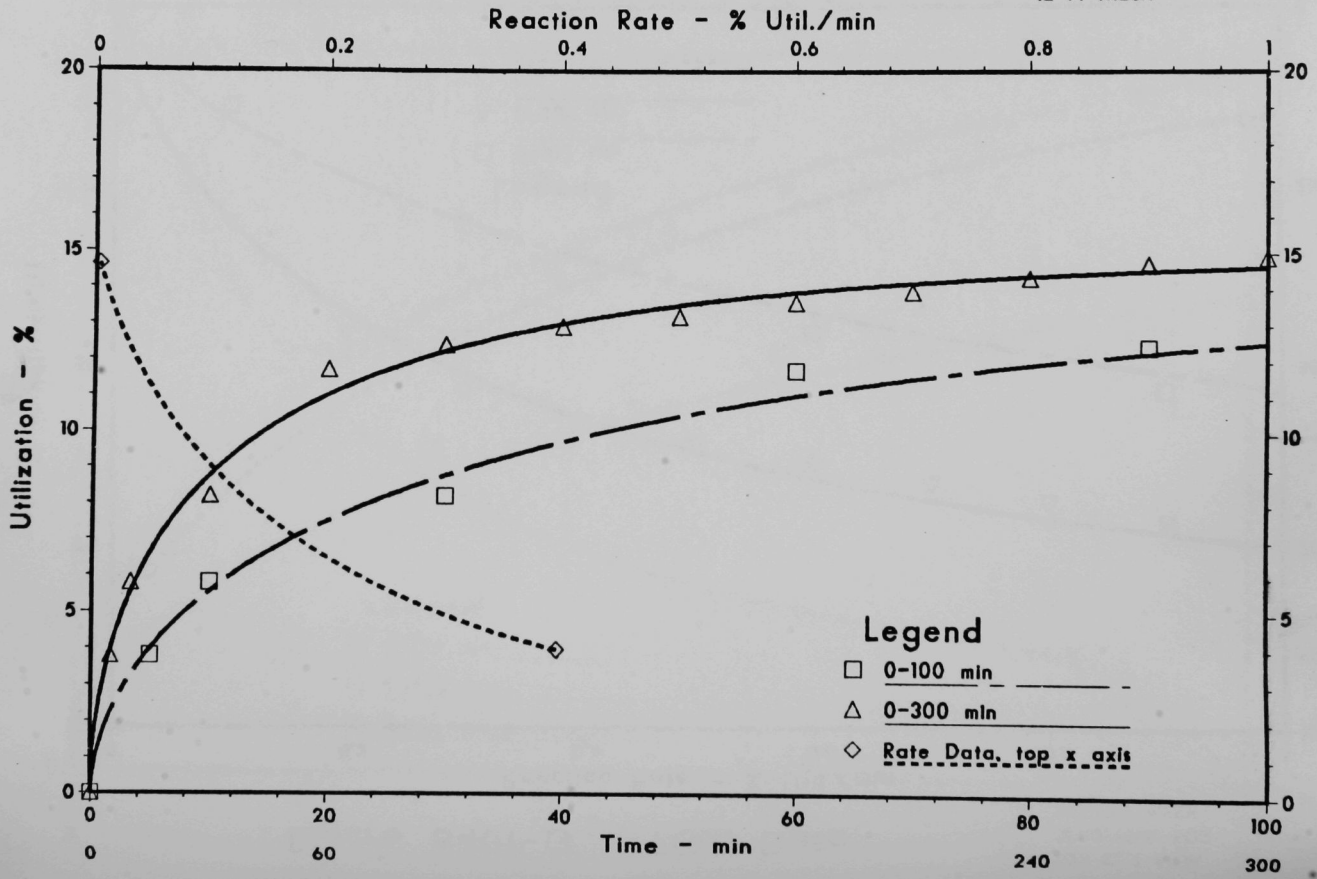

1. NAME: 1351 ANL-6101

   SOURCE: Jeffery Limestone Co., Parma, MI

2. CHEMICAL COMPOSITION, wt %

$CaCO_3$	$MgCO_3$	SiO_2	Fe_2O_3	Al_2O_3	Na_2O	K_2O
61.2	28.7	3.15	5.56	0.51	0.13	0.18

3. DENSITY: RAW SORBENT 2.466 g/cm^3 153.9 lb/ft^3

   CALCINED 1.443 g/cm^3 90.08 lb/ft^3

4. PETROGRAPHIC DESCRIPTION: AVERAGE GRAIN SIZE 40 μm, SEE FIG. 6701 A & B

   Fine-grained equigranular stone

5. PORE SIZE DISTRIBUTION: SEE FIG. 6101-C

   AVERAGE PORE DIAMETER - RAW SORBENT 0.277 μm

   CALCINED 0.091 μm

6. SURFACE AREA: RAW SORBENT 0.987 m^2/g 4.82 x 10^3 ft^2/lb

   CALCINED 20.47 m^2/g 9.99 x 10^4 ft^2/lb

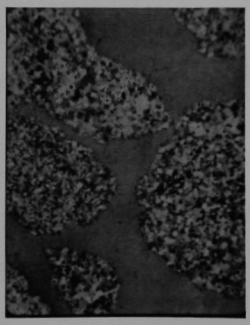

Fig. 6101A
Raw Dolomite
50X

Fig. 6101B
Calcined Dolomite 1 h 850°C
1100X

7. TOTAL POROSITY: RAW SORBENT 0.061 cm^3/g 9.8×10^{-4} ft^3/lb

CALCINED 0.454 cm^3/g 7.27×10^{-3} ft^3/lb

8. THERMOGRAVIMETRIC ANALYSIS: SEE FIG. 6101-D

(1123 K, 1 atm, 3000 ppm SO_2, -18 +20 mesh)

FRACTIONAL UTILIZATION = $\alpha(t, \text{min}) = 0.689\ [1 - \exp(-0.0205\ t^{0.967})]$

ANL PARAMETERS: D = 0.684 b = 137.3

9. ATTRITION: SEE FIG. 6101-E

Bed loss due to calcination breakup (%) = 1.1

Bed mass lost in linear portion (%/min.) = 1.22×10^{-3}

Attrition constant, λ_4 (sec^{-1}) = 2.77×10^{-7}

ATTRITION DATA

	Grams Total	wt %	
		Ca	S
Initial Bed	160.001	24.8	0.0
Final Bed	126.032	29.0	10.6
Total Overhead	1.812	36.0	6.0
Overhead, 5 min	0.599	36.0	6.0
10 min	0.257	36.0	6.0
15 min	0.115	36.0	6.0
30 min	0.117	36.0	6.0
1 h	0.047	36.0	6.0
1.5 h	0.104	36.0	6.0
2 h	0.129	36.0	6.0
4 h	0.146	36.0	6.0
6 h	0.152	36.0	6.0
8 h	0.177	36.0	6.0

Attrition Data, continued for Sorbent 6101

Weight in Grams, Particle Diameter, μm

Sample	-1000 +840	-841 +707	-707 +595	-595 +420	-420 +297	-297 +250
Overhead, first 30 min	0.000	0.000	0.006	0.002	0.003	0.016
Overhead, remaining 7.5 h	0.000	0.000	0.000	0.000	0.001	0.001
Final Bed, post test	119.813	3.524	0.316	0.171	0.134	0.025

Sample	-250 +210	-210 +74	-74 +63	-63 +53	-53 +44	-44 +37	-37 +0
Overhead, first 30 min	0.053	0.216	0.004	0.025	0.034	0.037	0.054
Overhead, remaining 7.5 h	0.003	0.027	0.000	0.003	0.002	0.003	0.000
Final Bed, post test	0.032	0.111	0.000	0.000	0.000	0.000	0.000

Figure 6101-C
Pore Size Distribution

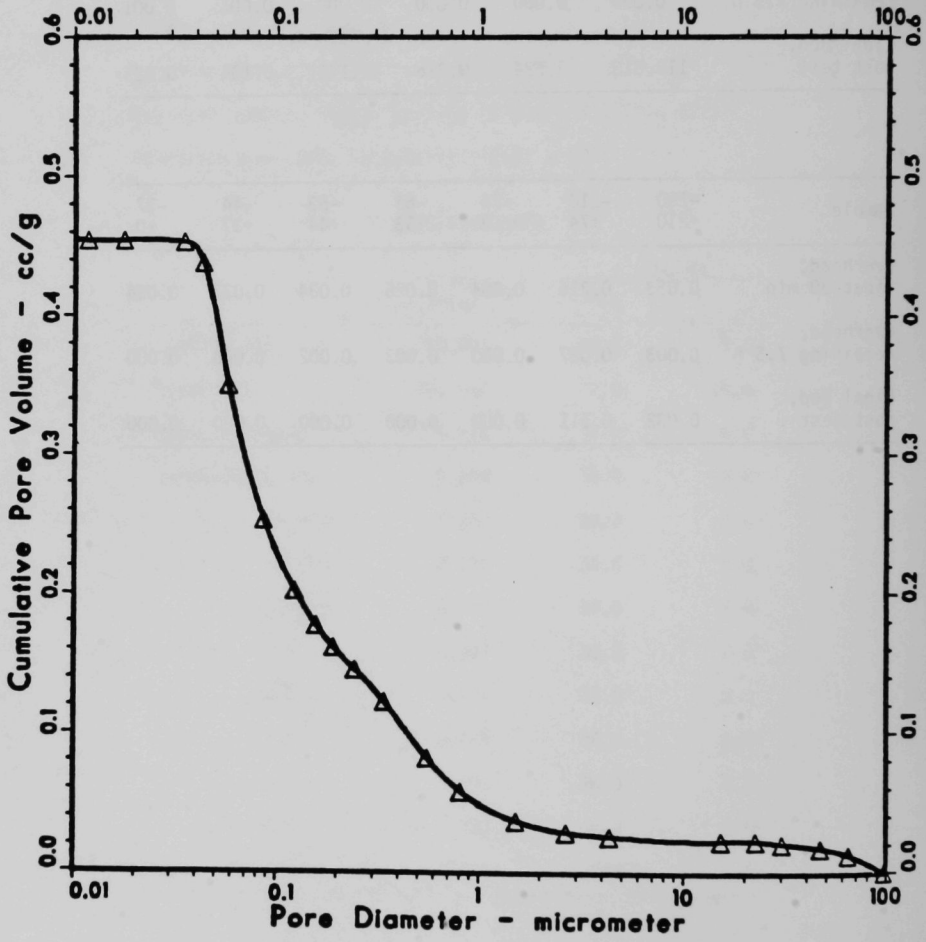

Figure 6101-D TGA Data

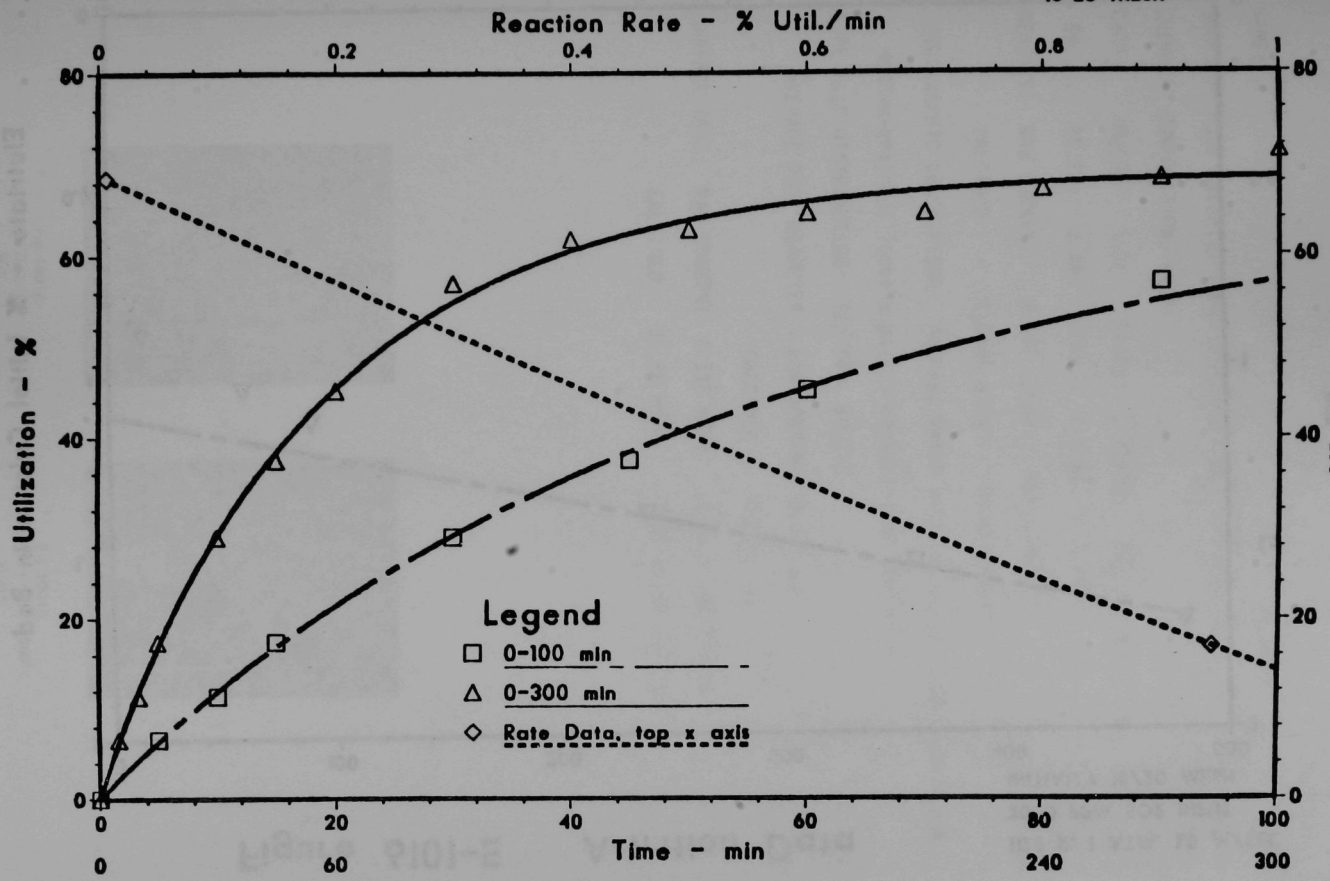

Figure 6101-E Attrition Data

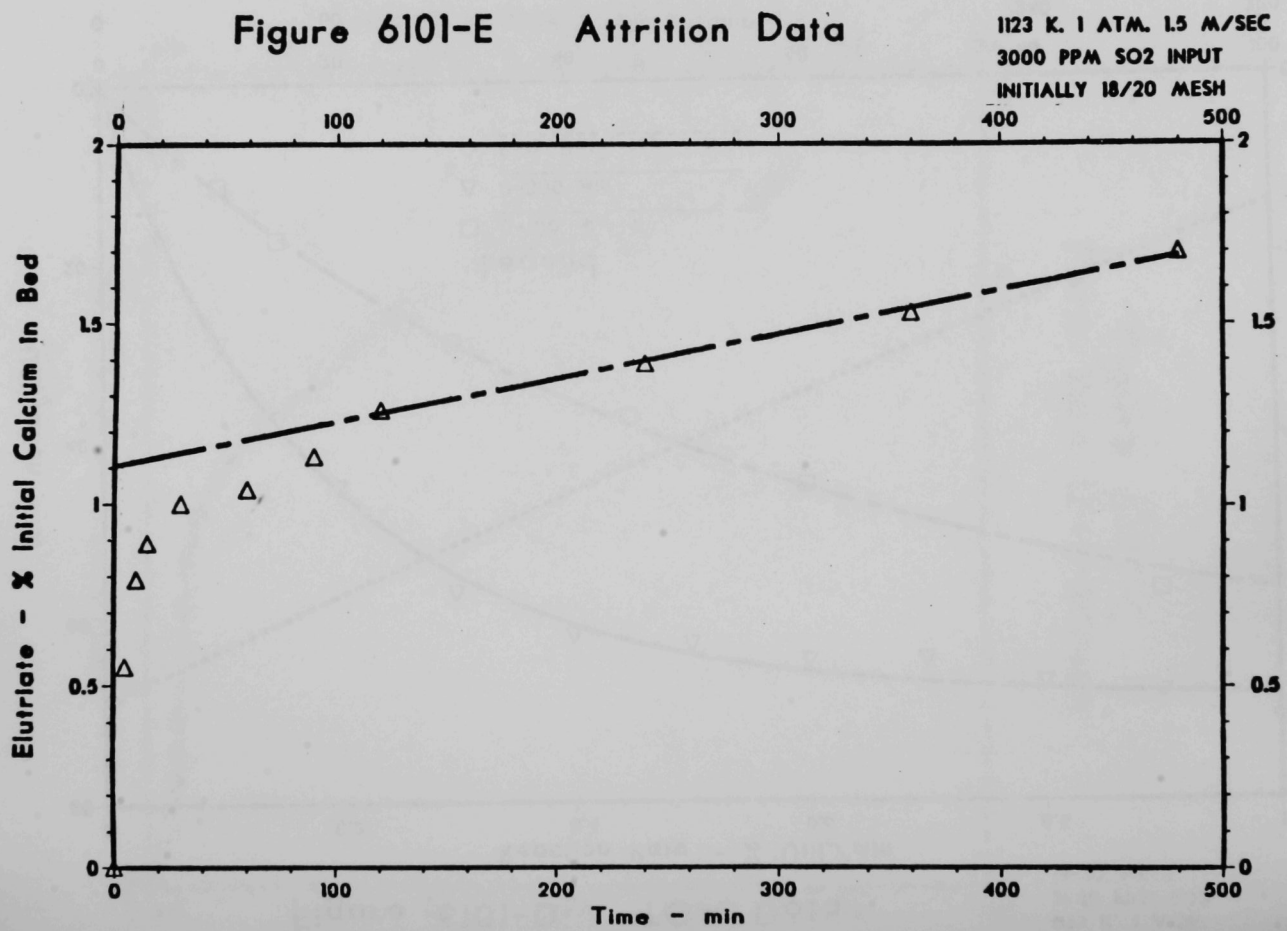

1. NAME: ANL-5901

SOURCE: Road Material (Medusa Aggregates), Burlington, IA

2. CHEMICAL COMPOSITION, wt %

$CaCO_3$	$MgCO_3$	SiO_2	Fe_2O_3	Al_2O_3	Na_2O	K_2O
59.1	35.72	3.48	0.68	0.34	0.27	0.53

3. DENSITY: RAW SORBENT 2.557 g/cm^3 159.6 lb/ft^3

CALCINED 1.4495 g/cm^3 90.49 lb/ft^3

4. PETROGRAPHIC DESCRIPTION: AVERAGE GRAIN SIZE 75 μm, SEE FIG. 5901 A & B

Medium-grained; loosely packed equigranular particles.

5. PORE SIZE DISTRIBUTION: SEE FIG. 5901-C

AVERAGE PORE DIAMETER - RAW SORBENT 0.852 μm

CALCINED 0.0461 μm

6. SURFACE AREA: RAW SORBENT 0.116 m^2/g 5.66 x 10^2 ft^2/lb

CALCINED 31.66 m^2/g 1.56 x 10^5 ft^2/lb

Fig. 5901A
Raw Dolomite
50X

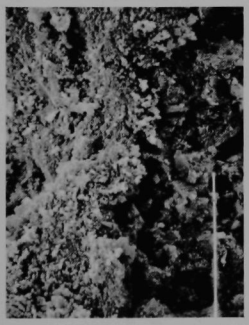

Fig. 5901B
Calcined Dolomite 1 h 850°C
1100X

7. TOTAL POROSITY: RAW SORBENT 0.0272 cm^3/g 4.36×10^{-4} ft^3/lb

CALCINED 0.370 cm^3/g 5.93×10^{-3} ft^3/lb

8. THERMOGRAVIMETRIC ANALYSIS: SEE FIG. 5901-D

(1123 K, 1 atm, 3000 ppm SO_2, -18 +20 mesh)

FRACTIONAL UTILIZATION = $\alpha(t, min) = 0.459 [1 - exp (-0.116 t^{0.639})]$

ANL PARAMETERS: D = 0.411 b = 246.1

9. ATTRITION: SEE FIG. 5901-E

Bed loss due to calcination breakup (%) = 0.63

Bed mass lost in linear portion (%/min.) = 1.72×10^{-3}

Attrition constant, λ_4 (sec^{-1}) = 4.0×10^{-7}

ATTRITION DATA

	Grams Total	wt % Ca	wt % S
Initial Bed	161.746	23.64	0.00
Final Bed	114.179	35.7	7.67
Total Overhead	1.932	28.0	7.66
Overhead, 5 min	0.380	28.0	7.66
10 min	0.094	28.0	7.66
15 min	0.083	28.0	7.66
30 min	0.099	28.0	7.66
1 h	0.154	28.0	7.66
1.5 h	0.129	28.0	7.66
2 h	0.145	28.0	7.66
4 h	0.383	28.0	7.66
6 h	0.254	28.0	7.66
8 h	0.209	28.0	7.66

Attrition Data, continued for Sorbent 5901

Weight in Grams, Particle Diameter, μm

Sample	-1000 +840	-841 +707	-707 +595	-595 +420	-420 +297	-297 +250
Overhead, first 30 min	0.001	0.000	0.000	0.000	0.004	0.016
Overhead, remaining 7.5 h	0.002	0.000	0.002	0.009	0.050	0.057
Final Bed, post test	88.881	22.481	0.694	0.474	0.510	0.175

Sample	-250 +210	-210 +74	-74 +63	-63 +53	-53 +44	-44 +37	-37 +0
Overhead, first 30 min	0.021	0.252	0.008	0.029	0.058	0.052	0.033
Overhead, remaining 7.5 h	0.115	0.732	0.011	0.029	0.040	0.024	0.012
Final Bed, post test	0.187	0.642	0.010	0.034	0.059	0.017	0.011

Figure 5901-C
Pore Size Distribution

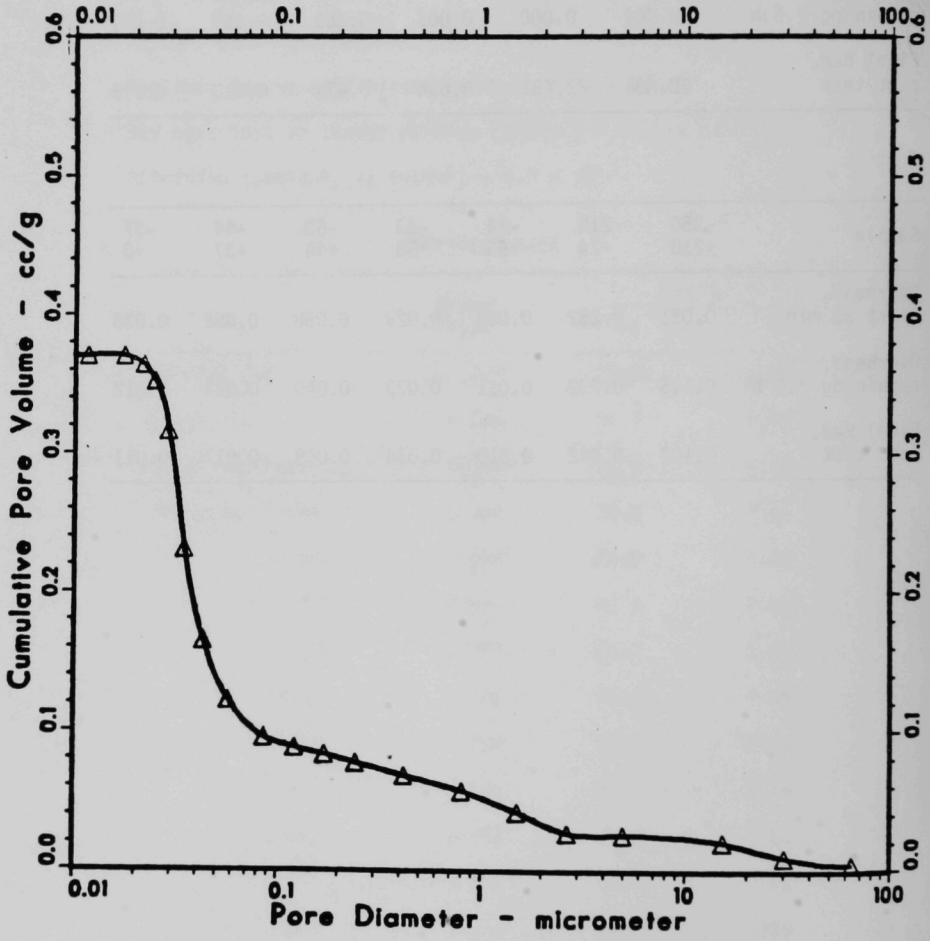

Figure 5901-D TGA Data

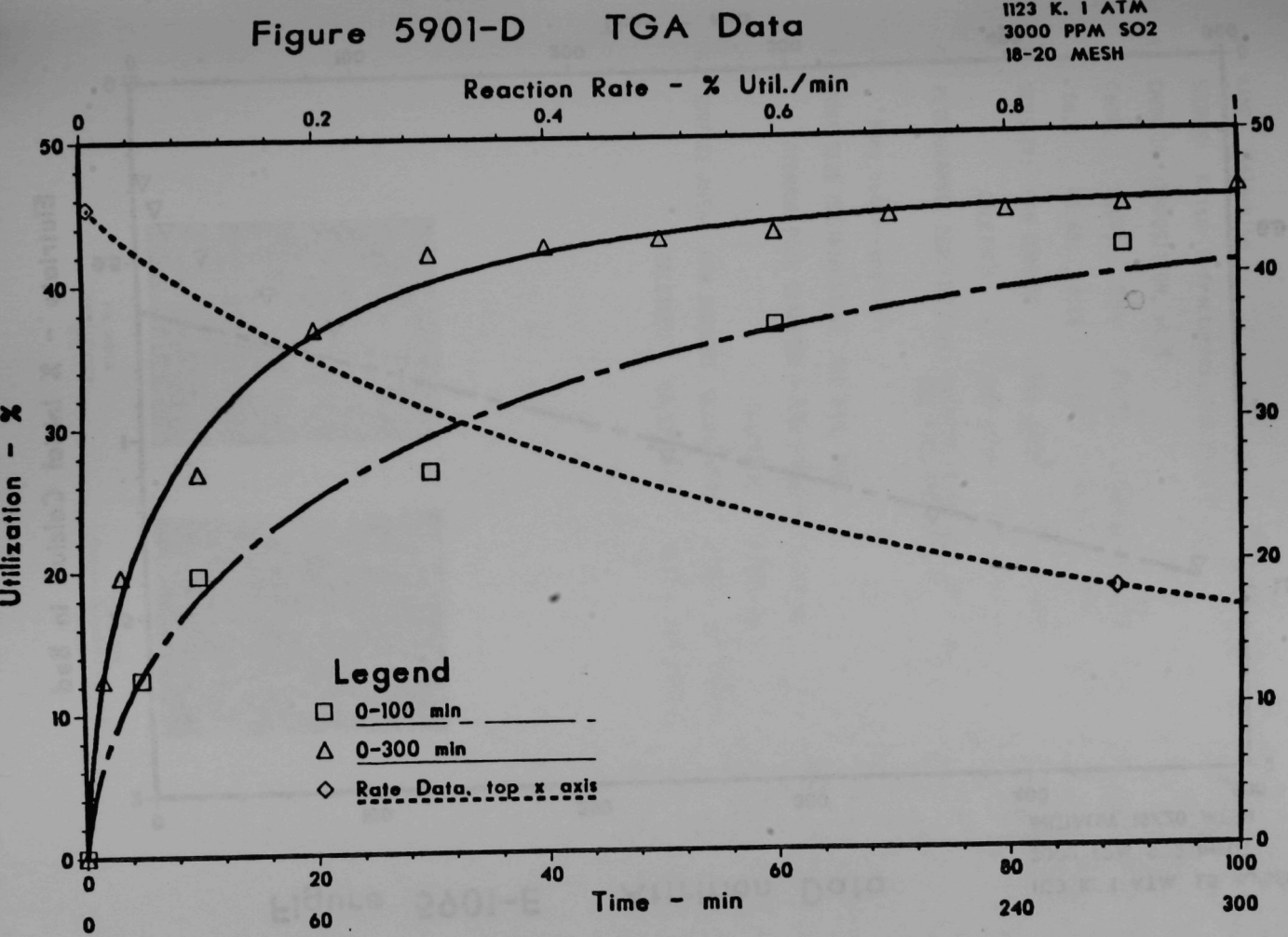

Figure 5901-E Attrition Data

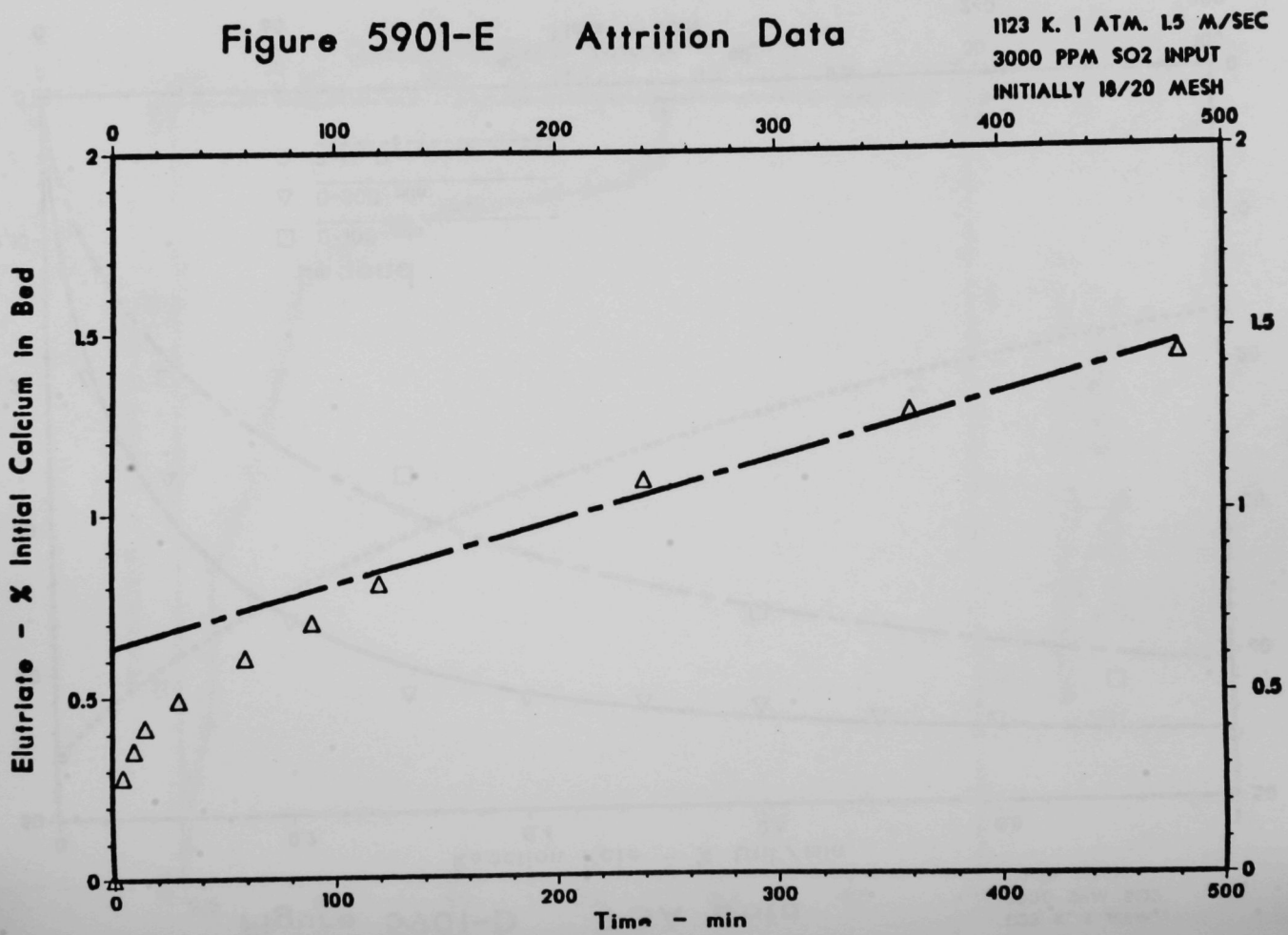

1. NAME: Dolowhite ANL-5601

   SOURCE: Kaiser Refractories, Salinas, CA

2. CHEMICAL COMPOSITION, wt %

$CaCO_3$	$MgCO_3$	SiO_2	Fe_2O_3	Al_2O_3	Na_2O	K_2O
56.8	45.62	0.18	0.09	0.01	0.02	0.01

3. DENSITY: RAW SORBENT 2.969 g/cm^3 185.3 lb/ft^3

   CALCINED 1.630 g/cm^3 101.8 lb/ft^3

4. PETROGRAPHIC DESCRIPTION: AVERAGE GRAIN SIZE >250 μm, SEE FIG. 5601 A & B

   Very coarse-grained.

5. PORE SIZE DISTRIBUTION: SEE FIG. 5601-C

   AVERAGE PORE DIAMETER - RAW SORBENT 0.119 μm

   CALCINED 0.034 μm

6. SURFACE AREA: RAW SORBENT 0.060 m^2/g 2.95 x 10^2 ft^2/lb

   CALCINED 43.17 m^2/g 2.11 x 10^5 ft^2/lb

Fig. 5601A
Raw Dolomite
50X

Fig. 5601B
Calcined Dolomite 1 h 850°C
1100X

7. TOTAL POROSITY: RAW SORBENT 0.002 cm^3/g 3.7×10^{-5} ft^3/lb

CALCINED 0.360 cm^3/g 5.77×10^{-3} ft^3/lb

8. THERMOGRAVIMETRIC ANALYSIS: SEE FIG. 5601-D

(1123 K, 1 atm, 3000 ppm SO_2, -18 +20 mesh)

FRACTIONAL UTILIZATION = $\alpha(t, min) = 0.149 [1 - exp (-0.091 t^{0.594})]$

ANL PARAMETERS: D = 0.0745 b = 746.7

9. ATTRITION: SEE FIG. 5601-E

Bed loss due to calcination breakup (%) = 5.9

Bed mass lost in linear portion (%/min.) = 1.69×10^{-3}

Attrition constant, λ_4 (sec^{-1}) = 4.82×10^{-7}

ATTRITION DATA

	Grams Total	wt %	
		Ca	S
Initial Bed	160.004	22.72	0.00
Final Bed	89.620	37.4	3.97
Total Overhead	7.838	31.05	4.42
Overhead, 5 min	3.177	31.05	4.42
10 min	1.445	31.05	4.42
15 min	0.912	31.05	4.42
30 min	0.544	31.05	4.42
1 h	0.384	31.05	4.42
1.5 h	0.273	31.05	4.42
2 h	0.360	31.05	4.42
4 h	0.321	31.05	4.42
6 h	0.170	31.05	4.42
8 h	0.251	31.05	4.42

Attrition Data, continued for Sorbent 5601

Weight in Grams, Particle Diameter, μm

Sample	-1000 +840	-841 +707	-707 +595	-595 +420	-420 +297	-297 +250
Overhead, first 30 min	0.000	0.006	0.001	0.004	0.187	0.000
Overhead, remaining 7.5 h	0.004	0.002	0.001	0.012	0.247	0.251
Final Bed, post test	54.686	9.233	8.399	9.590	5.660	1.070

Sample	-250 +210	-210 +74	-74 +63	-63 +53	-53 +44	-44 +37	-37 +0
Overhead, first 30 min	0.000	2.875	0.022	0.129	0.296	0.134	0.408
Overhead, remaining 7.5 h	0.347	0.855	0.009	0.039	0.096	0.046	0.118
Final Bed, post test	0.684	0.288	0.002	0.002	0.003	0.001	0.002

10. OTHER DATA: TGA Data: 1123 K, 1 atm, 3000 ppm SO_2

See Fig. 5601-F $\alpha(t,min) = 0.236\ [1 - \exp(-0.161\ t^{0.357})]$

-50 +70 mesh $D = 0.0931$ $b = 988$

See Fig. 5601-G $\alpha(t,min) = 0.346\ [1 - \exp(-0.137\ t^{0.438})]$

-140 +170 mesh $D = 0.182$ $b = 498$

Figure 5601-C
Pore Size Distribution

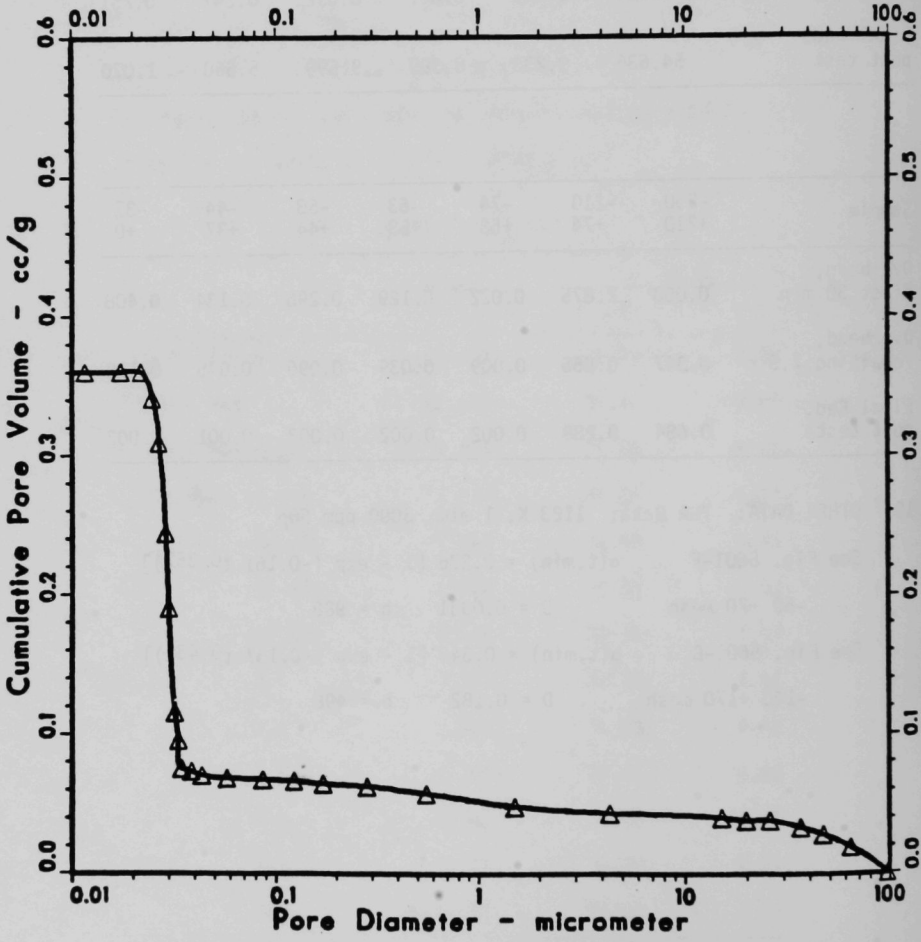

Figure 5601-D TGA Data

1123 K. 1 ATM
3000 PPM SO2
18-20 MESH

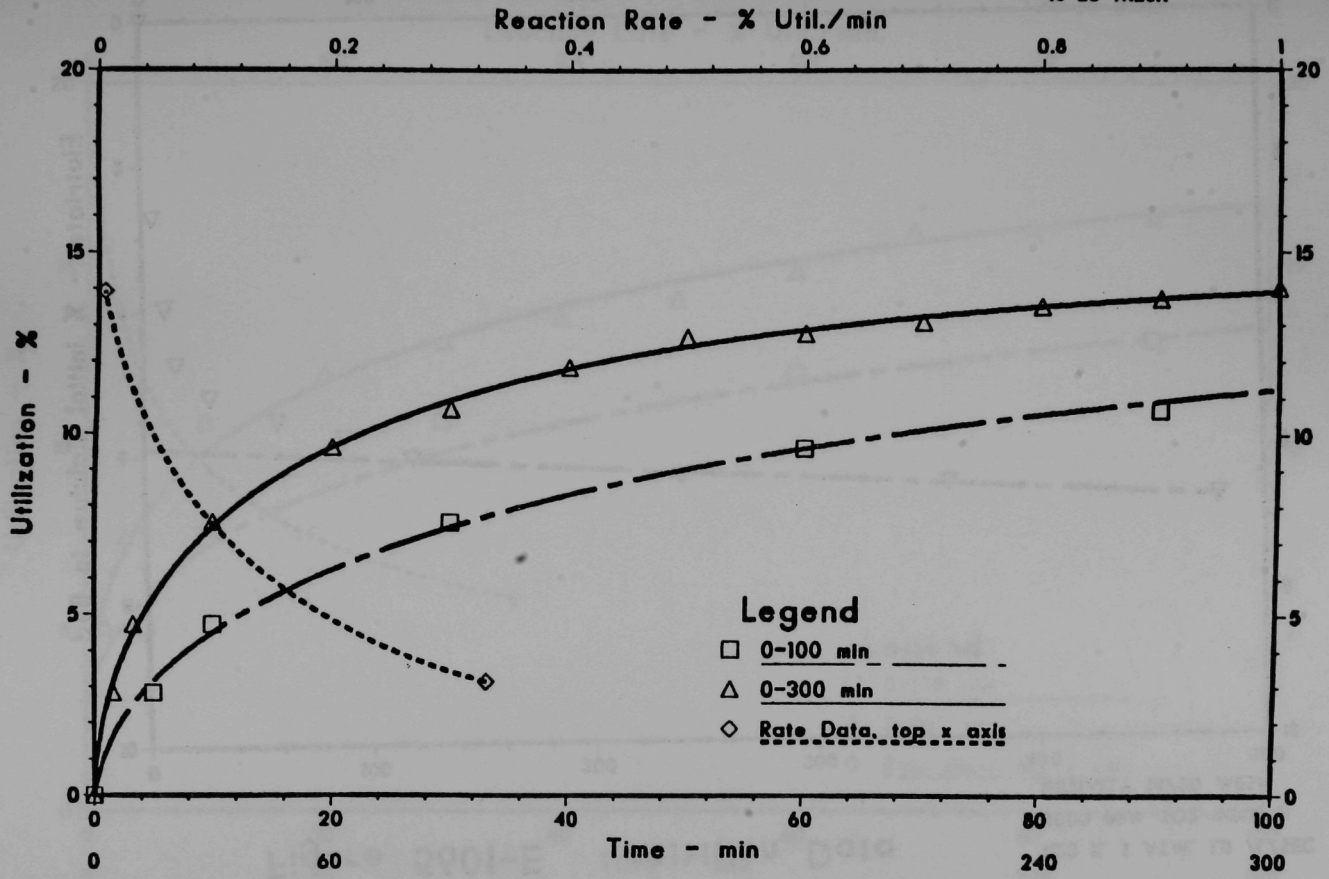

Figure 5601-E Attrition Data

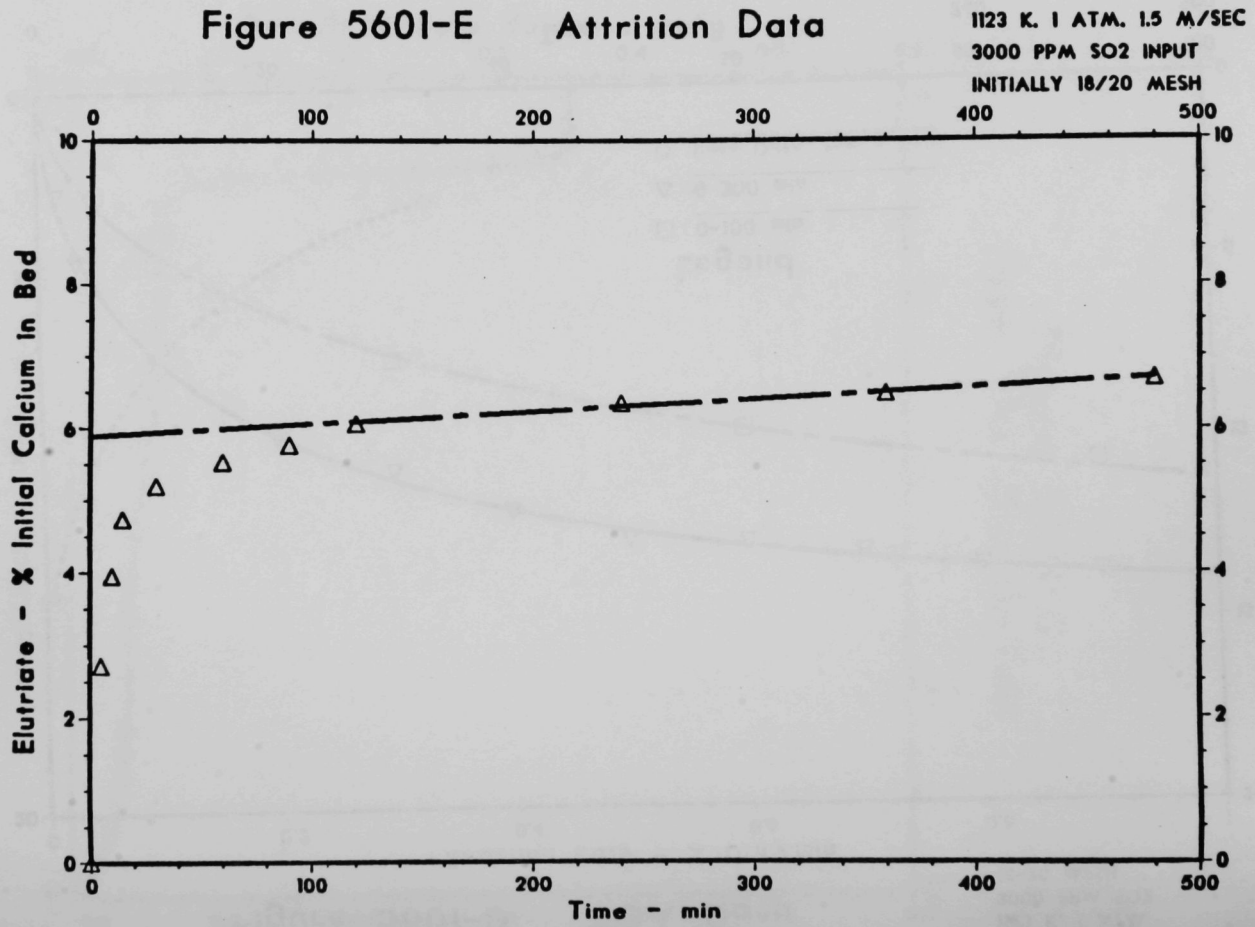

Figure 5601-F TGA Data

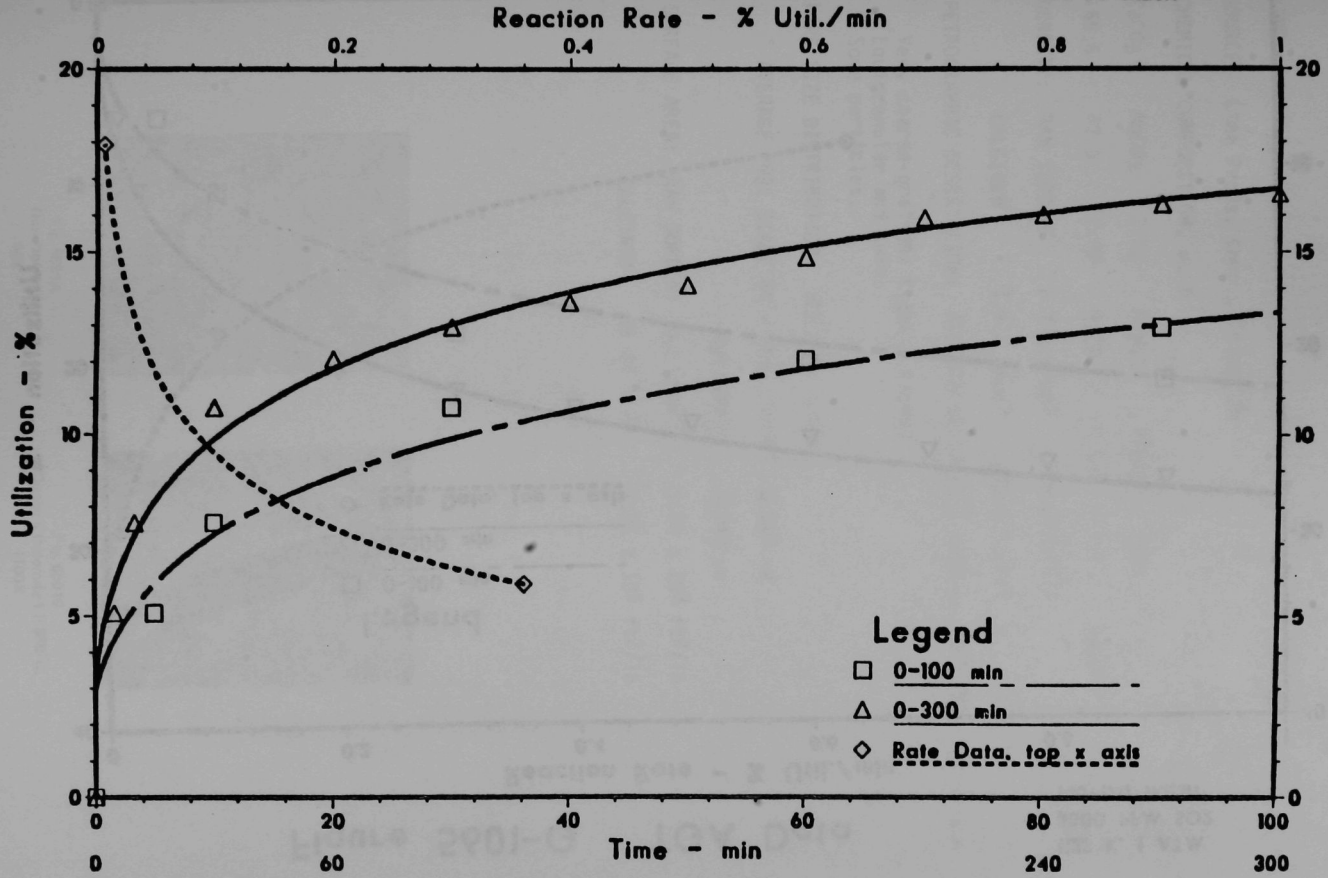

Figure 5601-G TGA Data

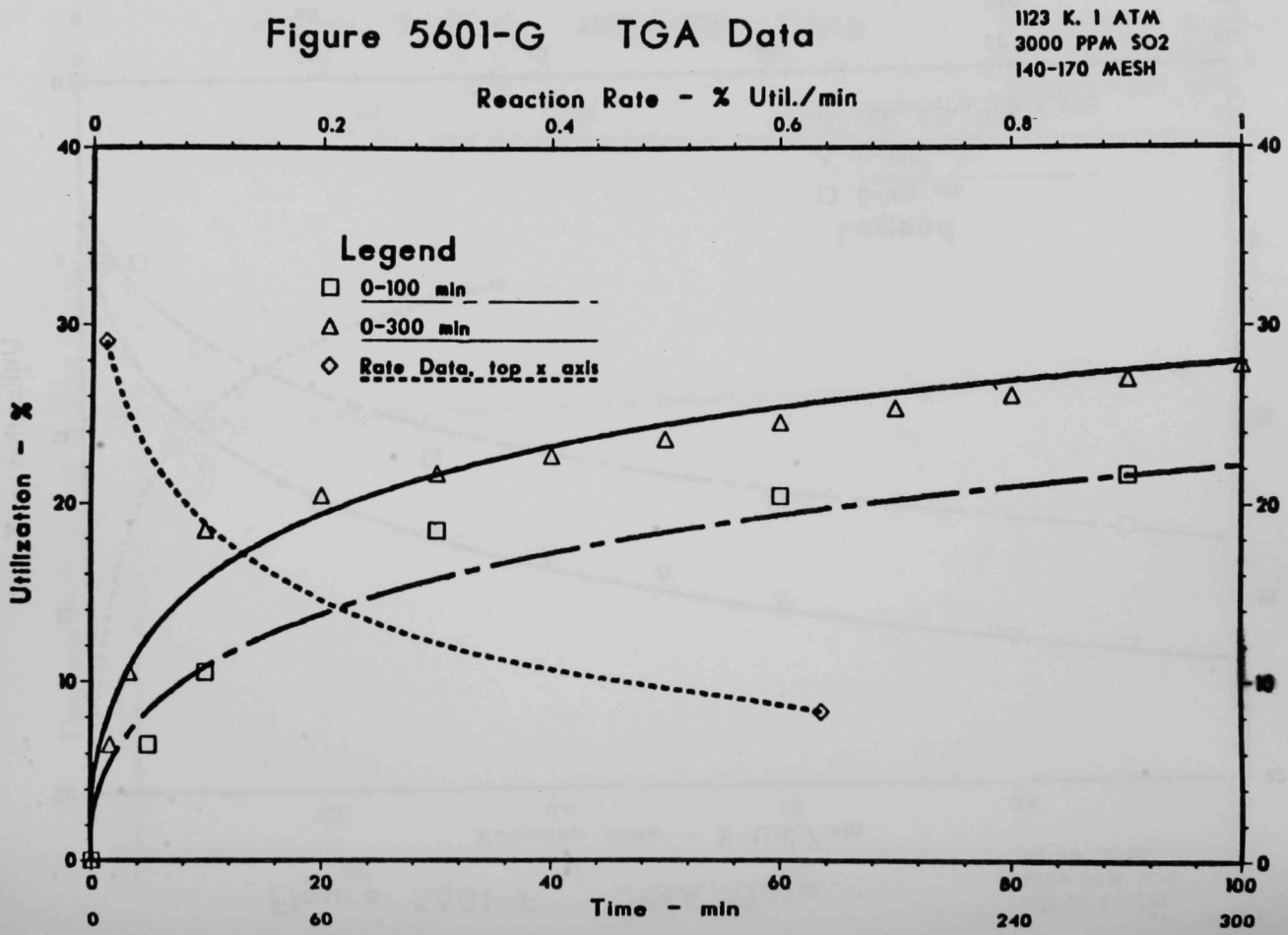

1. NAME: ANL-5501

SOURCE: Lime Prods. Corp., Union, ME

2. CHEMICAL COMPOSITION, wt %

$CaCO_3$	$MgCO_3$	SiO_2	Fe_2O_3	Al_2O_3	Na_2O	K_2O
55.6	43.3	2.97	0.23	0.18	0.03	0.03

3. DENSITY: RAW SORBENT 2.832 g/cm^3 176.8 lb/ft^3

CALCINED 1.974 g/cm^3 123 2 lb/ft^3

4. PETROGRAPHIC DESCRIPTION: AVERAGE GRAIN SIZE >250 μm, SEE FIG. 5501 A & B

Very coarse-grained; tightly packed.
Equigranular and twin.
Some particles.

5. PORE SIZE DISTRIBUTION: SEE FIG. 5501-C

AVERAGE PORE DIAMETER - RAW SORBENT 0.119 μm

CALCINED 0.048 μm

6. SURFACE AREA: RAW SORBENT 0.233 m^2/g 1.14 x 10^3 ft^2/lb

CALCINED 26.78 m^2/g 1.31 x 10^5 ft^2/lb

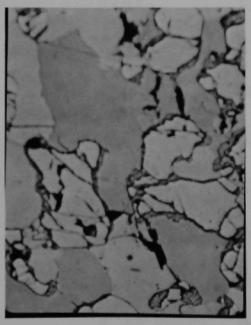

Fig. 5501A
Raw Dolomite
50X

Fig. 5501B
Calcined Dolomite 1 h 850°C
1100X

7. TOTAL POROSITY: RAW SORBENT 0.008 cm^3/g 1.2×10^{-4} ft^3/lb

CALCINED 0.334 cm^3/g 5.35×10^{-3} ft^3/lb

8. THERMOGRAVIMETRIC ANALYSIS: SEE FIG. 5501-D

(1123 K, 1 atm, 3000 ppm SO_2, -18 +20 mesh)

FRACTIONAL UTILIZATION = $\alpha(t, \text{min}) = 0.209\ [1 - \exp(-0.100\ t^{0.676})]$

ANL PARAMETERS: D = 0.164 b = 420.9

9. ATTRITION: SEE FIG. 5501-E

Bed loss due to calcination breakup (%) = 3.9

Bed mass lost in linear portion (%/min.) = 3.29×10^{-3}

Attrition constant, λ_4 (sec^{-1}) = 9.0×10^{-7}

ATTRITION DATA

	Grams Total	wt % Ca	wt % S
Initial Bed	160.436	22.24	0.00
Final Bed	97.256	29.2	4.20
Total Overhead	6.583	29.3	5.50
Overhead, 5 min	2.102	29.3	5.50
10 min	0.702	29.3	5.50
15 min	0.365	29.3	5.50
30 min	0.642	29.3	5.50
1 h	0.594	29.3	5.50
1.5 h	0.414	29.3	5.50
2 h	0.282	29.3	5.50
4 h	0.666	29.3	5.50
6 h	0.387	29.3	5.50
8 h	0.428	29.3	5.50

Attrition Data, continued for Sorbent 5501

Weight in Grams, Particle Diameter, μm

Sample	-1000 +840	-841 +707	-707 +595	-595 +420	-420 +297	-297 +250
Overhead, first 30 min	0.000	0.000	0.000	0.008	0.026	0.090
Overhead, remaining 7.5 h	0.025	0.009	0.004	0.011	0.207	0.361
Final Bed, post test	66.224	10.855	5.230	2.932	4.186	1.931

Sample	-250 +210	-210 +74	-74 +63	-63 +53	-53 +44	-44 +37	-37 +0
Overhead, first 30 min	0.370	2.018	0.046	0.120	0.160	0.105	0.078
Overhead, remaining 7.5 h	0.556	1.613	0.017	0.074	0.139	0.068	0.119
Final Bed, post test	2.413	3.329	0.002	0.029	0.015	0.004	0.002

Figure 5501-C
Pore Size Distribution

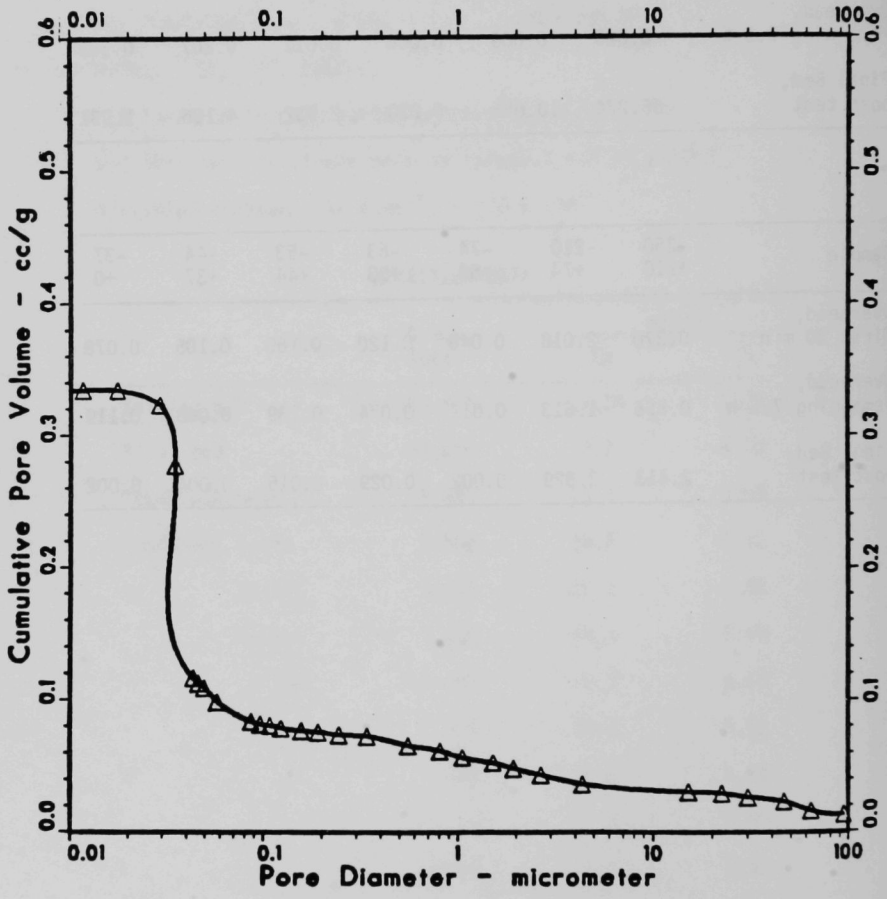

Figure 5501-D TGA Data

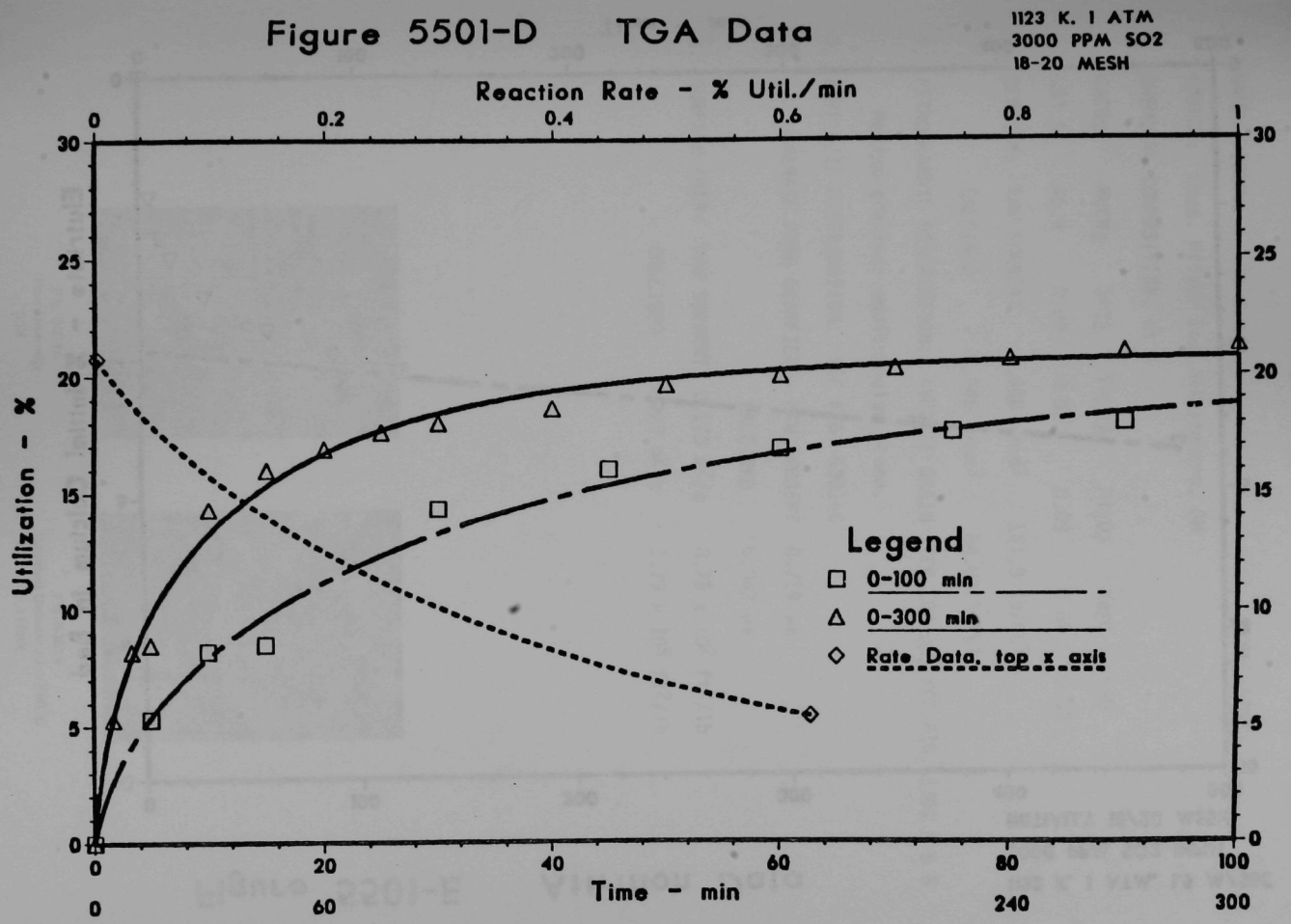

Figure 5501-E Attrition Data

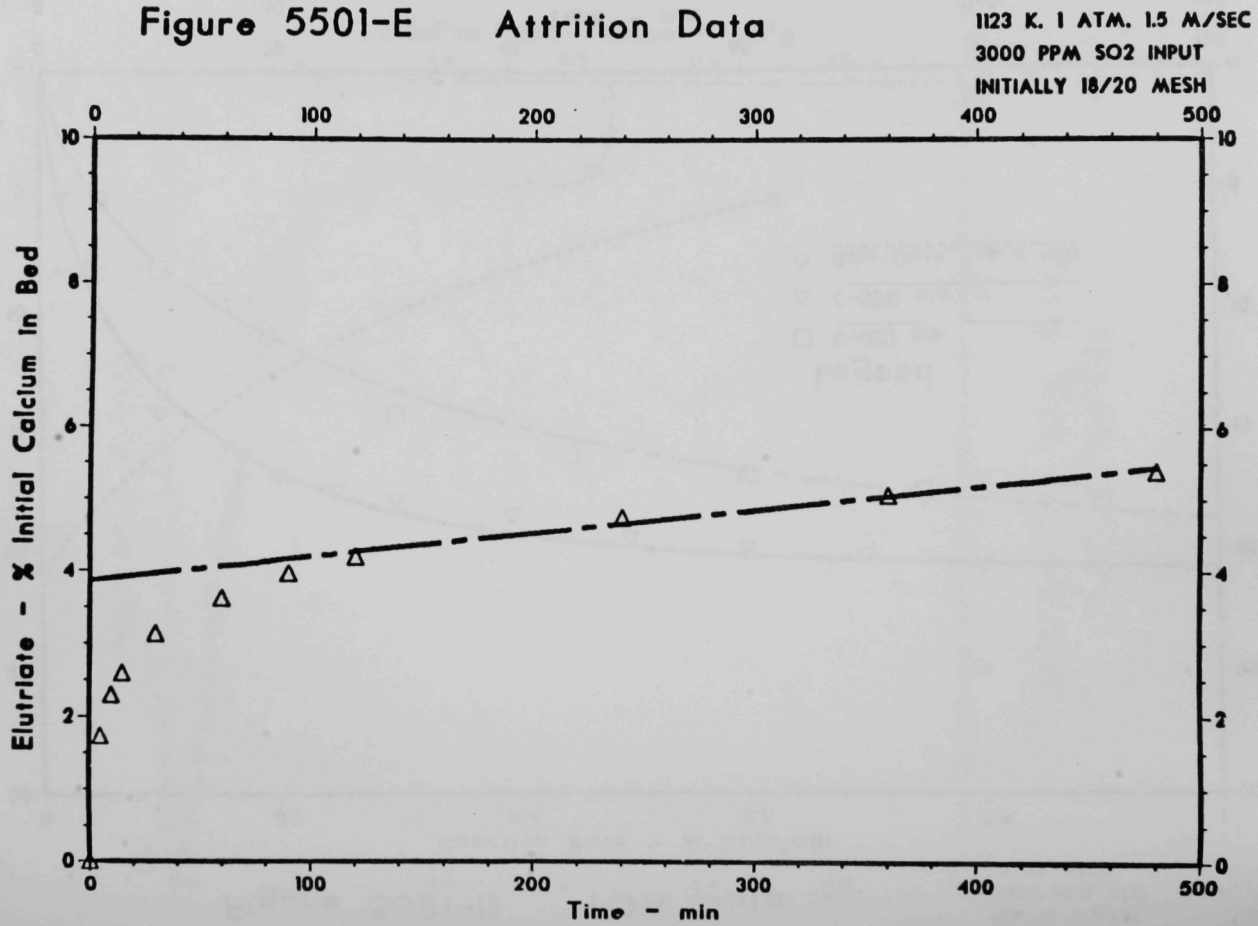

1. NAME: 1337 ANL-5301

SOURCE: Chas. Pfizer Co., Gibsonburg, OH

2. CHEMICAL COMPOSITION, wt %

$CaCO_3$	$MgCO_3$	SiO_2	Fe_2O_3	Al_2O_3	Na_2O	K_2O
53.4	45.4	0.69	0.07	0.08	0.05	0.03

3. DENSITY: RAW SORBENT 2.688 g/cm^3 167.8 lb/ft^3

CALCINED 1.346 g/cm^3 84.03 lb/ft^3

4. PETROGRAPHIC DESCRIPTION: AVERAGE GRAIN SIZE 100 μm, SEE FIG. 5301 A & B

Medium-grained; equigranular stone.

5. PORE SIZE DISTRIBUTION: SEE FIG. 5301-C

AVERAGE PORE DIAMETER - RAW SORBENT 0.719 μm

CALCINED 0.047 μm

6. SURFACE AREA: RAW SORBENT 0.179 m^2/g 8.75 x 10^2 ft^2/lb

CALCINED 36.75 m^2/g 1.79 x 10^5 ft^2/lb

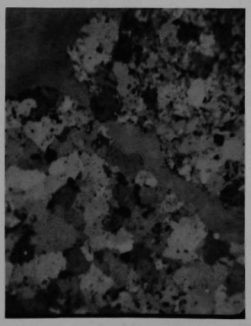

Fig. 5301A
Raw Dolomite
50X

Fig. 5301B
Calcined Dolomite 1 h 850°C
1100X

7. TOTAL POROSITY: RAW SORBENT 0.033 cm^3/g 5.3×10^{-4} ft^3/lb

CALCINED 0.430 cm^3/g 6.89×10^{-3} ft^3/lb

8. THERMOGRAVIMETRIC ANALYSIS: SEE FIG. 5301-D

(1123 K, 1 atm, 3000 ppm SO_2, -18 +20 mesh)

FRACTIONAL UTILIZATION = $\alpha(t, \text{min}) = 0.630\ [1 - \exp(-0.0355\ t^{0.825})]$

ANL PARAMETERS: D = 0.586 b = 134.8

9. ATTRITION: SEE FIG. 5301-E

Bed loss due to calcination breakup (%) = 10.0

Bed mass lost in linear portion (%/min.) = 1.07×10^{-3}

Attrition constant, λ_4 (sec^{-1}) = 2.54×10^{-7}

ATTRITION DATA

	Grams Total	wt % Ca	wt % S
Initial Bed	160.010	21.36	0.00
Final Bed	104.613	30.8	10.7
Total Overhead	10.480	34.4	2.23
Overhead, 5 min	1.331	34.4	2.23
10 min	3.493	34.4	2.23
15 min	2.000	34.4	2.23
30 min	2.284	34.4	2.23
1 h	0.708	34.4	2.23
1.5 h	0.191	34.4	2.23
2 h	0.059	34.4	2.23
4 h	0.164	34.4	2.23
6 h	0.118	34.4	2.23
8 h	0.132	34.4	2.23

Attrition Data, continued for Sorbent 5301

Weight in Grams, Particle Diameter, μm

Sample	-1000 +840	-841 +707	-707 +595	-595 +420	-420 +297	-297 +250
Overhead, first 30 min	0.001	0.003	0.001	0.004	0.004	0.015
Overhead, remaining 7.5 h	0.001	0.002	0.001	0.005	0.046	0.183
Final Bed, post test	90.850	8.063	2.268	1.172	0.994	0.204

Sample	-250 +210	-210 +74	-74 +63	-63 +53	-53 +44	-44 +37	-37 +0
Overhead, first 30 min	0.081	3.654	0.169	0.662	0.704	0.388	0.722
Overhead, remaining 7.5 h	0.453	1.903	0.011	0.175	0.272	0.095	0.175
Final Bed, post test	0.065	0.496	0.005	0.030	0.031	0.040	0.003

10. OTHER DATA: TGA Data: 1123 K, 1 atm, 3000 ppm SO_2

See Fig. 5301-F $\alpha(t,min) = 0.819\ [1 - \exp(-0.057\ t^{0.646})]$

-50 +70 mesh $D = 0.668$ $b = 116$

See Fig. 5301-G $\alpha(t,min) = 0.920\ [1 - \exp(-0.0574\ t^{0.625})]$

-140 +170 mesh $D = 0.7400$ $b = 104$

Figure 5301-C
Pore Size Distribution

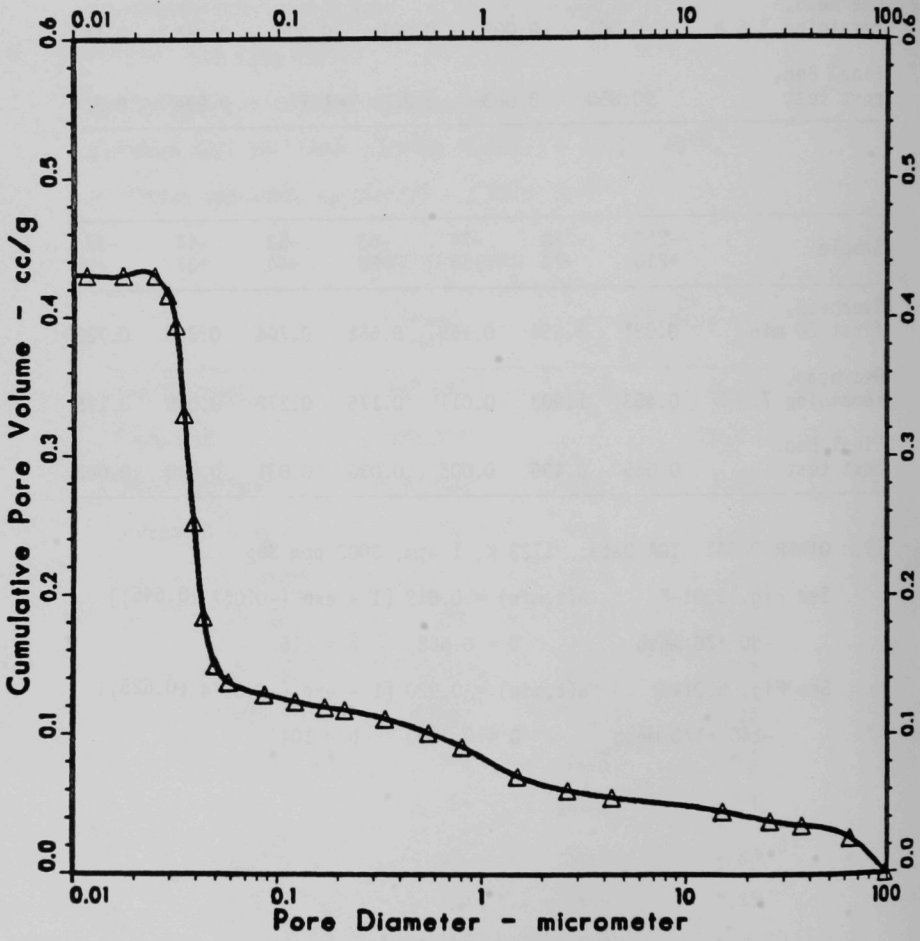

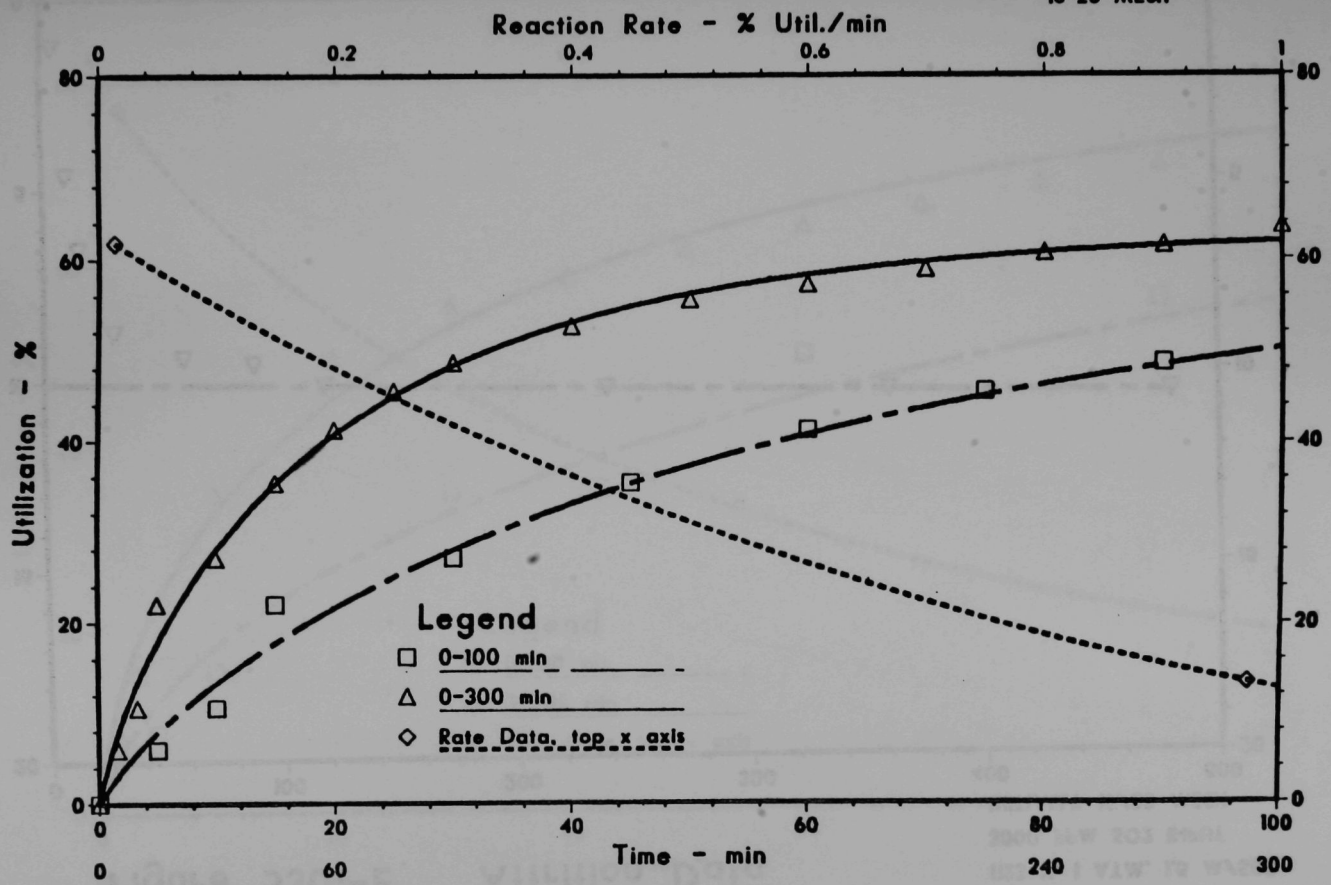
Figure 5301-D TGA Data
1123 K. 1 ATM
3000 PPM SO2
18-20 MESH
Reaction Rate - % Util./min
0
0.2
0.4
0.6
0.8
1
Utilization - %
80
60
40
20
0
Legend
0-100 min
0-300 min
Rate Data, top x axis
0
20
40
60
80
100
Time - min
0
60
240
300

Figure 5301-E. Attrition Data

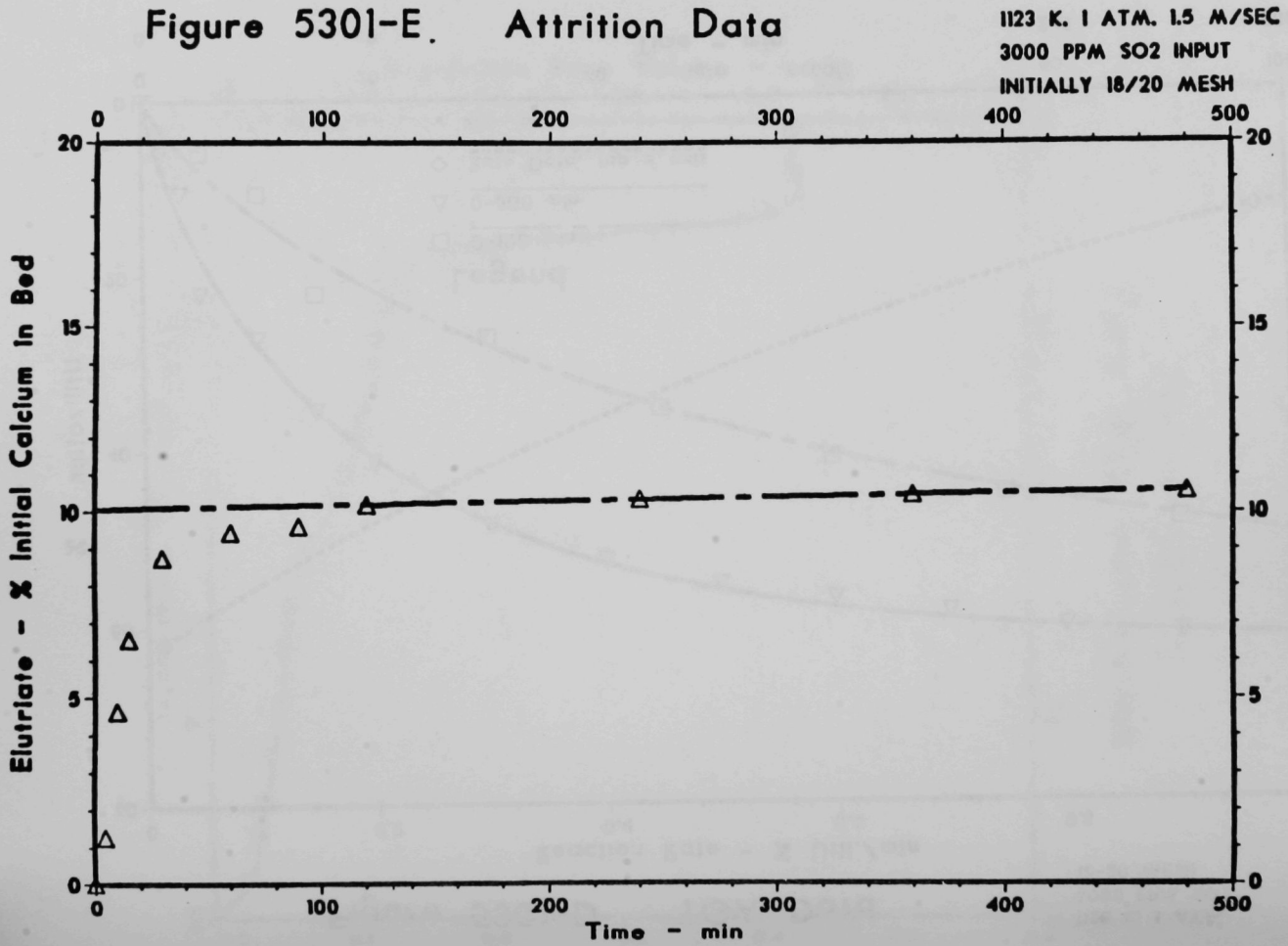

Figure 5301-F TGA Data

1123 K. 1 ATM
3000 PPM SO2
50-70 MESH

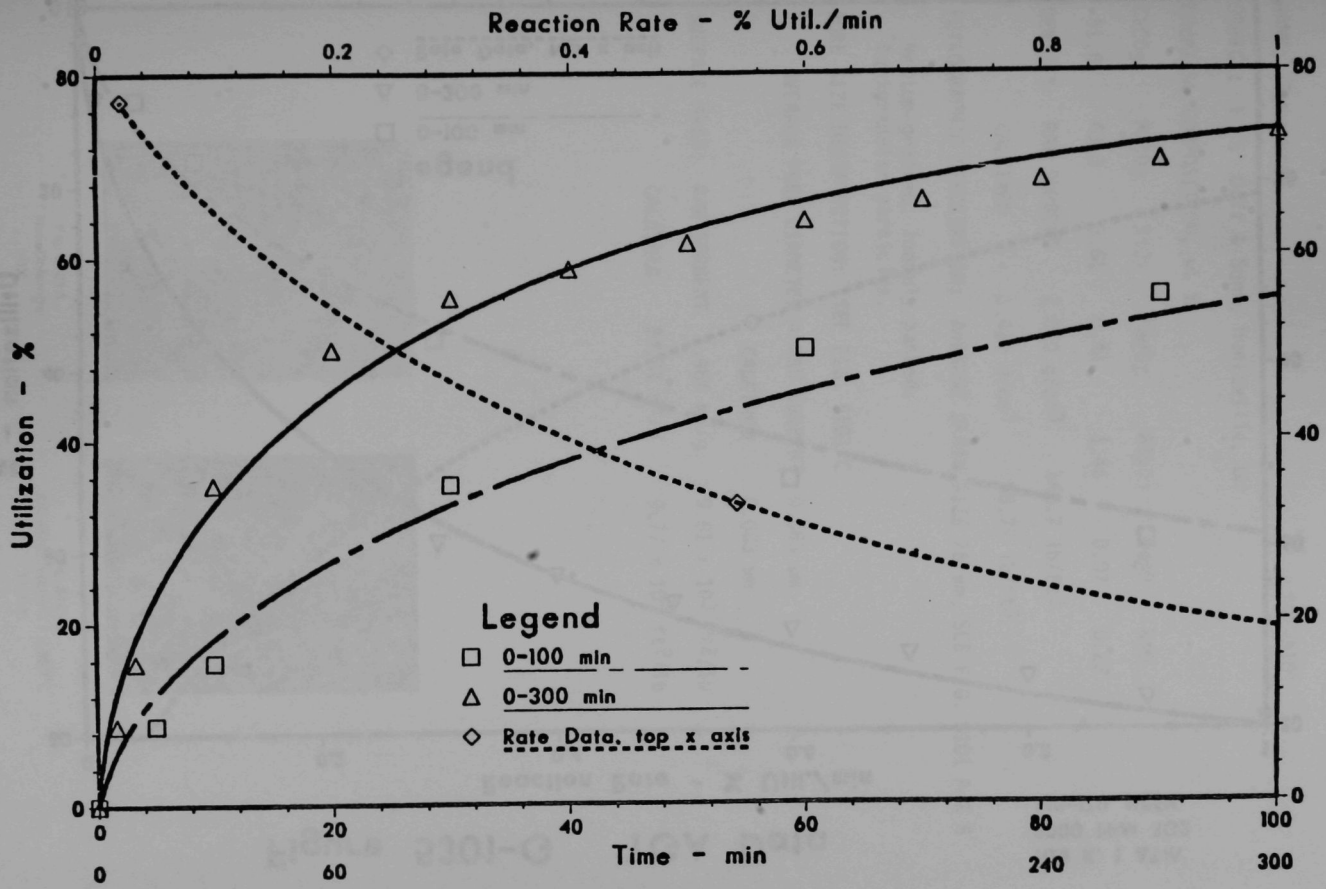

Figure 5301-G TGA Data

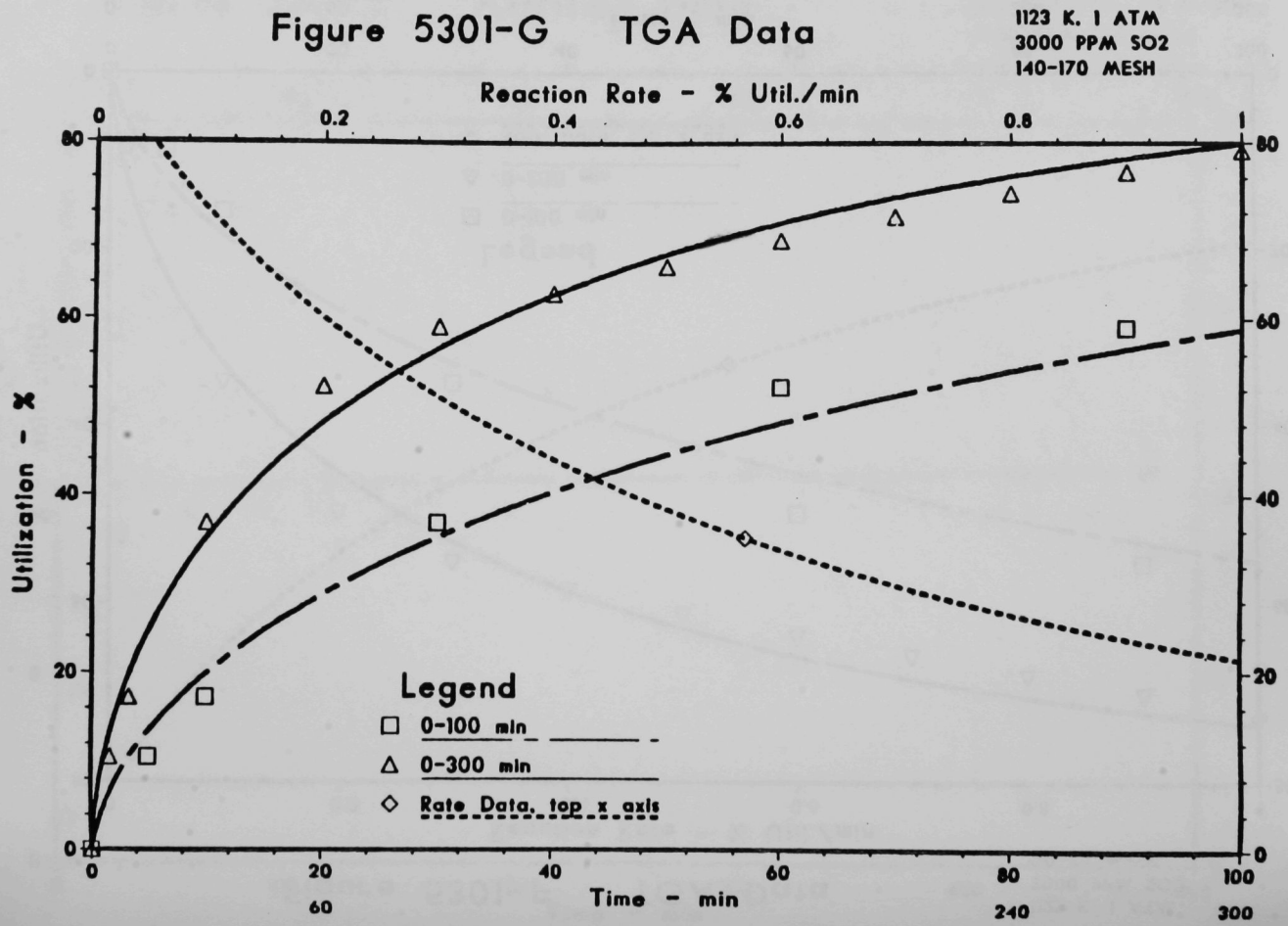

1. NAME: Tymochtee ANL-5101

   SOURCE: E. E. Duff & Sons, Huntsville, OH

2. CHEMICAL COMPOSITION, wt %

$CaCO_3$	$MgCO_3$	SiO_2	Fe_2O_3	Al_2O_3	Na_2O	K_2O
51.8	43.3	3.61	0.41	1.46	0.07	0.22

3. DENSITY: RAW SORBENT 2.670 g/cm^3 166.7 lb/ft^3

   CALCINED 1.422 g/cm^3 88.77 lb/ft^3

4. PETROGRAPHIC DESCRIPTION: AVERAGE GRAIN SIZE 75 µm, SEE FIG. 5101 A & B

   Medium-grained; loosely packed.
   Equigranular particles.

5. PORE SIZE DISTRIBUTION: SEE FIG. 5101-C

   AVERAGE PORE DIAMETER - RAW SORBENT 0.065 µm

   CALCINED 0.083 µm

6. SURFACE AREA: RAW SORBENT 1.969 m^2/g 9.61 x 10^3 ft^2/lb

   CALCINED 20.01 m^2/g 9.77 x 10^4 ft^2/lb

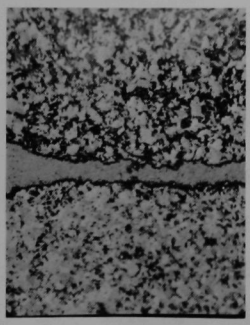

Fig. 5101A
Raw Dolomite
50X

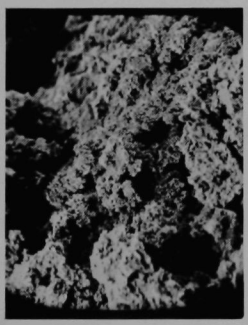

Fig. 5101B
Calcined Dolomite 1 h 850°C
1100X

7. TOTAL POROSITY: RAW SORBENT 0.037 cm^3/g 5.9×10^{-4} ft^3/lb

CALCINED 0.422 cm^3/g 6.76×10^{-3} ft^3/lb

8. THERMOGRAVIMETRIC ANALYSIS: SEE FIG. 5101-D

(1123 K, 1 atm, 3000 ppm SO_2, -18 +20 mesh)

FRACTIONAL UTILIZATION = $\alpha(t, \text{min}) = 0.950\ [1 - \exp(-0.0422\ t^{0.782})]$

ANL PARAMETERS: D = 0.899 b = 115.1

9. ATTRITION: SEE FIG. 5101-E

Bed loss due to calcination breakup (%) = 0.67

Bed mass lost in linear portion (%/min.) = 1.66×10^{-5}

Attrition constant, λ_4 (sec^{-1}) = 3.79×10^{-9}

ATTRITION DATA

	Grams Total	wt %	
		Ca	S
Initial Bed	165.451	20.72	0.00
Final Bed	129.455	25.9	11.2
Total Overhead	1.385	18.4	4.07
Overhead, 5 min	1.105	18.4	4.07
10 min	0.131	18.4	4.07
15 min	0.125	18.4	4.07
30 min	0.0038	18.4	4.07
1 h	0.0037	18.4	4.07
1.5 h	0.0036	18.4	4.07
2 h	0.0035	18.4	4.07
4 h	0.0034	18.4	4.07
6 h	0.0033	18.4	4.07
8 h	0.0032	18.4	4.07

Attrition Data, continued for Sorbent 5101

Weight in Grams, Particle Diameter, μm

Sample	-1000 +840	-841 +707	-707 +595	-595 +420	-420 +297	-297 +250
Overhead, first 30 min	0.000	0.000	0.000	0.002	0.011	0.022
Overhead, remaining 7.5 h	0.000	0.000	0.000	0.000	0.056	0.049
Final Bed, post test	127.113	1.828	0.250	0.220	0.121	0.018

Sample	-250 +210	-210 +74	-74 +63	-63 +53	-53 +44	-44 +37	-37 +0
Overhead, first 30 min	0.041	0.304	0.200	0.100	0.097	0.089	0.000
Overhead, remaining 7.5 h	0.040	0.101	0.094	0.040	0.027	0.005	0.000
Final Bed, post test	0.015	0.116	0.001	0.014	0.024	0.006	0.000

10. OTHER DATA: TGA Data: 1123 K, 1 atm, $\alpha(t,min) = C_1[1 - \exp(-C_2 t^{C_3})]$

Fig.	ppm SO_2	Mesh	C_1	C_2	C_3	D	b
5101-F	3,000	50/70	0.966	0.0357	0.862	0.944	135
5101-G	3,000	140/170	0.995	0.0194	0.965	0.989	117
5101-H	10,000	18/20	0.980	0.128	0.645	0.835	98.9
5101-I	5,000	18/20	0.940	0.0409	0.843	0.892	96.3
5101-J	2,000	18/20	0.868	0.0296	0.667	0.648	94.8
5101-K	1,000	18/20	0.857	0.0070	1.049	0.861	197
5101-L	500	18/20	1.015	0.0054	0.791	0.723	101

See Figs. 5101-M and 5101-N for decrepitation data.

Figure 5101-C
Pore Size Distribution

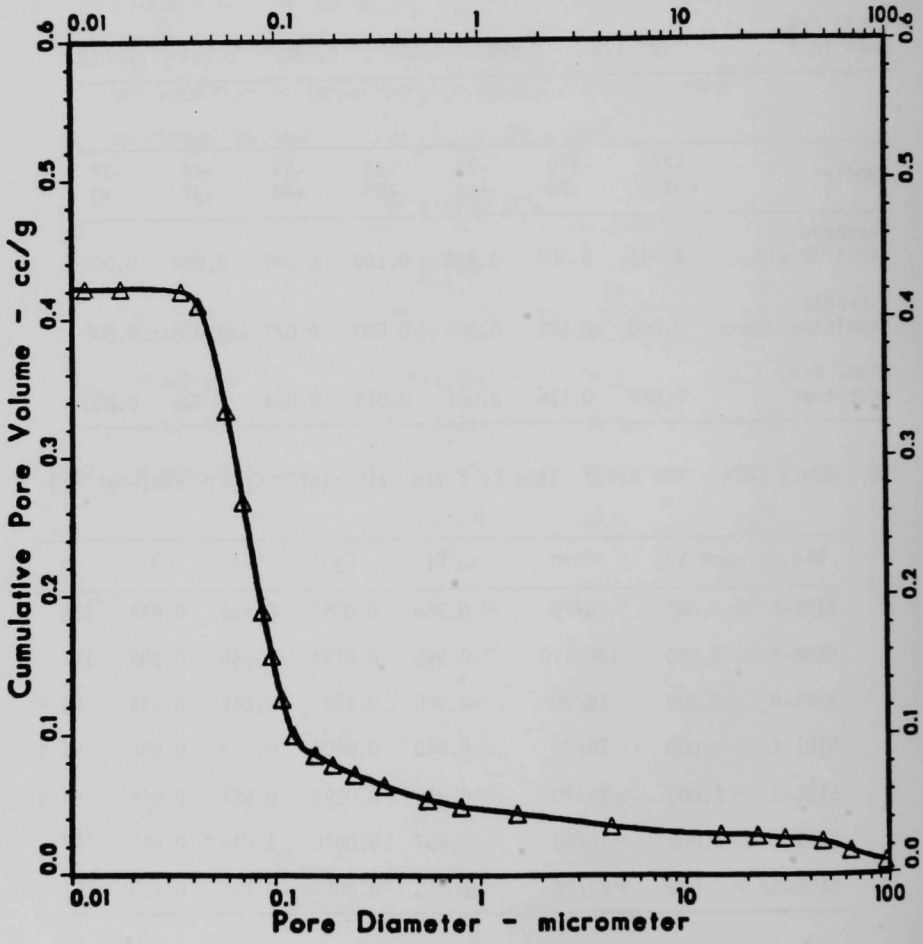

Figure 5101-D TGA Data

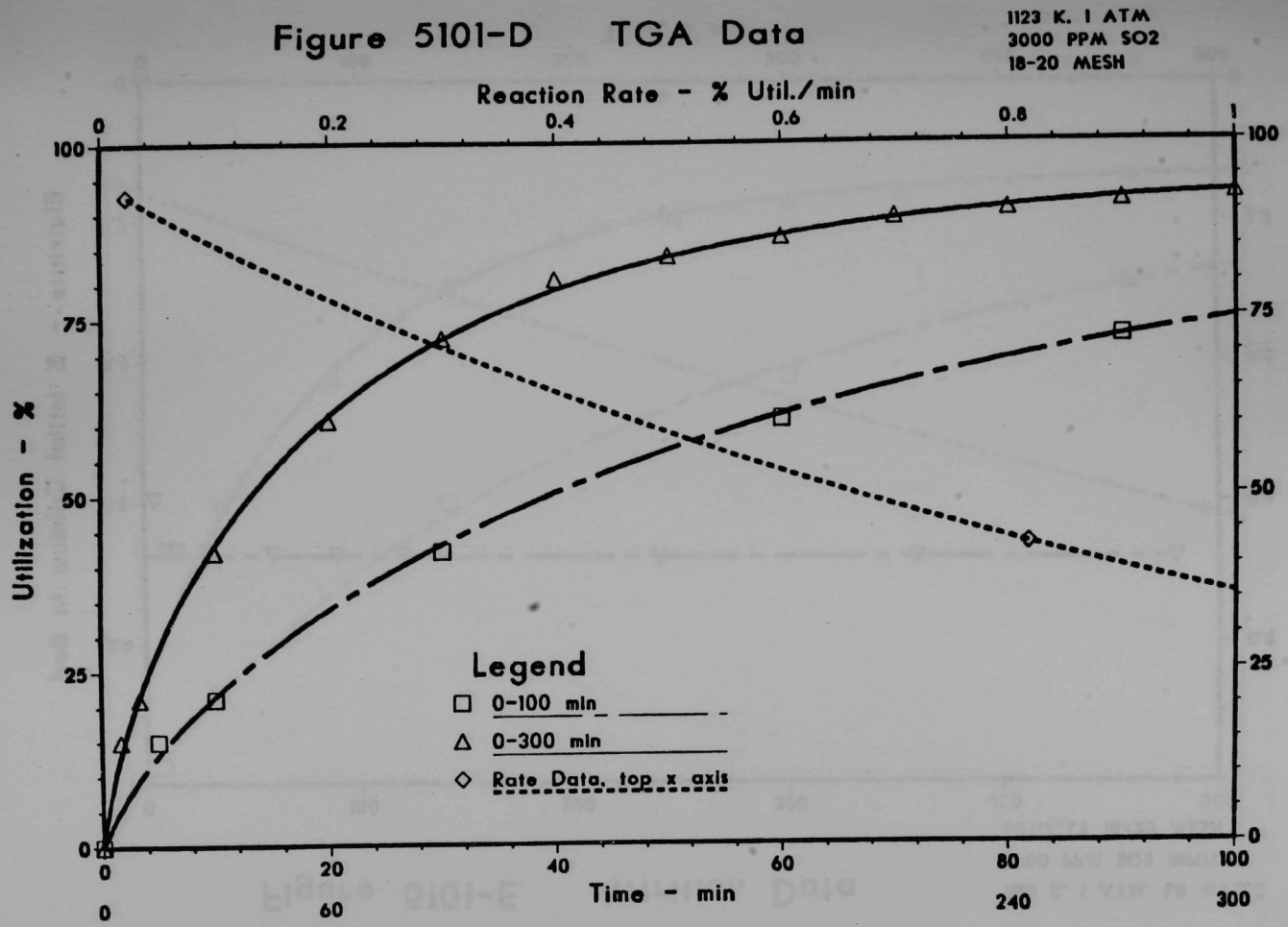

Figure 5101-E Attrition Data

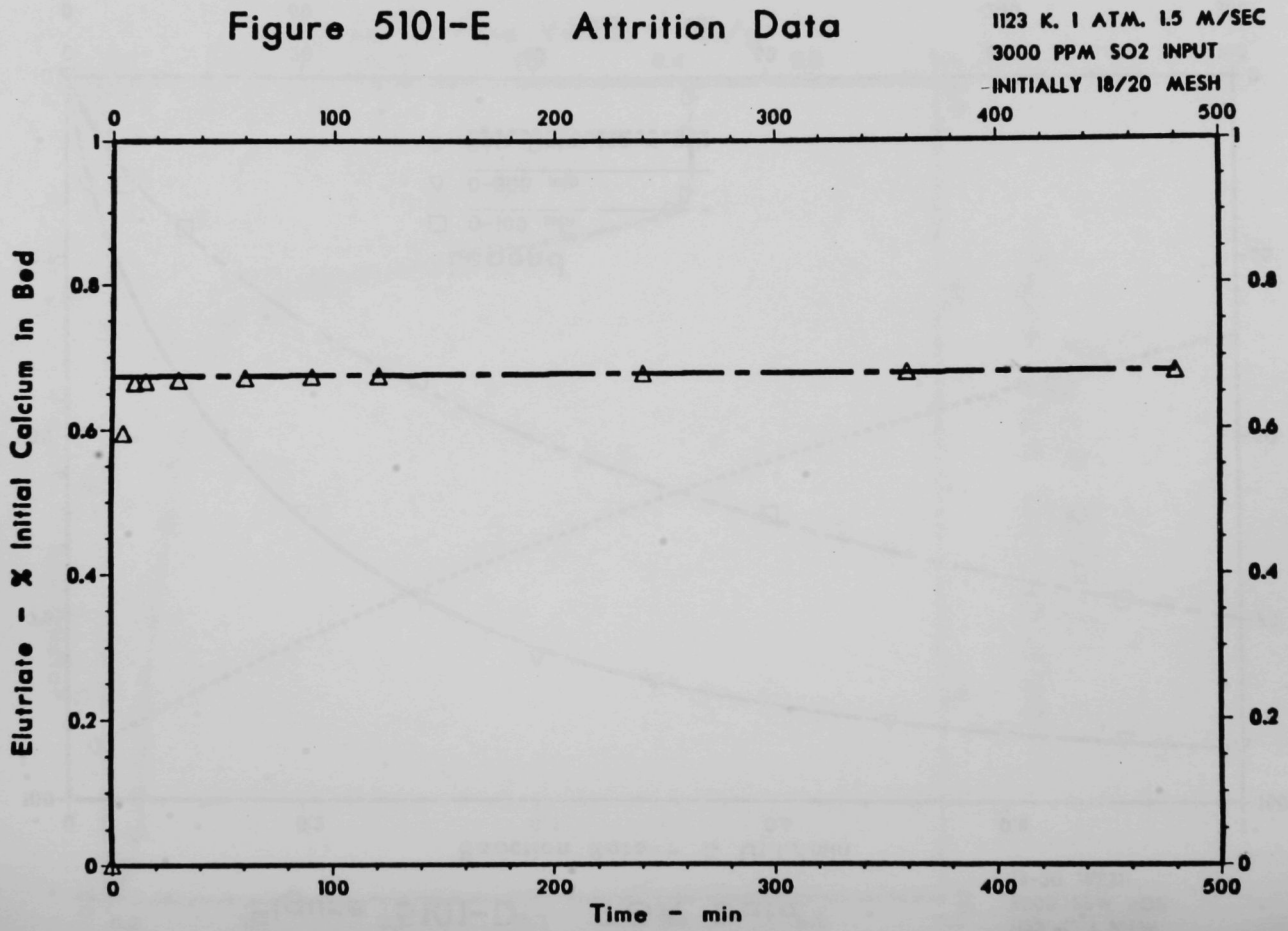

Figure 5101-F TGA Data

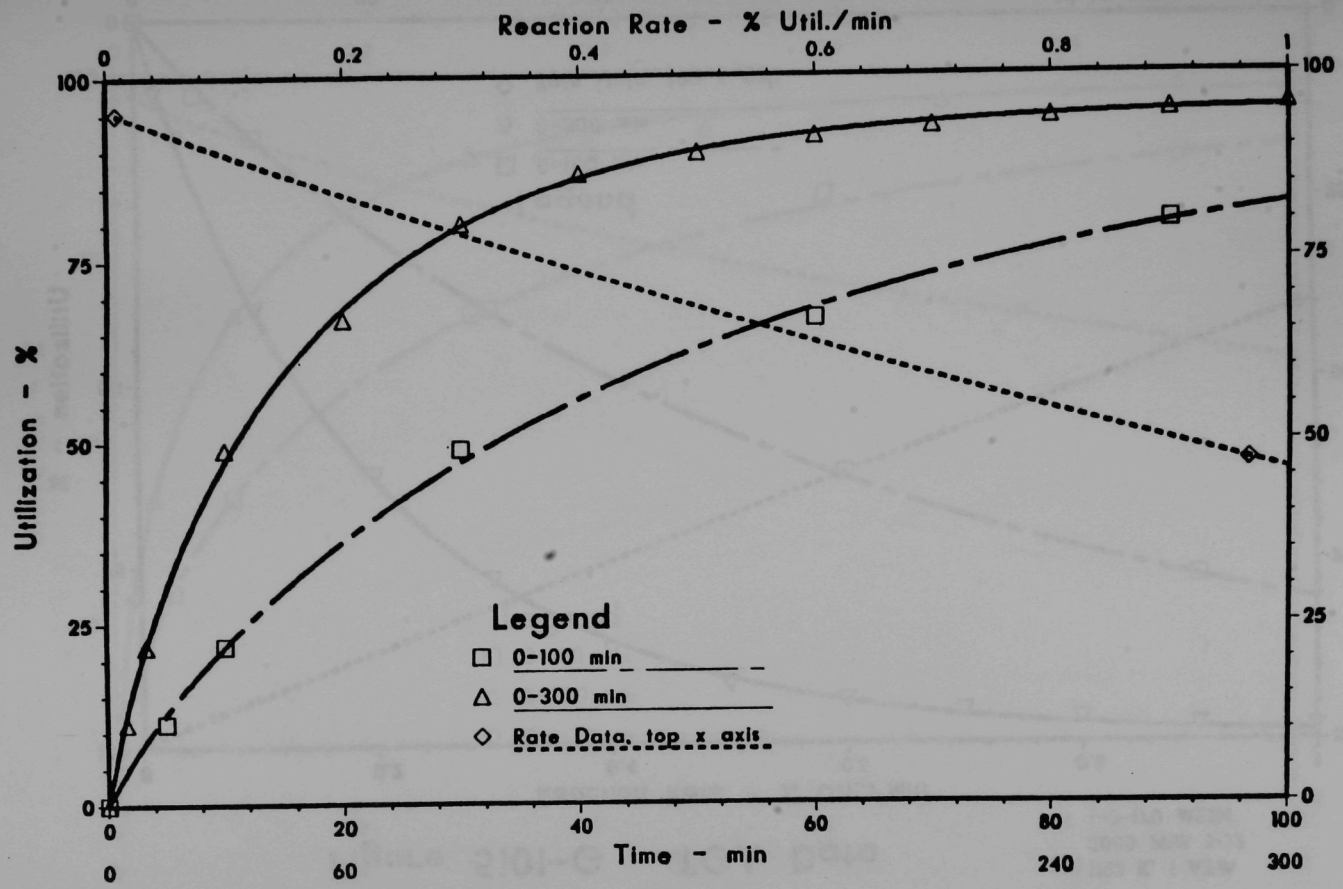

Figure 5101-G TGA Data

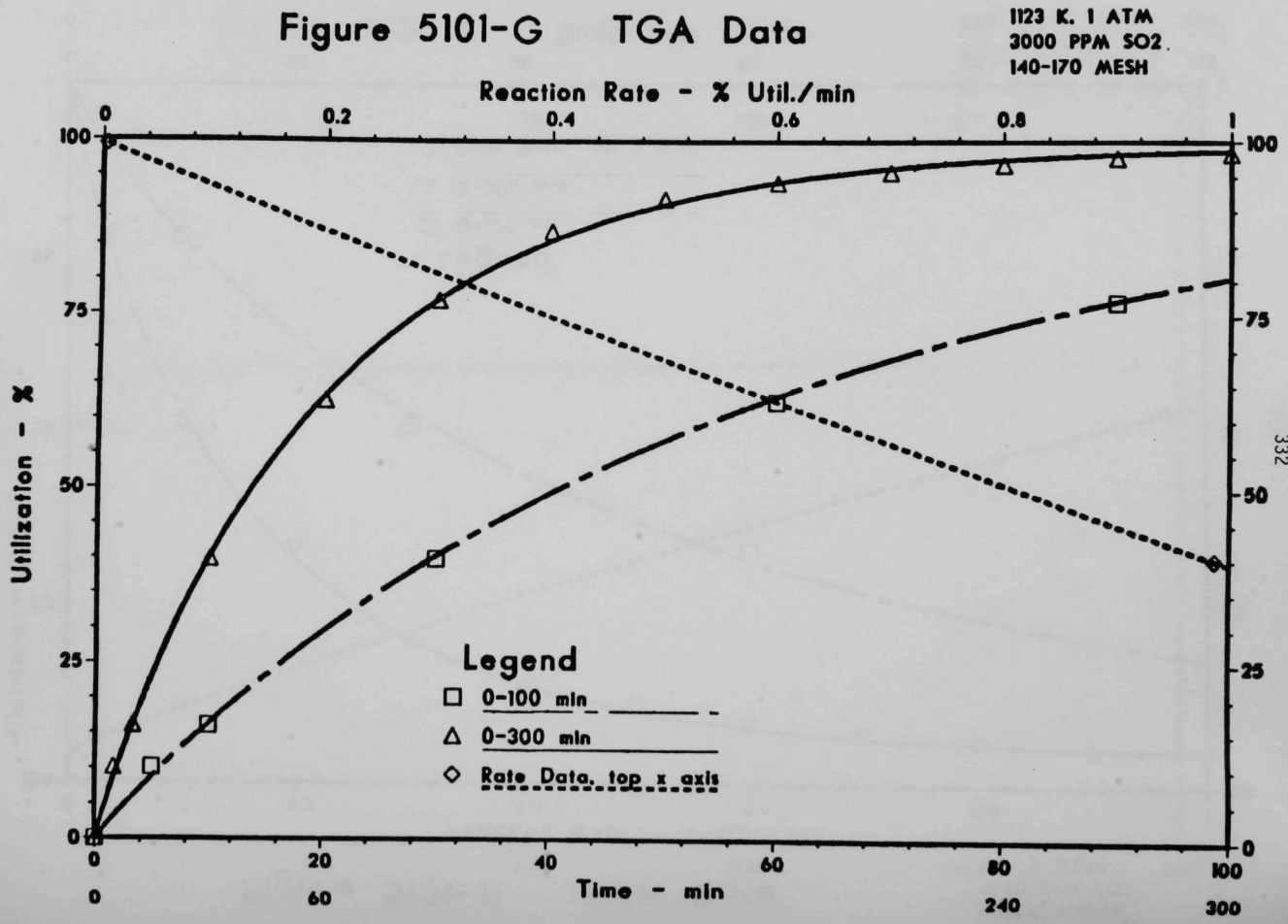

Figure 5101-H TGA Data

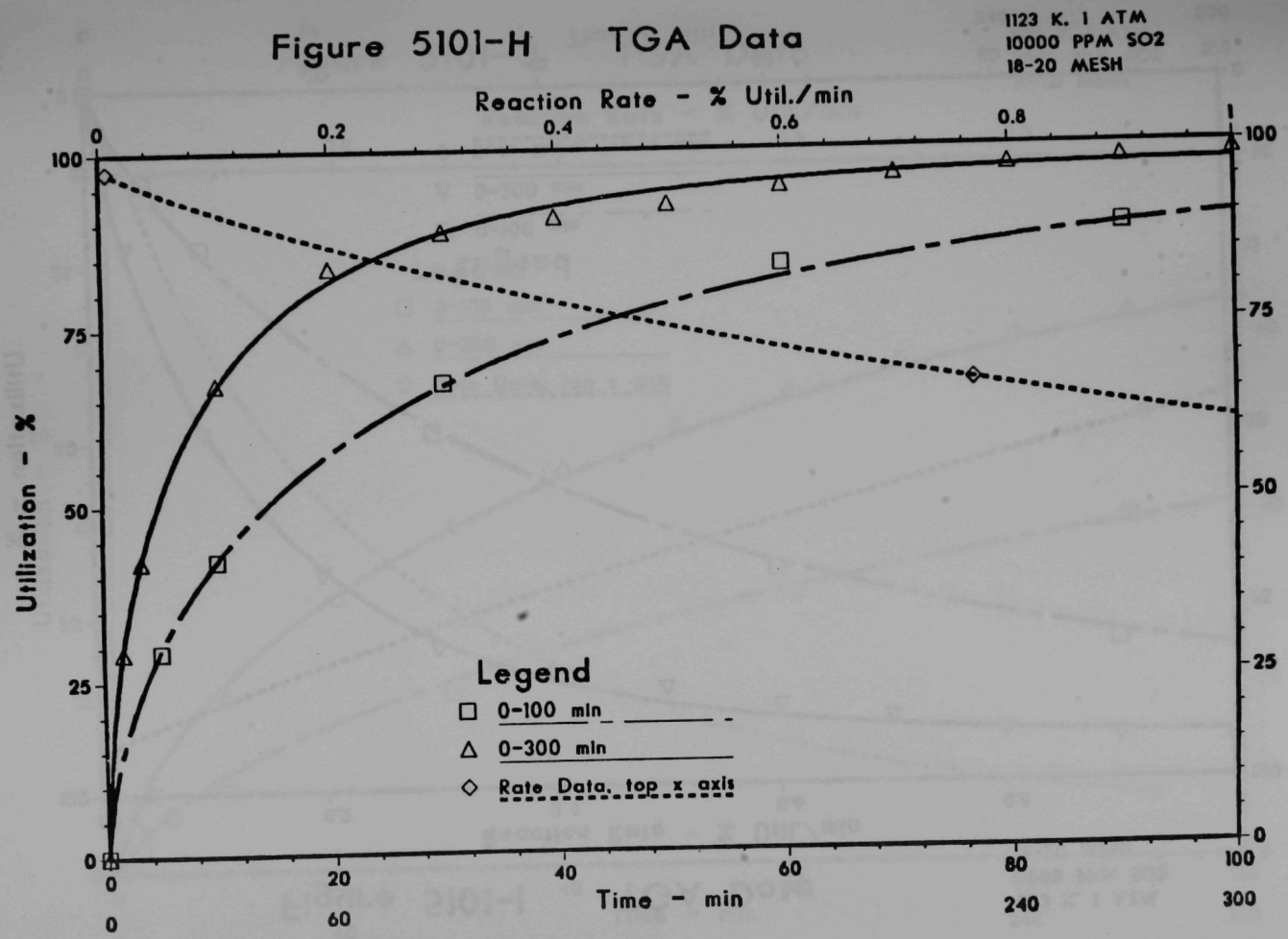

Figure 5101-1 TGA Data

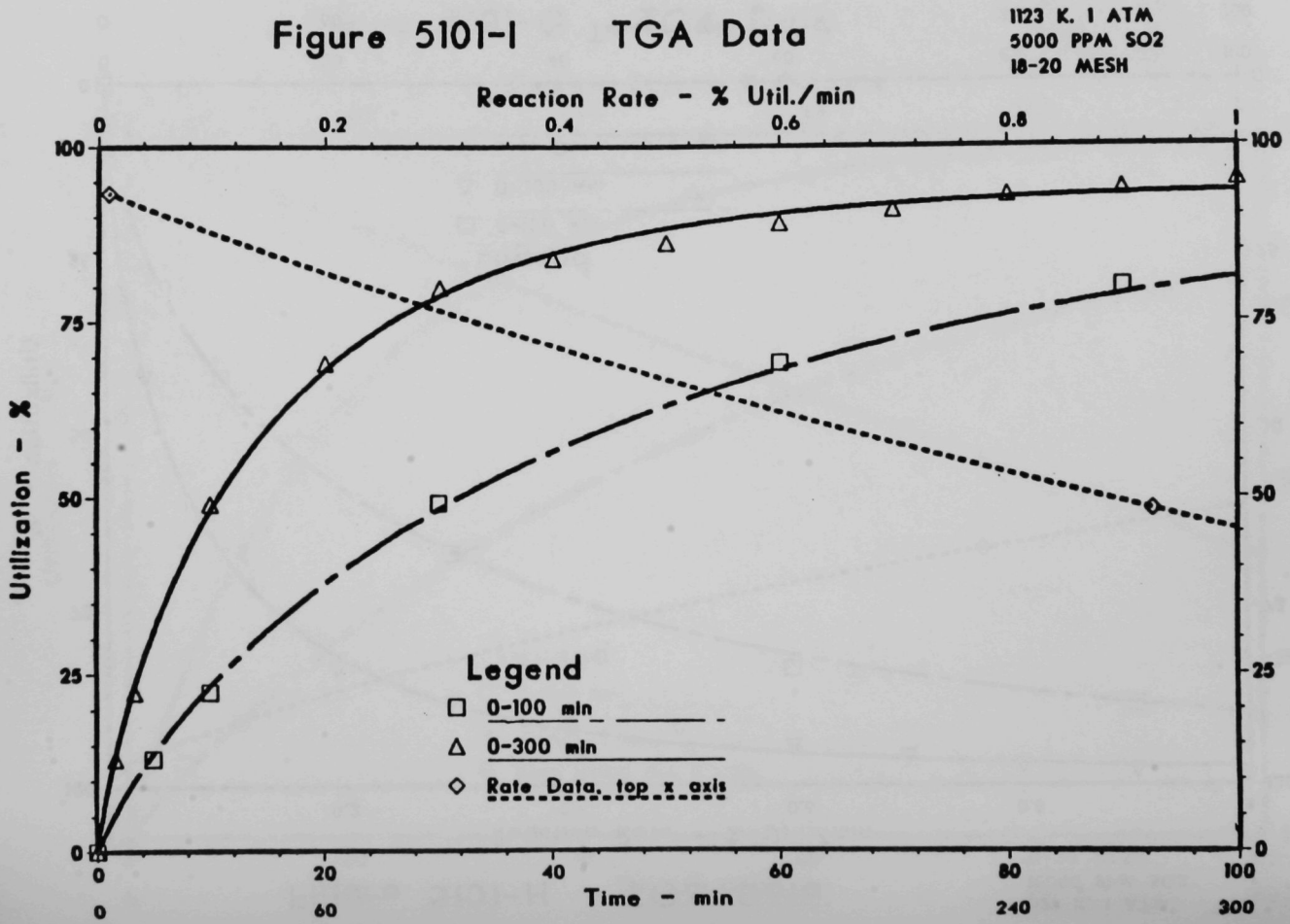

Figure 5101-J TGA Data

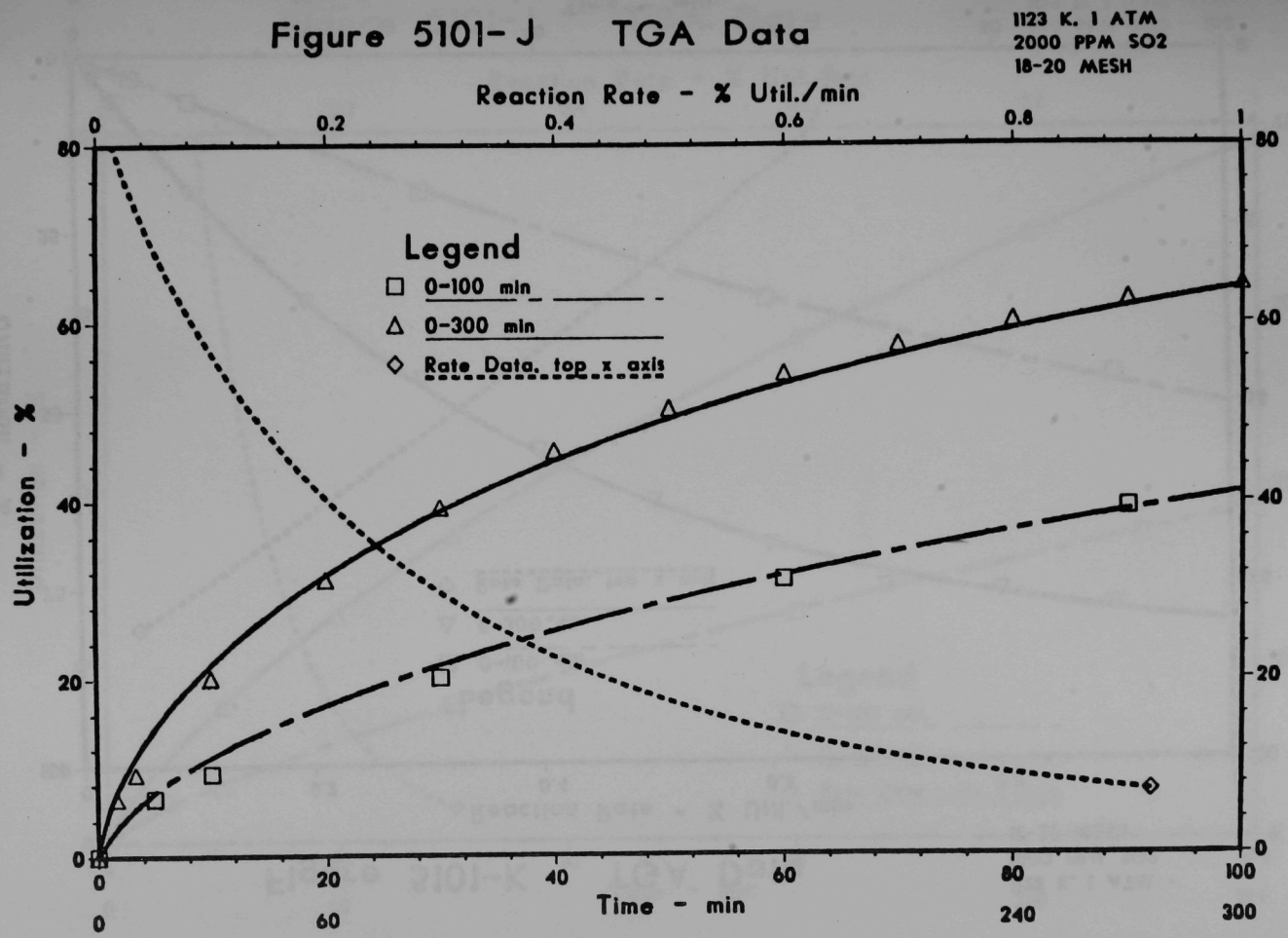

Figure 5101-K TGA Data

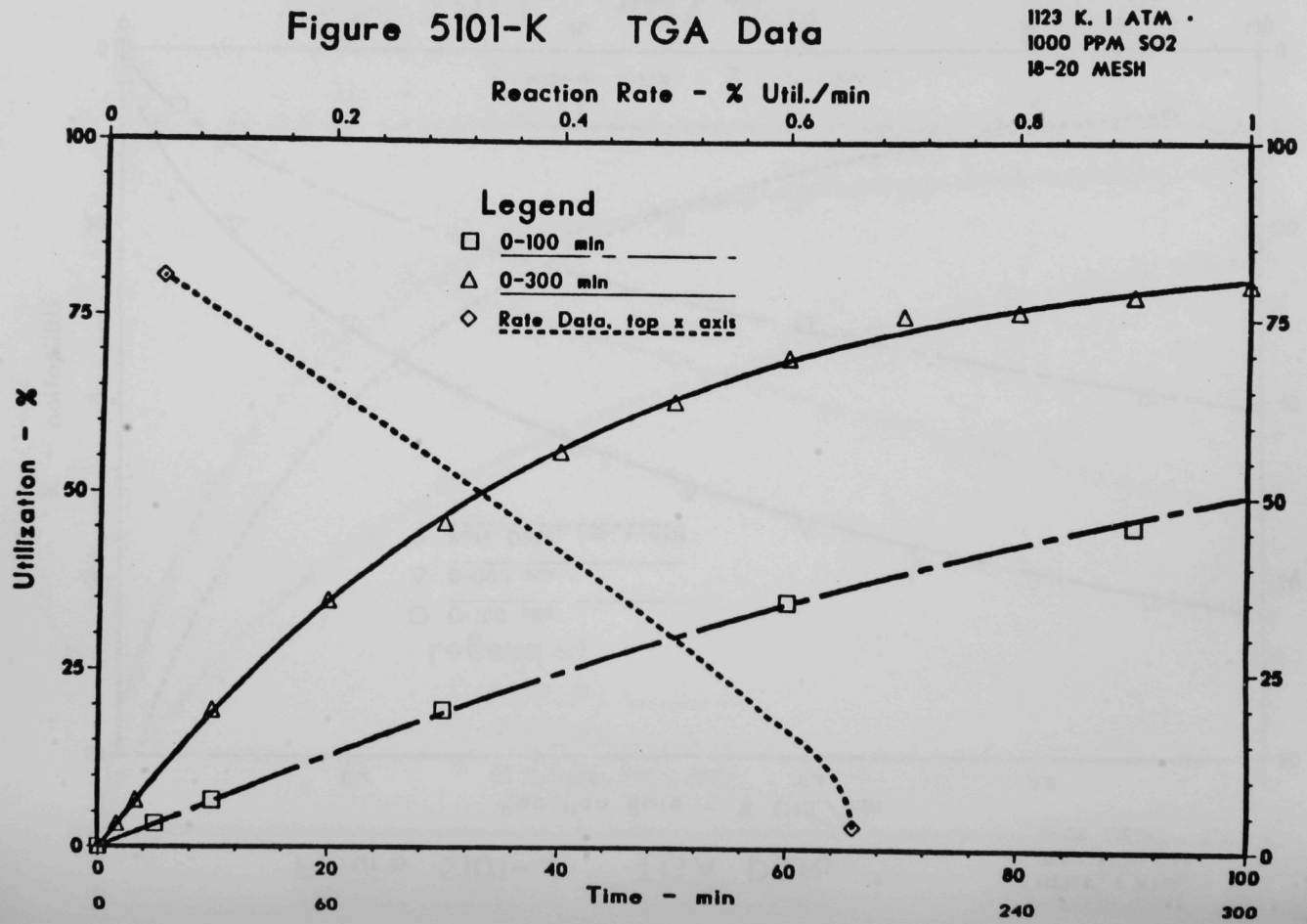

Figure 5101-L TGA Data

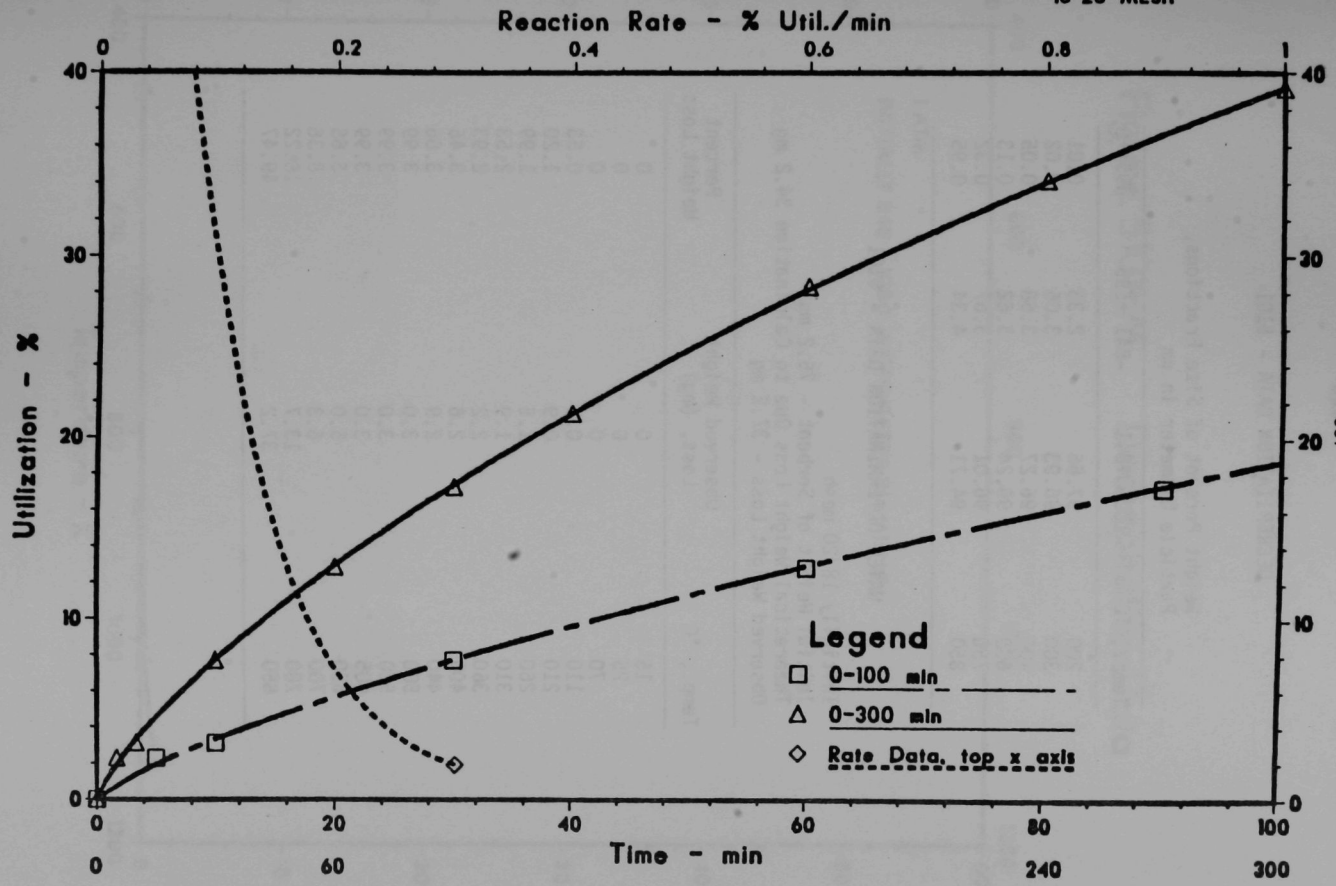

DECREPITATION DATA - 5101

Temp., °C	Weight Percent of Size Fractions, Particle Diameter in μm -1000 +841	-841 +595	-595 +0
200	97.66	2.33	0.01
300	96.93	3.06	0.02
400	96.27	3.68	0.05
600	96.24	3.62	0.13
750	96.01	3.67	0.32
850	94.71	4.34	0.95

WATER DETERMINATION DATA - 5101

Initially 18/20 mesh
Initial Weight of Sorbent - 75.2 mg
Theoretical Weight Loss Due to Calcination 34.2 mg
Observed Weight Loss - 37.2 mg

Temp., °C	Observed Weight Loss, (mg)	Percent Weight Loss
15	0	0
25	0	0
70	0	0
110	0.4	0.53
210	0.9	1.20
260	1.5	1.99
310	1.9	2.53
360	2.2	2.93
400	2.6	3.46
440	2.9	3.86
500	3.0	3.99
550	3.0	3.99
605	3.0	3.99
650	5.0	6.65
700	6.3	8.38
780	13.7	18.22
850	37.2	49.47

Figure 5101-M Decrepitation Data

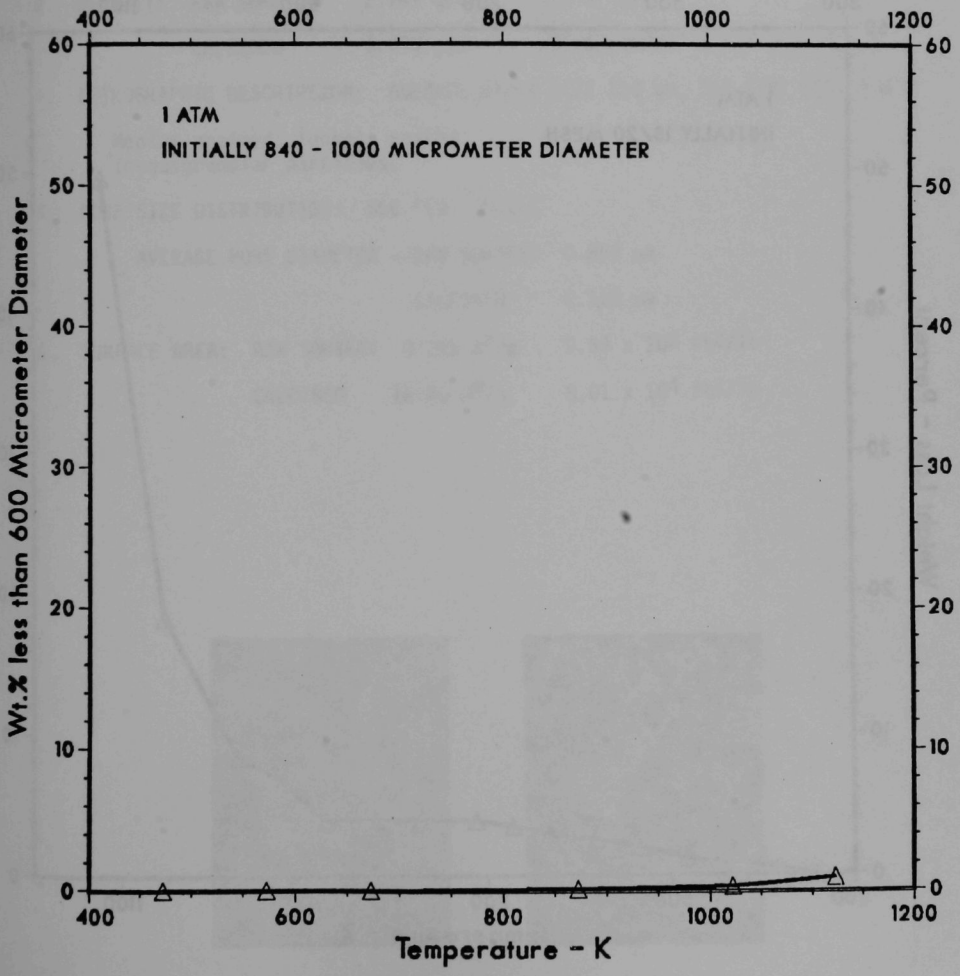

Figure 5101-N Water Loss Data

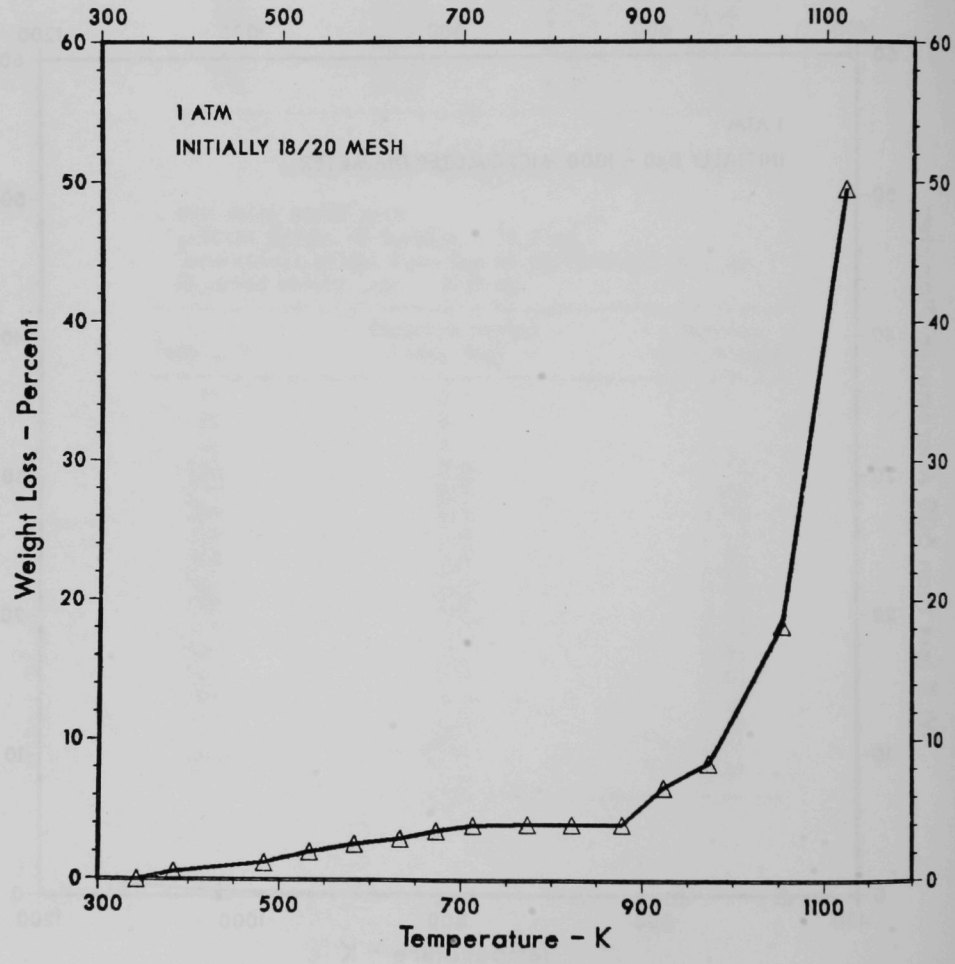

1. NAME: ANL-5001

   SOURCE: Harris Limestone Co., Piedmont, MO

2. CHEMICAL COMPOSITION, wt %

$CaCO_3$	$MgCO_3$	SiO_2	Fe_2O_3	Al_2O_3	Na_2O	K_2O
50.4	43.0	3.52	0.37	0.98	0.34	0.10

3. DENSITY: RAW SORBENT 2.749 g/cm^3 171.6 lb/ft^3

   CALCINED 1.435 g/cm^3 89.67 lb/ft^3

4. PETROGRAPHIC DESCRIPTION: AVERAGE GRAIN SIZE 110 μm, SEE FIG. 5001 A & B

   Medium-grained; loosely packed.
   Inequigranular particles.

5. PORE SIZE DISTRIBUTION: SEE FIG. 5001-C

   AVERAGE PORE DIAMETER - RAW SORBENT 0.554 μm

   CALCINED 0.115 μm

6. SURFACE AREA: RAW SORBENT 0.195 m^2/g 9.53 x 10^2 ft^2/lb

   CALCINED 16.40 m^2/g 8.01 x 10^4 ft^2/lb

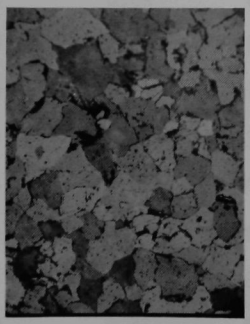

Fig. 5001A
Raw Dolomite
50X

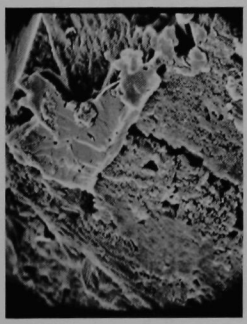

Fig. 5001B
Calcined Dolomite 1 h 850°C
1100X

7. TOTAL POROSITY: RAW SORBENT 0.032 cm^3/g 5.13×10^{-4} ft^3/lb

CALCINED 0.498 cm^3/g 31.09 ft^3/lb

8. THERMOGRAVIMETRIC ANALYSIS: SEE FIG. 5001-D

(1123 K, 1 atm, 3000 ppm SO_2, -18 +20 mesh)

FRACTIONAL UTILIZATION = $\alpha(t, \text{min}) = 0.807\ [1 - \exp(-0.0504\ t^{0.668})]$

ANL PARAMETERS: D = 0.669 b = 112.7

9. ATTRITION: SEE FIG. 5001-E

Bed loss due to calcination breakup (%) = 61.6

Bed mass lost in linear portion (%/min.) = 5.39×10^{-3}

Attrition constant, λ_4 (sec^{-1}) = 1.48×10^{-6}

ATTRITION DATA

	Grams Total	wt % Ca	wt % S
Initial Bed	160.040	20.16	0.00
Final Bed	47.684	24.4	8.11
Total Overhead	82.878	25.0	6.33
Overhead, 5 min	65.837	25.0	6.33
10 min	11.238	25.0	6.33
15 min	2.035	25.0	6.33
30 min	0.490	25.0	6.33
1 h	0.308	25.0	6.33
1.5 h	0.252	25.0	6.33
2 h	0.210	25.0	6.33
4 h	0.828	25.0	6.33
6 h	0.808	25.0	6.33
8 h	0.873	25.0	6.33

Attrition Data, continued for Sorbent 5001

Weight in Grams, Particle Diameter, μm

Sample	-1000 +840	-841 +707	-707 +595	-595 +420	-420 +297	-297 +250
Overhead, first 30 min	0.000	0.036	0.030	0.028	0.162	3.141
Overhead, remaining 7.5 h	0.000	0.000	0.000	0.000	0.079	0.386
Final Bed, post test	31.853	5.106	2.989	2.783	3.266	1.030

Sample	-250 +210	-210 +74	-74 +63	-63 +53	-53 +44	-44 +37	-37 +0
Overhead, first 30 min	5.591	58.153	1.284	1.100	2.656	0.328	1.124
Overhead, remaining 7.5 h	0.424	1.539	0.061	0.172	0.261	0.307	0.000
Final Bed, post test	0.306	0.323	0.006	0.027	0.034	0.016	0.007

10. OTHER DATA

See Figs. 5001-F and 5001-G for decrepitation data.

Figure 5001-C
Pore Size Distribution

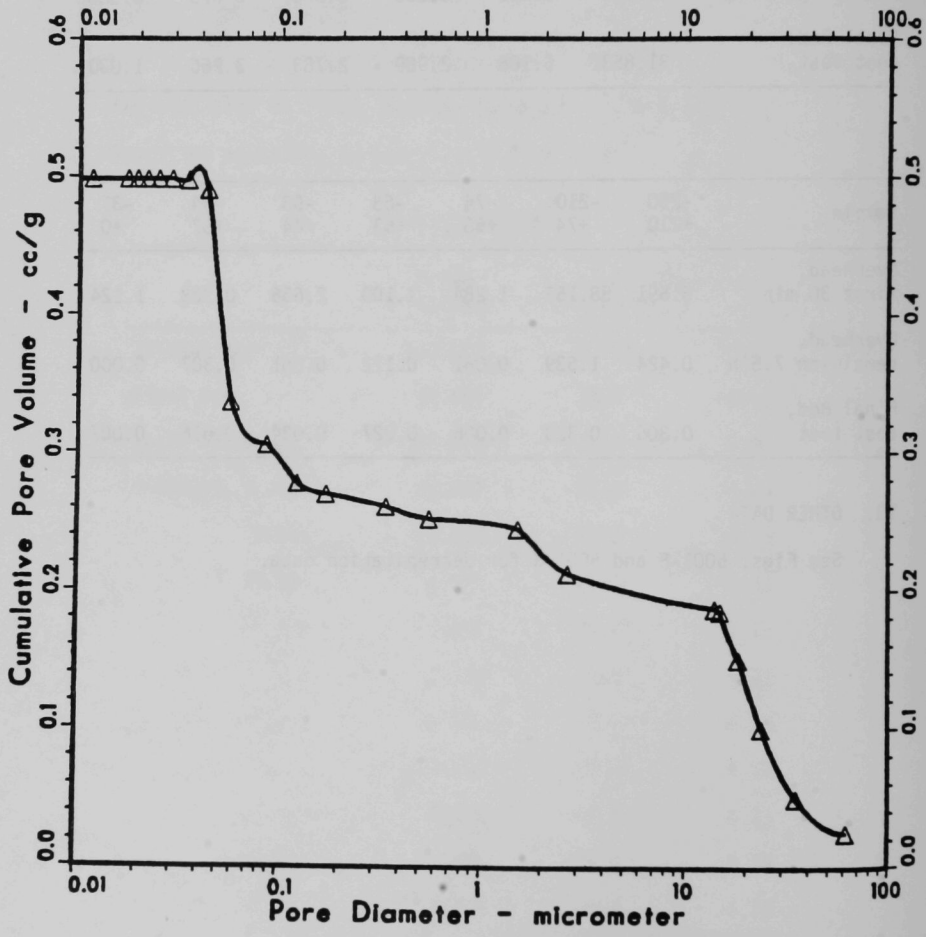

Figure 5001-D TGA Data

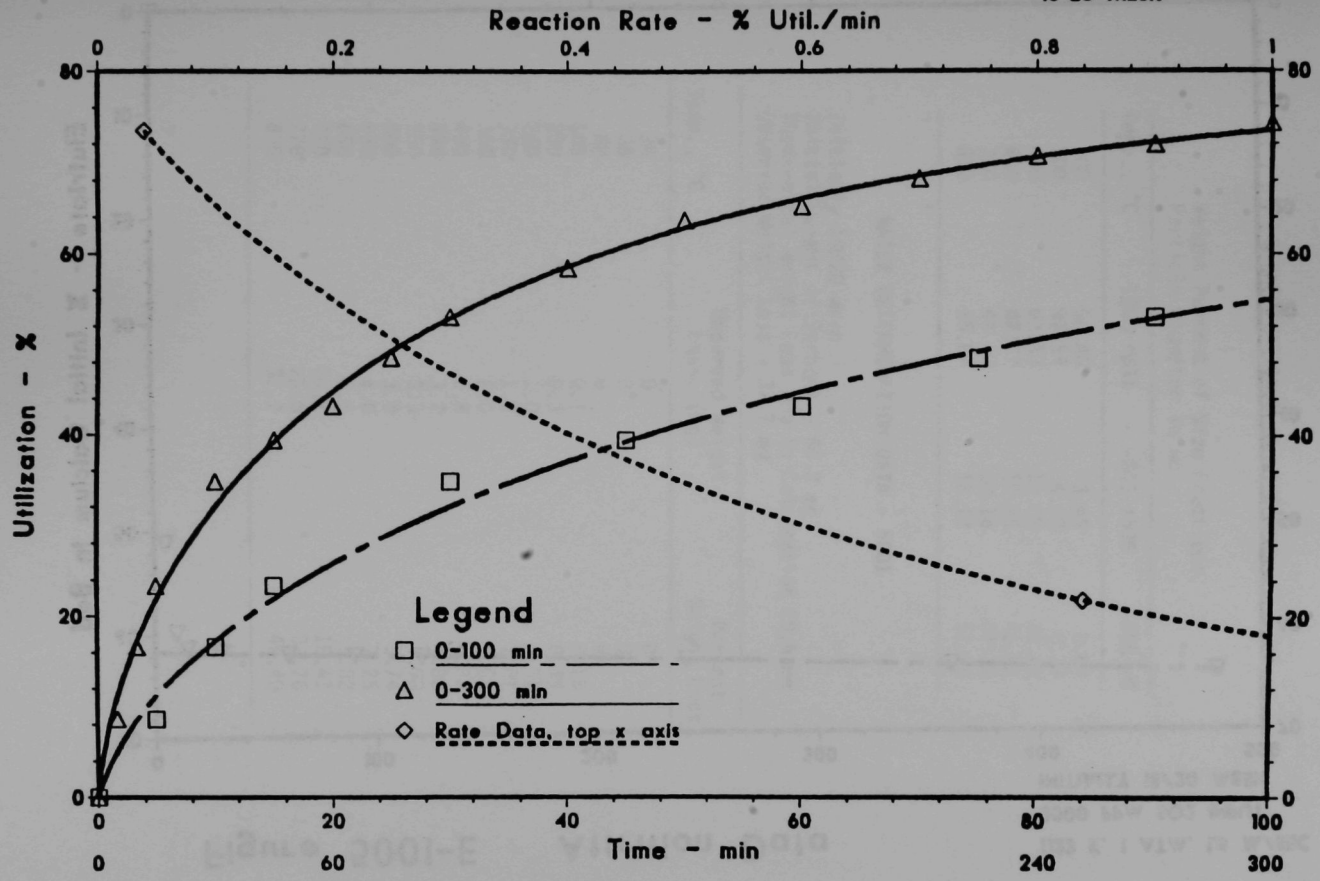

Figure 5001-E Attrition Data

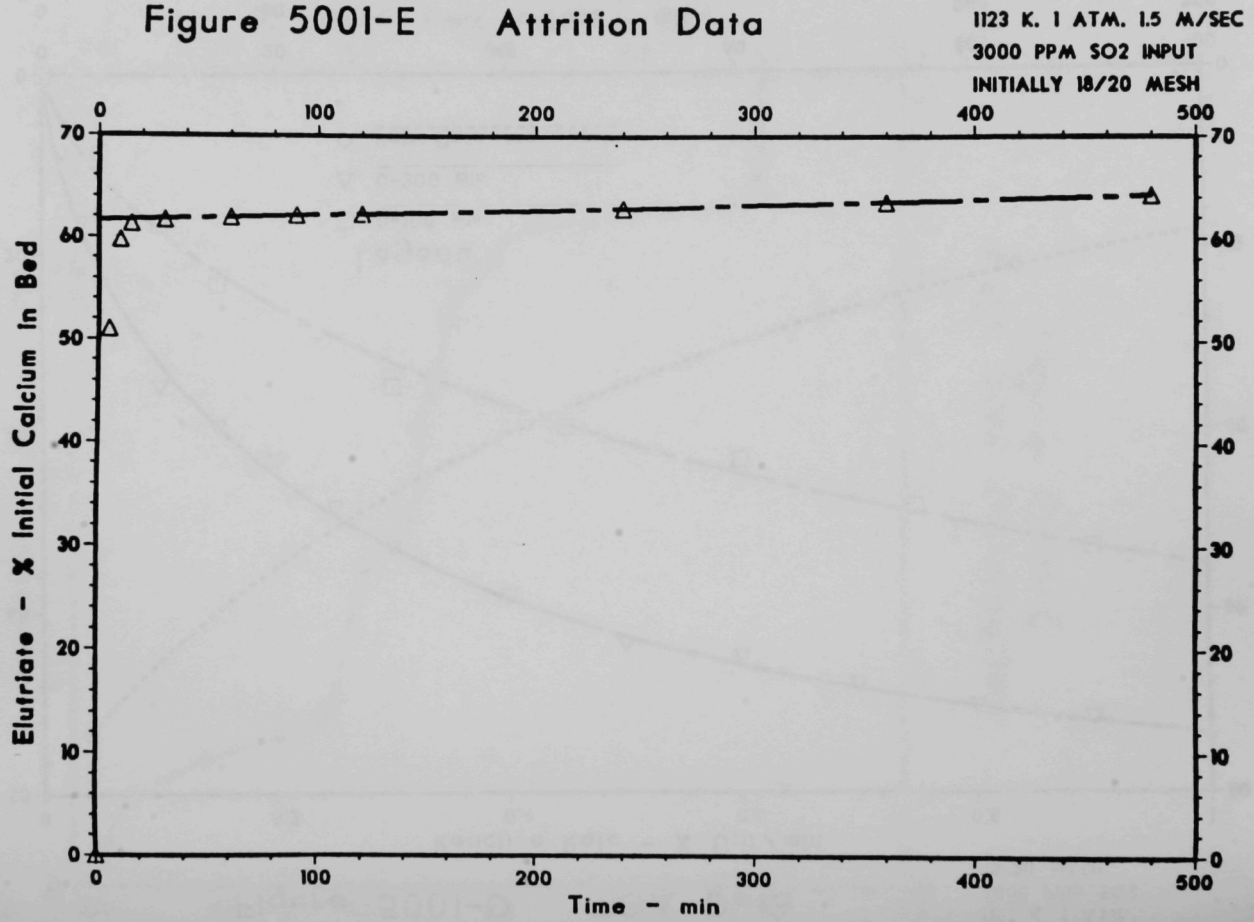

DECREPITATION DATA - 5001

Temp., °C	Weight Percent of Size Fractions, Particle Diameter in µm -1000 +841	-841 +595	-595 +0
200	96.46	3.48	0.06
300	95.54	4.08	0.37
400	62.43	12.08	25.49
600	42.77	10.25	46.98
750	42.48	10.16	47.36
850	35.57	12.12	52.31

WATER DETERMINATION DATA - 5001

Initially 18/20 mesh
Initial Weight of Sorbent - 66.2 mg
Theoretical Weight Loss Due to Calcination 29.6 mg
Observed Weight Loss - 37.7 mg

Temp., °C	Observed Weight Loss, (mg)	Percent Weight Loss
20	0	0
30	0	0
60	0	0
100	0.1	0.15
200	0.3	0.45
260	1.0	1.51
320	1.2	1.81
380	2.0	3.02
430	2.8	4.23
495	3.2	4.83
550	3.3	4.98
600	3.8	5.74
650	4.8	7.25
680	6.5	9.82
720	10.2	15.41
770	25.0	37.76
850	37.7	49.40

Figure 5001-F Decrepitation Data

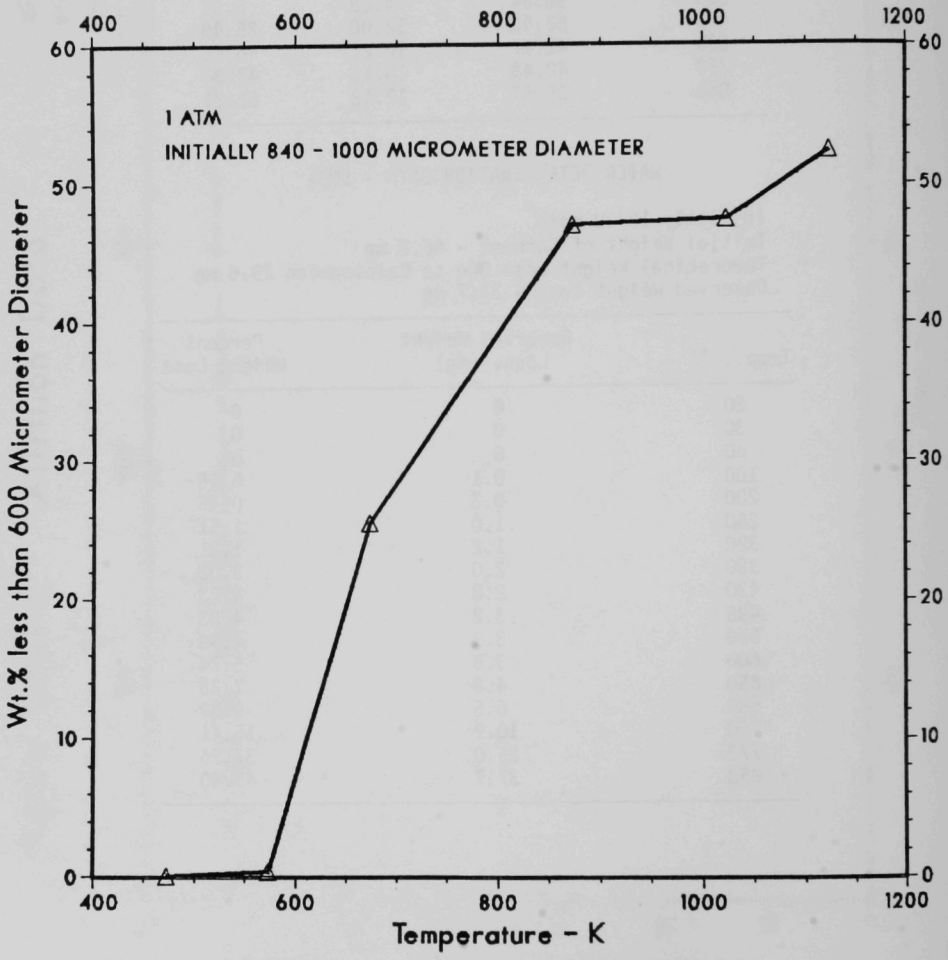

Figure 5001-G Water Loss Data

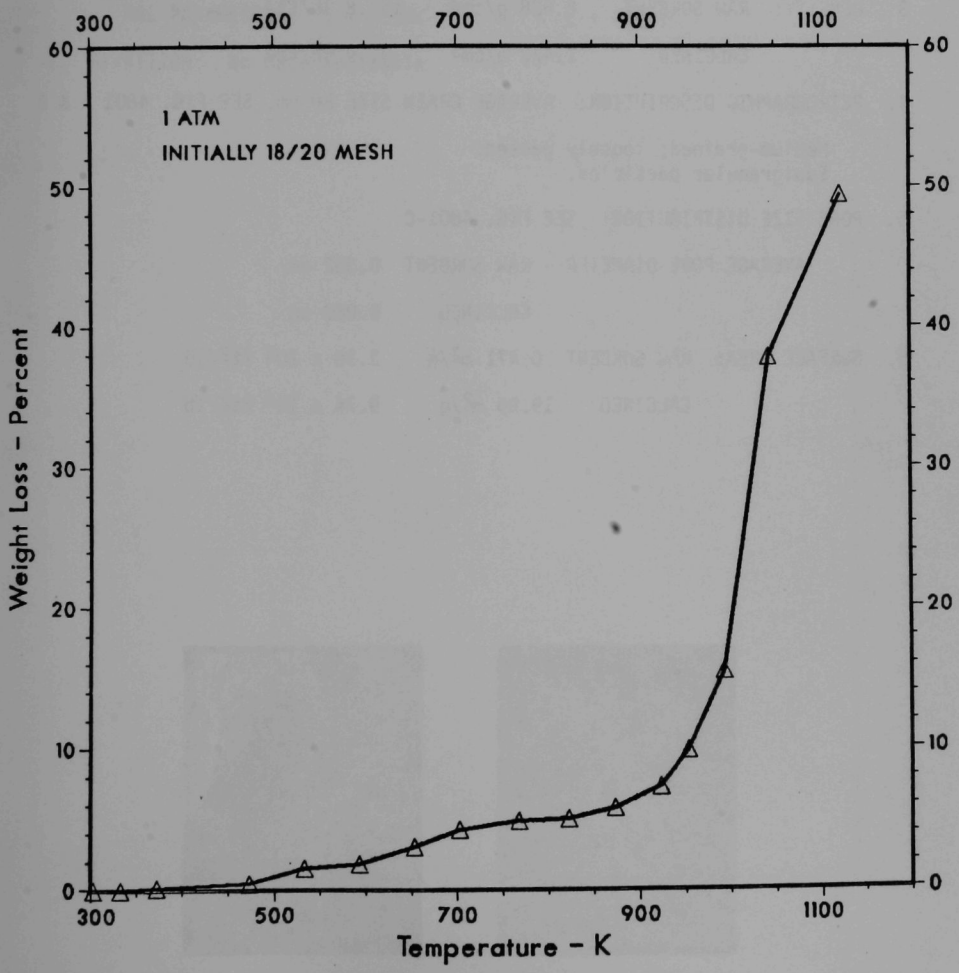

1. NAME: ANL-4801

SOURCE: Midwest Aggregates Corp., Fort Wayne, Indiana

2. CHEMICAL COMPOSITION, wt %

$CaCO_3$	$MgCO_3$	SiO_2	Fe_2O_3	Al_2O_3	Na_2O	K_2O
48.7	40.2	7.02	0.66	1.81	0.99	0.38

3. DENSITY: RAW SORBENT 2.688 g/cm^3 167.8 lb/ft^3

CALCINED 1.472 g/cm^3 91.9 lb/ft^3

4. PETROGRAPHIC DESCRIPTION: AVERAGE GRAIN SIZE 80 μm, SEE FIG. 4801 A & B

Medium-grained; loosely packed.
Equigranular particles.

5. PORE SIZE DISTRIBUTION: SEE FIG. 4801-C

AVERAGE PORE DIAMETER - RAW SORBENT 0.382 μm

CALCINED 0.080 μm

6. SURFACE AREA: RAW SORBENT 0.471 m^2/g 2.30 x 10^3 ft^2/lb

CALCINED 19.95 m^2/g 9.74 x 10^4 ft^2/lb

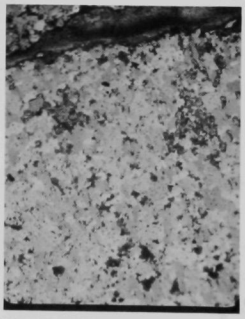

Fig. 4801A
Raw Dolomite
50X

Fig. 4801B
Calcined Dolomite 1 h 850°C
1100X

7. TOTAL POROSITY: RAW SORBENT 0.050 cm^3/g 8.0×10^{-4} ft^3/lb

CALCINED 0.406 cm^3/g 6.59×10^{-3} ft^3/lb

8. THERMOGRAVIMETRIC ANALYSIS: SEE FIG. 4801-D

(1123 K, 1 atm, 3000 ppm SO_2, -18 +20 mesh)

FRACTIONAL UTILIZATION = $\alpha(t, \text{min}) = 0.894\ [1 - \exp(-0.0152\ t^{1.130})]$

ANL PARAMETERS: D = 0.904 b = 186.1

9. ATTRITION: No data available

Figure 4801-C
Pore Size Distribution

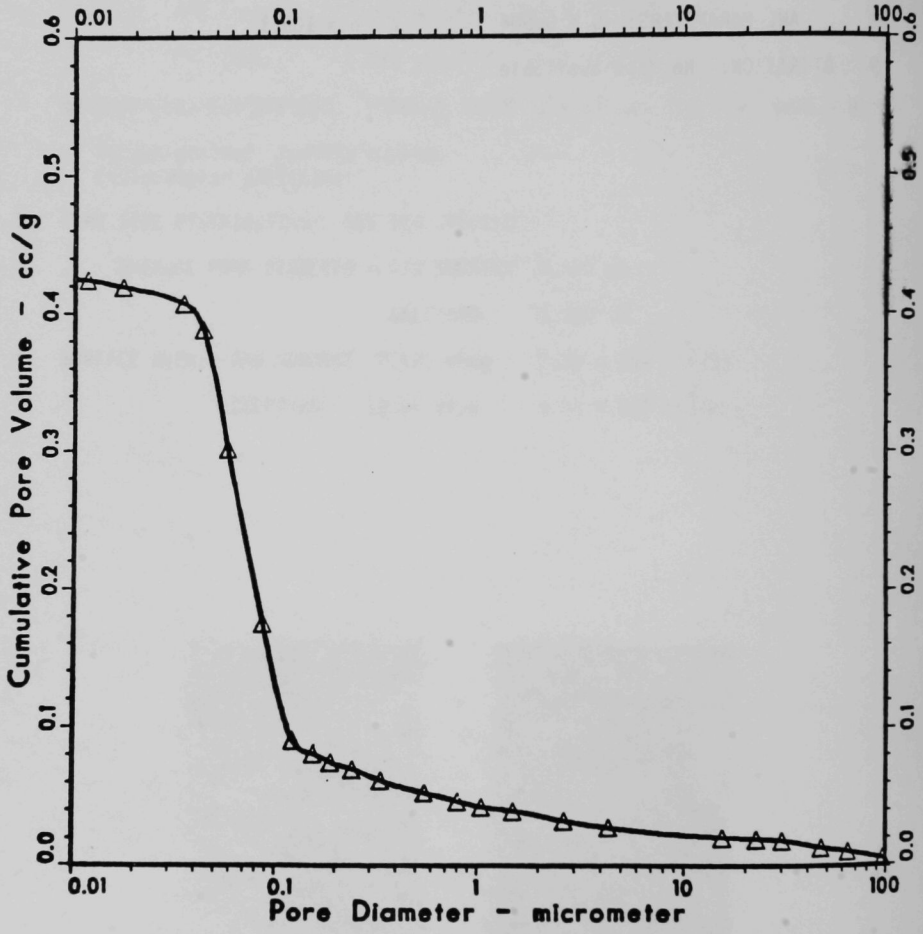

Figure 4801-D TGA Data

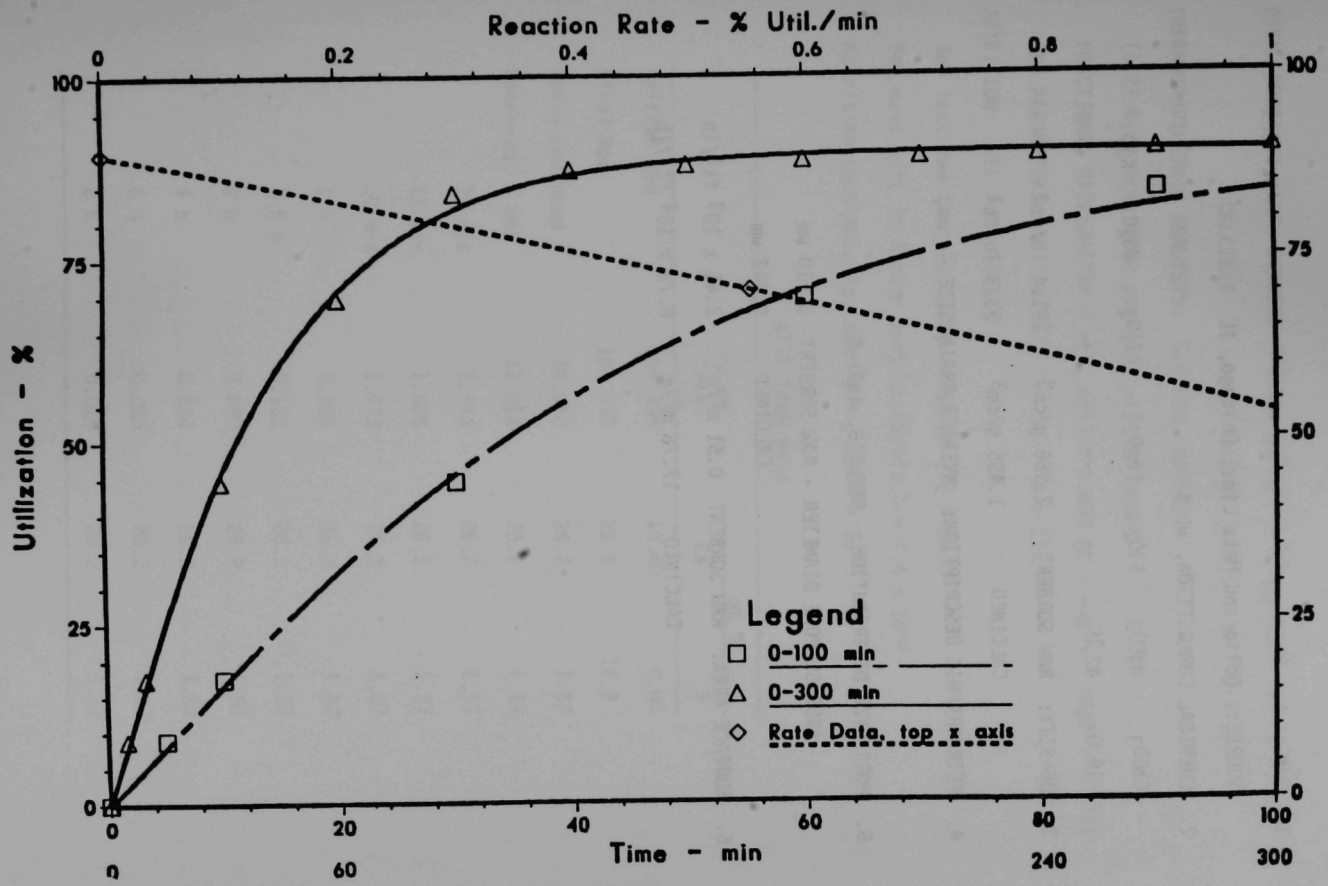

1. NAME: ANL-4601

   SOURCE: Dolio and Metz Ltd., Chicago, IL

2. CHEMICAL COMPOSITION, wt %

$CaCO_3$	$MgCO_3$	SiO_2	Fe_2O_3	Al_2O_3	Na_2O	K_2O
46.0	42.0	--	--	--	--	--

3. DENSITY: RAW SORBENT 2.586 g/cm^3 161.4 lb/ft^3

   CALCINED 1.495 g/cm^3 93.3 lb/ft^3

4. PETROGRAPHIC DESCRIPTION: AVERAGE GRAIN SIZE -- μm, --

5. PORE SIZE DISTRIBUTION: SEE FIG. 4601-C

   AVERAGE PORE DIAMETER - RAW SORBENT 0.610 μm

   CALCINED 0.042 μm

6. SURFACE AREA: RAW SORBENT 0.51 m^2/g 2.41 x 10^3 ft^2/lb

   CALCINED 17.78 m^2/g 8.73 x 10^4 ft^2/lb

7. TOTAL POROSITY: RAW SORBENT 0.053 cm^3/g 8.5×10^{-4} ft^3/lb

CALCINED 0.420 cm^3/g 6.7×10^{-3} ft^3/lb

8. THERMOGRAVIMETRIC ANALYSIS: SEE FIG. 4601-D

(1123 K, 1 atm, 3000 ppm SO_2, -18 +20 mesh)

FRACTIONAL UTILIZATION = $\alpha(t, \text{min}) = 0.838\ [1 - \exp(-0.0557\ t^{0.665})]$

ANL PARAMETERS: D = 0.7673 b = 110

9. ATTRITION: SEE FIG. 4601-E

Bed loss due to calcination breakup (%) = 16.0

Bed mass lost in linear portion (%/min.) = 7.4×10^{-4}

Attrition constant, λ_4 (sec^{-1}) = 1.6067×10^{-7}

ATTRITION DATA

	Grams Total	wt % Ca	wt % S
Initial Bed	159.995	18.40	0.00
Final Bed	108.942	23.5	12.2
Total Overhead	18.916	26.2	1.57
Overhead, 5 min	13.012	26.2	1.57
10 min	2.843	26.2	1.57
15 min	1.075	26.2	1.57
30 min	1.073	26.2	1.57
1 h	0.355	26.2	1.57
1.5 h	0.181	26.2	1.57
2 h	0.080	26.2	1.57
4 h	0.184	26.2	1.57
6 h	0.085	26.2	1.57
8 h	0.029	26.2	1.57

Attrition Data, continued for Sorbent 4601

Weight in Grams, Particle Diameter, μm

Sample	-1000 +840	-841 +707	-707 +595	-595 +420	-420 +297	-297 +250
Overhead, 8 h	0.000	0.000	0.000	0.016	0.018	0.035
Final Bed, post test	92.867	7.605	2.178	1.780	1.959	0.712

Sample	-250 +210	-210 +74	-74 +63	-63 +53	-53 +44	-44 +37	-37 +0
Overhead, 8 h	0.311	13.413	0.158	0.500	1.360	1.357	1.732
Final Bed, post test	0.803	0.904	0.011	0.039	0.049	0.029	0.009

Figure 4601-C
Pore Size Distribution

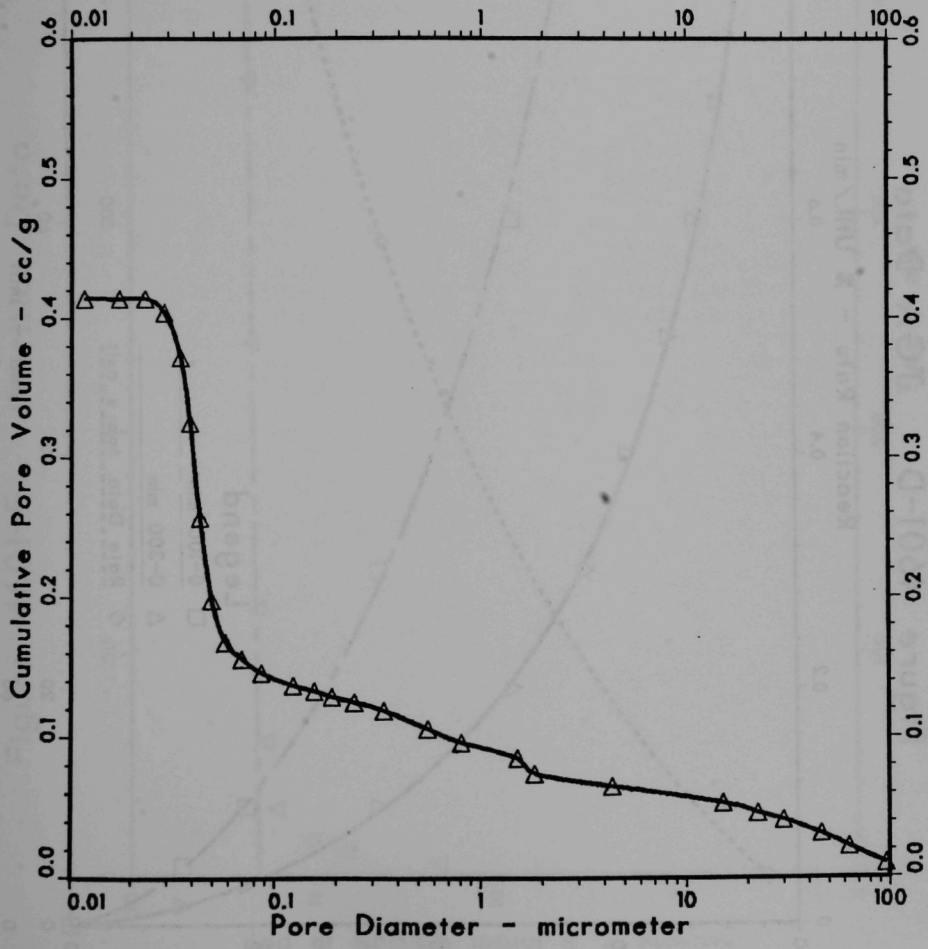

Figure 4601-D TGA Data

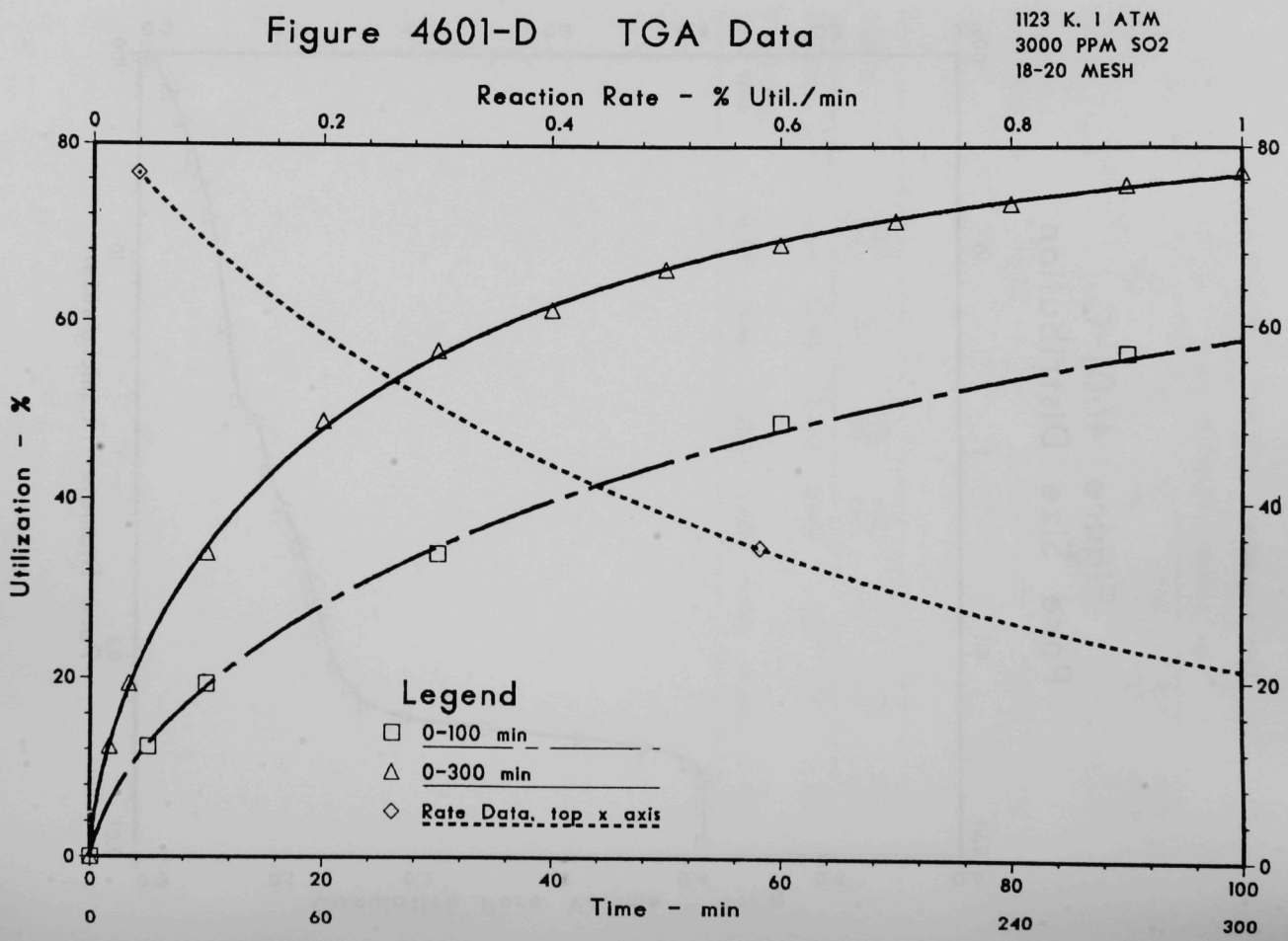

Figure 4601-E Attrition Data

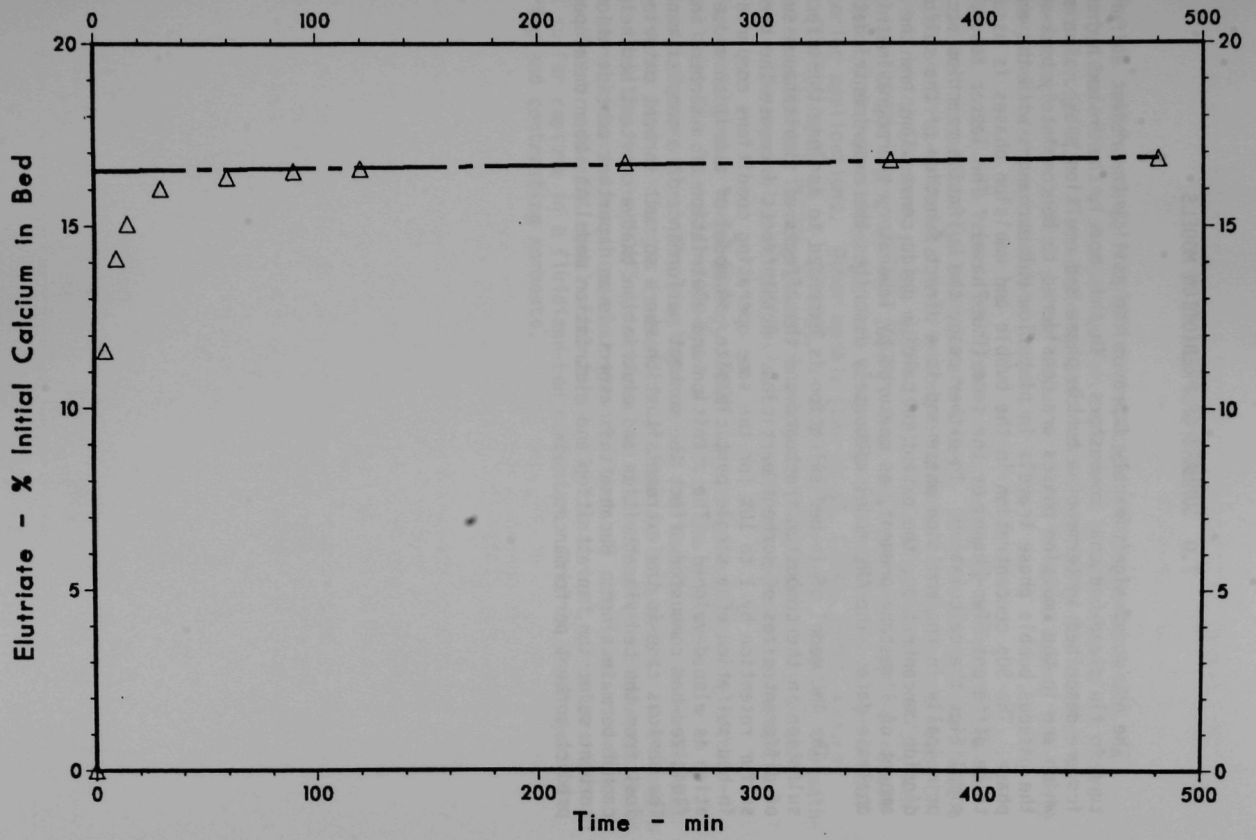

7.0 SUMMARY OF PREDICTION MODELS

The ANL model significantly improves the ability to predict sulfur capture in fluidized-bed coal combustors. In this model, the in-bed hydrodynamics are described in terms of a bubble phase and emulsion phase. The solids, which are in the emulsion phases are considered to be completely back-mixed; the gaseous bubble phase travels in plug flow but exchanges with the emulsion phase. The SO_2 concentration in the bubble and emulsion phases is assumed to be different (Two-Phase) or the same (One-Phase). The latter assumption simplifies the calculation. In either case, the sulfation reaction occurs principally in the emulsion phase and is a direct function of the sulfur dioxide concentration, the extent of calcium oxide conversion, and the amount of limestone present, as measured by laboratory thermogravimetric analysis data. The ANL model adequately describes the experimental data.

The ANL model of in-bed sulfation is extended to include the effects of sulfation in the combustor freeboard and the effects of simultaneous sulfation of different sizes of sorbent particles. Both effects increase the predicted sulfur retention by 1 to 10% for the same operating conditions compared to the in-bed sulfation of a single particle size. A model of attrition and elutriation is also developed. The attrition and elutriation of a sorbent in a fluidized-bed combustor affect the sorbent performance in a complex manner. The obvious case is the extreme situation where so much sorbent material is lost from the bed via attrition and elutriation that a constant bed height cannot be maintained. Because this aspect is an important consideration in sorbent selection, an attrition and elutriation model has been developed to predict sorbent performance.

7.1 IN-BED SULFATION

The ANL model greatly simplifies prediction of the sorbent feed rate necessary to achieve the desired sulfur capture in an atmospheric fluidized-bed combustor (AFBC). The simple equation shows explicity the sorbent and AFBC parameters which affect sulfur capture. This is advantageous in rapidly screening and selecting candidate sorbents.

The ANL model is a recent addition to the models of sulfur capture in fluidized-bed combustors [all model references]. Many of the previous models are based on first-principle descriptions of chemical diffusion and reaction process kinetics [Hartman et al. (1974-1979), Pigford and Sliger (1973), Wen and Ishida (1973), Horio and Wen (1976), Chen and Saxena (1977)] that result in mathematical expressions that are generally too complicated for practical engineering applications. Other models [Lee et al. (1980, 1981), Keairns et al. (1975), Newby et al. (1980)], as does the ANL model, simplify the mathematics by utilizing thermogravimetric analysis (TGA) data of the sorbent-sulfur dioxide reactivity as the basis for predicting sorbent performance.

The Westinghouse model (Newby, 1980) represent the pioneering effort that utilizes TGA data as the basis of a model of the sulfur capture in a fluidized-bed combustor. The Westinghouse and ANL models are similar in that the residence time of the gas is explicitly shown in both models. Both models predict that the required Ca/S to achieve the desired sulfur capture decreases as the gas residence time increases, provided that all other factors remain fixed. However, the ANL model shows explicitly the sorbent parameters that affect sulfur capture in a fluidized-bed combustor. This is advantageous in comparing and contrasting sorbents.

The ANL model is based on the following simplifying assumptions:

1. The mechanism which dominates the rate of SO_2 capture,

$$CaO(s) + SO_2(g) + 1/2\ O_2(g) \rightarrow CaSO_4(s) \qquad 1$$

   in a fluidized bed is diffusion resistance in the pores of the sorbent particle.

2. Laboratory-scale thermogravimetric techniques accurately simulate this rate-limiting mechanism and therefore, in principle, can be used to predict sorbent requirements in a fluidized bed.

3. The fluidized-bed consists of two phases: an emulsion phase and a bubble phase; non-uniform mixing of SO_2 gas between these two phases is assumed. All sulfur from the coal is uniformly released in the emulsion phase as SO_2.

4. The emulsion phase, which contains the solids, can be regarded as a loose approximation to an idealized continuous stirred tank reactor (CSTR); that is, the solids are well mixed. In addition, the sorbent size distribution of this emulsion phase is the same as the over-flow materials.

5. Sulfur removal by a wide particle size distribution in a fluidized bed can be predicted utilizing the sulfation rate data of a narrow particle size fraction representing the average particle size in the bed.

6. The reaction of SO_2 with sorbent is first order in SO_2. This assumption is supported by data in this work (see TEST Results, Section 4.1), [Borgwardt (1970, 1972), Yang, et al., (1975), James and Hughes (1976)].

7. The bulk of the sulfur dioxide is captured in the fluidized bed rather than in the freeboard region above the bed. There are, however, indications that the freeboard region makes a significant contribution (as high as 25%) to sulfur capture [Babcock and Wilcox, (1979)].

By use of these simplifying assumptions, the sorbent feed rate necessary to achieve the desired sulfur capture can readily be projected. The average conversion, $\bar{\alpha}$, of the sorbent in the fluidized bed may be calculated from the equation

$$\bar{\alpha} = \int_0^\infty E\ \alpha\ dt \qquad 2$$

where E is the age distribution of sorbent stone in the bed and α is the extent of conversion of the sorbent at time, t [Kunii and Levenspiel (1969)]. The age distribution function is taken as

$$E = \frac{1}{\tau} e^{-t/\tau} \qquad 3$$

where τ is the average residence time of sorbent stone in the bed (i.e., τ is the moles of calcium in the bed divided by the calcium feed rate). The extent of conversion, α is taken from TGA data (see Section 4.1) as

$$\alpha = D \left[1 - \exp \left(\frac{-bC_g t}{\rho_c} \right) \right] \qquad 4$$

and

$$\frac{d\alpha}{ct} = \frac{b}{\rho_c} C_g \left[D - \alpha \right] \qquad 5$$

Substituting Eqs. 3 and 4 into Eq. 2, letting $b' = \frac{b}{\rho_c} C_g$ and integrating results in

$$\bar{\alpha} = \frac{Db'\tau}{\tau b' + 1} \qquad 6$$

Now R = fractional retention of SO_2 = $(Ca/S)\bar{\alpha}$

$$= \frac{(Ca/S)\ Db' \left[\frac{Ca_{bed}}{(Ca/S)\ S_{in}} \right]}{b' \left[\frac{Ca_{bed}}{(Ca/S)\ S_{in}} \right] + 1} \qquad 7$$

where Ca_{bed} = moles of calcium in the bed

S_{in} = molar feed rate of sulfur to the bed (moles/sec)

(Ca/S) = calcium to sulfur molar ratio of the feed

Manipulating Eq. 7 gives

$$\frac{1}{Ca/S} = \frac{D}{R} - \frac{S_{in}}{b' Ca_{bed}} \qquad 8$$

Now

$$Ca_{bed} = AH(1 - \beta)\ \rho_c \text{ moles} \qquad 9$$

where A - area of fluidized bed (m^2)
H - height of fluidized bed (m)
β = fractional volume-in the bed not occupied by sorbent particles (including the fractional volumes of the bubbles (δ), emulsion voidage (ϵ) heat exchanger tubes (F_H), and inert solids in the bed (F_I).

$$(1 - \beta) = (1 - \delta)(1 - \epsilon)(1 - F_H)(1 - F_I) \qquad 10$$

Thus from Eq. 8

$$Ca/S = \left(\frac{D}{R} - \frac{S_{in}}{(b/\rho_c)\ C_1\ Ca_{bed}} \right)^{-1} \qquad 11$$

where C_1 and C_2 are the SO_2 concentration (moles/m^3) in the emulsion phase and bubble phase, respectively.

The SO_2 concentrations are different in the bubble and emulsion phases. To calculate the difference, it is assumed that the two-phase theory can be applied to simulate the performance of the reactor. Thus, the superficial velocities of gas entering the emulsion phase and the bubble phase are U_{mf} and $U - U_{mf}$, respectively, where U_{mf} is the minimum fluidization velocity (m/sec). The material balance for the total sulfur in the bubble phase gives rise to

$$(U - U_{mf}) \frac{dC_2}{dz} = k_L\ \delta(C_1 - C_2) \qquad 12$$

where K_L is the interfacial mass transfer coefficient between the bubble phase and the emulsion phase, sec^{-1}, δ is the volume fraction of the bubble phase, and z is the axial distance above the gas distributor plate.

The boundary conditions for Eq. 12 are

$$z = 0,\ C_2 = 0 \qquad 13$$

From Eqs. 12 and 13, it can be shown that

$$C_2 = C_1 \left[1 - \exp \left(- \frac{k_L \delta z}{U - U_{mf}} \right) \right] \qquad 14$$

The total sulfur balance in the emulsion phase becomes

$$S_{in} = A\ C_1 U_{mf} + \int_0^H k_L\ A\delta(C_1 - C_2)\ dz + RS_{in} \qquad 15$$

Substituting Eq. 14 into Equation 15 yields:

$$S_{in} = A\ C_1 U_{mf} + C_1 \left[1 - \exp \left(- \frac{k_L \delta H}{U - U_{mf}} \right) \right] (U - U_{mf}) + RS_{in} \qquad 16$$

Rearranging Eq. 16 leads to

$$C_1 = \frac{S_{in}\ (1 - R)}{A\ U_{mf} + A \left[1 - \exp \left(- \frac{k_L \delta H}{U - U_{mf}} \right) \right] (U - U_{mf})} \qquad 17$$

Rearranging Eq. 17 gives

$$C_1 = \frac{S_{in}\ (1 - R)}{A\gamma U} \qquad 18$$

where

$$\gamma = \left\{ U_{mf} + \left[1 - \exp\left(- \frac{k_L \delta H}{U - U_{mf}} \right) \right] (U - U_{mf}) \right\} \frac{1}{U} \qquad 19$$

Generally, γ is less then unity and TWO PHASE is the descriptor given to the bed. However, when k_L is infinitely large, γ becomes equal to unity, there is uniform gas mixing between bubble and emulsion phases, ($C_1 = C_2$), and ONE PHASE is the descriptor given to the bed.

Substituting Eqs. 9 and 18 into Eq. 11 yields

$$Ca/S = \left[\frac{D}{R} - \frac{\gamma H}{U\ b\ (1 - R)(1 - \beta)} \right]^{-1} \qquad 20$$

The SO_2 concentration in the flue gas above the bed, C_e, can be calculated by

$$C_e = \frac{C_1\ U_{mf} + C_2\ (U - U_{mf})}{U} \qquad 21$$

Substituting Eqs. 14 and 17 into Eq. 21 gives

$$C_e = \frac{S_{in}\ (1 - R)}{AU} \qquad 22$$

as would be expected from sulfur material balance considerations.

The three additional parameters, U_{mf}, k_L and δ used in describing the TWO-PHASE (fast bubble) regime are estimated as follows. U_{mf}, the minimum fluidization velocity (m/sec) is calculated from the empirical correlations proposed by Wen and Fan (1974). The equations have the form:

$$(N_{Re})_{mf} = 0.00134\ (N_{Ga})^{0.89};\ \text{for } 18 < 10^5$$

$$(N_{Re})_{mf} = 0.0426\ (N_{Ga})^{0.602};\ \text{for } N_{ga} > 10^5 \qquad 23$$

where $(N_{Re})_{mf}$, defined as $\frac{d_p\ U_{mf}\ \rho_g}{\mu}$, is the Reynolds number at the minimum

fluidization condition. N_{Ga} is the Galileo number, defined as

$$N_{Ga} = \frac{d_p^3(\rho_p - \rho_g)\rho_g\, g}{\mu^2} \qquad 24$$

where d_p is the particle diameter (m), ρ_g is the gas density (kg/m^3), ρ_g is the particle density (kg/m^3), μ is the viscosity of the gas (kg/m sec) and g is the acceleration of gravity. On rearranging Eqs. 23 and 24, U_{mf} is given by

$$U_{mf} = \frac{0.00134\ \mu}{d_p \rho_g} \left[\frac{d_p^3\ (\rho_p - \rho_g)\rho_g\ g}{\mu^2} \right]^{0.89} \qquad 25$$

for $18 < N_{Ga} < 10^5$

$$= \frac{0.0426\ \mu}{d_p \rho_g} \left[\frac{d_p^3\ (\rho_p - \rho_g)\rho_g\ g}{\mu^2} \right]^{0.602}$$

for $N_{Ga} > 10^5$

The gas exchange coefficient, k_L, between the bubble phase and emulsion phase (sec^{-1}), is estimated from Kobayaski, et al. (1967) as

$$k = \frac{0.11}{\bar{D}_B} \qquad 26$$

where $\bar{D}_B$ (m) is the average bubble diameter in the bed. The correlation equations of Mori and Wen (1975) are used to calculate for the average bubble diameter at the location of H/2. The equations have the form:

$$\bar{D}_B = D_{Bm} - (D_{Bm} - D_{BO}) \exp \left(- 0.30 \frac{Z}{D_R} \right) \qquad 27$$

where Z = H/2 and D_{Bm} (m) is the maximum bubble diameter which can be expressed by

$$D_{Bm} = 1.64\ [A\ (U - U_{mf})]^{2/5} \qquad 28$$

or

D_{Bm} = bed diameter (D_R,m) whichever is smaller.

D_{BO} is the initial bubble diameter (m) which can be expressed by

$$D_{BO} = \begin{cases} 0.871 \left[\dfrac{\dot{A}\ (U - U_{mf})}{N_D} \right]^{2/5} ; \text{ for a perforated plate or bubble cap} \\ 0.376\ (U - U_{mf})^2 ; \text{ for a porous plate} \end{cases} \qquad 29$$

where N_D is the total number of orifice openings on the distributor. The bed average bubble diameter has also been assumed to occur at the location of $H_{mf}/2$ where H_{mf} is the bed height (m) at minimum fluidization [Kato and Wen (1969), Fan and Fan (1979)].

In the fluidized bed operation, the height of bed expansion, H, is normally a known parameter, which is taken as the height of the outlet for the spent sorbent. Assuming that the heat transfer tubes are uniformly distributed in the bed, the height of the bed at the minimum fluidization conditions, H_{mf}, can, thus, relate to H from the mass balance of the gas in the bubble phase [Mori and Wen (1975)] as

$$H_{mf} = \frac{U_b - (U - U_{mf})}{U_b} H \qquad 30$$

where U_b (m/sec) is the linear bubble velocity which can be estimated by the equation of Davidson and Harrison (1963)

$$U_b = U - U_{mf} + 0.711\ (g\ \bar{D}_B)^{0.5} \qquad 31$$

Thus

$$H_{mf} = \left[\frac{0.711\ (g\ \bar{D}_B)^{0.5}}{U - U_{mf} + 0.711\ (g\ \bar{D}_B)^{0.5}} \right] H \qquad 32$$

The final parameter δ, the volume fraction of the bubble phase in the bed, is obtained by

$$\delta = \frac{H - H_{mf}}{H} = \frac{U - U_{mf}}{U_b} \qquad 33$$

How to Calculate γ and $(1 - \beta)$

The quantity $(1 - \beta)$ is calculated from Eq. 10. Estimated values for F_H, F_I and E are used; typical values are shown in the Numerical Example which follows. The value of δ is calculated from Eq. 33. The quantity γ is calculated from Eq. 19 using the desired fluidizing gas, U, and bed height, H. The other values put into Eq. 19 are obtained as follows. U_{mf} is obtained from Eq. 25; k_L from Eqs. 25 to 29. The calculation of γ and $(1 - \beta)$ as well as the use of the ANL model of in-bed sulfation is illustrated in the following example.

Numerical Example

The nominal values of the operating parameters for the fluidized-bed combustor and limestone ANL-9202 employed in this example are given in Table 7.1.1. With these values, the other parameters in the model can be computed using Eqs. 23 through 33. These are:

Galileo number, N_{Ga} = 2874

Maximum bubble diameter = 1.82 m (bed diameter)

Minimum fluidization velocity, U_{mf} = 0.219 m/sec

Initial bubble diameter, D_{BO} = 0.072 m

Average bubble diameter, $\bar{D}_B$ = 0.237 m

Gas exchange coefficient, k_L = 0.522 sec^{-1}

Linear bubble velocity, U_b = 2.85 m/sec

Bed height at minimum fluidization, H_{mf} = 0.454 m

Volume fraction of bubble phase, δ = 0.64

β (defined by Eq. 10) = 0.82

γ (defined by Eq. 19) = 0.26

For the desired fraction retention, R, the required Ca/S molar ratio of the feed to the bed is calculated using Eq. 20. For example, for R = 0.85, Ca/S = 4.76. (Additional results are shown in Fig. 7.1.1.) In contrast, for the case of uniform gas mixing between the emulsion and bubble phase (γ = 1 in Eq. 19) and for the same operating conditions, with R = 0.85, Ca/S = 10.61. The large difference between the predicted Ca/S feed requirements for the two-phase case (γ = 0.26, Ca/S = 4.76) and the uniform mixing, one-phase case (γ= 1.00, Ca/S = 10.61) results from the predictions being based on the flat portion of the retention versus Ca/S curve (Fig. 7.1.1). In the flat region, large increases in the Ca/S feed produce only small increases in the sulfur retention. This insensitivity to Ca/S ratio produces the large difference in feed requirements at R = 0.85. The two-phase case and the uniform mixing, one-phase case result in close predictions at lower retention values which are not in the flat portion. For example, at R = 0.60, Ca/S = 3.37 and 2.94 for the one-phase and two-phase predictions, respectively.

Table 7.1.1. Nominal Values Employed for the Numerical Example Using ANL-9202

Bed height	:	$H = 1.00$ meters
Fluidizing velocity	:	$U = 2.00$ meter/sec
Maximum fractional conversion of sorbent	:	$D = .213$
Reaction rate constant	:	$b = 465\ sec^{-1}$
Volume fraction of voidage in emulsion phase	:	$\epsilon = 0.45$ estimated*
Volume Fraction of inerts in bed	:	$F_I = 0.05$ estimated
Volume fraction of heat exchange tubes in bed	:	$F_H = 0.04$ estimated
Average sorbent particle diameter	:	$d_p = 0.0010$ meter
Sorbent particle density	:	$\rho_p = 1{,}800\ kg/m^3$
Gas density	:	$\rho_g = 0.33\ kg/m^3$
Acceleration of gravity	:	$g = 9.80\ m/sec^2$
Gas viscosity	:	$\mu = 4.5 \times 10^{-10}$ kg/m-sec
Bed diameter	:	$D_R = 1.82$ meter
Number of orifice openings in distributor plate	:	$N_D = 3580$
Bed area	:	$A = 3.34\ m^2$

*See Kunii and Levenspiel (1969).

DISCUSSION

The equations which can be used to predict sorbent performance differ only in that γ, the gas exchange parameter is less than unity for two-phase regime and equals unity for the slow bubble regime. In both cases the equation shows explicitly the sorbent and FBC parameters which affect sulfur capture. Three conclusions are immediately obvious. First, the maximum fractional sorbent utilization parameter, D, is extremely important. If the sorbent reacts infinitely rapid with SO_2 (i.e., $b \to \infty$), the

$$\frac{\gamma U}{H\, b\, (1 - R)(1 - \beta)}$$

term becomes zero and the required (Ca/S) ratio is R/D. This is the minimum Ca/S ratio for the sorbent in question to achieve the desired sulfur retention, R. Further, a plot of retention versus (Ca/S) ratio has a slope of D. For finite values of b, the

$$\frac{\gamma U}{H\, b\, (1 - R)(1 - \beta)}$$

term is non-negligible and (Ca/S) > R/D. The D value depends not only on the particular sorbent but often depends on the sorbent particle size as well (see Test Results, Section 4.1). In many cases, smaller sorbent particles are sulfated to a greater extent (higher D values). A typical example of the particle size effect on sorbent feed requirements is shown in Fig. 7.1.2. The second conclusion is that the gas residence time in the bed, H/U, is important. Increasing the gas residence time decreases the Ca/S ratio required as shown in Fig. 7.1.3 (provided, of course, that these changes in the H/U ratio are over an interval small enough so that β is constant). The final conclusion is the intuitively obvious one--namely, for two stones with the same maximum sulfation (D) values and the same combustor operating conditions, the more reactive stone with the larger b value will require a smaller (Ca/S) ratio in the feed to achieve the same sulfur capture, R.

For the two-phase regime, exchange of gas between bubble and emulsion is less than infinitely rapid, γ is less than unity. As a result, the concentration of SO_2 in the emulstion phase is higher than for the slow bubble case (see Eq. 18). This increases the amount of sulfur captured because the rate of sulfur capture increases linearly with increasing SO_2 pressure. As a consequence, lower sorbent requirements to achieve the same fractional sulfur retention are predicted for the two-phase regime compared to the one-phase regime. Use of the two-phase approach ($\gamma < 1$) is slightly more difficult than use of the one-phase approach ($\gamma = 1$) because three additional parameters, k_L, δ, and U_{mf}, must be calculated. Further, the accuracy of these calculated parameters cannot be easily verified experimentally. However, the projected sorbent requirements using the two-phase treatment are not extremely sensitive to the k_L, δ, and U_{mf} values. So errors in calculating these parameters do not detract from the general trend (discussed above) of lowering the predicted sorbent feed required for a desired sulfur retention.

Fig. 7.1.1

Projected Performance of Sorbent 9202

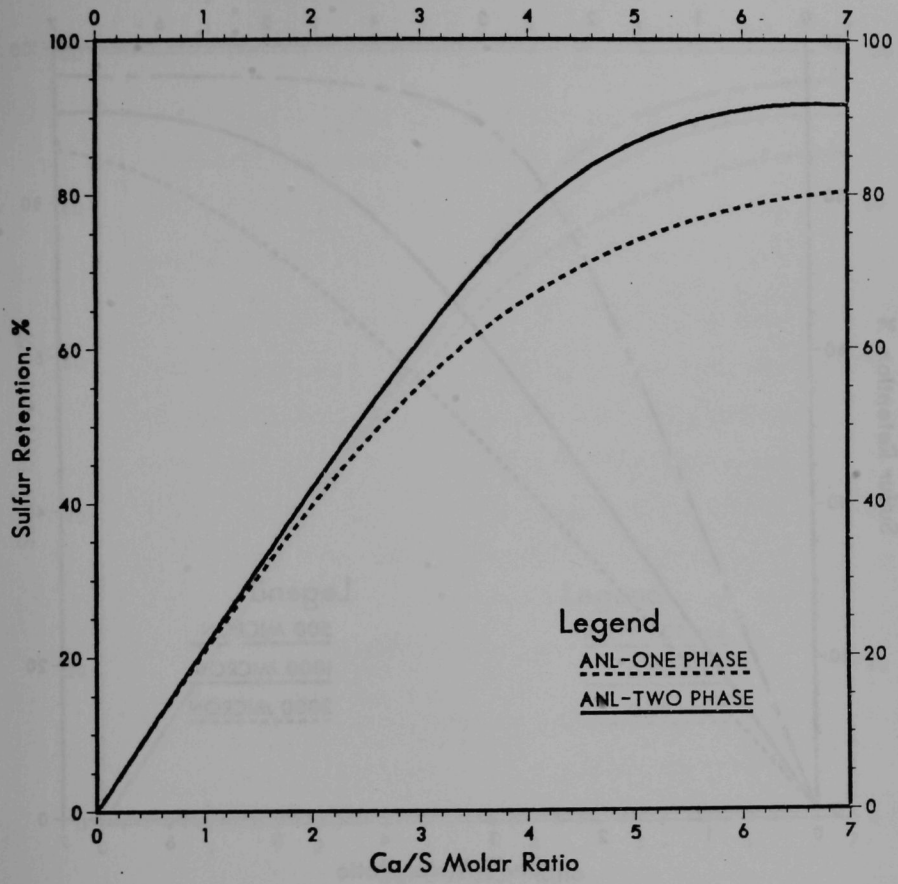

Fluidized Bed Operating Conditions

Temperature = 850. C = 1562. F

Pressure = 101. kPa = 1.0 atm

Fluidizing Velocity = 2.00 Meters/sec = 6.56 ft/sec

Bed Height = 1.00 Meters = 3.28 ft

Coal Feed Rate = 897.6 kg/hr = 1977.0 lb/hr

Sulfur Content in Coal = 2.58 wt%

Bed Area = 3.34 sq. meter = 36.0 sq.ft.

Sorbent Particle Dia. = 1000. micron = 0.0394 inch

Fig. 7.1.2

Particle Size Effects on Projected Performance of Sorbent 9202

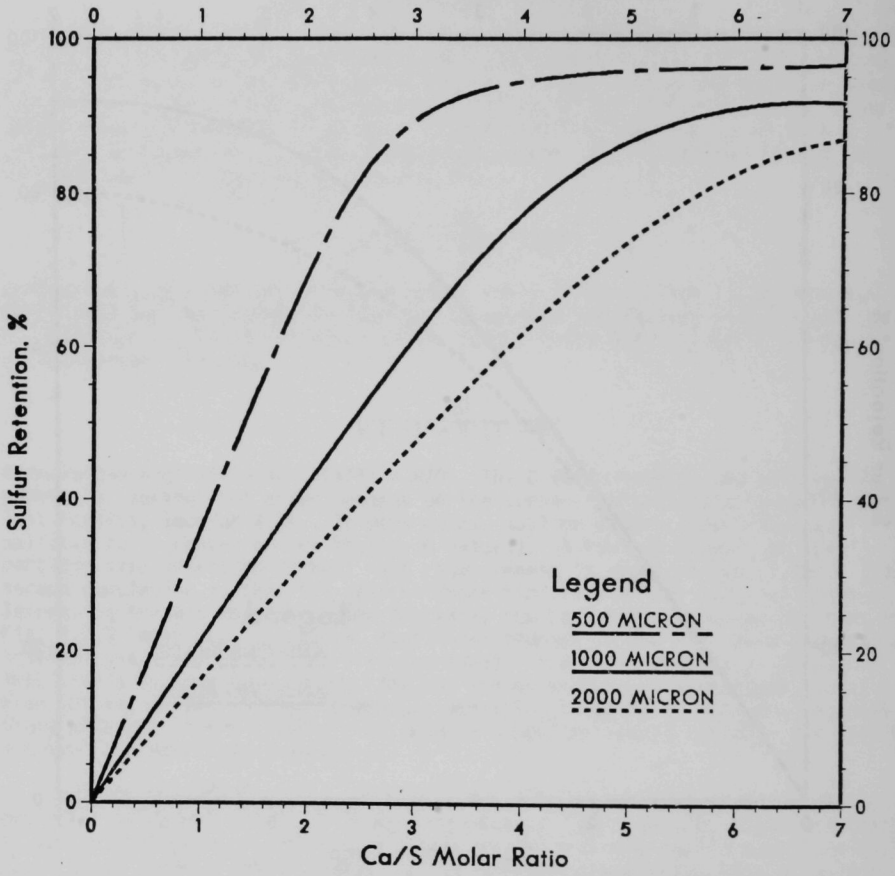

Fluidized Bed Operating Conditions

Temperature = 850. C = 1562. F

Pressure = 101. kPa = 1.0 atm

Fluidizing Velocity = 2.00 Meters/sec = 6.56 ft/sec

Bed Height = 1.00 Meters = 3.28 ft

Coal Feed Rate = 897.6 kg/hr = 1977.0 lb/hr

Sulfur Content in Coal = 2.58 wt%

Bed Area = 3.34 sq. meter = 36.0 sq.ft.

Fig. 7.1.3

Effects of Gas Residence Time on Projected Performance of Sorbent 9202

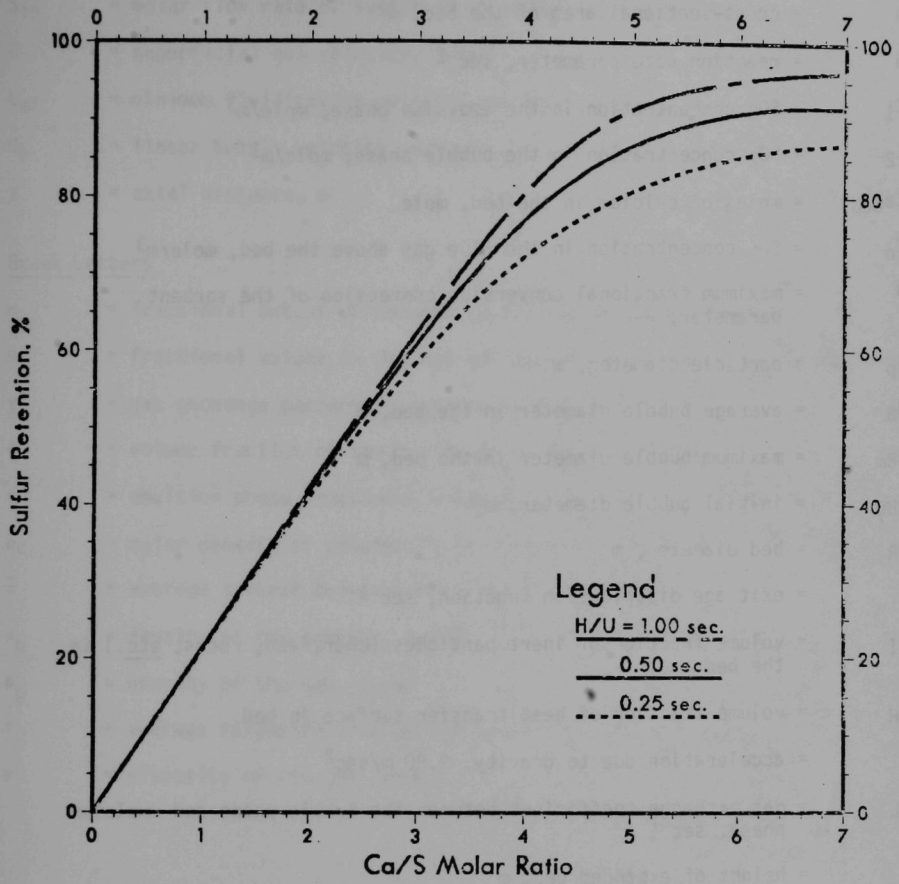

Fluidized Bed Operating Conditions

Temperature = 850. C = 1562. F

Pressure = 101. kPa = 1.0 atm

Fluidizing Velocity = 2.00 Meters/sec = 6.56 ft/sec

Coal Feed Rate = 897.6 kg/hr = 1977.0 lb/hr

Sulfur Content in Coal = 2.58 wt%

Bed Area = 3.34 sq. meter = 36.0 sq.ft.

Sorbent Particle Dia. = 1000. micron = 0.0394 inch

NOMENCLATURE

A = cross-sectional area of the bed, m^2

b = reaction rate parameter, sec^{-1}

C_1 = SO_2 concentration in the emulsion phase, $mole/m^3$

C_2 = SO_2 concentration in the bubble phase, $mole/m^3$

Ca_{bed} = moles of calcium in the bed, mole

C_e = SO^2 concentration in the flue gas above the bed, $mole/m^3$

D = maximum fractional conversion conversion of the sorbent parameter, ---

d_p = particle diameter, m

$\bar{D}_B$ = average bubble diameter in the bed, m

D_{Bm} = maximum bubble diameter in the bed, m

D_{BO} = initial bubble diameter, m

D_R = bed diameter, m

E = exit age distribution function, sec^{-1}

F_I = volume fraction of inert particles (char, ash, rocks, etc.) in the bed

F_H = volume fraction of heat transfer surface in bed

g = acceleration due to gravity, 9.80 m/sec^2

k_L = gas exchange coefficient between the bubble phase and emulsion phase, sec^{-1}

H = height of expanded bed, m

H_{mf} = bed height at the minimum fluidization condition, m

$(N_{Re})mf$ = Reynolds number at the minimum fluidization condition, ---

N_{Ga} = Galileo number

N_D = total number of orifice openings on the distributor, ---

R = fractional sulfur retention in the bed, ---

t = time

S_{in} = molar flow rate of sulfur at the bed-inlet, mole/sec

U = superficial gas velocity, m/sec

U_{mf} = minimum fluidization velocity, m/sec

U_b = linear bubble velocity, m/sec

z = axial distance, m

Greek Letters

α = fractional extent of sorbent conversion at time t, ---

β = fractional volume in the bed not occupied by sorbent particles, ---

γ = gas exchange parameter, defined by Eq. 19

δ = volume fraction of the bubble phase in the bed, ---

ε = emulsion phase fractional voidage, ---

ρ_c = molar density of calcium in the sorbent, mole/m^3

$\bar{\alpha}$ = average sorbent conversion at the bed-outlet, ---

ρ_p = density of the sorbent, kg/m^3

ρ_g = density of the gas, kg/m^3

τ = average residence time of the sorbent in the bed, sec

μ = viscosity of the gas, kg/m sec

References for Section 7.1

In-Bed Sulfation

R. H. Borgwardt, Environ. Sci. Technol., 4, 59 (1970).

R. H. Borgwardt, Environ. Sci. Technol., 6, 350 (1972).

J. F. Davidson and D. Harrison, Fluidized Particles, Cambridge Univ. Press (1963).

L. T. Fan and L.-S. Fan, Chem. Eng. Sci., 34, 171 (1979).

N. J. James and R. Hughes, 2nd Int. Conf. on the Control of Gaseous Sulfur and Nitrogen Compound Emission (Vol. I), Salford, United Kingdom, April 6-8, 1976.

K. Kato and C. Y. Wen, Chem. Eng. Sci., 24, 1351 (1969).

H. Kobayashi, F. Arai, T. Sunagawa, Chem. Eng. (Japan), 31, 239 (1967).

D. Kunii and O. Levenspiel, Fluidization Engineering, Wiley & Sons, New York (1969), Chapter 15.

LR:78:4775:03 Fluidized Bed Combustion Facility and Commercial Utility AFBC Design Assessment, Babcock & Wilcox Annual Report 1978 (1979).

S. Mori and C. Y. Wen, AIChE J. 21, 109 (1975).

C. Y. Wen and L.-S. Fan, Ind. Eng. Chem. Process Des. Dev., 13, 194 (1974).

R. T. Yang, P. T. Cunningham, W. I. Wilson and S. A. Johnson, Adv. Chem., 139, 149 (1975).

Sulfur Capture Models

T. P. Chen and S. C. Saxena, Fuel 56, 401 (1977).

M. Hartman, Int. Chem. Eng. 16, 86 (1976).

M. Hartman and R. W. Coughlin, Ind. Eng. Chem. Process Des. Dev. 13, 248 (1974).

M. Hartman and R. W. Coughlin, AIChE J. 23, 490 (1976).

M. Hartman, J. Hejna and Z. Beran, Chem. Eng. Sci. 34, 475 (1979).

M. Hartman, J. Pata and R. W. Coughlin, Ind. Eng. Chem., Process Des. Dev. 17, 411 (1978).

M. Horio and C. Y. Wen, "Analysis of Fluidized-Bed Combustion of Coal with Limestone Injection," Fluidization Technology, Vol 2 (D. L. Keairns, ed.), 1976.

D. L. Keairns, et al., EPA 650/2-75-027-C, Westinghouse Research Laboratory, September 1975.

D. C. Lee, J. L. Hodges and C. Georgakis Chem, Eng. Sci. 35, 302 (1980).

D. C. Lee and C. Georgakis, AIChE Journal, 27, 472 (1981).

R. A. Newby, N. H. Ulerich, and D. L. Keairns, "A Technique to Project the Sulfur Removal Performance of Fluidized-Bed Combustors," 6th International Conference on Fluidized-Bed Combustion, Atlanta, Georgia, April 9-11, 1980 Conf. 800428 (1980) p 803.

R. L. Pigford and G. Sliger, Ind. Eng. Chem. Process Des. Dev. 12, 85 (1973).

C. Y. Wen and M. Ishida, Environ. Sci. Tech. 1, 703 (1973).

J. Zheng, J. G. Yates, and P. N. Rowe, Chem. Eng. Sci. 37, 167 (1982).

7.2 FREEBOARD AND IN-BED SULFATION

The ANL model of in-bed sulfation (Section 7.1) has been extended to account for sulfur capture in the freeboard of a fluidized-bed coal combustor (FBC). Other than the recent work of Chen and Wen (1981), none of the models for predicting sulfur retention in an FBC [Bethell et al. (1973), Keairns et al. (1975), Daniel et al. (1980), Lee et al. (1980, 1981), Fee et al. (1981), and Zheng et al. (1982)] have taken into account the possible reactions in the free board region despite limited experimental evidence that the sulfur capture above the bed may be significant (Babcock and Wilcox Annual Report, 1979).

The proposed model considers the fluidized bed and the freeboard region to be coupled continuously stirred tank reactors as shown in Fig. 7.2.1. The dense phase or in-bed region is modeled according to the modified two phase theory, that is, the bed consists of two phases namely, bubble phase and emulsion phase. The superficial gas flow for the bubble phase is $\lambda(U-U_{mf})$ and that for the emulsion phase is $(1-\lambda)U + \lambda U_{mf}$.

Other assumptions include: (i) the sorbent particle size distribution can be represented by the average particle size. (ii) Reaction in the bubble phase is negligibly small. The bubble phase moves in plug flow and exchanges gas with the emulsion phase. (iii) The major freeboard reaction takes place in the freeboard transition region where all the entrained sorbent returns to the bed; this region is modeled as a completely back-mixed reactor. (iv) The sorbent-SO_2 reactivity is given from laboratory thermogravimetric analyzer data as

$$\frac{d\alpha}{dt} = \frac{bC_g}{\rho}[D - \alpha],\ \alpha = D[1 - \exp(-b'C_g t)] \text{ where } b' = b/\rho. \qquad 1$$

The basic mathematical expressions describing the system at the steady state are as follows (see Fig. 7.2.1):

The sorbent balance in the in-bed region gives rise to

$$F + (1 - \alpha_f)F_e - (1 - \alpha_1)F - (1 - \alpha_1)F_e - M_f b'C_1(D - \alpha_1) = 0. \qquad 2$$

The sorbent balance in the transition region of the freeboard yields

$$F_e(1 - \alpha_1) - F_e(1 - \alpha_f) - M_f b'C_f(D - \alpha_f) = 0. \qquad 3$$

The SO_2 balance in the freeboard can be written as

$$UA(C_{fin} - C_f) = M_f b'C_f(D - \alpha_f). \qquad 4$$

Combining Eq. 3 and Eq. 4, we obtain

$$-F_e\alpha_1 + F_e\alpha_f = UA(C_{fin} - C_f). \qquad 5$$

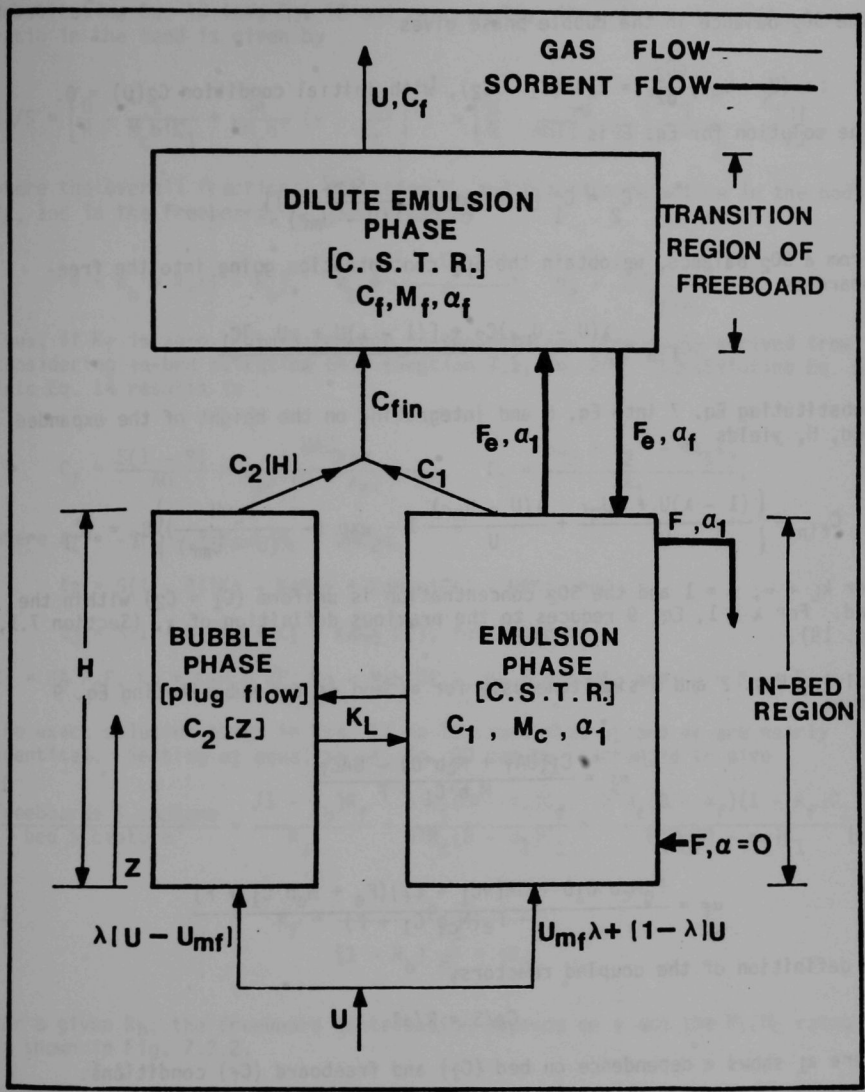

Fig. 7.2.1 Schematic Representation of the Combustor Model

The SO_2 balance in the bubble phase gives

$$\lambda\ (U - U_{mf})\frac{dC_2}{dz} = k_L\delta\ (C_1 - C_2), \text{ with initial condition } C_2(0) = 0. \qquad 6$$

The solution for Eq. 6 is

$$C_2 = C_1\ [1 - \exp\ (-\frac{k_L wZ}{\lambda(U - U_{mf})})] \qquad 7$$

From a SO_2 balance, we obtain the SO_2 concentration going into the freeboard as

$$C_{fin} = \frac{\lambda(U - U_{mf})C_2 + [(1 - \lambda)U + \lambda U_{mf}]C_1}{U} \qquad 8$$

Substituting Eq. 7 into Eq. 8 and integrating on the height of the expanded bed, H, yields

$$C_{fin} = \left\{\frac{(1 - \lambda)U + \lambda U_{mf}}{U} + \frac{\lambda(U - U_{mf})}{U}\ 1 - \exp\ (-\frac{k_L wH}{\lambda(U - U_{mf})})\right\}C_1 = \gamma C_1\ . \qquad 9$$

For $k_L \to \infty$, $\gamma = 1$ and the SO_2 concentration is uniform ($C_1 = C_2$) within the bed. For $\lambda = 1$, Eq. 9 reduces to the previous definition of γ, (Section 7.1, Eq. 19).

Solving Eqs. 2 and 5 simultaneously for α_1 and α_f and substituting Eq. 9 gives

$$\alpha_1 = \frac{C_1(UA\gamma + M_c b'D) - UAC_f}{M_c b'C_1 + F} \qquad 10$$

and

$$\alpha_f = \frac{F_e M_c b'C_1 D + UA(\gamma C_1 - C_f)(F_e + M_c b'C_1 + F)}{F_e(M_c b'C_1 + F)} \qquad 11$$

By definition of the coupled reactors,

$$Ca/S = R/\alpha l, \qquad 12$$

where a_1 shows a dependence on bed (C_1) and freeboard (C_f) conditions.

Substituting Eq. 10 into Eq. 12 and rearranging, the calcium to sulfur molar ratio in the feed is given by

$$Ca/S = \left[\frac{D}{R} - \frac{S}{M_c b' C_1} + \frac{UA}{RM_c b'}\left(\gamma - \frac{C_f}{C_1}\right)\right]^{-1} = \left[\frac{D}{R} - \frac{\gamma U}{Hb(1-\beta)}\left(\frac{1}{1-R_b} - \frac{R_f}{R}\right)\right]^{-1}, \qquad 13$$

where the overall fractional retention R, and fraction retention in the bed, R_b, and in the freeboard, R_f, are given by

$$R = R_b + R_f(1 - R_b), \quad R_b = \frac{S - C_{fin}UA}{S}, \quad R_f = \frac{C_{fin} - C_f}{C_{fin}}. \qquad 14$$

Thus, if R_f is zero, Eq. 13 reduces to the equation previously derived from considering in-bed sulfation only (Section 7.1, Eq. 20). Substituting Eq. 11 into Eq. 14 results in

$$C_f = \frac{S(1-R)}{AU} = \frac{UAC_{fin}}{M_f b'(D - \alpha_f) + UA}, \quad C_1 = \frac{-\xi_2 - \xi_2^{\,2} - 4\xi_1\xi_3}{2\xi_1}, \qquad 15$$

where $\xi_1 = -S(1 - R)K_4\gamma b'M_c - UAK_2q.$ 16

$\xi_2 = S(1 - R)(K_2 - K_4K_5\gamma + K_4M_b b'C_f) - UAK_1$, and 17

$\xi_3 = S(1 - R)(K_3 + K_1 + K_4K_5\, C_f)$, furthermore 18

$K_1 = UA\, F_eF$, $K_2 = K_1M_c b'/F$, $K_3 = M_f b'DF_eF$, $K_4 = M_f b'UA$, and $K_5 = F_e + F$. 19

The exact solution given in Eqs. 15 to 19 shows that α_1 and α_f are nearly identical. Setting α_1 equal to α_f, Eq. 20 can be rearranged to give

$$\frac{\text{freeboards S capture}}{\text{bed S capture}} = \frac{(1 - R_b)R_f}{R_b} = \frac{b'M_f(D - \alpha_f)C_f}{b'M_c(D - \alpha_1)C_1} = \frac{b'M_f(D - \alpha_f)(1 - R_f\gamma C_1}{b'M_c(D - \alpha_1)C_1} \qquad 20$$

$$R_f = \frac{\gamma R_b}{(1 - R_b)\dfrac{M_c}{M_f} + \gamma R_b} \qquad 21$$

For a given R_b, the freeboard contribution depends on γ and the M_f/M_c ratio as shown in Fig. 7.2.2.

Fig. 7.2.2

Freeboard Sulfur Capture at In-Bed Sulfur Capture of 80% Sulfur fed to Bed

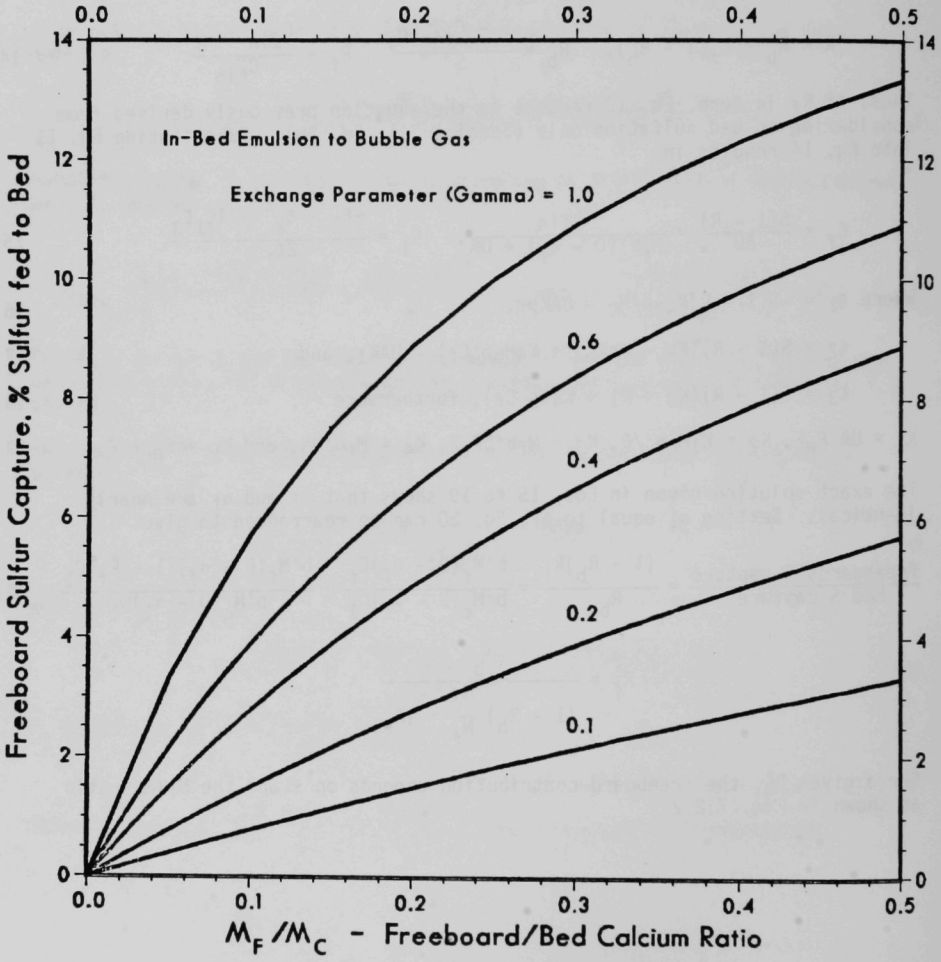

ESTIMATION OF MODEL PARAMETERS

The model parameters for the bed are estimated in the manner previously described (Section 7.1) with the chief exception of the excess gas velocity in the bubble phase, λ. Cranfield and Geldart (1974) have found that for systems with particles from 1000 to 2000 μm the bubble flow rate is approximately 55% (λ = 0.55) of the excess gas flow. Xavier et al. (1978), using particles of 158 μm to 885 μm found that only 80% (λ = 0.8) of the excess gas, goes to the bubble phase. The former work used small velocities; $U - U_{mf}$ from 0.15 m/s to 0.32 m/s; the latter work used higher velocities $U - U_{mf}$ up to 0.8 m/s. However, discrepancies still remain on the deviations from the two-phase theory and little has been done with large particles to allow the use of reliable correlations. Thus, λ = 0.75 will be used as a representative value, and the large particle correlations for bubble diameter (Cranfield and Geldart, 1974) will be employed for the large particle case. Note that the modified equations of the two phase theory describing the system are reduced to their classical form for the fine particle systems when λ = 1.0. For the small particle case, the average bubble diameter is evaluated using the expression of Mori and Wen (1975) at a bed height of $H_{mf}/2$, where H_{mf} and the bubble diameter are calculated in an iterative manner until a consistent set of values are determined. In Section 7.1 an approximation was made by calculating the bubble diameter at H/2. The bubble velocity for both fine and large particle cases is evaluated using the correlation of Cranfield and Geldart (1974).

The entrainment of the sorbent into the freeboard is estimated according to the correlation of Wen and Chen (1980). The holdup in the freeboard is related to the entrainment, F_e, and the average holdup time, θ, of the sorbent particles in the freeboard by

$$M_f = F_e\,\theta. \qquad 22$$

The value of θ is obtained from the integration of the motion equations of the particles from the time they depart at the bed surface to the time they return to it (Zenz and Weil, 1958 and Do et al., 1972).

The departing velocity distribution of the sorbent entering the freeboard is estimated by combining the maximum projected height of the particles, as given by the equations of motion and the empirical equation for the entrainment, obtained under the assumption of its exponential decay along the height in the transition region. A cross plot allowed cumulative frequency distribution of the departing velocities of the sorbent to be obtained (Wen and Chen, 1980). From the departing velocity distribution, the average departing velocity was calculated.

In performing this calculation in an exact manner, a value for the sulfur retention R, is set and C_f calculated with Eq. 14. Then a value for F is assumed, the SO_2 concentration of the emulsion phase, C_1, is calculated with Eq. 15, and the Ca/S ratio (and F) is calculated with Eq. 13. The value of F calculated in this manner is compared with the assumed value and an iterative procedure is followed until both values coincide. The iterative procedure can be circumvented by using Eq. 21 to approximate R_f for given values of the R_b and the M_f/M_c ratio. Following on, R is determined from R_f and R_b using Eq. 14 and the Ca/S ratio is calculated from Eq. 13.

RESULTS AND DISCUSSION

The model indicates that significant sulfur capture can occur in the freeboard region. As shown in Fig. 7.2.3, as much as 9% of the total sulfur fed to the bed is predicted to be captured within the freeboard above a 1.8 m by 1.2 m high bed of 1200 μm diameter limestone particles fluidized at 2.4 m/s. Further, as shown in Fig. 7.2.4, as much as 10% of the total sulfur fed to the bed is predicted to be captured within the freeboard above a 1.0 m by 1.0 m by 0.4 m high bed of 1130 μm diameter particles fluidized at 2.5 m/s. In Figs. 7.4.3 and 7.4.4, the "large particle" case and the "small particle" case are shown for in-bed retention only and combined in-bed and freeboard reactions. The relative contribution of the freeboard to sulfur retention is lower when descriptions of bed hydrodynamics based on small particle data are used.

As shown in Eq. 20, for the same overall retention, R, (and consequently, the same outlet SO_2 concentration, C_f) the SO_2 concentration in the emulsion phase, C_1, is higher for the small particle, nonuniform SO_2 description ($\gamma < 1$) than in the large particle, uniformly mixed SO_2 description ($\gamma = 1$). Further, because of the different calculated bed hydrodynamics, less sorbent is ejected into the freeboard and the lower C_f/C_1 and M_f/M_c ratios result in a reduced freeboard contribution to sulfur capture in the small particle description. However, for both small and large particle descriptions, increasing the fluidizing velocity or decreasing the particle size increases the freeboard holdup and, thus, increases the sulfur retention in the freeboard versus the bed.

The contribution of the freeboard is much less in this model than in the model of Chen and Wen (1981). Although, the calculated overall retention in Figs. 7.2.3 and 7.2.4 compare favorably with the combustor data, the calculations show that the freeboard captures only 9-10% of the total sulfur fed to the bed. In contrast, in the model of Chen and Wen, 60% of the total sulfur fed to the bed is captured in the freeboard in the 1.8 m x 1.8 m AFBC under conditions similar to Fig. 7.2.3. Babcock and Wilcox data show that the freeboard may be responsible for capturing as much as 25% of the total sulfur fed to the bed (Babcock and Wilcox, 1978). The model presented here differs from that of Chen and Wen in several additional aspects. First, Chen and Wen use experimental data on the extent of sulfation in the bed to predict the sulfur capture in the freeboard. This model predicts both the in-bed and freeboard sulfur capture based on sorbent behavior in laboratory tests. Second, the Chen and Wen model predicts that sulfur capture by the elutriated fines is 10% of the total captured in the freeboard. This model can be readily extended to show that the elutiated fines account for negligible sulfur capture. Lastly, there are differences between the models in predictions of the sorbent holdup in the freeboard and reactivity of the sorbent. Compared to the model of Chen and Wen, this model predicts greater sorbent holdup in the freeboard but lowered sulfur dioxide-sorbent reactivity (based on laboratory rate data).

Fig. 7.2.3 Projected Performance of Sorbent 9202
Babcock & Wilcox 6 x 6 Ft Combustor

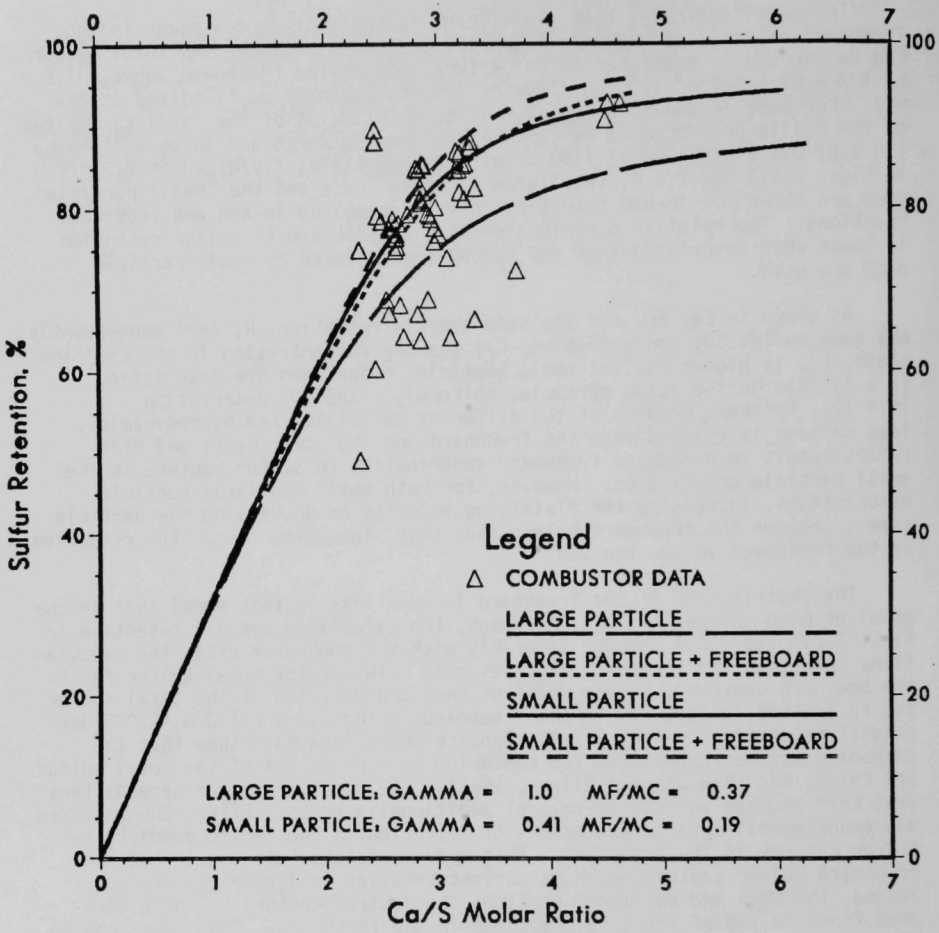

Fluidized Bed Operating Conditions

Temperature = 850. C = 1562. F

Pressure = 101. kPa = 1.0 atm

Fluidizing Velocity = 2.44 m/sec = 8.00 ft/sec

Bed Height = 1.20 Meters = 3.93 ft

Coal Feed Rate = 900.0 kg/hr = 1982.4 lb/hr

Sulfur Content in Coal = 3.60 wt%

Bed Area = 3.34 sq. meter = 36.0 sq. ft.

Sorbent Particle Dia. = 1200. micron = 0.0472 inch

Fig. 7.2.4 Projected Performance of Sorbent 9202
Babcock & Wilcox 3 x 3 Ft Combustor

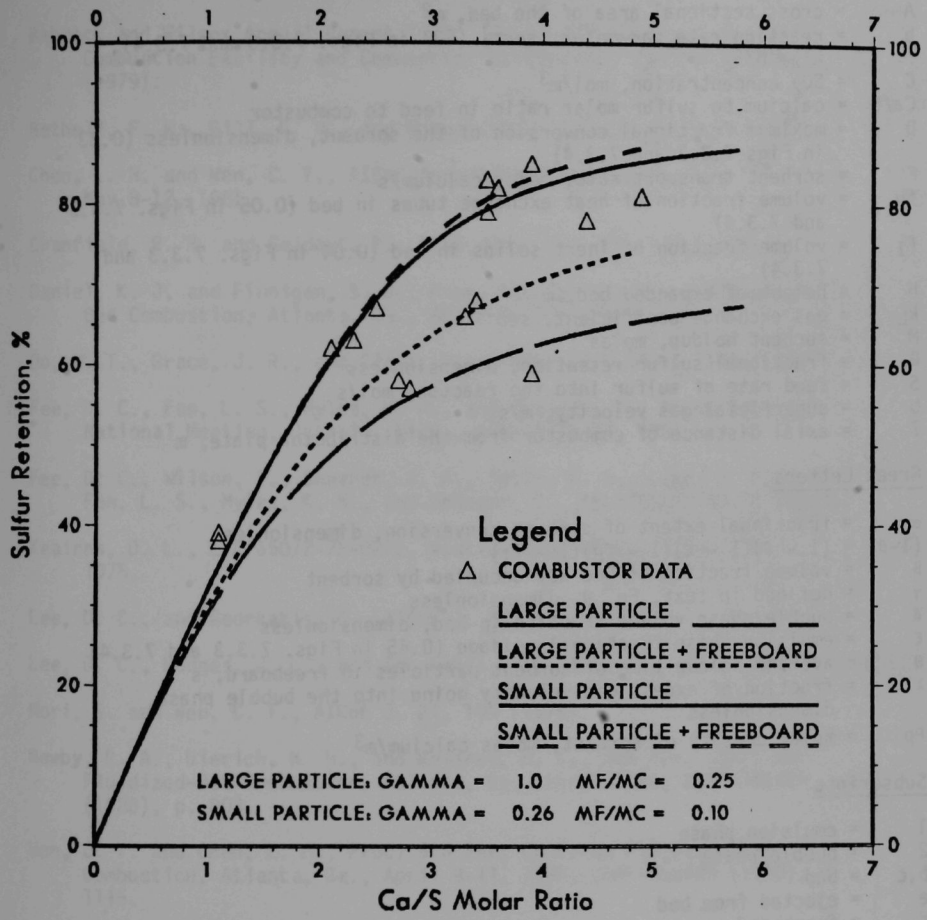

Fluidized Bed Operating Conditions

Temperature = 850. C = 1562. F

Pressure = 101. kPa = 1.0 atm

Fluidizing Velocity = 2.54 m/sec = 8.33 ft/sec

Bed Height = 0.42 Meters = 1.38 ft

Coal Feed Rate = 221.0 kg/hr = 486.9 lb/hr

Sulfur Content in Coal = 3.00 wt%

Bed Area = 0.98 sq. meter = 10.5 sq. ft.

Sorbent Particle Dia. = 1130. micron = 0.0445 inch

Nomenclature

A = cross sectional area of the bed, m^2
b = reaction rate parameter, sec^{-1} (437 in Figs. 7.3.3 and 7.3.4), $b' = b/\rho_p$
C = SO_2 concentration, mol/m^3
Ca/S = calcium to sulfur molar ratio in feed to combustor
D = maximum fractional conversion of the sorbent, dimensionless (0.33 in Figs 7.3.3 and 7.3.4)
F = sorbent transport rate, moles calcium/s
f_H = volume fraction of heat exchange tubes in bed (0.05 in Figs. 7.3.3 and 7.3.4)
f_I = volume fraction of inert solids in bed (0.04 in Figs. 7.3.3 and 7.3.4)
H = height of expanded bed, m
k_L = gas exchange coefficient, sec^{-1}
M = sorbent holdup, moles
R = fractional sulfur retention, dimensionless
S = feed rate of sulfur into the reactor, mol/s
U = superficial gas velocity, m/s
Z = axial distance of combustor from the distributor plate, m

Greek Letters

α = fractional extent of sorbent conversion, dimensionless
$(1-\beta)$ = $(1 - \delta)(1 - \xi)(1 - f_H)(1 - f_I)$
β = volume fraction of bed not occupied by sorbent
γ = defined in text, Eq. 9, dimensionless
δ = bubble phase volume fraction in bed, dimensionless
ξ = emulsion phase fractional voidage (0.45 in Figs. 7.3.3 and 7.3.4)
θ = average holdup time of sorbent particles in freeboard, s
λ = fraction of excess gas velocity going into the bubble phase, dimensionless
ρ_p = molar density of sorbent, moles calcium/m^3

Subscripts

1 = emulsion phase
2 = bubble phase
b,c = bed
e = ejected from bed
f = freeboard
fin = freeboard inlet
g = gas phase in TGA
mf = minimum fluidization

References for Section 7.2

Babcock and Wilcox Annual Report 1978. LR:78:4775:03 Fluidized Bed Combustion Facility and Commercial Utility AFBC Design Assessment (1979).

Bethell, F. W., Gill, D. W., and Morgan, B. B., Fuel 52, 121 (1973).

Chen, L. H. and Wen, C. Y., AIChE Annual Meeting, New Orleans, LA, Nov.8-12, 1981.

Cranfield, R. R. and Geldart, D., Chem. Eng. Sci. 29, 935 (1974).

Daniel, K. J. and Finnigan, S. D., Proc. 6th Int. Conf. on Fluidized Bed Combustion, Atlanta, Ga., April 9-11, 1980.

Do, H. T., Grace, J. R., and Clift, R., Powder Technol. 6, 195 (1972).

Fee, D. C., Fan, L. S., Myles, K. M., and Johnson, I., AIChE 91st National Meeting, Detroid, Mich., August 16-19, 1981.

Fee, D. C., Wilson, I., Shearer, J. A., Smith, G. W., Lenc, J. F., Fan, L. S., Myles, K. M., and Johnson, I., ANL/CEN/FE-80-10 (1980).

Keairns, D. L., EPA 650/2-75-027c, Westinghouse Research Lab., Sept. 1975.

Lee, D. C., and Georkakis, C., AIChE J. 27, 472 (1981).

Lee, D. C., Hodges, J. L., and Georkakis, C., CHem. Eng. Sci. 35, 302 (1980).

Mori, S. and Wen, C. Y., AIChE J. 21, 109 (1975).

Newby, R. A., Ulerich, N. H., and Keairns, D. L., 6th Int. Conf. on Fluidized-Bed Combustion, Atlanta, Ga., April 1980, CONF-800428 (1980), p. 803.

Wen, C. Y. and Chen, L. H., Proc. 6th Int. Conf. on Fluidized-Bed Combustion, Atlanta, Ga., April 9-11, 1980, CONF-800428 (1980), p. 1115.

Xavier, A. M., Lewis, D. A., and Davidson, J. F., Trans Inst. Chem. Engrs. 56, 274 (1978).

Zenz, F. A. and Weil, N. A., AIChE J. 4, 472 (1978).

Zheng, J., Yates, J. G., and Rowe, P. N., Chem. Eng. Sci. 37, 167 (1982).

7.3 IN-BED SULFATION: MULTIPLE PARTICLE SIZES

The Argonne National Laboratory model of in-bed sulfation (Section 7.1) has been extended to account for different size sorbent particles in the bed. Because the overall rate of sulfation changes appreciably with particle sizes, this effect may be significant when compared to the single particle size descriptions of in-bed and freeboard sulfation given in Sections 7.1 and 7.2.

In addition to the various assumptions made previously for the single-size in-bed sulfation model, the bed sorbent material is divided into several narrow size ranges and each size fraction is represented by an average particle diameter. The Ca/S ratio necessary to achieve a desired sulfur retention can be projected as follows. Starting with a given sorbent size fraction in the bed, its average conversion may be represented by the equation below:

$$\bar{\alpha}_i = \int_0^\infty E_i \alpha_i dt \qquad 1$$

where $\bar{\alpha}_i$ = average conversion for a given size fraction of sorbent in the bed.

E_i = age distribution of the size fraction i.

α_i = extent of sorbent conversion of size i.

For a continuous stirred-tank reactor, CSTR, the age distribution of a particle size i at time t can be written as:

$$E_i = 1/\tau_i \exp(-t/\tau_i) \qquad 2$$

where τ_i represents the average residence time of the particle size i.

For a given particle size, i, the kinetics of the sulfation reaction may be expressed as follows:

$$\frac{d\alpha_i}{dt} = \frac{b_i}{\rho_c} C_g (D_i - \alpha_i) \qquad 3$$

where α_i is the extent of sorbent conversion at time t, D_i is the maximum fractional conversion of sorbent parameter, b_i is the reaction rate parameter (sec^{-1}), ρ_c is the concentration of the calcium in the sorbent ($moles/m^3$) and C_g is the SO_2 concentration ($mole/m^3$) around the sorbent particle. Note that Eq. 3 described the rate of sorbent conversion to be first order in SO_2 concentration and relied on the TGA data to determine the b_i and D_i values. (See Test Results, Section 4.1)

Within the broad range of particle sizes found in FBC, Eq. 3 generally provides an adequate representation of their reaction behavior based on TGA experiments. Applying the initial conditions of $t = 0$, $\alpha_i = 0$, an expression for α_i can be found:

$$\alpha_i = D_i \left[1 - \exp\left(-\frac{b_i}{\rho_c} C_g t\right)\right] \qquad 4$$

By substituting Eqs. 2 and 4 into 1 and letting $b_i' = \frac{b_i}{\rho_c} C_g$, one obtains the following expression for $\bar{\alpha}_i$ after integration:

$$\bar{\alpha} = \frac{D_i b_i' \tau_i}{b_i' \tau_i + 1} \qquad 5$$

For

$$R = \text{fraction retention of } SO_2 = (Ca/S)\bar{\alpha} \qquad 6$$

and

$$\bar{\alpha} = \text{average conversion of the bed} = \sum_i f_i \bar{\alpha}_i \qquad 7$$

Substituting Eq. 5 into 7 and the resultant into Eq. 6, the following results:

$$R = (Ca/S) \sum_i \frac{f_i D_i b_i' \tau_i}{b_i' \tau_i + 1} \qquad 8$$

If one assumes that the sorbent size distribution of the bed remains relatively unchanged with respect to the product, then

$$\tau = \frac{Ca_{bed}}{(Ca/S) S_{in}} \qquad 9$$

where: Ca_{bed} = moles of calcium in the bed

S_{in} = molar feed rate of sulfur to the bed (moles/sec)

(Ca/S) = calcium to sulfur molar ratio of the feed

Putting Eq. 8 into 7 and manipulating the resultant expression, one obtains:

$$\frac{1}{(Ca/S)} = \sum f_i D_i \left(\frac{1}{R} - \frac{S_{in}}{Ca_{bed} \sum f_i D_i b_i} \right) \qquad 10$$

Following the same approach as illustrated previously for the single-size model, the following expression can be derived from Eq. 10:

$$Ca/S = \frac{1}{\sum f_i D_i \left(\frac{1}{R} - \sum \frac{U_\gamma}{f_i D_i b_i H(1-R)(1-\beta)} \right)} \qquad 11$$

To use this methodology:

1. Determine the size distribution of the sorbent in a fluidized-bed. For each size category, determine the corresponding weight fraction and average particle size.

2. Determine the sorbent parameters D_i and b_i for each size interval of a given stone. These parameters are tabulated in the TEST RESULTS section of this handbook for selected sorbents at different particle sizes.

3. Determine the fluidized-bed parameter $(1-\beta)$ and γ using the equations from Section 7.1 and an averaged bed particle size. Because of the less dominate effect γ and $(1-\beta)$ played in projecting the sorbent performance, a more vigorous treatment to calculate γ and $(1-\beta)$ from a multiple-sized-particle bed is not warranted.

4. Select the desired fractional sulfur retention R. For the New Source Performance Standards of 90% removal of the sulfur in the coal feed, R = 0.90.

5. Calculate the predicted Ca/S ratio for the bed height, H, and fluidizing gas velocity, U, of the AFBC, using Eq. 11.

Numerical Example

The nominal values of the operating parameters for the fluidized-bed combustor and limestone ANL-9202 employed in this example are given in Table 7.3.1. The calculated values of other model parameters are also given in Table 7.3.1. The variation of sorbent parameters D (maximum fractional sulfation) and b (rate, sec^{-1}) with particle size is shown in Fig. 7.3.1. The size distribution of bed material used in this example is shown in Table 7.3.2.

Table 7.3.1 Values Employed for the Numerical Example Using ANL-9202

Operating Parameters		
Bed height	:	$H = 1.20$ meters
Fluidizing velocity	:	$U = 2.40$ meter/sec
Volume fraction of voidage in emulsion phase	:	$\varepsilon = 0.45$ estimated*
Volume fraction of inerts in bed	:	$F_I = 0.05$ estimated
Volume fraction of heat exchange tubes in bed	:	$F_H = 0.04$ estimated
Average sorbent particle diameter	:	$d_p = 0.00093$ meter
Sorbent particle density	:	$\rho_c = 1{,}800$ kg/m^3
Gas density	:	$\rho_g = 0.33$ kg/m^3
Acceleration of gravity	:	$g = 9.80$ m/sec^2
Gas viscosity	:	$\mu = 4.5 \times 10\text{-}5$ kg/m-sec
Bed diameter	:	$D_R = 1.82$ meter
Number of orifice openings in distributor plate	:	$N_D = 3580$
Bed area	:	$A = 3.34$ m^2

Calculated Data

Galileo number, $N_{Ga} = 2312$

Maximum bubble diameter, $D_{Bm} = 1.82$ m (bed diameter)

Minimum fluidization velocity, $U_{mf} = 0.194$ m/sec

Initial bubble diameter, $D_{BO} = 0.072$ m

Average bubble diameter, $\bar{D}_B = 0.237$ m

Gas exchange coefficient, $k_L = 0.453$ sec^{-1}

Linear bubble velocity, $U_b = 2.85$ m/sec

Bed height at minimum fluidization, $H_{mf} = 0.454$ m

Volume fraction of bubble phase, $\delta = 0.67$

β (defined by Eq. 7.1-10) = 0.83

γ (defined by Eq. 7.1-19) = 0.22

*See D. Kunii and O. Levenspiel, Fluidization Engineering, Wiley & Sons, New York (1969), Chapter 15.

Fig. 7.3.1

Particle Size Effect on Sorbent Parameters

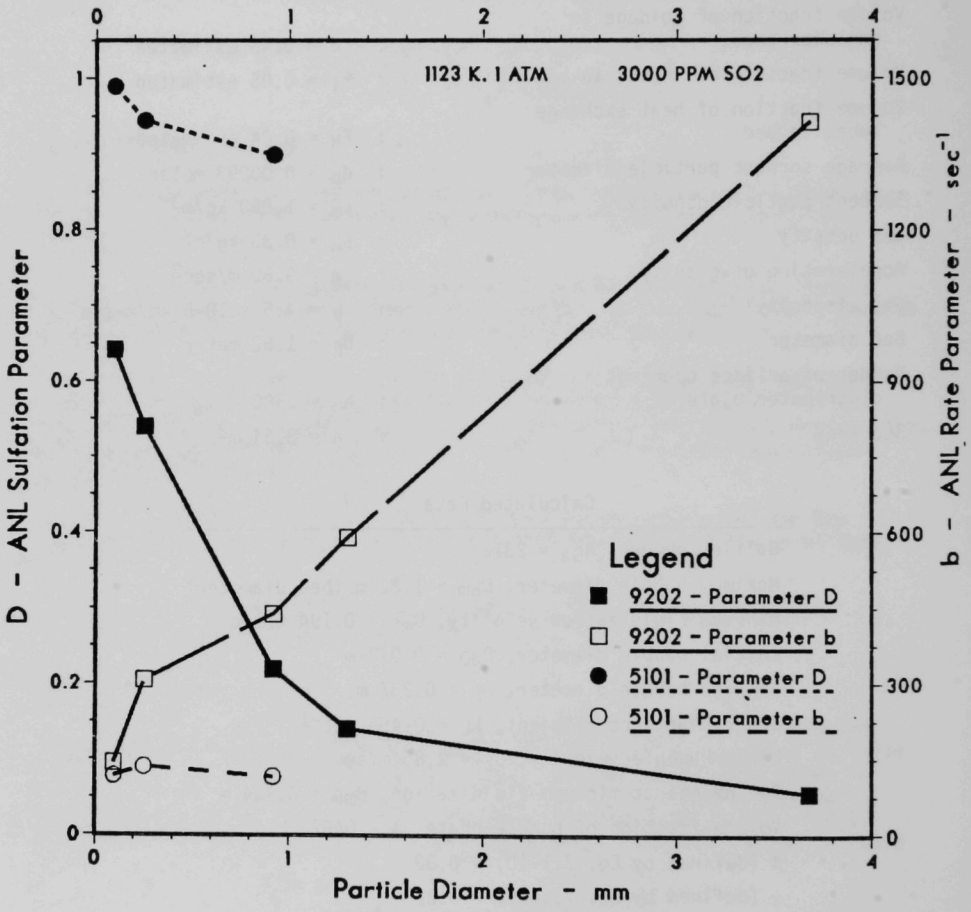

Fig. 7.3.2

Comparison of Single with Multiple Size Models on Projected Performance of Sorbent 9202

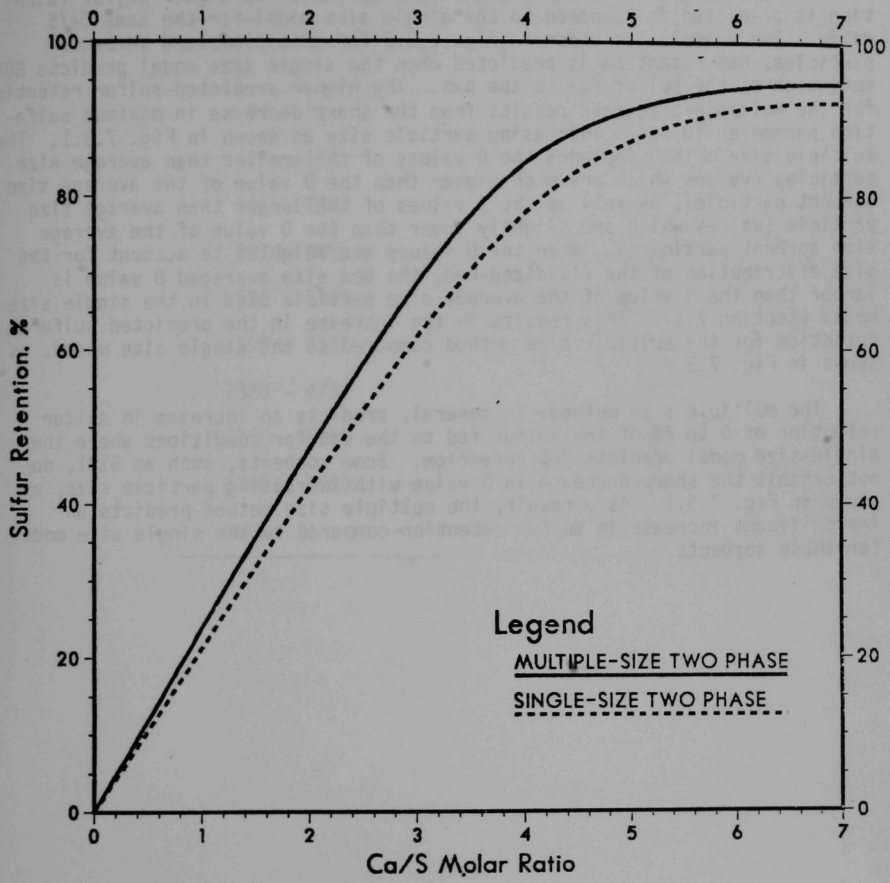

Fluidized Bed Operating Conditions

Temperature = 850. C = 1562. F

Pressure = 101. kPa = 1.0 atm

Fluidizing Velocity = 2.40 Meters/sec = 7.87 ft/sec

Bed Height = 1.20 Meters = 3.93 ft

Coal Feed Rate = 889.5 kg/hr = 1961.0 lb/hr

Sulfur Content in Coal = 3.87 wt%

Bed Area = 3.34 sq. meter = 36.0 sq.ft.

Sorbent Particle Dia. = 930. micron = 0.0394 inch

Discussion

For multiple-size sorbent particles a consistently higher sulfur retention is predicted as compared to the single size model for the same Ca/S ratio. For example, as shown in Fig. 7.3.2 for multiple-sized sorbent particles, 86% retention is predicted when the single size model predicts 80% retention of the sulfur fed to the bed. The higher predicted sulfur retention for the multiple-size case results from the sharp decrease in maximum sulfation parameter (D) with increasing particle size as shown in Fig. 7.3.1. The multiple size method includes the D values of the smaller than average size particles (values which are much higher than the D value of the average size sorbent particle), as well as the D values of the larger than average size particle (values which are slightly lower than the D value of the average size sorbent particles). When the D values are weighted to account for the size distribution of the fluidized-bed, the bed size averaged D value is larger than the D value of the average size particle used in the single size model (Section 7.1). This results in the increase in the predicted sulfur retention for the multiple size method compared to the single size model, as shown in Fig. 7.3.2.

The multiple size method, in general, predicts an increase in sulfur retention of 0 to 6% of the sulfur fed to the bed for conditions where the single-size model predicts 80% retention. Some sorbents, such as 5101, do not exhibit the sharp decrease in D value with increasing particle size, as shown in Fig. 7.3.1. As a result, the multiple size method predicts an insignificant increase in sulfur retention compared to the single size model for these sorbents.

Table 7.3.2 Particle Size Distribution for the Babcock & Wilcox 6 x 6 ft Combustor Series 4, Test 1

Particle Diameter d_p, μm	Weight Fraction
44 - 74	0
74 - 149	0.001
149 - 297	0
297 - 595	0.001
595 - 1190	0.247
1190 - 2380	0.389
2380 - 4750	0.281
4750 - 6350	0.073
6350 - 9500	0.008
9500+	0

NOMENCLATURE

A = cross-sectional area of the bed, m^2

b_i = reaction rate parameter of sorbent particle size fraction i, sec^{-1}

Ca_{bed} = moles of calcium in the bed, mole

D_i = maximum fractional conversion parameter of the sorbent particle size fraction i, ---

d_p = particle diameter, m

$\bar{D}_B$ = average bubble diameter in the bed, m

D_{Bm} = maximum bubble diameter in the bed, m

D_{BO} = initial bubble diameter, m

D_R = bed diameter, m

E = exit age distribution function, sec^{-1}

F_I = volume fraction of inert particles (char, ash, rocks, etc.) in the bed

F_H = volume fraction of heat transfer surface in bed

g = acceleration due to gravity, 9.80 m/sec^2

k_L = gas exchange coefficient between the bubble phase and emulsion phase, sec^{-1}

H = height of expanded bed, m

H_{mf} = bed height at the minimum fluidization condition, m

$(N_{Re})mf$ = Reynolds number at the minimum fluidization condition, ---

N_{Ga} = Galileo number

N_D = total number of orifice openings on the distributor, ---

R = fractional sulfur retention in the bed, ---

t = time

S_{in} = molar flow rate of sulfur at the bed-inlet, mole/sec

U = superficial gas velocity, m/sec

U_{mf} = minimum fluidization velocity, m/sec

U_b = linear bubble velocity, m/sec

Greek Letters

α_i = fractional extent of sorbent conversion at time t, ---

β = fractional volume in the bed not occupied by sorbent particles, ---

γ = gas exchange parameter, defined by Eq. 19

δ = volume fraction of the bubble phase in the bed, ---

ϵ = emulsion phase fractional voidage, ---

ρ_C = molar density of calcium in the sorbent, mole/m^3

$\bar{\alpha}_i$ = conversion of sorbent particle size fraction

ρ_p = density of the sorbent, kg/m^3

ρ_g = density of the gas, kg/m^3

τ_i = average residence time in the bed of the sorbent of sorbent particle size fraction i

μ = viscosity of the gas, kg/m sec

7.4 LIMITATIONS OF THERMOGRAVIMETRIC ANALYZER DATA

The ANL model predictions of sorbent performance in a fluidized-bed combustor is based on thermogravimetric analyzer (TGA) data. However, even though great care is taken in an attempt to make the conditions identical in the TGA and combustor in terms of temperature, CO_2, SO_2, and N_2 pressure, etc., the calcination/sulfation conditions are apparently different in the TGA and in the fluidized-bed combustors.

Part of the difference between TGA and FBC appears in the utilization of the calcium in the sorbent. The maximum calcium utilization achieved in the combustor is higher than in the TGA test. For example, Lowellville limestone achieves a maximum utilization of only 32% of the calcium in the TGA test while utilizations of 36% were reported in the B&W 6' x 6' combustor at steady-state conditions [Babcock and Wilcox (1978)]. A difference in the maximum utilization of this magnitude would increase the predicted sulfur retention for sorbent 9202, at a Ca/S feed ratio of 3.0, of 5 to 8% of the sulfur fed to the bed operated under the conditions shown in Table 7.4.1. A similar difference in maximum calcium utilization between a small laboratory fixed bed reactor and combustor has been noted previously [Bethell et al. (1973)].

Table 7.4.1 Fluidized Bed Operating Conditions[a,b]

	B&W 6' x 6'
Fluidizing Velocity, m/sec	2.44
Bed Height, m	1.20
Bed Area, m^2	3.34
Coal Feed Rate, kg/h	900
Sulfur Content in Coal, %	3.6
Avg. Sorbent Particle Diameter in Bed, mm	1.0

[a]Temperature - 850°C, pressure - 1 atm, sorbent - Lowellville limestone (93 wt % $CaCO_3$; 2 wt % $MgCO_3$; calcine density - 1700 kg/m^3)

[b]Additional data used in the comparison are as follows: $\varepsilon = 0.45$, $F_I = 0.05$, $F_H = 0.04$, $\mu = 4.5 \times 10^{-5}$ kg/m-s, $\rho_g = 0.33$ kg/m^3, and $N_D/A = 1070$ openings/m^2

These differences between the standard TGA test results and the fluidized-bed combustor results may arise from differences in calcination/sulfation conditions, the presence of coal ash, oxidizing and reducing zones and/or sorbent particle attrition in the combustor, and/or difficulties in characterizing a particular quarry based on a limited number of samples.

Calcination/Sulfation Conditions

The reaction of limestone ($CaCO_3$) with SO_2 as a fairly simple process. The reaction generally takes place in two separate steps: the $CaCO_3$ is first calcined at a high temperature to form CaO and the resultant product subsequently reacts with SO_2 to form $CaSO_4$. The two chemical reactions involved are:

$$CaCO_3(s) \rightarrow CaO(s) + CO_2(g) \qquad 1$$

$$CaO(s) + SO_2(g) + 1/2\ O_2(g) \rightarrow CaSO_4(s) \qquad 2$$

The pore structure which forms due to CO_2 loss on calcination plays a dominant role in determining the sulfation capacity and the reactivity of the sorbent with sulfur dioxide. The $CaSO_4$ produced, which has a high molar volume, blocks the gas diffusional paths along pores in the sorbent particles, causing reaction to virtually cease. In general, not all of the CaO in the sorbent reacts with SO_2 (i.e., sorbent utilization is less than 100%).

Stones calcined/sulfated in a combustor have a larger average pore diameter than when calcined in a simulated flue gas in a TGA. The larger pore diameter is consistent with the higher capacity for sulfur dioxide in that more sulfation may occur before the pore plugs. The pore structure depends on temperature, carbon dioxide pressure and impurity level.

The lower temperature limit for calcination is set from thermodynamic considerations. Calcinations by Dowdy et al. (1976) reveal that calcination of $CaCO_3$ will cease at temperatures lower than about 770°C. Consequently, if the fluidized bed is operated below this critical temperature, the reaction of SO_2 will take place by direct involvement of limestone,

$$CaCO_3(s) + SO_2(g) + 1/2\ O_2(g) \rightarrow CaSO_4(s) + CO_2(g) \qquad 3$$

Since the sulfur capture rate of CaO is much faster in comparison to $CaCO_3$ under the same conditions, the temperature of limestone utilization is set above the calcination temperature of $CaCO_3$.

Increasing the calcination temperature increases the capacity of the sorbent for sulfur dioxide retention under the same sulfation conditions as shown in Fig. 7.4.1. Calcining the sorbent at 950°C brings about a 31% increase in maximum sulfation compared to calcination at 850°C. The sorbent sulfation

Fig. 7.4.1 Sorbent 9202 TGA Data

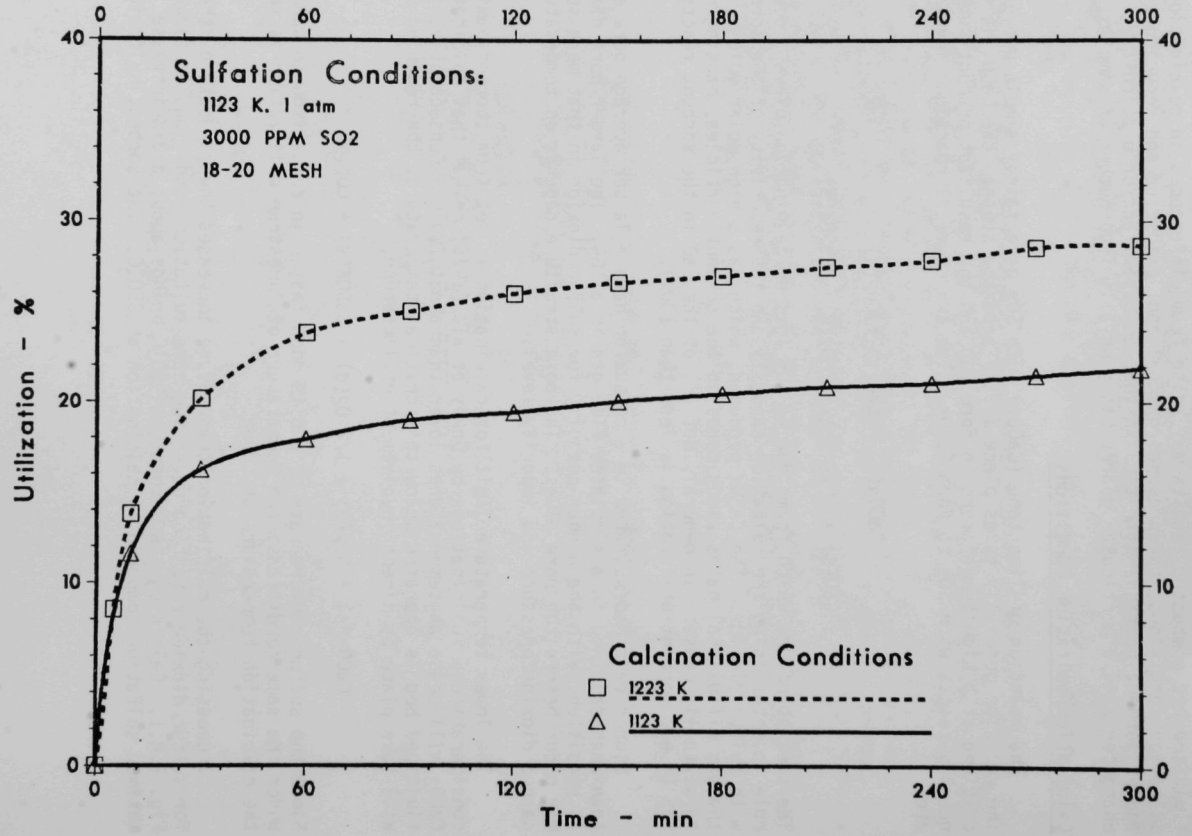

capacity is also expected to increase with increasing P_{CO_2} up to the thermodynamic equilibrium [O'Neil et al. (1976)]. The sorbent sulfation capacity is affected, in addition, by the the impurity level, principally in the form of coal ash.

Coal Ash

The sorbent behavior depends on the type of coal as shown in Fig. 7.4.2. The temperature of maximum sulfation is different for different coals although the same sorbent and some operating conditions (3 ft/sec fluidizing velocity, 3% excess O_2, limestone 1359) were used. This different temperature of maximum sulfation may depend on the characteristics of the coal ash. At lower temperatures, the rise in sulfur retention is probably set by the rates of calcination and reaction of SO_2 with CaO to form $CaSO_4$. The reason for the decrease in sulfur retention at temperatures above the maximum is not yet well understood. One theory is that the coal ash begins to slag and fill the pores of the sorbent, and thus reducing its sulfation capacity. A second theory focuses on sintering where the crystal structure of the sorbent changes to a less reactive form with decreasing porosity as the temperature is increased. Both theories tend to imply that the process is irreversible, although results from the National Coal Board [NCB (1979)] suggest otherwise.

Calcination/sulfation in the presence of coal ash affects the TGA results (Fig. 7.4.3) in addition to the combustor results (Fig. 7.4.2). Experiments were carried out to study the effect of coal ash on calcination/sulfation. A sample of the sorbent (9202 Lowellville) was mixed with Sewickley coal ash (previously oxidized at 800°C in air) in a ratio of 1 to 1 by weight. The standard ANL procedure for testing sorbents with a TGA was used (see STANDARD TESTS, Section 3.1). Table 7.4.2 lists the composition of the Sewickley coal ash and Lowellville limestone that were used.

Figure 7.4.3 shows the sorbents' sulfation reactivity and capacity in the presence of coal ash. The maximum sulfation is nearly 40% or more for stone sulfated with the ash than without. This is contrary to the expectation of poremouth plugging by ash during the reaction. Further studies using larger particle size (5-6 mesh) confirm this observation (Fig. 7.4.4) where a 61% increase in sorbent sulfation with the coal ash is observed.

Additives such as NaCl, $CaCl_2$, Na_2CO_3, etc. are known to alter the pore structure of limestone in a way beneficial to sulfation [Shearer et al, (1979, 1979[a], 1980)]. Study of the coal and ash compositions reveals the presence of several of these elements (Na, K, Cl, etc.) at concentration levels sufficient to produce effects of enhancement. Further, Yang et al, (1978) studied the catalytic effect of Fe_2O_3 on the CaO sulfation reaction with SO_2. A two-fold increase in the sorbent sulfation capacity with 4 wt % Fe_2O_3 was reported. Mixing sorbent with the coal ash from Illinois No. 6 showed similar improvement. Thus the effect of coal ash on sorbent properties may contribute to the difference between TGA and combustor results.

Table 7.4.4 Chemical Analysis

Mineral Analysis	Sewickley Coal Ash	Lowellville Limestone
$CaCO_3$	--	93.2
$MgCO_3$	--	1.58
SiO_2	40.37	1.84
Al_2O_3	22.10	1.12
TiO_2	0.76	--
Fe_2O_3	19.86	0.718
CaO	4.14	--
MgO	2.07	--
K_2O	1.40	0.18
Na_2O	0.57	0.032
SO_3	6.69	--
P_2O_5	0.24	--
SrO	0	--
BaO	0.14	--
Mn_3O_4	1.57	--

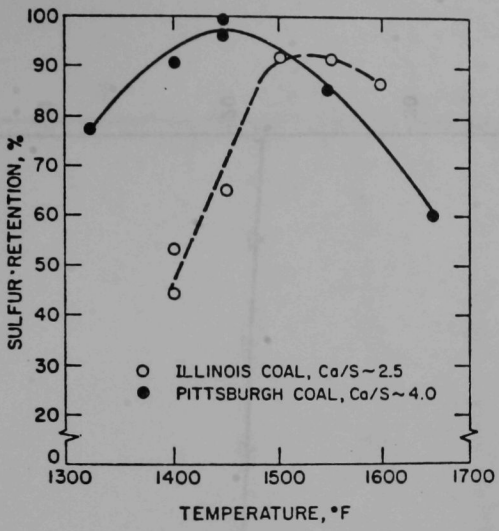

Fig. 7.4.2. Effect of Fluidized-Bed Temperature on Sulfur Retention in a 6-in. Combustor (gas velocity, 3 ft/sec excess oxygen, about 3%, limestone no. 1359). [Joulle, et al. (1972)].

Fig. 7.4.3 Sorbent 9202 TGA Data

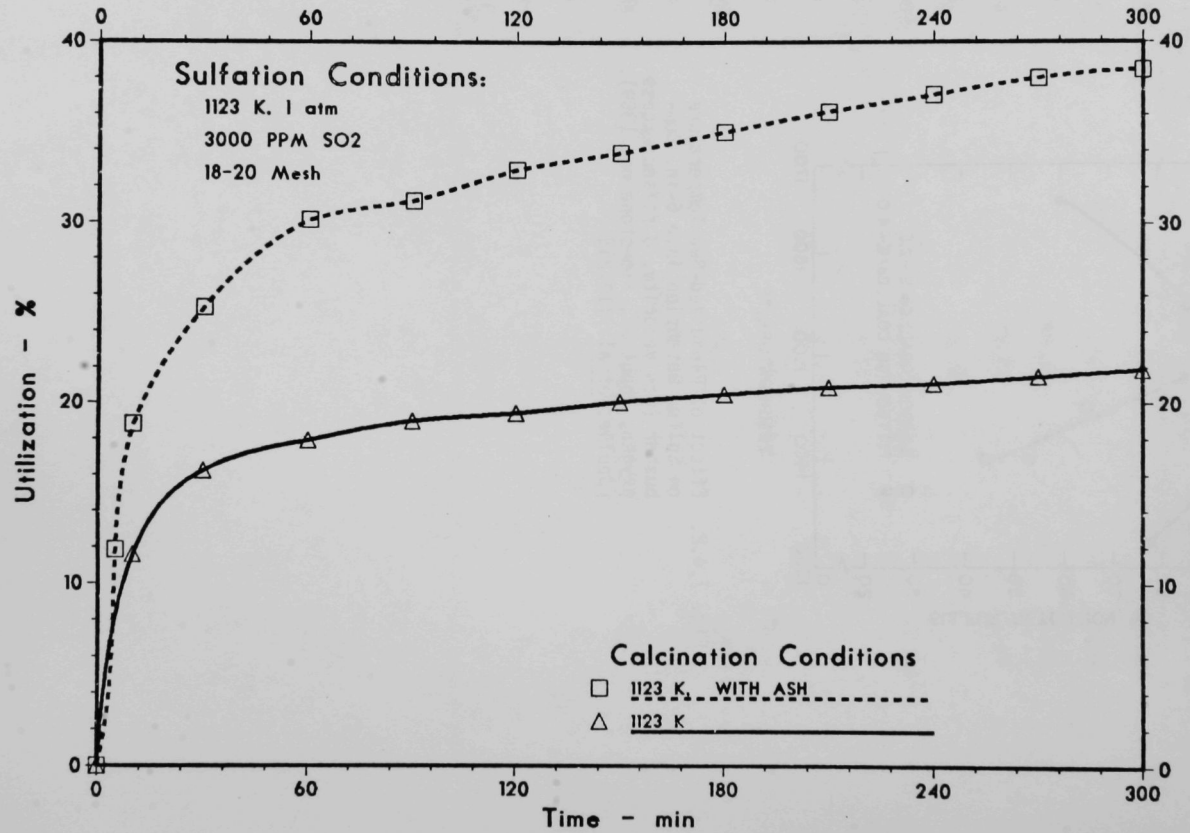

Fig. 7.4.4 Sorbent 9202 TGA Data

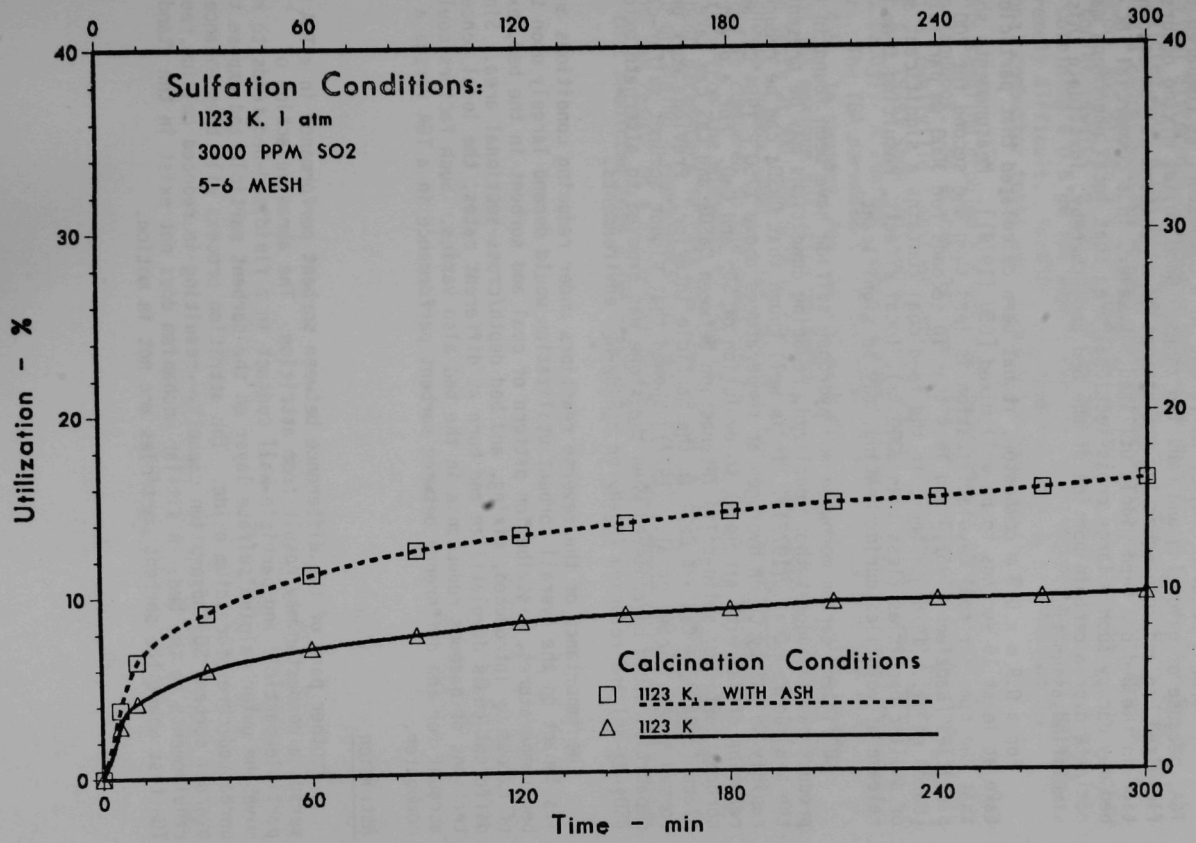

Oxidizing and Reducing Zones

The sorbent behavior may be different in a combustor, as compared to a TGA, because of oxidizing and reducing zones. Good solids mixing occurs in fluidized bed and, consequently, the assumption of uniform solids concentration in the bed has been widely utilized. However, in a commercial FBC, the bed may occupy such a large cross-sectional area that local phenomena may dominate over a certain portion of the bed and, thereby, invalidate this simplified assumption.

For a 0.9 m x 0.9 m combustor, it has been calculated that particles take at least 15 seconds to be well mixed [OSU (1979)]. Measurements show that the time for coal devolatilization is less than one second for 200 μm particles [Badzioch (1961)] and less than 10 seconds for 3000 μm particles [Baron et al., (1978)]. Thus, if the feed coal contains a significant amount of smaller particles (less than 3000 μm), local effects, resulting from the release of volatiles during heating, may be significant.

Sufficient carbon monoxide and hydrogen sulfide have been found in the product gas to suggest that localized, reducing conditions may be present in the bed [Jonke et al. (1972)]. It is well known that $CaSO_4$ can be reduced rapidly to CaS by CO or hydrogen at temperatures above 1750°F (954°C), and reaction of CaS with air leads to evolution of SO_2 and CaO. For a given sorbent particle, solid-solid interaction between $CaSO_4$ and CaS can take place ($3\ CaSO_4 + CaS \rightarrow 4\ CaO$) in the particle interior. Previous work performed by ANL [Vogel et al., (1977)] showed that higher sorbent sulfur-capture capacities could be achieved when the stone was exposed to alternate oxidizing (SO_2-O_2-N_2) and reducing (H_2-N_2 or H_2S-H_2-N_2) environments.

The importance of the reverse reactions under reducing conditions and its impact on the overall sorbent utilization would depend largely upon the bed temperatures, distribution pattern of coal and sorbent in the bed, extent of excess O_2 introduced, mixing, and bed depth/cross-sectional area. Since different coals devolatilize and burn at different rates, the local concentrations of gaseous reductants in the bed also varies. Such factors could account for the difference between sorbent performance in a TGA versus a combustor.

Attrition

Another part of the difference between sorbent performance in a TGA versus a combustor may result from attrition. The abrasive action of particle-particle and particle-wall contact in a fluidized-bed tends to remove the outer calcium sulfate layer on the sorbent particle and expose the unreacted core of calcium oxide. The attrition process will thus enhance the overall sorbent SO_2 adsorption capacity--resulting in reduced calcium feed requirements to the bed. A similar mechanism does not exist in the standard TGA test where the sorbent particles are not in motion.

Sampling

A final difference between sorbent performance in a combustor versus that predicted from a TGA experiment may be due to the inherent problem of obtaining a representative sorbent sample for TGA analysis. For example, in the Babcock and Wilcox 6 x 6 ft AFBC at Alliance, Ohio, a sorbent feed rate of 0.5 ton/hr results in 100 tons of sorbent usage in a typical 200 hour test. Obtaining a 0.5 gm TGA sample which is representative of the 100 tons is extremely difficult. Further, the sampling problem is compounded by additional combustor tests over a period of many years.

This sampling problem has not been addressed in preparing the TGA data in this handbook. No attempt has been made for example, to obtain a representative Lowellville limestone sample, even though Babcock and Wilcox data (Apa et al. 1979) show considerable variability in the limestone (87 to 93 wt % $CaCO_3$). A limited number of Lowellville samples have been analyzed, however. The TGA parameters for two such Lowellville samples are shown in Fig. 7.4.5. In summary, for -18 +20 mesh (840-1000 μm), the value of the critical TGA maximum sulfation parameter, D, varied from 0.22 to 0.28 in limited tests at ANL and 0.22 to nearly 0.40 in more extensive tests at Westinghouse (Newby, 1981). The combustor performance data of Lowellville limestone is compared to the predicted values using the (TGA derived) sorbent parameters from the midpoint of this range. Obviously, the large variability of sorbent parameters in this one case indicates that some attention must be paid to obtaining a representative sample for TGA analysis in the future. Sampling can result in a difference between sorbent performance in a combustor versus that predicted from a TGA experiment.

Fig. 7.4.5

Comparison of Parameters for Two Samples of Sorbent 9202

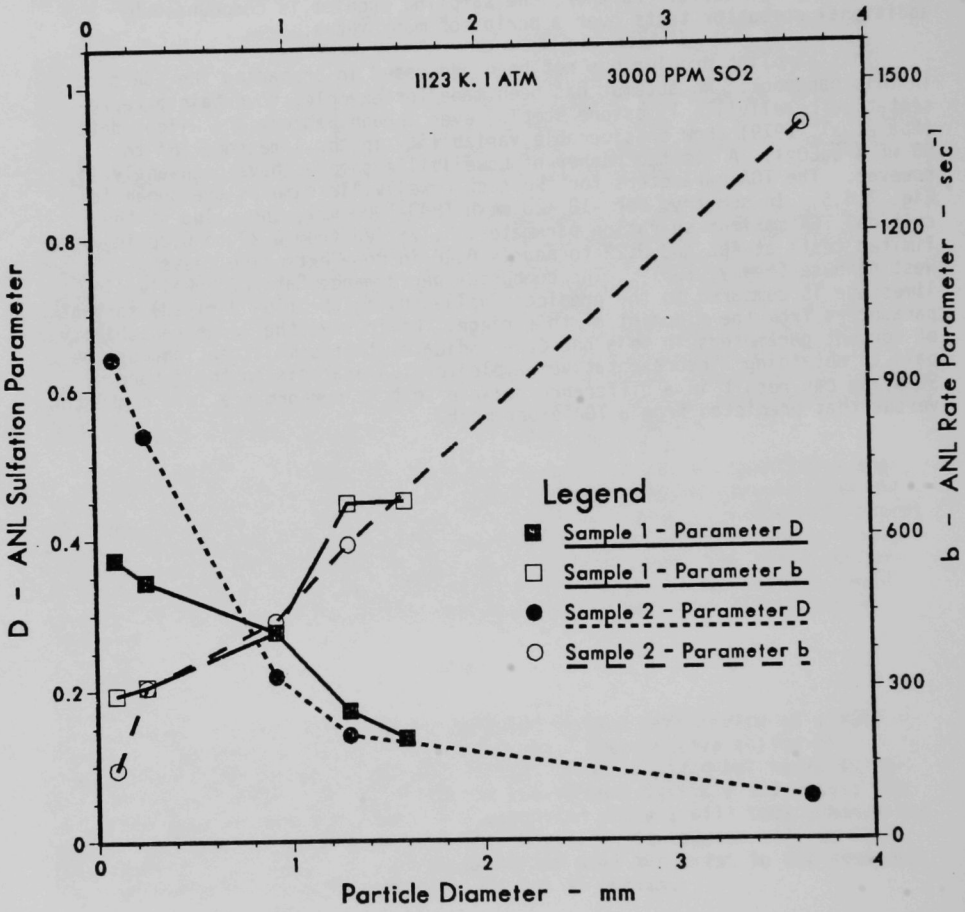

References for Section 7.4

Apa, R. P. et al., "Fluidized-Bed Combustion Development Facility and Commercial Utility AFBC Design Assessment," Babcock & Wilcox Quarterly Report, LR:79:4775:01, January-March 1979.

Badzioch, S., British Coal Utilization Reserch Association Monthly Bulletin 25, 285 (1961).

Baron, R. E., J. L. Hodges, and A. F. Sarofim, AIChE Symposium Series 74, 176 (1978).

Dowdy et al., EPRI PFP-308, Vol. III: Appendices 3A-1 to 3A-3 and 6A-1 to 6A-9 (1976).

Jonke, A. A. et al., "Pollution Control Capabilities of Fluidized-Bed Combustion, AIChE Symposium Series 68(126) 241 (1972).

NCB, "Reduction of Atmospheric Pollution," National Coal Board Report, Vol 1, September 1979.

Newby, R. A., Westinghouse R&D Center, Pittsburgh, PA, private communication, March 1981.

OSU Quarterly Progress Report for January 1, 1979 to March 31, 1979, Supplement to Babcock and Wilcox Quarterly Report, 1979.

O'Neill, E. P., D. L. Keairns, and W. F. Kittle, Thermochem. Acta 14, 209 (1976).

Shearer, J. A., J. F. Lenc, Irving Johnson, and C. B. Turner, "The Effect of Sodium Carbonate on the Reaction of SO_2/O_2 Mixtures with Carbonate Rocks," Argonne National Laboratory Report No. ANL/CEN/FE-79-11, July 1979.

Shearer, J. A., Irving Johnson, and C. B. Turner, "Effects of Sodium Chloride on Limestone Calcination and Sulfation in Fluidized-Bed Combustion," Environ. Sci. Tech. 13, 1113-1118 (1979).

Shearer, J. A., Irving Johnson and C. B. Turner, "The Effects of $CaCl_2$ on Limestone Sulfation in Fluidized-Bed Coal Combustion," Thermochem. Acta 35, 105-109 (1980).

Vogel, G. J. et al. "Supportive Studies in Fluidized-Bed Combustion," Argonne National Laboratory Report, ANL/ES-CEN-1019 and FE-1780-7 (1977).

Yang, R. T., M. Shen, and M. Steinberg, Environ. Sci. Tech. 12, 915 (1978).

7.5 ATTRITION

For both pneumatic transport to the bed and fluidization in the bed the attrition characteristics of a sorbent are an important consideration in determining the overall suitability of the sorbent. Attrition is the process whereby the particle size is reduced either by abrasion (the wearing away of surface material) or by breakup due to particle-particle or particle-wall collisions, or by breakup arising from thermal shock and decrepitation during calcination. Small diameter particles produced by attrition are rapidly elutriated from the bed. In severe cases, replacing the attrition losses (so as to maintain a constant bed height) requires a higher sorbent feed rate than necessary for sulfur capture. Avoiding this unwarranted additional operating cost requires consideration of the attrition behavior of a sorbent. A model has been developed which deals with both aspects of attrition as follows [Fan and Strivastava (1981), Wilson et al. (1981)]:

a) Abrasion and Collision-Induced Breakup - The ANL attrition model can be applied equally well to attrition both in the fluidized bed and in the pneumatic transport lines carrying sorbent to the bed.

b) Calcination Induced Breakup - The amount of sorbent breakup arising from thermal shock and decrepitation during calcining is derived from the standard attrition test.

A. Abrasion and Collision-Induced Breakup

The theories in the literature describing the rate of disintegration of solid particles due to attrition are primarily based on the population balance models of grinding and comminuation processes [Merrick and Highly (1974), Austin et al. (1976), Wei et al. (1977)]. models, in essence, are deterministic. Recently, Fan and Srivastava (1981) proposed a stochastic model to account for the particle disintegration based on the grinding mechanism for attrition. Because the process of attrition is a complex phenomenon which involves various factors such as hardness, abrasion resistance and the impact elasticity of the crystallites, and imperfections in the structure, it appears that the model based on the probabilistic approach can be considered to be a viable alternative to the deterministic models.

The following assumptions are used in the development of the probabilistic model:

(1). The particles in the system can be divided into four size fractions where size 4 is the largest and size 1 is the smallest as follows:

Size, k	Average Diameter (m)	Average Weight at Time, t (g)
1	D_1	$W_1(t)$
2	D_2	$W_2(t)$
3	D_3	$W_3(t)$
4	D_4	$W_4(t)$

(2) The particle disintegration is such that the abrasive removal of material occurs only from the surface of the particle. Thus, the disintegration of particles of size k (k = 4, 3) will generate a particle of size k-1 and a large number of particles of size 1.

Disintegration of a Particle of Size k. Since the total mass of the system remains unchanged during the course of particle disintegration, the following equation holds for particle disintegration from size k to size k-1:

$$X_{k1}D_1^3 + D_{kk-1}^3 = D_k^3 \qquad 1$$

where X_{k1} is the number of particles of size 1 generated from the disintegration of a particle from size k to k-1.

Thus, X_{k1} can be expressed by

$$X_{k1} = \frac{D_k^3 - D_{k-1}^3}{D_1^3}, \quad k = 3,4 \qquad 2$$

and X_{21} can be expressed by

$$X_{21} = \frac{D_2^3}{D_1^3} \qquad 3$$

The total number of particles of size 1 generated by particle disintegration from size k to size 1 becomes:

$$X^*_{k,1} = \sum_{i=0}^{k=2} X_{(k-1)1}, \quad k = 3,4 \qquad 4$$

It is assumed that the probability of transition size i → size i - 1 in the time interval (t, t + h) is $\lambda_i h + O(h)$, where λ_i is a constant and O(h) is a function of h such that $O(h)/h \to 0$ as $h \tau 0$. It is also assumed that the probability of a transition size i → size i - j, j > 1 in the time interval (t, t + h) is O(h).

Let

$P_{ki}(t)$ = Prob. (the particle is in size i at time t given that it was in size k at time t = 0); i = 1,....k. 5

Taking a probability balance over size k yields

$$p_{kk}(t+h) = P_{kk}(t) \quad [1-\lambda_k h + o(h)] \qquad 6$$

When h approaches zero, Eq. 6 becomes

$$\frac{dP_{kk}(y)}{dt} = -\lambda_k P_{kk}(t) \qquad 7$$

The initial condition for Eq. 7 is

$$P_{kk}(0) = 1 \qquad 8$$

Equations 7 and 8 yield

$$P_{kk}(t) = e^{-\lambda_k t} \qquad 9$$

Likewise, the probability balance over size k-1 gives rise to

$$P_{k(k-1)}\ (t + h) = P_{k(k-1)}(t)\ [1 - \lambda_{k-1}h + o(h)] + P_{kk}\ (t)\lambda_k h + o(h) \qquad 10$$

When h approaches zero, Eq. 10 becomes

$$\frac{dP_{k(k-1)}(t)}{dt} = \lambda_{k-1}\ P_{k(k-1)}\ (t) + \lambda_k P_{kk}(t) \qquad 11$$

Substituting Eq. 10 into Eq. 11, we have

$$\frac{dP_{k(k-1)}(t)}{dt} + \lambda_{k-1} P_{k(k-1)}(t) = \lambda_k\ e^{-\lambda_k t} \qquad 12$$

The initial condition for Eq. 12 is

$$P_{k(k-1)}(0) = 0 \tag{13}$$

Thus, Eqs. 12 and 13 give rise to the solution for $P_{k(k-1)}$ as

$$P_{k(k-1)}(t) = (-1)\lambda_k \left\{ \frac{e^{-\lambda_k t}}{\lambda_k - \lambda_{k-1}} + \frac{e^{-\lambda_{k-1} t}}{\lambda_{k-1} - \lambda_k} \right\} \tag{14}$$

The expression for $P_{k(k-2)}(t)$ can be obtained in a similar manner as follows:

$$P_{k(k-2)}(t) = \lambda_k \lambda_{k-1} \left\{ \frac{e^{-\lambda_k t}}{(\lambda_k - \lambda_{k-1})(\lambda_k - \lambda_{k-2})} + \frac{e^{-\lambda_{k-1} t}}{(\lambda_{k-1} - \lambda_k)(\lambda_{k-1} - \lambda_{k-2})} + \frac{e^{-\lambda_{k-2} t}}{(\lambda_{k-2} - \lambda_{k-1})(\lambda_{k-2} - \lambda_k)} \right\} \tag{15}$$

Thus, for k of 2, 3 and 4, Eqs. 9, 14 and 15 give rise to:

$$P_{44}(t) = e^{-\lambda_4 t} \tag{16}$$

$$P_{43}(t) = \lambda_4 \left\{ \frac{e^{-\lambda_4 t}}{\lambda_4 - \lambda_3} + \frac{e^{-\lambda_3 t}}{\lambda_3 - \lambda_4} \right\} \tag{17}$$

$$P_{42}(t) = \lambda_4 \lambda_3 \left\{ \frac{e^{-\lambda_4 t}}{(\lambda_4 - \lambda_3)(\lambda_4 - \lambda_2)} + \frac{e^{-\lambda_3 t}}{(\lambda_3 - \lambda_4)(\lambda_3 - \lambda_2)} + \frac{e^{-\lambda_2 t}}{(\lambda_2 - \lambda_3)(\lambda_2 - \lambda_4)} \right\} \tag{18}$$

$$P_{33}(t) = e^{-\lambda_3 t} \tag{19}$$

$$P_{32}(t) = -\lambda_3 \left\{ \frac{e^{-\lambda_3 t}}{\lambda_3 - \lambda_2} + \frac{e^{-\lambda_2 t}}{\lambda_2 - \lambda_3} \right\} \qquad 20$$

$$P_{22}(t) = e^{-\lambda_2 t} \qquad 21$$

It is reasonably postulated that the larger the particle size, the greater is the rate of disintegration for the particle. [Merrick and Highly (1974), Wei et al. (1977)]. Thus, the following inequality is valid:

$$\lambda_4 > \lambda_3 > \lambda_2 \qquad 22$$

Assuming that the intensity of disintegration for size i particle, λ_i, is linearly proportional to the volume of the same size particle and the proportionality constants for all size particles are identical, we have

$$\lambda_{i-1} = \left(\frac{D_{i-1}}{D_i}\right)^3 \lambda_i, \; i = 2, 3, 4 \qquad 23$$

and

$$\lambda_1 = 0$$

Thus, λ_4 is the only undetermined or adjustable parameter in the model. Further, λ_4 can be correlated as functions of operating parameters and the physical characteristics of the sorbent.

Disintegration of Multi-Sized Particles. The disintegration of multi-sized particles in the system is also described by this model. Suppose at time t = 0, there are $N_i(0)$, i = 2, 3, 4, particles in size i in the system. We will assume that the particles behave independently during the integration process [Fan and Srivastava (1981), Fan et al. (1979), Nassar et al. (1980)].

Let $N_i(t)$, i = 2, ... k, denote the number of particles in size i at time t > 0. $N_{ij}(t)$ denotes the number of particles in size j at time t > 0 resulting from $N_i(0)$ in size i at time t = 0.

Given the initial number of particles in size k and number of particles in size i, i = 2 ... k, at time t, the number of particles in size 1 at time t can readily be obtained from the mass balance of the particles. Thus we have:

$$N_{k1}(t) = E\,[N_{k1}(t)] = [N_k(0) - n_{kk}(t)]\, X_{k1} + [N_k(0) - n_{kk}(t) - n_{k(k-1)}(t)]\, X_{(k-1)i} + \ldots + [N_k(0) - n_{kk}(t) \ldots - n_{k2}(t)]\, X_{21} \qquad 24$$

where n_{ki} is the expected value of N_{ki}.

The expected number of particles in size i at time t can be obtained from binominal consideration as:

$$n_{kj}(t) = E\,[N_{kj}(t)] = N_k\,(0)\;\; P_{kj}(t),\; j = 2, \ldots k \qquad 25$$

The expected total weight of the particles in size j at time t thus becomes

$$w_{kj}(t) = n_{kj}(t)\,\frac{\pi}{6}\,D_j^3\,\rho_p \qquad 26$$

and

$$w_{k1}(t) = n_{k1}(t)\,\frac{\pi}{6}\,D_1^3\,\rho_p \qquad 27$$

where n_{k1} is given by Eq. 24 and ρ_p is the density of the particle.

Let $N_{k1}(t)$ denote the number of particles in size j. Clearly, we have

$$N_j(t) = \sum_{i=j}^{k} N_{ij}(t) \qquad 28$$

The expected number of particles of size j at time t can be obtained from binomial consideration as

$$n_j(t) = \sum_{i=j}^{k} N_i(0)\;P_{ij}\;(t),\; j = 2, \ldots, k \qquad 29$$

For example, for four particle sizes this becomes

$$n_j(t) = \sum_{i=j}^{4} N_i(0)\;P_{ij}(t),\; j = 2, 3, 4 \qquad 30$$

$$n_4(t) = N_4(0)\;P_{44}(t) \qquad 31$$

$$n_3(t) = N_4(0)\;P_{43}(t) + N_3(0)\;P_{33}(t) \qquad 32$$

$$n_2(t) = N_4(0)\;P_{42}(t) + N_3(0)\;P_{32}(t) + N_2(0)\;P_{22}(t) \qquad 33$$

The expected weight of the particles in class j at time t thus becomes

$$w_j(t) = E\,[w_j(t)] = n_j(t)\,\frac{\pi}{6}\,\rho_p\,D_j^3 \qquad 34$$

The initial total weight in the system $W_T(0)$ is given by

$$w_T(t) = \sum_{i=1}^{k} W_1(0) = \sum_{i=1}^{k} N_i\ (0)\frac{\pi}{6}\ \rho_p\ {}_iD^3 \qquad 35$$

Thus, the weight of particles in class 1 at time t can be readily obtained from the mass balance as

$$w_1(t) = w_T(0) - \sum_{i=2}^{k} W_1(t) \qquad 36$$

and

$$n_1(t) = \frac{6w_1(t)}{\pi\rho_p\ D_1^3} \qquad 37$$

B. Calcination Induced Breakup

Breakup of sorbent material due to thermal shock and decrepitation during calcining (after being introduced to a fluidized-bed) also produces finely sized material. The extent of breakup due to shock calcination is determined from the standard attrition test as discussed in the TEST RESULTS SECTION.

C. Numerical Example

The data in Table 7.5.1 are the nominal values of the particle properties which are employed for two numerical examples. The examples deal with attrition resulting from abrasion and collision-induced breakup. The first example is for attrition during pneumatic transport. The second example is for attrition of the fluidized-bed material.

Pneumatic Transport. Given λ_4 and D_i in the table, λ_2 and λ_3 can be evaluated by Eq. 23 as follows:

$$\lambda_2 = 0.04550$$

$$\lambda_3 = 0.1866 \qquad 38$$

Table 7.5.1. Nominal Values of the Particle Properties in the Feed Hopper Employed for the Numerical Example

$\lambda_4 = 1$, sec^{-1}

$\rho_p = 2$, kg/m^3

	D_i, μ			
	50 (i = 1)	250 (i = 2)	400 (i = 3)	700 (i = 4)
$N_i(0)$	20	50	70	100
$w_i(0)$, kg	2.618×10^{-9}	8.180×10^{-7}	4.690×10^{-6}	3.590×10^{-5}

For the given t of 1, the probability that the particle is in size i at time t was in size k at time zero, p_{ki} (t), can be obtained by Eqs. 16 through 21 as given below:

$$P_{44}(1) = 0.3679$$

$$P_{43}(1) = 0.5678$$

$$P_{42}(1) = 0.06300$$

$$P_{33}(1) = 0.8298$$

$$P_{32}(1) = 0.1660$$

$$P_{22}(1) = 0.9555 \qquad 39$$

Likewise, the probability $P_{ki}(t)$ for the given t of 5 can be obtained as given below:

$$P_{44}(5) = 0.006738$$

$$P_{43}(5) = 0.4753$$

$$P_{42}(5) = 0.4656$$

$$P_{33}(5) = 0.3934$$

$$P_{32}(5) = 0.5332$$

$$P_{22}(5) = 0.7965 \qquad 40$$

The expected total weight of the particles in size i can readily be calculated from Eqs. 25 through 37. The variations of the weight distribution for the particles at t of 0, 1, and 5 are shown in Fig. 7.5.1. As can be seen, attrition during pneumatic transport can greatly increase the amount of fine particles fed to the bed. In fact, attrition during pneumatic transport is believed to be an important factor in determining the overall attrition behavior of a sorbent.

In-bed Attrition. The preceding numerical example also illustrates how the model is used to calculate the amount of fines produced by in-bed attrition. However, for in-bed attrition, the attrition constants and time scales are altered, but in opposite directions. The λ_4 attrition constant is typically decreased to around 10^{-6} sec^{-1} rather than 1 sec^{-1} in Table 7.5.1. The time (t) is increased to (0.2 to 1) x 10^5 sec rather than 1 to 5 sec in Fig. 7.5.1. These opposing changes tend to cancel. As a result, the model predicts significant production of fine particles (size 1) from in-bed attrition although certainly not to the extent shown in Fig. 7.5.1. In fact, the model predicts that in an hour only 1 to 4% of the larger size particles are abraded and broken into size 1 particles. However, given the large mass of the bed, the fines produced from in-bed attrition amount to 0 to 90% of the sorbent feed to the bed in the same period. Thus, in some cases the sorbent feed rate is determined by the desire to maintain the bed height, not from sulfur capture considerations.

Fig. 7.5.1

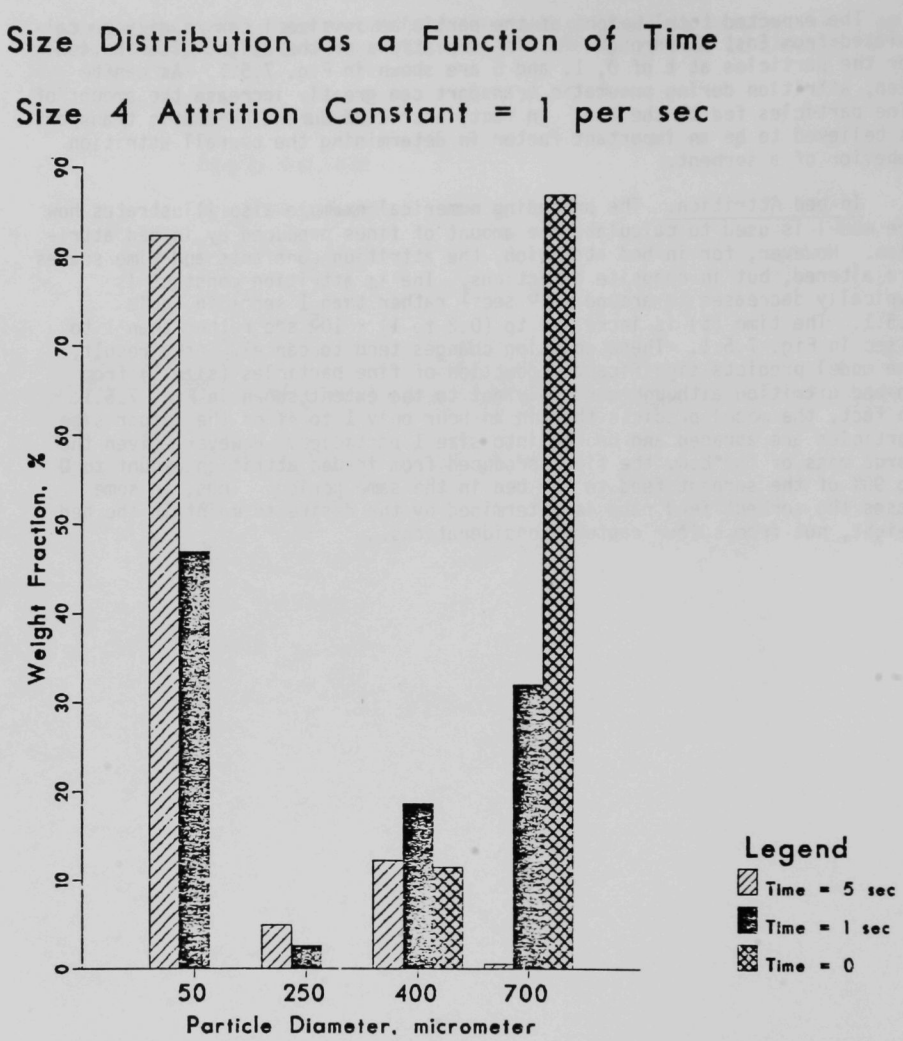
Size Distribution as a Function of Time
Size 4 Attrition Constant = 1 per sec
Weight Fraction, %
0
10
20
30
40
50
60
70
80
90
50
250
400
700
Particle Diameter, micrometer
Legend
Time = 5 sec
Time = 1 sec
Time = 0

Nomenclature

D_i = diameter of the particle in size i, i = 1 ... 4

λ_k = intensity of particle disintegration from size k to k-1

$N_{ij}(t)$ = random variable representing the number of particles in size j at time t that were in size i at time zero

$n_{ij}(t)$ = expected number of paarticles in size j at time t that were in size i at time zero

$N_i(t)$ = random variable representing the number of particles in size i at time t, $N_i(0)$ = the initial number particle of size i

$n_i(t)$ = expected number of particles in size i at time t

$P_{ki}(t)$ = probability that the particle is in size i at time t that were in size k at time zero

t = time

w_i = random variable representing the weight of the particles in size i

X_{i1} = number of particles in size 1 which is generated from the disintegration of a particle from size i to size i - 1

ρ_p = density of particle

References Section 7.5

L. Austin, K. Shoji, V. Bhatia, V. Jindal, and K. Savage, "Some Results on the Description of Size Reduction as a Rate Process in Various Mille," I & EC Process Des. Dev. 15, 187 (1976).

L. S. Fan and R. C. Strivastava, "A Stochastic Model for Particle Disintegration I. Grinding Mechanism," Chem. Eng. Sci., 36, 1091 (1981).

L. T. Fan, L. S. Fan, and R. F. Nassar, "A Stochastic Model of the Unsteady Age Distribution in a Flow System," Chem. Eng. Sci., 34, 1172 (1979).

D. Merrick and J. Highly, "Particle Reduction and Elutriation in a Fluidized-Bed Process," AIChE Symposium Series No. 137, Vol. 70, p. 366 (1974).

R. F. Nassar, L. T. Fan, and L. S. Fan, "A Stochastic Treatment of Unimolecular Reactions in a Flow System," Chem. Eng. Sci., 36, 1094-1096 (1981).

J. Wei, W. Lee, and R. F. Krambeck, "Catalyst Attrition and Deactivation in Fluid Catalytic Cracking System," Chem. Eng. Sci. 32, 1211 (1977).

W. I. Wilson, D. C. Fee, and K. M. Myles, "Standardized Test Methods for Investigating Attrition and Elutriation Characteristics of Natural Sorbents in Fluidized-Bed Coal Combustors," Proc. Int. Powder and Bulk Solids Handling and Processing Conference, Rosemont, IL, May 12-14, 1981, Cohners Exposition Group (1981) p. 127.

7.6 ELUTRIATION

Elutriation is a phenomenon which must be given careful consideration during the operation of a fluidized bed. Particles of bed material become entrained in the fluidizing gas and are elutriated (i.e., carried from the bed). The extent of elutriation depends on the mass and diameter of the particles and the velocity of the fluidizing gas. For the same fluidizing gas velocity and solids density, the lighter sorbent particles with the smaller diameters tend to be elutriated to a greater degree. This affects the sulfur capture ability of the sorbent in two ways. First, the small particles react more rapidly and, thus, capture more sulfur for the same total weight of sorbent in the bed. Further, for the same sorbent, the maximum sorbent utilization increases as the particle size decreases. So selective elutriation of the small-size sorbent particles decreases the sulfur capture ability of the bed. Second, selective elutriation of the finer size sorbent particles affects sulfur capture by increasing the average residence time of the larger particles in the bed because fewer of the larger particles need be removed through the overflow to maintain the bed height. Thus, the larger particles survive to achieve higher utilizations (and lower reactivities) than would occur in the absence of elutriation. A higher feed rate of sorbent is then required to reduce the average residence time of the larger particles to the level where the desired sulfur capture is achieved. Because of the relationship between elutriation and sulfur capture, a model of elutriation in a fluidized bed has been developed.

The elutriation calculations being used are a modification of those presented in the literature [Levenspiel (1972), Levenspiel et al. 1968-69), Yagi and Kuni (1961a,b,c,)]. For the fluidized bed shown in Figure 7.6.1, the overall steady state mass balance for no reaction can be written as

$$F_0 = F_1 + F_2 \qquad 1$$

Where F_0 is the feed to the bed, F_1 is the overflow, and F_2 is the carry-over (elutriation). In the absence of particle abrasion and breakage, the mass balance can be written for a discrete size interval i, to give

$$X_{0i}F_0 = X_{1i}F_1 + X_{2i}F_2 \qquad 2$$

where X_{0i}, X_{1i}, and X_{2i} are the mass fractions of material in size interval i for streams 0, 1, and 2 respectively. The elutriation rate constant necessary to solve the above can be defined in terms of discrete intervals as

$$K_i = \frac{F_2 \; X_{2i}}{W \; X_{bi}} \qquad 3$$

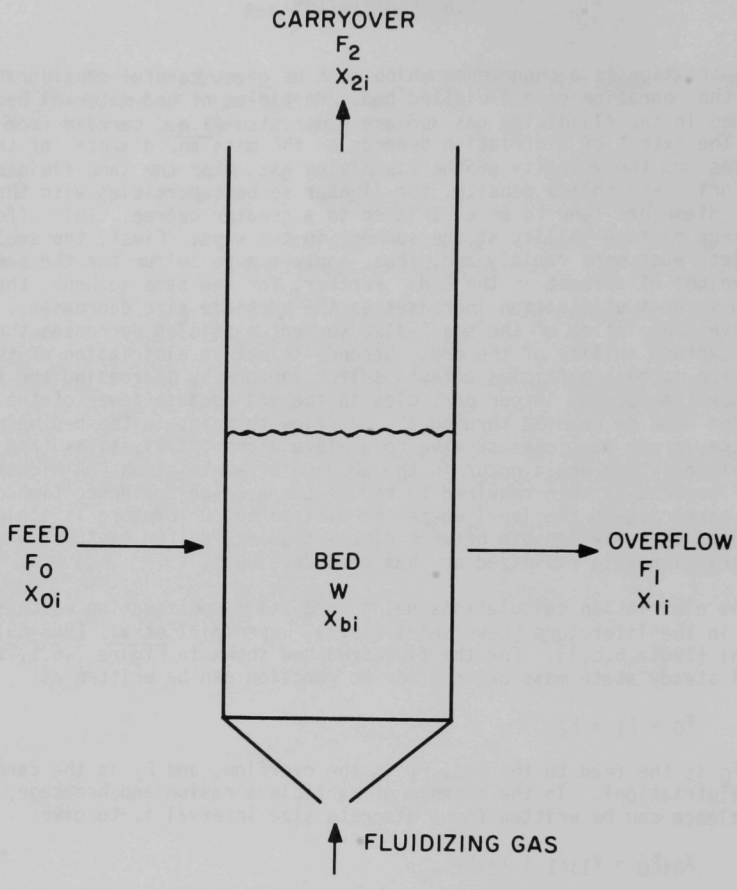
CARRYOVER
F_2
x_{2i}
FEED
F_0
x_{0i}
BED
W
x_{bi}
OVERFLOW
F_1
x_{1i}
FLUIDIZING GAS

Fig. 7.6.1

where W is the mass of the bed, and X_{bi} is the mass fraction of material in size interval i in the bed. For well mixed flow within the bed, the mass fraction within the overflow and the bed are identical (i.e., $X_{1i} = X_{bi}$), so the mass balance for size interval i becomes

$$X_{0i}F_0 = X_{1i}F_1 + K_i W X_{1i} \qquad 4$$

and the elutriation rate of particles of size i is given by

$$F_{2i} = K_i \, W X_{1i} \qquad 5$$

The total elutriation rate is the sum of the elutriation rate from each size interval

$$F_2 = \sum_i F_{2i} \qquad 6$$

Several empirical correlations for the elutriation rate constant, K_i, are available in the literature [Colakyan et al. (1979), Merrick and Highly (1974), Yagi and Aochi (1955), Wen and Hassinger (1960), Tanaka and Shinohara (1972)]. Those are summarized in Table 7.6.1. The correlation developed by Colakyan et al. was selected as the most appropriate because it was based on data from a large fluidized bed (1 m x 1 m) with in-bed tubes and a large freeboard section (8 m). In addition, the (ambient temperature) data was collected for large limestone particles and high gas velocities typical of what would be used in an AFBC.

The terminal velocity of the elutriated particle, V_T, is essential for calculating the elutriation rate using any of the correlations in Table 7.6.1. The terminal velocity of a particle is reached when the gravitational force on the particle is counter balanced by the fluid drag and buoyant forces on the particle [Leva (1959), Perry and Chilton (1973)]. The gravitational force is given by

$$F_g = \frac{\pi}{6} D_p^3 \rho_p \, g \qquad 7$$

where F_g is the gravitational force, D_p is the average particle diameter in size interval i, ρ_p is the particle density, and g is the gravitational acceleration. The term $\pi D_p^3 \rho_p/6$ represents the mass of the particle while g represents the acceleration in Newton's first law F = ma. The buoyant force results from the fluid displaced by the particle and is given by

$$F_b = \frac{\pi}{6} D_p^3 \rho_g \, g \qquad 8$$

where ρ_g is the density of the displaced gas. The relative motion between the fluid and the particle exerts a drag upon the particle. The drag force upon the particle is given by

$$F_d = \frac{1}{2} C_D \rho_g \frac{\pi D_p^2}{4} V^2 \qquad 9$$

where V is the relative velocity between the fluid and the particle and C_D is the dimensionless drag coefficient.

Table 7.6.1 Correlations for Elutriation

Colakyan et al.

$$K^* = 33.9\ (1 - V_t/U)^2$$

Geldhart et al.

$$\frac{K^*}{\rho_e U} = 23.7 \exp\left(-5.4\ \frac{V_t}{U}\right)$$

Merrick and Highley

$$\frac{K^*}{\rho_g U} = A + 130 \exp\left[-10.4\left(\frac{V_t}{U}\right)^{0.5}\left(\frac{U_{mf}}{U - U_{mf}}\right)^{0.25}\right]$$

Yagi and Aochi

$$K^* g d^2/\mu(U - V_t)^2 = 0.0015 Re_t^{0.6} + 0.01 Re_t^{1.2}$$

Wen and Hashinger

$$\frac{K^*}{\rho_g(U - V_t)} = 1.7 \times 10^{-5}\left[\frac{(U - V_t)^2}{gd}\right]^{0.5} Re_t^{0.725}\left(\frac{\rho_p - \rho_g}{p_g}\right)^{1.15}\left(\frac{U - V_t}{V_t}\right)^{0.1}$$

Tanaka and Shinohara

$$\frac{K^*}{\rho_g(U - V_t)} = 4.6 \times 10^{-2}\left[\frac{(U - V_t)^2}{gd}\right]^{0.5} Re_t^{0.3}\left(\frac{\rho_p - \rho_g}{p_g}\right)^{0.15}$$

When the terminal velocity, V_t, is reached, the buoyant and drag forces balance the gravitational force so that

$$F_g = F_b + F_d \qquad 10$$

Substituting for the above terms allows solution for the terminal velocity

$$V_t = \sqrt{\frac{4gD_p(\rho_p - \rho_g)}{3\rho_g C_D}} \qquad 11$$

The drag coefficient depends on the flow geometry and fluid properties described by the particle Reynolds number:

$$N_{Re} = \frac{D_p \rho_g V}{\mu} \qquad 12$$

where μ is the gas viscosity. For laminar flow about a sphere ($N_{Re} < 0.3$), Stokes law applies and

$$C_D = 24/N_{Re} \qquad 13$$

For turbulent flow about the sphere ($1000 < N_{Re} < 200{,}000$), Newton's law applies and

$$C_D = 0.44 \qquad 14$$

In the transition region ($0.3 < N_{Re} < 1000$) the drag coefficient relationship can be approximated by

$$C_D = 18.5\ N_{Re}^{-0.6} \qquad 15$$

An empirical relation providing better fit to the experimental data in the transition region has been applied by Do, Grace, and Clift (1972,1978). The correlation applies for $N_{Re} < 10^5$ and is given by

$$C_D = \frac{24}{N_{Re}}\left(1 + 0.15\ N_{Re}^{0.687}\right) + \frac{0.42}{1 + 42500\ N_{Re}^{-1.16}} \qquad 16$$

The above correlation has Stokes law as its limiting form as N_{Re} approaches zero; Newton's law is the limiting form of this correlation for large N_{Re}. Thus, the single Eq. 16 can be used in place of the three equations, 13 to 15.

Numerical Example

The physical properties for the elutriation calculations are given in Table 7.6.2. The first step requires the calculation of the terminal velocities for use in the calculation of k_i. An initial estimate of the drag coefficient, C_D, is used with Eq. 11 to obtain an estimate for V_t. The velocity V_t is used to calculate the particle Reynolds number in Eq. 12. A refined drag coefficient can then be obtained from Eq. 16 for further refinement of the value of V_t. Typical values are shown in Table 7.6.3.

Table 7.6.2. Nominal Values Employed for Numerical Example

Combustor cross section:	$A =$	$0.209\ m^2$
Fluidizing velocity	$U =$	$1.86\ m/sec$
Solid particle density:	$\rho_s =$	$2 \times 10^3\ kg/m^3$
Gas density:	$\rho_g =$	$0.3\ kg/m^3$
Gas viscosity:	$\mu =$	$4.5 \times 10^{-5}\ kg/m\ sec$
Bed weight:	$W =$	$300\ kg$

Table 7.6.3. Calculation of Terminal Velocities and Elutriation Constants

Interval	Particle Diameter, D_i μm	Bed Mass Fraction, X_{bi}	Particle Reynolds Number, N_{Re}	Drag Coefficient, C_D	Terminal Velocity, V_t m/sec	Elutriation Constant, k_i sec^{-1}	Carry-over F_2 kg/sec
1	50	0.002	0.0200	1212	0.599	0.0225	0.135
2	250	0.20	2.05	14.6	1.22	0.00284	0.170
3	400	0.58	6.67	5.59	2.50	$O(V_t>U)$	0
4	700	0.20	23.7	2.35	5.09	$O(V_t>U)$	0

Total F_2 = 0.305

Symbols Used

A	= cross-sectional area of bed (m^2)
d	= particle diameter, m
g	= acceleration of gravity
K	= elutriation rate constant (s^{-1}) ($K = K^* A/W$)
K^*	= carryover rate constant ($kg\ m^{-2} s^{-1}$)
Re_t	= Reynolds number of a particle at its terminal velocity ($\rho_g V_t d/\mu$)
U	= superficial gas velocity ($m\ s^{-1}$)
U_{mf}	= minimum fluidization velocity ($m\ s^{-1}$)
V_t	= terminal velocity of a particle ($m\ s^{-1}$
μ	= viscosity
ρ_g	= gas density ($kg\ m^{-3}$)
ρ_p	= mass of a single particle divided by the volume of the particle ($kg\ m^{-3}$)
ρ_e	= effective density of gas ($kg\ m^{-1}$)

References for Section 7.6

R. Clift, J. R. Grace and M. E. Weber, Bubbles, Drops and Particles, Academic Press, (1978) p. 111.

M. Colakyan, N. Catipovic, G. Jovanovic and T. Fitzgerald, "Elutriation from a Large Particle Fluidized Bed with and without Immersed Heat Transfer Tubes," Paper presented at the 72nd Annual Meeting, American Institute of Chemical Engineers, San Francisco, CA, November 25-29, 1979.

H. T. Do, J. R. Grace and R. Clift, Powder Technol. 6, pp. 195-200 (1972).

D. Geldart, J. Cullinan, S. Georghiades, D. Gilvray and D. J. Pope, Trans. I Chem. E. 57, 269-275 (1979).

M. Leva, Fluidization, McGraw-Hill, pp. 120-123 (1959).

O. Levenspiel, Chemical Reaction Engineering, 2nd Edition, John Wiley and Sons, 1972.

O. Levenspiel, D. Kuni and T. Fitzgerald, Power Technol. 2, 87-96 (1968/1969).

D. Merrick and J. Highley, "Particle Size Reduction and Elutriation in a Fluidized Bed Process," AIChE Symposium Series, 137, Vol. 70, 366 (1974).

R. H. Perry and C. H. Chilton, Eds., Chemical Engineers' Handbook, Fifth Edition, McGraw-Hill, pp. 5-61, 5-62 (1973).

I. Tanaka and H. Shinohara, Mem. Faculty Eng. Kyushu Univ. Japan, 32, 117 (1972).

C. Y. Wen and R. F. Hashinger, AIChE J. 6, 220 (1960).

S. Yagi and T. Aochi, Soc. Chem Eng. Japan, Spring Meeting, 1955.

S. Yagi and D. Kuni, Chem. Eng. Sci. 16, 364-371 (1961).

S. Yagi and D. Kuni, Chem. Eng. Sci. 16, 372-379 (1961).

S. Yagi and D. Kuni, Chem. Eng. Sci. 16, 380-391 (1961).

7.7 ELUTRIATION COUPLED WITH ATTRITION

Attrition and elutriation are closely coupled phenomena which affect sulfur capture by increasing and renewing the reactive surface area of the sorbent and by decreasing the residence time of the fine sorbent particles in the bed. The following model deals with this interrelationship by performing the following sequence of calculations.

1. Determine four size categories - The four sorbent particle diameter size categories used by the attrition and elutriation models are determined from the sorbent feed size distribution. Size category one is always 0 to 150 μm. This range is typical of the cyclone catch from a fluidized-bed combustor [LR:79:4775:01 (Babcock and Wilcox (1979)]. Further, the calculations show that particles in this size range are not usually retained in the bed. Sizes 2, 3, and 4 are equal in size and span the range from 150 μm to the upper limit of sorbent particle diameter in the feed hopper.

2. Partition the sorbent material - The sorbent feed is partitioned into the four size categories based on the sieve analysis of the material in the sorbent feed hopper. This feed distribution is also used as the initial estimate for the steady state distribution of particle sizes in the fluidized-bed.

3. Determine fines production rate from attrition - The production rate of fines from abrasion and collision is determined from the attrition model and the particle size distribution in the bed. The attrition constant, λ_4, is determined from standard laboratory attrition tests. An adjustment is made to λ_4 for the difference in diameter of size 4 particles between the laboratory test and the fluidized-bed combustor that is being modeled. Further, an adjustment is also made for the difference in fluidization conditions between the standard laboratory attrition test and the fluidized-bed combustor.

The adjustment for different particle size (see Section 7.5) and different fluidization conditions [Perry (1963), Merrick and Highly (1974)] has the following form

$$\lambda_4^{FBC} = \lambda_4^{test} \left(\frac{D_4^{FBC}}{D_4^{test}} \right)^3 \left(\frac{U^{FBC} - U_{mf}^{FBC}}{U^{test} - U_{mf}^{test}} \right) \qquad 1$$

where FBC refers to the fluidized-bed combustor being modeled, test refers to the fluidized-bed used for the attrition test, D_4 is the average particle diameter of size 4 particles (m), U is the fluidization velocity (m/sec), and U_{mf} is the minimum fluidization velocity (m/sec). Equations to calculate U_{mf} are found in Section 7.1, IN-BED SULFATION.

4. Determine fines feeding rate - Finely sized particles are introduced into the bed via feeding followed by calcination. The production of fines during calcination is also determined from the standard laboratory attrition test. The test showed the fraction of the sorbent which breaks up to produce fines during calcination. This fraction of sorbent feed sizes 2, 3, and 4 is subtracted from these larger size categories and added to the size 1 category to yield the amount of fines (size 1) arising from shock calcination and from sorbent feeding.

5. Determine elutriation constant - The elutriation constant is determined using the elutriation model. The solids density value which is input to the model is taken as the average density of the bed. This average density depends on the extent of sulfation of the sorbent which is determined using one of the models of in-bed sulfation.

6. Determine elutriation rate - The elutriation rate (kg/sec) of partially sulfated sorbent material is determined from the elutriation model (see ELUTRIATION). The elutriation rate of calcium is compared to the feed rate of calcium. If the feed rate exceeds the elutriation rate, the difference represents the amount of material removed by the bed drain. If the feed rate is less than the elutriation rate, the difference represents the amount of additional sorbent feed required to maintain a constant bed height.

7. Determine steady state conditions - Steady state conditions are achieved by iterating through steps 3 to 6 until the particle size distribution in the bed is constant. For example, a constant bed weight fraction of size 4 indicates that the feed rate of size 4 particles (reduced by shock calcination losses) balances the removal of size 4 particles due to attrition. During this iteration step, a constant bed height is maintained.

The foregoing sequence of calculation gives the rate at which sorbent material is elutriated from the bed. The elutriation rate is then compared with the sorbent feed rate required to achieve the desired sulfur capture. Obviously more sorbent must be added in situation where the sorbent feed rate is less than the elutriation rate.

Numerical Example

Tables 7.7.1 and 7.7.2 give the fixed dimensions of the fluidized-bed combustor and other data that are used in this example. The sequence of calculation is as follows:

1. Determine four size categories - The maximum size particle in the sorbent feed (Table 7.7.1) is 2500 μm. Size 1 is always 0 to 150 μm. Sizes 2, 3 and 4 are equal in size and span the range 150 to 930 μm, 930 to 1720 μm and 1720 to 2500 μm for sizes 2, 3 and 4, respectively. The average particle diameter for each size is taken as the midpoint of the size range, namely 75, 540, 1325, 2110 μm.

2. Partition the Sorbent Material - The sorbent feed material is partitioned into the four size categories based on sieve analysis. As calculated from data given in Table 7.7.1, this is 12 wt % in size 1, 38 wt % in size 2, 38 wt %, in size 3, and 12 wt % in size 4.

3. Determine fines production rate from attrition - The fines produced by attrition are determined using the attrition model. Two inputs are required for the attrition model. First, the weight fraction of each size category in the bed must be known. The initial estimate is taken as the feed size distribution calculated above. Second, the attrition constant for the size 4 particles must be calculated; this is determined using Eq. 1,

D_4^{FBC} = 2110 μm (step 1)

where $\lambda_4^{test} = 5.7 \times 10^{-7}$ sec^{-1} (Table 7.7.2)

D_4^{test} = 858 μm. (ANALYSIS OF ATTRITION DATA)

U^{FBC} = 2.00 m/sec (see Table 7.7.1)

U_{mf}^{FBC} = 0.22 m/sec (Calculated)

U^{test} = 1.5 m/sec (see STANDARD TESTS)

U_{mf}^{test} = 0.19 m/sec (Calculated)

Thus,

$$\lambda_4^{FBC} = 1.1 \times 10^{-5} \text{ sec}^{-1}$$

Having calculated the attrition constant for the size 4 particles in the FBC, the attrition constants for the smaller size categories are calculated as follows) see ATTRITION, Eq. 23).

$$\lambda_3^{FBC} = 2.7 \times 10^{-6} \text{ sec}^{-1} = \left(\frac{1325}{2110}\right)^3 \lambda_4^{FBC}$$

and

$$\lambda_2^{FBC} = 1.8 \times 10^{-7}\ \text{sec}^{-1} = \left(\frac{540}{2110}\right)^3 \lambda_4^{FBC}$$

Using these attrition constants the attrition probabilities after t = 60 sec are as follows (see Section 7.5, Eqs. 16 through 21)

$P_{44} = 0.99934$
$P_{43} = 6.558 \times 10^{-4}$
$P_{42} = 5.34 \times 10^{-8}$
$P_{33} = 0.99984$
$P_{32} = 1.628 \times 10^{-4}$
$P_{22} = 0.99988$

The bed weight, (w), calculated from the bed dimensions and the estimated density of the partially sulfated sorbent, is 1400 kg. Using this bed weight, the bed size distribution determined in step 2 above, and the attrition probabilities determined above, results in a calculated formation of 1.69 kg of new size 1 particles from attrition per minute (0.028 kg/sec).

4. Determine fines feeding rate - The size 1 particles entering the bed are the initial size 1 particles in the feed (12 wt %) plus new size 1 particles produced by calcination. The new size 1 particles produced by calcination are determined by multiplying the fraction of sorbent breakup due to attrition (0.18 for sorbent 9601, see Table 7.7.2) times the feed size distribution for size 2, 3 and 4. Thus, the size distribution of material fed to the bed when breakup due to calcination is taken into account is as follows:

size 1 feeding rate 12 + 0.18(38) + 0.18(38)+ 0.18(12) = 27.8 wt %
size 2 feeding rate = 38(1 - 0.18) = 31.1 wt %
size 3 feeding rate = 38(1 - 0.18) = 31.1 wt %
size 4 feeding rate = 12(1 - 0.18) = 9.8 wt %

5. Determine elutriation constant - The elutriation constant is determined for each size category using the elutriation model, Section 7.6, and the average particle diameters for each size. These are

$K_1 = 0.071\ \text{sec}^{-1}$
$K_2 = 0$
$K_3 = 0$
$K_4 = 0$

The elutriation constants for size 2, 3 and 4 are zero because the terminal velocity, V_t, is greater than the fluidizing velocity, U. Thus, the larger

particles are not entrained and carried over from the bed.

6. Determine elutriation rate - The elutriation rate of size i particles, F_{2i}, (kg/sec) is calculated using Eq. 2

$$F_{2i} = K_i W_i \qquad 2$$

where W_i is the weight of size i particles in the bed of total weight, W (kg). Using an initial estimate of a bed weight fraction of size 1 particles of 0.12 gives W_i = 0.12(1400kg) = 168 kg initially in the bed. One second later, at a Ca/S ratio of 4.5, 0.053 kg of sorbent has been fed to the bed of which 27.8 wt % (from step 4) is size 1 particles. Further, after one second, 0.028 kg of size 1 particles have been formed from attrition (step 3). Thus, after 1 sec the weight of size 1 particles is 168 + 0.278(0.053) + 0.028 = 168.04 kg. The elutriation rate is (0.071) (168.04) = 11.93 kg/sec. The weight fraction of size 1 particles left in the bed is (168 - 11.93)/(1400 - 11.93) = 0.112. This is the trial value to be used in the next iteration, starting again with a bed weight of 1400 kg.

7. Determine steady state conditions - The steady state conditions, determined by iterating through steps 3 to 6 until the particle size distribution in the bed is constant, is $X_{b1} = 2.03 \times 10^{-4}$, X_{b2} = 0.434, X_{b3} = 0.432, X_{b4} = 0.134. The steady state elutriation rate is 0.020 kg/sec.

8. After adjusting for the different calcium weight fractions in the sorbent feed (0.687) and the partially sulfated sorbent material (0.547), 33% of the calcium fed to the bed is calculated to be eluted at 85% retention. Thus, the bed height appears to be easily maintained in this example.

Table 7.7.1. Nominal Values Employed for Numerical Example

Temperature = 850°C = 1562 °F

Pressure = 101 kPa = 1.0 atm

U_{FBC} = Fluidizing Gas Velocity = 2.00 m/sec = 6.56 ft/sec

Bed Height = 1.20 meters = 3.93 ft

Coal Feed Rate = 897.6 kg/hr = 1977.0 lb/hr

Sulfur Content of Coal = 2.58 wt %

Bed Area = 3.34 sq meter = 36.0 sq ft

Volume fraction voidage in emulsion phase:	ε	= 0.45 estimated
Volume fraction inerts in bed:	F_I	= 0.05 estimated
Volume fraction heat exchange tubes in bed:	F_H	= 0.04 estimated
Gas density:	ρ_g	= 0.33 kg/m^3
Acceleration of gravity:	g	= 9.80 m/sec^2
Gas viscosity:	μ	= 4.5 x 10^{-5} kg/m -sec (450 micropoise)
Bed diameter:	D_R	= 1.82 meter (6 ft)
Number of orifice openings in distributor plate	N_D	= 3580
Freeboard height	7.9 m (26 ft)	

Table 7.7.2. Properties of Sorbent 9601

Attrition constant from standard test, $\lambda_4(sec^{-1}) = 5.7 \times 10^{-7}$

Sorbent breakup due to calcination (%) = 18

Density: raw sorbent 2.54 g/cm^3

calcined 1.49 g/cm^3

Chemical composition: 96.0 wt % $CaCO_3$

Sorbent size distribution:

average size in bed = 1000 μm

feed size - weight percentage less than

Micron	%
9500	100
6350	100
4750	100
2500	100
1720	88
1330	72
930	50
600	34
300	21
150	12
75	6

References for Section 7.7

LR:79:4775:01, "Fluidized Bed Combustion Facility and Commercial Utility AFBC Design Assessment," Babcock and Wilcox Quarterly Technical Progress Report - January through March, 1979. (1979)

D. Merrick and J. Highly, "Particle Reduction and Elutriation in a Fluidized-Bed Process," AIChE Symposium Series No. 137, Vol. 70, p. 366 (1974).

J. H. Perry (ed.), "Chemical Engineers Handbook," McGraw-Hill, New York (1963) Chapter 8.

8.0 FBC PLANT DATA

The literature has been reviewed to extract data on sorbent utilization in fluidized-beds combustors. (See ANL/FE-10; Addendum, "Sulfur Control in Fluidized-Bed Combustors: Methodology for Predicting the Performance of Limestone and Dolomite Sorbents," Compilation of Sorbent Performance Data from Atmospheric Fluidized-Bed Combustors, supersedes ANL/CEN/FE-80-10, "Sulfur Control in Fluidized-Bed Combustors: Sorbent Utilization Prediction Methodology," 1980.) The principle focus is the larger combustors, combustors greater than 18-inch in diameter. Although somewhat arbitrary, the choice of this size of combustor as a basis for comparing sulfur capture predictions with experiment is based on two conflicting goals. The first goal is to eliminate potential problems of scale-up to future large commercial FBC's. Potential problems arise from the different bed hydrodynamics between small fluidized-beds (dominated by slugging and other wall effects) and large commercial prototypes. The second goal is to compare the sulfur capture predictions with as much combustor data as possible. Restricting the comparison only to the two or three extant commercial scale fluidized-bed combustors eliminates the interesting variety of sorbents and operating conditions examined with the smaller combustors. (For this reason, selected data from fluidized-bed combustors smaller than 18-inch in diameter have been included in the review, although sulfur capture predictions are not made for these small combustors.) Thus, the data on sorbent utilization in fluidized-bed combustors have been compiled largely on units greater than 18-inch in diameter. Further, the performance data included in the review represents the data available at the time of publication either in the open literature or by private arrangement with the combustor operators and Morgantown Energy Technology Center.

Distribution for ANL/FE-80-10

Internal:

L. Burris
E. L. Carls
D. C. Fee
J. E. Helt
R. Henry
H.-S. Huang
I. Johnson
A. A. Jonke
S. H. D. Lee
J. F. Lenc
S. A. Miller
K. M. Myles
P. Nelson
M. Petrick
W. F. Podolski
J. J. Roberts
J. A. Shearer
S. D. Smith
G. W. Smith
E. B. Smyk
W. M. Swift
F. G. Teats
W. I. Wilson (65)
J. E. Young
ANL Patent Dept.
ANL Contract File
ANL Libraries
TIS Files (6)

External:

DOE-TIC, for distribution per UC-90e (367)
Manager, Chicago Operations Office, DOE
V. H. Hummel, DOE/CH
Chemical Technology Division Review Committee:
C. B. Alcock, U. Toronto
S. Baron, Burns and Roe, Inc., Oradell, N. J.
T. Cole, Jet Propulsion Lab.
M. N. Delgass, Purdue U.
H. Perry, Resources of the Future, Washington
W. L. Worrell, U. Pennsylvania
J. J. Markowsky, American Electric Power Service, New York City
T. Modrak, Babcock and Wilcox, Alliance, O.
J. Tang, Babcock and Wilcox, Alliance, O.
H. Raymond Hoy, BCURA Ltd., Leatherhead, England
S. Farbstein, B. F. Goodrich, Cleveland
H. Nack, Battelle Columbus Labs.
E. Kimell, Burns and Roe, Inc., Oradell, N. J.
W. Norcross, Combustion Engineering, Windsor, Conn.
A. Leon, Dorr-Oliver, Stamford, Conn.
S. Ehrlich, Electric Power Research Inst., Palo Alto
J. Porter, Energy and Environmental Engineering, Cambridge, Mass.
D. DeCoursin, Fluidyne Engineering, Minn.
R. Gamble, Foster Wheeler, Livingston, N. J.
P. Fennelly, GCA Corp., Bedford, Mass.
S. Callahan, General Atomic Co., San Diego
C. Thoennes, General Electric Co., Schenectady
G. M. Goblirsch, Grand Forks Energy Technology Center
D. Farrell, Illinois Dept. of Energy, Springfield
Librarian, Illinois Institute of Natural Resources, Champaign
B. R. Hutchinson, Johnston Boiler, Ferrysburg, Mich.
J. M. Beer, Massachusetts Inst. Technology
S. Mori, Nagoya Inst. of Technology, Nagoya, Japan
S.. H. Wong, Northern Petrochemical Co., Morris, Ill.
J. Salmela, Northern States Power Co., Minneapolis
L.-S. Fan, Ohio State U.
V. Buck, Pope, Evans, and Robbins, New York City
T. Stringfellow, Pope, Evans, and Robbins, Rivesville, W. Va.

L. Tignac, Rockwell International, Canoga Park
A. M. Manaker, Tennessee Valley Authority, Chattanooga
H. Withers, Tennessee Valley Authority, Chattanooga
J. Highley, U. K. National Coal Bd., Gloucestershire, England
J. Byam, U. S. Department of Energy (METC), Morgantown, W. Va.
L. Carpenter, U. S. Department of Energy (METC), Morgantown, W. Va.
A. Hall, U. S. Department of Energy (METC), Morgantown, W. Va.
J. Halow, U. S. Department of Energy (METC), Morgantown, W. Va.
Library, Morgantown Energy Technology Center
K. Markel, Jr., U. S. Department of Energy (METC), Morgantown, W. Va.
J. McClung, U. S. Department of Energy (METC), Morgantown, W. Va.
J. Mei, U. S. Department of Energy (METC), Morgantown, W. Va.
J. Notestein, U. S. Department of Energy (METC), Morgantown, W. Va.
J. Wilson, U. S. Department of Energy (METC), Morgantown, W. Va.
J. Geffken, U. S. Department of Energy, Washington
W. Siskind, U. S. Department of Energy, Washington
G. Weth, U. S. Department of Energy, Washington
D. Henschel, U. S. Environmental Protection Agency, Research Triangle Park
F. Boenig, United Technologies Corp., South Windsor, Conn.
S. Saxena, U. Illinois, Chicago
T. Furusawa, U. Tokyo, Tokyo, Japan
R. Bailie, West Virginia U., Morgantown, W. Va.
D. Keairns, Westinghouse Research and Development Center, Pittsburgh
R. Newby, Westinghouse Research and Development Center, Pittsburgh
A. Wormser, Wormser Engineering, Middleton, Mass.

ARGONNE NATIONAL LAB WEST
3 4444 00029707 7
X

B